

EXTENDING ARTIFICIAL METALLOENZYMES FOR THE UNCAGING OF DRUGS ON CELLS

Inauguraldissertation

zur Erlangung der Würde eines Doktors der Philosophie

vorgelegt der

Philosophisch-Naturwissenschaftlichen Fakultät

der Universität Basel

von

Boris Lozhkin

2022

Originaldokument gespeichert auf dem Dokumentenserver der Universität Basel
edoc.unibas.ch

Genehmigt von der Philosophisch-Naturwissenschaftlichen Fakultät

auf Antrag von

Prof. Dr. Thomas Ward, Prof. Dr. Christof Sparr und Prof. Dr. Asier Unciti-Broceta.

Basel, den 18.10.2022

Prof. Dr. Marcel Mayor

(Dekan)

Die vorliegende Arbeit wurde von Januar 2018 bis September 2022 an der Universität Basel unter Leitung von Prof. Dr. Thomas Ward angefertigt. Teile dieser Arbeit wurden veröffentlicht:

Lozhkin, B.; Ward, T. R. Bioorthogonal Strategies for the *in Vivo* Synthesis or Release of Drugs. *Bioorganic & medicinal chemistry* **2021**, 45, 116310

Lozhkin, B., Ward, T. R. A Close-to-Aromatize Approach for the Late-Stage Functionalization through Ring Closing Metathesis. *Helvetica Chimica Acta* **2021**, 104(5), e2100024

Christoffel, F., Igareta, N., Pellizzoni, M. M., Tiessler-Sala, L., **Lozhkin, B.**, Spiess, D. C., Lledos, A., Marechal, J.-D., Peterson, R. L., Ward, T. R.; Design and Evolution of Chimeric Streptavidin for Protein-Enabled Dual Gold Catalysis. *Nature Catalysis* **2021**, 4 (8), 643-653

Let's go. In and out. 20 minutes adventure.

Rick and Morty S3:E6

Acknowledgements

First and foremost, I would like to thank *Prof. Dr. Thomas R. Ward* for accepting me as a PhD student and giving me the opportunity to work on such a fascinating research topic. I really appreciate your support and assistance over these almost five years. You always inspired and motivated me, especially during difficult times. I am very thankful that I had a chance to improve myself both professionally and personally.

I would sincerely like to thank *Prof. Dr. Christof Sparr* for agreeing to become the co-referee for this dissertation and *Prof. Dr. Asier Unciti-Broceta* for accepting to be the external expert.

Moreover, I want to acknowledge my colleagues from the WARD group for the great working atmosphere. *Johannes Rebelein*, *Brett Garabedian*, *Alina Stein*, and *Robin Vinck*, thank you for your tenacity in a project that no one believed in. *Zhi (Robin) Zou* and *Elinor Morris*, thank you for the hope I have at the end of my journey here. I would also like to acknowledge *Ryo Tachibana* for our short but very informative conversations about things in which I did not understand anything but learned a lot. Thank you, *Jaicy Vallapurackal*, for the amazing time we had at the film festival in Locarno. I also want to acknowledge all the postdoc labmates *Alexandria Deliz Liang*, *Daniel Brodbeck*, and *Yoann Cotelte* for the opportunity to learn from you. And last but not least, I would like to thank all other current and former group members for the time we had together and for being a part of my life even if we didn't talk much. Thank all of you guys for your support in the lab and beyond!

I would sincerely like to thank *Prof. Dr. David Baker* for the chance to work on a very challenging but interesting project and *Dr. Indrek Kalvet* for his contribution to my research.

I would also like to acknowledge Marie Skłodowska-Curie European Training Network for partially funding this project and the opportunity to meet amazing people and learn a lot. If not for pandemic, we would have achieved much more.

The research would not have been possible without the entire staff of the Chemistry Department. I would like to thank *Prof. Dr. Daniel Häussinger* for the support concerning NMR experiments and *Dr. Michael Pfeffer* for performing HRMS measurements. I am also grateful to the whole Werkstatt team and *Jonas Zurflüh* for solving problems with instruments and lab equipment and to the IT support, especially *Dr. Bernhard Jung*, for figuring out all the technical issues. I would like to thank *Esther Stalder* and *Claudia Stadelmann-Prescha* for your help with administrative questions and your kind words.

Over the last five years, I have met so many amazing people from the chemistry department who also became my friends. Many thanks go to *Dzmitry Miarzlou*, *Egor Nalivaiko*, *Snizhana Zaitseva*, and *Oleksandr Vyhivskyi*. Thank you, guys, for our cozy parties and celebrations! It was always great to feel at home. I am also incredibly grateful to *Oleks* for his professional help.

A special thank deserves *Mariia Beliaeva*, who is my colleague and neighbor. Thank you for the introduction to protein production and for being such a great person and friend.

My most important thanks are to my fiancée, *Daria*. Thank you for making me better every day, for your support and for always being by my side. I wouldn't have made it without you. Love you, Dr. Куся.

Last but not least, I want to thank my mom *Irina* and my friends *Stepan*, *Mikhail*, and *Roman* for your beliefs in me, and for our joint past and future.

Table of Contents

1. Introduction.....	1
1.1. Summary of the publication	1
1.2. Manuscript Reprint	3
2. Objectives of This Thesis.....	17
3. Results and Discussion.....	18
3.1. Deallylation project	18
Bioorthogonal activation of a prodrug on cells.....	18
Ru-deallylation.....	19
Fluorinated anchors.....	21
Azolamide derivatives and experiments on cells.....	25
Prodrugs synthesis and evaluation	29
Outlook	34
3.2. Ring-Closing Metathesis Project	35
A Close-to-Aromatize Approach for the Late-Stage Functionalization through Ring-Closing Metathesis.....	35
Abstract of the publication.....	35
Potential substrates for <i>in vivo</i> synthesis of bioactive molecules.	40
Close-to-release approach (phenols).....	44
Close-to-release approach (carbamates)	48
MINFLUX project	49
Dendritic approach.....	53
Side projects.....	60
3.3. <i>De Novo</i> Artificial Metalloenzymes	63
Brief summary of existing approaches to abiotic enzymatic reactions.....	63
On the way to fully engineered ArMs.....	65
Synthesis of the carbene precursor XVII	67
Synthesis of metal cofactors	73
RuTRPs.....	79
AuTRPs.....	81
4. Summary and Outlook	83
5. Supplementary Information	84
5.1. Deallylation Project	84
8-(Allyloxy)quinoline-5-carboxylic acid derivatives.....	84

α,ω -Aminothiols.....	87
2,5,6-Trifluorobenzenesulfonamides	89
Azolamide derivatives	98
Drug and prodrug synthesis	105
Dimeric caging.....	108
5.2. RCM Project.....	112
Substrates for the <i>in vivo</i> synthesis	112
Click-to-release approach (phenols)	115
Close-to-release approach (carbamates)	120
MINFLUX project	122
Dendritic approach.....	130
Alternative ligands	135
Alternative anchors	137
5.3. <i>De Novo</i> ArMs Project	140
Synthesis of NHC precursor DB13	140
Alternative routes' products	144
Gold cofactors.....	148
Ru-cofactors	150
Alternative routes' products	156
Substrates and products for catalytic assays	163
6. Index of Abbreviations	165
7. Literature References	169
8. Reprint Permissions.....	174
9. Appendix.....	175

1. Introduction

1.1. Summary of the publication

A previous review “*In Vivo* Catalyzed New-to-Nature Reaction” published by the Ward group included the advances in bioorthogonal transformations inside living cells and organisms by mid-2017.¹ The review reproduced below “Bioorthogonal strategies for the *in vivo* synthesis or release of drugs” summarizes the key achievements in this field from 2017 to 2021 and underlines the importance of biocompatible metal catalysts as elements of the anticancer therapy. The range of active catalytic metal species used to carry out new-to-nature reactions on cells and tissues has grown significantly. At the same time, the toolkit of protecting groups and modalities used for the drug caging-uncaging, as well as the targeted delivery of prodrugs to diseased cells, has also been expanded.

Bioorthogonal catalysts can be divided into two classes: heterogeneous and homogeneous. The indisputable advantages of heterogeneous catalysts include their stability in cells and living organisms. This makes it possible to achieve high TONs and, consequently, high concentrations of bioactive molecules upon selective uncaging of cytotoxins in tumors. For example, the Unciti-Broceta group in 2018 reported the first clinically-relevant result for the release of doxorubicin in an animal model (zebrafish). Resin nanoparticles (NPs) loaded with Pd were implanted in an animal body and then used for the depropargylation of the caged drug *in vivo*. Subsequently, this approach was significantly extended to other metals and prodrugs. In addition to Pd- and Au-catalyzed depropargylation, it is also worth noting significant achievements in the field of bioorthogonal catalysis by groups: Gu (deallylation by Pd-coated TiO₂ in mice), Qu (enantioselective hydrogenation by neutrophil-coated silica NPs embedded with Pd and chiral alkaloids in mice), Suzuki-Miyaura cross coupling by photosensitive Pd-loaded silica NPs in HeLa cells, azide-alkyne cycloaddition by Cu-loaded MOFs in *C.elegans.*), Weissleder (Heck reaction and deallylation by Pd(II) complex encapsulated in polymer NPs in mice), Palmans (depropargylation and deallylation by Pd(II) and Cu(I) in single-chain NPs in HeLa cells), Mascareñas (depropargylation by Pd-loaded hollow silica spheres and MOFs), Pané (depropargylation by Fe-Pd-nanowires in mice), Zhang (azide-alkyne cycloaddition by Cu-loaded lipoic acid NPs in HeLa cells), Rotello (azide reduction by Fe-loaded polyzymes in bacteria biofilms).

Despite the clear advantages of the above catalytic systems, their use is limited by the need to accurately implant a heterogeneous catalyst in the tumor region, which is not always possible (for example, for metastatic cancers). In addition, the high stability of these catalysts can become a disadvantage if the drug needs to be released to treat another tumor.

Homogeneous transition metal catalysis aims to overcome these limitations due to the potential for the precise targeted delivery of the cofactor to the surface or into cancer cells. In addition, the possibility of modifying the first coordination sphere of the metal opens up possibilities for fine tuning the properties of the catalyst (activity, selectivity). Thus, the Lin, Chen, and Davis groups used water-soluble palladium salts for a previously undescribed Sonogashira reaction in addition to Suzuki-Miyaura reaction in *E. coli*, *Shigella*, and HEK293 cells. Bernardes et al. demonstrated the applicability of a bioorthogonal approach to drug release from antibody-drug conjugates using Pd(cod)Cl₂.

The most innovative modalities have been developed for water-soluble gold complexes. Thus, Mascareñas and coworkers demonstrated the intramolecular hydroarylation leading to a highly

fluorescent product formation in HeLa cells. Tanaka and coworkers developed a new protecting group for amines (2-alkynylbenzamide, Ayba). Despite limited reactivity *in vivo*, this group is specifically cleaved only by gold complexes and is not reactive for other metal catalysts, which has been demonstrated in various cell lines. The same group developed an HSA-specific cofactor for catalytic hydroamination, which demonstrated an unprecedented efficiency (211 TON) in the presence of cell components.

Ruthenium is another promising metal for *in vivo* catalysis. The Mascareñas group demonstrated the orthogonality of Au-catalyzed hydroarylation and Ru-catalyzed deallylation in HeLa cells. The same group then showed that deallylation catalysts also catalyze [2+2+2]-cycloadditions both in intra- and intermolecular manners. Ru(IV) complexes have also been found to promote isomerization of allyl alcohols to ketones giving fluorescent products.

Ward and coworkers developed artificial metathesases for ring-closing metathesis of diolefins, which was further expanded by Tanaka group in the synthesis of an anticancer drug. The Ru-cofactor bound to glycosylated HAS significantly reduced viability of various cells lines by cyclization of umbelliprenin precursor.

In vivo RCM was further expanded by Ward and coworkers. A Ru-cleavable diolefin protecting group can be used for caging of various functional groups for a wide range of bioactive molecules.

Other metals were also used for homogeneous bioorthogonal catalysis by groups: Chen (depropargylation of ADCs by Cu(I)BTAA), Do (transfer hydrogenation by IrCp* complexes in NIH-3T3), Sadler (perturbation of the redox homeostasis of cells by Ru(II), Os(II), Ir(III) complexes), Bernardes (pentynoyl cleavage from ADCs by Pt(II) complexes in HeLa cells and zebrafish).

Many of the bioorthogonal reactions mentioned have not been applied to drug release but have only been tested on fluorogenic substrates in cells. Despite this, these findings provide an innovative arsenal with great potential. Optimizing existing methods and developing new ones could lead to breakthroughs in new therapies for cancer and other diseases.

1.2. Manuscript Reprint

Bioorg. Med. Chem. 45 (2021) 116310



Contents lists available at ScienceDirect

Bioorganic & Medicinal Chemistry

journal homepage: www.elsevier.com/locate/bmcBioorthogonal strategies for the *in vivo* synthesis or release of drugs

Boris Lozhkin, Thomas R. Ward*

Department of Chemistry, University of Basel, BPR 1096, Mattenstrasse 24a, Biopark Rosental, 4058 Basel, Switzerland

ARTICLE INFO

Keywords:

Bioorthogonality
Prodrug activation
Drug delivery
Catalysis
Artificial metalloenzymes

ABSTRACT

The site-specific delivery of antitumor agents is a rapidly developing field that relies on prodrug activation and uncaging strategies. For this purpose, a wide range of homogeneous and heterogeneous biocompatible activators/catalysts have been developed to convert caged drugs with low toxicity and high stability in physiological settings into active substances in a bioorthogonal manner. The current methods allow for the site-specific delivery of activators and prodrugs to organelles, target cells, or tumors in living organisms. Here, we present an overview of the latest advances in catalytic drugs, highlighting the expanding toolbox of bioorthogonal activation strategies made possible by transition metals acting as activators or catalysts.

1. Introduction

Until recently, the spectrum of *in-vivo* cleavable protecting groups amenable to minimize the toxicity of drugs (anti-inflammatory, anti-tumor, and others) was strictly limited by the repertoire of natural enzymes. –The term *in vivo* will be used throughout to describe catalytic systems performed in the presence of living cells (e.g. cell cultures). Whether the catalytic event occurs “inside” or “outside” of the cells will be specified in each case. – For example, native hydrolases and oxidoreductases, among others, can be used to uncage a drug *in vivo*. Since such enzymes are widely distributed in most tissues in the body, it is challenging to site-specifically uncage a bioactive molecule where its therapeutic action is most desirable (see Fig. 1).

The pronounced toxicity of many antitumor drugs, both for diseased and healthy cells, calls for strategies to minimize these severe side effects where the drug is not needed. The term *bioorthogonality* was introduced by Hang et al. in 2003 and is used to describe “chemical reactions that neither interact with nor interfere with a biological system”.¹ The presence of a large number of functionalities in cells and intercellular space complicates the identification of such reactions and reagents that do not interact with the native biological environment.

In the early 2000s, there were very few reactions displaying low reactivity in biological systems and high specificity of binding to the target substrate. Among these, the Staudinger ligation, developed in 2003,¹ and the metal-free click reaction, reported in 2007,² occupies a prominent place. Capitalizing on these tools, it proved possible to label cells, tissues and microorganisms using fluorescent probes via reaction of organic azides with esters and triple bonds, respectively.

Despite their high specificity, these approaches are strictly stoichiometric and therefore cannot be used to generate high concentrations of free fluorophores or potentially bioactive molecules.

In 2006, Streu and Meggers³ reported an important milestone in metal-catalyzed bioorthogonal reactions: the cleavage of allylcarbamates by [Cp*Ru(cod)Cl] (Cp* = pentamethylcyclopentadienyl, cod = 1,5-cyclooctadiene) (Fig. 2a). This uncaging reaction was demonstrated for the first time in HeLa cells. This achievement marked the starting point in the development of bioorthogonal organometallic catalysis as tool for new-to-nature reactions performed *in vivo*.

From this point on, the number of publications dedicated to bioorthogonal transformations in cells, tissues, and organisms has grown significantly (Fig. 3).

This area of research has developed primarily along two avenues: i) metal-free click-chemistry and ii) metal-catalyzed uncaging of drugs. The first approach allows for the site-specific delivery of activators and prodrugs to organelles and tissues. For this purpose, antibody-drug conjugates (ADCs) have been widely used. The metal-free click reaction has been expanded to a click-and-release strategy, whereby an inverse-electron-demand Diels-Alder reaction generates an intermediate that spontaneously undergoes tautomerization to release its cargo. This elegant strategy was developed by Robillard and coworkers in 2013⁴ and demonstrated in a mouse model by Wu and coworkers,⁵ wherein they developed a system that simultaneously releases the anticancer agent camptothecin and a NIR-fluorophore, allowing real-time monitoring of the drug release event. In another study, Xie and coworkers⁶ used pH-responsive polymers to target the delivery of the prodrug doxorubicin to tumor areas. Strictly speaking, the click-and-release

* Corresponding author.

E-mail address: Thomas.ward@unibas.ch (T.R. Ward).<https://doi.org/10.1016/j.bmc.2021.116310>

Received 21 May 2021; Received in revised form 6 July 2021; Accepted 9 July 2021

Available online 15 July 2021

0968-0896/© 2021 The Authors. Published by Elsevier Ltd. This is an open access article under the CC BY-NC-ND license

<http://creativecommons.org/licenses/by-nc-nd/4.0/>

approach is not catalytic as it requires stoichiometric amounts of diene and alkene (or alkyne). The advantages and disadvantages of recent advances in this area are discussed in detail in the reviews by Wang and coworkers⁷ and together with catalytic systems by many other researchers.^{8–13}

From a synthetic organic chemistry perspective, the most versatile means of carrying out chemical reactions *in vivo* is catalysis by transition metal complexes. The biocompatibility and bioorthogonality of these complexes have led to various applications in a cellular environment for the production or release of fluorophores and, more importantly, drugs. In this arena, an important milestone was achieved by the Bradley group.^{14–15} They reported that palladium nanoparticles anchored to the surface of polystyrene microspheres (approx. 0.5 μm) are effective for allylcarbamate cleavage and Suzuki–Miyaura coupling. These beads can penetrate the cell membrane and maintain their bioorthogonal activity in the cytoplasm. The Pd-nanodevices were used to uncage rhodamine 110 and separately synthesize a mitochondria-specific fluorophore.¹⁴ This approach was adapted by the Unciti-Broceta group by applying these Pd nanoparticles to uncage antitumor drugs.^{16–17} They showed that both caged 5-fluorouracil (5FU)⁹ and gemcitabine⁹ could be depropargylated in PBS in the presence of HCT116 or BxPC-3 and BxPC-3 or Mia PaCa-2 cells, respectively. Importantly, the propargylated and allylated gemcitabine was found to be 23–67 times less active than the free drug and pro-5FU showed no toxicity at all ($\text{EC}_{50} > 1 \text{ mM}$) for various cell lines. In each case, the prodrug-Pd nanoparticles combination had similar cytotoxicity to the unmodified drug. Additionally, zebrafish embryos injected with PEGylated Pd nanoparticles grew and developed without any noticeable negative effect.⁸

An alternative to nanoparticle catalysis is the use of transition metal complexes to carry out homogeneous catalysis *in vivo*, which does not require the implantation of solid particles into the body. Sánchez et al. reported on the unmasking of DNA-intercalating agents (DAPI and ethidium bromide) using $[\text{Cp}^*\text{Ru}(\text{cod})\text{Cl}]$ in the presence of an excess of the nucleophile.¹⁸ Building on the original work of Meggers and coworkers,² the same group developed new ruthenium catalysts that are competent for uncaging of allyl carbamate-protected amines with turnover numbers (TONs) as high as 270, representing more than a 33-fold increase over the parent $[\text{Cp}^*\text{Ru}(\text{cod})\text{Cl}]$ (i.e. 8 TON).¹⁹ In particular, using glutathione as a nucleophile, they demonstrated that the complex $[\text{Cp}^*\text{Ru}(\text{QA-NMe}_2)(\eta^3\text{-allyl})]\text{PF}_6$ (QA-NMe₂ = 4-(*N,N*-dimethylamino)-2-quinolinecarboxylate) (Fig. 2b) is significantly more active than $[\text{Cp}^*\text{Ru}(\text{cod})\text{Cl}]$ in releasing doxorubicin from its allyloxycarbonyl-protected form.

In subsequent years, the list of bioorthogonal reactions has expanded significantly as a result of the work of Weissleder,²⁰ Rotello,^{21–22} Bernardes,²³ Qu,²⁴ Chen,²⁵ Unciti-Broceta,^{26–29} Ward,^{30–32} Mascareñas,^{33–35} Tanaka,^{36–38} and others.^{39–40} The development of such

a diverse repertoire of bioorthogonal catalyst- and substrate-pairs has made it possible to expand the class of biocompatible protective groups for *in vivo* applications (Scheme 1) (see Scheme 2).

In addition to the above-mentioned drugs, the field of bioorthogonal chemistry has been applied to the uncaging/synthesis of ciprofloxacin,²¹ endoxifen,³⁷ monomethyl auristatin E (MMAE)^{23,41} SN-38 (the active metabolite of irinotecan),⁴² paclitaxel,²⁷ floxuridine,⁴³ resatorvid,⁴⁴ cisplatin,³⁹ panabinstat,²⁸ etoposide,⁴⁵ and others.

Here, we present a review of catalytic release of bioactive molecules in *cellulo* and *in vivo* and the potential prospects for this area of research from the perspective of heterogeneous and homogeneous catalysis.

2. Heterogeneous transition metal catalysts

2.1. Palladium-based heterogeneous *in vivo* catalysts

As mentioned above, one of the key breakthroughs in the field of bioorthogonal catalysis in living systems was the development of Pd⁰ nanoparticles embedded in polystyrene beads. First described in 2011 for allyl and allyloxycarbonyl cleavage,^{14–15} this approach has been expanded by Unciti-Broceta group to the cleavage of propargyl, propargyloxycarbonyl and propargyloxyaryl groups.^{29,42,46} For example, propargyloxyaryl-protected SN-38 (Table 1, Entry 1) (an analogue of topoisomerase I inhibitor) and the previously known 1-propargyl-5-fluorouracil (Table 1, Entry 5)^{17,47} were uncaged using entrapped Pd-nanodevices in HCT116 and U-87 cancer cells.⁴² This work was the first example of the simultaneous release of a combination of therapeutic agents from their caged forms using bioorthogonal reactions. The TON could not be determined in this and subsequent studies, since the exact amount of catalyst is not known, and the amount of products formed can only be roughly estimated using fluorescence analysis for dyes/prodrugs or cell viability for drugs/prodrugs.

Unciti-Broceta and coworkers used this approach for the catalytic release of doxorubicin protected by *para* and *ortho* propargyloxybenzyl groups (Table 1, Entry 2).⁴⁶ The novel caged drug featuring the *ortho* group afforded the greatest therapeutic window (150–350 times less toxic than free doxorubicin for various cell lines) and was not cardiotoxic to zebrafish larvae, even at concentrations much higher than would be achieved with maximum drug dosage. In addition to biocompatibility, the functionality of the system was also investigated. Nanoparticles of different sizes (10 μm –110 μm) were tested under the conditions of catalytic depropargylation of rhodamine. The particles with 110 μm and 30 μm sizes displayed the highest activity and stability (>20 months when stored at 4 °C). The catalytic activity of size-optimized Pd-particles was studied on U87 glioblastoma cells and DU145 prostate cancer cells in mice. The nanoparticles retained their activity three weeks after implantation into the body. The initial concept

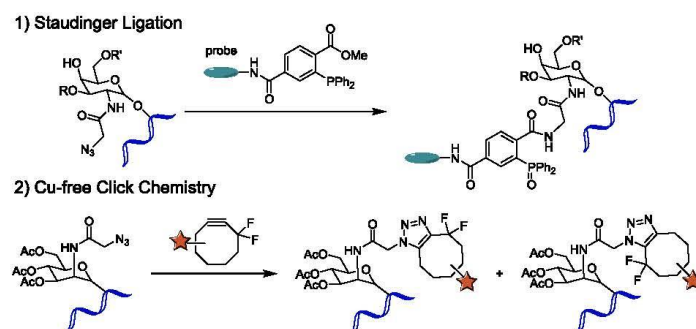


Fig. 1. Pioneering reactions applicable in the context of bioorthogonal chemistry.

laid on a solid proof: experiments on zebrafish have become the first clinically-relevant result for the release of a drug (doxorubicin) in a bioorthogonal manner in an animal model. Experiments on mice have confirmed the possibility of precise injection of Pd-nanodevices directly into the tumor area. All this opens up broad prospects for the use of bioorthogonal systems for cancer therapy.

Recently, Unciti-Broceta and coworkers devised a creative “Trojan horse” approach to enable targeted delivery of palladium catalyst into A549 and U-87 cells.²⁹ They succeeded in growing palladium nanosheets inside the respective cell exosomes, and showed that these hybrid systems selectively penetrate into their parent cells to deliver catalyst with high activity for the uncaging of the drug panobinostat (Table 1, Entry 4). Unciti-Broceta and coworkers²⁷ capitalized on the above work and designed palladium nanosheets encapsulated in biocompatible hydrogel networks that are highly effective for the depargylation of a caged paclitaxel prodrug, as demonstrated from treating A549 and U87 cells (Table 1, Entry 12).

Numerous other groups have continued to work towards palladium-catalyzed reactions *in vivo*. For example, Wang et al.²⁴ developed photosensitive Pd-loaded microporous silica nanoparticles functionalized with azobenzene and capped with cyclodextrin. Upon exposure to UV light, the *trans* to *cis* azobenzene photoisomerization results in the release of cyclodextrin from the surface of the NPs and thus catalyst activation. This process is reversible upon irradiation with visible light. As demonstrated in HeLa cells, this system is able to cleave allyloxycarbonyl-protected rhodamine 110, catalyze bimolecular Suzuki-Miyaura cross-coupling to generate a mitochondria-specific probe, and convert 5-fluoro-1-propargyl-uracil into 5-fluorouracil. Such light-gated heterogeneous transition metal catalysis could be broadly applied to the selective release/synthesis of anticancer drugs using UV light irradiation (Table 1, entries 16, 19).

Gu and coworkers developed new devices based on titanium oxide

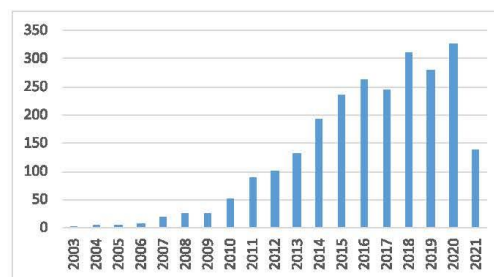


Fig. 3. Number of publications that include the topic *bioorthogonality*.

coated with palladium nanoparticles.⁴³ Biocompatible and easy-to-use patches easily penetrate the area of a tumor and release the active compound with high efficiency and precise localization (without leakage of toxic agents into healthy tissues). This model has been tested on B16-F10 tumor in mice treated with the allyloxycarbonyl-DOX (Table 1, Entry 17) and has shown the potential of such bioorthogonal systems in cancer-targeted therapy compared to passive drug-releasing systems.

Qu and coworkers⁴⁹ designed novel catalysts capable of the targeted synthesis of chiral drugs in inflamed tissue. These catalysts consist of neutrophil-coated mesoporous silica nanoparticles embedded with palladium and chiral alkaloids (cinchonidine, cinchonine, quinine, and quinidine). The cinchonidine variant was shown to catalyze the enantioselective reduction of 2-(4-isobutylphenyl)acrylic acid to (*S*)-ibuprofen with an enantiomeric excess (*ee*) of 78% (Table 1, Entry 22). These catalysts were shown to be effective in reducing inflammation in RAW264.7 cells and mouse paw tissue.

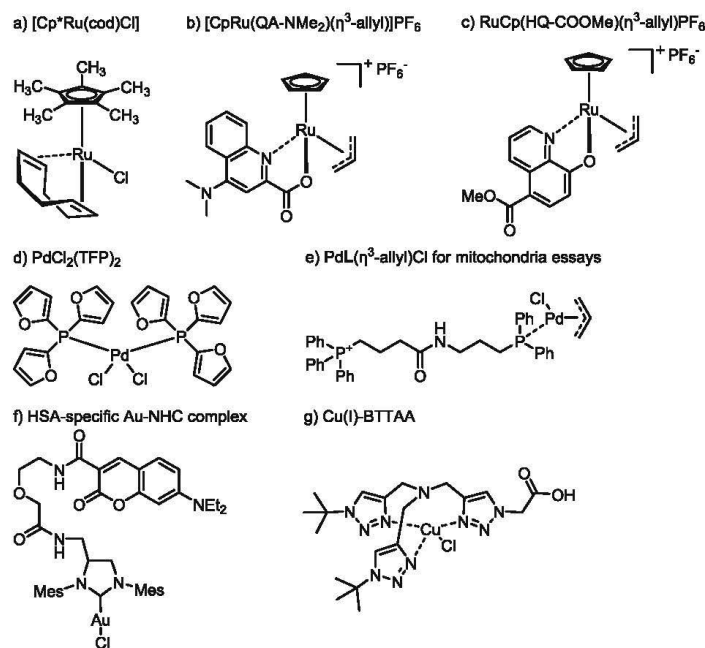
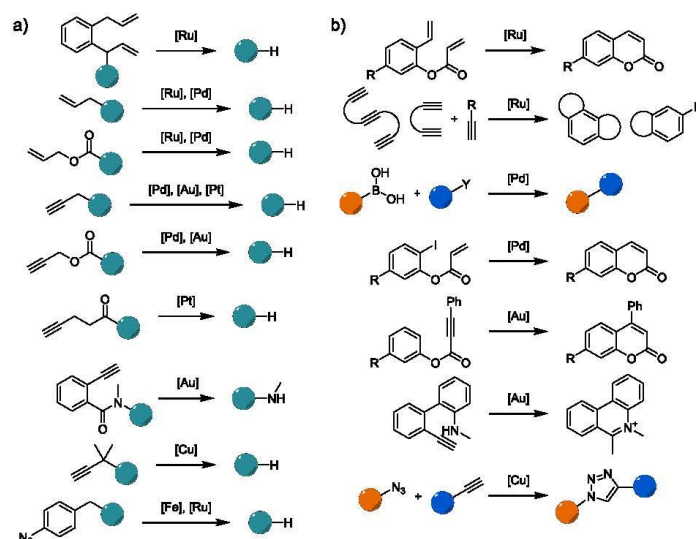
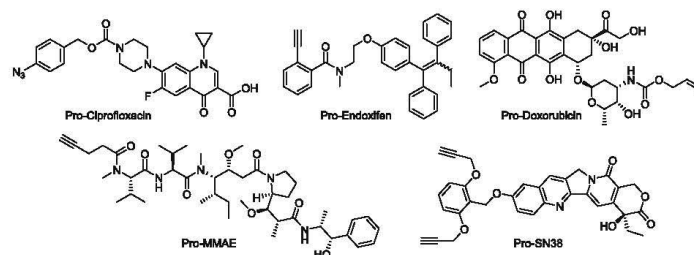


Fig. 2. Structures of selected organometallic catalysts used in bioorthogonal chemistry.



Scheme 1. Bioorthogonal reactions used *in vivo* for a) the uncaging of a product (blue-green sphere); b) the synthesis of bioactive molecules or fluorophores.



Scheme 2. Selection of caged drugs.

TentaGel resins, known for their biocompatibility and metal retention, are widely used in biomedical applications. Kane and coworkers⁴⁴ used palladium nanoparticles immobilized on TentaGel resins in a TLR4 reporter cell assay to release propargyl- and propargyloxycarbonyl-protected resatorvid (Table 1, Entries 7, 13).

Weissleder and coworkers²⁰ created a biocompatible catalyst featuring $\text{PdCl}_2(\text{TFP})_2$ (TFP = tri(2-furyl)phosphine) (Fig. 2d) encapsulated in poly(lactic-co-glycolic acid)-polyethyleneglycol nanoparticles. Under physiological conditions, the encapsulated complex is reduced to Pd^0 , and this species was used to synthesize fluorescent 7-diethylaminocoumarin via an intramolecular Heck reaction, carried out *in vivo* for the first time (Table 1, Entry 21). To date, the reaction has not found use in the synthesis and release of a drug, however it shows another unique reactivity achievable via Pd-catalysis. Weissleder and coworkers³³ has shown this catalytic micelle system to be effective in deallylation reactions leading to the release of rhodamine 110 and doxorubicin into HT1080 fibrosarcoma cells in mice (Table 1, Entry 17), as well as the delivery and activation of MMAE and doxorubicin prodrugs. Notably, the protective group reduces the toxicity of MMAE by more than four orders of magnitude (Table 1, Entry 18).

The use of polymers for encapsulating palladium has been pursued Palmans and coworkers.⁵⁰ They developed self-assembling micelles,

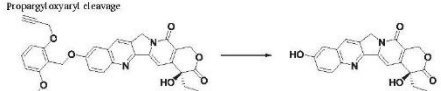
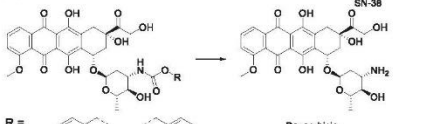
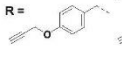
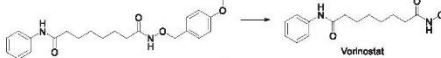
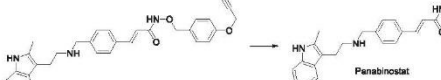

formed by block-copolymers carrying ligands for binding to Pd(II) and copper(I) (see below), which were used for depropargylation and deallylation of caged-fluorophores in HeLa cells (Table 1, Entry 14).

Significant contributions to the use of scaffold structures for the delivery of palladium into the cellular environment were made by Mascareñas group,^{35,51} who used Pd-loaded mesoporous hollow SiO_2 spheres and core-shell Pd/metal-organic framework nanoreactors to depropargylate caged-fluorophores in HeLa cells (Table 1, Entries 6, 11, 20).

Purely inorganic catalytic systems for *in vivo* bioorthogonal transformations have been developed by Pané and coworkers.⁵² They synthesized iron-palladium-nanowires via a template-assisted electrode position, which showed high biocompatibility and moderate efficiency for the activation of 5-fluoro-1-propargyl-uracil in MDA-MB-231 cells in mice (Table 1, Entry 5).

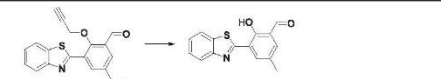
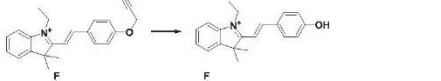
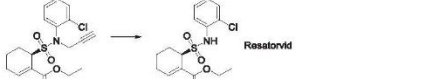
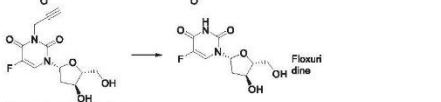
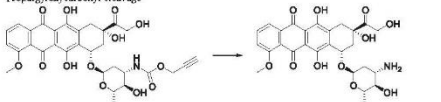
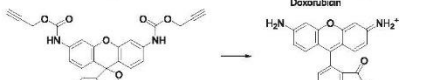

Rubio-Ruiz and coworkers²⁶ developed a palladium-coated titanium catalyst and tested its activity in propargyl and propargyloxycarbonyl cleavage. These biocompatible and reusable devices were shown to be highly efficient in the release of rhodamine 110 and the anticancer drug Vorinostat (Table 1, Entries 3, 10), illustrating the promise of metal-based devices for clinical therapy.

Table 1

Entry	Reaction	Catalyst	Organism/organelle	Ref.
1	Propargyl oxaryl cleavage 	Pd-devices	HCT116 U-87 U-251 In combination with 5FU	42
2	 R =  Doxorubicin	Pd devices 10–110 nm Au-resins	Zebrafish U87 DU145 prostate cancer in mice A549 cells	48 43
3	 Vorinostat	Au-resins (Pd) loaded titanium (Ti) devices	A549 cells A549 cells	43 28
4	 Panabiosat	Cancer derived exosomes Pd-Exo ⁴⁵⁻⁴⁹	A549 and U87 cells	29
5	Propargyl cleavage 	Pd-devices FePd nanowires Au-PHIER	HCT116 U-87 U-251 In combination with SN-38 MDA-MB-231 cells in mice LHCat, MDA-MB-231 cells	42 51 46

(continued on next page)

Table 1 (continued)

Entry	Reaction	Catalyst	Organism/organelle	Ref.
6		Pd loaded mesoporous hollow SiO ₂ sphere Core-shell Pd/MOF Nanoreactor	HeLa cells HeLa cells	51 51
7	 Resatorvid	Pd NPs immobilized on TetraGel resins	TLR4 reporter cell assay	44
8	 Floaxuridine	Au-resins	A549 cells	42
9	Propargyl oxycarbonyl cleavage 	Pd-devices 10–110 nm	Zebrafish U87 DU145 prostate cancer in mice	48
10	 Doxorubicin	(Pd) loaded titanium (Ti) devices Pd-PHIER Au-resins	A549 cells LHCat, MDA-MB-231 cells A549 cells	28 46 43
11		Core-shell Pd/MOF Nanoreactor	HeLa cells	51
12		Pd-nanosheet-hydrogel network	A549, U87 cells and HRVFs	27

(continued on next page)

Table 1 (continued)

Entry	Reaction	Catalyst	Organism/organelle	Ref.
13		Pd NPs immobilized on Tentagel resins	TLR4 reporter cell assay	44
14		Pd(II) SCPNs	HeLa cells	55
15		Cu(I) SCPNs	HeLa cells	56
16		Microporous silica nanoparticles (DMSH) + Photosensitizer + Pd + cyclodextrin	HeLa Mitochondria of HeLa cells	24
17		Pd NP (PdCl ₂ TFP ₂) + PLGA-PBG micelles Pd-NPs on TiO ₂ nanosheets	HT1080 fibrosarcoma cells in mice B16-F10 in mice	20 48

(continued on next page)

Table 1 (continued)

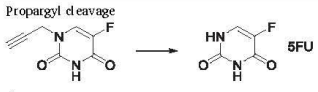
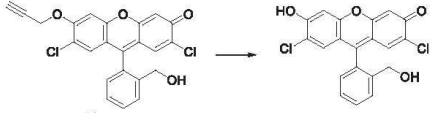
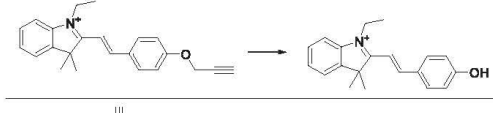
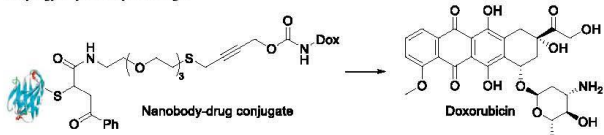
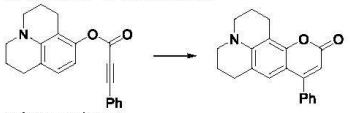
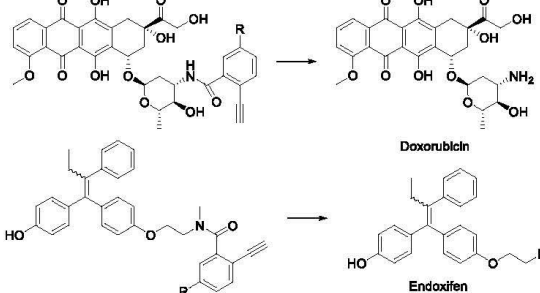
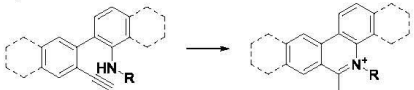
Entry	Reaction	Catalyst	Organism/organelle	Ref.
18		Pd NP (PdCl ₂ TFP ₂) + PLGA-PBG micelles	HT1080 fibrosarcoma cells in mice	41
19		Pd-loaded photosensitive microporous silica nanoparticles (DMSH)	HeLa Mitochondria of HeLa cells	24
20		Pd-loaded mesoporous hollow SiO ₂ sphere	HeLa cells	22
21		Pd NP (PdCl ₂ TFP ₂) + PLGA-PBG micelles	HT1080 fibrosarcoma cells in mice	20

(continued on next page)

Table 1 (continued)

Entry	Reaction	Catalyst	Organism/organelle	Ref.
22	Reduction 	Neutrophil- membrane-coated chiral Pd catalysts	RAW264.7 cells	49
23	[3 + 2]-Cycloaddition 	Cu crosslinked lipic acid NPs MOF-Cu catalyst	HeLa cells C. elegans MCF-7 cells Mitochondria	55 60
24		MOF-Cu catalyst	C. elegans MCF-7 cells	60
25	Azide reduction 	Fe-polymers	Bacterial biofilms (E. coli)	22
26		Fe-polymers	E. coli and P. aeruginosa biofilms NIH 3T3 fibroblast cells	21

Table 2

Entry	Reaction	Catalyst	Organism/ organelle	Ref.
1	Propargyl cleavage 	Biocompatible NHC-Pd catalysts K_2PtCl_6 , cisplatin	MCF-7 cells HeLa cells Zebrafish	68 23 68
2		Biocompatible NHC-Pd catalysts	MCF-7 cells	68
3		Cl^- Pd^{II} L^- -labeled for mitochondria assays $PdCl_2 \cdot btrHis_2$	Cell lysate Vero cells HeLa cells	69 70
4	Propargyloxycarbonyl cleavage 	$Pd(COD)Cl_2$	HEK293 and MCF-7 cells	71
5	Au-activated C–C–bond formation 	Water-soluble Au (I)-catalysts	HeLa cells	73
6	Ayba-group cleavage 	Au-NHC complexes HSA-based Gold ArMs	PBS buffer	37
7	Hydroamination 	$NaAuCl_4$ Au-NHC complexes HSA-based Gold ArMs	A549 cells	38

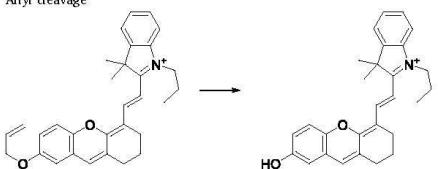
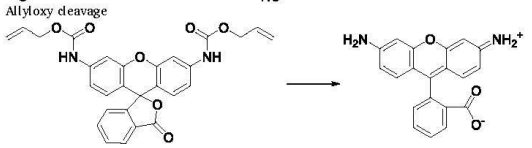
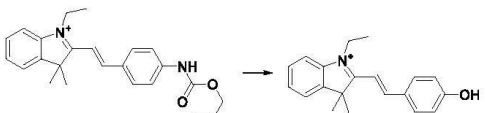
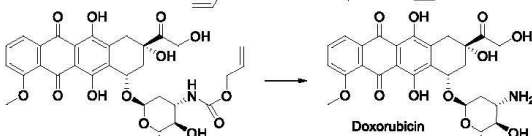
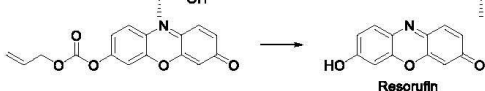
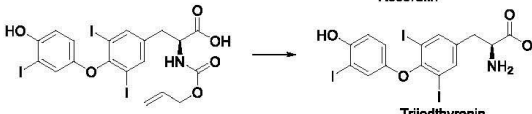
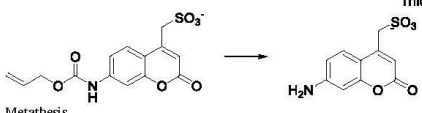
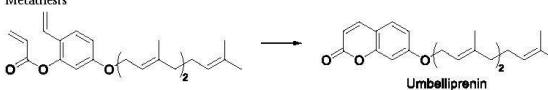
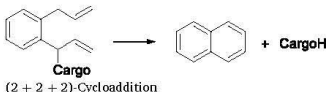
(continued on next page)

2.2. Heterogeneous gold, copper, and iron catalysts

The use of heterogeneous catalysts is not limited to palladium or its compounds. Indeed, in principle, any metals that are biocompatible and stable under physiological conditions may be promising as bio-orthogonal catalysts. After palladium, gold was the next metal to feature

prominently in the catalysis of new-to-nature reactions. Until 2017, gold nanoparticles were used as a basis for the immobilization of chemically-active agents. Thus, Rotello and coworkers showed that $[Cp^*Ru(cod)Cl]$, entrapped on the surface of gold nanoparticles in a HeLa cell culture medium, catalyzes deallylation of pro-rhodamine 110, and $Pd(dppf)Cl_2$ – depropargylation of pro-5FU.⁵³ Unciti-Broceta and

Table 2 (continued)

Entry	Reaction	Catalyst	Organism/ organelle	Ref.
8	Allyl cleavage 	CpRu(QA)(η^3 -allyl)-complex	HeLa cells	73
9	Allyloxy cleavage 	CpRu(QA)(η^3 -allyl)-complex Cl L labeled for mitochondria essays [RuCp*Cl(COD)]-based nanozymes Ru-based nanozymes w/ or w/o protein corona	HeLa cells HeLa and Vero cells mitochondria HeLa and Raw 264.7 cells Serum HeLa cells	19,34,74 69 85 86
10		Cl Pd L	Cell lysate	69
11		CpRu(QA)(η^3 -allyl)-complex	HeLa cells	19,74
		[RuCp*Cl(COD)]-based nanozymes	HeLa and Raw 264.7 cells	85
12		Artificial deallylase based on SAV and Ru cofactor	HEK-293 T cells	75
13		Artificial deallylase based on SAV and Ru cofactor	C. reinhardtii	32
14	Metathesis 	Artificial metathesase based on HSA and Ru cofactor	SW620, A549, and HeLa cells	36
15	 (2 + 2 + 2)-Cycloaddition	Ru Hoveyda-Grubbs 2nd generation catalyst	HeLa cells, E. coli	31

(continued on next page)

coworkers⁴³ developed cell-penetrating Au-resins that can release doxorubicin, floxuridine, and vorinostat within A549 cancer cells and significantly reduce cell viability (Table 1, Entries 2, 3, 8) via catalytic depropargylation and depropargyloxyarylation. Gold nanoparticles implanted in the brain of zebrafish have been shown to be effective for

the release of the fluorescent rhodamine 110 (Table 1, Entry 10). Lee and coworkers⁴⁰ synthesized a family of new plasmonically integrated nanoreactors (PINERs) that can be doped with gold, as well as palladium (Table 1, Entry 10) and platinum. These catalysts are activated upon near IR irradiation, and effectively release 5FU and rhodamine 110 upon

Table 2 (continued)

Entry	Reaction	Catalyst	Organism/ organelle	Ref.
16	<p>Redox Isomerization</p>	[RuCp*Cl(COD)], RuCp(QA)(η³-allyl)	HeLa cells	76
17	<p>Diacylpropargyl cleavage</p>	[Ru(η³-η³-C₁₀H₁₆) Cl(μ²-O₂O-O₂CMe)]	HeLa, Vero and A549 cells	33
18	<p>Doxorubicin</p> <p>Etoposide</p>	Cu(I)-BTAA	HeLa and SKBR-3 cells	45
19	<p>Transfer hydrogenation</p>	Cp*Ir(N,N')- complexes	NIH-3T3 cells	80
20	<p>Pentynoyle cleavage</p> <p>R = H, Antibody</p> <p>MMAE</p>	K₂PtCl₄, cisplatin	HeLa cells Zebrafish	23
21	<p>Azide reduction</p>	Ru(bpy)₂(phen)- derivatives Ru(bpy)₂(phen)- derivatives	HEK293T, MCF-7 cells Zebrafish	77 78

propargyl cleavage in LNCaP and MDA-MB-231 cells (Table 1, Entry 5).

The diversity of bioorthogonal chemistry that can be carried out using copper makes it possible to break bonds and remove protective groups and also to create key fragments of fluorophores and cytotoxic agents.^{54–57} Additionally, it has been shown that the incorporation of copper compounds into polymer shells reduces the intrinsic toxicity of copper compounds.⁵⁸

Copper bound by single-chain polymeric nanoparticles⁵⁹ removes 1,1-dialkylpropargyl protecting groups catalytically. Palladium, which is effective in propargyl cleavage, is significantly less active in 1,1-dialkylpropargyl cleavage than copper, highlighting the relative orthogonality in the reactivity of the two metals. For example Cu-based nanoparticles were shown to uncage rhodamine 110 in HeLa cells (Table 1, Entry 15).

Zhang and coworkers⁵⁹ used nanocopper-doped cross-linked lipoic acid nanoparticles (Cu@CLNP) for the copper-catalyzed azide-alkyne cycloaddition. A potent coumarin-based fluorophore and tubulin polymerization inhibitor (IC50 15 μ M) displayed in Table 1, Entry 23 was synthesized in HeLa cells using Cu@CLNP via an intermolecular [3 + 2] cycloaddition.

Qu and coworkers⁶⁰ developed a Cu-loaded metal-organic framework for targeted azide-alkyne cycloaddition in mitochondria. The corresponding products are displayed in Table 1, Entries 23 and 24. The resveratrol analogue (Table 1, Entry 23) significantly decreased the viability of MCF-7 cells, and the catalyst was also shown to be biocompatible with *C. elegans*.

Another metal of interest in the context of bioorthogonality is iron. Rotello and coworkers^{21–22} used self-assembling polyzymes based on a quaternary ammonium polymer possessing hydrophobic alkyl side chains and [Fe(TPP)]Cl for the catalytic reduction of aryl azides to anilines, followed by 1,6-elimination of fluorophores and cytotoxic agents. The activity of the polyzymes was established during experiments on NIH 3T3 fibroblast cells, as well as *E. coli* and *P. aeruginosa* biofilms. The polyzymes had no adverse effects on cells, and researchers showed that these catalysts can be used to release moxifloxacin and ciprofloxacin, reducing cell viability with IC₅₀ ~ 10 μ M (Table 1, Entries 25, 26).

3. Homogeneous transition metal catalysts

3.1. Homogeneous palladium catalysts

In light of its versatility in homogeneous catalysis, Pd occupies a place of choice in bioorthogonal chemistry. Lin and coworkers reported a water soluble catalyst for *in cellulo* cross-coupling reactions.⁶² The Lin, Chen and Davis groups used this catalyst (as well as other water-soluble Pd(II) salts) for Sonogashira and Suzuki-Miyaura cross-couplings for labeling *E. coli*, *Shigella*, and HEK293 cells.^{63–65}

Following this work, research shifted toward the development of complexes for protection/deprotection reactions.^{25,62,66–67} Biocompatible *N*-heterocyclic carbene (NHC)-Pd catalysts developed by the Bradley group are effective for propargyl and propargyloxycarbonyl cleavage.^{67–68} These catalysts were used to release rhodamine 110 in PC-3 cells and 2,7-dichlorofluorescein and 5-fluorouracil in MCF-7 cells (Table 2, Entries 1, 2).⁶⁸

Mascareñas and coworkers synthesized a family of PdL(η^3 -allyl)Cl complexes (L = pyridine, triphenylphosphine, and phosphonium ions, etc., Fig. 2e) and studied their activity in deprotection reactions in PBS, cell culture media, and *in vivo*.⁶⁹ Depending on the identity of L and the reaction environment, the catalyst's performance varied significantly. Complexes featuring phosphine or phosphonium-ion ligands were found to localize preferentially in the mitochondria of HeLa and Vero cells, and catalyzed depropargylation and deallylation reactions, leading to the formation and accumulation of fluorophores in the cytoplasm and on the mitochondrial surface (Table 2, Entries 3, 9, 10).

Mascareñas and coworkers also described the use of metallopeptides containing palladium coordinated to two histidine residues.⁷⁰ This

example is the first example of a so-called “bottom-up” strategy to generate metalloproteins displaying a synergistic effect. The histidine residues coordinate to Pd and increase the catalyst's activity, while the short peptide plays a protective role, preventing the degradation of the catalytic activity. Experiments on HeLa cells highlighted the efficiency for the uncaging of dyes which were unreactive using other palladium (II) catalysts (Table 2, Entry 3).

The use of antibody-drug conjugates for the delivery of prodrugs in the vicinity of target tissues/cells/organelles offers an alternative to targeted-catalyst delivery. In this case, the catalyst can circulate freely in the body or cellular environment. Bernardes and coworkers⁷¹ demonstrated this approach for the first time. For this purpose, they relied on a bifunctional PEGylated caged doxorubicin, featuring a thioether group for directing palladium-mediated depropargylation and a carbonylacrylic group that reacts with cysteine to form a nanobody-drug conjugate. In the presence of non-toxic amounts of Pd(cod)Cl₂, the caged doxorubicin combined with the Pd-catalyst proved as effective at killing MCF-7 cells as doxorubicin (Table 2, Entry 4). As the authors note, new palladium catalysts will need to be developed to optimize cell selectivity and minimize toxicity.

3.2. Homogeneous gold catalysts

Until recently, the use of water-soluble gold complexes in bioorthogonal chemistry was limited to the formation of amide bonds and was used only for attaching fluorescent labels to proteins.⁷² However, in 2018, Mascareñas and coworkers⁷³ reported that C–C bond formation can be catalyzed by a water-soluble Au(I) complex in HeLa cells. In particular, a phenylpropionic acid ester was converted to a highly fluorescent 7-aminocoumarin derivative in the presence of complexes with phosphine and phenanthroline ligands as well as either NaAuCl₄ or HAuCl₄ (Table 2, Entry 5).

Recently, Tanaka and coworkers developed the new protecting group 2-alkynylbenzamide (Ayba) for uncaging prodrugs via Au-triggered bioorthogonal chemistry.⁴⁷ They showed that gold(I)-NHC complexes are effective for converting pro-endoxifen and pro-doxorubicin, protected with Ayba (Table 2, Entry 6) to the active molecules in different cancer cell lines. Although the uncaging reactions do not display multiple turnovers, they were highly specific and unreactive to either palladium or ruthenium catalysts.

The same group subsequently reported the use of Na[AuCl₄] and Au-NHC complexes as catalysts in the hydroamination of 2'-alkynyl-*N*-methyl-2-aminobiphenyls to form phenanthridinium derivatives (Table 2, Entry 7).³⁹ Using an Au-NHC (Fig. 2f), they created new human serum albumin (HSA)-based gold artificial metalloenzyme (ArM) that results from the incorporation of an NHC-gold cofactor bearing an aminocoumarin moiety enabling its anchoring in HSA. The resulting ArM exhibits high efficiency (up to 211 TON) even in the presence of highly reactive cell components, such as glutathione, lysine, and arginine.

3.3. Homogeneous ruthenium catalysts

Thanks to its biocompatibility and chemical versatility, ruthenium is a valuable metal in the context of bioorthogonal chemistry. It gained attention following the proof-of-principle report on catalytic allylcarbamate cleavage by [Cp*Ru(cod)Cl] in the presence of strong nucleophiles.^{3,18} Subsequent work described the use of RuCp(QA-R)(η^3 -allyl) (QA = 2-quinolinecarboxylate) and RuCp(HQ-R)(η^3 -allyl) (HQ = 8-hydroxyquinoline) (Fig. 2c) as catalyst for the deallylation of a wide range of substrates *in vivo* (Table 2, Entries 9, 11).^{19,34,74}

Mascareñas and coworkers⁷³ demonstrated that deallylation and hydroarylation of different substrates can be carried out concurrently and orthogonally in HeLa cells, using [RuCp(QA-R)(η^3 -allyl)]PF₆ (Table 2, Entry 8) and a gold-phosphine catalyst, respectively.

Ward and coworkers⁷⁵ designed a cell-penetrating artificial

deallylase based on streptavidin (SAV) and biotinylated Ru-cofactor for the catalytic deallylation of allyloxycarbonyl-triiodothyronine in HEK-293 T cells (Table 2, Entry 12). The efficacy of the thyroid hormone release was optimized through directed mutagenesis, and the consumption of the released triiodothyronine was monitored by furimazine luminescence. A similar catalytic system was used by Gademann and coworkers.³² They developed a SAV-based Ru-deallylase that was shown to convert allyloxycarbonyl-protected 7-aminocoumarin to a fluorescent product on *C. reinhardtii* cells (Table 2, Entry 13).

A significant advance in the use of the ruthenium to catalyze bio-orthogonal reactions was pioneered by Ward and coworkers.³⁰ They developed and evolved an ArM that catalyzes olefin metathesis *in vivo*. This area of research has since been expanded over by a number of groups. Tanaka and coworkers³⁶ used ring-closing metathesis to synthesize the anticancer drug umbelliprenin (Table 2, Entry 14). Glycosylated HSA was used to shield the ruthenium metathesis cofactor from glutathione. The activation of umbelliprenin *in vivo* reduced the viability of SW620, A549, and HeLa cells.

Ward and coworkers³¹ used Ru-catalyzed ring-closing metathesis to release caged molecules from diolefins-containing substrates with TONs up to 260. This method introduces the prospect of efficient and bio-orthogonal release of fluorophores and drugs (Table 2, Entry 15).

The deallylation catalysts of the type RuCp(QA-R)(η^3 -allyl) and [Cp*Ru(cod)Cl] also promote [2 + 2 + 2]-cycloadditions *in vivo*, as reported by Mascareñas and coworkers (Table 2, Entry 16).⁷⁶ The approach is highly versatile, facilitating intra- and intermolecular reactivity and the *in vivo* generation of anthraquinones that exhibit aggregate-induced emission, which cannot otherwise be introduced into cells directly.

Finally, Ru(IV) bis-allyl complexes catalyze the isomerization of allyl alcohols to ethyl ketones.³³ This approach has been applied for the synthesis of fluorescent molecules in HeLa, Vero, and A549 cells (Table 2, Entry 17).

Luminescent ruthenium complexes synthesized by Winssinger and coworkers have also been used to photocatalyze azide-reductions (Table 2, Entry 21) in HEK293T and MCF-7 cells⁷⁷ and in zebrafish,⁷⁸ similarly to the above-mentioned Fe-polyzymes reductions. However, this approach has not been significantly developed and applied recently.

3.4. Homogeneous copper, platinum and iridium catalysts

The rest of the biocompatible metals are poorly represented in the topic of homogeneous bioorthogonality. For example, since 2017, only one article has been published in which a water-soluble copper compound is used for bioorthogonal deprotection/drug conversion. Chen and coworkers⁴⁵ used Cu(I)-BTAA (BTAA⁷⁹ = 2-[4-((bis(1-*tert*-butyl-1H-1,2,3-triazol-4-yl)methyl)amino)methyl]-1H-1,2,3-triazol-1-yl]acetic acid, Fig. 2g) for dialkylpropargyl cleavage of doxorubicin and etoposide from antibody-drug conjugates (Table 2, Entry 18). The released drugs are 120 times more toxic than the ADCs, making this a promising approach to drug delivery and release.

As of this writing, the last report on the use of iridium in the field of new-to-nature reactions *in vivo* was published in 2017. In that study, Do and coworkers⁸⁰ reported that aldehydes can be converted to alcohols using unprotected transfer hydrogenation catalysts [Cp*Ir(*N*-phenyl-2-pyridinecarboxamidate)Cl], [Cp*Ir(2,2'-bipyridine)Cl], and [Cp*IrCl₂]₂, reactivity that was monitored in NIH-3T3 cells using a fluorogenic Bodipy substrate (Table 2, Entry 19). In a series of elegant studies,^{81–82} Sadler and coworkers have investigated the use of d₆-piano-stool complexes Ru(II), Os(II), Ir(III) *in vivo* to perturb the redox status of cells. Excellent reviews have recently been published on the topic.^{83–84}

In 2020, Bernardes and coworkers showed that K₂PtCl₄ and cisplatin are effective catalysts for pentynoyl and propargyl cleavage.²³ The biocompatibility of these complexes was studied using HeLa cells and zebrafish. Despite its toxicity, cisplatin selectively deprotected 5-

fluorouracil and MMAE (Table 2, Entries 1 and 20, respectively).

4. Conclusions

Since 2017, there has been substantial progress in the development of bioorthogonal reactions catalyzed by transition metals. Homogeneous and heterogeneous catalysts have become significantly more diverse and effective. The ability of solid nanoparticles to cross the membrane of cancer cells has been enhanced by the use of cancer cell-derived markers. New polymeric self-assembling nanoparticles with zero cytotoxicity and high specificity have been shown to be effective for the release of anticancer drugs. Homogeneous catalysts, the use of which was limited by the presence of a large number of reactive components in cells, significantly expanded the field of application. For example, scaffolds of native proteins and their mutants play the role of shells that protect the metal cofactor, increase the penetrating ability and, at the same time, improve the selectivity of catalysis. The number of new-to-nature reactions in biological media has increased significantly. The development of new anticancer drugs and their prodrugs (caged drugs, antibody-drug conjugates, precursors for *in vivo* synthesis) expand the tools for targeted delivery of bioactive molecules to the area of action. In tandem with the increasing progress in the development of catalysts with reduced cytotoxicity and increased efficacy, the wealth of research within recent years opens up exciting prospects for new therapies for cancer and other diseases.

Declaration of Competing Interest

The authors declare that they have no known competing financial interests or personal relationships that could have appeared to influence the work reported in this paper.

Acknowledgement

Work related to drug uncaging *in vivo* in the Ward group is generously funded by the European Union's Horizon 2020 research and innovation program including i) the Marie Skłodowska-Curie grant agreement no. 765497 (THERACAT) and ii) the ERC (the dREAM, grant agreement 694424); as well as the NCCR Molecular Systems Engineering.

References

- Hang HC, Yu C, Kato DL, et al. A metabolic labeling approach toward proteomic analysis of mucin-type O-linked glycosylation. *Proc Natl Acad Sci USA*. 2003;100:14846–14851.
- Baskin JM, et al. Copper-free click chemistry for dynamic *in vivo* imaging. *Proc Natl Acad Sci USA*. 2007;104:16793–16797.
- Streu C, Meggers E. Ruthenium-induced allylcarbamate cleavage in living cells. *Angew Chemie - Int Ed*. 2006;45:5645–5648.
- Versteegen RM, Rossin R, Ten Hoeve W, et al. Click to release: Instantaneous doxorubicin elimination upon tetrazine ligation. *Angew Chemie - Int Ed*. 2013;52:14112–14116.
- Xie X, et al. Bioorthogonal Nanosystem for Near-Infrared Fluorescence Imaging and Prodrug Activation in Mouse Model. *ACS Mater Lett*. 2019;1:549–557.
- Zuo L, et al. Coordinating bioorthogonal reactions with two tumor-microenvironment-responsive nanovehicles for spatiotemporally controlled prodrug activation. *Chem Sci*. 2020;11:2155–2160.
- Ji X, et al. Click and release: Bioorthogonal approaches to 'on-demand' activation of prodrugs. *Chem Soc Rev*. 2019;48:1077–1094.
- Wang J, Wang X, Fan X, et al. Unleashing the Power of Bond Cleavage Chemistry in Living Systems. *ACS Cent Sci*. 2021. <https://doi.org/10.1021/acscentsci.1c00124>.
- Liu Y, Bai Y. Design and Engineering of Metal Catalysts for Bio-orthogonal Catalysis in Living Systems. *ACS Appl Bio Mater*. 2020;3:4717–4746.
- Martínez-Calvo M, Mascareñas JL. Organometallic catalysis in biological media and living settings. *Coord Chem Rev*. 2018;359:57–79.
- Destito P, Vidal C, López F, et al. Transition Metal-Promoted Reactions in Aqueous Media and Biological Settings. *Chem - A Eur J*. 2021;27:4789–4816.
- Nguyen DP, Nguyen HTH, Do LH. Tools and Methods for Investigating Synthetic Metal-Catalyzed Reactions in Living Cells. *ACS Catal*. 2021;11:5148–5165. <https://doi.org/10.1021/acscatal.1c00438>.

- 13 van de L'Isle MOH, Ortega-Liebana MC, Unciti-Broceta A. Transition metal catalysts for the bioorthogonal synthesis of bioactive agents. *Curr Opin Chem Biol.* 2021;61:32–42.
- 14 Yusop RM, Unciti-Broceta A, Johansson EMV, et al. Palladium-mediated intracellular chemistry. *Nat Chem.* 2011;3:239–243.
- 15 Unciti-Broceta A, Johansson EMV, Yusop RM, et al. Synthesis of polystyrene microspheres and functionalization with Pd0 nanoparticles to perform bioorthogonal organometallic chemistry in living cells. *Nat Protoc.* 2012;7:1207–1218.
- 16 Weiss JT, et al. Extracellular palladium-catalysed dealkylation of 5-fluoro-1-propargyl-uracil as a bioorthogonally activated prodrug approach. *Nat Commun.* 2014;5.
- 17 Weiss JT, et al. Development and bioorthogonal activation of palladium-labile prodrugs of gemcitabine. *J Med Chem.* 2014;57:5395–5404.
- 18 Sánchez MI, Penas C, Vázquez ME, et al. Metal-catalyzed uncaging of DNA-binding agents in living cells. *Chem Sci.* 2014;5:1901–1907.
- 19 Völker T, Denpawolff E, Graumann PL, et al. Progress towards bioorthogonal catalysis with organometallic compounds. *Angew Chemie - Int Ed.* 2014;53:10536–10540.
- 20 Miller MA, et al. Nano-palladium is a cellular catalyst for in vivo chemistry. *Nat Commun.* 2017;8:1–13.
- 21 Huang R, et al. Polymer-Based Bioorthogonal Nanocatalysts for the Treatment of Bacterial Biofilms. *J Am Chem Soc.* 2020;142:10723–10729.
- 22 Cao-Millán R, et al. Thermally Gated Bio-orthogonal Nanozymes with Supramolecularly Confined Porphyrin Catalysts for Antimicrobial Uses. *Chem.* 2020;6:1113–1124.
- 23 Oliveira BL, et al. Platinum-Triggered Bond-Cleavage of Pentynol Amide and N-Propargyl Handles for Drug-Activation. *J Am Chem Soc.* 2020;142:10869–10880.
- 24 Wang F, Zhang Y, Du Z, et al. Designed heterogeneous palladium catalysts for reversible light-controlled bioorthogonal catalysis in living cells. *Nat Commun.* 2018;9.
- 25 Li J, et al. Palladium-triggered deprotection chemistry for protein activation in living cells. *Nat Chem.* 2014;6:352–361.
- 26 Torres-Sánchez C, Pérez-López AM, Alqahtani MN, et al. Design and manufacture of functional catalyst-carrier structures for the bioorthogonal activation of anticancer agents. *New J Chem.* 2019;43:1449–1458.
- 27 Pérez-López AM, et al. Bioorthogonal Uncaging of Cytotoxic Paditaxel through Pd Nanosheet-Hydrogel Frameworks. *J Med Chem.* 2020;63:9650–9659.
- 28 Rubio-Ruiz B, Weiss JT, Unciti-Broceta A. Efficient Palladium-Triggered Release of Vorinostat from a Bioorthogonal Precursor. *J Med Chem.* 2016;59:9974–9980.
- 29 Sancho-Albero M, et al. Cancer-derived exosomes loaded with ultrathin palladium nanosheets for targeted bioorthogonal catalysis. *Nat Catal.* 2019;2:864–872.
- 30 Jeschek M, et al. Directed evolution of artificial metalloenzymes for in vivo metathesis. *Nature.* 2016;537:661–665.
- 31 Sabatino V, Rebelein JG, Ward TR. 'Close-to-Release': Spontaneous Bioorthogonal Unloading Resulting from Ring-Closing Metathesis. *J Am Chem Soc.* 2019;141:17048–17052.
- 32 Szponarski M, Schwizer F, Ward TR, et al. On-cell catalysis by surface engineering of live cells with an artificial metalloenzyme. *Commun Chem.* 2018;1.
- 33 Vidal C, Tomás-Gamasa M, Gutiérrez-González A, et al. Ruthenium-Catalyzed Redox Isomerizations Inside Living Cells. *J Am Chem Soc.* 2019;141:5125–5129.
- 34 Tomás-Gamasa M, Martínez-Calvo M, Couceiro JR, Mascareñas JL. Transition metal catalysis in the mitochondria of living cells. *Nat Commun.* 2016;7.
- 35 Destito P, et al. Hollow nanoreactors for Pd-catalyzed Suzuki-Miyaura coupling and O-propargyl cleavage reactions in bio-relevant aqueous media. *Chem Sci.* 2019;10:2598–2603.
- 36 Ede S, et al. Biocompatibility and therapeutic potential of glycosylated albumin artificial metalloenzymes. *Nat Catal.* 2019;2:780–792.
- 37 Vong K, Yamamoto T, Chang TC, et al. Bioorthogonal release of anticancer drugs: Via gold-triggered 2-alkynylbenzamide cyclization. *Chem Sci.* 2020;11:10928–10933.
- 38 Chang TC, Vong K, Yamamoto T, et al. Prodrug Activation by Gold Artificial Metalloenzyme-Catalyzed Synthesis of Phenanthridinium Derivatives via Hydroamination. *Angew Chemie - Int Ed.* 2021. <https://doi.org/10.1002/anie.202100369>.
- 39 Mazzei LE, et al. Toward supramolecular nanozymes for the photocatalytic activation of Pt(IV) anticancer prodrugs. *Chem Commun.* 2020;56:10461–10464.
- 40 Kumar A, et al. Plasmonically Coupled Nanoreactors for NIR-Light-Mediated Remote Stimulation of Catalysis in Living Cells. *ACS Catal.* 2019;9:977–990.
- 41 Miller MA, et al. Modular Nanoparticulate Prodrug Design Enables Efficient Treatment of Solid Tumors Using Bioorthogonal Activation. *ACS Nano.* 2018;12:12814–12826.
- 42 Adam C, et al. Bioorthogonal Uncaging of the Active Metabolite of Irinotecan by Palladium-Functionalized Microdevices. *Chem - A Eur J.* 2018;24:16783–16790.
- 43 Pérez-López AM, et al. Gold-Triggered Uncaging Chemistry in Living Systems. *Angew Chemie - Int Ed.* 2017;56:12548–12552.
- 44 Plunk MA, et al. Design and Catalyzed Activation of Tak-242 Prodrugs for Localized Inhibition of TLR4-Induced Inflammation. *ACS Med Chem Lett.* 2020;11:141–146.
- 45 Wang X, et al. Copper-Triggered Bioorthogonal Cleavage Reactions for Reversible Protein and Cell Surface Modifications. *J Am Chem Soc.* 2019;141:17133–17141.
- 46 Bray TL, et al. Bright insights into palladium-triggered local chemotherapy. *Chem Sci.* 2018;9:7354–7361.
- 47 Clavdetscher J, Indrijo E, Chankeshwara SV, et al. In-Cell Dual Drug Synthesis by Cancer-Targeting Palladium Catalysts. *Angew Chemie - Int Ed.* 2017;56:6864–6868.
- 48 Chen Z, et al. Bioorthogonal catalytic patch. *Nat Nanotechnol.* 2021. <https://doi.org/10.1038/s41565-021-00910-7>.
- 49 Du Z, et al. Neutrophil-Membrane-Directed Bioorthogonal Synthesis of Inflammation-Targeting Chiral Drugs. *Chem.* 2020;6:2060–2072.
- 50 Liu Y, et al. Catalytically Active Single-Chain Polymeric Nanoparticles: Exploring Their Functions in Complex Biological Media. *J Am Chem Soc.* 2018;140:3423–3433.
- 51 Martínez R, et al. Core-Shell Palladium/MOF Platforms as Diffusion-Controlled Nanoreactors in Living Cells and Tissue Models. *Cell Reports Phys Sci.* 2020;1.
- 52 Hoop M, et al. Mobile Magnetic Nanocatalysts for Bioorthogonal Targeted Cancer Therapy. *Adv Funct Mater.* 2018;28:1–8.
- 53 Tonga GY, et al. Supramolecular regulation of bioorthogonal catalysis in cells using nanoparticle-embedded transition metal catalysts. *Nat Chem.* 2015;7:597–603.
- 54 Tornøe CW, Christensen C, Meldal M. Peptidotriazoles on solid phase: 1,2,3-Triazoles by regioselective copper(I)-catalyzed 1,3-dipolar cycloadditions of terminal alkynes to azides. *J Org Chem.* 2002;67:3057–3064.
- 55 Rostovtsev VV, Green LG, Fokin VV, et al. A stepwise huisgen cycloaddition process: Copper(I)-catalyzed regioselective 'ligation' of azides and terminal alkynes. *Angew Chemie - Int Ed.* 2002;41:2596–2599.
- 56 Bai Y, et al. A Highly Efficient Single-Chain Metal-Organic Nanoparticle Catalyst for Alkyne-Azide 'click' Reactions in Water and in Cells. *J Am Chem Soc.* 2016;138:11077–11080.
- 57 Clavdetscher J, et al. Copper Catalysis in Living Systems and In Situ Drug Synthesis. *Angew Chemie - Int Ed.* 2016;55:15662–15666.
- 58 Liang L, Astruc D. The copper(I)-catalyzed alkyne-azide cycloaddition (CuAAC) 'click' reaction and its applications. An overview. *Coord Chem Rev.* 2011;255:2933–2945.
- 59 Huang J, et al. Nanocopper-Doped Cross-Linked Lipid Acid Nanoparticles for Morphology-Dependent Intracellular Catalysis. *ACS Catal.* 2018;8:5941–5946.
- 60 Wang F, et al. A Biocompatible Heterogeneous MOF-Cu Catalyst for In Vivo Drug Synthesis in Targeted Subcellular Organelles. *Angew Chemie - Int Ed.* 2019;58:6987–6992.
- 61 Fernández-Caro H, et al. Supramolecular caging for cytosolic delivery of anionic probes. *Chem Sci.* 2019;10:8930–8938.
- 62 Li N, Lim RKV, Edwardraja S, et al. Copper-free sonogashira cross-coupling for functionalization of alkyne-encoded proteins in aqueous medium and in bacterial cells. *J Am Chem Soc.* 2011;133:15316–15319.
- 63 Spicer CD, Triemer T, Davis BG. Palladium-Mediated Cell-Surface Labeling. *J Am Chem Soc.* 2012;800–803.
- 64 Li J, et al. Ligand-free palladium-mediated site-specific protein labeling inside gram-negative bacterial pathogens. *J Am Chem Soc.* 2013;135:7330–7338.
- 65 Li N, Ramil CP, Lim RKV, et al. A genetically encoded alkyne directs palladium-mediated protein labeling on live mammalian cell surface. *ACS Chem Biol.* 2015;10:379–384.
- 66 Wang J, et al. Palladium-Triggered Chemical Rescue of Intracellular Proteins via Genetically Encoded Allene-Caged Tyrosine. *J Am Chem Soc.* 2016;138:15118–15121.
- 67 Indrijo E, et al. Intracellular delivery of a catalytic organometallic complex. *Chem Commun.* 2017;53:6712–6715.
- 68 Cherukaraveedu D, Cowling PT, Birch GP, et al. Solid-phase synthesis of biocompatible N-heterocyclic carbene-Pd catalysts using a sub-monomer approach. *Org Biomol Chem.* 2019;17:5533–5537.
- 69 Martínez-Calvo M, et al. Intracellular Deprotection Reactions Mediated by Palladium Complexes Equipped with Designed Phosphine Ligands. *ACS Catal.* 2018;8:6055–6061.
- 70 Learte-Aymarné S, Vidal C, Gutiérrez-González A, et al. Intracellular Reactions Promoted by Bis(histidine) Miniproteins Stapled Using Palladium(II) Complexes. *Angew Chemie - Int Ed.* 2020;59:9149–9154.
- 71 Stenton BJ, Oliveira BL, Matos MJ, et al. A thioether-directed palladium-cleavable linker for targeted bioorthogonal drug deaging. *Chem Sci.* 2018;9:4185–4189.
- 72 Tsubokura K, et al. In Vivo Gold Complex Catalysis within Live Mice. *Angew Chemie - Int Ed.* 2017;56:3579–3584.
- 73 Vidal C, Tomás-Gamasa M, Destito P, López F, Mascareñas JL. Concurrent and orthogonal gold(I) and ruthenium(II) catalysis inside living cells. *Nat Commun.* 2018;9:1–9.
- 74 Völker T, Meggers E. Chemical Activation in Blood Serum and Human Cell Culture: Improved Ruthenium Complex for Catalytic Uncaging of Alloc-Protected Amines. *ChemBioChem.* 2017;18:1083–1086.
- 75 Okamoto Y, et al. A cell-penetrating artificial metalloenzyme regulates a gene switch in a designer mammalian cell. *Nat Commun.* 2018;9:1–7.
- 76 Miguel-Avila J, Tomás-Gamasa M, Mascareñas JL. Intracellular Ruthenium-Promoted (2+2+2) Cycloadditions. *Angew Chemie - Int Ed.* 2020;59:17628–17633.
- 77 Sadhu KK, Lindberg E, Winsinger N. In cellulo protein labelling with Ru-conjugate for luminescence imaging and bioorthogonal photocatalysis. *Chem Commun.* 2015;51:16664–16666.
- 78 Holtzer L, et al. Nucleic acid templated chemical reaction in a live vertebrate. *ACS Cent Sci.* 2016;2:394–400.
- 79 Besanceney-Webler C, et al. Increasing the efficacy of bioorthogonal click reactions for bioconjugation: A comparative study. *Angew Chemie - Int Ed.* 2011;50:8051–8056.
- 80 Bose S, Ngo AH, Do LH. Intracellular Transfer Hydrogenation Mediated by Unprotected Organotitrium Catalysts. *J Am Chem Soc.* 2017;139:8792–8795.
- 81 Soldevila-Barreda JJ, Romero-Canelón I, Habtemariam A, et al. Transfer hydrogenation catalysis in cells as a new approach to anticancer drug design. *Nat Commun.* 2015;6.
- 82 Coverdale JPC, et al. Asymmetric transfer hydrogenation by synthetic catalysts in cancer cells. *Nat Chem.* 2018;10:347–354.
- 83 Ian M, et al. Photosensitizers for Photodynamic Therapy. *Adv Healthc Mater.* 2019;8:1–37.

B. Loshkin and T.R. Ward

Bioorganic & Medicinal Chemistry 45 (2021) 116310

- 84 Huang C, et al. Recent advances in endoplasmic reticulum targeting metal complexes. *Coord Chem Rev.* 2020;408, 213178.
- 85 Das R, et al. Control of Intra- versus Extracellular Bioorthogonal Catalysis Using Surface-Engineered Nanozymes. *ACS Nano.* 2019;13:229–235.

- 86 Zhang X, et al. Intracellular Activation of Bioorthogonal Nanozymes through Endosomal Proteolysis of the Protein Corona. *ACS Nano.* 2020;14:4767–4773.

2. Objectives of This Thesis

Since the discovery of Ru-catalyzed deallylation as a biocompatible new-to-nature reaction, the topic of bioorthogonality has been constantly growing. Several thousand publications in less than 20 years have demonstrated a wide variety of methods for activating fluorogenic and anticancer agents in cells and living organisms. However, the problem of precise targeted delivery and release of drugs has only been partially addressed using heterogeneous catalysts or ADCs. Homogeneous catalysts, as well as low-molecular delivery-vehicles, have not yet found application in this area.

Thus, this work aims to develop approaches to anticancer therapy, using bioorthogonal uncaging of a prodrug specifically on cancer cells. Known deallylation catalysts must be modified with selective binders to create metal cofactors for cancer-specific membrane proteins. In this work, we propose the synthesis of such metal complexes, as well as a test of their ability to a) discriminate against cancer cells in the presence of healthy ones, b) activate the prodrug. We also aim to design and synthesize a library of caged drugs to reduce the vital properties of diseased cells upon protecting-group cleavage.

The Ward group has a wealth of experience with other bioorthogonal reactions. In particular, the group demonstrated the first example of Ru-mediated olefin metathesis *in vivo*. However, at the start of this project, this reaction had never been used to activate prodrugs. Thus, another objective of this work is to design and develop substrates for *in vivo* ring-closing metathesis as the most promising intramolecular Ru-catalyzed reaction. We aim to assess RCM of prodrugs on different cell lines in the presence of water-soluble Hoveyda-Grubbs-like catalysts. The activation of fluorogenic substrates will be assessed by fluorescence spectroscopy and high-resolution microscopy.

Cancer cell proteins as scaffolds for ArMs have a strictly determined structure and, therefore, have limited functionality and selectivity. However, other proteins (streptavidin, HSA, and others) that can be modified by existing methods of protein engineering have been used to catalyze highly efficient and selective new-to-nature reactions. Another goal of this work is to expand the catalytic possibilities of artificial metathesases by rational design and directed evolution of protein scaffolds. In collaboration with Prof. David Baker (University of Washington), we set out to create a fully engineered artificial metalloenzyme based on *de novo* protein. The resulting ArMs will be optimized by directed evolution to increase regio-, enantio-, atropo- and other selectivities of RCM.

3. Results and Discussion

3.1. Deallylation project

Bioorthogonal activation of a prodrug on cells

This introduction details the application of bioorthogonal catalysis for *in vivo* drug and fluorophore release. The range of metals, ligands, and prodrugs used for cell and animal experiments is expanding every year. Despite the great potential of this approach in cancer therapy, to date, none of the developed methods has completed all clinical trials and has not been approved by the FDA. One of the most effective ways to activate caged prodrugs is heterogeneous Pd- and Au-catalysis, developed by, among others, the Unciti-Broceta group. Following implantation in mice and zebrafish, nanoparticles loaded with metal ions, catalyze the deallylation and depropargylation of many caged drugs and fluorophores.²⁻⁴ In this case, the challenge of selective drug delivery is circumvented by the precise implantation of a heterogeneous catalyst at the tumor site, where it remains active for several months.

Obviously, there are several other approaches towards tumor-specific drug delivery. One of the most relevant methods for targeting small molecules is the use of monoclonal antibodies as delivery vehicles in antibody-drug conjugates (ADCs). Antibodies specifically bind to membrane-bound proteins of cancer cells, after which the active molecule is released. Although the FDA has approved the use of 12 ADCs to date, this approach has several drawbacks:

- 1) Cancer cells can develop resistance to ADC in the same way as to other therapies.
- 2) Due to their large size, antibodies have low kinetics and cannot penetrate deep into the tumor.
- 3) Antibodies may trigger an immune response in the patient.

To overcome these challenges, antibodies can be loaded with drugs with orthogonal mechanisms of action. In particular, mutant antibodies containing selenocysteine for orthogonal conjugation of different drugs to one carrier have been developed but not yet validated in clinical trials investigated.

Also under development are peptide- and small molecule-drug conjugates that target cell-surface markers: integrins, membrane receptors, and others. Peptides and small molecules have the advantage of lower immunogenicity and improved tissue penetration, but they have poor pharmacokinetic properties (shorter half-life relative to ADCs). A small number of peptide- and small molecule-drug conjugates are currently in late-stage clinical trials.

By combining several established strategies of targeted drug-delivery and bioorthogonal catalysis, we propose an alternative approach to discriminate cancer from healthy cells, thus enabling a more precise cancer therapy.

Using small molecules – inhibitors or antagonists of cancer cell-membrane proteins – as delivery vehicles, we aim to label cancer cells with a bioorthogonal cofactor. In contrast, healthy cells should accumulate less cofactor as these display lower levels of the targeted cell-membrane proteins. Upon addition of a caged drug, the cofactor-catalyzed uncaging leads to the site-specific release of the uncaged drug, thereby deploying its action in the proximity of the cancer cells.

There are many cancer-specific membrane proteins. These include: i) human epidermal growth factor receptor 2 (HER2), ii) vascular endothelial growth factor receptors (VEGFRs), iii) epidermal growth

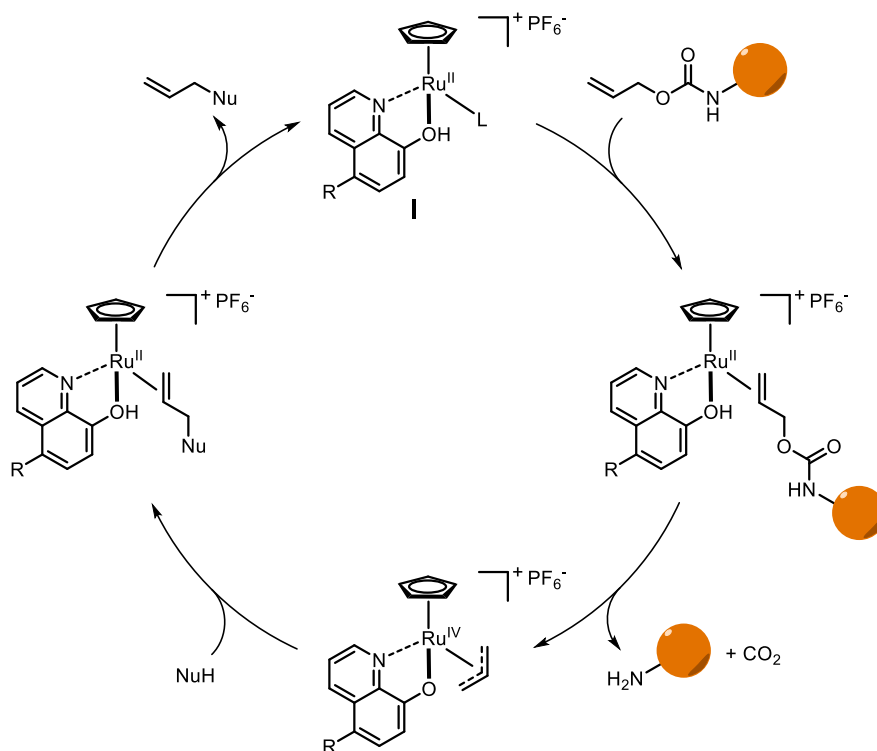
factor receptor (EGFR), iv) fibroblast activation protein (FAP), v) epithelial cell adhesion molecule (EpCAM), vi) human carbonic anhydrase IX (hCAIX) and many others. For each of them, low-molecular agonists and antagonists have been developed. These can potentially be used as an anchor to accumulate metal cofactors which catalyze the bioorthogonal uncaging of highly potent anti-cancer drugs.

As surface-displayed protein, we selected the cancer-specific variant of the human carbonic anhydrase (hCAIX), which is specifically expressed on cancer cells under hypoxic (<1% O₂) conditions. Using the difference in expression under hypoxic and normoxic (21% O₂) conditions, we can use a single cell line as a model for both diseased and healthy cultures.

Ru-deallylation

Meggers' 3rd generation Ru-deallylation catalyst **I** was selected as the catalytic moiety to target hCAIX which is overexpressed on the surface of many cancers. This Ru half-sandwich complex **I** displayed the highest efficiency in *in vivo* studies due to its higher activity and tolerance to cellular components.

The Ru(II)-complex with 8-hydroxyquinoline moiety **I** cleaves the alloc-moiety from caged fluorophores and drugs by a mechanism which proceeds via i) η^2 -coordination of the alkene, ii) oxidative addition of the allyl group, followed by iii) nucleophilic attack of the η^3 -allyl to afford iii) the Ru(II)(η^2 -alkene) which after ligand displacement closes the catalytic cycle (**Scheme A1**). Deallylation is irreversible due to the elimination of CO₂. When the reaction is performed in a cellular environment the free amino group of the drug/fluorophore is hypothesized not to act as a nucleophile on the Ru(IV)(η^3 -allyl) as other nucleophiles (e.g., GSH, OH⁻) are present in vast excess in the cytoplasm.

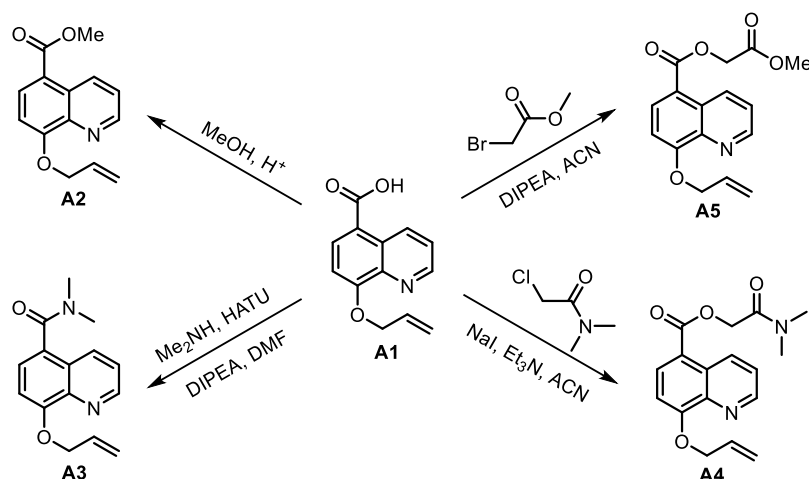


Scheme A1. Proposed catalytic cycle for the deallylation with Ru half-sandwich complexes.

The electronic properties of the substituents in the quinoline core significantly affect the activity of the catalyst **I**. For example, it is known that if **R** is a carboxylic acid derivative, then its esters lead to more

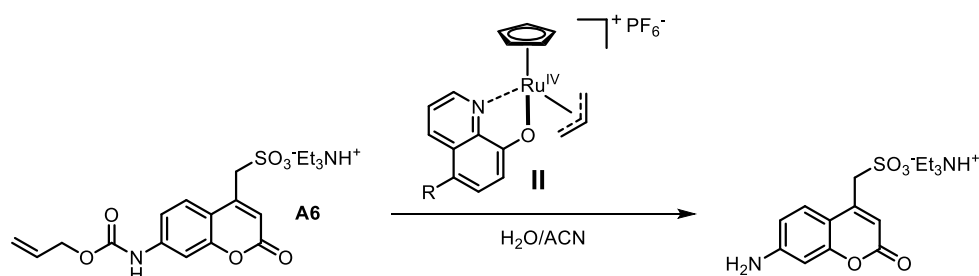
effective catalysts that the corresponding amide-bearing hydroxyquinoline. Assuming that amide coupling of the ligand with an hCAIX-specific anchor is used for the metal cofactor, it was necessary to identify the optimal spacer that does not significantly affect i) the binding of the anchor to hCAIX and ii) the catalytic properties of the Ru-complexes.

For this purpose, a series of 8-allyloxyquinoline ligands **A2-5** was synthesized for subsequent catalytic activity tests (**Scheme A2**).



Scheme A2. A family of 8-allyloxyquinolines for catalysis study.

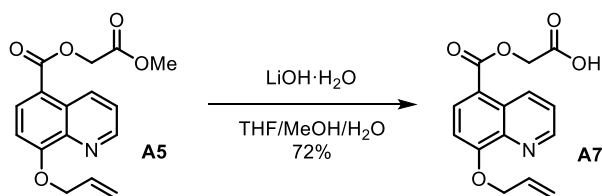
All ligands were mixed with $[\text{CpRu}(\text{NCMe})_3]\text{PF}_6$ as a Ru source. The uncaging activity of the resulting Ru(IV) complexes **II** was evaluated for the catalytic deallylation of caged 7-aminocoumarin **A6** (**Scheme A3**).



Scheme A3. Catalytic deallylation of **A6**.

The results of these experiments confirmed the initial hypothesis about the influence of substituents.

Complexes with ligands **A2**, **A4**, and **A5** revealed nearly the same activity since they are esters of **A1**. Amide **A3** turned out to be approximately 10 times less active. Therefore, acid **A7** was synthesized as a result of partial alkaline hydrolysis of **A5** for subsequent amide coupling with an appropriate protein binder (**Scheme A4**).



Scheme A4. Synthesis of ligand **A7**.

Fluorinated anchors

The next goal within the framework of this project was the identification of optimal antagonists of hCAIX for the selective accumulation of the metal cofactor to cancer cells which overexpress hCAIX.

Since all carbonic anhydrases are zinc-dependent enzymes, the most effective inhibitors contain an arylsulfonamide which binds tightly to the Zn-ion (**Fig. A1**).

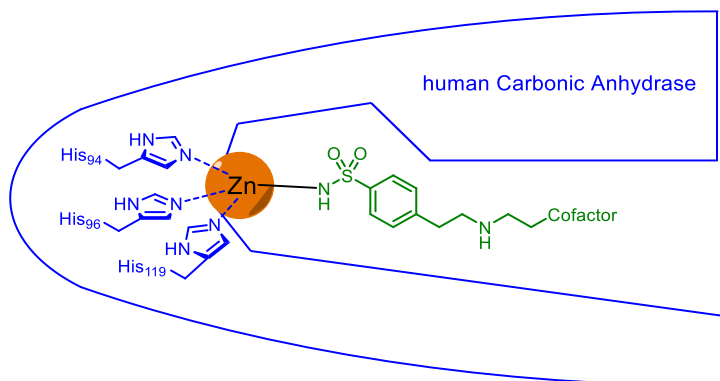


Figure A1. Schematic representation of arylsulfonamide binding to hCA binding site.

However, hCAs are also widely present in healthy cells of the human body. In order to enable the cofactor to distinguish between cancer and normal cells, it is necessary to minimize its binding to the most abundant anhydrases (hCAII) and maintain its affinity for cancer-specific proteins. Matulis Daumantas et al. reported a family of perfluoroarylsulfonamides (**Fig. A2**) as selective inhibitors of hCAIX.⁵

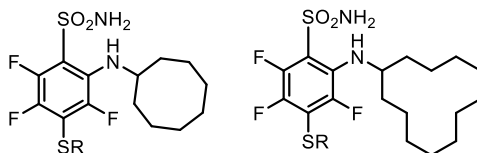
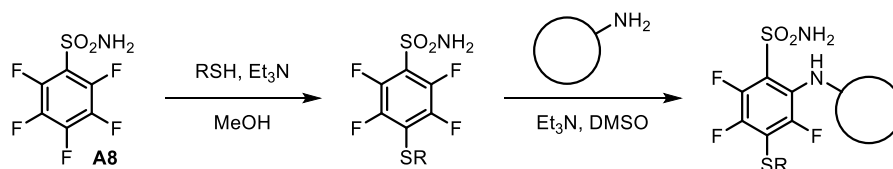


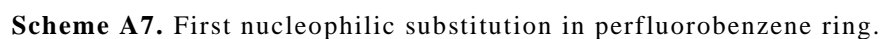
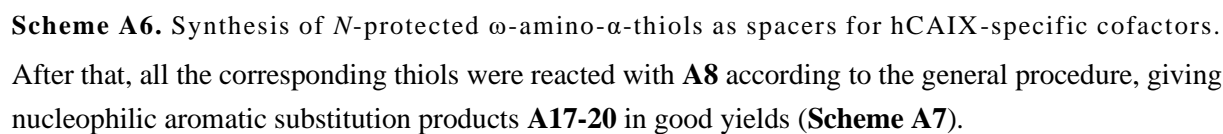
Figure A2. Potential delivery vehicles for Ru-deallylation cofactor.

Inspired by this study, we synthesized a family of hCAIX-specific anchors for subsequent conjugation with **A1** and a fluorophore for live-cell imaging. Fluorescent markers can also be used to assess the target protein expression level under hypoxic and normoxic conditions. Since nucleophilic aromatic substitution in 2,3,4,5,6-pentafluorobenzenesulfonamide **A8** is facilitated by activation of the *ortho*- and *para*-positions, the following general scheme for synthesizing hCAIX inhibitors was developed (**Scheme A5**).

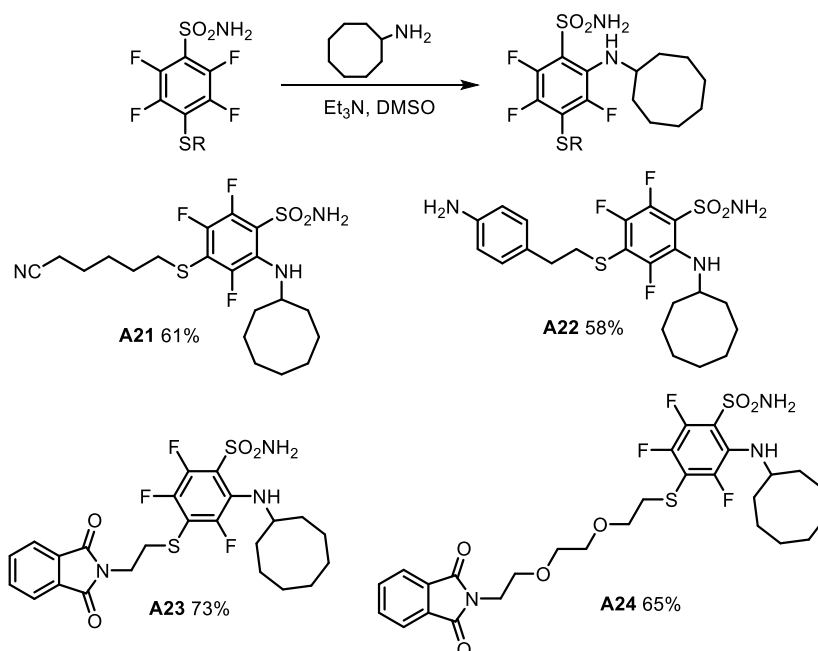


Scheme A5. General approach to hCAIX polyfluorinated inhibitors.

Next, *N*-protected α,ω -aminothiols **A9,11,14,16** with different chain lengths and polarities, were selected as spacers and were synthesized in several steps (**Scheme A6**).



22



Scheme A8. Second nucleophilic aromatic substitution.

Finally, all protecting groups were removed under various conditions (see SI) to afford the corresponding free amines **A22,25-27** (**Fig. A3**).

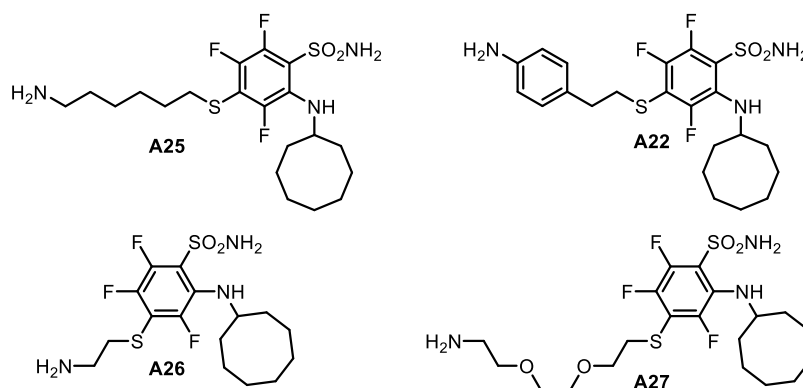
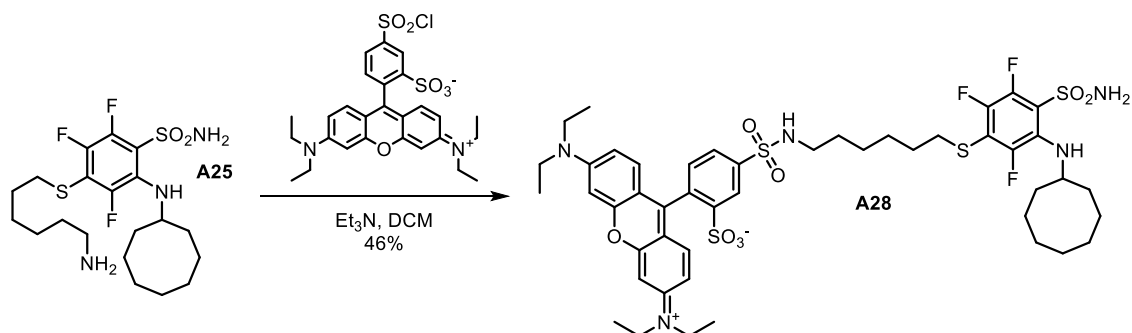


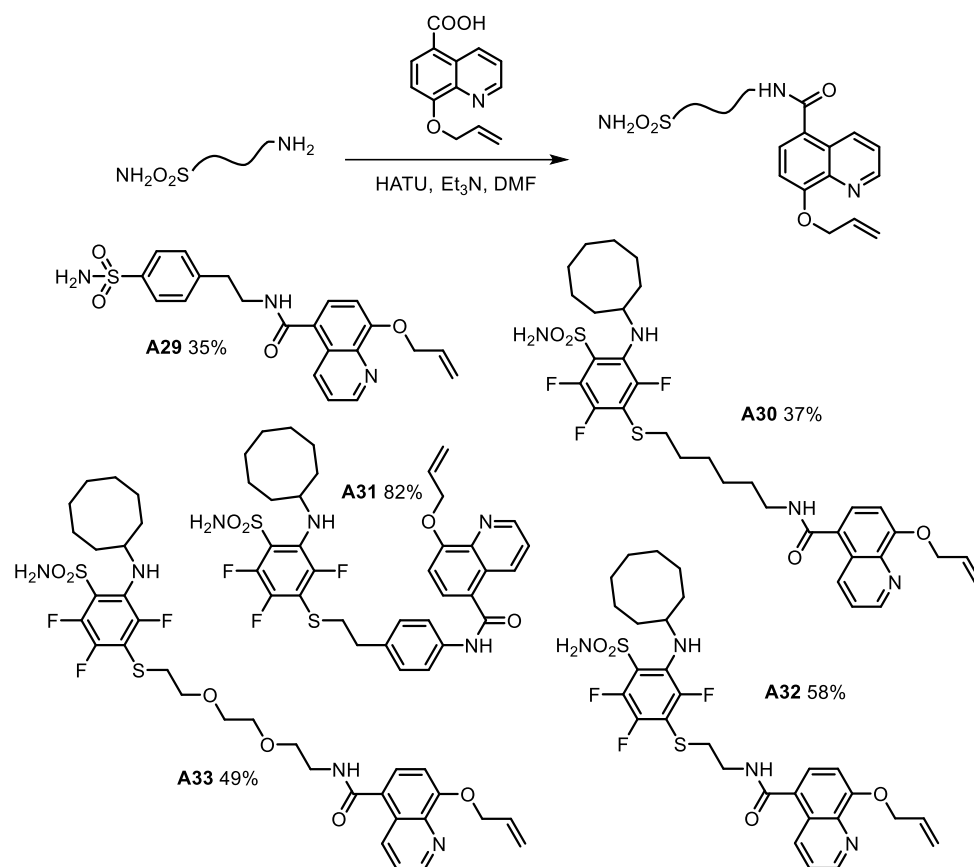
Figure A3. A family of potential hCAIX-specific anchors.

One of the anchors **A25** was modified with Sulforhodamine B (Kiton Red 620), a water-soluble fluorophore widely used for cell experiments. The corresponding fluorescent inhibitor **A28** can be used to monitor arylsulfonamide binding to surface-expressed hCAIX (**Scheme A9**).



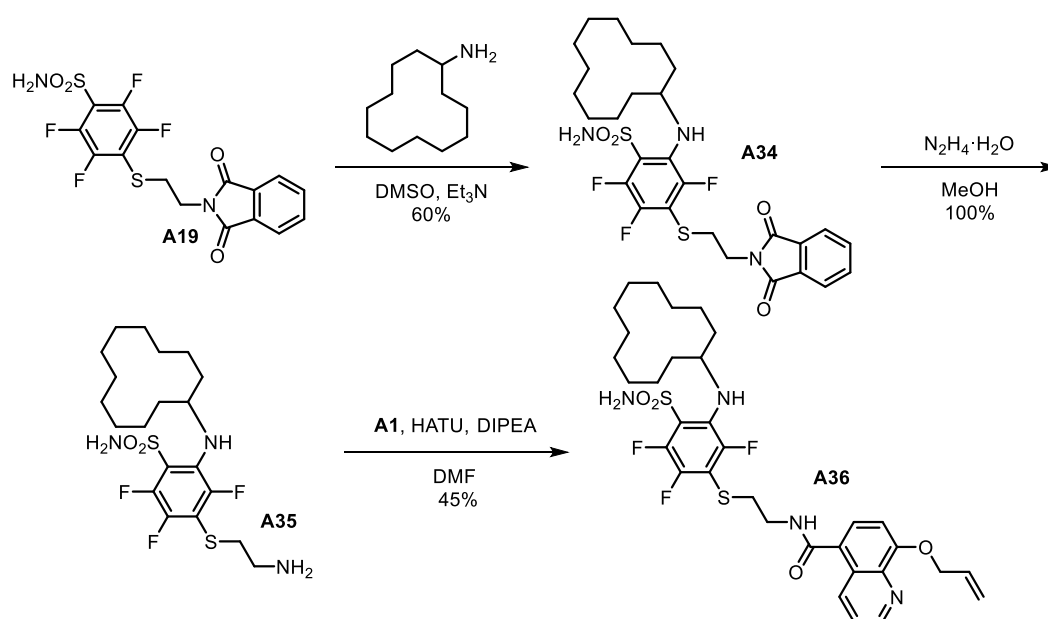
Scheme A9. Synthesis of fluorescent marker for hCAIX imaging.

Despite its lower catalytic potential, **A1** was selected as a ligand, since it is available on a larger scale. For proof-of-concept studies, **A1** was linked to the anchors **A22,25-27** by amide coupling, yielding Ru-deallylation cofactors precursors **A30-33**. To compare their activity with a cofactor bearing an hCAII-specific anchor, the benzenesulfonamide derivative **A29** was prepared as well (**Scheme A10**).



Scheme A10. Synthesis of hCA-targeted ligands for Ru-catalyzed deallylation.

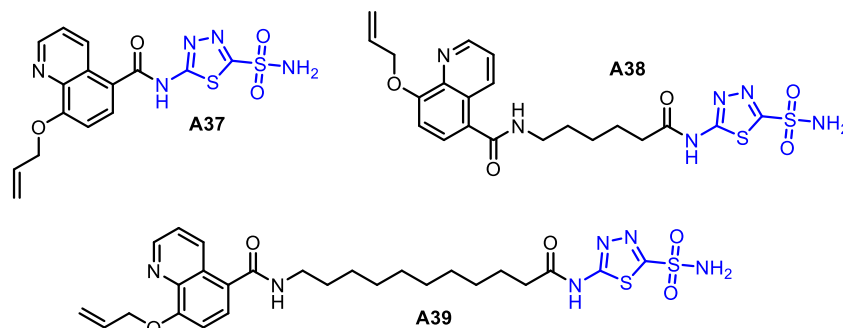
With optimized reaction conditions at hand, ligand **A36**, the cyclododecyl analog of **A32**, was synthesized in 3 steps from **A19** (**Scheme A11**).



Scheme A11. Synthesis of **A36**.

Azolamide derivatives and experiments on cells

Building on a report by Neri and coworkers,⁶ we synthesized acetazolamide-bearing inhibitors as these display high affinity (typically sub nM) for various CAs. Thus, the azolamide derivatives **A37-39** with spacers of varying lengths (**Scheme A12**) were prepared according to the general procedure (see SI).



Scheme A12. A1-azolamide conjugates. The azolamide fragment highlighted in blue.

The biological results presented in this chapter as well as probes for cellular studies were obtained in collaboration with Brett Garabedian.

For initial experiments, all synthesized ligands were pre-mixed with [CpRu(NCMe)₃]PF₆ and tested in the deallylation of the caged fluorophore **A6** in a cell-free medium either under hypoxic or normoxic conditions (corresponding to < 1% O₂ vs 21% O₂ respectively).

Control reactions (caged coumarin **A6** (100 μM), quinoline ligand (2 μM), [CpRu(NCMe)₃]PF₆ (2 μM)) were run both under hypoxic and normoxic conditions in a) DMSO as a negative control; b) PBS buffer; and c) PBS buffer in the presence of 2 μM hCAII as a model protein (**Fig. A4**). All complexes revealed high catalytic activity (from 21 to 50 turnovers), both as a free cofactor and in the presence of hCAII.

It has also been found that azolamide-bearing derivatives with a short spacer (**A37-38**) yielded the best results (i.e., fluorescence). Importantly, oxygen had a marked detrimental effect on the catalytic deallylation of **A6**.

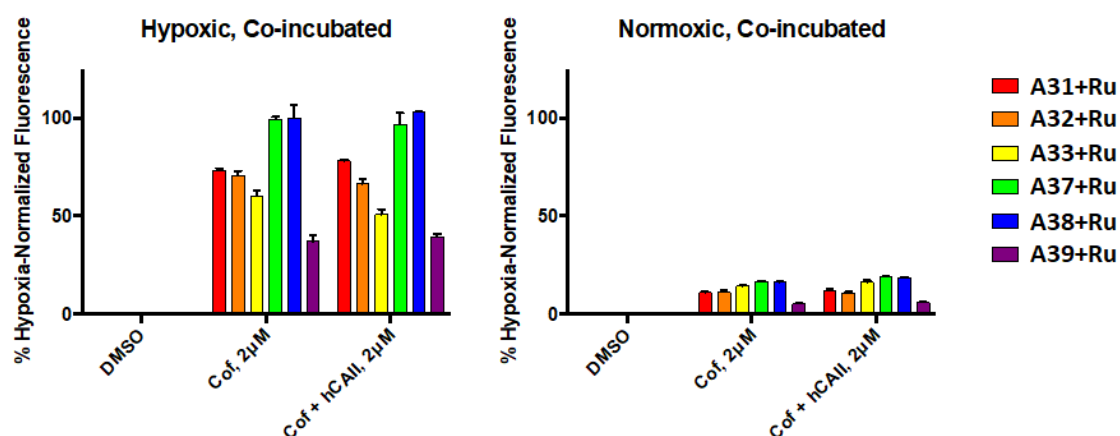


Figure A4. Deallylation of caged fluorophore **A6** catalyzed by [CpRu]-complexes. Conditions: ligand (2 μM), [CpRu(NCMe)₃]PF₆ (2 μM), **A6** (100 μM), PBS buffer, 37 °C, 24 h.

The experiment was then repeated in the presence of HeLa cells according to the following protocol:

- 1) Seed 10,000 cells/well.
- 2) Grow culture at 1% or 21% oxygen, 37°C, 24 h.

- 3) Bind cofactor, 37°C, 15 min (1 to 10 μM).
- 4) Wash cells 2x with PBS.
- 5) Add alloc-coumarin **A6** (100 μM).
- 6) Incubate at 1% or 21% oxygen, 37°C, 24 h.

From the hypoxic experiments, the fluorescence correlates with the concentration of the cofactor (**Fig. A5**). However, even at 10 μM cofactor concentration, only 2 μM of the product is formed, corresponding to TON = 0.2. Under normoxic conditions, nonspecific binding of the cofactor leads to high background fluorescence at all initial concentrations of Ru.

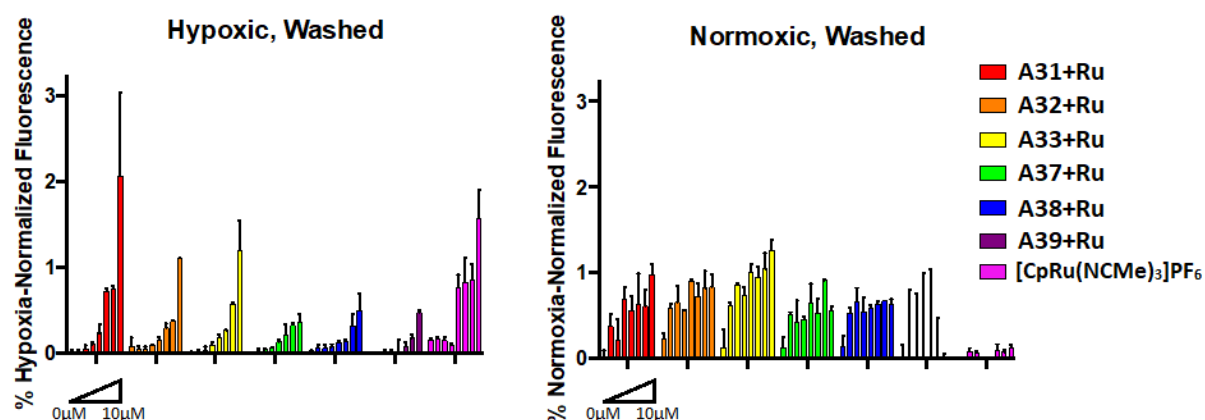


Figure A5. On-cell catalytic deallylation. Conditions: ligand preincubated with [CpRu(NCMe)₃]PF₆ (1:1 ratio, with concentrations varying from 1 to 10 μM), **A6** (100 μM), PBS buffer, HeLa cells, 37 °C, 24 h.

Next, the workflow was modified to test the non-specific binding hypothesis by increasing the cofactor concentration and decreasing the oxygen content to increase catalysis activity (**Fig. A6**):

- 1) Seed 10,000 cells/well.
- 2) Grow culture at 1% or 21% oxygen, 37°C, 24 h.
- 3) Bind cofactor, 37°C, 30 min (1 to 100 μM).
- 4) Wash cells 2x with PBS.
- 5) Add alloc-coumarin **A6** (100 μM).
- 6) Incubate at 1% oxygen, 37°C, 24 h.

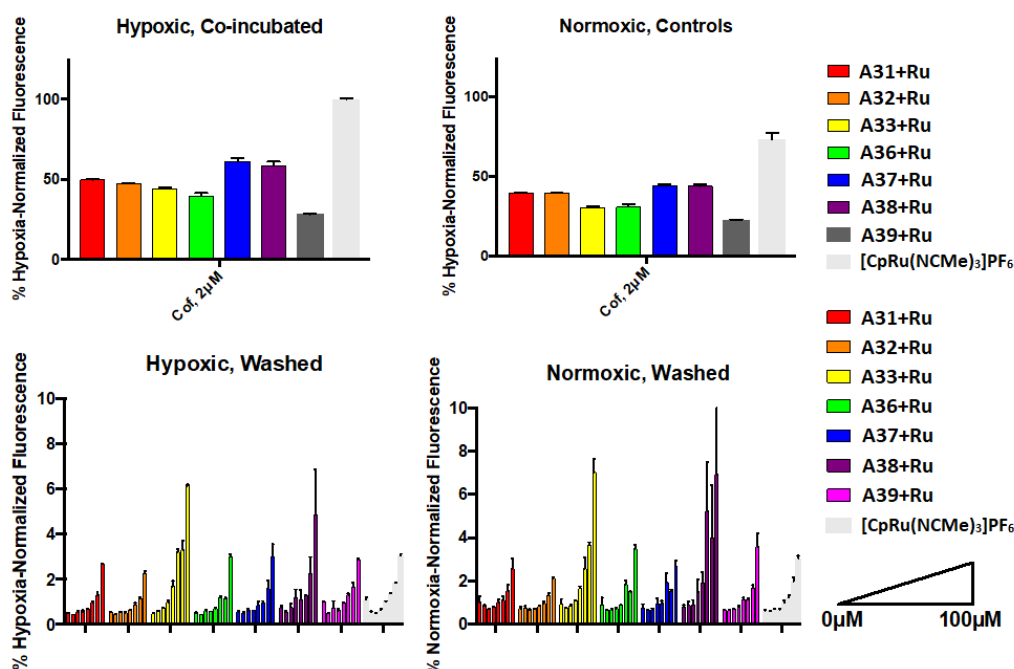


Figure A6. On cell catalytic deallylation. Conditions: ligand preincubated with [CpRu(NCMe)₃]PF₆ (1 to 100 μM), **A6** (100 μM), PBS buffer, HeLa cells, 37 °C, 1% O₂, 24 h.

This series of experiments suggested that cofactors bearing inhibitors **A31-A39** do not accumulate significantly on the surface of hypoxic cells. Thus, we set out to design a cofactor with increased affinity towards hCAIX

In 2015, groups of Neri and Scheuermann reported a new hCAIX inhibitor **A40** with a subnanomolar affinity ($K_d \approx 0.2$ nM for hCAIX) identified using a DNA-encoded library.⁶ In addition to the azolamide fragment, it contains a bisphenol A moiety, which significantly improves the binding selectivity. Accordingly, inhibitor **A40** was synthesized using solid-phase peptide synthesis according to the literature procedure (see SI). After that, the following derivatives of **A40** were synthesized for experiments on cells (**Fig. A7**):

- 1) **A40-SRB** – fluorescently-labeled inhibitor for *in vivo* imaging;
- 2) **A40-QA** – amide of **A1** with **A40** for *in vivo* catalysis;
- 3) **A40-COCH₂-QA** – amide of **A7** with **A40** for *in vivo* catalysis;
- 4) **A40-p-I** – amide of *p*-iodobenzoic acid with **A40** for ICP-MS analysis;
- 5) **A40-p-Sn** – amide of *p*-(tributyltin)benzoic acid with **A40** for ICP-MS analysis;
- 6) **A40-DRDGG-QA** – **A40** attached to **A1** *via* DRDGG linker to prevent internalization of the cofactor for *in vivo* catalysis;
- 7) **A40-DRDGG-SRB** – fluorescently-labeled inhibitor with DRDGG linker for *in vivo* imaging.

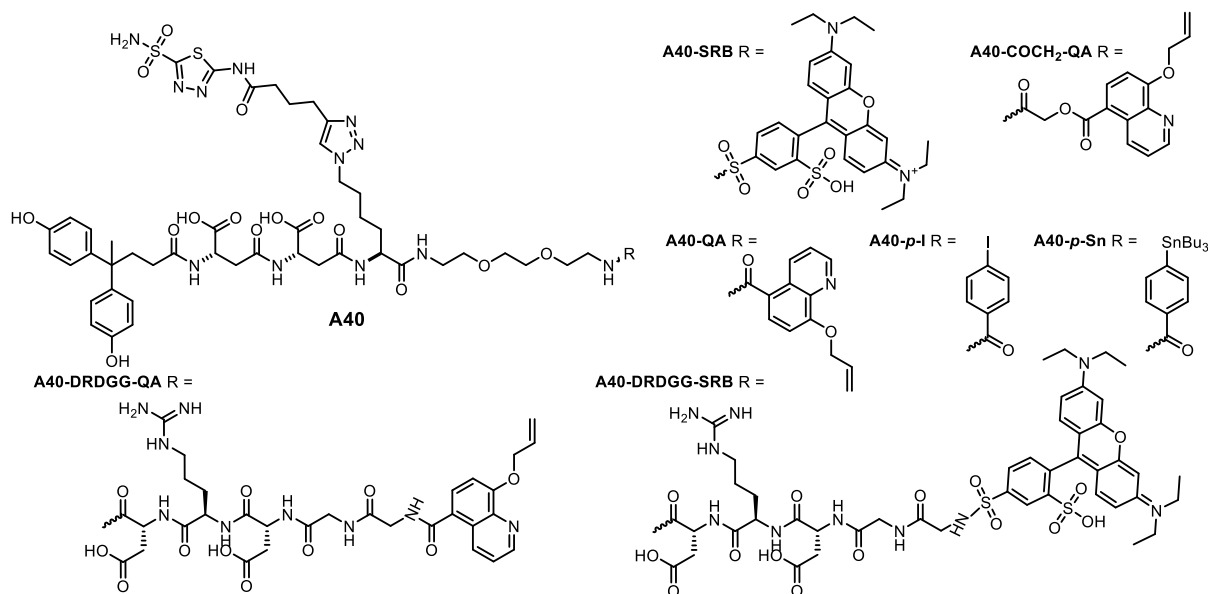


Figure A7. Structures of inhibitor **A40** adducts for cell experiments.

A40-SRB conjugate was used to assess the selectivity of **A40** binding to the surface of cancer cells. For this, **A40-SRB** was co-incubated with cells grown under hypoxic (**Fig. A8.A-C**) and normoxic (**Fig. A8.D**) conditions. In experiment **A**, the cells were also incubated with primary anti-hCAIX-antibodies and secondary antibodies labeled with FITC. Primary antibodies were not added in experiment **B**. In experiment **C**, a large excess of acetazolamide (AAZ) was used to inhibit the binding sites of hCAIX, which did not interfere with the binding of antibodies to proteins. In experiment **D**, all fluorescent markers of hCAIX were used on cells grown at normal oxygen concentration. After co-incubation for 30 minutes, cell cultures were washed twice with cell media to remove free binders.

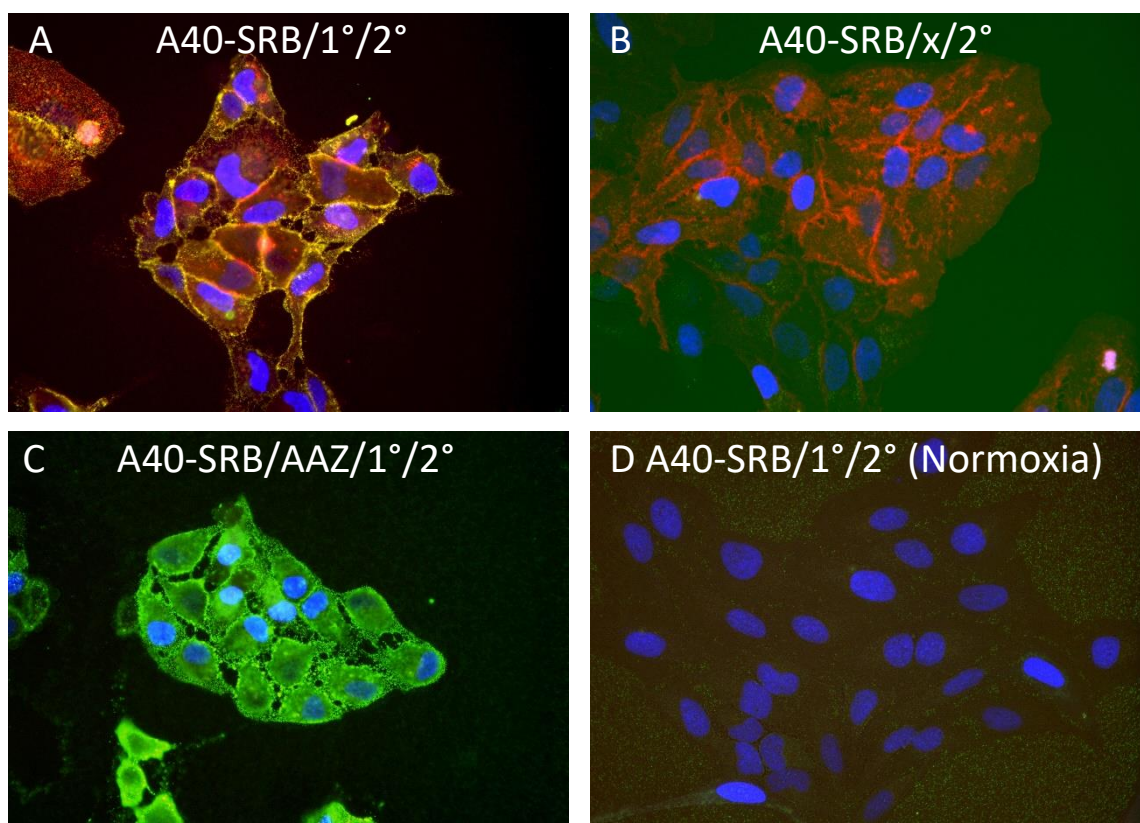
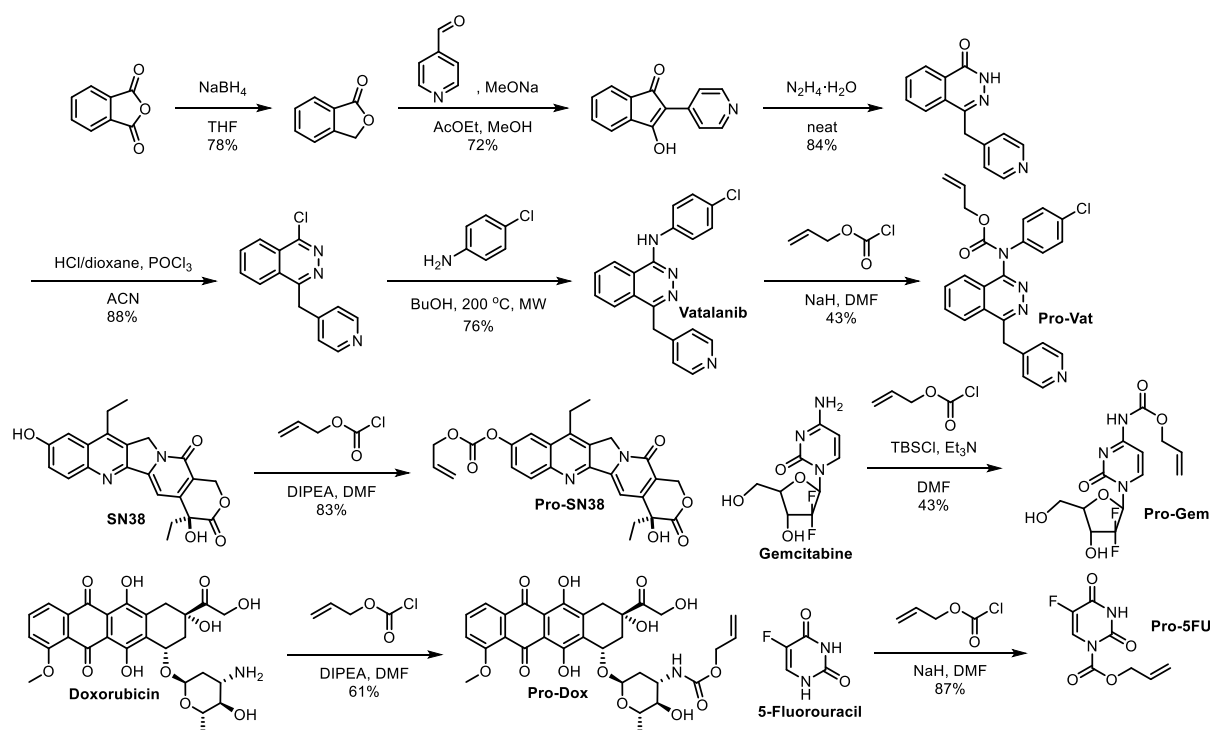


Figure A8. Live-cell imaging study of binder localization on the cell membrane. Nuclei – blue, DAPI. CAIX – green (FITC) and red (**A40-SRB**).

With these promising results in hand, we set out to synthesize a family of alloc-protected drugs for subsequent testing in cancer cell cultures.

Prodrugs synthesis and evaluation

There are many existing methods to reduce the vital functions of cancer cells. For this project, we selected representatives of various classes of anticancer drugs: SN-38 (topoisomerase inhibitor), doxorubicin (anthracycline), vatalanib (protein kinase inhibitor), gemcitabine and 5-fluorouracil (antimetabolites). Allyloxy and propargyloxy protecting groups are known to significantly reduce the cytotoxicity of bioactive small molecules.^{4,7,8} SN-38, doxorubicin, gemcitabine, and 5-fluorouracil were purchased from suppliers and used without further purification. Vatalanib was synthesized in 5 linear steps from commercially available reagents. Within the framework of this project, we relied on the classic approach to caging selected drugs by direct modification of their functional groups (OH, NH₂) (Scheme A13).



Scheme A13. Synthesis of vatalanib and Pro-Vat, Pro-SN38, Pro-Gem, Pro-Dox, and Pro-5FU.

For each of these caged prodrugs, the toxicity was compared with the parent drug. For this, various cultures of cancer cells were incubated for 7 days with solutions of drugs and prodrugs at different concentrations (Table A1).

Table A1. IC₅₀ values of drugs and prodrugs tested on various cell lines.

	IC ₅₀ , μ M		
	HeLa	A549	HT29
Dox	0.09	0.32	0.14
Pro-Dox	1.78	20.4	21.9
SN38	0.17	0.30	0.08
Pro-SN38	0.89	0.30	0.08
Vatalanib	5.39	29.5	23.6
Pro-Vatalanib	6.34	29.6	21.7
5FU	1.24	2.83	16.5
Pro-5FU	1.24	2.40	47.4
Gem	0.08	0.07	0.07
Pro-Gem	0.31	0.43	1.65

As can be appreciated from these data, the following prodrugs showed the most promising results:

- 1) **Pro-Dox**: 20 times less toxic for HeLa, 64 times less toxic for A549, and 21 times less toxic for HT29.
- 2) **Pro-Gem**: 21 times less toxic for HT29.

All other prodrugs do not provide a sufficiently wide therapeutic window since the prodrug has comparable cytotoxicity to the parent drug.

After that, hCAIX expression was assessed in all cell lines compared to HeLa cells in the presence of various stimuli (**Fig. A9.A**). It was found that HT29 cells cannot be used in this project because they express hCAIX under both hypoxic and normoxic conditions without stimuli. HeLa cells express, on average, 100,000-400,000 copies of hCAIX per hypoxic cell (**Fig. A9.A**), which confirms the promise of this protein for the targeted accumulation of an azolamide-bearing catalyst.

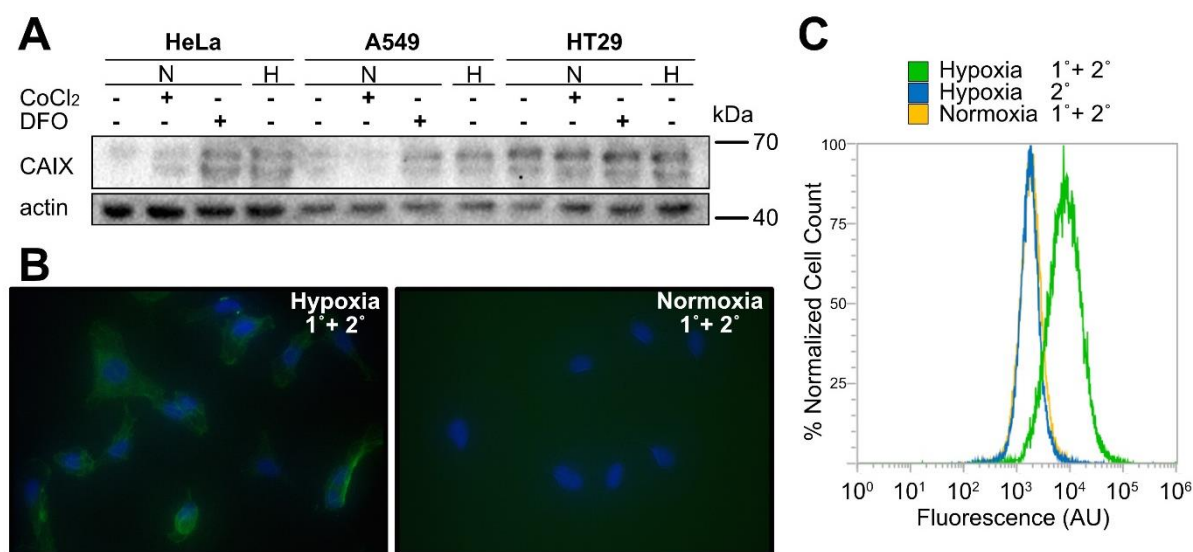


Figure A9. **A.** CAIX expression levels of cancer cell lines under various stimuli. **B.** Live-cell imaging study of hCAIX expression with primary and secondary antibodies. Nuclei – **blue**, DAPI. hCAIX – **green**, FITC. **C.** FACS sorting of CAIX expressing cells.

The high level of hCAIX expression in normoxic HT29 precludes the use of this cell line as a model in this project. In this regard, HeLa cells and **A6** and **Pro-Dox** were selected as substrates for subsequent experiments. Catalysis was performed using a 100 nM solution of [A40-COCH₂-QA+[CpRu(NCMe)₃]PF₆] a) in the presence and absence of an inhibitor (AAZ); b) with or without washing after co-incubation with a catalyst; c) on cells grown under either normoxic or hypoxic conditions; d) in hypoxic and normoxic conditions during catalysis.

It was found that the highest catalytic activity was achieved when the cells were not washed after co-incubation with the catalyst. Indeed, the uncaging aminocoumarin in the presence of cells that were washed after incubation with the cofactor was six times lower – as reflected by increased fluorescence.— This suggests that the cells lose ruthenium during washing, which is obviously detrimental to catalytic activity. In general, the reaction is not tolerant to oxygen, which was confirmed by the minimal increase in fluorescence when the reaction was performed in the presence of air.

Despite the low catalytic activity of the cofactor bound to hCAIX, a similar experiment was carried out with **Pro-Dox** as a substrate. Cells were preincubated with 100 nM cofactor solution, after which **Pro-Dox** was added at various concentrations immediately or after washing. The efficiency of catalysis was monitored by MTT test enabling the monitoring of cell viability.

The decrease in IC₅₀ that we observed in this experiment suggests the following: washed cells adsorb about $5 \cdot 10^9$ Ru atoms per well (IC₅₀^{normoxia} 35.8 nM, IC₅₀^{hypoxia} 33.7 nM); unwashed cells contain about $6 \cdot 10^{12}$ Ru atoms per well (IC₅₀^{normoxia} 34.6 nM, IC₅₀^{hypoxia} 19.2 nM) (**Fig. A10**).

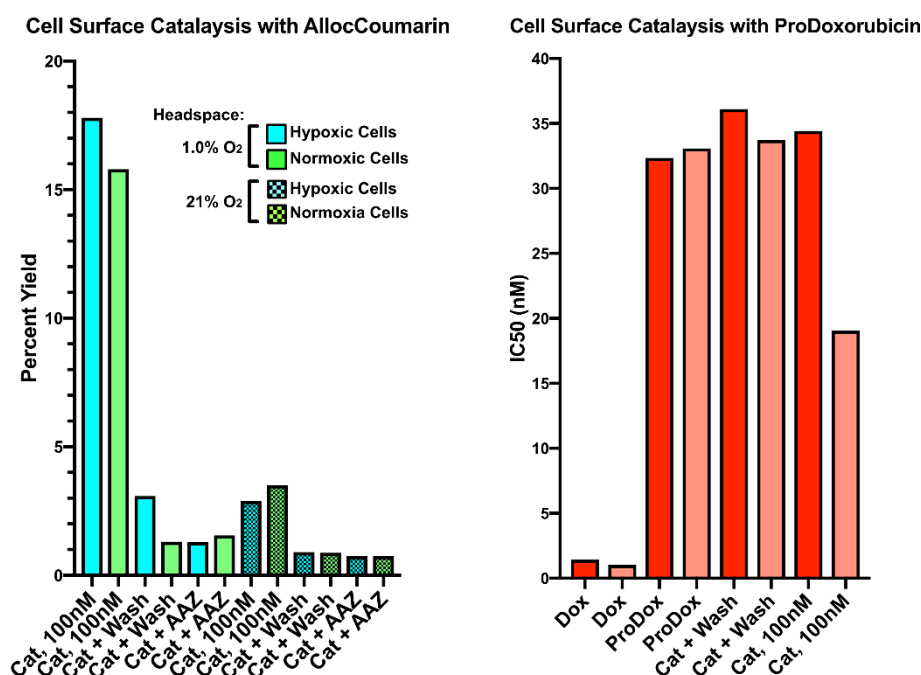


Figure A10. Cell surface deallylation of **A6** and **Pro-Dox**.

The low catalytic activity leads to the fact that the required "lethal" concentration of doxorubicin cannot be achieved as a result of **Pro-Dox** deallylation. However, the visible and reproducible difference in catalysis between hypoxic and normoxic cells opens up opportunities for further system improvement.

One of the approaches to address this challenge may be to uncage a more potent drug as a result of Ru-catalyzed deallylation. Nanomolar drug activity must be sufficient to achieve IC_{50} under Ru-deallylation conditions.

For this project, the antimitotic agent monomethyl auristatin E (**MMAE**), blocking the polymerization of tubulin, was selected (**Fig. A11**). Due to its high toxicity, it is not used as a drug itself but conjugated with monoclonal antibodies that direct its delivery to the tumor.

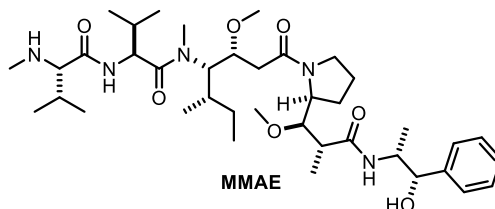


Figure A11. Structure of monomethyl auristatin E **MMAE**.

Existing ADCs rely on bioenzymatic cleavage of the valine-citrulline (Val-Cit) dipeptide resulting in a cascade elimination of PAB and free **MMAE**. For this project, alloc-protected **MMAE** (**alloc-MMAE**) was synthesized and tested on various cells (**Fig. A12**). Unfortunately, this protecting group turned out to be too small to alter the marked cytotoxic properties of the parent drug significantly. The IC_{50} of **alloc-MMAE** was found to be 4 nM, which is only 4 times higher than the IC_{50} of **MMAE**.

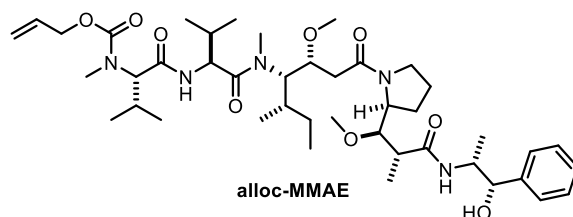


Figure A12. Structure of **alloc-MMAE**.

To reduce the toxicity of the prodrug even further, we set out to develop a new alloc-like protecting group that would allow the synthesis of a caged drug-drug conjugate. The prodrug with reduced bioavailability would release both drug molecules under bioorthogonal catalysis. The simplest allyl diols **A41-43** were selected as a "bridge" between the two **MMAE** fragments (**Fig. A13**).

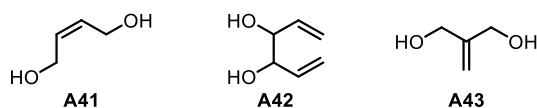
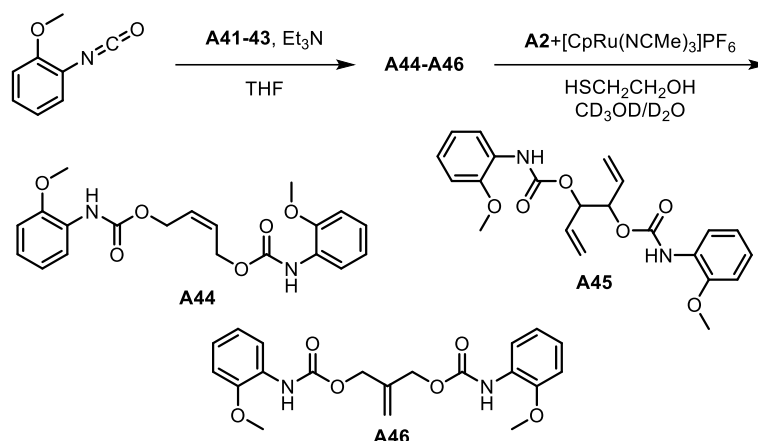


Figure A13. Structures of potential Ru-cleavable allyl moiety between two **MMAE** moieties.

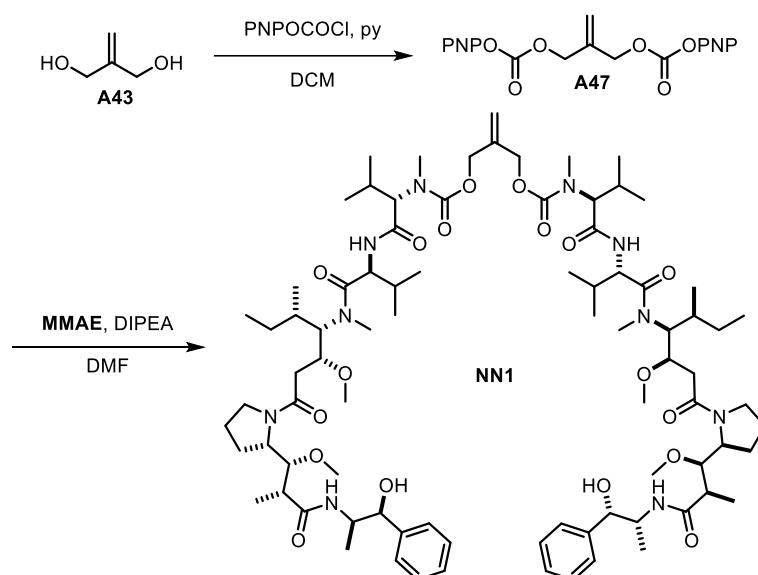
All diols were reacted with 2-methoxyphenyl isocyanate, and the resulting dicarbamates were tested in presence of $[A2 + [CpRu(NCMe)_3]PF_6]$ as a catalyst and 2-mercaptoethanol as a nucleophile (**Scheme A14**). As a negative control, the stability of substances was tested in the presence of a catalyst without a nucleophile and in the presence of a nucleophile without a catalyst.

Only the **A43** linker led to complete conversion of the model substrate to *o*-anisidine using 5 mol% of the cofactor and two equivalents of the nucleophile. In the absence of the nucleophile, the maximum achieved conversion was lower than 10%. The reaction did not proceed in the absence of a catalyst, highlighting the compound's resistance to hydrolysis under aqueous conditions.



Scheme A14. Synthesis of caged *o*-anisidines **A44-46** and their catalytic deallylation.

In order to obtain two **MMAE** units linked with the cleavable bridging allyl group, the alcohol groups of **A43** were first activated with PNP-carbonates (**A47**), after which **MMAE** was conjugated with the **A47**, affording the pure **NN1** dimer after reversed-phase HPLC purification (**Scheme A15**).



Scheme A15. Synthesis of dimeric **MMAE** (**NN1**).

The toxicity of **NN1** was determined for three cancer cell lines (HeLa, A549, HT29). For each of them, a significant increase in IC_{50} (up to more than 20 times) was found (**Fig. A14**). Given that this molecule is a dimer of **MMAE**, it results in about a 40-fold decrease in toxicity per drug molecule.

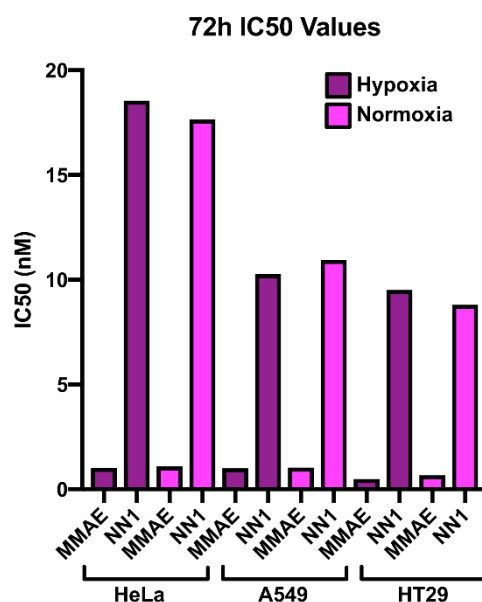
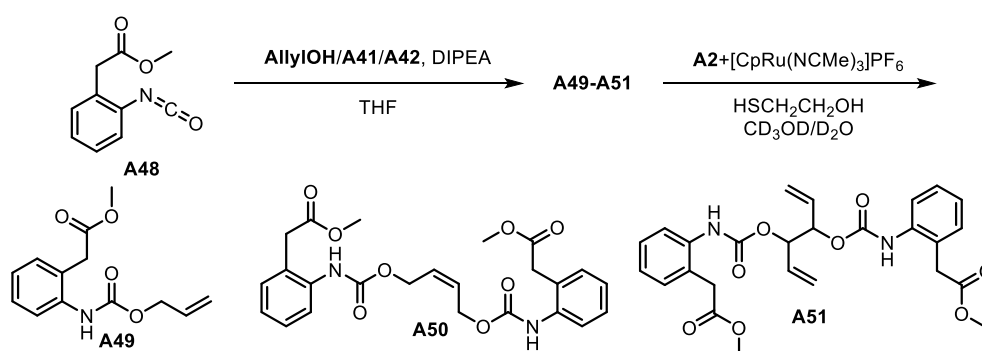


Figure A14. IC₅₀ values of MMAE and NN1 for various cancer cell lines.

We also tried to design a protecting group for the norephedrine moiety of MMAE because it has a stronger effect on drug potency. For this, several deallylation substrates **A49-51** containing an *o*-aminophenylacetic acid moiety have been synthesized since it is known that the released amino group can lead to aminolysis of the ester. However, under the model reaction conditions, deallylation was not followed by lactamization (**Scheme A16**).



Scheme A16. Synthesis of caged *o*-aminophenylacetic esters **A51-53** and their catalytic deallylation.

Outlook

Since anchor **A40** revealed high affinity to hCAIX allowing discrimination of cancer cells in presence of healthy cells, ligands **A40-COCH₂-QA** and **A40-QA** will be further used for generation of Ru-deallylation cofactor *in cellulo*. The prodrug **NN1** will be used as the most promising prodrug candidate.

Upon generating positive results, cell viability can also be tested in the presence of a mixture of **NN1** and other prodrugs at concentrations far below IC₅₀. The synergistic effect of combinatorial therapy may allow a milder dosage regimen.

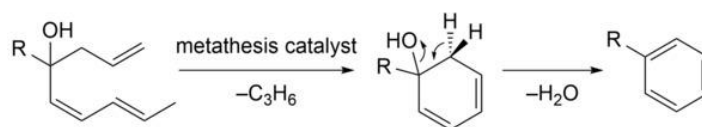
3.2. Ring-Closing Metathesis Project

A Close-to-Aromatize Approach for the Late-Stage Functionalization through Ring-Closing Metathesis

The next reaction of practical interest in the context of ruthenium-catalyzed bioorthogonal transformations is metathesis. The number of structural fragments present in bioactive molecules that can be obtained as a result of intra- or intermolecular metathesis is limited. As a part of this project, a family of substrates that convert to mono-substituted aromatic compounds under mild conditions has been developed.

Abstract of the publication

An efficient approach for the synthesis of monosubstituted aromatic compounds relying on a ring-closing metathesis followed by spontaneous 1,2-elimination is presented. The efficiency for late-stage functionalization is highlighted in various solvents (up to 920 TON). This approach is compatible with strained cycles and other multiple bonds in the substrate.





DOI: 10.1002/hlca.202100024

COMMUNICATION

HELVETICA
CHIMICA ACTA

A Close-to-Aromatize Approach for the Late-Stage Functionalization through Ring Closing Metathesis

Boris Lozhkin^a and Thomas R. Ward^{*a}^a Department of Chemistry, University of Basel, Building 1096, Mattenstrasse 24a, Biopark Rosental, CH-4058 Basel, Switzerland, e-mail: Thomas.ward@unibas.ch

© 2021 The Authors. Helvetica Chimica Acta published by Wiley-VHCA AG. This is an open access article under the terms of the Creative Commons Attribution Non-Commercial NoDerivs License, which permits use and distribution in any medium, provided the original work is properly cited, the use is non-commercial and no modifications or adaptations are made.

An efficient approach for the synthesis of monosubstituted aromatic compounds relying on a ring-closing metathesis followed by spontaneous 1,2-elimination is presented. The efficiency for late-stage functionalization is highlighted in various solvents (up to 920 TON). This approach is compatible with strained cycles and other multiple bonds in the substrate.

Keywords: elimination, late-stage functionalization, metathesis, ring closing metathesis.

Introduction

Aromatic fragments are present in a vast majority of organic compounds. For the late-stage introduction of aromatic fragments, common methods include various cross-coupling and C–H activation strategies.^[1–6] Herein, we exploit ring closing metathesis of a readily accessible triene-ol to access monosubstituted benzene derivatives.

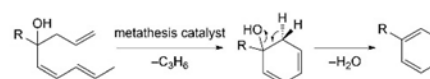
Numerous strategies to produce aromatic rings as a result of ring-closing metathesis (RCM) have been reported.^[7–14] Most of these, however, require harsh oxidants to produce the aromatic ring.^[15–20] We were inspired by a report by *Sabatino et al.*^[21] who reported a ‘close-to-release’ approach whereby aromatization resulting from a 1,4-elimination serves as driving force for the generation of naphthalene, with the concomitant release of a cargo-molecule. Herein we report our efforts to extend this methodology to RCM followed by the 1,2-elimination of water to generate monosubstituted benzene moieties (*Scheme 1*).

Results and Discussion

To test the generality of this approach, we identified the triene-one **1** as a key building block. Subsequently, a *Grignard*-type addition to the ketone functionality allows tethering this masked benzene to a variety of fragments.

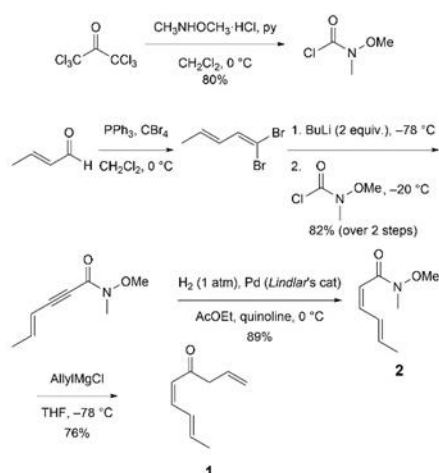
Synthesis of (5*Z*,7*E*)-nona-1,5,7-trien-4-one **1** was carried out according to the general procedure reported by *Cossy* and coworkers that they used in the total synthesis of (–)-*muricatacin* and related compounds.^[22] Reaction of *Weinreb* amide **2** with allyl-magnesium chloride afford triene **1** in > 75% yield (*Scheme 2*). The γ,δ -double bond is highly reactive, which, together with the (*Z*)-configuration of the α,β -double bond, opens up the possibility of an intramolecular reaction.

The biphenyl precursor **3a** was selected for the optimization of the cyclization conditions. The reaction proceeds in low yields in polar solvents (*Table 1*, *Entries 1–3*), including in water using *AquaMet* as catalyst (*Table 1*, *Entries 4–6*). This may be traced back to



Scheme 1. Concomitant ring-closing metathesis followed by 1,2-elimination of water for the synthesis of monosubstituted benzene derivatives.

Supporting information for this article is available on the WWW under <https://doi.org/10.1002/hlca.202100024>



Scheme 2. Synthesis of (5Z,7E)-nona-1,5,7-trien-4-one 1.

the very low solubility of the triene **3a** in aqueous media. The most effective solvent proved to be dichloromethane, in which all reagents are readily soluble. The

reaction yield is affected by the nature of the catalyst, with the *Hoveyda-Grubbs* second-generation (HG-II) performing best (Table 1, Entries 7–14). Strikingly, the yield of biphenyl **3** increases with decreasing catalyst loading from 5 mol-% to 1 mol-%. This can be traced back to the cross-metathesis between the diolefinic substrate **3a** and the *ortho*-isopropoxy-benzylidene moiety of HG-II catalyst. The yield of this cross-metathesis product is affected by catalyst loading. The resulting disubstituted olefin does not further participate in productive ring-closing metathesis, thus contributing to erode the yield of biphenyl **3** with increasing catalyst loading.

Near quantitative conversion was achieved using 0.1% catalyst, corresponding to >900 TON. ¹H-NMR Monitoring reveals that the equilibrium is reached after six hours at room temperature using 5 mol-% HG-II (Figure 1). To reach (near) full conversion, nine and twenty hours of reaction time are necessary using 1 mol-% and 0.1 mol-% HG-II, respectively (Figure 1).

With these optimized conditions at hand, monosubstituted benzenes **3–10** were synthesized without the requirement of isolating the alcohol resulting from the *Grignard* addition to (5Z,7E)-nona-1,5,7-trien-4-one (**1**). The syntheses were carried out in two steps: 1) the reaction of ketone **1** with a *Grignard* derivative and

Table 1. Optimization of cyclization conditions.

Entry ^[a]	Solvent	Catalyst	Cat. load. [%]	yield [%] ^[b]	TON
1	DMSO	HG-II	5	5 ± 1	1 ± 0
2	ACN	HG-II	5	20 ± 4	4 ± 1
3	Acetone	HG-II	5	26 ± 6	5 ± 2
4	DMSO/H ₂ O	AquaMet	5	n.d.	0
5	ACN/H ₂ O	AquaMet	5	3 ± 0	1 ± 0
6	Acetone/H ₂ O	AquaMet	5	9 ± 4	2 ± 1
7	CH ₂ Cl ₂	G-I	5	58 ± 5	12 ± 1
8	CH ₂ Cl ₂	G-II	5	63 ± 6	13 ± 1
9	CH ₂ Cl ₂	HG-I	5	71 ± 9	14 ± 2
10	CH ₂ Cl ₂	Umicore-M1	5	57 ± 7	11 ± 1
11	CH ₂ Cl ₂	Schrock ^[c]	5	35 ± 1	7 ± 0
12	CH ₂ Cl ₂	HG-II	5	92 ± 3	18 ± 1
13	CH ₂ Cl ₂	HG-II	1	97 ± 2	97 ± 2
14	CH ₂ Cl ₂	HG-II	0.1	92 ± 4	920 ± 40

^[a] Reaction conditions: solvent (1 M), catalyst, r.t., 6 h. ^[b] Yields were determined by ¹H-NMR as the average of three independent experiments. ^[c] 2,6-Diisopropylphenylimidoneophylidene molybdenum(VI) bis(hexafluoro-*tert*-butoxide).

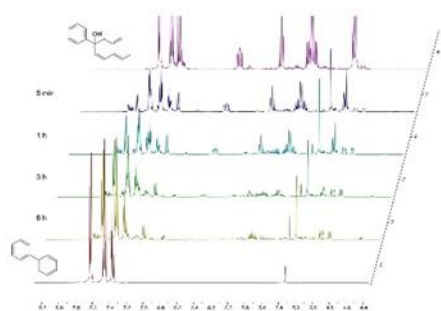
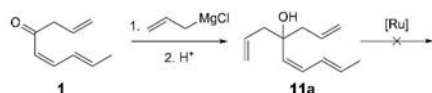


Figure 1. ^1H -NMR Monitoring of the cyclization (CH_2Cl_2 , 1 M), 5 mol-% HG-II, r.t.). None of the diene-ol intermediates is detected by ^1H -NMR.



Scheme 3. Evaluating the regioselectivity of RCM using tetraene-ol **11a**.

2) ring-closing metathesis with spontaneous 1,2-elimination of H_2O (Table 2).

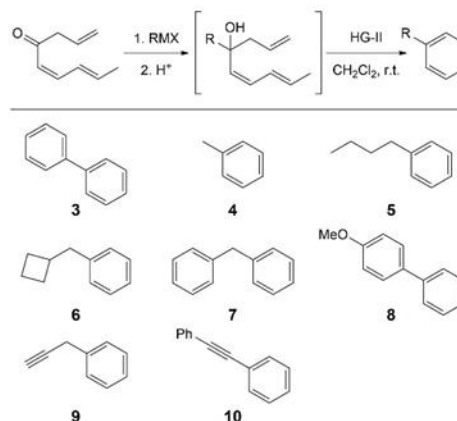
The metallated substrates were obtained from the corresponding halides and alkynes by adding either Mg or BuLi in ether. The monosubstituted benzene products **3–10** resulting from RCM and 1,2-elimination were isolated by column chromatography. Gratifyingly, the above reaction sequence tolerates a variety of (cyclic) aliphatic and aliphatic substituents, including cyclobutane (Table 2, Entries 1–6). Alkynes do not participate in metathesis as no product mixtures could be detected (Entries 7 and 8).

The regioselectivity was evaluated by subjecting the tetraene-ol substrate **11a** to RCM. Under standard conditions (CH_2Cl_2 , 1 M), 5 mol-% HG-II, r.t.), no RCM product was detected. Upon increasing catalyst loading to 50%, only cross-metathesis with the styrene fragment of the HG-II catalyst could be isolated, along with the starting material **11a**. We could not find any rationale for this unexpected lack of reactivity (Scheme 3).

Conclusions

An efficient method for the synthesis of monosubstituted aromatic compounds with saturated and unsaturated

Table 2. Substrate scope for the synthesis of monosubstituted benzene derivatives through RCM.



Entry ^[a]	RMX	Product	Yield [%] (over 2 steps) ^[b]
1	MeMgI	4	65
2	BuMgBr	5	78
3	cyclobutyl- CH_2MgBr	6	56
4	BnMgBr	7	75
5	PhMgBr	3	83
6	<i>p</i> -MeOPhMgBr	8	72
7	$\text{HC}\equiv\text{CCH}_2\text{MgBr}$	9	70
8	$\text{PhC}\equiv\text{CLi}$	10	47

^[a] The first step was carried out with ketone **1** and corresponding Grignard reagent (diethyl ether (0.5 M), 0°C , 2 h) without isolating the corresponding trien-4-ol. The second step was performed with crude alcohols using HG-II catalyst (5 mol-%) in CH_2Cl_2 (1 M) for 6 h. ^[b] Yield of isolated product.

aliphatic and aromatic substituents was developed. The key step proceeds in almost quantitative yields with low catalyst loading (0.1 mol-%, up to 920 TON). This method can be used to introduce an aromatic moiety at a late stage if alternative cross-coupling schemes prove challenging. The synthesis of the key intermediate can be carried out on a multi-gram scale with a total yield of > 52% over five steps. The strategy outlined herein, relying on more elaborate Weinreb amides,^[22,23] should allow to introduce various poly-substituted benzene moieties as a result of ring-closing metathesis. The strategy to introduce a masked benzene moiety as a result of RCM is limited by the following features: 1) The substrates must not contain any functional group that can interfere with the metalating reagent and 2) The



metalated derivative must have sufficient nucleophilicity to react with the carbonyl group of the unsaturated ketone.

We are currently capitalizing on this strategy to generate drugs *in vivo* (e.g. tamoxifen) as a result of ring-closing metathesis from inactive precursors.^[21]

Acknowledgements

This project has received funding from the European Union's Horizon 2020 research and innovation program under the Marie Skłodowska-Curie (grant agreement no. 765497 (THERACAT)).

Author Contribution Statement

T. R. W. and B. L. designed the concept. T. R. W. supervised the work which was carried out by B. L.; B. L. and T. R. W. discussed the results and wrote the manuscript. Both authors have given approval to the final version of the manuscript.

References

- [1] Y. Zhu, M. Bauer, J. Ploog, L. Ackermann, 'Late-Stage Diversification of Peptides by Metal-Free C–H Arylation', *Chem. Eur. J.* **2014**, *20*, 13099–13102.
- [2] Y. Zhu, M. Bauer, L. Ackermann, 'Late-Stage Peptide Diversification by Bioorthogonal Catalytic C–H Arylation at 23 °C in H₂O', *Chem. Eur. J.* **2015**, *21*, 9980–9983.
- [3] P. S. Fier, J. F. Hartwig, 'Synthesis and Late-Stage Functionalization of Complex Molecules through C–H Fluorination and Nucleophilic Aromatic Substitution', *J. Am. Chem. Soc.* **2014**, *136*, 10139–10147.
- [4] T. Oshima, I. Yamanaka, A. Kumar, J. Yamaguchi, T. Nishiwaki-Ohkawa, K. Muto, R. Kawamura, T. Hirota, K. Yagita, S. Irle, S. A. Kay, T. Yoshimura, K. Itami, 'C–H Activation Generates Period-Shortening Molecules That Target Cryptochrome in the Mammalian Circadian Clock', *Angew. Chem. Int. Ed.* **2015**, *54*, 7193–7197.
- [5] W. R. Gutekunst, P. S. Baran, 'Total Synthesis and Structural Revision of the Piperarbornenines via Sequential Cyclobutane C–H Arylation', *J. Am. Chem. Soc.* **2011**, *133*, 19076–19079.
- [6] J. Xie, C. Zhu, 'Sustainable C(sp³)-H Bond Functionalization', Springer, Heidelberg, 2016.
- [7] K. Yoshida, S. Horiuchi, N. Iwadate, F. Kawagoe, T. Imamoto, 'An Efficient Route to Benzene and Phenol Derivatives via Ring-Closing Olefin Metathesis', *Synlett* **2007**, 1561–1564.
- [8] X. Yang, A. Althammer, P. Knochel, 'Selective Functionalization in Positions 2 and 3 of Indole via an Iodine-Copper Exchange Reaction', *Org. Lett.* **2004**, *6*, 1665–1667.
- [9] K.-S. Huang, E.-C. Wang, 'A novel synthesis of substituted naphthalenes via Claisen rearrangement and RCM reaction', *Tetrahedron Lett.* **2001**, *42*, 6155–6157.
- [10] K. Huang, E. Wang, 'Synthesis of Substituted Indenes from Isovanillin via Claisen Rearrangement and Ring-Closing Metathesis', *J. Chin. Chem. Soc.* **2004**, *51*, 383–391.
- [11] T. J. Donohoe, A. J. Orr, K. Gosby, M. Bingham, 'A Metathesis Approach to Aromatic Heterocycles', *Eur. J. Org. Chem.* **2005**, 1969–1971.
- [12] M.-L. Bannasar, E. Zulaica, S. Tummers, 'A synthetic entry to 2,3-fused ring indole derivatives by ring-closing metathesis reactions', *Tetrahedron Lett.* **2004**, *45*, 6283–6285.
- [13] Y. Chen, H. V. R. Dias, C. J. Lovely, 'Synthesis of fused bicyclic imidazoles by ring-closing metathesis', *Tetrahedron Lett.* **2003**, *44*, 1379–1382.
- [14] W. A. L. van Otterlo, E. L. Ngidi, E. M. Cayanis, C. B. de Koning, 'Ring-closing metathesis for the synthesis of benzofused bicyclic compounds', *Tetrahedron Lett.* **2003**, *44*, 311–313.
- [15] S. Kotha, K. Mandal, 'A Retrospective on the Design and Synthesis of Novel Molecules through a Strategic Consideration of Metathesis and Suzuki–Miyaura Cross-Coupling', *Chem. Asian J.* **2009**, *4*, 354–362.
- [16] S. Kotha, S. Halder, E. Brahmachary, 'Synthesis of highly functionalized phenylalanine derivatives via cross-ene metathesis reactions', *Tetrahedron* **2002**, *58*, 9203–9208.
- [17] S. Kotha, S. Halder, E. Brahmachary, T. Ganesh, 'Synthesis of Unusual α -Amino Acid Derivatives via Cross-Enyne Metathesis Reaction', *Synlett* **2000**, 853–855.
- [18] S. Kotha, V. R. Shah, K. Mandal, 'Formation of Arenes via Diallylarenes: Strategic Utilization of Suzuki–Miyaura Cross-Coupling, Claisen Rearrangement and Ring-Closing Metathesis', *Adv. Synth. Catal.* **2007**, *349*, 1159–1172.
- [19] K. Yoshida, T. Toyoshima, I. Tsunoo, 'Synthesis of Aromatic Compounds Using Combinations of Ring-Closing Olefin Metathesis, Dehydration, Oxidation, and Tautomerization', *Bull. Chem. Soc. Jpn.* **2008**, *81*, 1512–1517.
- [20] S. K. Chattopadhyay, B. K. Pal, S. Maity, 'Combined Multiple Claisen Rearrangement and Ring-closing Metathesis as a Route to Naphthalene, Anthracene, and Anthracene Ring Systems', *Chem. Lett.* **2003**, *32*, 1190–1191.
- [21] V. Sabatino, J. G. Rebelein, T. R. Ward, 'Close-to-Release': Spontaneous Bioorthogonal Uncaging Resulting from Ring-Closing Metathesis', *J. Am. Chem. Soc.* **2019**, *141*, 17048–17052.
- [22] B. Ferrié, S. Reymond, P. Capdevielle, J. Cossy, 'Concise Total Synthesis of (–)-Muricatacin and (–)-iso-Cladospolide B Using Chemoselective Cross-Metathesis', *Synlett* **2007**, 2891–2893.
- [23] K. Kawai, Y. Bunno, T. Yoshino, S. Matsunaga, 'Weinreb Amide Directed Versatile C–H Bond Functionalization under (η^5 -Pentamethylcyclopentadienyl)cobalt(III) Catalysis', *Chem. Eur. J.* **2018**, *24*, 10231–10237.
- [24] F. Li, C. Yu, J. Zhang, G. Zhong, 'Weinreb amide directed cross-coupling reaction between electron-deficient alkenes catalyzed by a rhodium catalyst', *Org. Biomol. Chem.* **2017**, *15*, 1236–1244.

Received February 10, 2021

Accepted March 30, 2021

Potential substrates for *in vivo* synthesis of bioactive molecules.

The research on the synthesis of monosubstituted aromatic compounds described in the previous chapter was a follow-up study of the design of substrates capable of RCM under ruthenium catalysis in water and a cellular environment. Existing protecting groups, removable in a bioorthogonal manner, do not significantly change the toxicity of the parent drug. Thus, we aimed to develop new *in vivo* synthetic methods in the framework of this project.

RCM is one of the most promising reactions for experiments on living cells, due to its compatibility with water and cell media, and low toxicity. Some Ru-catalysts have revealed their effectiveness in a number of studies.⁹⁻¹² However, since at the beginning of this project there were no FDA-approved drugs containing an internal double bond, it was decided to develop a substrate containing a benzene ring precursor. Aromatic compounds can be obtained under RCM conditions, however, previously reported studies typically required aromatization as the last step. Classical conditions (DDQ, toluene, 70 °C) are incompatible with living cells.¹³ The work of Sabatino et al.¹² as well as the results described in the preceding chapter¹⁴ suggest that the use of leaving groups (OH, OR) may offer fascinating opportunities for spontaneous aromatization.

For example, (5*Z*,7*E*)-nona-1,5,7-trien-4-one, after the addition of a suitable nucleophile forms a triene-ol system, which is a versatile benzene-ring precursor.

With these preliminary results in hand, we selected tamoxifen as the target molecule (**Fig. M1**). This non-steroidal drug, developed in 1962 for the treatment of breast cancer, is still widely used today. For example, in 2018 alone, over a million prescriptions for this drug were filled in the USA. The World Health Organization has included tamoxifen on its list of essential medicines.¹⁵

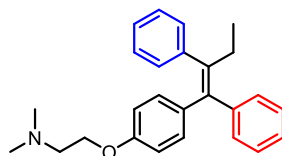


Figure M1. Structure of tamoxifen. Monosubstituted benzene rings are highlighted in blue (top) and red (bottom).

Despite its proven effectiveness, this drug can cause severe side effects associated with the toxicity of the compound to healthy cells. *In vivo* synthesis of one of the aromatic rings can reduce the overall toxicity of the drug, opening the possibility for its activation on cancer cells whose surface proteins are associated with an olefin metathesis cofactor.

Since there are several drugs containing a triphenylethylene moiety, the "upper" ring was selected as the target benzene ring since this is a common fragment for all compounds of this family (**Fig. M2**).

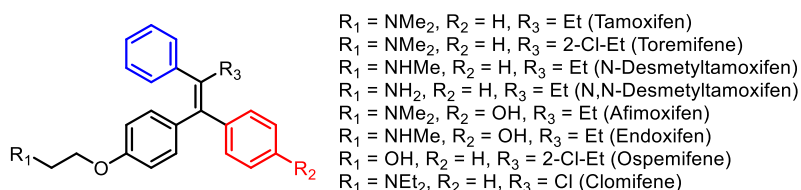
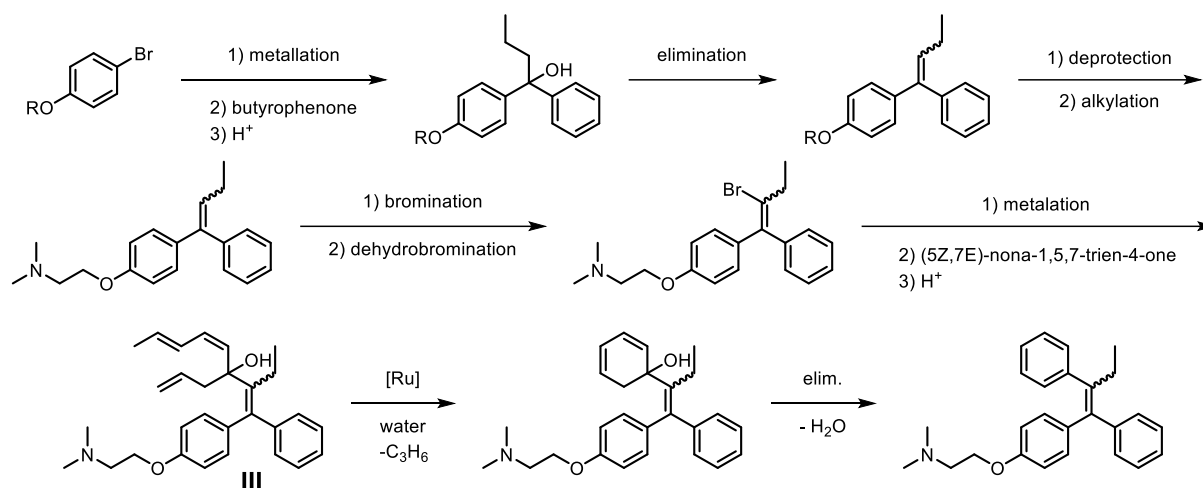


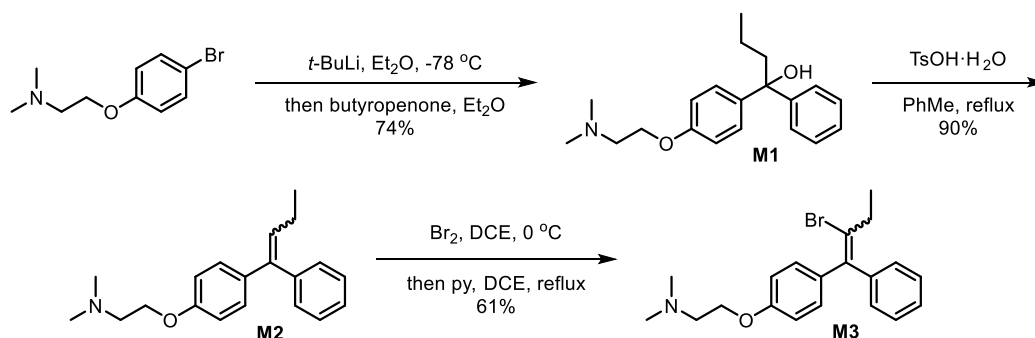
Figure M2. Nonsteroidal selective estrogen-receptor modulators.

In order to transform (5*Z*,7*E*)-nona-1,5,7-trien-4-one into the desired prodrug, an approach to 1,1-diaryl-2-bromobutene-1 was developed (**Scheme M1**).



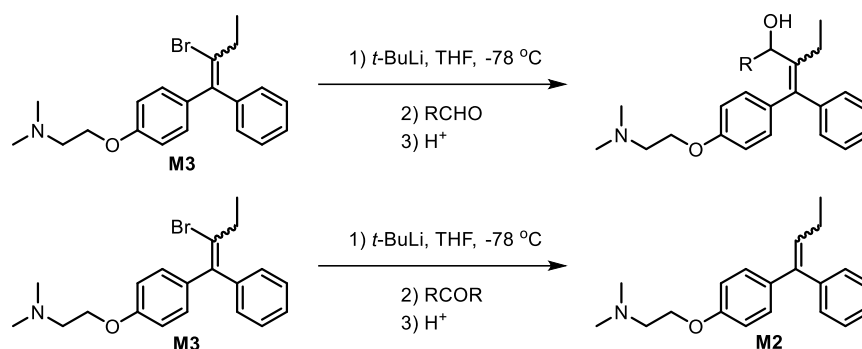
Scheme M1. Proposed synthesis of a tamoxifen precursor **III** and Ru-mediated RCM leading to tamoxifen.

Initially, synthetic approaches were optimized for alkylated derivatives of 4-bromophenol (R = Me, Bn). However, it was found that all steps tolerate the Me₂N-CH₂-CH₂ group, which simplified the synthetic scheme. The desired bromide **M3** was obtained in 4 linear steps (**Scheme M2**). The metalation of the starting aryl bromide was carried out using *tert*-butyllithium. Indeed, the use of magnesium led to low yields (<20%); while *n*-butyllithium, following metalation and conversion to 1-bromobutane, irreversibly alkylated the amino group of the product **M1**. The elimination of water, which usually requires catalytic amounts of *p*-toluenesulfonic acid, was carried out in the presence of 1.2 equivalents of acid since the amino group deprotonates it quantitatively. **M2** was obtained as a mixture of *cis*- and *trans*-isomers (1:1 ratio) in high yield. Finally, it was brominated and dehydrobrominated using pyridine as a base, giving product **M3** as a mixture of *cis*- and *trans*-isomers (5:4 ratio).



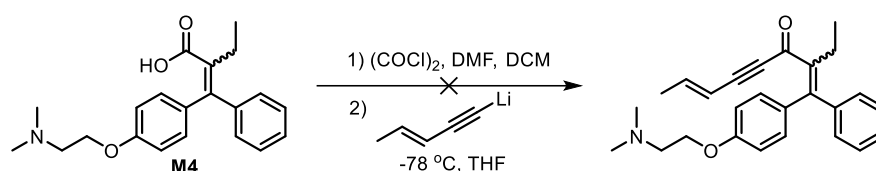
Scheme M2. Optimized synthesis of 1,1-diaryl-2-bromobutene-1 **M3**.

Unfortunately, all attempts to metalate **M3** and add it to (5Z,7E)-nona-1,5,7-trien-4-one failed. The only product of this reaction was the dehalogenation product **M2**. Aliphatic and aromatic aldehydes and ketones were tested as carbonyl compounds. It was found that the reactivity of lithiated **M3** is limited by reactions with an aldehyde (**Scheme M3**). Thus, the proposed approach cannot be used for the synthesis of the tamoxifen precursor **III**.



Scheme M3. Reactivities of **M3** with various carbonyl compounds.

To evaluate other possibilities, the carboxylic acid **M4** was synthesized, and its acyl chloride was added to lithium acetylide, as described in the previous chapter (**Scheme M4**). However, the desired product was not obtained in this reaction. We thus concluded that this approach is not suitable for the synthesis of the tamoxifen precursor **III**.



Scheme M4. Alternative synthetic route to tamoxifen precursor **III**.

At this time, we found out that the Janus kinase inhibitor pacritinib (**Fig. M3**) – which received FDA priority review, fast track – had entered the second stage of clinical trials. In addition to its potential medicinal properties, its structure is ideal for use in this project, as pacritinib is a macrocyclic compound with an internal double bond.

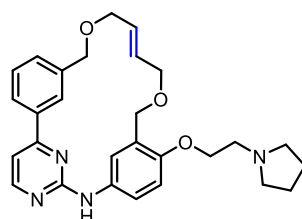
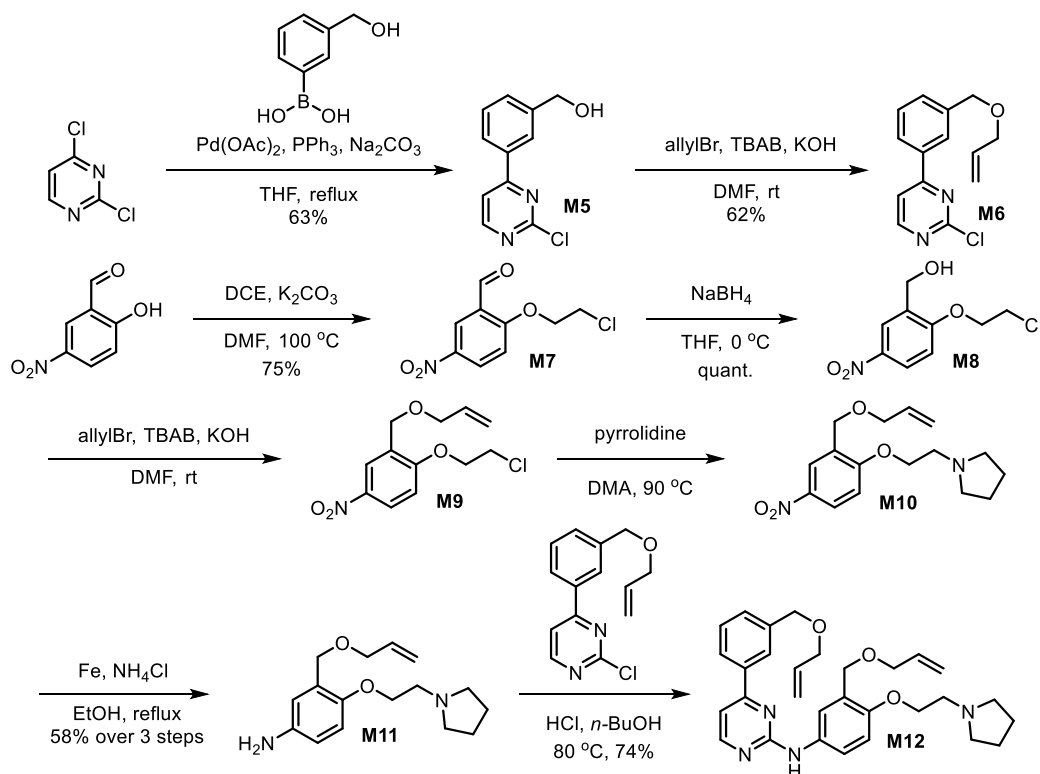
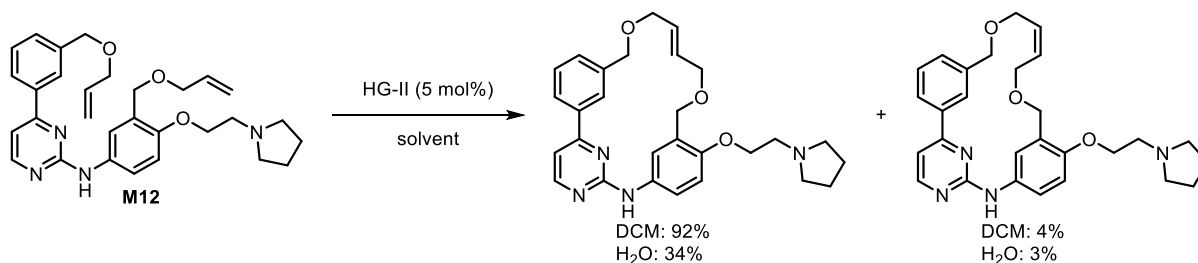


Figure M3. Structure of pacritinib. The target *trans*-internal double bond is highlighted in blue. The diolefin precursor of pacritinib **M12** was synthesized in 8 steps (6 LLS) from commercially available reagents (**Scheme M5**).



Scheme M5. Synthesis of pacritinib precursor **M12**.

Preliminary experiments in organic solvents and in water highlighted that RCM using Hoveyda-Grubbs 2nd generation catalysts lead to the formation of a mixture of *cis*- and *trans*-macrocyclization products with a predominance of the desired *trans*-product (**Scheme M6**).



Scheme M6. Ru-mediated macrocyclization of **M12** leading to pacritinib.

Recent studies suggest that the yield and selectivity of olefin metathesis can be significantly improved by lowering the pH, opening the way for *in vivo* synthesis of pacritinib.¹⁶

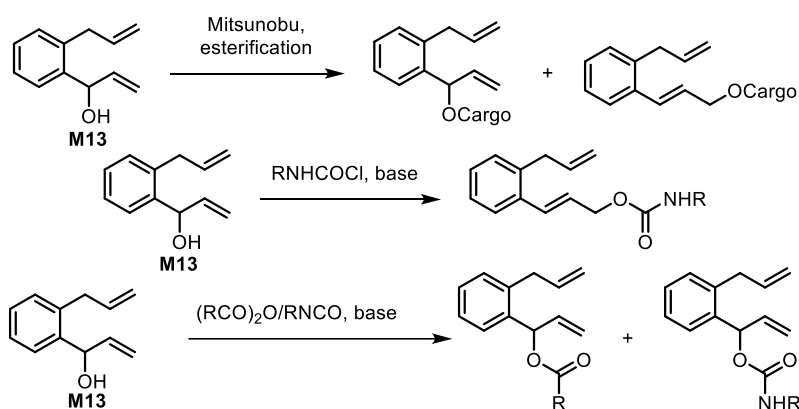
However, at the time when this synthesis and preliminary experiments were carried out in our group (mid-2019), clinical trials of pacritinib showed a number of severe toxic side effects, and the drug was withdrawn from further clinical trials. Therefore, we decided not to focus on its use as a model drug and instead pursue a more classic approach to reducing drug toxicity, namely caging drugs with a cleavable protecting group.

Unexpectedly, in early 2022, the FDA granted accelerated approval for pacritinib to treat adults who have a rare form of a bone marrow disorder with intermediate or high-risk primary or secondary myelofibrosis. This fact allows us to reconsider our decision to use pacritinib precursor **M12** as a model for proof-of-concept studies of *in vivo* drug synthesis.

Close-to-release approach (phenols)

The work of Sabatino et al. was a big step towards Ru-mediated *in vivo* drug release. Although there was only one example of a caged drug in the original publication (alofanib, now in Phase 2 of clinical trials), the naphthalene precursor can be considered as a protecting group for many other compounds. This chapter outlines a new approach to the synthesis of 1,2-diallylnaphthalene derivatives for various applications, as well as attempts to develop a universal approach to drug synthesis, allowing the rapid development of a prodrugs' library for experiments on cancer cells.

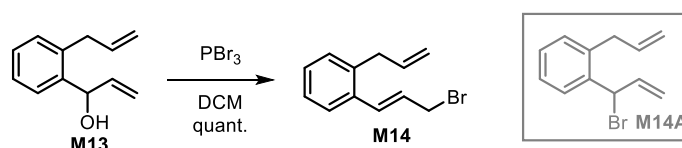
Alcohol **M13**, which can be obtained in 2 steps from commercially available reagents, is a universal starting material for the synthesis of caged fluorophores and drugs (**Scheme M7**). However, Mitsunobu reaction conditions or esterification and other modifications lead to a mixture of branched and linear products. The structures of the products share many similarities, and therefore their separation by column chromatography is most often very challenging. In addition, some products rearrange on the column from the less stable branched product to the more stable linear one, further reducing the yield of the desired product. It was also found that the use of chlorocarbamates in the synthesis of carbamates leads to the formation of a predominantly linear product. Anhydrides and isocyanates give higher yields of branched products.



Scheme M7. Caging of alcohols, phenols, carboxylic acids, and amines using the naphthalene precursor **M13**.

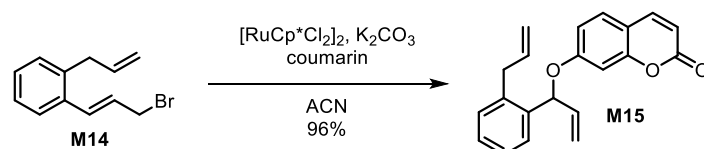
Since the most common functional groups of fluorophores and drugs are phenols and amino groups, there is a need for general methods for their protection (caging).

Droplet experiments in our group (performed by Dr. Jaicy Vallapurackal) required large amounts of fluorogenic compounds. However, the modification of **M13** with 7-hydroxycoumarin under the Mitsunobu reaction conditions proceeded with low selectivity. Importantly, on a larger scale (1 mmol) the selectivity decreases further. As an alternative, we considered the possibility of converting the OH group into a halide for use in direct alkylation. However, all attempts to convert the alcohol **M13** to the branched bromide **M14A** were unsuccessful, since linear cinnamyl bromide **M14** was formed in a quantitative yield (**Scheme M8**).



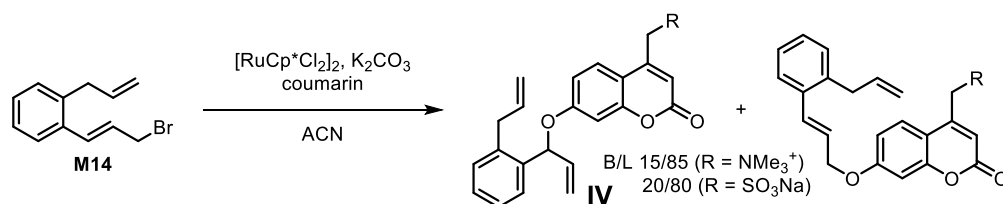
Scheme M8. Synthesis of the linear bromide **M14** from the branched alcohol **M13**.

There are few examples of the synthesis of branched esters, ethers, and other derivatives of 1-phenylprop-2-en-1-ol in the literature.^{17–20} They usually involve metal-catalyzed rearrangements and the use of ligands that hinder the formation of a linear product. One of these approaches, which uses cheap and commercially available $[\text{RuCp}^*\text{Cl}_2]_2$ as a catalyst, was applied to the bromide **M14** and 7-hydroxycoumarin as the nucleophile (**Scheme M9**). The first attempts revealed the formation of a predominantly branched product. Further optimization of the conditions, including the choice of solvent, determination of the water content, as well as the order of addition and the amounts of reagents, made it possible to obtain **M15** with a 96% yield (300 mg scale) in solid form. The purity of **M15** was regularly tested highlighting its stability in the fridge after more than 2 years.



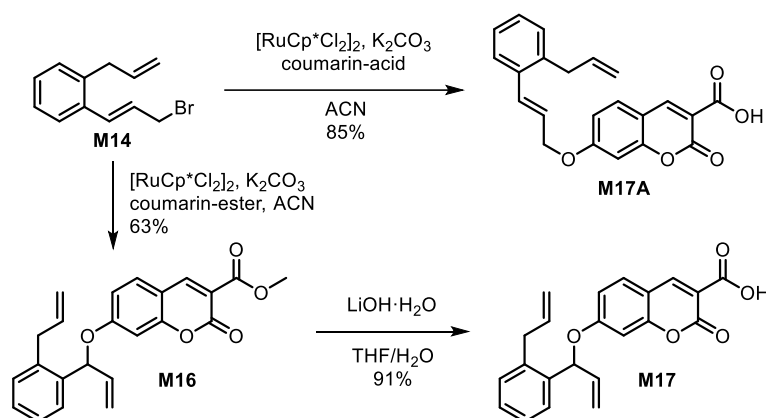
Scheme M9. Synthesis of caged coumarin **M15**.

Due to the need for a water-soluble substrate, hydroxycoumarins containing charged and polar groups were tested as nucleophiles. Unfortunately, the presence of such groups significantly reduced the selectivity of the rearrangement. In addition, the purification of the charged molecules **IV**, proved extremely challenging, rendering this approach unsuitable for our purposes (**Scheme M10**).



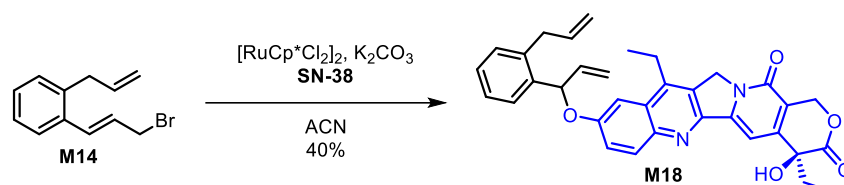
Scheme M10. Synthesis of water-soluble caged fluorophores (B/L represents branched/linear ratio).

However, if the polar group is protected or introduced after the formation of ether, then the desired product **M16** can be obtained in high yield (**Scheme M11**). The reaction of **M14** with 7-hydroxycoumarin-3-carboxylic acid led to linear product **M17A**.



Scheme M11. Synthesis of the caged fluorophore with polar group.

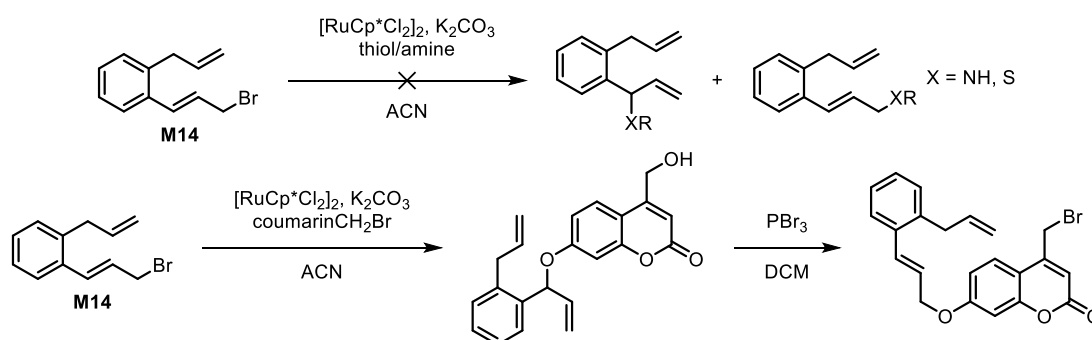
Additionally, the topoisomerase inhibitor SN-38, which is an active metabolite of irinotecan widely used in cancer therapy, was tested as a nucleophile. Despite the complexity of the molecule, the desired branched product **M18** was obtained under standard conditions in 40% yield (**Scheme M12**).



Scheme M12. Synthesis of caged SN-38. The SN-38 structure is highlighted in blue.

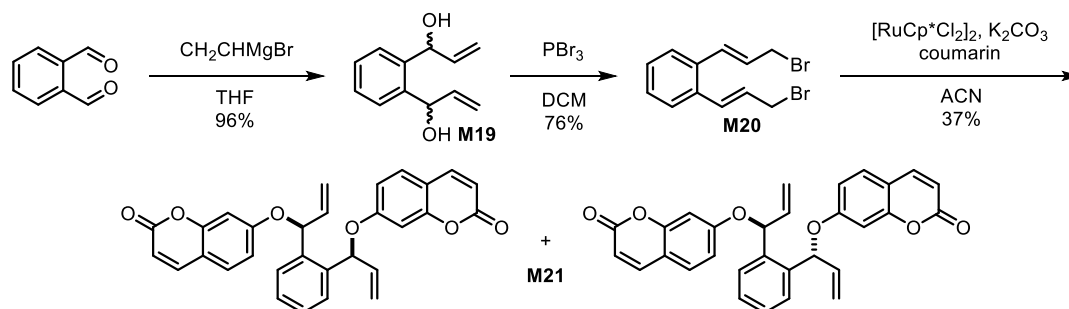
It is worth noting some limitations of this method, in addition to general intolerance to charged fragments, which may be the result of traces of water. This method is also not applicable to hetero-nucleophiles (thiols, amines) and other halides.

Thus, for example, a product containing a tetraalkylammonium cation can theoretically be obtained from the corresponding halide. However, under reaction conditions, the benzyl bromide was transformed into the corresponding benzyl alcohol. The product, upon addition of halogenating reagents, rearranges into a linear derivative, which can no longer be converted into the desired branched product (**Scheme M13**).



Scheme M13. Limitations of the approach.

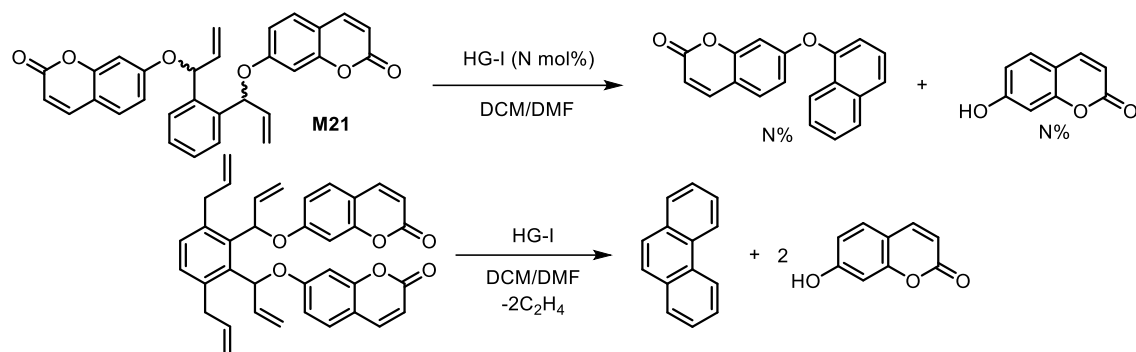
To test the effectiveness of the method for generating substrates bearing multiple fluorophores, the approach illustrated in **Scheme M14** was used.



Scheme M14. Synthesis of symmetrical diethers.

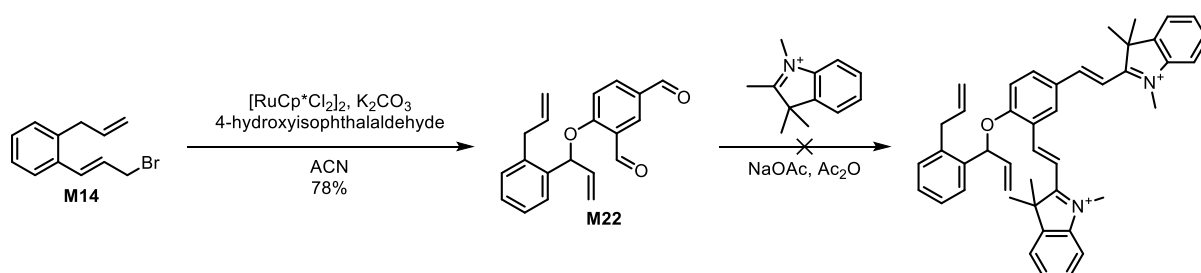
Due to the low solubility of the product **M21**, which partially precipitates during the reaction, RCM for this particular substrate requires the addition of significant amounts of DMSO or DMF to homogenize the solution. The highest achieved activity of the ruthenium catalyst was $\text{TON} = 1$ (**Scheme M15**). However, the introduction of allyl groups in both *ortho*-positions can potentially lead to the release of

both fluorophores and the formation of phenanthrene. Nevertheless, this approach can be used for the caging of multiple molecules.



Scheme M15. RCM of the diolefin **M21**.

An attempt to synthesize caged cyanine dye for *in vivo* imaging was also made. Caged dialdehyde **M22** was obtained in a high yield. However, the branched fragment showed high acid and base sensitivity and rearranged into the undesired linear product (**Scheme M16**).

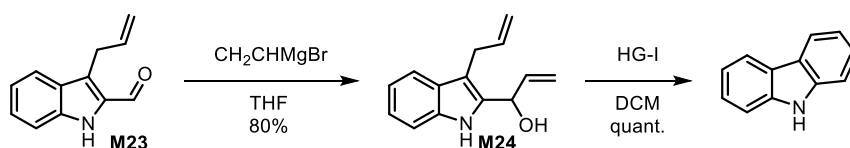


Scheme M16. An attempt to synthesize a caged cyanine dye.

Summarizing the above:

- 1) Alcohol **M13** is a promising substrate for the direct modification of the OH group (esterification, carbamoylation).
- 2) Bromide **M14** is more promising in the synthesis of ethers from phenols in the absence of certain functional groups in the nucleophile (charged groups, halogens).
- 3) Post-rearrangement modification of branched products is severely limited due to the tendency of the products to rearrange into their linear form.

As a close-to-release proof of concept, the known 3-allylindole derivative **M23** was synthesized. Following a Grignard reaction with vinylmagnesium bromide, it was converted to 9H-carbazole under RCM conditions (**Scheme M17**). This synthesis of indole derivatives is the last missing approach to the synthesis of these compounds under RCM conditions. Due to the frequent appearance of the indole fragment in biologically active molecules, this approach can potentially be used for bioorthogonal prodrug activation.



Scheme M17. Close-to-release approach in 9H-carbazole synthesis.

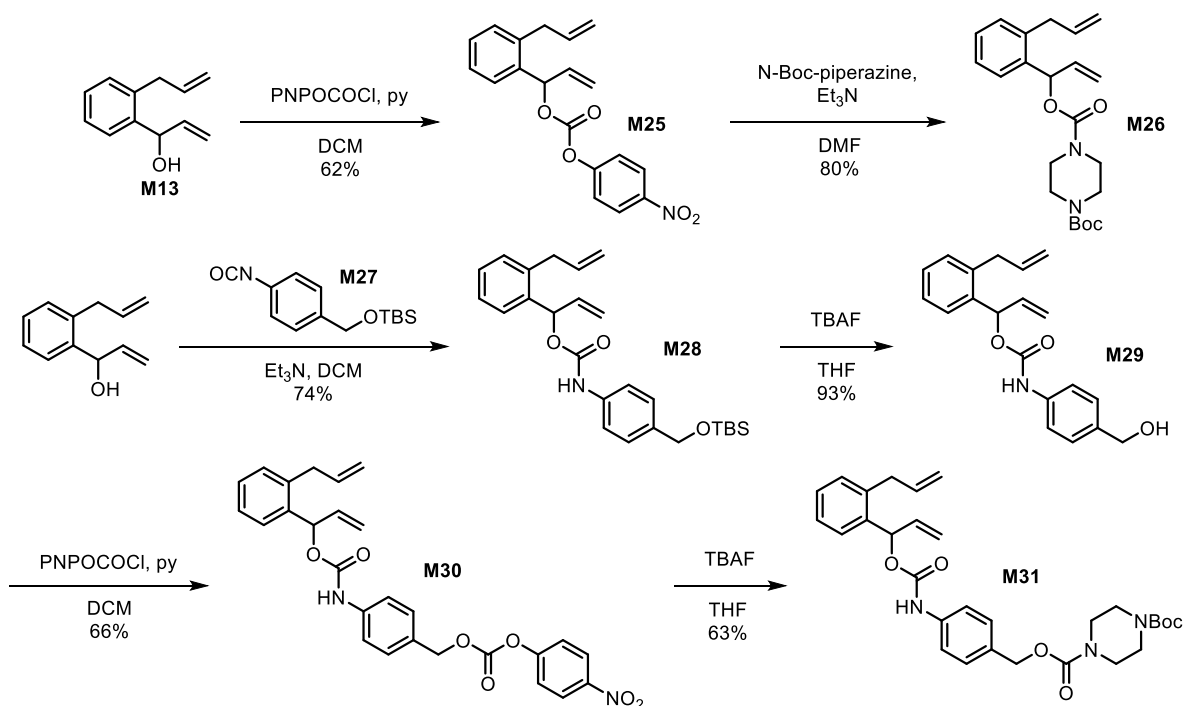
Close-to-release approach (carbamates)

In the previous chapter, the synthesis of caged phenols was considered. However, amino groups are more common in drug and fluorophore molecules. Moreover, the binding of these groups leads to a much greater drop in bioactivity or fluorescence than with the "protection" of OH groups. Since there are not many biocompatible protecting groups, which can be cleaved bioorthogonally (amides, carbamates), it was decided to use **M13** alcohol derivatives to cage a wide range of functional molecules. This project was developing in parallel with the deallylation of caged **MMAE** as the most bioactive and highly toxic drug. Therefore, the main focus of this chapter was devoted specifically to attempts to synthesize a prodrug that releases **MMAE** under conditions of ruthenium olefin metathesis.

In medicinal chemistry, there are two main ways to synthesize carbamates: a) addition of alcohols to isocyanates; b) addition of amines to *p*-nitrophenyl carbonates or CDI derivatives.

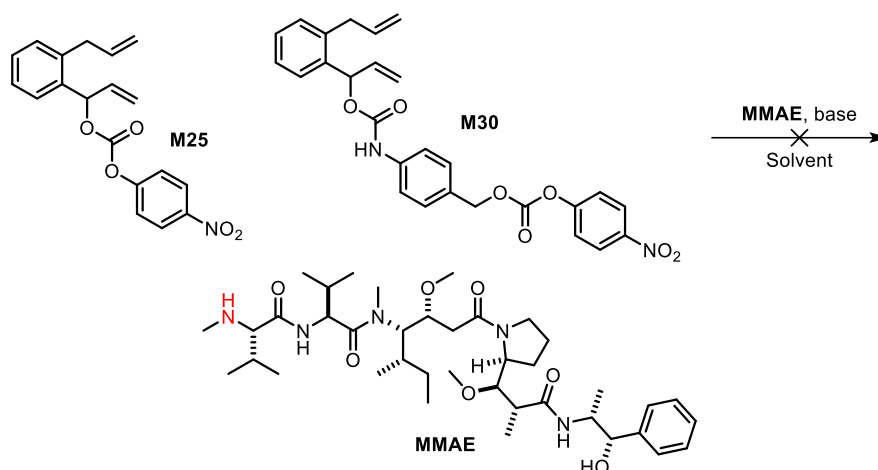
Both approaches have been used for the synthesis of protecting group precursors. Below, we omit long preparatory experiments and highlight only the optimized methods that open access to caged drugs.

The alcohol **M13** was activated with *p*-nitrophenyl chloroformate directly and *via* a PAB linker to afford products **M25** and **M30** (Scheme M18). The reactivity of these compounds was tested with N-Boc-piperazine. Both substrates showed high reactivity, affording **M26** and **M31** in 80% and 63% yield, respectively.



Scheme M18. Synthesis of PNP-activated protecting groups **M25** and **M30** and evaluation of their reactivity towards amines.

Next, **M25** and **M30** were reacted with **MMAE**, but the target product could not be detected under any conditions (Scheme M19). We could not find any rationale for this unexpected lack of reactivity, as in the deallylation project, we used PNP-carbonates to attach the **MMAE** to the protecting group.



Scheme M19. **M25** and **M30** reactivity test with **MMAE**. The target secondary amine highlighted in red.

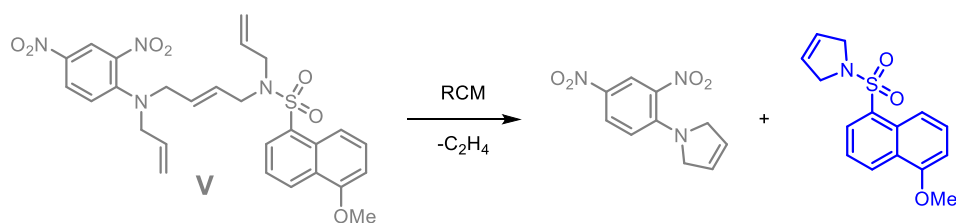
Since this was the main goal of this project, the resulting compounds were not further used to protect other drugs. However, they are still of high interest for caging amino groups of drugs and fluorophores and may be used in the future.

MINFLUX project

A particular challenge of bioorthogonal activation of prodrugs inside living cells is the difficulty of localizing the catalytic reaction and, consequently, the drug release. The development of microscopy-tools allows scrutinizing deeper into a single cell. This makes possible single-molecule detection using a fluorophore with a high quantum yield and a suitable wavelength. One of these technologies is MINFLUX, which enables tracking the movement of single molecules in real-time with ultra-high resolution.²¹ This opens up fascinating prospects for understanding the action of metal cofactors in either the periplasm, the outer-membrane or the cytoplasm of *E. coli*. Importantly, it may enable the precise localization of both a (fluorescently labeled) cofactor as well as the reaction product if this latter is fluorescent. Importantly, however, the newly developed MINFLUX requires the use of dyes with very high near-infrared fluorescence and must be completely quenched with an appropriate protecting group prior to the uncaging event. Unfortunately, such near-infrared dyes, suitable for MINFLUX –cyanines, rhodamines, and heterorhodamines– are very difficult to quench. Accordingly, using conventional protecting groups will most probably result in very high background fluorescence caused by the presence of the caged fluorophore.

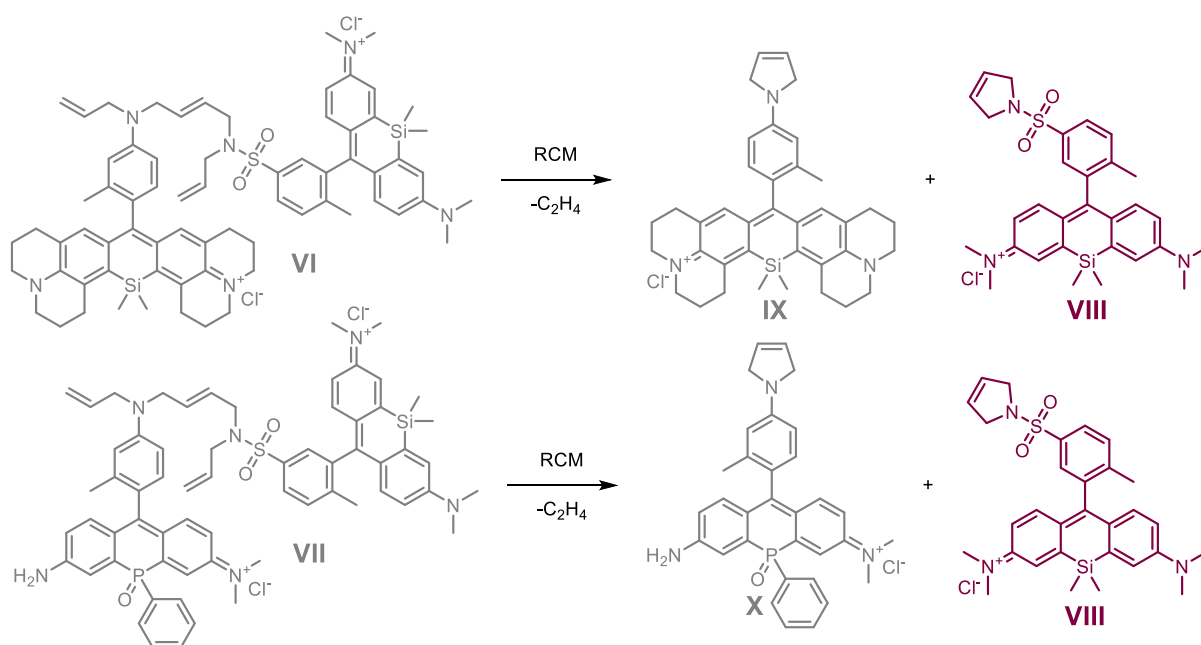
One of the most efficient methods of energy transfer from a fluorescent molecule is Förster resonance energy transfer (FRET), which allows the energy of an excited particle to be quickly transferred within a covalently bound complex. Most often, FRET is used in the study of the structure of macromolecules and intermolecular interactions. However, this effect can be used to quench the fluorescence of a strong fluorophore if a moiety with high absorbance, but low fluorescence is selected as acceptor. In this case, both molecules must be covalently linked through a cleavable bridge.

In this project, we were inspired by previous work in the group, in which Reuter et al. developed a fluorogenic probe **V** for RCM using quenching of 5-methoxynaphthalene-1-sulfonamide with a 2,4-dinitroaniline derivative.²² Upon relay ring-closing metathesis, the fluorophore and quencher were disconnected, resulting in the formation of a fluorescent product (**Scheme M20**).



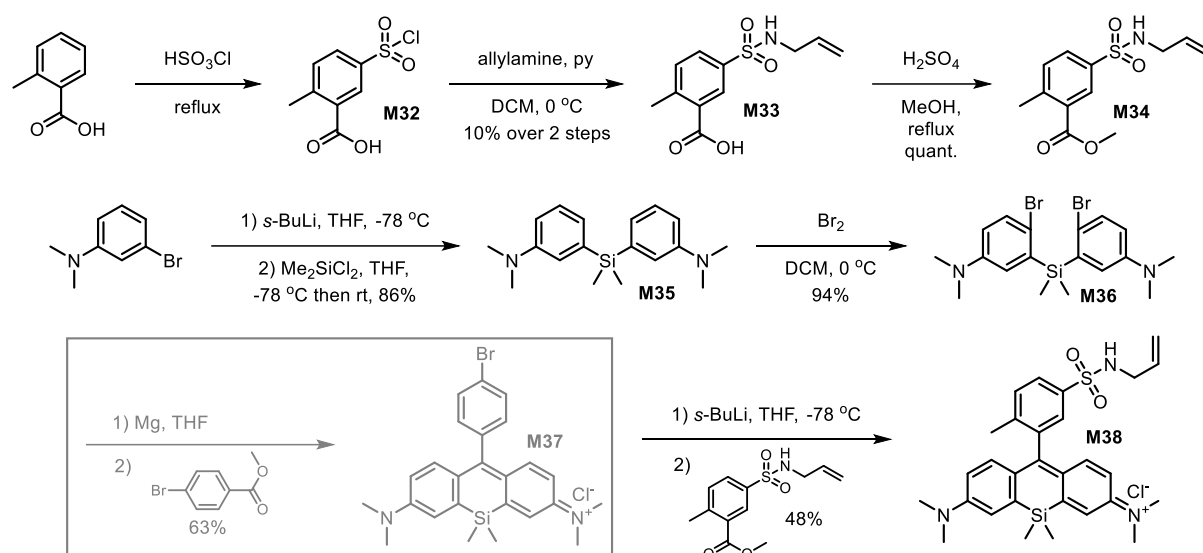
Scheme M20. Profluorescent substrate and its activation upon RCM.

Substituting the fluorophore and quencher fragments with more efficient near-infrared dyes may provide a fluorogenic substrate for MINFLUX. Dr. Ryo Tachibana, experienced in dye design and synthesis, proposed several potential structures **VI**, **VII** for this project using the same approach to release the fluorescent molecule **VIII** (**Scheme M21**). Both moieties contain the same fragment of silicorhodamine, which is widely used in cell experiments. Quenchers **IX** and **X** are not described in the literature, but computational prediction suggests that they display very high absorption, coinciding with the emission wavelength of the fluorescent fragment. Their own fluorescence is quenched by the amino group on the "upper" aromatic ring.



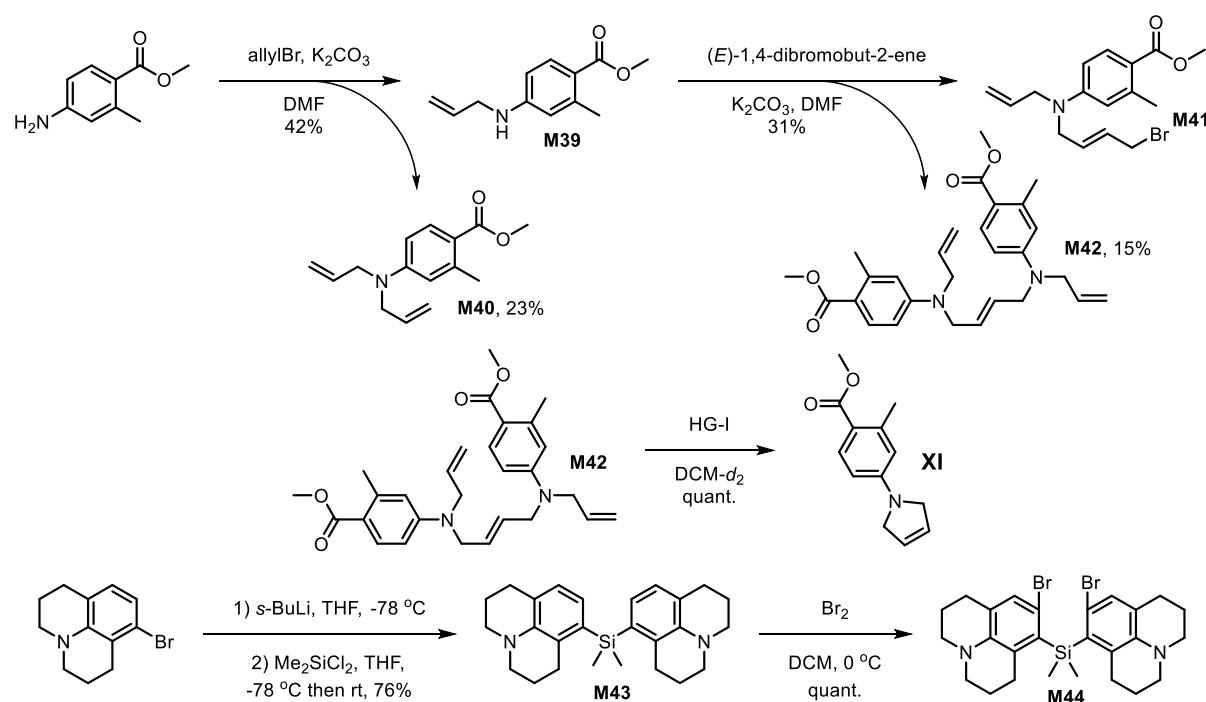
Scheme M21. Proposed structures of coupled FRET-pairs and their activation resulting from RCM. The fluorescent fragment is highlighted in magenta.

The first fluorescent core was obtained in several linear steps. First, *o*-toluic acid was sulfochlorinated, to afford the known product **M32**. After sulfonylation of allylamine (**M33**) and esterification, **M34** was obtained in a high yield. Using the approach of Fischer et al.,²³ we obtained a silicon derivative **M35** which was brominated to give **M36**. The reactivity of bis(magnesium bromide) obtained by mixing **M36** with magnesium was tested in reaction with *p*-bromobenzoic acid (**M37**). However, the reaction of **M36** with **M34** required lithiation, affording the monoallylic product **M38** in moderate yield (**Scheme M22**).



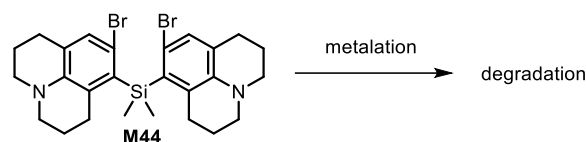
Scheme M22. Synthesis of the first fluorescent core **M38**.

For the synthesis of the second fragment, we hoped to use the same approach, so compounds **M39-44** were synthesized for subsequent metalation and nucleophilic addition (**Scheme M23**). A by-product **M42** was used to test relay RCM. Complete conversion of **M42** to the corresponding 2,5-dihydro-1*H*-pyrrole **XI** was achieved in less than 5 min in the presence of HG-I (5 mol%).



Scheme M23. Synthesis of precursors for dibromide-to-ester approach.

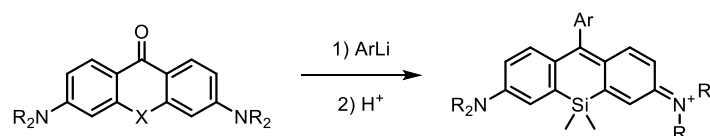
However, despite thorough screening of **M44** metalation conditions and nucleophilic addition to **M41**, **M44** was found to degrade upon metalation to form polyaryl by-products (**Scheme M24**). In addition, compounds **M43** and **M44** are unstable in the light, which complicates their purification and handling.



Scheme M24. Unsuccessful metalation of **M44**.

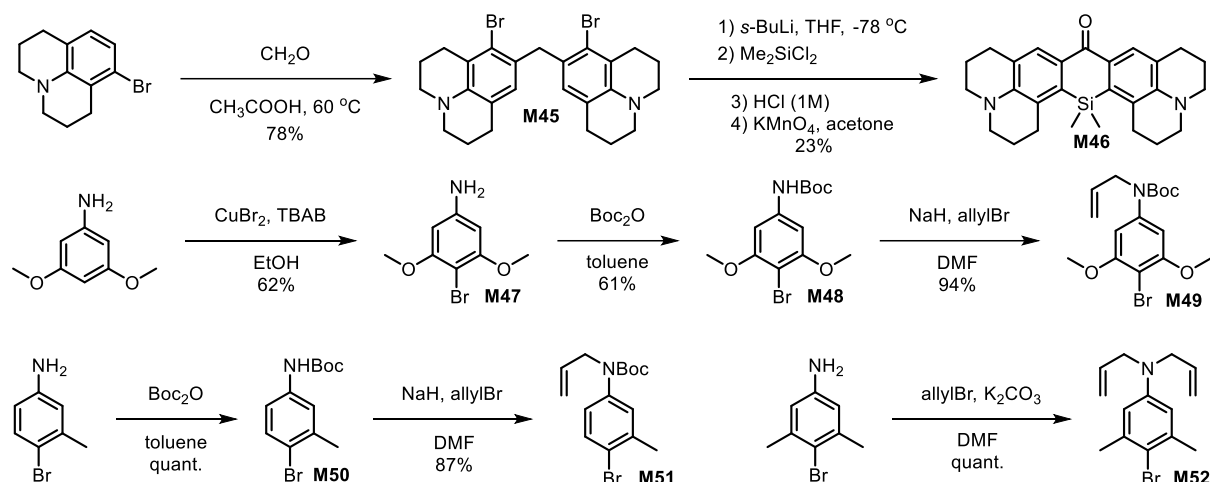
Summarizing the above, **M44** is not suitable for the synthesis of silicorhodamine derivatives. We thus set out to devise an alternative synthesis.

Another strategy to obtain rhodamines is the addition of aryllithium to phenones, followed by the elimination of water under acidic conditions, leading to the aromatization of the molecule (**Scheme M25**).



Scheme M25. Alternative approach to rhodamines.

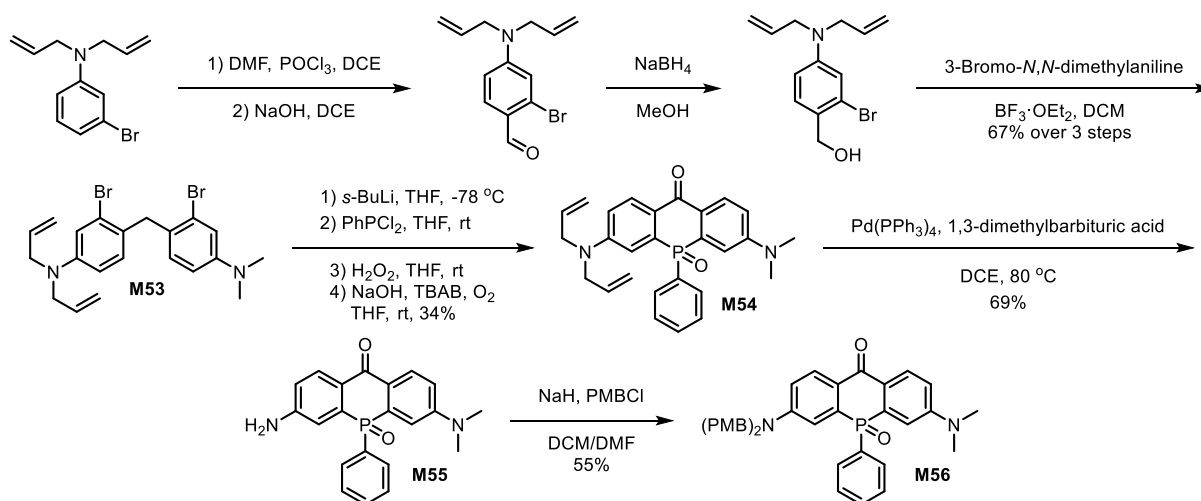
In order to obtain the target compound or its analogs, phenone **M46** and aryl halides **M49**, **M51**, and **M52** were synthesized. The amino group is used to quench fluorescence and bind to another fluorescent core. All introduced substituents, according to computational studies performed by Dr. Ryo Tachibana, should not change the electronic- and hence the fluorescent properties (**Scheme M26**).



Scheme M26. Synthesis of precursors for the aryllithium-to-phenone approach.

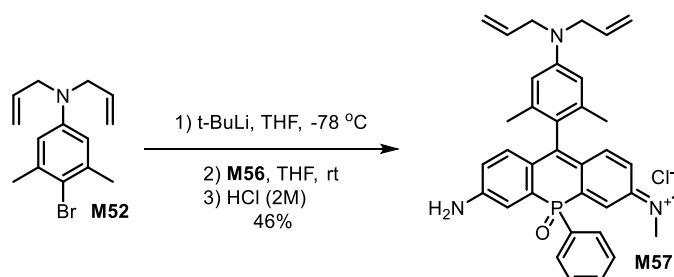
However, the challenges arose on the side of the aryl halides. The nucleophilicity of metalated **M49** and **M51** was not strong enough to react with phenone **M46** at -78°C , and heating the reaction mixture to room temperature led to the cleavage of the Boc-group. Metalated **M52** did not react with **M46** at room temperature, and heating to 50°C led to degradation of the phenone.

In order to overcome these limitations, we set out to synthesize an alternative phenone **M56** as a precursor of phosphonorhodamine. The required intermediate was obtained in 6 steps, including replacing the allyl protection with *p*-methoxybenzyl (PMB) (**Scheme M27**).



Scheme M27. Synthesis of the phosphonorhodamine precursor.

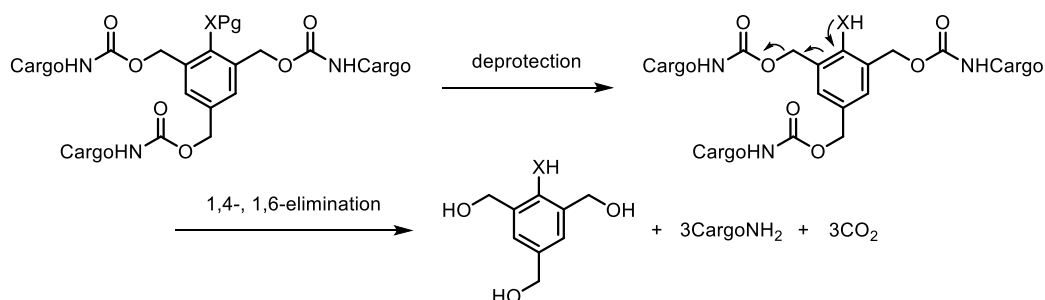
The previously-prepared aryl halides **M49**, **M51**, and **M52** were metalated and reacted with **M56**. As with **M46**, the reactivity of the aryllithium derivatives was found to be low, with loss of the Boc-group and degradation at room temperature. The product of the addition of metalated **M52** to **M56** was the only success of this approach (**Scheme M28**). However, the PMB protecting group was quantitatively removed upon acidic hydrolysis during the workup. Since it was originally proposed to partially remove the allyl group for subsequent binding to the first fluorescent core, this approach was also not suitable for the synthesis of target compounds.



Scheme M28. Synthesis of the phosphonorodamine **M57**.

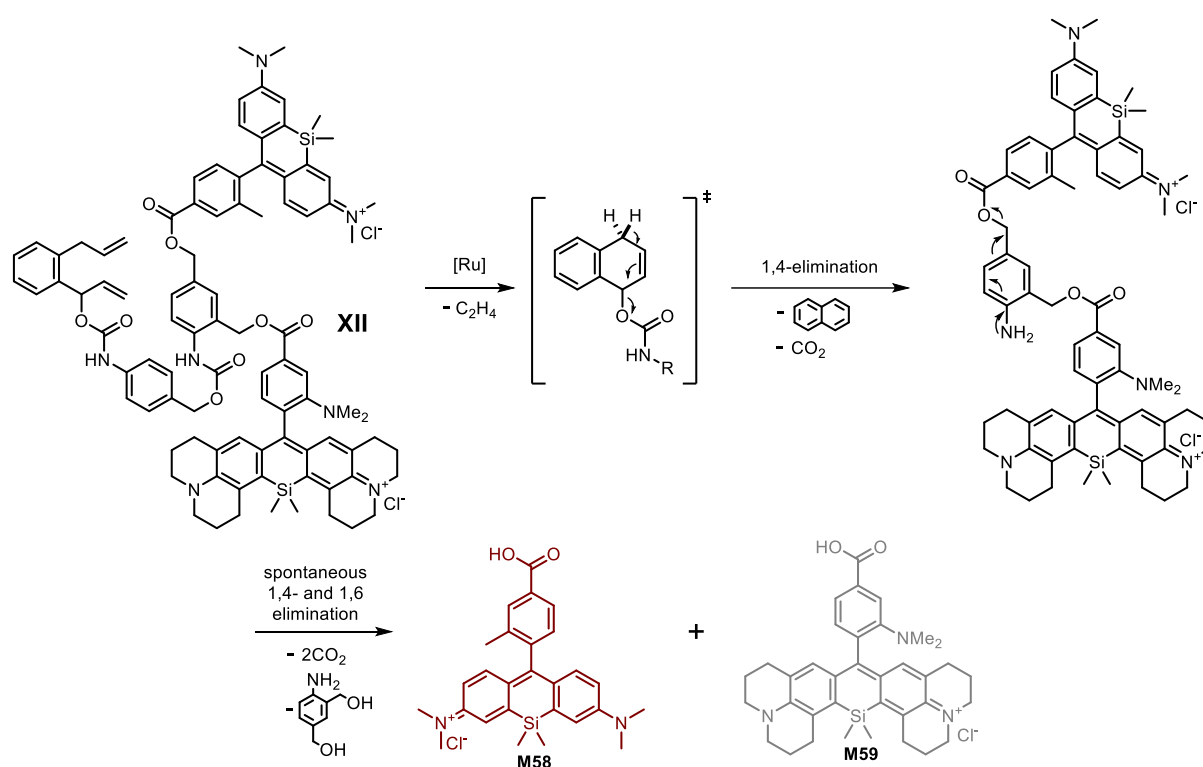
Dendritic approach

Since the triolefin approach proved challenging, we sought for alternative methods leading to the release of multiple molecules. Self-immolative branched linkers, first reported by Shabat in 2003,²⁴ were significantly improved in 2007 by the replacement of phenol with aniline.²⁵ These linkers provide various degrees of branching and, upon protecting-group cleavage, spontaneously release from two to nine caged-molecules (**Scheme M29**).



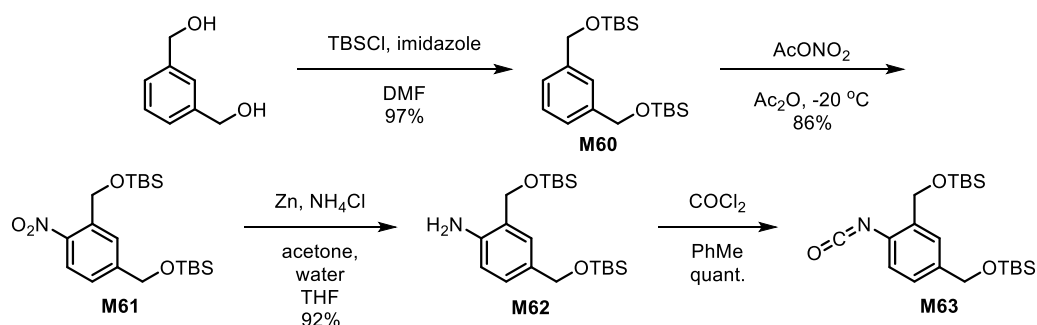
Scheme M29. Multiple releases upon single deprotection resulting from self-immolation.

This approach has been used to create dendrimers carrying multiple drug copies, but never for fluorescence studies. For example, the use of dendrimer-bearing quenched fluorophore and caged drug can provide multiple responses on the effectiveness of catalysis and cytotoxic effect. To prove the concept and to achieve the goal set in the previous chapter, we set out to synthesize a dendritic substrate **XII** with **M13** as a protecting group. The close-to-release sequence, leading to the release of both cargoes as a result of the spontaneous 1,4-elimination and self-immolation of the tri-substituted self-immolative core is presented in **Scheme M30**. Accordingly, the FRET-pair consisting of the fluorophore **M58** and the quencher **M59** were connected to the trisubstituted aromatic core. As a result of RCM, we predicted that both fluorophore **M58** and quencher **M59** should be released, thus enabling the monitoring of RCM *in cellulo*.



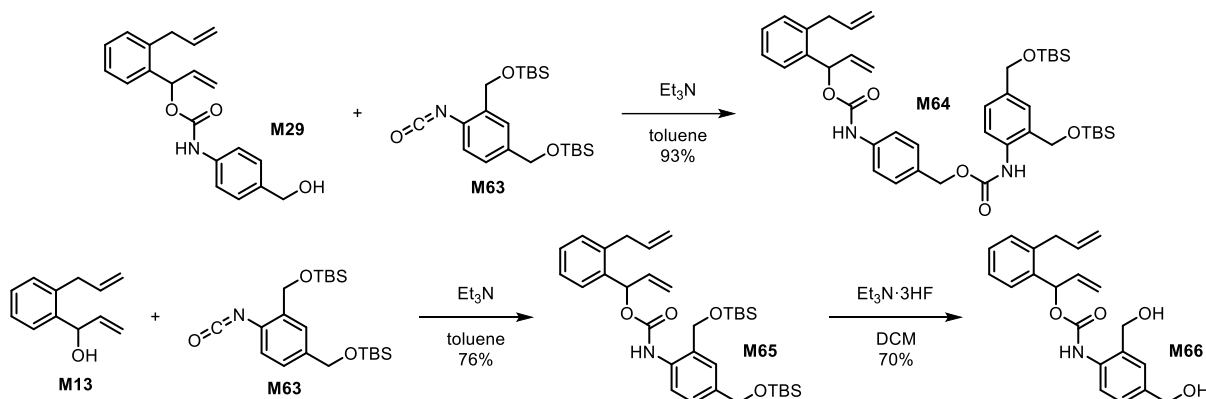
Scheme M30. Proposed dendritic substrate and its activation upon RCM to release the fluorophore **M58** and the quencher **M59**.

To complete the synthesis, the tri-substituted core, **M63** was prepared in a high yield on a multi-gram scale in 4 steps from commercially available reagents (**Scheme M31**).



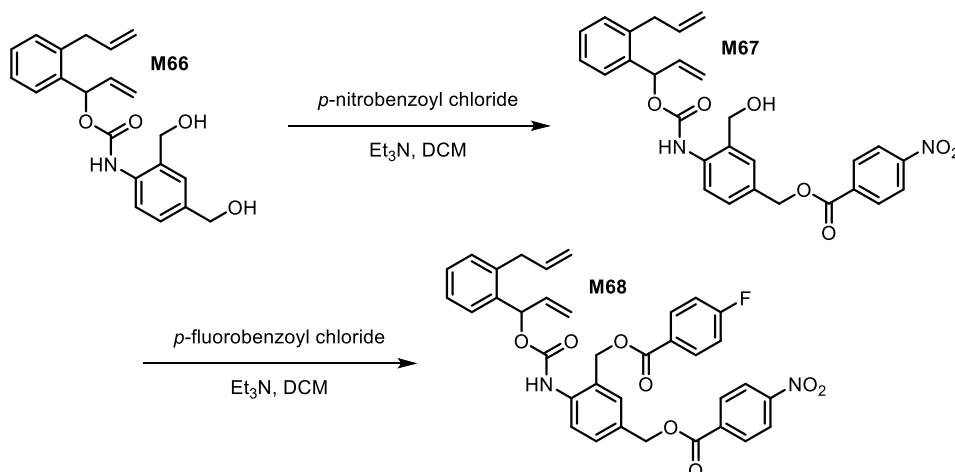
Scheme M31. Synthesis of dendritic building block **M63**.

Since it is not known how much the charged fragments of fluorophores will affect the efficiency of RCM, in addition to the direct adduct of **M63** to **M13**, its analog containing a PAB-linker was prepared by reaction of **M63** with **M29**. Since the synthesis of **M65** proceeds with a higher overall yield, this compound was selected for preliminary screening of the conditions for subsequent reactions (**Scheme M32**). For example, the removal of TBS-protection from benzyl alcohol in the *ortho*-position to **M13** is sterically challenging. Accordingly, it cannot be removed by TBAF or Amberlyst-H. If necessary, this may be used for orthogonal sequential modification of the dendrimer. As a result of intensive screening, Et₃N·3HF was found as the best reagent for quantitative cleavage of silyl ethers. In comparison to acidic solutions, it does not lead to a rearrangement of the branched carbamate into a linear one.



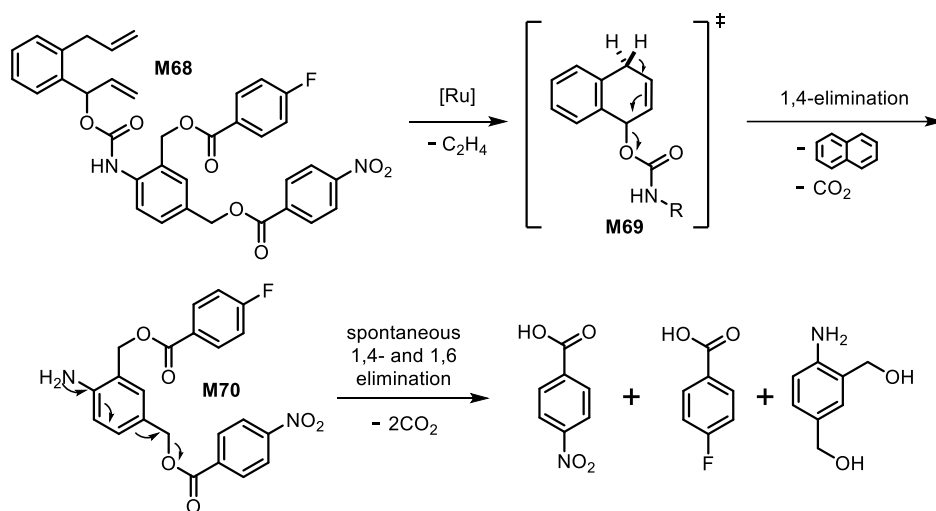
Scheme M32. Synthesis of caged dendritic precursors **M64** and **M66**.

Since it is known that the introduction of a free amino group into the dye structure significantly complicates the synthesis, a carboxylic acid was selected as the functional group for the attachment to the dendrimer. In this case, the sterically-hindered ester was protected from spontaneous hydrolysis in an aqueous environment, making this substrate suitable for experiments in cells. To test the concept, the substrate **M68** bearing two different carboxylic acids on *para*- and *ortho*-benzyl alcohols was synthesized (**Scheme M33**).



Scheme M33. Synthesis of generation-0 dendrimer for mechanistic studies.

To evaluate RCM of diolefin and the concurrent release of both cargoes, **M68** was dissolved in CD₂Cl₂, the Hoveyda-Grubbs 2nd gen. catalyst (5 mol%) was added, and the reaction progress was monitored for 72 hours to determine the kinetics of the transformations by the ¹H and ¹⁹F NMR spectroscopy (**Scheme M34**, **Fig. M3-4**).



Scheme M34. RCM of **M68** followed by cascade elimination.

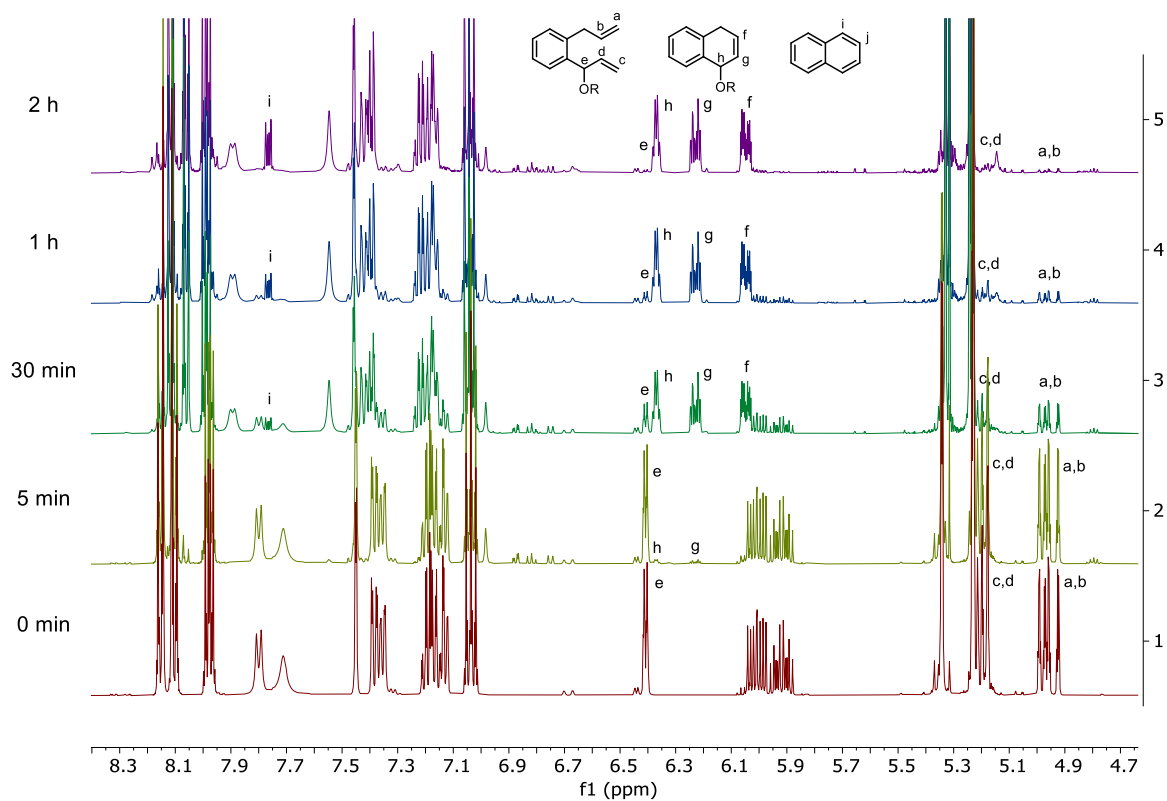


Figure M3. ^1H -NMR analysis of RCM of **M68**, followed by spontaneous elimination within 2 hours.

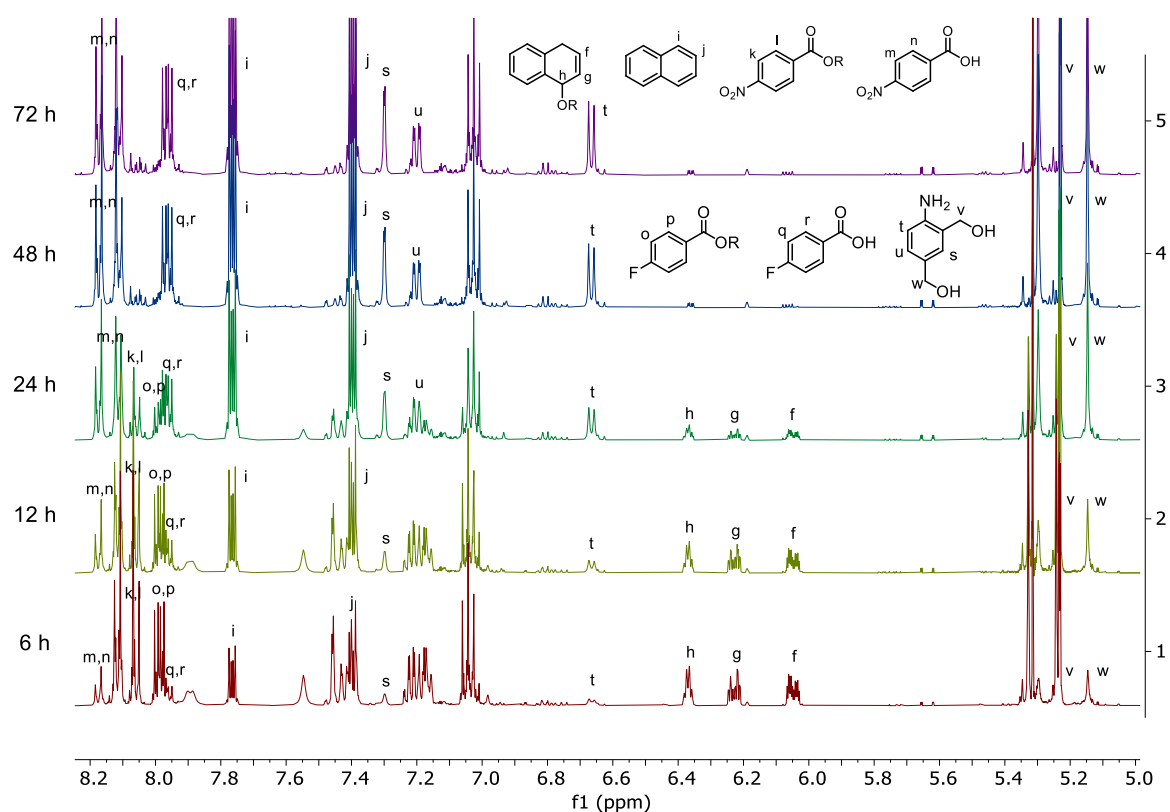


Figure M4. ^1H -NMR analysis of the cascade elimination within 72 h.

The results of the NMR spectra analysis led us to the following conclusions:

- 1) In an organic solvent, RCM proceeds quantitatively in less than 2 hours.
- 2) Complete 1,4-elimination leading to naphthalene proceeds in 48 hours.
- 3) The rate of cleavage of carboxylic acids is much higher than the rate of cleavage of naphthalene since the amount of naphthalene is equal to the amount of free benzoic acids.
- 4) The reaction proceeds cleanly and without by-products, which is highlighted by the formation of (4-amino-1,3-phenylene)dimethanol.

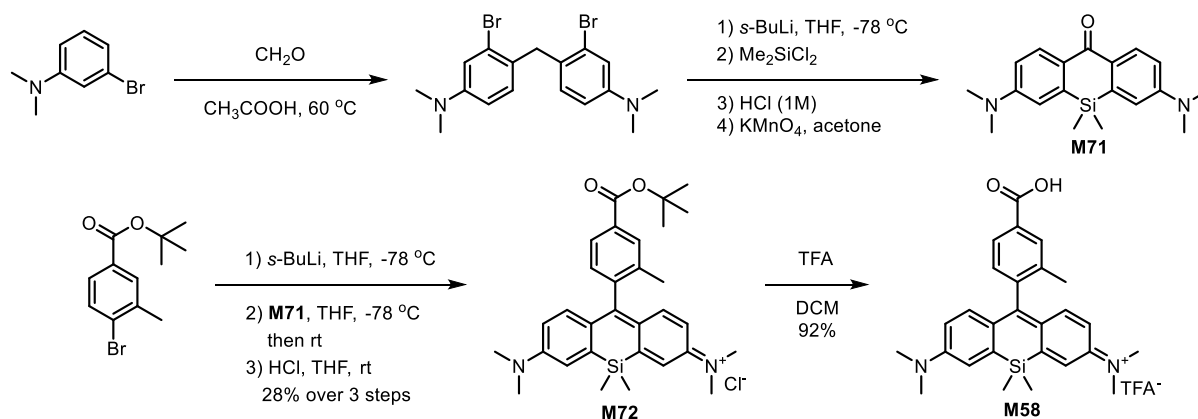
Then, a similar experiment was carried out in a mixture of D_2O - $\text{DMF-}d_7$ (the organic solvent was added to increase the solubility of the lipophilic substrate **M68**). Due to the use of a solvent mixture, calibration of the NMR spectrometer was challenging. Accordingly, the reaction mixture was analyzed at several time points after sampling and extraction of the products from the aqueous phase.

Based on the results of this experiment, the following conclusions can be drawn:

- 1) The reaction proceeds much more slowly due to the presence of both water and DMF.
- 2) The maximum conversion achieved is 65% (13 TON) in 12 hours.
- 3) Intermediates **M69** and **M70** were not detected at any time point, which confirms the potential of this approach within the framework of this project.

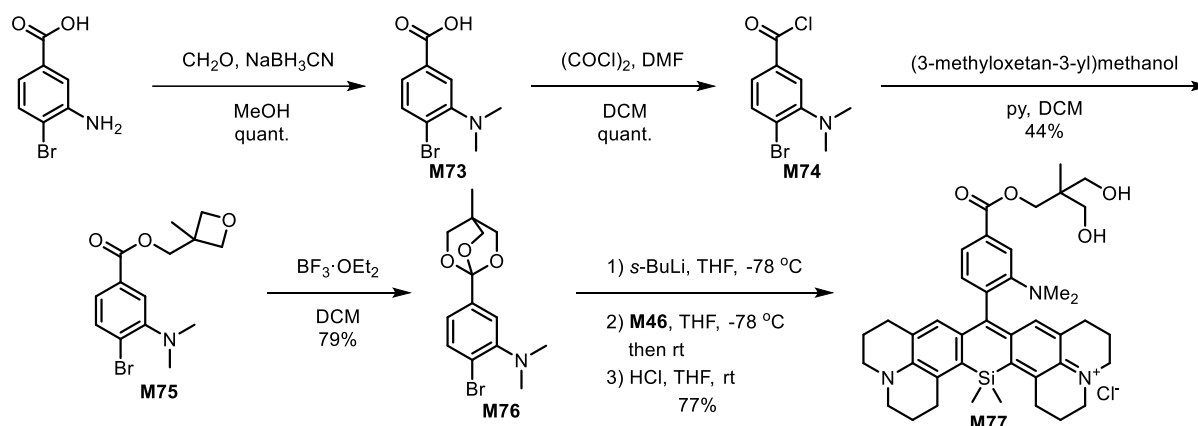
The reaction of the test substrate in an aqueous medium revealed no delay between RCM and the release of uncaged molecules (in contrast to the reaction carried out in an organic solvent). Accordingly, we set out to modify the diol **M66** with a fluorophore and a quencher to yield a water-soluble FRET-substrate.

Silicorhodamine carboxylic acid **M58** was prepared according to a literature method in high yields (**Scheme M35**).²⁶



Scheme M35. Synthesis of carboxylic acid **M58**.

At the time of writing this thesis, the synthesis of the quencher **M59** was carried out to the penultimate step. The *tert*-butyl ester proved as an unsuitable protecting group in the metallation of 4-bromo-3-dimethylaminobenzoic acid **M73**. The carboxyl group was protected as an orthoester **M76**. After metallation, nucleophilic addition, and aromatization, the product **M77** was obtained in high yield (**Scheme M36**).



Scheme M36. Synthesis of ester **M77**.

After alkaline hydrolysis of **M77**, both carboxylic acids **M58** and **M59** will be attached to the diol **M66** under Yamaguchi-esterification conditions, and the resulting diester will be tested on living cells in the presence of Ru-cofactors.

In order to quickly check whether the resulting compounds form a FRET pair and whether the **M77** ester is an appropriate quencher for **M72**, the optical and fluorescent properties of the compounds were measured (**Fig. M5-7**).

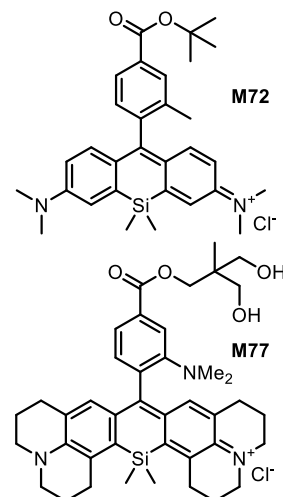
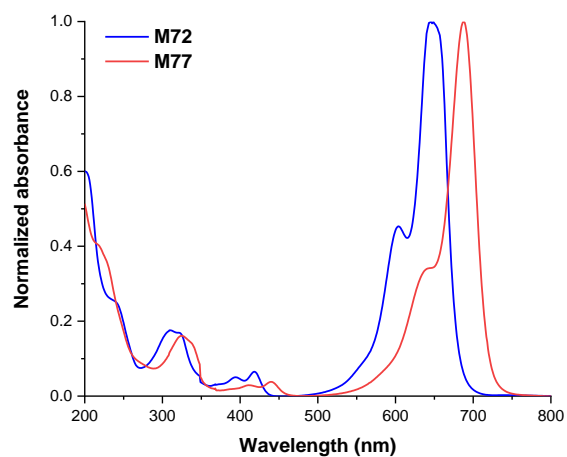


Figure M5. UV-Vis spectra of esters **M72** and **M77**.

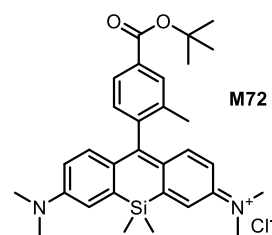
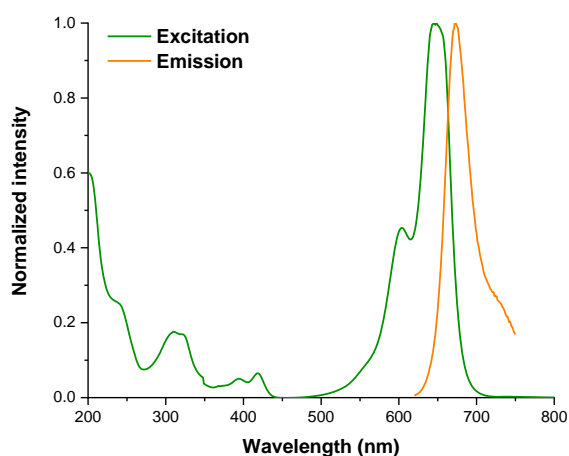


Figure M6. Normalized absorption and fluorescence spectra of **M72**.

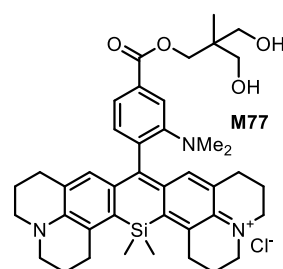
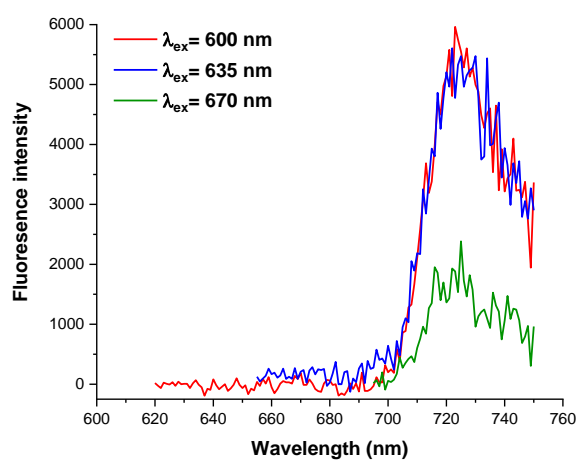
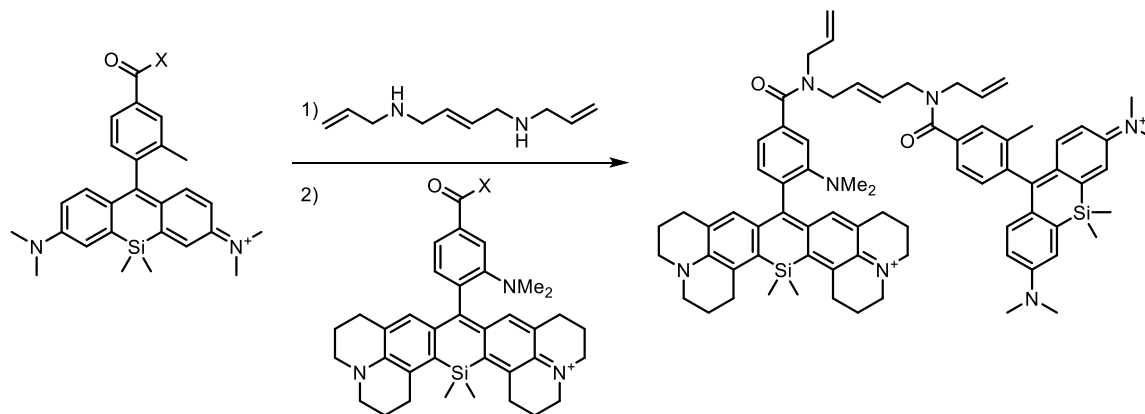


Figure M7. Fluorescence spectra of **M77** with different excitation wavelengths.

As can be appreciated from these spectra, the **M72** and **M77** are indeed ideal candidates for a FRET pair, so this will be the highest priority after the thesis submission.

It should be emphasized that these carboxylic acids **M58** and **M59** may be used to implement the triolefin approach. (*E*)-*N*¹,*N*⁴-dialylbut-2-ene-1,4-diamine can be coupled sequentially to both carboxylic acids by acid chloride acylation or amide coupling to afford the desired product. Upon relay RCM, both FRET partners are released, leading to fluorescence (**Scheme M37**).



Scheme M37. Alternative application of carboxylic acids **M58** and **M59**.

However, the dendritic approach seems more versatile as it allows the addition of any number of molecules of interest, while the triolefin approach is limited to two.

Side projects

Prior to this project, Ward Group's experimental experience in artificial metatheses was limited to streptavidin, HaloTag, and hCAII, with the following cofactors **MRu1-3** used to create metalloenzymes (**Fig. M8**).

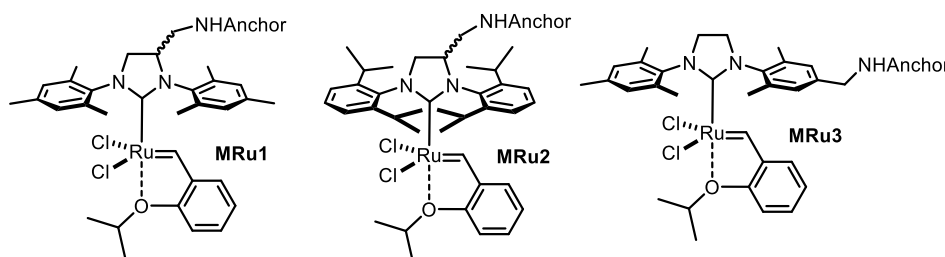
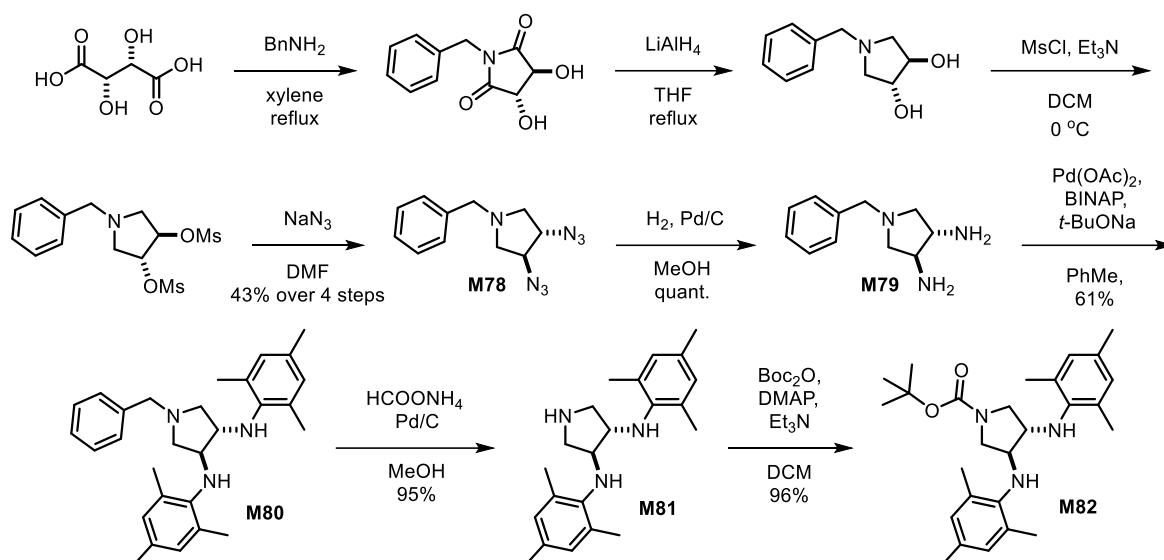


Figure M8. Structures of the cofactors used in Ward Group.

As can be seen from the structures of the cofactors **MRu1** and **MRu2**, they are prepared as racemates. Since it is still not clear whether the absolute configuration affects the cofactor binding to the host protein, and hence the efficiency and selectivity of catalysis, there is a need to synthesize single enantiomers to evaluate their catalytic properties. Dr. Fadri Christoffel tried a number of approaches to the separation of the enantiomers of N-heterocyclic carbenes for gold complexes, but without success.

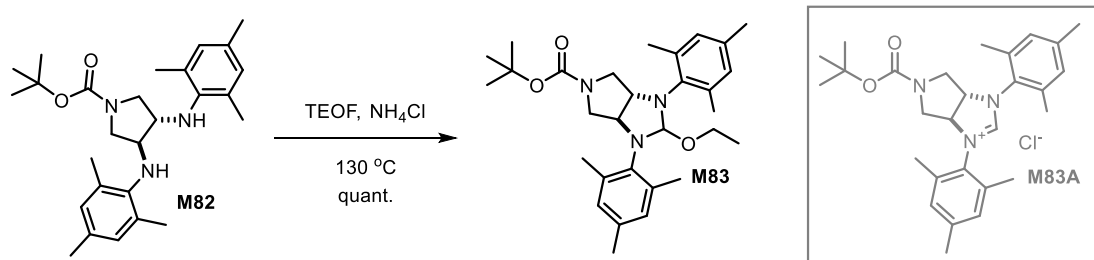
In order to obtain enantiomerically pure ligands for subsequent metal coordination, the following synthetic scheme was developed (**Scheme M38**).



Scheme M38. Synthesis of enantiopure trans-3,4-(bisarylamino)-pyrrolidine **M82**.

Both enantiomers of **M82** were synthesized starting from both enantiomers of tartaric acid.

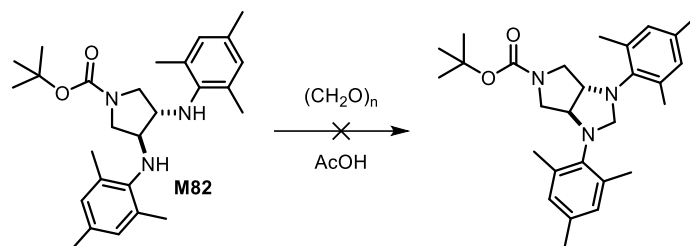
After that, it was decided to prepare the N-heterocyclic carbene precursor under standard conditions (TEOF, NH_4Cl , 130 °C). However, this resulted in the formation of the only product **M83** instead of the expected imidazolium salt **M83A** (Scheme M39).



Scheme M39. The reaction of **M82** with TEOF.

Despite the fact that the product **M83A** was not formed as a result of the reaction, it is known that the adducts of the corresponding imidazoles with methanol and *tert*-butanol can be used as starting materials in the synthesis of ruthenium complexes.²⁷ However, all tested sources of ruthenium, temperature conditions, and stoichiometric ratios did not lead to a complex with the enantiopure NHC bound to the metal.

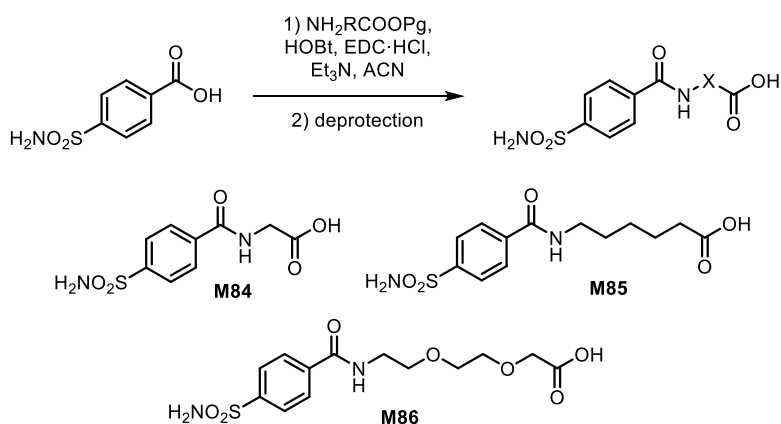
During the work on the project described in the next chapter, it was found that 1,2-(bisarylamino)ethanes react with paraformaldehyde under acidic conditions to form the corresponding imidazolidines in high yields. However, after mixing **M82** with paraformaldehyde in acetic acid, the starting material was quantitatively recovered, and the desired product was not detected (Scheme M40).



Scheme M40. Attempt to synthesize saturated imidazolidine for subsequent oxidation to NHC precursor.

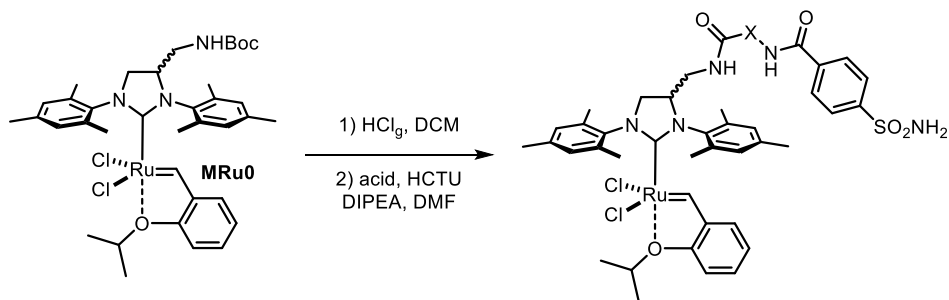
Most likely, a *trans*-disubstituted five-membered ring cannot be fused with another unsaturated five-membered ring due to steric hindrance since similar *cis*-adducts are known in the literature.

Also, for hCAII-specific cofactors, a family of arylsulfonamide anchors was produced for subsequent amide coupling with **MRu1** and **MRu2** cofactors (**Scheme M41**).



Scheme M41. Synthesis of novel hCAII-specific anchors.

The resulting carboxylic acids **M84–86** were reacted with the deprotected **MRu0** cofactor in the presence of HCTU and DIPEA (**Scheme 42**). However, despite moderate conversions, the polarity of the resulting cofactors turned out to be very close to those of the starting acids. Various purification methods failed to remove impurities, and since the cofactor must not be contaminated with a protein inhibitor, these mixtures were not used for experiments with purified proteins and in cells.



Scheme M42. Synthesis of novel hCAII specific Ru-cofactors.

3.3. *De Novo* Artificial Metalloenzymes

Brief summary of existing approaches to abiotic enzymatic reactions

Natural enzymes, as scaffolds for ArMs, are of particular interest in the field of *in vivo* drug release and synthesis. However, since the cell genotype strictly determines the structure of the protein, the catalytic activity of the metal cofactor cannot be improved by tuning the structure of the binding site. In this case, selectivity and TON are usually improved by modifying the first coordination sphere of the metal and electronic properties of the chemically engineered ligands. In addition, the design of prodrugs that are easily transformed into target bioactive molecules in bioorthogonal manner is another key to achieving high TONs.

However, the scope of ArMs is not limited to bioorthogonal drug release. Moreover, the medical applications are only a small part of the variety of ArMs' known and potential functions. Over the past decades, many groups working on the design, creation, and optimization of metalloenzymes have made significant contributions to fundamental science.^{28,29} In particular, they have expanded understanding of protein-small molecule interactions, structure-activity relationships, and the existing scope of biomimicking and new-to-nature reactions. Since the first use of avidin as a host for a metal cofactor in 1970s,^{30,31} the field has grown steadily, gradually involving more and more protein scaffolds and abiotic cofactors, resulting in over 80 ArMs to date.³² Researchers have developed a huge library of cofactors and metalloenzymes using four different anchoring strategies: covalent, supramolecular, dative, and metal substitution (**Fig. B1**).²⁸

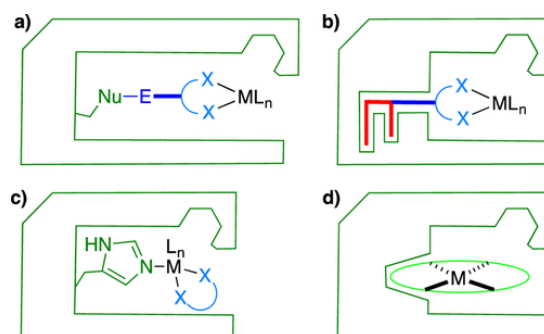


Fig. B1. Four anchoring strategies allow one to firmly localize an abiotic cofactor within a protein scaffold: (a) covalent, (b) supramolecular, (c) dative, and (d) metal substitution. The following color codes apply: protein and natural cofactor (green), supramolecular anchor (red), variable spacer and ligand (blue), and abiotic metal (black).

With the development of protein engineering and modification techniques, the variety of forms and functions of ArMs has expanded. Chimeric and other engineered ArMs display significantly higher TONs and selectivities as compared with wild-type-based ArMs. The discovery and development of directed evolution gave impetus for the explosive growth of the ArMs field since it provided the necessary tools for fine-tuning the structure and properties of the protein active site, and hence the resulting metalloenzyme. Some research groups have achieved unprecedented efficiencies in bioorthogonal catalysis using these methods.^{33–37}

However, all known ArMs use “natural proteins” as starting points for design and optimization. Due to this, the maximum achievable TON and e.r. (TON = turnover number and e.r = enantiomeric ratio, for enantioselective reactions) are limited by the characteristics of each parent protein, as well as by the

number of amino acid residues in the first and secondary coordination sphere of the metal. The latter can be optimized by rational design and directed evolution.

In order to overcome these limitations and have more degrees of freedom to further fine-tune the protein's structure to specific needs, *de novo* scaffolds can be used as hosts for engineer *de novo* ArMs.

Prof. Baker is the uncontested leader in the field of *de novo* protein design. The Rosetta software, originally introduced by the Baker group in 1998 as an *ab initio* approach to structure prediction, has evolved into several new computational methods and custom services such as Rosetta@Home and RoseTTAFold.

Since 2008, when Baker's lab published pioneering work, devoted to the computer-aided design of an enzyme for retro-aldol condensation (a reaction that had not been found in nature until then).³⁸ Since then, the importance of this approach to structure-property prediction and design of new-to-nature fragments of the tertiary structure have grown significantly. The capabilities of the predictive platform have led to several important advances, with clear and potentially highly-important practical applications. For example, the pharmaceutical industry is in dire need of establishing the structure of proteins to search for targets and leads. RoseTTAFold and AlphaFold (GoogleDeepMind deep learning program)³⁹ have come close to solving the problem of protein folding and are making predictions that are accurate enough to be used in drug discovery, increasing the speed of protein analysis, and reducing the need for X-ray crystallography and Cryo-EM. Also recently, the group of Prof. Baker published approaches to the design of miniproteins as protein binders with picomolar affinity to their targets, predicted from structural information alone,⁴⁰ as well as picomolar SARS-CoV-2 inhibitors.⁴¹ These advances can be directly used for precise drug delivery and other areas of medicine.

In a recent review, Baker and Hilvert⁴² identify four main approaches to constructing *de novo* metalloenzymes: i) supramolecular anchoring of the metal cofactor into host scaffolds; ii) introduction of new functionalities into natural metalloenzymes; iii) construction of simple protein mimics for subsequent evolutionary optimization; iv) design of new protein scaffold from scratch followed by metal cofactor binding.

The first two approaches are the most widely used and have been developed since the discovery of the first ArMs, demonstrating the implementation of top-down enzyme engineering of abiotic reactions. However, new protein design methods have made possible a bottom-up approach to artificial (metallo)enzymes. Significant improvement in computer modeling methods, together with the development of directed evolution, open prospects for the creation of fully engineered protein constructs. For example, catalytic dyads and triads for the hydrolysis of esters with $k_{\text{cat}}/K_{\text{m}} = 405 \text{ M}^{-1}\text{s}^{-1}$ were first described in 2012⁴³ and were completely revised and reassembled from short new peptides in 2022, resulting in Zn-dependent *de novo* metalloenzyme for enantiospecific ester cleavage with high catalytic efficiency ($k_{\text{cat}}/K_{\text{m}} = 10^6 \text{ M}^{-1}\text{s}^{-1}$).⁴⁴ In addition, based on the same principles, the Baker and Hilvert groups constructed metal-free *de novo* enzymes for the stereoselective Diels-Alder reaction,⁴⁵ aldol condensation⁴⁶ and others.⁴²

It is also worth noting the contribution of the Tezcan group to the development of *de novo* protein assemblies. Self-assembling agglomerates of monomeric redox proteins are capable of coordinating multiple (up to 8) Zn cations in its interface.^{47,48} The resulting *de novo* constructs act as esterases and beta-lactamases with unprecedented efficiency in the hydrolysis of ampicillin [$(k_{\text{cat}}/K_{\text{m}})/k_{\text{uncat}} 2.3 \cdot 10^6$].⁴⁹

Independently, the Lombardli group developed a family of *de novo* Fe-enzymes (Due Ferri) that allow exquisite control of the selectivity of dioxygen-dependent oxidation of aminophenols by fine tuning of protein structure.⁵⁰

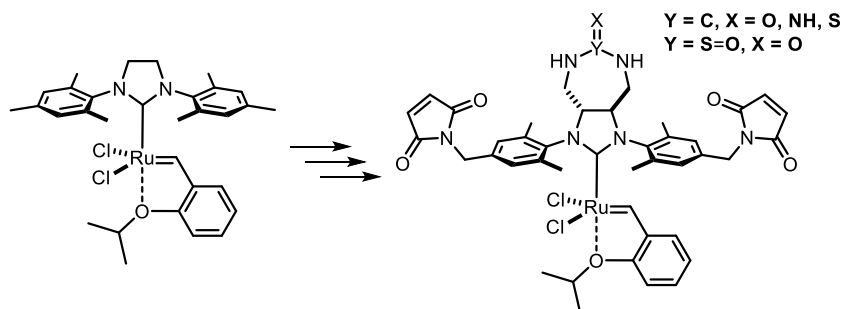
On the way to fully engineered ArMs

Inspired by previous advances in ArMs, as well as the expertise of the Baker group, we set out to construct a fully engineered ArM based on a Hoveyda-Grubbs-like metal cofactor, which is known to be a water-soluble and water-compatible catalyst. To achieve precise localization of the cofactor in the protein pocket, we aimed to modify the catalyst with a highly polar moiety for non-covalent interactions with amino acid residues of the binding site.

Since the general goal of this thesis is repurposing membrane proteins on the cell surface to abiotic reactions, the key requirement in the design of target protein should be its monomeric nature, enabling it to be displayed on a cell surface in its fully functional quaternary structure. Due to this, tandem repeat proteins^{51,52} were selected as the scaffolds. Their closed architectures and ease of handling and modification make them ideal hosts for abiotic metal cofactor.

The asymmetric structure of the parent catalyst requires to use a ligand with C₂ symmetry so that for any orientation inside the binding site it guarantees the same number of hydrogen (and covalent) bonds.

Inspired by the structure of the Hoveyda-Grubbs 2nd generation catalyst as the most air- and water-compatible catalyst, we proposed the following cofactor structures to our collaborators (**Scheme B1**).



Scheme B1. Initial cofactor concept for *de novo* scaffold optimization.

Trans-5,6-diamino-1,3-diazepane containing a fragment of urea (Y = C, X = O), guanidine (Y = C, X = NH or NH₂⁺), thiourea (Y = C, X = S) and sulfamide (Y = S=O, X = O) were proposed as non-covalent binders. For covalent binding, in *para*-positions of the mesityl moieties, we proposed maleimides, which have long been used in bioconjugation as a semi-reversible anchor to protein cysteines.

Dr. Indrek Kalvet from Baker's lab performed preliminary calculations of cofactor structures, which were then used for docking into the proposed protein scaffold. An intensive and complete screening for all possible mutants in the binding site led to the following conclusions:

1) sulfamide (-NH₂SO₂NH₂-) predictably turned out to be the most promising anchor for hydrogen bonding due to the presence of four electronegative atoms and two amide protons;

2) the interaction of the binding site with the polar anchor and aromatic rings provides sufficiently strong binding and eliminates the need for maleimide moieties for covalent binding;

3) depending on the set of mutations in the binding site, the cofactor is oriented differently, which opens up various possibilities for modifying the carbene fragment (for example, for Grela-like cofactors with fast initiation).

Thus, we identified and selected a cofactor containing one sulfamide moiety for non-covalent interactions with the host protein for binding and catalytic experiments. Also, for further experiments on cells and in droplets, we designed a cofactor modified at the *o*-isopropoxystyrene moiety remote from the binding site. To avoid quenching the fluorescence by the protein, the dye was attached to the cofactor by a long polar linker (**Fig. B2**).

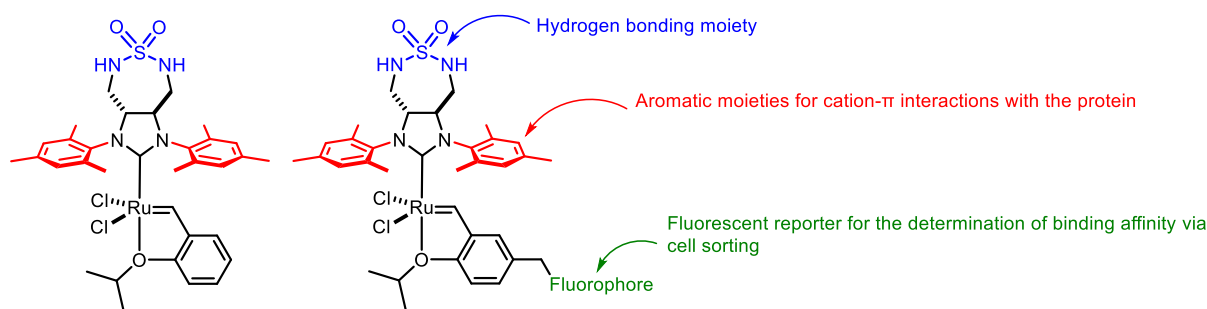
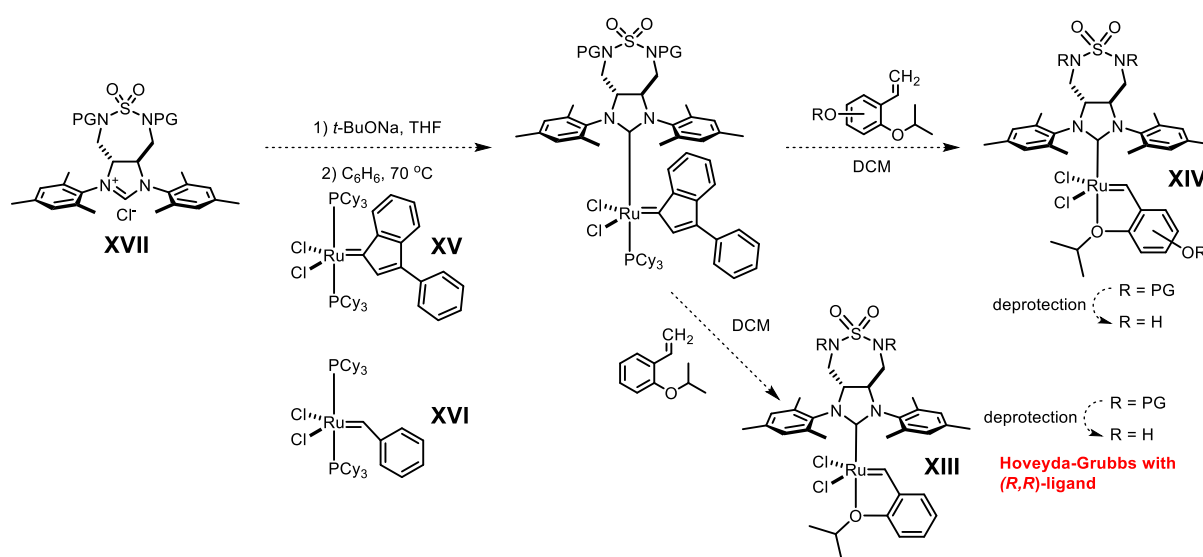


Figure B2. Selected structures of cofactors for catalytic and fluorescent essays to be used in conjunction with a *de novo* designed Tandem Repeat Protein.

Based on the literature data and the group's experience in the synthesis of olefin metathesis cofactors, we proposed the general strategy for the synthesis of desired compounds **XIII** and **XIV** (**Scheme B2**). Since it is not known whether the sulfamide moiety may coordinate to ruthenium, it must be protected to avoid side-reactions. We set out to deprotect these after coordination of the NHC to the Ru. The rest of the synthetic scheme is inspired by well-known approaches. It relies on the 3-phenyl-1*H*-inden-1-ylidene-based catalyst **XV** instead of the G-I catalyst **XVI**, as its more stable and synthetically available.

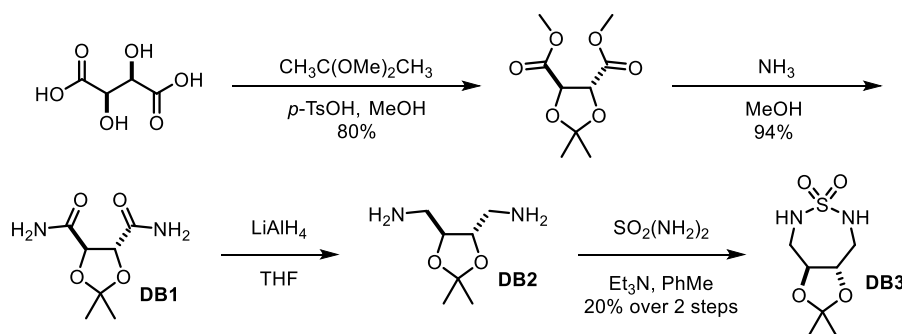
The N-heterocyclic carbene precursor **XVII** must be synthesized in enantiopure (*R,R*)-form, since this enantiomer was used by Indrek Kalvet to design the tailored TRPs.



Scheme B2. Proposed synthesis of Ru-cofactors **XIII** and **XIV**.

Synthesis of the carbene precursor **XVII**

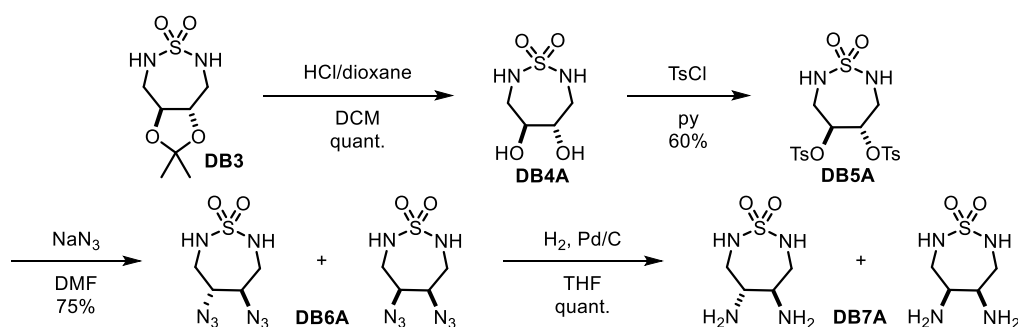
The synthesis of the 1,2,7-thiadiazepane 1,1-dioxide derivative (seven-membered sulfamide) was carried out according to literature procedures, starting from tartaric acid (**Scheme B3**).⁵³



Scheme B3. Synthesis of 7-membered cyclic sulfamide.

Starting from 50 g of L-tartaric acid, the diamide **DB1** could be obtained in two steps. It should be noted that the reduction of diamide **DB1** to diamine **DB2** followed by cyclization with sulfamide $\text{SO}_2(\text{NH}_2)_2$ proceeds in low yield, and the reaction scale had to be kept below 5 g of the starting diamide **DB1**. Therefore, the conversion of the diamide **DB1** to the cyclic sulfamide **DB3** required five repetitions of these reactions.

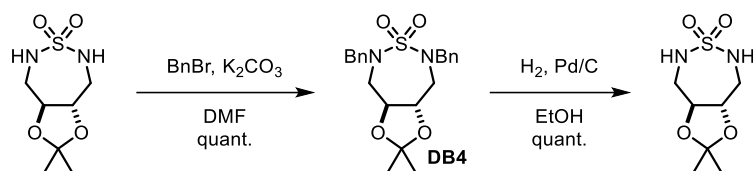
The resulting cyclic sulfamide **DB3** was deprotected under acidic conditions to afford the dihydroxy derivative **DB4A**. The hydroxyl groups were tosylated, giving **DB5A** which was subjected to nucleophilic substitution with azide (**Scheme B4**). All attempts of nucleophilic $\text{S}_\text{N}2$ substitution led to partial racemization of stereocenters, affording a mixture of *trans*- and *meso*-forms of the diazide **DB6A** in 1 to 1 ratio. Unfortunately, these proved inseparable by column chromatography. The products **DB7A** of catalytic reduction of diazides (H_2 , Pd/C) were also inseparable by column chromatography and by crystallization with enantiopure tartaric acid.



Scheme B4. Synthesis of diamino sulfamide **DB7A** via tosylation-azidation-reduction.

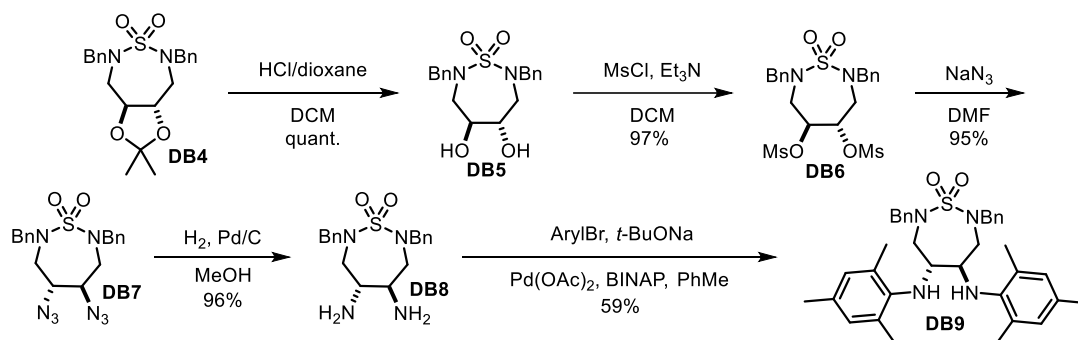
Assuming that the cause of racemization is the bulkiness of tosylate, we replaced the tosylate groups with mesylates as leaving groups. However, all solvents, temperature conditions and stoichiometric ratios led to the formation of mixtures of both O- and N-mesylation products.

Considering subsequent reactions involving acidic hydrolysis, nucleophilic substitutions, reductions, cross-couplings, condensations and carbene additions, we set out to protect the sulfamide nitrogen atoms with a group that unaffected by these multiple reactions. The two benzyl protecting groups were introduced in quantitative yield. Gratifyingly, these could be removed quantitatively in a test run by catalytic hydrogenolysis (**Scheme B5**).



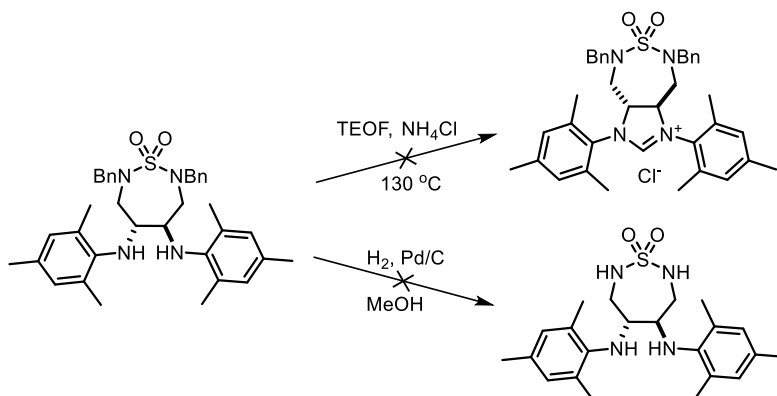
Scheme B5. Synthesis of protected sulfamide **DB4** and its deprotection by Pd-catalyzed hydrogenolysis.

The acetonide protecting group was hydrolyzed using the solution of HCl in dioxane (**Scheme B6**). The diol **DB5** was nearly quantitatively mesylated to afford **DB6**. Without further purification, it was reacted with NaN₃ in DMF. According to NMR data, no *meso*-product was formed, suggesting that both nucleophilic substitutions proceed exclusively via an S_N2 mechanism. After column chromatography, the diazide **DB7** was reduced to the diamine **DB8** using LiAlH₄. However, despite the complete conversion and purity of the crude material confirmed by ¹H-NMR, the preparative yield was <40%, probably due to the high polarity of the product. To overcome this limitation, catalytic hydrogenation was attempted. Surprisingly, the benzyl protection of **DB7** was tolerant to azide reduction conditions and remained intact. The crude diamine **DB8** was subjected to a Buchwald-Hartwig amination with bromomesitylene in the presence of Pd₂dba₃, (±)-BINAP, and *tert*-BuONa as a base. Despite steric hindrance of both substrates, the bis(arylamino) **DB9** was obtained in 59% yield (i.e., 77% per amino group) after column chromatography (**Scheme B6**).



Scheme B6. Synthesis of enantiopure bis(arylamino)sulfamide **DB9**.

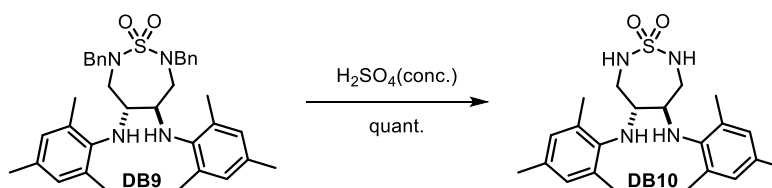
The classical method of the synthesis of imidazolinium salts from 1,2-bis(arylamino)ethanes requires heating the starting material in TEOF, in presence of ammonium salts. When applied to **DB9**, a complex mixture of products resulted. Unfortunately, the desired product could not be detected by LC-MS (**Scheme B7**). In addition, benzyl deprotection did not work on this substrate either.



Scheme B7. Unsuccessful reactivities of **DB9**.

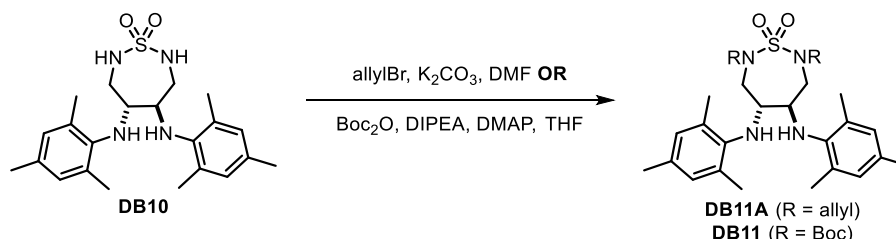
Thus, it was necessary to identify ways to generate a carbene precursor for subsequent coordination with the metal, as well as deprotection under metal-compatible conditions.

Intensive screening of reductive (H_2 , $HCOOH$ with Pd/C , $Pd(OH)_2$, PtO_2 , and others) and oxidative (DMP, NIS) methods for benzyl-group cleavage from amide nitrogen revealed no conversion under all tested pressures and temperatures: the starting material was quantitatively recovered. Surprisingly, treatment with 98-100% sulfuric acid proved very effective for deprotecting amide nitrogens from their benzyl protection, despite the fact that there is only one example in the literature (**Scheme B8**).⁵⁴ The crushed solid **DB9** was mixed with sulfuric acid and stirred for 1 hour. Following neutralization and extraction, the free sulfamide **DB10** was isolated in high purity.



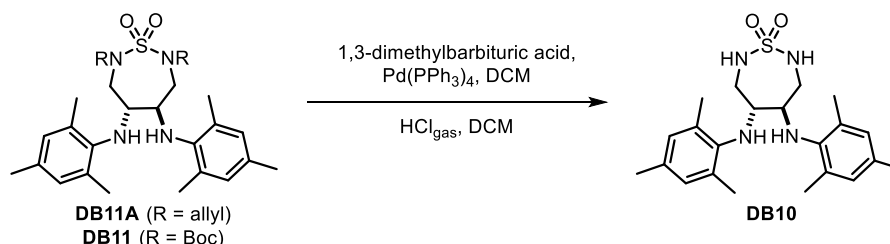
Scheme B8. H_2SO_4 -mediated benzyl cleavage.

Since this approach cannot be used for benzyl-deprotection in the presence of ruthenium, we set out to replace the protecting group – or use an unprotected sulfamide – for the generation of the N-heterocyclic carbene. As there were no data on the nucleophilicity of the nitrogen atoms present in **DB10**, the compound was allylated with two equivalents of allyl bromide. This led to the formation of a single product **DB11A** in a high yield (**Scheme B9**). NMR spectra and test reaction with Boc_2O revealed that a selective alkylation of both sulfamide nitrogens had taken place. $Fmoc\text{-}Cl$ was also evaluated to protect sulfamide **DB10**. However, only the Boc-protected **DB11** was found to be stable enough for chromatographic purification.



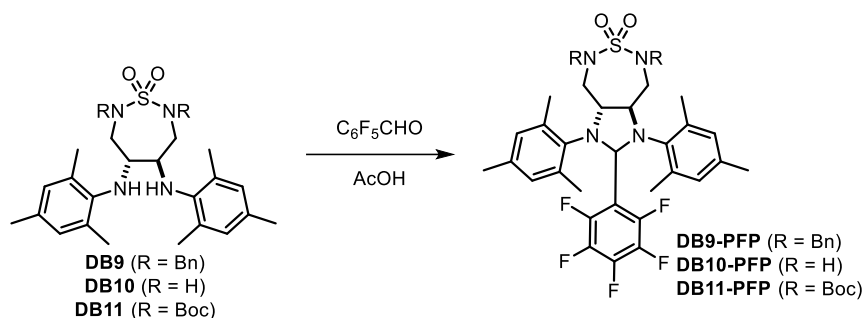
Scheme B9. Protection of sulfamide **DB10** required for the completion of the synthesis of the NHC precursor **XVII**.

Test deprotections under mild conditions highlighted the promise of this approach in the proposed reaction sequence (**Scheme B10**).



Scheme B10. Protecting-group cleavage from sulfamides **DB11A** and **DB11**.

To obtain NHC-metal complexes, imidazolidine-derived substrates with different leaving groups (LGs) were evaluated. These can generate a carbene under the action of base (LG = H) or thermally (LG = CCl₃, CO₂, OR₁, PFP and others). Since the direct method of obtaining the imidazolinium salt did not work, we set out to test various adducts for the thermal generation of the corresponding NHC. Chloroform, carbon dioxide, and alcoholate precursors require the synthesis of the H-derivative. These are therefore not suitable. To overcome this limitation, the products of the condensation of diamines **DB9**, **DB10**, and **DB11** with pentafluorobenzaldehyde were prepared according to **Scheme B11**.⁵⁵



Scheme B11. Condensation of bis(aryl amino)sulfamides **DB9**, **DB10**, and **DB11** with 2,3,4,5,6-pentafluorobenzaldehyde.

The resulting adducts **DB9-PFP**, **DB10-PFP**, and **DB11-PFP** were subjected to thermolysis in a series of NMR experiments evaluating various solvents and temperature regimes (**Table B1**). The course of the reaction was monitored by ¹H- and ¹⁹F-NMR spectra. Monitoring the formation of 1,2,3,4,5-pentafluorobenzene proved very useful. As can be appreciated from **Table B1**, the heat resistance of the adducts increases with decreasing dipole moment of the solvent, making standard solvents for the synthesis of NHC-Ru complexes (benzene, toluene, DCM) unsuitable for these starting materials.

Table B1. Results of thermolysis of PFP adducts in various solvents after 4 hours of the reaction time at 40 °C and 12 hours at 60 °C.

Solvent	Conversion, %	
	40 °C, 4h	60 °C, 12 h
Chloroform	0	0
DCM	0	0
Benzene	0	0
THF	0	43
ACN	7	95
Acetone	10	97

To test the other solvents in the synthesis of desired cofactors, the adducts were thermalized in THF, ACN, and acetone in the presence of G-I and CuCl. Unfortunately, none of the adducts coordinated the metal in any of the solvents. Accordingly, we sought for alternative ways to synthesize the imidazolinium **XVII**.

In order to make sure that such a five-membered cycle is thermodynamically stable, a calculation of the bond lengths and angles in the structure of the desired product was carried out using the PRIRODA software (**Figure B3**). The calculation revealed no particular challenge in generating the desired product.

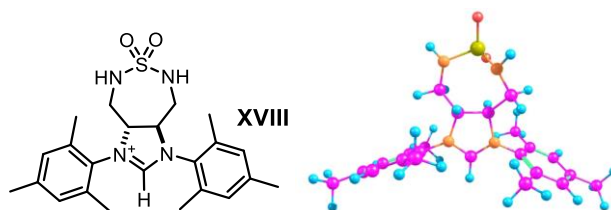
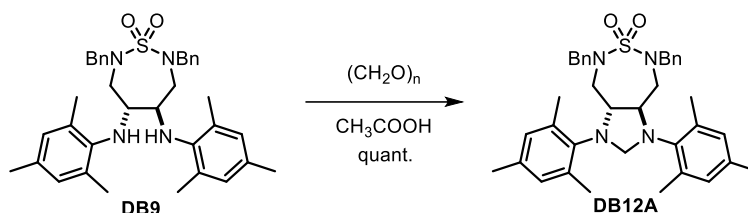


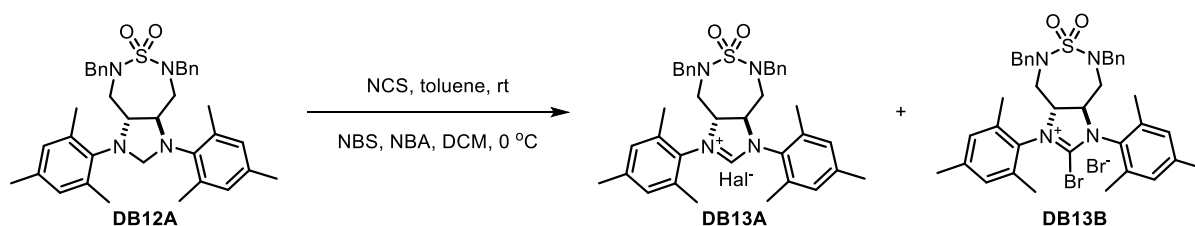
Figure B3. Calculated structure of the imidazolinium **XVIII**.

Then it was decided to first generate the saturated five-membered imidazolidine **DB12A** via condensation of bis(arylamino)sulfamides with paraformaldehyde (**Scheme B12**).⁵⁶



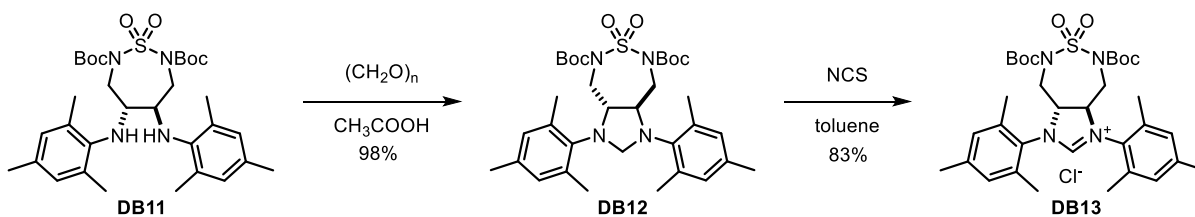
Scheme B12. Condensation of **DB9** with paraformaldehyde under acidic conditions.

There are several reported methods for the oxidation of imidazolidines to imidazolinium salts with radical halogenating reagents.^{57,58} The desired product **DB13A** was obtained using NCS at room temperature in toluene and using NBA in DCM at 0 °C (**Scheme B13**). NBS or a slight excess of NBA lead to overoxidation and formation of the bromo adduct **DB13B**.



Scheme B13. Oxidation of **D12A** by radical halogenating agents leading to imidazolinium salts **DB13A** and **DB13B**.

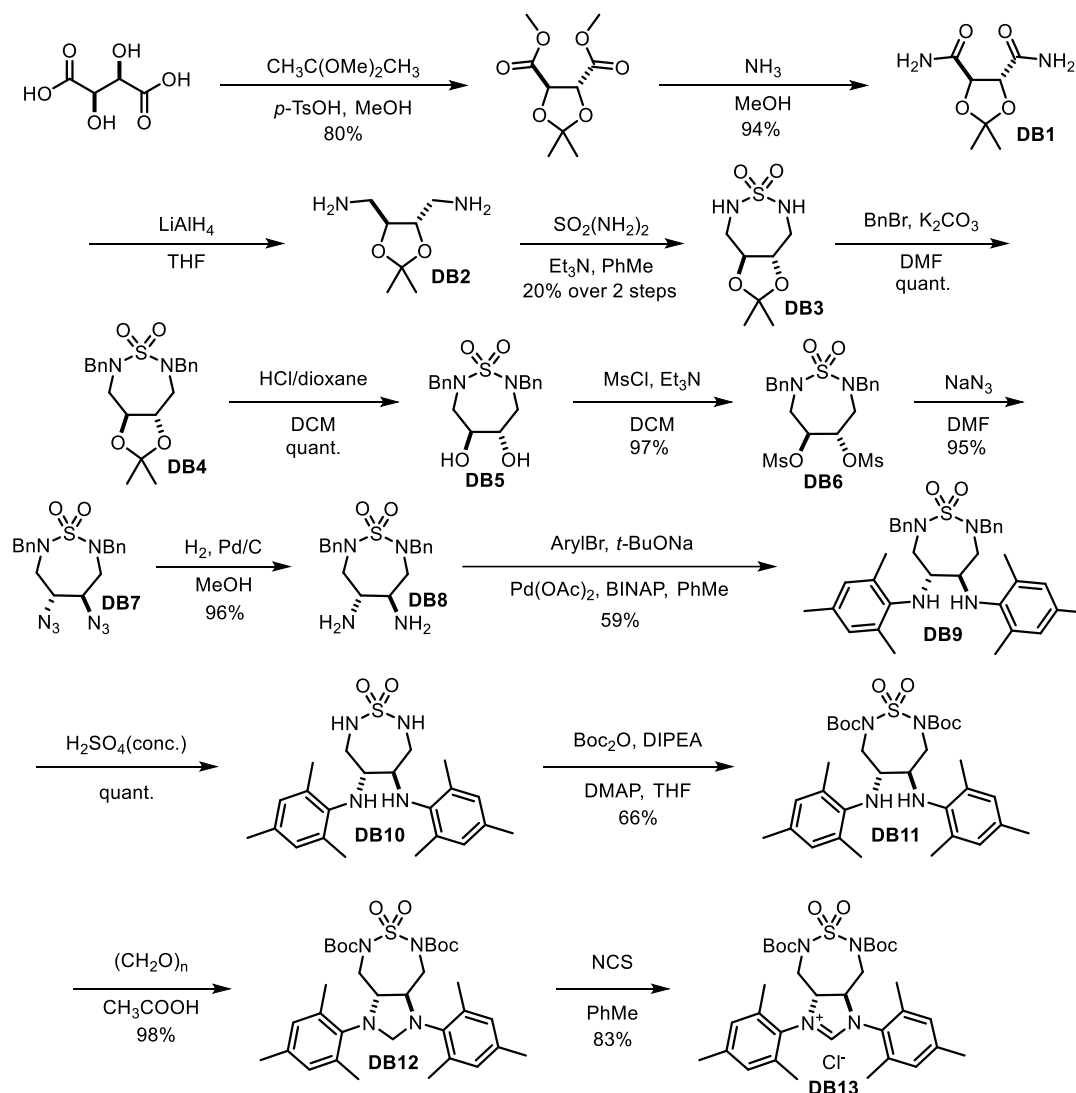
Since the optimization of the protecting group and the approach to the carbene were conducted simultaneously, **DB9** was used as a model substrate. Then, the Boc-protected NHC precursor **DB13** was similarly obtained from **DB11** after cyclization with paraform and subsequent oxidation with NCS (**Scheme B14**).



Scheme B14. Synthesis of NHC precursor **DB13**.

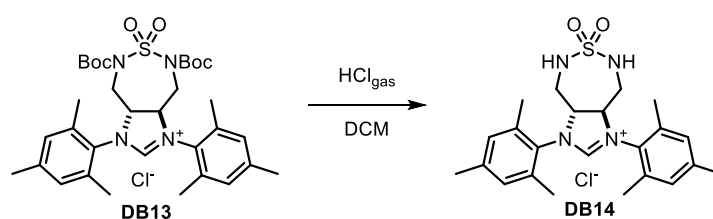
In summary, the heterocyclic carbene precursor **DB13** was obtained in fourteen linear steps with a total yield of 4%. Importantly, it only required three chromatographic purifications (**Scheme B15**). A weakness of this method is the low yield of sulfamide **DB3** (20% after diamide **DB2** reduction and cyclization) and the need to repeat this step several times due to poor scalability. All other steps give

moderate to high yields and do not require further purification. The imidazolinium **DB13** only requires reprecipitation and drying and can be used for subsequent steps.



Scheme B15. Complete synthesis of imidazolinium **DB13**.

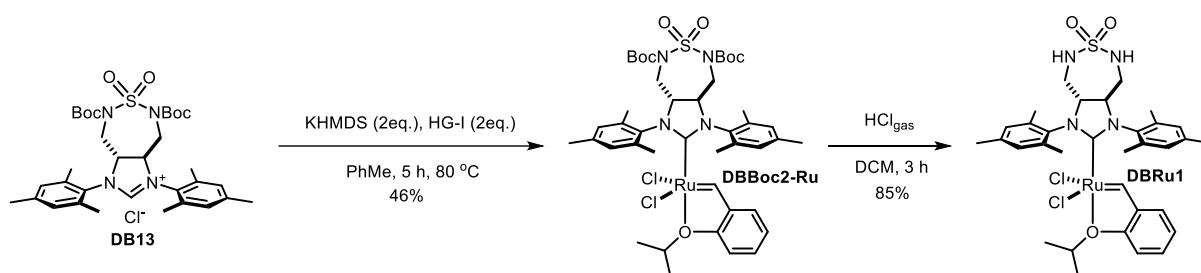
To evaluate the binding of the 7-membered sulfamides to the host protein, the deprotected imidazolinium **DB14** was generated by deprotection with HCl gas in DCM (**Scheme B16**). The quantitative conversion confirmed the potential of this approach towards the synthesis of various metal-containing cofactors.



Scheme B16. Synthesis of the imidazolinium **DB14** for binding studies.

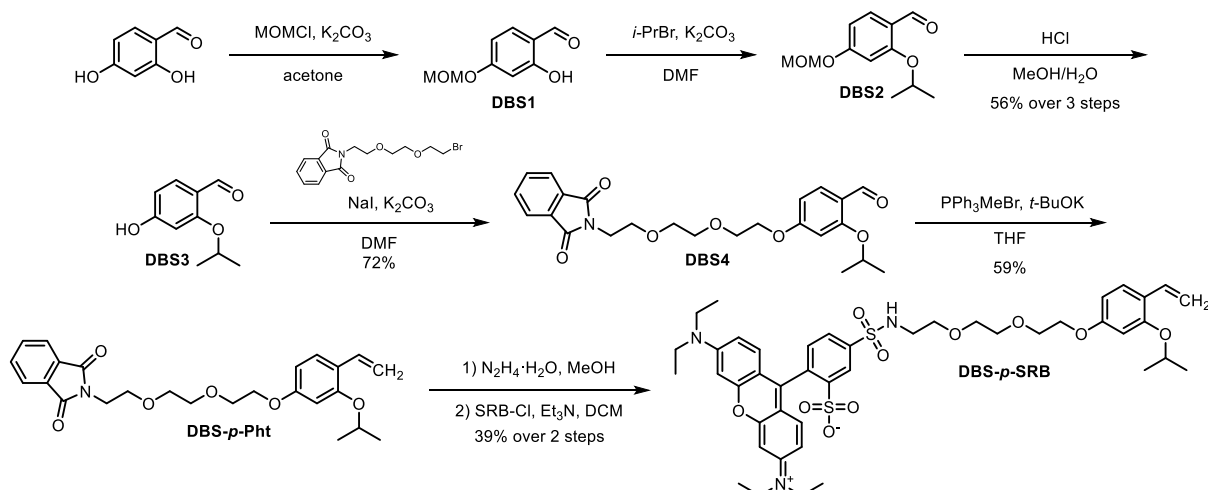
Synthesis of metal cofactors*Ru-cofactors*

The target olefin metathesis cofactor **DBRu1** was obtained in two linear steps from imidazolium **DB13** using a first generation Hoveyda-Grubbs catalyst as the ruthenium source. Following coordination, the Boc-protecting groups were removed with HCl gas (Scheme B17). The conditions for the carbene generation and its coordination to metal were optimized by extensive screening of bases, solvents, temperatures, and order of reagent's addition. Complex **DBBoc2-Ru** was prepared using two equivalents of solid KHMDS and HG-I, which gave a 46% yield, significantly surpassing the efficiency of many other known approaches. Complete deprotection followed by chromatographic purification afforded the product **DBRu1** in an overall yield of 39% over two steps.

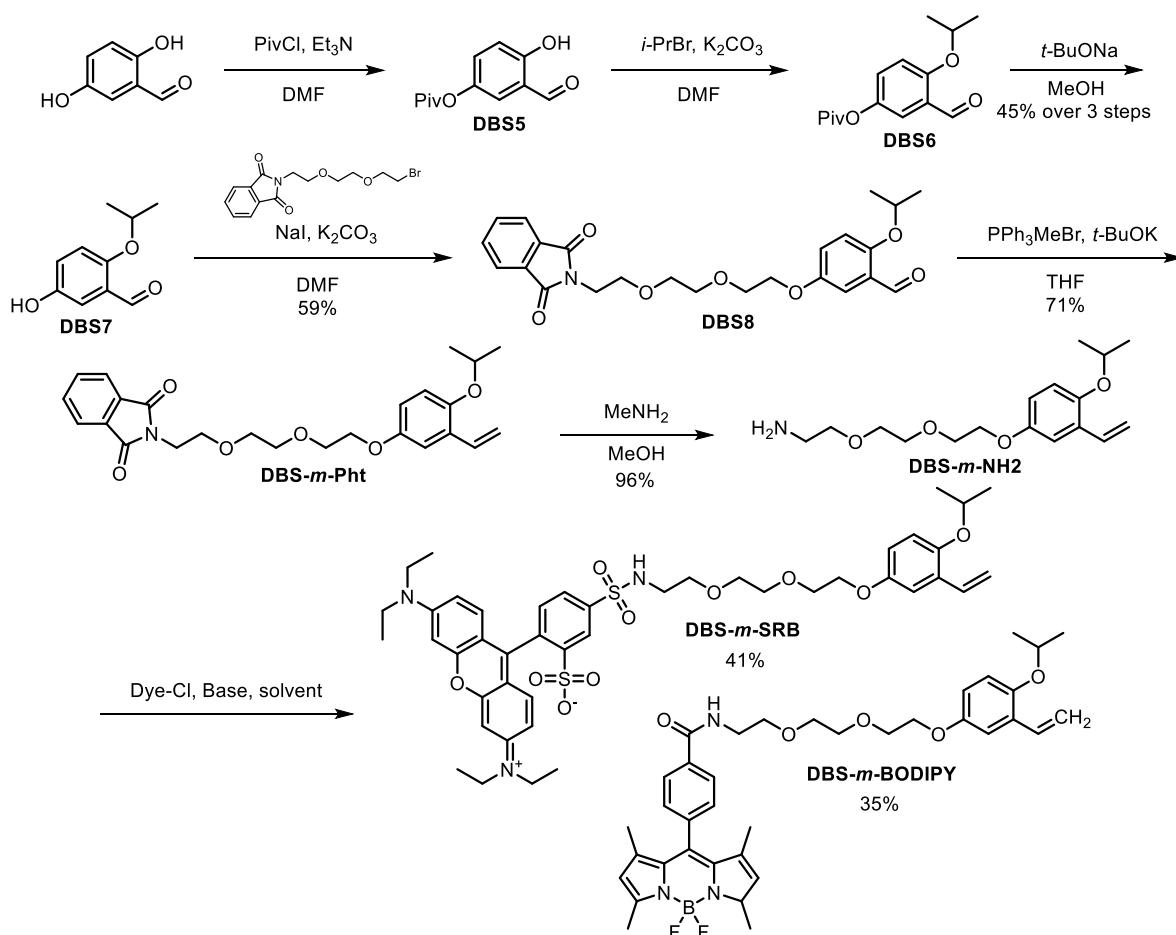


Scheme B17. Synthesis of the cofactor **DBRu1**.

While working on the synthesis of ligand **DB13**, we synthesized a series of functionalized *o*-isopropoxystyrenes for subsequent conjugation with a dye for the synthesis of fluorescent cofactors **DBS-*p*-SRB**, **DBS-*m*-SRB**, and **DBS-*m*-BODIPY** (Schemes B18-19).

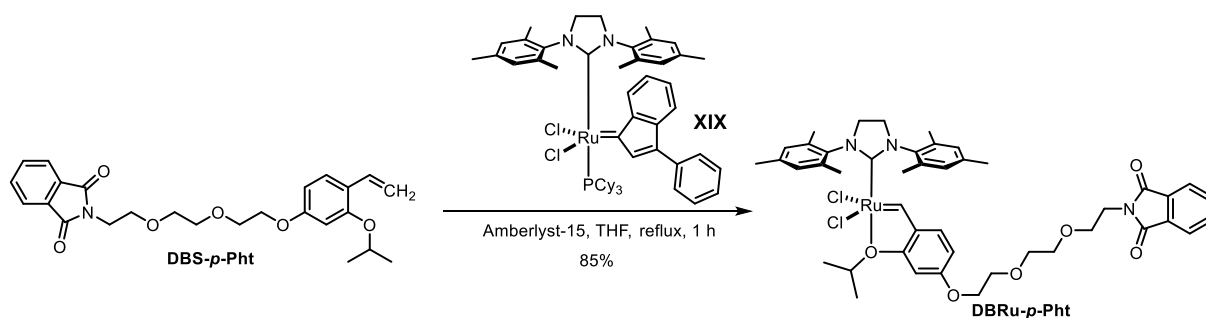


Scheme B18. Synthesis of styrene **DBS-*p*-SRB**.



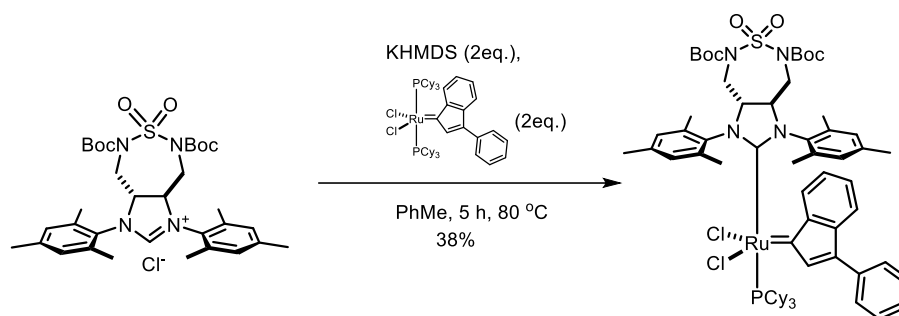
Scheme B19. Synthesis of styrenes **DBS-*m*-SRB** and **DBS-*m*-BODIPY**.

To evaluate the reactivity of 3-phenyl-1*H*-inden-1-ylidene-containing complexes, commercially available Grubbs Catalyst® M101 (**XIX**) was reacted with the protected styrene **DBS-*p*-Pht** (**Scheme B20**). The desired product **DBRu-*p*-Pht** was obtained in high yield and purity, highlighting the promise of the synthetic route.



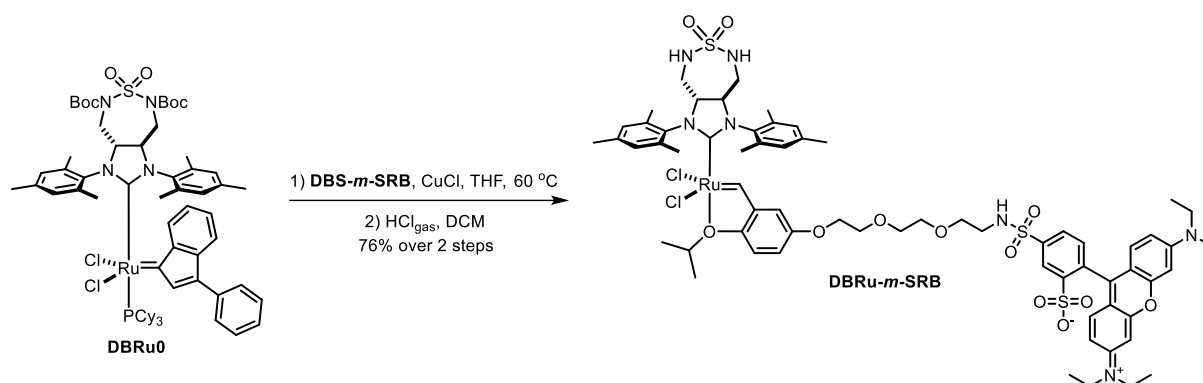
Scheme B20. Alkylidene exchange in the synthesis of Hoveyda-Grubbs-like catalysts.

For simple and efficient synthesis of the flourophore bearing cofactors, intermediate **DBRu0** containing the required ligand and an easily cleavable 3-phenyl-1*H*-inden-1-ylidene fragment was obtained (**Scheme B21**).



Scheme B21. Synthesis of intermediate **DBRu0**.

The structure of the binding site, predicted by computer modelling, suggested that introduction of substituent in *meta*-position of the benzylidene group should be favoured. The fluorescent cofactor **DBRu-*m*-SRB** was obtained by heating a mixture of styrene **DBS-*m*-SRB**, intermediate **DBRu0**, and CuCl in THF, followed by deprotection with HCl in DCM (**Scheme B22**).

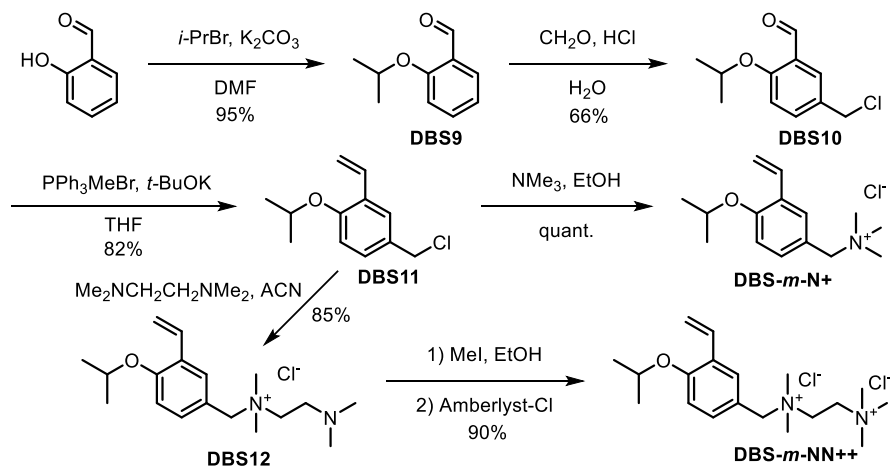


Scheme B22. Synthesis of fluorescent cofactor **DBRu-*m*-SRB**.

Charged Ru-cofactors

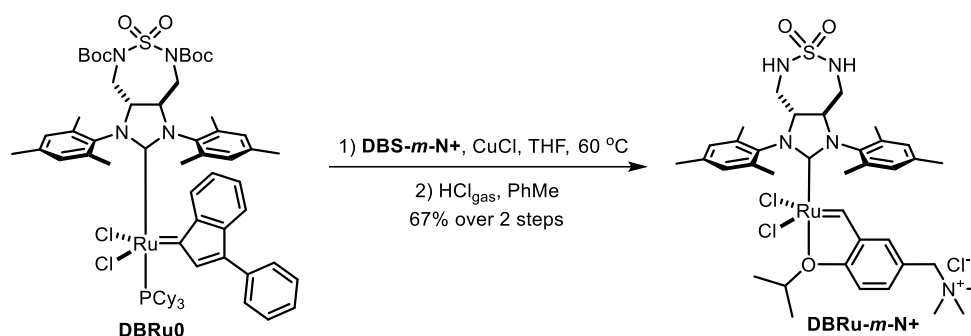
Preliminary experiments with purified proteins, performed by Dr. Zhi Zou revealed that cofactor **DBRu1** has insufficient solubility in water, thus rendering the screening experiments challenging. To overcome this challenge, we set out to increase the polarity of the cofactor by adding one or two positive charges to the *o*-isopropoxybenzylidene moiety.

Charged *o*-isopropoxystyrenes were obtained according to literature methods (**Scheme B23**).⁵⁹



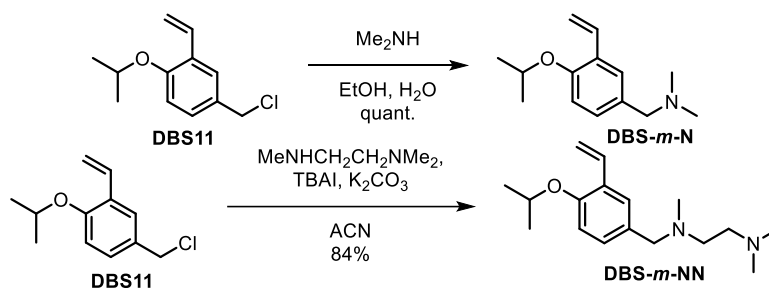
Scheme B23. Synthesis of charged styrenes **DBS-*m*-N⁺** and **DBS-*m*-NN⁺⁺**.

The resulting styrenes **DBS-*m*-N⁺** and **DBS-*m*-NN⁺⁺** were mixed with the intermediate **DBRu0** in THF in the presence of CuCl, after which they were subjected to column chromatography. Due to the high polarity of the initial styrenes and the expected products, neutral alumina was selected as a sorbent, which allowed to obtain pure complex **DBBoc₂Ru-*m*-N⁺** after double purification. **DBBoc₂Ru-*m*-NN⁺⁺**, despite its presence in the reaction mixture (according to NMR and LC-MS), could not be eluted from alumina. **DBRu-*m*-N⁺** was obtained after deprotection with HCl and two column purifications (**Scheme B24**). The product **DBRu-*m*-N⁺** turned out to be insoluble in DCM, but soluble in MeOH and water proving initial hypothesis about high solubility of charged Ru-complexes.



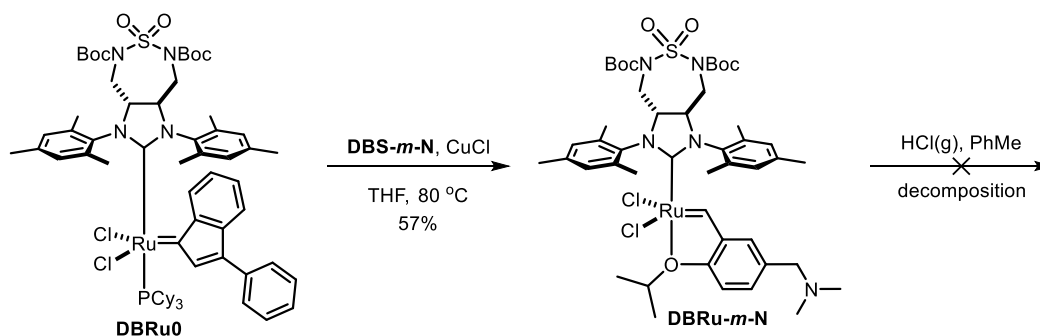
Scheme B24. Synthesis of charged cofactor **DBRu-*m*-N⁺**.

Due to the difficulty encountered in the synthesis of **DBRu-*m*-N⁺**, we developed an alternative approach for the synthesis of water-soluble cofactors. For this, we introduced the charge during the last synthetic step, facilitating chromatographic purification. For this, mono- and diamino styrenes **DBS-*m*-N** and **DBS-*m*-NN** were prepared (**Scheme B25**).



Scheme B25. Synthesis of aminostyrenes **DBS-*m*-N** and **DBS-*m*-NN**.

The interaction of styrene **DBS-*m*-N** with the intermediate **DBRu0** resulted in the formation of the desired complex **DBRu-*m*-N**, which completely decomposed upon removal of the Boc protection, demonstrating the unsuitability of this approach for the synthesis of charged cofactors (**Scheme B26**).

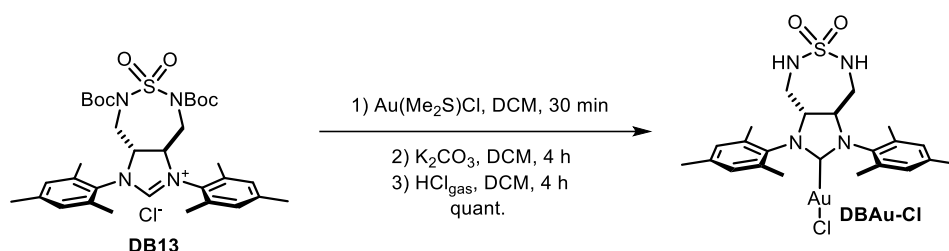


Scheme B26. Alternative approach for the synthesis of charged cofactors.

At this time, Dr. Zhi Zou found that minimal addition of ACN and DMF sufficiently increase the solubility of cofactor **DBRu1** without changing the properties of the host protein, which eliminated the need in charged olefin metathesis cofactors.

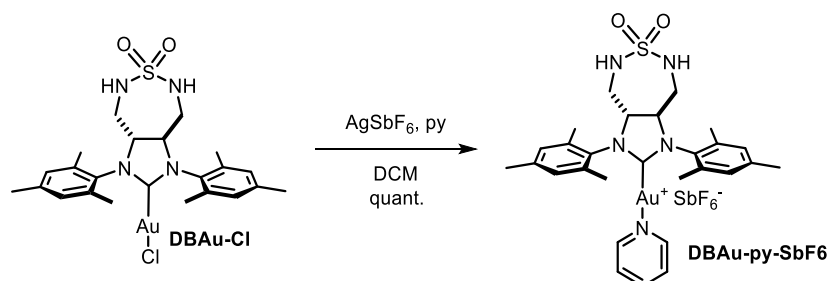
Au-cofactors

Since heterocyclic carbenes can coordinate to a variety of metals, we set out to expand this project with the chemistry of gold as another catalyst with a wide range of bioorthogonal reactivities. Using the same NHC precursor **DB13**, after extensive screening and optimization of conditions, we synthesized a Boc-protected Au-cofactor **DBBoc2-Au-Cl** by simple mixing **DB13** with Au(Me₂S)Cl in the presence of base. The deprotection with HCl afforded cofactor **DBAu-Cl** in a quantitative yield after two steps (**Scheme B27**).



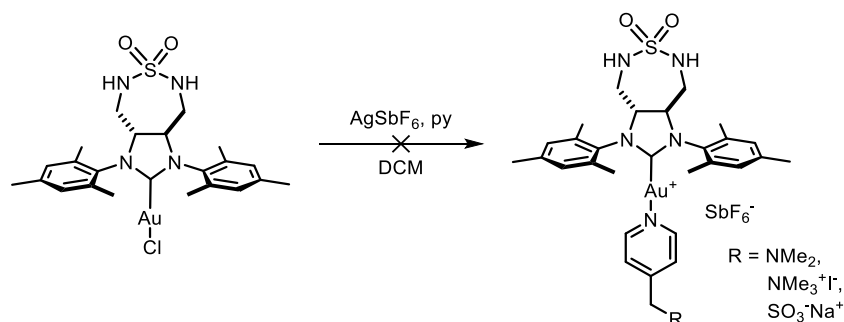
Scheme B27. Synthesis of Au-NHC-complex **DBAu-Cl**.

Preliminary experiments performed by Elinor Morris revealed insufficient solubility of **DBAu-Cl**. To overcome this challenge, we prepared the pyridine complex **DBAu-py-SbF₆** by replacing the chloride in the presence of soluble silver salt and pyridine (**Scheme B28**).



Scheme B28. Synthesis of water-soluble complex **DBAu-py-SbF₆**.

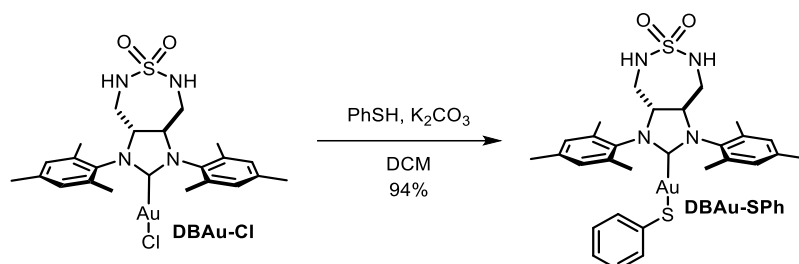
To further increase solubility, we synthesized a family of charged and polar pyridines, however they did not form a stable complex with NHC-Au (**Scheme B29**).



Scheme B29. Attempts to synthesize charged Au-py complexes.

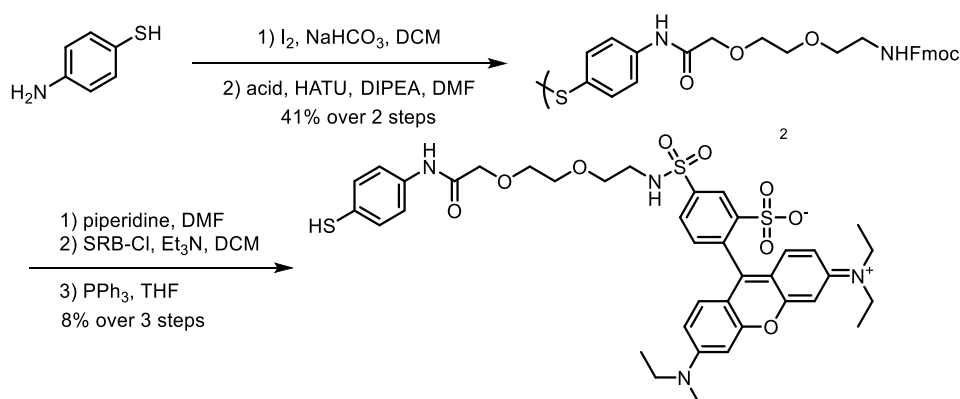
Nevertheless, the cofactor **DBAu-py-SbF₆** revealed sufficient solubility in water, thus enabling the screening and evolving of gold-containing TRPs.

The high affinity of gold for sulfur opens prospects for the preparation of thiol-containing gold. We hypothesized that these may not be catalytically active but may allow to introduce a fluorescent reporter that could enable fluorescence-based sorting. This may be required to evolve the affinity of the cofactor for the TRP: ideally the cofactors should display $K_d < 1$ mM for the various TRPs. As a proof of concept, **DBAu-SPh** was obtained by simple mixing **DBAu-Cl** with thiophenol and potassium carbonate, followed by precipitation in diethyl ether (**Scheme B30**).



Scheme B30. Synthesis of covalent complex **DBAu-SPh**.

The thiophenol with a fluorescent moiety was obtained in a few simple steps (**Scheme B31**).



Scheme B31. Synthesis of thiophenol **DBHS-SRB** modified with fluorophore.

Despite all attempts to coordinate **DBAu-Cl** to the fluorescent thiophenol **DBHS-SRB**, the product could never be obtained. Thankfully however, the K_d of **DBAu-Cl** could be determined by Isothermal Titration Calorimetry, albeit not a high-throughput method.

All obtained cofactors and ligands were tested for the binding and catalytic activity by Dr. Zhi Zou and Elinor Morris. Preliminary data are presented in the next chapter.

RuTRPs

As it was mentioned above, homohexameric TRP was selected as a scaffold for ArMs construction, and **DBRu1** was chosen as a metal cofactor. Docking studies were carried out by Dr. Indrek Kalvet and resulted in 21 designs of *de novo* TRPs (**Fig. B4**).

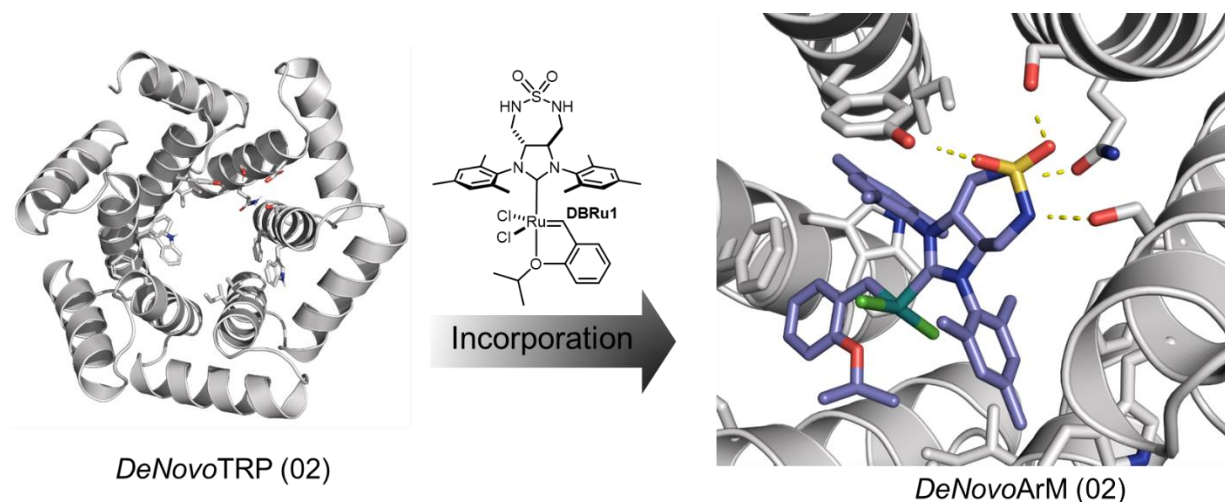


Figure B4. Proposed interactions of the cofactor **DBRu1** and donut-shaped *de novo* designed α -helical tandem repeat proteins (DeNovoTRPs).

Twenty out of 21 designs were solubly expressed in *E. coli*, purified, and characterized (HRMS) by Dr. Zhi Zou.

Binding affinity of the cofactor **DBRu1** were preliminarily determined by fluorescence quenching (**Fig. B5**). Since cofactor itself revealed negligible fluorescence, **DBRu1** was used for titration of the protein. K_d determined for two pH values was found as micromolar, proving the design's success.

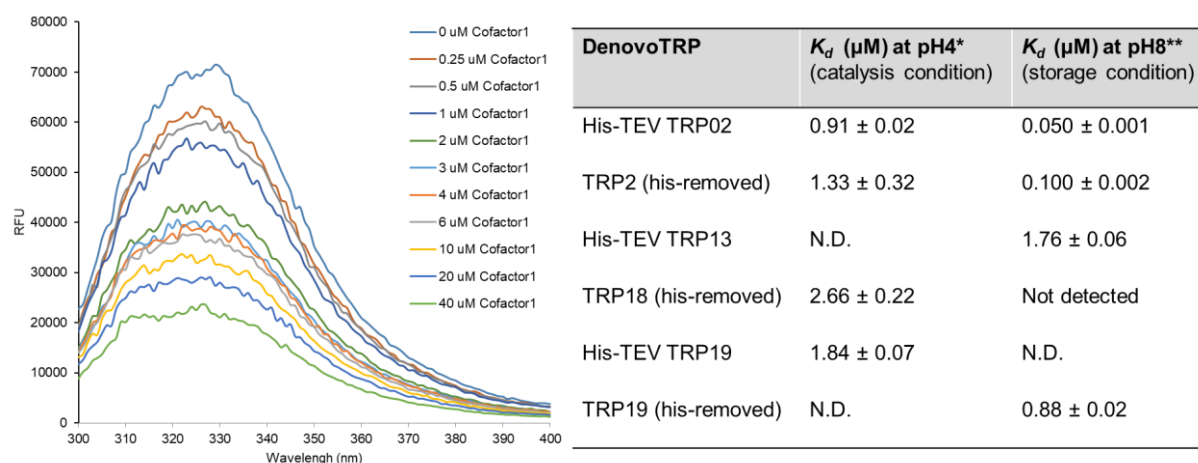


Figure B5. Fluorescence scan of TRP02 (1 μM) in presence of different concentrations of **DBRu1**.

Then, catalytic activity of metalloenzymes was investigated for various TRPs with the cationic diolefin **XX**. The free cofactor revealed moderate TON = 17. In order to completely bind the cofactor **DBRu1** Dr. Zhi Zou used 20 eq. of protein. In presence of protein cofactor demonstrated lower TONs (**Fig. B6**).

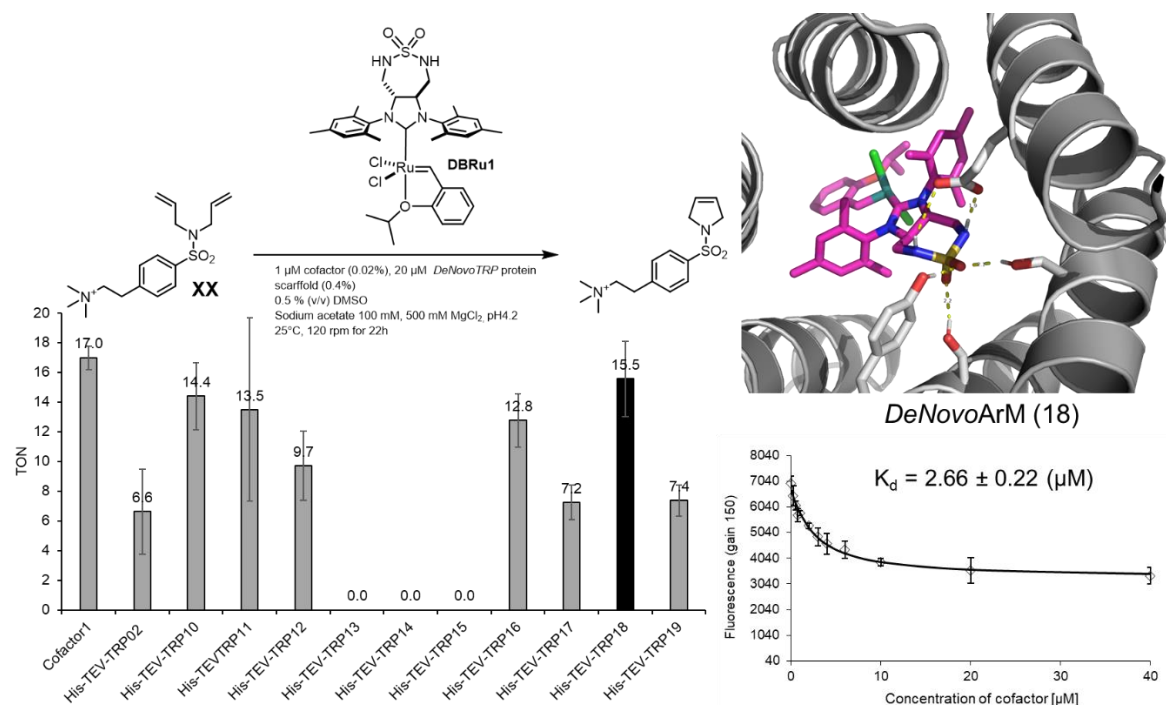


Figure B6. RCM of the diolefin **XX** in presence of **DBRu1** and TRPs.

Assuming that the protein surface is positively charged at pH 4.2 and cationic substrate is electrostatically repelled, the neutral diolefin **XXI** was tested (**Fig. B7**) under similar conditions (DMSO additive was increased for better substrate solubility). Despite the known negative effect of DMSO on the aqueous RCM, the catalytic activity of unbound cofactor reached 52 turnovers. Surprisingly, almost all RuTRPs demonstrated higher activity (up to 188 turnovers). This can be explained by the fact that the hydrophobic binding site protects the cofactor from water and DMSO.

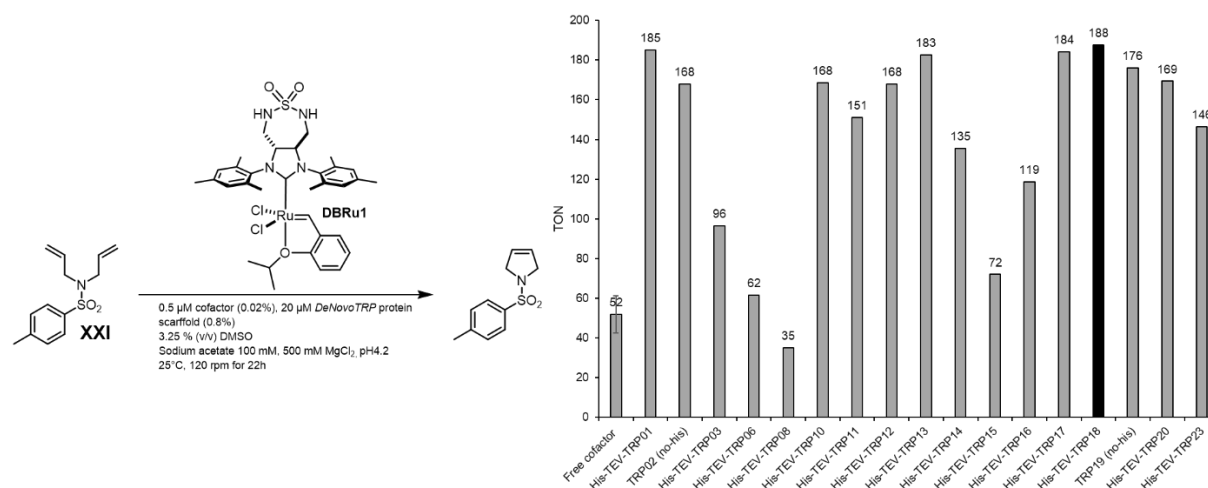


Figure B7. RCM of the diolefin **XXI** in presence of **DBRu1** and TRPs.

For TRP18, a quick-and-dirty evolutionary experiment was performed by random substitutions of amino acids at positions in close proximity to Ru cofactor (L115, G17, E39, F43, L78) (**Fig. B8**). Some of the substitutions led to a significant decrease in catalytic activity. However, the mutant L115S revealed a noticeable and reproducible improvement, which opens the way for further, more systematic structure optimization.

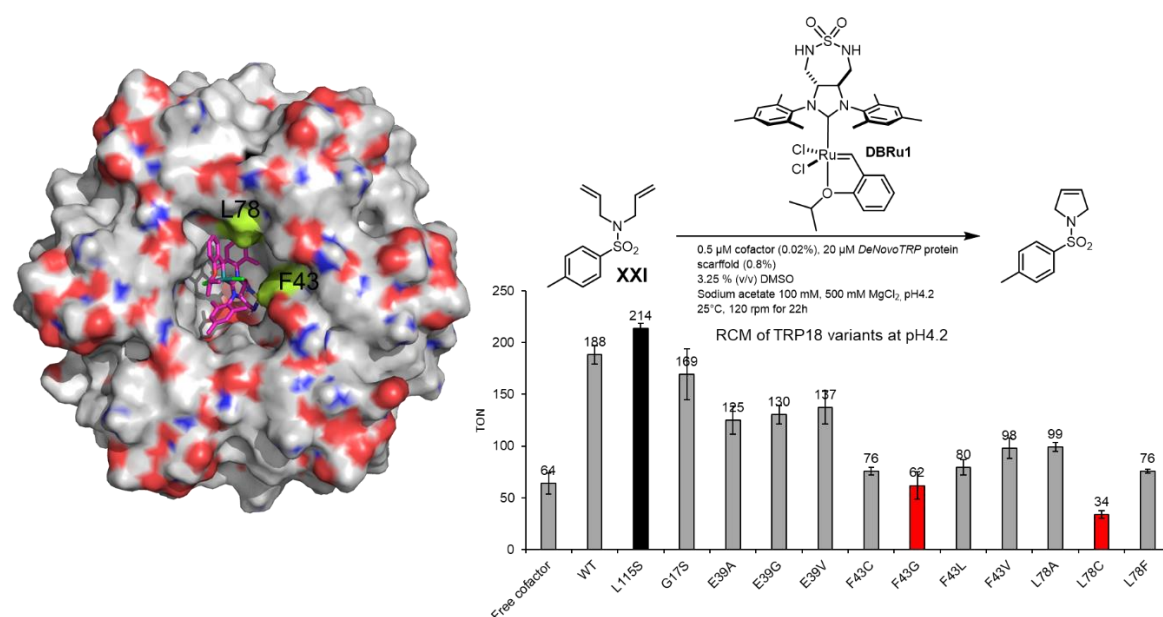


Figure B8. RCM of the diolefin **XXI** in presence of **DBRu1** and TRP18 mutants.

AuTRPs

Preliminary studies of Au-TRP metalloenzymes were performed by Elinor Morris and Dr. Sophie Basler. Catalytic activity of ArMs was evaluated in hydroamination of 2-ethynylaniline **XXII** as yields of indole (determined by UPLC). As can be seen from **Figure B9**, constructs 16, 17, and 18 demonstrate significant improvement in catalytic activity.

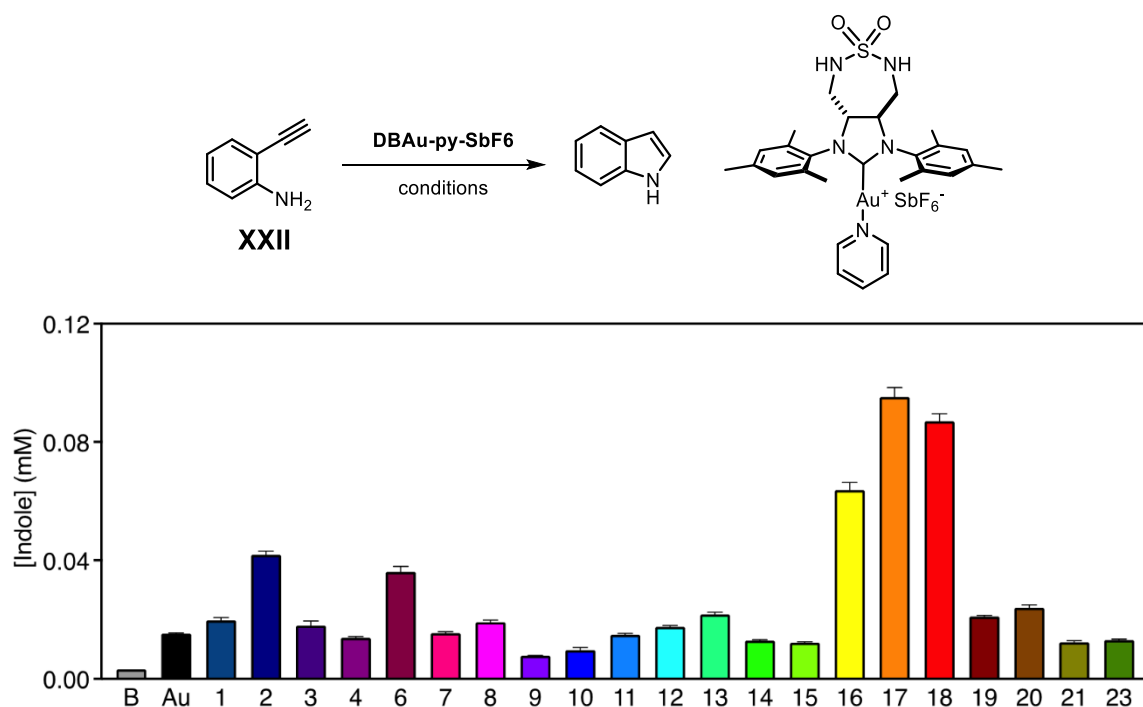


Figure B9. Intramolecular hydroamination of 2-ethynylaniline **XXII** in the presence of **DBAu-py-SbF6** (Au) and TRPs. Reaction conditions: TRP (10 μ M), cofactor (10 μ M), substrate (1 mM), pH 5, MES (40 mM), NaCl (300 mM), ACN (12.5%), 25 °C.

For the further assessment of the catalytic activity of the gold complex **DBAu-py-SbF6**, two substrates **DBSb1** and **DBSb2** were prepared (**Fig. B10**). Upon gold-catalyzed hydroarylation, aminocoumarin

derivatives are generated which can be readily monitored by fluorescence allowing high-throughput screening.

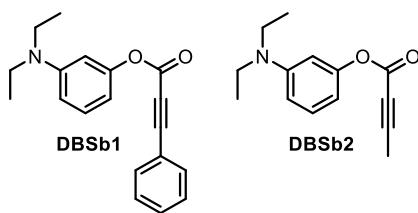


Figure B10. Substrates for Au-catalyzed hydroarylation.

The results obtained by Dr. Zhi Zou and Elinor Morris confirm the initial hypothesis about interaction between cofactor and *de novo* protein. The expressed and purified proteins will be further investigated by ITC for precise determination of K_d values. After all preliminary experiments, selected proteins will be assessed in various reactions. Selectivities (regio-, enantio-, atropo-, diastereo-, and others) as well as TONs will be improved by directed evolution.

4. Summary and Outlook

Bioorthogonal transformations are of particular interest in the context of cancer therapy. Acting like conventional batch catalysts, metal cofactors allow new-to-nature reactions inside living cells or in tumor tissue.

In this work, we present a Ru-deallylation cofactor associated with a low-molecular, highly specific binder of hCAIX (a known marker of various cancer cell lines). The ability of HeLa cells to express hCAIX exclusively under hypoxic conditions made it possible to use this cell line as a single model for healthy and diseased cells. The specificity of binding of the anchor to the tumor marker was demonstrated by FACS and super-resolution microscopy. A library of new prodrugs capable of Ru-catalyzed uncaging was also synthesized. Due to the limited applicability of conventional alloc-protection for highly potent cytotoxins, a new protecting group that allows caging of two drug molecules has been developed. The obtained results open-up prospects for further study of this catalytic system for targeted delivery of the Ru-cofactor to the cell surface, discriminating diseased cells against healthy ones.

In addition, as part of the work on designing the substrate for *in vivo* synthesis of bioactive molecules, we developed an approach to monosubstituted benzenes under RCM conditions. Unfortunately, this method was inapplicable for the synthesis of the tamoxifen precursor. However, this approach complements and completes the arsenal of methods for the synthesis of aromatic compounds under Ru-catalysis. A precursor of pacritinib has also been synthesized. It has been shown that this bioactive molecule can be obtained by RCM in various solvents, including water. Due to the controversial clinical status of the drug in 2019, it was not then tested on cancer cells. Even so, in early 2022 it was approved by the FDA, and therefore is a potential subject for further *in vivo* studies.

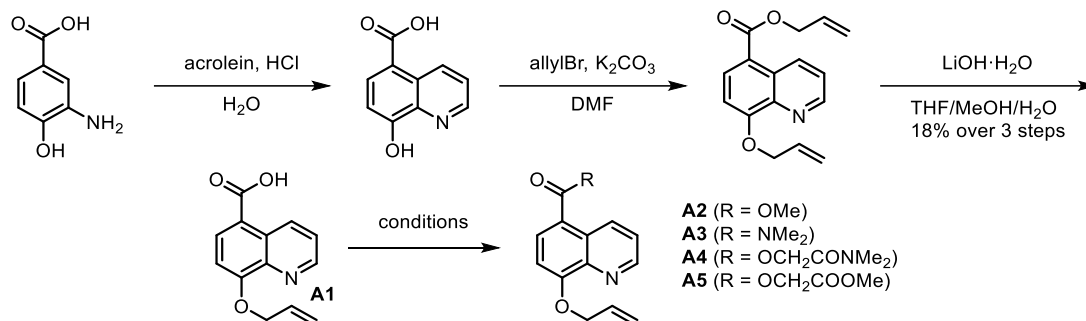
New approaches to caging phenols and amines relying on a Ru-cleavable protecting group have also been developed. In particular, **SN-38** caged by naphthalene diolefin precursor was synthesized. A dendritic approach to caging of multitude of molecules was also demonstrated for the first time in a bioorthogonal manner. Finally, we developed a substrate for live-cell imaging of RCM using MINFLUX technology. The synthesis of the target substrate has been brought to the final stage. In the near future, all synthesized building blocks will be combined, and the resulting substrate will be tested in living cells in the presence of water-soluble ruthenium complexes.

With the aim of developing monomeric ArMsAs that can readily be evolved on a cell surface, we are collaborating with Prof. David Baker. Having designed a suitable cofactor bearing a sulfamide moiety, we have synthesized an optically active NHC as well as ruthenium and gold complexes for bioorthogonal reactions. These cofactors display a micromolar affinity to engineered *de novo* scaffolds. The next stage of this study includes optimization of the structure of binding sites, after which all cofactors will be tested on a wide range of substrates to evaluate regio-, atropo-, enantio- and other types of selectivity. Thereafter, each of these reactions will be individually optimized by directed evolution to achieve the best-in-class activities and selectivities.

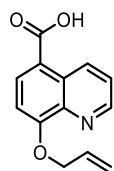
5. Supplementary Information

5.1. Deallylation Project

8-(Allyloxy)quinoline-5-carboxylic acid derivatives



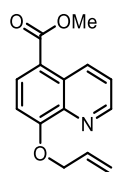
8-(Allyloxy)quinoline-5-carboxylic acid (**A1**)



The carboxylic acid **A1** was prepared according to a reported procedure.⁶⁰

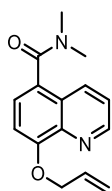
¹H NMR (500 MHz, DMSO-*d*₆): δ 12.95 (s, 1H), 9.41 (dd, J = 8.8, 1.7, 1H), 8.91 (dd, J = 4.0, 1.7, 1H), 8.27 (d, J = 8.4, 1H), 7.67 (dd, J = 8.7, 4.0, 1H), 7.27 (d, J = 8.4, 1H), 6.18 (ddt, J = 17.1, 10.7, 5.4, 1H), 5.53 (dq, J = 17.2, 1.6, 1H), 5.35 (dq, J = 10.5, 1.5, 1H), 4.85 (dt, J = 5.4, 1.5, 2H).

Methyl 8-(allyloxy)quinoline-5-carboxylate (**A2**)



The carboxylic acid **A1** (70 mg, 0.3 mmol) was dissolved in methanol (5 mL) and thionyl chloride (70 μ L, 0.96 mmol) was added. The reaction mixture was refluxed for 16 h and then concentrated under reduced pressure. The residue was dissolved in diethyl ether (10 mL) and washed with a saturated solution of NaHCO₃ (2 \times 5 mL), water (50 mL), and brine (10 mL), dried over anhydrous sodium sulfate and filtered. The organic solvent was removed under reduced pressure to give the methyl ester **A2** as an off-white solid (68 mg, 93%).

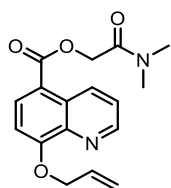
¹H NMR (500 MHz, CDCl₃) δ 9.46 (dd, J = 8.8, 1.7 Hz, 1H), 8.99 (dd, J = 4.1, 1.7 Hz, 1H), 8.30 (d, J = 8.4 Hz, 1H), 7.56 (dd, J = 8.8, 4.1 Hz, 1H), 7.05 (d, J = 8.4 Hz, 1H), 6.20 (ddt, J = 17.2, 10.8, 5.5 Hz, 1H), 5.49 (dq, J = 17.3, 1.5 Hz, 1H), 5.38 (dd, J = 10.5, 1.3 Hz, 1H), 4.94 (dt, J = 5.4, 1.3 Hz, 3H), 3.97 (s, 3H).

8-(Allyloxy)-N,N-dimethylquinoline-5-carboxamide (**A3**)

The carboxylic acid **A1** (69 mg, 0.3 mmol) was dissolved in DMF (5 mL), and HATU (384 mg, 1 mmol) and DIPEA (350 μ L, 2 mmol) were added at room temperature. The reaction mixture was stirred for 30 min, and dimethylamine hydrochloride (40 mg, 0.5 mmol) was added. The reaction mixture was stirred for 16 h, concentrated under reduced pressure, and purified by silica gel column chromatography (60% EtOAc in cyclohexane) to give the amide **A3** as a colourless liquid (43 mg, 56%).

^1H NMR (500 MHz, CDCl_3) δ 8.98 (dd, J = 4.1, 1.7 Hz, 1H), 8.18 (dd, J = 8.5, 1.7 Hz, 1H), 7.47 (dd, J = 8.5, 4.1 Hz, 1H), 7.42 (d, J = 8.0 Hz, 1H), 7.06 (d, J = 8.0 Hz, 1H), 6.20 (ddt, J = 17.2, 10.7, 5.4 Hz, 1H), 5.48 (dd, J = 17.3, 1.4 Hz, 1H), 5.36 (dd, J = 10.5, 1.3 Hz, 1H), 4.90 (dt, J = 5.4, 1.3 Hz, 2H), 3.23 (s, 3H), 2.86 (s, 3H).

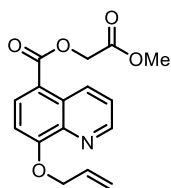
^{13}C NMR (126 MHz, CDCl_3) δ 170.02, 155.18, 149.87, 140.35, 133.65, 132.88, 126.58, 125.48, 122.49, 118.81, 108.41, 70.11, 39.34, 35.26.

2-(Dimethylamino)-2-oxoethyl 8-(allyloxy)quinoline-5-carboxylate (**A4**)

The carboxylic acid **A1** (69 mg, 0.3 mmol), 2-chloro-N,N-dimethylacetamide (50 mg, 0.35 mmol), NaI (30 mg, 0.2 mmol) were mixed in DMF (1 mL). Et_3N (83 μ L, 0.6 mmol) was added at room temperature, and the mixture was stirred for 16 h. The reaction mixture was diluted with water (10 mL) and extracted with diethyl ether (3 \times 10 mL). The combined organic phase was washed with saturated NaHCO_3 solution (2 \times 10 mL), water (10 mL), and brine (20 mL), dried over anhydrous sodium sulfate and filtered. The organic solvent was removed under reduced pressure. The residue was purified by silica gel column chromatography (60% EtOAc in cyclohexane) to give the amide **A4** as a colourless liquid (89 mg, 94%).

^1H NMR (500 MHz, CDCl_3) δ 9.49 (dd, J = 8.8, 1.6 Hz, 1H), 8.98 (dd, J = 4.1, 1.6 Hz, 1H), 8.44 (d, J = 8.4 Hz, 1H), 7.55 (dd, J = 8.8, 4.1 Hz, 1H), 7.06 (d, J = 8.4 Hz, 1H), 6.20 (ddt, J = 16.0, 10.7, 5.5 Hz, 1H), 5.52 – 5.45 (m, 1H), 5.43 – 5.32 (m, 1H), 5.03 (s, 2H), 4.94 (d, J = 5.4 Hz, 2H), 3.08 (s, 3H), 3.03 (s, 3H).

^{13}C NMR (126 MHz, CDCl_3) δ 166.68, 166.14, 158.64, 149.58, 140.28, 134.83, 133.33, 132.44, 128.95, 123.24, 119.13, 117.83, 107.77, 70.22, 61.76, 36.07, 35.79.

2-Methoxy-2-oxoethyl 8-(allyloxy)quinoline-5-carboxylate (**A5**)

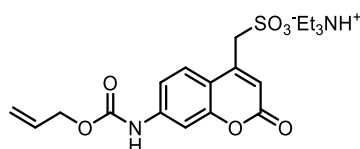
The carboxylic acid **A1** (140 mg, 0.6 mmol), methyl bromoacetate (107 mg, 0.65 mmol), NaI (30 mg, 0.2 mmol) were mixed in DMF (1 mL). Et_3N (170 μ L, 1.2 mmol) was added at room temperature, and

the mixture was stirred for 16 h. The reaction mixture was diluted with water (10 mL) and extracted with diethyl ether (3×10 mL). The combined organic phase was washed with saturated NaHCO₃ solution (2×10 mL), water (10 mL), and brine (20 mL), dried over anhydrous sodium sulfate and filtered. The organic solvent was removed under reduced pressure to give the diester 2-methoxy-2-oxoethyl 8-(allyloxy)quinoline-5-carboxylate **A5** as a pale yellow oil (141 mg, 78%) which was used in the next step without further purification.

¹H NMR (500 MHz, CDCl₃) δ 9.45 (dd, *J* = 8.8, 1.6 Hz, 1H), 8.99 (dd, *J* = 4.1, 1.6 Hz, 1H), 8.42 (d, *J* = 8.4 Hz, 1H), 7.56 (dd, *J* = 8.8, 4.1 Hz, 1H), 7.07 (d, *J* = 8.5 Hz, 1H), 6.20 (ddd, *J* = 22.7, 10.7, 5.5 Hz, 1H), 5.49 (dd, *J* = 17.3, 1.3 Hz, 1H), 5.38 (dd, *J* = 10.5, 1.2 Hz, 1H), 4.95 (d, *J* = 5.4 Hz, 2H), 4.92 (s, 2H), 3.82 (s, 3H).

¹³C NMR (126 MHz, CDCl₃) δ 168.67, 165.63, 158.89, 149.67, 140.31, 134.60, 133.39, 132.37, 128.99, 123.36, 119.19, 117.17, 107.73, 70.26, 61.06, 52.51.

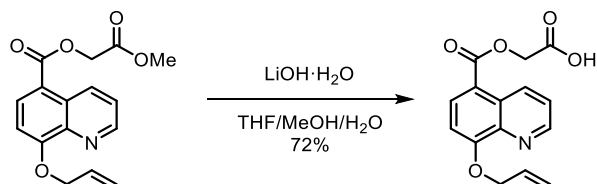
(7-(((Allyloxy)carbonyl)amino)-2-oxo-2*H*-chromen-4-yl)methanesulfonic acid triethylammonium salt (**A6**)



The coumarin **A6** was prepared according to a reported procedure.⁶¹

¹H NMR (500 MHz, DMSO-*d*₆) δ 10.23 (s, 1H), 7.85 (d, *J* = 8.8 Hz, 1H), 7.55 (d, *J* = 2.0 Hz, 1H), 7.34 (dd, *J* = 8.8, 2.1 Hz, 1H), 6.25 (s, 1H), 6.00 (ddt, *J* = 17.2, 10.6, 5.5 Hz, 1H), 5.38 (dt, *J* = 17.2, 1.6 Hz, 1H), 5.26 (dt, *J* = 10.5, 1.4 Hz, 1H), 4.65 (dt, *J* = 5.5, 1.4 Hz, 2H), 4.01 (s, 2H).

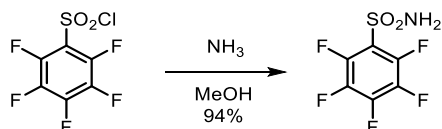
2-((8-(Allyloxy)quinoline-5-carbonyl)oxy)acetic acid (**A7**)



To a stirred solution of the diester **A5** (135 mg, 0.45 mmol) in methanol (3.5 mL) a solution of LiOH·H₂O (18 mg, 0.43 mmol) in water (300 μL) was added at room temperature. The mixture was stirred for 16 h at room temperature, and acetic acid (3 mL) was added dropwise at 0 °C. Solids were filtered, washed with acetic acid, and dried *in vacuo* to give the carboxylic acid **A7** as an off-white powder (89 mg, 72%). The crude product was used in the next step without further purification.

¹H NMR (500 MHz, DMSO-*d*₆) δ 13.20 (s, 1H), 9.29 (d, *J* = 8.4 Hz, 1H), 8.95 (s, 1H), 8.34 (d, *J* = 8.3 Hz, 1H), 7.71 (dd, *J* = 8.5, 3.7 Hz, 1H), 7.33 (d, *J* = 8.4 Hz, 1H), 6.19 (td, *J* = 10.8, 5.2 Hz, 1H), 5.54 (d, *J* = 17.1 Hz, 1H), 5.36 (d, *J* = 10.4 Hz, 1H), 4.88 (s, 4H).

2,3,4,5,6-Pentafluorobenzenesulfonamide (**A8**)



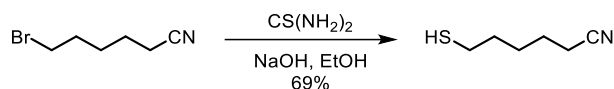
2,3,4,5,6-pentafluorobenzenesulfonamide **A8** was prepared according to a reported procedure.⁶²

¹H NMR (500 MHz, DMSO-*d*₆) δ 8.46 (s, 2H).

^{19}F NMR (471 MHz, $\text{DMSO}-d_6$) δ -138.77 – -139.23 (m), -148.82 (tt, J = 22.5, 5.2 Hz), -160.46 (tt, J = 22.6, 5.5 Hz).

α,ω -Aminothiols

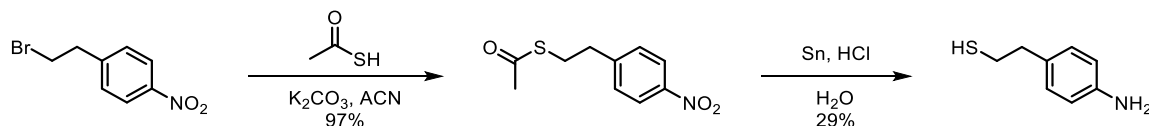
6-Mercaptohexanenitrile (**A9**)



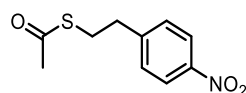
6-bromohexanenitrile (1.76 g, 10 mmol) and thiourea (910 mg, 12 mmol) were heated in ethanol (25 mL) under reflux for 4 h. The reaction mixture was cooled to room temperature, and a 10% NaOH solution (20 mL) was added, and the mixture was heated to reflux for additional 16 h. The organic solvent was removed under reduced pressure, and the aqueous phase was extracted with diethyl ether (3×20 mL). The combined organic phase was washed with water (20 mL) and brine (20 mL), dried over anhydrous sodium sulfate and filtered. The organic solvent was removed under reduced pressure to give the thiol **A9** as a pale-yellow liquid (896 mg, 69%). The crude product was used without further purification.

^1H NMR (500 MHz, CDCl_3) δ 2.54 (q, J = 7.1 Hz, 2H), 2.35 (t, J = 7.0 Hz, 2H), 1.73 – 1.61 (m, 4H), 1.59 – 1.51 (m, 2H), 1.35 (t, J = 7.8 Hz, 1H).

Synthesis of the thiol **A11**



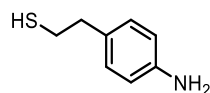
S-(4-Nitrophenethyl) ethanethioate (**A10**)



1-(2-Bromoethyl)-4-nitrobenzene (1.06 g, 4.6 mmol), K_2CO_3 (760 mg, 5.5 mmol), and thioacetic acid (390 μL , 5.5 mmol) were mixed in ACN (10 mL) and stirred at room temperature for 4 h. The organic solvent was removed under reduced pressure, and the residue was redissolved in diethyl ether (50 mL). The organic phase was washed with saturated NaHCO_3 solution (20 mL), water (20 mL) and brine (20 mL), dried over anhydrous sodium sulfate and filtered. The organic solvent was removed under reduced pressure to give the thioester **A10** as a pale-yellow oil (1 g, 97%). The crude product was used in the next step without further purification.

^1H NMR (500 MHz, CDCl_3) δ 8.20 – 8.10 (m, 1H), 7.44 – 7.34 (m, 1H), 3.14 (dd, J = 8.4, 6.6 Hz, 1H), 2.98 (t, J = 7.5 Hz, 1H), 2.33 (s, 1H).

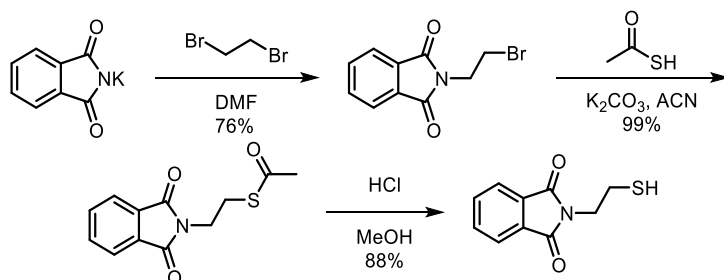
2-(4-Aminophenyl)ethane-1-thiol (**A11**)



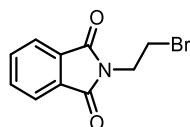
The thioester **A10** (1 g, 4.4 mmol) was mixed with 2M HCl solution (30 mL) and Sn dust (2.5 g, 21 mmol) was added in portions at room temperature. The reaction mixture was stirred for 16 h and then filtered through a pad of celite. The aqueous phase was extracted with diethyl ether (3×20 mL), washed with a saturated NaHCO_3 solution (20 mL), water (20 mL) and brine (20 mL), dried over anhydrous sodium sulfate and filtered. The organic solvent was removed under reduced pressure to give the thiol **A11** as a yellow oil (195 mg, 29%). The crude product was used in the next step without further purification.

^1H NMR (500 MHz, CDCl_3) δ 6.99 (d, J = 8.3 Hz, 2H), 6.64 (d, J = 8.4 Hz, 2H), 2.89 – 2.78 (m, 2H), 2.77 – 2.67 (m, 2H), 1.37 (t, J = 7.7 Hz, 1H).

Synthesis of the thiol **A14**

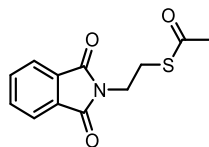


2-(2-Bromoethyl)isoindoline-1,3-dione (**A12**)



The bromide **A12** was prepared according to a reported procedure.⁶³

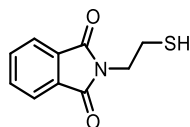
S-(2-(1,3-Dioxoisoindolin-2-yl)ethyl) ethanethioate (**A13**)



The bromide **A12** (2.32 g, 9.1 mmol), K_2CO_3 (1.51 g, 10.9 mmol), and thioacetic acid (780 μL , 10.9 mmol) were mixed in ACN (20 mL) and heated to reflux for 3 h. The organic solvent was removed under reduced pressure, and the residue was redissolved in diethyl ether (100 mL). The organic phase was washed with a saturated NaHCO_3 solution (50 mL), water (50 mL) and brine (50 mL), dried over anhydrous sodium sulfate and filtered. The organic solvent was removed under reduced pressure to give the thioester **A13** as an off-white solid (2.24 g, 99%). The crude product was used in the next step without further purification.

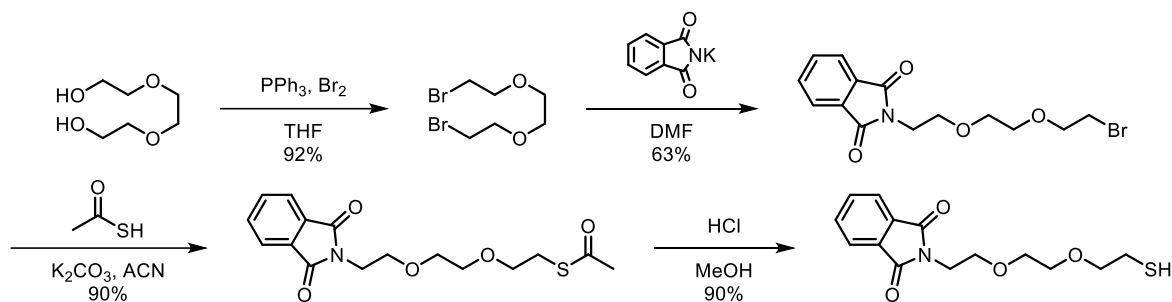
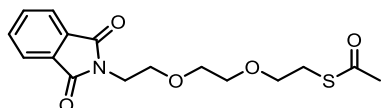
^1H NMR (500 MHz, CDCl_3) δ 7.84 (dd, J = 5.4, 3.0 Hz, 2H), 7.71 (dd, J = 5.5, 3.0 Hz, 2H), 3.90 (t, J = 6.5 Hz, 2H), 3.20 (t, J = 6.5 Hz, 2H), 2.31 (s, 3H).

2-(2-Mercaptoethyl)isoindoline-1,3-dione (**A14**)



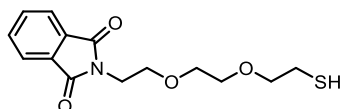
The thioester **A13** (2.24 g, 9 mmol) was dissolved in MeOH (30 mL) and conc. HCl (4 mL) was added at room temperature. The reaction mixture was stirred for 3 h and then concentrated under reduced pressure. The residue was redissolved in ethyl acetate (100 mL), and the organic phase was washed with saturated NaHCO_3 solution (50 mL), water (50 mL) and brine (50 mL), dried over anhydrous sodium sulfate and filtered. The organic solvent was removed under reduced pressure to give the thiol **A14** as a pale-yellow solid (1.64 g, 88%). The crude product was used in the next step without further purification.

^1H NMR (500 MHz, CDCl_3) δ 7.86 (dd, J = 5.5, 3.0 Hz, 2H), 7.73 (dd, J = 5.5, 3.0 Hz, 2H), 3.93 – 3.81 (m, 3H), 2.84 (ddd, J = 8.5, 7.2, 6.4 Hz, 3H), 1.43 (t, J = 8.6 Hz, 1H).

Synthesis of the thiol **A16**

 S-(2-(2-(2-(1,3-Dioxoisindolin-2-yl)ethoxy)ethoxy)ethyl) ethanethioate (**A15**)


The thioester **A15** was prepared according to a reported procedure.⁶⁴

¹H NMR (500 MHz, CDCl₃) δ 7.84 (dd, *J* = 5.4, 3.1 Hz, 2H), 7.71 (dd, *J* = 5.5, 3.0 Hz, 2H), 3.90 (t, *J* = 5.8 Hz, 2H), 3.74 (t, *J* = 5.8 Hz, 2H), 3.66 – 3.49 (m, 6H), 3.01 (t, *J* = 6.4 Hz, 2H), 2.31 (s, 3H).

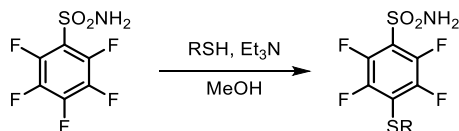
 2-(2-(2-(2-Mercaptoethoxy)ethoxy)ethyl)isindoline-1,3-dione (**A16**)


The thioester **A15** (1.4 g, 4.1 mmol) was dissolved in MeOH (50 mL) and conc. HCl (2 mL) was added at room temperature. The reaction mixture was heated under reflux for 3 h and then concentrated under reduced pressure. The residue was redissolved in ethyl acetate (100 mL), and the organic phase was washed with a saturated NaHCO₃ solution (50 mL), water (50 mL) and brine (50 mL), dried over anhydrous sodium sulfate and filtered. The organic solvent was removed under reduced pressure to give the thiol **A15** as a pale-yellow oil (1.1 g, 90%). The crude product was used in the next step without further purification.

¹H NMR (500 MHz, CDCl₃) δ 7.84 (dd, *J* = 5.4, 3.0 Hz, 2H), 7.71 (dd, *J* = 5.5, 3.0 Hz, 2H), 3.90 (t, *J* = 5.8 Hz, 1H), 3.75 (t, *J* = 5.8 Hz, 2H), 3.66 – 3.61 (m, 2H), 3.61 – 3.56 (m, 2H), 3.54 (t, *J* = 6.4 Hz, 2H), 2.60 (dt, *J* = 8.2, 6.4 Hz, 2H), 1.53 (t, *J* = 8.2 Hz, 1H).

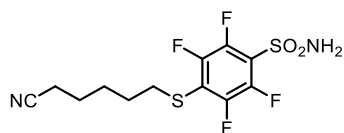
2,5,6-Trifluorobenzenesulfonamides

General procedure for the synthesis of **A17-A20** (**GP1**)⁶²



The sulfonamide **A8** (1 eq.), Et₃N (1.01 eq.) and the nucleophile (1.1 eq.) were dissolved in MeOH (0.133M). The reaction mixture was refluxed for 16 h. The reaction mixture was concentrated under reduced pressure, and the residue was purified to afford the desired product.

4-((5-Cyanopentyl)thio)-2,3,5,6-tetrafluorobenzenesulfonamide (**A17**)

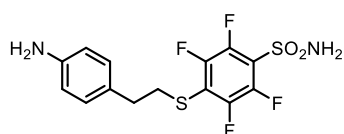


The sulfonamide **A17** was synthesized according to the general procedure **GP1** and purified by silica gel column chromatography (25% EtOAc in cyclohexane) to give the title compound as a white solid (1.28 g, 90%).

^1H NMR (500 MHz, CDCl_3) δ 5.44 (s, 2H), 3.07 (t, $J = 7.0$ Hz, 2H), 2.36 (t, $J = 6.9$ Hz, 2H), 1.67 (p, $J = 7.1$ Hz, 4H), 1.63 – 1.55 (m, 2H).

^{19}F NMR (471 MHz, CDCl_3) δ -131.81 – -132.11 (m), -138.02 – -138.50 (m).

4-((4-Aminophenethyl)thio)-2,3,5,6-tetrafluorobenzenesulfonamide (**A18**)

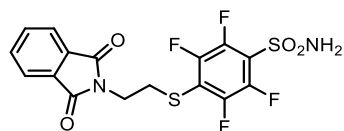


The aniline **A18** was synthesized according to the general procedure **GP1** and purified by silica gel column chromatography (33% EtOAc in cyclohexane) to give the title compound as a white solid (192 mg, 69%).

^1H NMR (500 MHz, CDCl_3) δ 6.92 (d, $J = 8.3$ Hz, 2H), 6.50 (d, $J = 8.4$ Hz, 2H), 6.35 (s, 2H), 3.64 (s, 2H), 3.40 – 3.30 (m, 2H), 2.98 (dd, $J = 7.1, 5.0$ Hz, 2H).

^{19}F NMR (471 MHz, CDCl_3) δ -130.53 – -131.14 (m), -139.59 – -140.02 (m).

4-((2-(1,3-Dioxoisindolin-2-yl)ethyl)thio)-2,3,5,6-tetrafluorobenzenesulfonamide (**A19**)

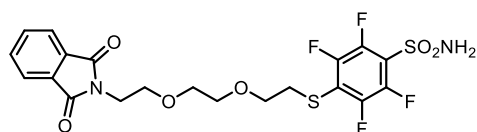


The sulfonamide **A19** was synthesized according to the general procedure **GP1** and purified by silica gel column chromatography (33% EtOAc in cyclohexane) to give the title compound as a white solid (1.44 g, 83%).

^1H NMR (500 MHz, CDCl_3) δ 7.84 (dd, $J = 5.5, 3.0$ Hz, 2H), 7.75 (dd, $J = 5.5, 3.0$ Hz, 2H), 5.38 (s, 2H), 3.92 (t, $J = 6.5$ Hz, 2H), 3.44 (t, $J = 6.5$ Hz, 2H).

^{19}F NMR (471 MHz, CDCl_3) δ -131.17 – -131.59 (m), -137.93 – -138.29 (m).

4-((2-(2-(2-(1,3-dioxoisindolin-2-yl)ethoxy)ethoxy)ethyl)thio)-2,3,5,6-tetrafluorobenzenesulfonamide (**A20**)



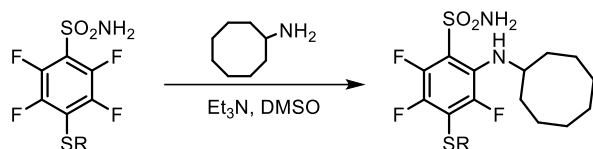
The sulfonamide **A20** was synthesized according to the general procedure **GP1** and purified by silica gel column chromatography (50% EtOAc in cyclohexane) to give the title compound as a white solid (1.09 g, 87%).

^1H NMR (500 MHz, CDCl_3) δ 7.83 (dd, $J = 5.4, 3.1$ Hz, 2H), 7.72 (dd, $J = 5.5, 3.0$ Hz, 2H), 6.02 (s, 2H), 3.83 (t, $J = 5.8$ Hz, 2H), 3.64 (td, $J = 5.8, 3.4$ Hz, 4H), 3.48 (s, 4H), 3.11 (t, $J = 5.8$ Hz, 2H).

^{19}F NMR (471 MHz, CDCl_3) δ -131.29 – -131.80 (m), -138.83 – -139.13 (m).

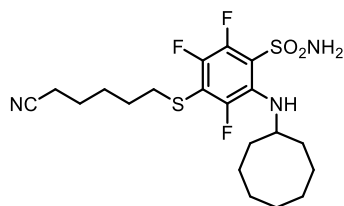
^{13}C NMR (126 MHz, CDCl_3) δ 168.67, 134.26, 132.07, 123.48, 121.29, 71.24, 70.51, 70.15, 67.96, 37.44, 34.02.

Synthesis of **A21-24 (GP2)**⁶⁵



A mixture of 2,3,5,6-tetrafluoro-4-[thio]benzenesulfonamide (1 eq.), Et_3N (1.04 eq), DMSO (5 mL/mmol), and cyclooctylamine (1.04 eq.) was stirred at 60 °C for 16 h. The mixture was then diluted with EtOAc and extracted with EtOAc three times. The combined organic phase was dried over MgSO_4 and concentrated under reduced pressure. The product was purified to give the desired product.

4-((5-Cyanopentyl)thio)-2-(cyclooctylamino)-3,5,6-trifluorobenzenesulfonamide (**A21**)



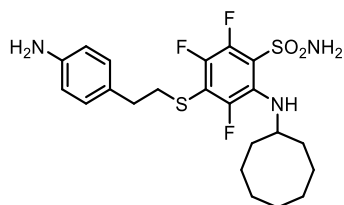
The cyclooctylaniline **A21** was synthesized according to the general procedure **GP2** and purified by silica gel column chromatography (20% EtOAc in cyclohexane) to give the title compound as a colourless oil (285 mg, 61%).

^1H NMR (500 MHz, CDCl_3) δ 6.16 (d, $J = 7.3$ Hz, 1H), 5.29 (s, 2H), 3.80 (dd, $J = 7.8, 3.5$ Hz, 1H), 2.98 (t, $J = 6.9$ Hz, 2H), 2.35 (t, $J = 6.9$ Hz, 2H), 1.86 (ddt, $J = 12.0, 8.4, 3.0$ Hz, 2H), 1.76 – 1.44 (m, 18H).

^{19}F NMR (471 MHz, CDCl_3) δ -119.81 (dd, $J = 11.4, 3.2$ Hz), -138.06 (dd, $J = 25.9, 11.4$ Hz), -144.58 (dd, $J = 25.9, 3.2$ Hz).

^{13}C NMR (126 MHz, CDCl_3) δ 132.65, 119.49, 56.22, 56.13, 33.81, 33.78, 33.75, 32.98, 29.34, 27.53, 27.37, 25.67, 24.98, 23.58, 17.24.

4-((4-Aminophenethyl)thio)-2-(cyclooctylamino)-3,5,6-trifluorobenzenesulfonamide (**A22**)



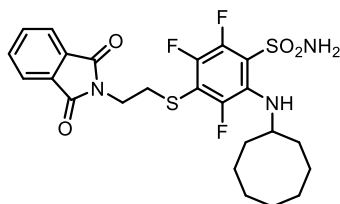
The cyclooctylaniline **A22** was synthesized according to the general procedure **GP2** and purified by silica gel column chromatography (25% EtOAc in cyclohexane) to give the title compound as a white solid (37 mg, 58%).

^1H NMR (500 MHz, CDCl_3) δ 6.94 (d, $J = 8.3$ Hz, 2H), 6.51 (d, $J = 8.4$ Hz, 2H), 5.98 (s, 2H), 3.74 (s, 1H), 3.58 (s, 2H), 3.24 (dd, $J = 7.1, 5.8$ Hz, 2H), 2.95 – 2.85 (m, 2H), 1.92 – 1.80 (m, 2H), 1.76 – 1.45 (m, 12H).

^{19}F NMR (471 MHz, CDCl_3) δ -119.63 (dd, J = 11.2, 3.2 Hz), -139.54 (dd, J = 26.1, 11.2 Hz), -143.25 (dd, J = 26.1, 3.2 Hz).

^{13}C NMR (126 MHz, CDCl_3) δ 143.65, 130.31, 129.88, 115.88, 56.29, 56.21, 37.41, 34.41, 33.16, 27.41, 27.06, 25.70, 23.64.

2-(Cyclooctylamino)-4-((2-(1,3-dioxisoindolin-2-yl)ethyl)thio)-3,5,6-trifluorobenzenesulfonamide (**A23**)



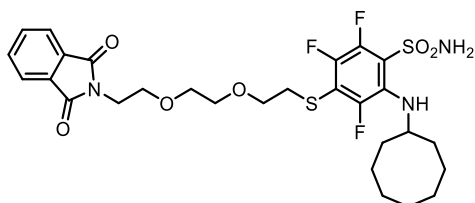
The cyclooctylaniline **A23** was synthesized according to the general procedure **GP2** and purified by silica gel column chromatography (25% EtOAc in cyclohexane) to give the title compound as a white solid (261 mg, 73%).

^1H NMR (500 MHz, CDCl_3) δ 7.82 (dd, J = 5.4, 3.1 Hz, 2H), 7.73 (dd, J = 5.5, 3.0 Hz, 2H), 6.11 (d, J = 8.4 Hz, 1H), 5.30 (d, J = 1.6 Hz, 2H), 3.91 (t, J = 6.7 Hz, 2H), 3.83 – 3.63 (m, 1H), 3.35 (t, J = 6.7 Hz, 2H), 1.93 – 1.76 (m, 2H), 1.74 – 1.61 (m, 2H), 1.59 – 1.53 (m, 8H).

^{19}F NMR (471 MHz, CDCl_3) δ -119.46 (dd, J = 11.3, 3.8 Hz), -138.00 (dd, J = 25.8, 11.4 Hz), -144.36 (dd, J = 25.8, 3.8 Hz).

^{13}C NMR (126 MHz, CDCl_3) δ 168.03, 134.36, 131.84, 123.51, 60.56, 56.22, 56.14, 37.77, 32.98, 31.70, 31.67, 31.64, 27.39, 27.05, 25.66, 23.56, 21.19, 14.33.

2-(Cyclooctylamino)-4-((2-(2-(2-(1,3-dioxisoindolin-2-yl)ethoxy)ethoxy)ethyl)thio)-3,5,6-trifluorobenzenesulfonamide (**A24**)

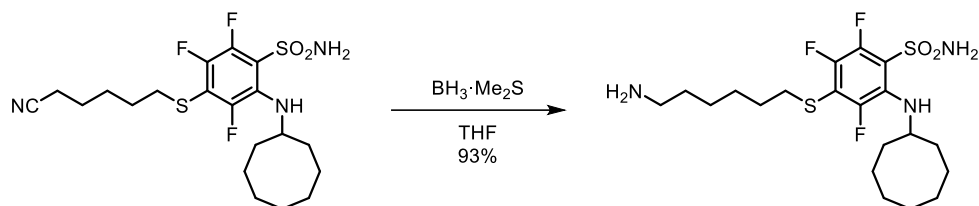


The cyclooctylaniline **A24** was synthesized according to the general procedure **GP2** and purified by silica gel column chromatography (40% EtOAc in cyclohexane) to give the title compound as a white solid (237 mg, 65%).

^1H NMR (500 MHz, CDCl_3) δ 7.84 (dd, J = 5.4, 3.0 Hz, 2H), 7.71 (dd, J = 5.4, 3.0 Hz, 2H), 6.13 (d, J = 7.9 Hz, 1H), 5.61 (s, 2H), 3.84 (t, J = 5.8 Hz, 2H), 3.77 (d, J = 3.8 Hz, 1H), 3.66 (t, J = 5.8 Hz, 2H), 3.60 (t, J = 6.2 Hz, 2H), 3.56 – 3.48 (m, 4H), 3.05 (t, J = 6.2 Hz, 2H), 1.83 (ddt, J = 11.9, 5.2, 2.8 Hz, 2H), 1.69 – 1.44 (m, 10H).

^{19}F NMR (471 MHz, CDCl_3) δ -119.45 (dd, J = 11.4, 3.0 Hz), -138.41 (dd, J = 26.1, 11.4 Hz), -144.00 (dd, J = 26.1, 3.0 Hz).

^{13}C NMR (126 MHz, CDCl_3) δ 168.57, 134.18, 132.16, 123.46, 70.94, 70.55, 70.15, 67.95, 56.22, 56.13, 37.40, 33.83, 33.80, 32.94, 27.37, 27.05, 25.64, 23.55.

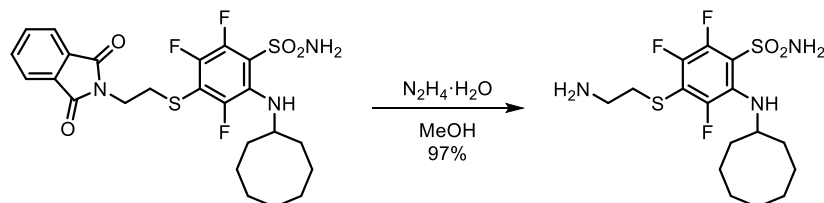
Synthesis of amines **A25-27**4-((6-Aminoethyl)thio)-2-(cyclooctylamino)-3,5,6-trifluorobenzenesulfonamide (**A25**)

The cyclooctylaniline **A21** (285 mg, 0.6 mmol) was dissolved in THF (10 mL) and $\text{BH}_3 \cdot \text{Me}_2\text{S}$ complex (570 μL , 6 mmol) was added dropwise at room temperature. The reaction mixture was stirred for 16 h, and then quenched by addition of HCl (1M, 25 mL). The reaction mixture was stirred for 30 min and then 2 M NaOH (15 mL) was added. The organic solvent was removed under reduced pressure and water phase was extracted with diethyl ether (5×20 mL). The combined organic phase was washed with water (20 mL) and brine (20 mL), dried over anhydrous sodium sulfate, filtered, and the organic solvent was removed under reduced pressure to give the amine **A25** as a colourless oil (261 mg, 93%). The crude product was used in the next step without further purification.

^1H NMR (500 MHz, CDCl_3) δ 6.16 (d, $J = 8.2$ Hz, 1H), 5.30 (s, 2H), 3.80 (tq, $J = 8.5, 4.7$ Hz, 1H), 2.98 (t, $J = 6.9$ Hz, 2H), 2.35 (t, $J = 6.9$ Hz, 2H), 1.86 (ddd, $J = 12.3, 5.7, 3.1$ Hz, 2H), 1.76 – 1.41 (m, 20H).

^{19}F NMR (471 MHz, CDCl_3) δ -119.82 (dd, $J = 11.4, 3.3$ Hz), -138.06 (dd, $J = 25.9, 11.4$ Hz), -144.59 (dd, $J = 25.9, 3.3$ Hz).

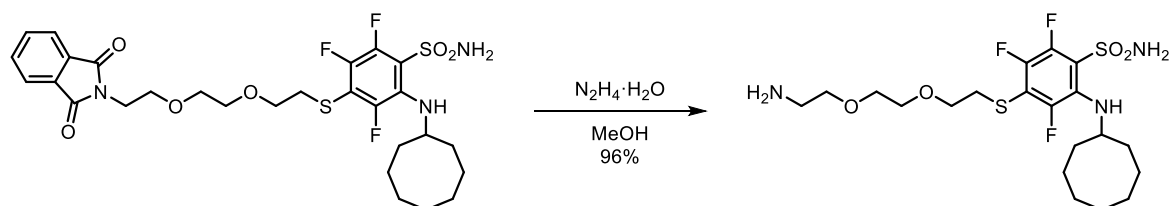
^{13}C NMR (126 MHz, CDCl_3) δ 119.49, 56.21, 56.13, 33.81, 33.78, 32.98, 29.34, 27.52, 27.37, 25.67, 24.98, 23.58, 17.24, 2.05.

4-((2-Aminoethyl)thio)-2-(cyclooctylamino)-3,5,6-trifluorobenzenesulfonamide (**A26**)

The cyclooctylaniline **A23** (108 mg, 0.2 mmol) was dissolved in MeOH (10 mL), and hydrazine hydrate (200 μL , 4 mmol) was added dropwise. The reaction mixture was stirred at room temperature for 16 h and then concentrated under reduced pressure. Chloroform (10 mL) was added, and the resulting suspension was sonicated for 5 min, and filtered through a pad of celite. The organic solvent was removed under reduced pressure to give the amine **A26** as a colourless oil (82 mg, 97%).

^1H NMR (500 MHz, CDCl_3) δ 6.17 (d, $J = 8.5$ Hz, 1H), 3.85 – 3.75 (m, 1H), 3.04 (t, $J = 6.2$ Hz, 2H), 2.86 (t, $J = 6.2$ Hz, 2H), 1.93 – 1.82 (m, 2H), 1.75 – 1.41 (m, 10H).

^{19}F NMR (471 MHz, CDCl_3) δ -119.51 (dd, $J = 11.5, 3.3$ Hz), -138.02 (dd, $J = 26.1, 11.5$ Hz), -144.31 (dd, $J = 26.1, 3.3$ Hz).

4-((2-(2-(2-Aminoethoxy)ethoxy)ethyl)thio)-2-(cyclooctylamino)-3,5,6-trifluorobenzenesulfonamide (**A27**)

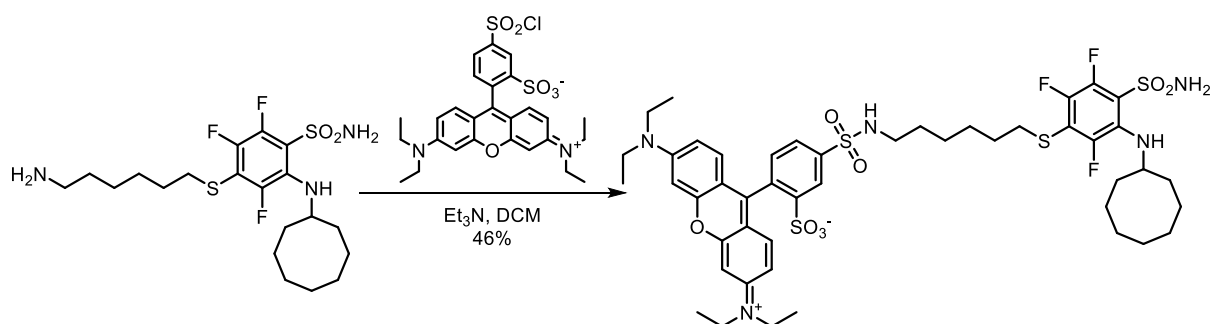
The cyclooctylaniline **A24** (126 mg, 0.2 mmol) was dissolved in MeOH (10 mL), and hydrazine hydrate (200 μ L, 4 mmol) was added dropwise. The reaction mixture was stirred at room temperature for 16 h and then concentrated under reduced pressure. Chloroform (10 mL) was added, and the resulting suspension was sonicated for 5 min, and filtered through a pad of celite. The organic solvent was removed under reduced pressure to give the amine **A27** as a colourless oil (100 mg, quant.). The crude product was used in the next step without further purification.

^1H NMR (500 MHz, CDCl_3) δ 3.78 (d, J = 3.3 Hz, 1H), 3.70 (t, J = 5.7 Hz, 2H), 3.55 – 3.49 (m, 2H), 3.46 (dt, J = 6.3, 3.1 Hz, 2H), 3.33 (t, J = 5.2 Hz, 2H), 3.11 (t, J = 5.7 Hz, 2H), 2.78 – 2.68 (m, 2H), 1.95 – 1.81 (m, 2H), 1.74 – 1.64 (m, 2H), 1.63 – 1.44 (m, 8H).

^{19}F NMR (471 MHz, CDCl_3) δ -119.43 (dd, J = 11.6, 2.8 Hz), -139.26 (dd, J = 26.3, 11.5 Hz), -143.74 (dd, J = 26.3, 2.9 Hz).

^{13}C NMR (126 MHz, CDCl_3) δ 72.74, 72.17, 70.78, 70.74, 56.25, 50.99, 41.27, 33.92, 33.04, 27.40, 25.68, 23.62.

5-(*N*-(6-((3-(cyclooctylamino)-2,5,6-trifluoro-4-sulfamoylphenyl)thio)hexyl)sulfamoyl)-2-(6-(diethylamino)-3-(diethyliminio)-3*H*-xanthen-9-yl)benzenesulfonate (**A28**)

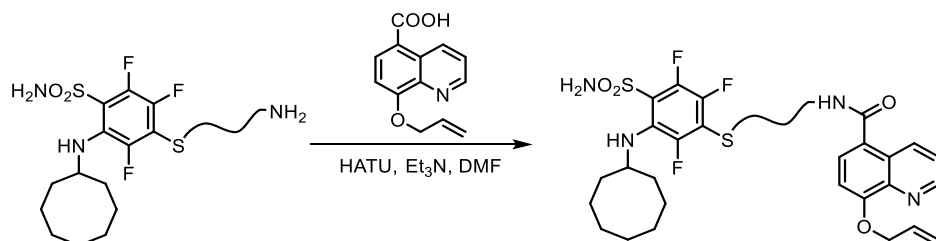


The amine **A25** (47 mg, 0.1 mmol), Sulforhodamine B acid chloride (58 mg, 0.1 mmol), and Et_3N (28 μ L, 0.2 mmol) were mixed in CH_2Cl_2 (5 mL) at room temperature. The reaction mixture was stirred for 16 h, concentrated under reduced pressure and purified by silica gel column chromatography (5% MeOH in CH_2Cl_2) to give the rhodamine **A28** as a mixture of two regioisomers as a pink solid (46 mg, 46%).

^1H NMR (500 MHz, CDCl_3) δ 8.75 – 8.53 (m, 1H), 8.10 – 7.91 (m, 1H), 7.39 – 7.13 (m, 2H), 7.06 (d, J = 7.8 Hz, 1H), 6.85 – 6.72 (m, 2H), 6.69 – 6.60 (m, 2H), 3.78 – 3.43 (m, 13H), 2.95 – 2.82 (m, 2H), 1.83 – 1.72 (m, 2H), 1.64 – 1.42 (m, 20H), 1.25 (t, J = 7.1 Hz, 12H).

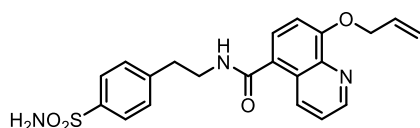
^{19}F NMR (471 MHz, CDCl_3) δ -119.59 – -120.56 (m), -137.22 – -138.22 (m), -143.96 – -145.12 (m).

General procedure for the synthesis of ligands **A29-33** (**GP3**)



The carboxylic acid **A1** (1 eq.) was dissolved in DMF (30 mL/mmol) and HATU (1.1 eq.) and Et_3N (1.2 eq.) were added. The mixture was stirred for 30 min and a solution of amine (1 eq.) in DMF (10 mL/mmol) was added dropwise. The reaction mixture was stirred at room temperature for 16 h, and then concentrated under reduced pressure. The residue was purified to give the desired product.

8-(Allyloxy)-*N*-(4-sulfamoylphenethyl)quinoline-5-carboxamide (**A29**)

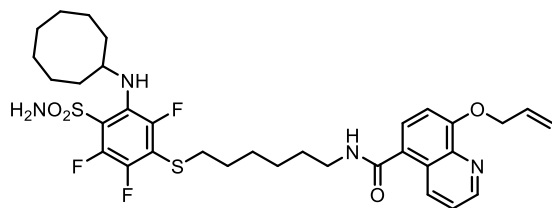


The arylsulfonamide **A29** was synthesized according to the general procedure **GP3** and purified by silica gel column chromatography (70% EtOAc in cyclohexane) to give the title compound as a white solid (29 mg, 35%).

^1H NMR (500 MHz, DMSO- d_6) δ 8.87 (dd, J = 4.0, 1.6 Hz, 1H), 8.58 (t, J = 5.6 Hz, 1H), 8.53 (dd, J = 8.6, 1.6 Hz, 1H), 7.76 (d, J = 8.2 Hz, 2H), 7.60 (d, J = 8.1 Hz, 1H), 7.56 (dd, J = 8.6, 4.1 Hz, 1H), 7.47 (d, J = 8.2 Hz, 2H), 7.31 (s, 2H), 7.20 (d, J = 8.2 Hz, 1H), 6.16 (ddd, J = 22.5, 10.5, 5.3 Hz, 1H), 5.51 (dd, J = 17.3, 1.6 Hz, 1H), 5.39 – 5.30 (m, 1H), 4.81 (d, J = 5.3 Hz, 2H), 3.58 (q, J = 6.8 Hz, 2H), 2.96 (t, J = 7.0 Hz, 2H).

^{13}C NMR (126 MHz, DMSO- d_6) δ 165.82, 153.63, 147.48, 142.15, 140.46, 137.84, 132.16, 131.71, 127.64, 124.98, 124.93, 124.45, 124.02, 120.59, 116.40, 116.32, 106.51, 67.39, 53.25, 53.25, 44.10, 33.12.

8-(Allyloxy)-*N*-(6-((3-(cyclooctylamino)-2,5,6-trifluoro-4-sulfamoylphenyl)thio)hexyl)quinoline-5-carboxamide (**A30**)

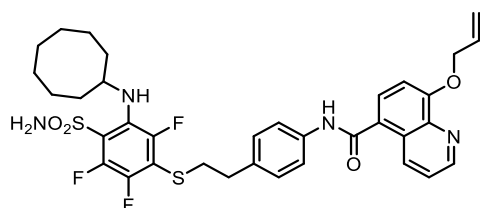


The arylsulfonamide **A30** was synthesized according to the general procedure **GP3** and purified by silica gel column chromatography (40% EtOAc in cyclohexane) to afford the title compound as a white solid (95 mg, 37%).

^1H NMR (500 MHz, CDCl_3) δ 8.94 (dd, J = 4.1, 1.6 Hz, 1H), 8.79 (dd, J = 8.6, 1.6 Hz, 1H), 7.59 (d, J = 8.0 Hz, 1H), 7.49 (dd, J = 8.6, 4.1 Hz, 1H), 6.97 (d, J = 8.1 Hz, 1H), 6.31 – 6.01 (m, 3H), 5.81 (s, 2H), 5.49 (dd, J = 17.3, 1.2 Hz, 1H), 5.43 – 5.34 (m, 1H), 4.86 (d, J = 5.5 Hz, 2H), 3.81 – 3.65 (m, 1H), 3.46 (q, J = 6.8 Hz, 2H), 2.97 (t, J = 7.1 Hz, 2H), 1.89 – 1.79 (m, 2H), 1.74 – 1.37 (m, 20H).

^{19}F NMR (471 MHz, CDCl_3) δ -120.04 (dd, J = 11.3, 3.2 Hz), -138.37 (dd, J = 26.0, 11.3 Hz), -144.77 (dd, J = 26.0, 3.2 Hz).

8-(Allyloxy)-*N*-(4-(2-((3-(cyclooctylamino)-2,5,6-trifluoro-4-sulfamoylphenyl)thio)ethyl)phenyl)quinoline-5-carboxamide (**A31**)



The arylsulfonamide **A31** was synthesized according to the general procedure **GP3** and purified by silica gel column chromatography (60% EtOAc in cyclohexane) to give the title compound as a white solid (57 mg, 82%).

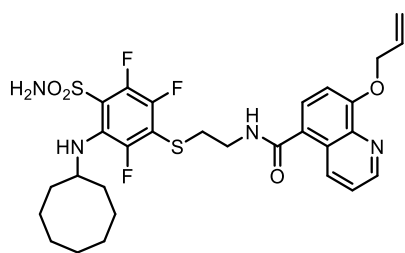
^1H NMR (500 MHz, CDCl_3) δ 8.87 (dd, J = 4.1, 1.6 Hz, 1H), 8.76 (dd, J = 8.6, 1.6 Hz, 1H), 8.31 (s, 1H), 7.68 (d, J = 8.1 Hz, 1H), 7.42 (dd, J = 8.6, 4.2 Hz, 3H), 7.09 (d, J = 8.4 Hz, 2H), 6.87 (d, J = 8.2

Hz, 1H), 6.23 (s, 2H), 6.20 – 5.98 (m, 2H), 5.45 (dd, $J = 17.3, 1.3$ Hz, 1H), 5.34 (dd, $J = 10.5, 1.2$ Hz, 1H), 4.77 (d, $J = 5.6$ Hz, 2H), 3.66 (s, 1H), 3.27 (t, $J = 6.7$ Hz, 2H), 2.95 (t, $J = 6.7$ Hz, 2H), 1.88 – 1.73 (m, 2H), 1.69 – 1.58 (m, 2H), 1.55 – 1.41 (m, 8H).

^{19}F NMR (471 MHz, CDCl_3) δ -119.43 (dd, $J = 11.1, 2.8$ Hz), -139.01 (dd, $J = 26.1, 11.2$ Hz), -144.22 (dd, $J = 26.2, 3.0$ Hz).

^{13}C NMR (126 MHz, CDCl_3) δ 171.34, 166.85, 156.26, 149.68, 139.85, 136.62, 135.37, 134.32, 132.39, 129.35, 127.21, 126.96, 125.75, 122.74, 120.34, 119.29, 107.45, 70.00, 60.52, 56.02, 55.94, 38.67, 37.06, 34.87, 32.98, 27.33, 27.01, 25.58, 23.53, 21.14, 14.28.

8-(Allyloxy)-*N*-(2-((3-(cyclooctylamino)-2,5,6-trifluoro-4-sulfamoylphenyl)thio)ethyl)quinoline-5-carboxamide (**A32**)

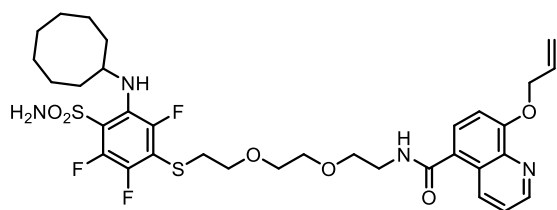


The arylsulfonamide **A32** was synthesized according to the general procedure **GP3** and purified by silica gel column chromatography (60% EtOAc in cyclohexane) to give the title compound as a white solid (72 mg, 58%).

^1H NMR (500 MHz, CDCl_3) δ 8.98 (dd, $J = 4.1, 1.5$ Hz, 1H), 8.89 (dd, $J = 8.6, 1.5$ Hz, 1H), 7.64 (d, $J = 8.1$ Hz, 1H), 7.53 (dd, $J = 8.6, 4.2$ Hz, 1H), 7.04 (d, $J = 8.1$ Hz, 1H), 6.48 (t, $J = 5.8$ Hz, 1H), 6.27 – 6.06 (m, 2H), 5.58 – 5.44 (m, 3H), 5.37 (d, $J = 9.5$ Hz, 1H), 4.89 (d, $J = 5.5$ Hz, 2H), 3.75 (s, 1H), 3.68 (q, $J = 5.9$ Hz, 2H), 3.26 (t, $J = 6.0$ Hz, 2H), 1.87 – 1.76 (m, 2H), 1.60 – 1.42 (m, 10H).

^{19}F NMR (471 MHz, CDCl_3) δ -120.01 (dd, $J = 11.6, 3.7$ Hz), -137.81 (dd, $J = 26.3, 11.6$ Hz), -144.67 (dd, $J = 26.3, 3.8$ Hz).

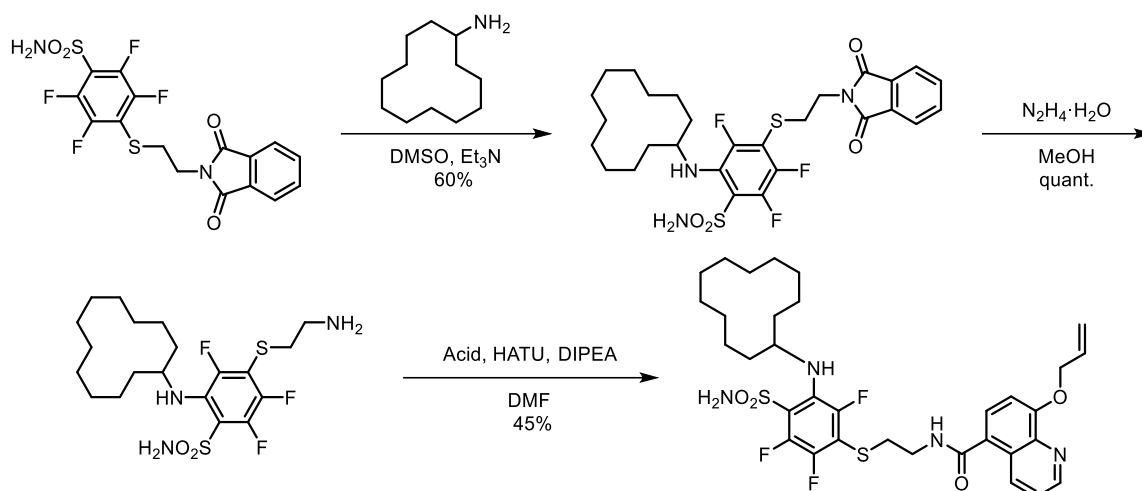
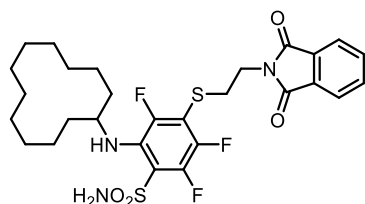
8-(Allyloxy)-*N*-(2-(2-(2-((3-(cyclooctylamino)-2,5,6-trifluoro-4-sulfamoylphenyl)thio)ethoxy)ethoxy)ethyl)quinoline-5-carboxamide (**A33**)



The arylsulfonamide **A33** was synthesized according to the general procedure **GP3** and purified by silica gel column chromatography (70% EtOAc in cyclohexane) to give the title compound as a white solid (70 mg, 49%).

^1H NMR (500 MHz, CDCl_3) δ 8.92 – 8.76 (m, 2H), 7.61 (d, $J = 8.0$ Hz, 1H), 7.45 (dd, $J = 8.6, 4.2$ Hz, 1H), 7.04 (s, 1H), 6.88 – 6.70 (m, 2H), 6.20 (ddt, $J = 16.3, 10.7, 5.8$ Hz, 1H), 5.86 (d, $J = 8.2$ Hz, 1H), 5.56 (d, $J = 17.2$ Hz, 1H), 5.49 – 5.40 (m, 1H), 4.69 (d, $J = 5.8$ Hz, 2H), 3.86 – 3.61 (m, 10H), 3.41 (s, 1H), 3.02 (t, $J = 5.6$ Hz, 2H), 1.86 – 1.34 (m, 12H).

^{19}F NMR (471 MHz, CDCl_3) δ -121.69 (dd, $J = 10.9, 3.3$ Hz), -138.79 (dd, $J = 26.1, 11.0$ Hz), -146.36 (dd, $J = 26.1, 3.3$ Hz).

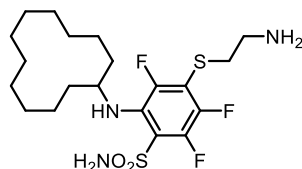
Synthesis of **A36**2-(Cyclododecylamino)-4-((2-(1,3-dioxoisindolin-2-yl)ethyl)thio)-3,5,6-trifluorobenzenesulfonamide (**A34**)

The cyclododecylaniline **A34** was synthesized according to the general procedure **GP2** and purified by silica gel column chromatography (40% EtOAc in cyclohexane) to give the title compound as a white solid (420 mg, 60%).

^1H NMR (500 MHz, $\text{DMSO}-d_6$) δ 8.06 (s, 2H), 7.90 – 7.74 (m, 4H), 6.13 (d, J = 8.2 Hz, 1H), 3.78 (t, J = 6.4 Hz, 2H), 3.62 (s, 1H), 3.35 (t, J = 6.4 Hz, 2H), 1.55 (d, J = 6.3 Hz, 2H), 1.39 – 1.24 (m, 20H).

^{19}F NMR (471 MHz, $\text{DMSO}-d_6$) δ -120.88 (dd, J = 11.3, 3.5 Hz), -137.15 (dd, J = 26.8, 11.5 Hz), -145.21 (dd, J = 26.8, 3.7 Hz).

^{13}C NMR (126 MHz, $\text{DMSO}-d_6$) δ 167.46, 134.54, 131.19, 122.92, 59.75, 52.40, 52.32, 37.58, 31.13, 30.10, 23.84, 23.62, 22.78, 22.64, 20.76, 20.57, 14.08.

4-((2-Aminoethyl)thio)-2-(cyclododecylamino)-3,5,6-trifluorobenzenesulfonamide (**A35**)

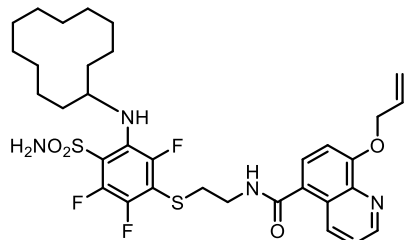
The cyclododecylaniline **A34** (210 mg, 0.35 mmol) was dissolved in MeOH (10 mL), and hydrazine hydrate (500 μL , 10 mmol) was added dropwise. The reaction mixture was stirred at room temperature for 16 h and then concentrated under reduced pressure. Chloroform (10 mL) was added, and the resulting suspension was sonicated for 5 min, and filtered through a pad of celite. The organic solvent was removed under reduced pressure to give the crude amine **A35** as a colourless oil (173 mg, quant.). The crude product was used in the next step without further purification.

^1H NMR (500 MHz, CDCl_3) δ 6.10 (d, J = 8.5 Hz, 1H), 3.78 (s, 1H), 3.03 (t, J = 6.1 Hz, 2H), 2.85 (t, J = 6.1 Hz, 2H), 1.62 (dt, J = 14.0, 6.0 Hz, 2H), 1.48 – 1.24 (m, 20H).

^{19}F NMR (471 MHz, CDCl_3) δ -119.54 (dd, J = 11.5, 3.3 Hz), -138.01 (dd, J = 26.1, 11.5 Hz), -144.52 (dd, J = 26.1, 3.4 Hz).

^{13}C NMR (126 MHz, CDCl_3) δ 149.65, 147.71, 143.98, 140.86, 133.25, 133.13, 117.31, 117.21, 53.43, 53.35, 41.36, 38.45, 38.42, 38.40, 30.83, 24.49, 24.21, 23.35, 23.22, 21.17.

8-(Allyloxy)-*N*-(2-((3-(cyclododecylamino)-2,5,6-trifluoro-4-sulfamoylphenyl)thio)ethyl)quinoline-5-carboxamide (**A36**)



The arylsulfonamide **A36** was synthesized according to the general procedure **GP3** and purified by silica gel column chromatography (33% EtOAc in cyclohexane) to give the title compound as a white solid (50 mg, 45%).

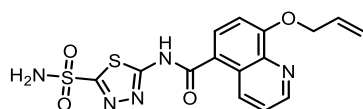
^1H NMR (500 MHz, $\text{DMSO}-d_6$) δ 8.88 (dd, $J = 4.1, 1.7$ Hz, 1H), 8.77 (dd, $J = 8.6, 1.7$ Hz, 1H), 8.62 (t, $J = 5.5$ Hz, 1H), 8.14 (s, 2H), 7.61 (d, $J = 8.1$ Hz, 1H), 7.57 (dd, $J = 8.6, 4.1$ Hz, 1H), 7.21 (d, $J = 8.2$ Hz, 1H), 6.26 – 6.09 (m, 2H), 5.51 (dq, $J = 17.3, 1.6$ Hz, 1H), 5.33 (dd, $J = 10.5, 1.6$ Hz, 1H), 4.82 (d, $J = 5.3$ Hz, 2H), 3.66 (s, 1H), 3.47 (q, $J = 6.5$ Hz, 2H), 3.24 (t, $J = 6.6$ Hz, 2H), 1.59 – 1.45 (m, 2H), 1.37 – 1.20 (m, 20H).

^{19}F NMR (471 MHz, $\text{DMSO}-d_6$) δ -120.48 (d, $J = 9.0$ Hz), -137.11 (dd, $J = 27.1, 11.5$ Hz), -144.89 – -145.21 (m).

^{13}C NMR (126 MHz, $\text{DMSO}-d_6$) δ 167.44, 155.49, 149.11, 139.52, 133.85, 133.32, 126.95, 126.67, 125.45, 122.21, 118.00, 108.08, 69.03, 30.19, 23.71, 23.46, 22.79, 22.63, 20.61.

Azolamide derivatives

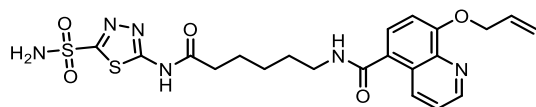
8-(Allyloxy)-*N*-(5-sulfamoyl-1,3,4-thiadiazol-2-yl)quinoline-5-carboxamide (**A37**)



The sulfonamide **A37** was synthesized according to general procedure **GP3** and purified by silica gel column chromatography (60% EtOAc in cyclohexane) to give the title compound as a white solid (50 mg, 61%).

^1H NMR (500 MHz, MeOD) δ 8.89 (dd, $J = 4.3, 1.6$ Hz, 1H), 8.25 (dd, $J = 8.5, 1.6$ Hz, 1H), 7.68 (dd, $J = 8.5, 4.3$ Hz, 1H), 7.57 – 7.49 (m, 1H), 7.29 (d, $J = 8.0$ Hz, 1H), 6.23 (dddd, $J = 16.0, 12.9, 6.6, 4.3$ Hz, 1H), 5.51 (dq, $J = 17.3, 1.6$ Hz, 1H), 5.38 – 5.31 (m, 1H), 4.90 (dt, $J = 5.4, 1.4$ Hz, 3H).

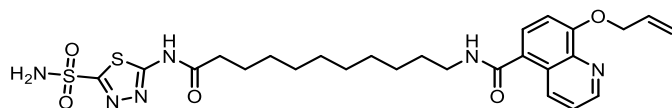
8-(Allyloxy)-*N*-(6-oxo-6-((5-sulfamoyl-1,3,4-thiadiazol-2-yl)amino)hexyl)quinoline-5-carboxamide (**A38**)



The sulfonamide **A38** was synthesized according to the general procedure **GP3** and purified by silica gel column chromatography (60% EtOAc in cyclohexane) to give the title compound as a white solid (41 mg, 41%).

^1H NMR (500 MHz, MeOD) δ 8.91 – 8.79 (m, 2H), 7.86 (d, J = 8.4 Hz, 1H), 7.67 (dd, J = 8.6, 4.3 Hz, 1H), 7.25 (d, J = 8.2 Hz, 1H), 6.21 (ddt, J = 16.1, 10.7, 5.4 Hz, 1H), 5.57 – 5.48 (m, 1H), 5.40 – 5.32 (m, 1H), 4.91 (d, J = 5.4 Hz, 2H), 3.44 (t, J = 7.1 Hz, 2H), 2.37 (t, J = 7.4 Hz, 2H), 1.68 (ddt, J = 11.1, 7.4, 3.9 Hz, 4H), 1.54 – 1.41 (m, 2H), 1.40 – 1.29 (m, 2H).

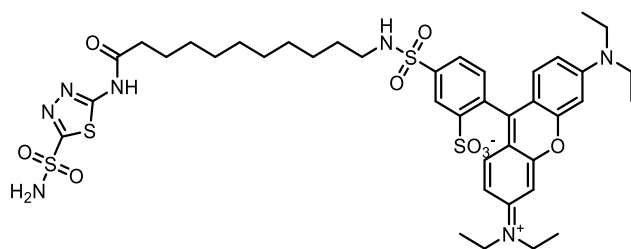
8-(Allyloxy)-*N*-(11-oxo-11-((5-sulfamoyl-1,3,4-thiadiazol-2-yl)amino)undecyl)quinoline-5-carboxamide (**A39**)



The sulfonamide **A39** was synthesized according to the general procedure **GP3** and purified by silica gel column chromatography (50% EtOAc in cyclohexane) to give the title compound as a white solid (38 mg, 33%).

^1H NMR (500 MHz, MeOD) δ 8.84 (d, J = 3.2 Hz, 1H), 8.77 (d, J = 8.6 Hz, 1H), 7.70 (d, J = 8.1 Hz, 1H), 7.61 (dd, J = 8.5, 4.1 Hz, 1H), 7.20 (d, J = 8.1 Hz, 1H), 6.22 (ddt, J = 16.1, 10.6, 5.3 Hz, 1H), 5.50 (d, J = 17.3 Hz, 1H), 5.33 (d, J = 10.5 Hz, 1H), 4.88 (d, J = 5.1 Hz, 2H), 3.43 (t, J = 7.1 Hz, 2H), 2.30 (t, J = 7.4 Hz, 2H), 1.72 – 1.55 (m, 4H), 1.51 – 1.27 (m, 12H)

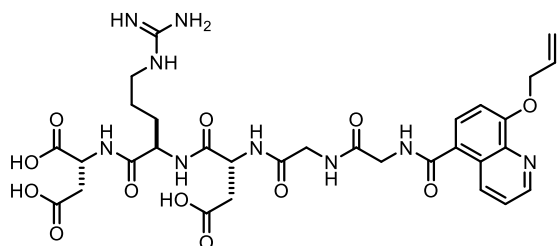
2-(6-(Diethylamino)-3-(diethyliminio)-3*H*-xanthen-9-yl)-5-(*N*-(11-oxo-11-((5-sulfamoyl-1,3,4-thiadiazol-2-yl)amino)undecyl)sulfamoyl)benzenesulfonate (**A39-SRB**)



11-Amino-*N*-(5-sulfamoyl-1,3,4-thiadiazol-2-yl)undecanamide (36 mg, 0.1 mmol), Sulforhodamine B acid chloride (58 mg, 0.1 mmol), and Et₃N (28 μL , 0.2 mmol) were mixed in CH₂Cl₂ (5 mL) at room temperature. The reaction mixture was stirred for 16 h, concentrated under reduced pressure and purified by silica gel column chromatography (5% MeOH in CH₂Cl₂) to give the rhodamine **A39-SRB** as a mixture of two regioisomers as a pink solid (38 mg, 42%).

^1H NMR (500 MHz, MeOD) δ 8.64 (d, J = 1.7 Hz, 1H), 8.10 (dd, J = 7.9, 1.7 Hz, 1H), 7.52 (d, J = 7.9 Hz, 1H), 7.11 (d, J = 9.5 Hz, 2H), 6.99 (dd, J = 9.5, 2.3 Hz, 2H), 6.94 (d, J = 2.3 Hz, 2H), 3.71 – 3.63 (m, 8H), 3.04 – 2.98 (m, 2H), 2.29 (t, J = 7.4 Hz, 2H), 1.65 – 1.48 (m, 4H), 1.37 – 1.28 (m, 24H).

(8-(Allyloxy)quinoline-5-carbonyl)glycylglycyl-*L*-aspartyl-*L*-arginyl-*L*-aspartic acid (**DRDGG-QA**)

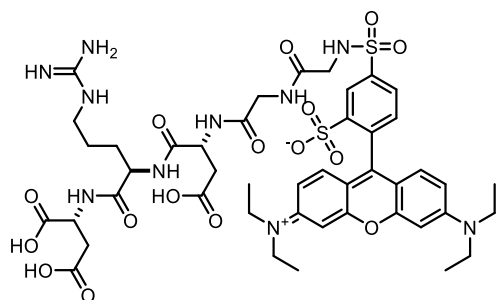


Commercially available pre-loaded Fmoc-Asp(OtBu)-OH on trityl resin (200 mg, 0.12 mmol) was swollen first in CH₂Cl₂ (3 \times 5 min \times 2 mL) and then in DMF (3 \times 5 min \times 2 mL). Then it was sequentially loaded with Fmoc-Arg(Pbf)-OH, Fmoc-Asp(OtBu)-OH, Fmoc-Gly-OH, Fmoc-Gly-OH, and **A1**. Analytical sample was obtained by cleavage with 20% TFA in CH₂Cl₂ and purification by reversed-

phase HPLC (95% A / 5% B to 30% A / 70% B over 30 min). After lyophilization the title compound was collected as a white powder.

¹H NMR (500 MHz, D₂O) δ 8.75 (dd, *J* = 4.3, 1.5 Hz, 1H), 8.65 (dd, *J* = 8.7, 1.6 Hz, 1H), 7.77 (d, *J* = 8.2 Hz, 1H), 7.58 (dd, *J* = 8.7, 4.3 Hz, 1H), 7.16 (d, *J* = 8.3 Hz, 1H), 6.13 (ddd, *J* = 22.8, 10.7, 5.5 Hz, 1H), 5.43 (dd, *J* = 17.3, 1.4 Hz, 1H), 5.31 (dd, *J* = 10.5, 1.2 Hz, 1H), 4.82 – 4.77 (m, 2H), 4.60 – 4.49 (m, 2H), 4.44 (t, *J* = 6.5 Hz, 1H), 4.20 (s, 2H), 4.07 – 3.91 (m, 2H), 3.74 (s, 2H), 3.13 – 2.96 (m, 3H), 2.76 – 2.46 (m, 8H), 2.31 – 2.20 (m, 2H), 1.46 (p, *J* = 7.6 Hz, 2H), 1.35 (p, *J* = 7.2 Hz, 2H), 1.15 (p, *J* = 7.4 Hz, 2H).

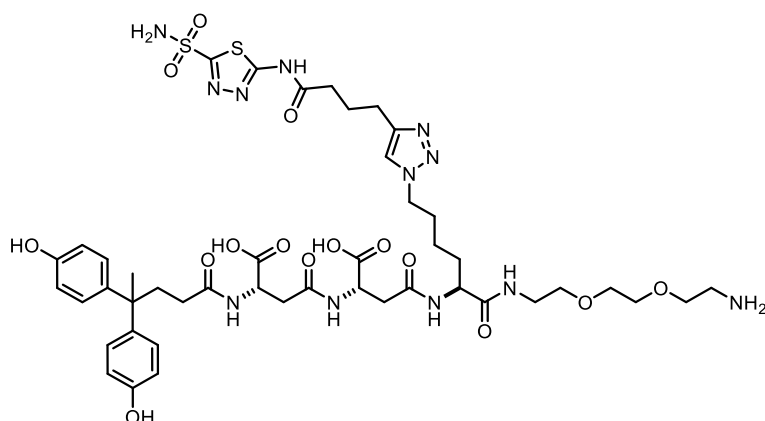
5-(*N*-(((6*S*,9*S*)-1-Amino-9-(carboxymethyl)-6-(((*S*)-1,2-dicarboxyethyl)carbamoyl)-1-imino-8,11,14-trioxo-2,7,10,13-tetraazapentadecan-15-yl)sulfamoyl)-2-(6-(diethylamino)-3-(diethyliminio)-3*H*-xanthen-9-yl)benzenesulfonate (**DRDGG-SRB**)



Commercially-available pre-loaded Fmoc-Asp(OtBu)-OH on trityl resin (200 mg, 0.12 mmol) was swollen first in CH₂Cl₂ (3 × 5 min × 2 mL) and then in DMF (3 × 5 min × 2 mL). Then it was sequentially loaded with Fmoc-Arg(Pbf)-OH, Fmoc-Asp(OtBu)-OH, Fmoc-Gly-OH, Fmoc-Gly-OH, and Sulforhodamine B acid chloride. An analytically pure sample was obtained by cleavage with 20% TFA in CH₂Cl₂ and purification by reversed-phase HPLC (95% A / 5% B to 20% A / 80% B over 30 min). After lyophilization the title compound was collected as a pink powder.

A40 and its derivatives

*N*⁴-((*S*)-1-((2-(2-(2-aminoethoxy)ethoxy)ethyl)amino)-1-oxo-6-(4-(4-oxo-4-((5-sulfamoyl-1,3,4-thiadiazol-2-yl)amino)butyl)-1*H*-1,2,3-triazol-1-yl)hexan-2-yl)-*N*²-((*S*)-3-(4,4-bis(4-hydroxyphenyl)pentanamido)-3-carboxypropanoyl)-*L*-asparagine (**A40**)



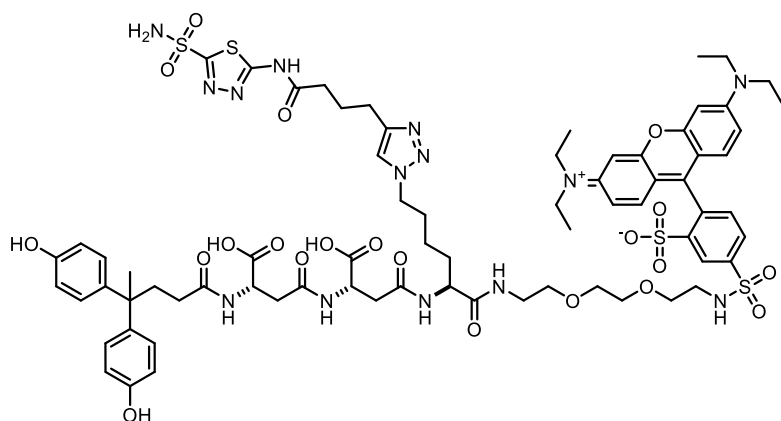
Commercially-available pre-loaded *O*-bis-(aminoethyl)ethylene glycol on trityl resin (200 mg, 0.12 mmol) was swollen first in CH₂Cl₂ (3 × 5 min × 2 mL) and then in DMF (3 × 5 min × 2 mL). Fmoc-protected azidolysine (142 mg, 0.36 mmol), HBTU (137 mg, 0.36 mmol), HOBt·H₂O (55 mg, 0.36 mmol) and DIPEA (119 μL, 0.72 mmol) were dissolved in DMF (2 mL), the mixture was allowed to stand at 22 °C for 15 min and then reacted with the resin for 1 h under gentle agitation. After washing with DMF (6 × 1 min × 2 mL) the Fmoc group was removed with 20% piperidine in DMF (1 × 2 min × 2 mL and 2 × 10 min × 2 mL) and the resin washed with DMF (6 × 1 min × 2 mL) before the peptide

was extended with 4,4-Bis(4-hydroxyphenyl)valeric acid (103 mg, 0.36 mmol) using the same coupling conditions (HBTU/HOBt-H₂O/DIPEA) described above. After the last peptide coupling step with the azidolysine, a solution of CuI (2.3 mg, 0.01 mmol), TBTA (6.4 mg, 0.01 mmol) and alkyne (99 mg, 0.36 mmol) in a mixture of DMF (1 mL) and THF (1 mL) was prepared and reacted with the resin at 22 °C for 2 h. After washing with DMF (6 × 1 min × 2 mL), the compound was cleaved by agitating the resin with a mixture of TFA (4.5 mL), TIPS (250 µL) and H₂O (250 µL) at 22 °C for 2 h. The resin was washed with TFA (1 × 5 min × 2 mL) and the combined cleavage and washing solutions added dropwise to ice cold diethyl ether (50 mL). The precipitate was collected by centrifugation and the product purified by reversed-phase HPLC (95% A / 5% B to 20% A / 80% B over 30 min). After lyophilization the title compound was collected as a white powder (52 mg, 61 µmol, 51% yield).

¹H NMR (500 MHz, DMSO-*d*₆): δ 13.01 (s, 1H), 9.20 (brs, 2H), 8.33 (s, 2H), 7.90 (t, *J* = 5.7 Hz, 1H), 7.88 (d, *J* = 8.0 Hz, 1H), 7.84 (s, 1H), 7.80 (brs, 3H), 6.93 (dd, *J* = 8.6, 1.4 Hz, 4H), 6.64 (d, *J* = 8.6 Hz, 4H), 4.25 (t, *J* = 7.1 Hz, 2H), 4.14 (td, *J* = 8.5, 5.4 Hz, 1H), 3.60 – 3.51 (m, 6H), 3.37 (t, *J* = 6.1 Hz, 2H), 3.17 (qd, *J* = 6.0, 2.0 Hz, 2H), 2.97 (sext, *J* = 5.6 Hz, 2H), 2.64 (t, *J* = 7.5 Hz, 2H), 2.58 (t, *J* = 7.4 Hz, 2H), 2.19 – 2.13 (m, 2H), 1.93 (pent, *J* = 7.5 Hz, 2H), 1.94 – 1.84 (m, 2H), 1.80 – 1.70 (m, 2H), 1.62 – 1.54 (m, 1H), 1.52 – 1.41 (m, 1H), 1.46 (s, 3H), 1.26 – 1.12 (m, 2H).

¹³C NMR (126 MHz, DMSO-*d*₆) δ 172.91, 172.87, 172.48, 172.16, 171.76, 169.33, 169.21, 164.41, 161.19, 158.43, 155.01, 146.17, 139.75, 139.68, 127.90, 121.95, 114.78, 69.74, 69.53, 68.90, 66.75, 52.45, 49.17, 48.79, 43.92, 38.80, 38.61, 37.20, 37.02, 34.34, 31.34, 29.48, 27.43, 24.47, 24.30, 22.34.

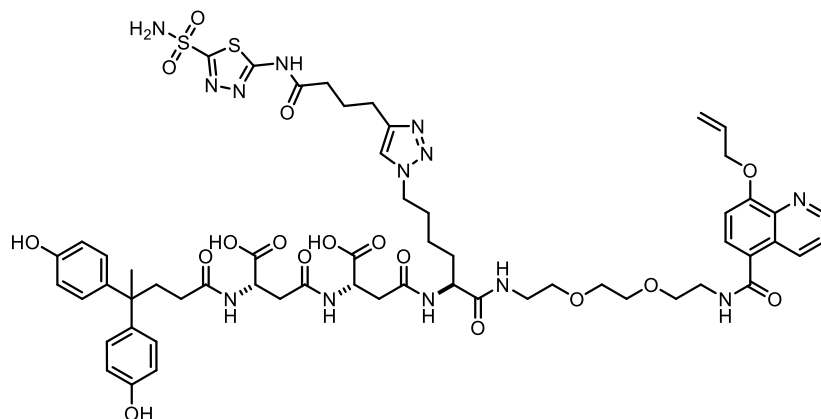
5-(*N*-((11*S*,15*S*,19*S*)-15,19-Dicarboxy-24,24-bis(4-hydroxyphenyl)-10,13,17,21-tetraoxo-11-(4-(4-oxo-4-((5-sulfamoyl-1,3,4-thiadiazol-2-yl)amino)butyl)-1*H*-1,2,3-triazol-1-yl)butyl)-3,6-dioxo-9,12,16,20-tetraazapentacosyl)sulfamoyl)-2-(6-(diethylamino)-3-(diethyliminio)-3*H*-xanthen-9-yl)benzenesulfonate (**A40-SRB**)



The amine **A40** (54 mg, 0.05 mmol), Sulforhodamine B acid chloride (34.5 mg, 0.06 mmol) and DIPEA (89 µL, 0.5 mmol) was dissolved in DMF and stirred for 16 h at room temperature. The reaction mixture was concentrated and purified by reversed-phase HPLC (95% A / 5% B to 30% A / 70% B over 40 min). After lyophilization the peptide **A40-SRB** was collected as a pink powder (49 mg, 61% yield).

¹H NMR (500 MHz, DMSO-*d*₆) δ 12.92 (s, 1H), 9.11 (s, 2H), 8.34 (s, 1H), 8.24 (s, 2H), 8.09 (d, *J* = 7.6 Hz, 1H), 7.98 (t, *J* = 5.7 Hz, 2H), 7.87 (d, *J* = 8.0 Hz, 1H), 7.82 (d, *J* = 7.5 Hz, 2H), 7.75 (s, 1H), 7.40 (d, *J* = 7.9 Hz, 1H), 7.21 (s, 1H), 7.11 (s, 1H), 7.01 (s, 1H), 6.95 (d, *J* = 9.6 Hz, 2H), 6.89 (d, *J* = 9.4 Hz, 2H), 6.84 (d, *J* = 7.9 Hz, 6H), 6.56 (d, *J* = 8.3 Hz, 4H), 6.16 (s, 1H), 4.48 – 4.32 (m, 2H), 4.21 – 4.04 (m, 2H), 2.97 – 2.90 (m, 2H), 2.58 – 2.48 (m, 6H), 2.13 – 2.05 (m, 2H), 1.90 – 1.80 (m, 2H), 1.67 (d, *J* = 6.2 Hz, 2H), 1.54 (s, 2H), 1.40 (s, 1H), 1.12 (t, *J* = 6.8 Hz, 12H).

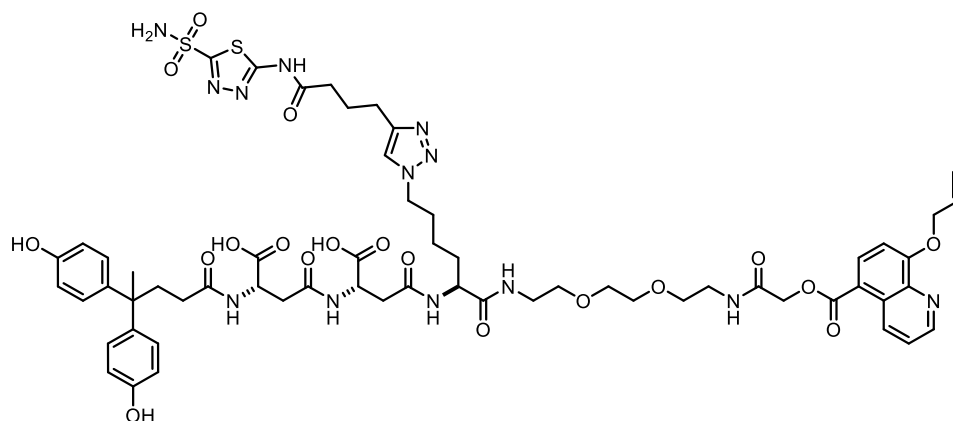
*N*⁴-((*S*)-1-(8-(Allyloxy)quinolin-5-yl)-1,12-dioxo-17-(4-(4-oxo-4-((5-sulfamoyl-1,3,4-thiadiazol-2-yl)amino)butyl)-1*H*-1,2,3-triazol-1-yl)-5,8-dioxo-2,11-diazaheptadecan-13-yl)-*N*²-((*S*)-3-(4,4-bis(4-hydroxyphenyl)pentanamido)-3-carboxypropanoyl)-*L*-asparagine (**A40-QA**)



To a solution of the carboxylic acid **A1** (23 mg, 0.1 mmol) in DMF (500 μ L), HATU (34 mg, 0.09 mmol) and DIPEA (16 μ L, 0.09 mmol) were added. The mixture was stirred for 30 min and a solution of the amine **A40** (54 mg, 0.05 mmol) in DMF (200 μ L) was slowly added. The reaction mixture was stirred for 8 h, concentrated and purified by reversed-phase HPLC (90% A / 10% B to 30% A / 70% B over 30 min). After lyophilization the title compound was collected as a white powder (53 mg, 82% yield).

¹H NMR (500 MHz, DMSO-*d*₆) δ 12.99 (s, 1H), 12.16 (brs, 1H), 9.13 (s, 2H), 8.96 – 8.92 (m, 1H), 8.89 (d, *J* = 8.5 Hz, 1H), 8.57 (t, *J* = 5.6 Hz, 1H), 8.32 (s, 2H), 8.16 (d, *J* = 8.0 Hz, 1H), 8.04 (d, *J* = 8.1 Hz, 1H), 7.93 – 7.87 (m, 2H), 7.82 (s, 1H), 7.74 (d, *J* = 8.1 Hz, 1H), 7.69 (dd, *J* = 8.4, 4.1 Hz, 1H), 7.30 (d, *J* = 8.2 Hz, 1H), 6.92 (d, *J* = 8.3 Hz, 4H), 6.64 (d, *J* = 8.3 Hz, 4H), 6.16 (ddt, *J* = 15.8, 10.6, 5.3 Hz, 1H), 5.52 (dd, *J* = 17.3, 1.6 Hz, 1H), 5.33 (dd, *J* = 10.5, 1.4 Hz, 1H), 4.85 (d, *J* = 5.1 Hz, 2H), 4.54 – 4.42 (m, 2H), 4.31 – 4.13 (m, 3H), 3.23 – 3.13 (m, 2H), 2.68 – 2.56 (m, 6H), 2.49 – 2.41 (m, 1H), 2.21 – 2.12 (m, 2H), 1.93 (p, *J* = 6.9, 6.4 Hz, 2H), 1.89 – 1.80 (m, 2H), 1.80 – 1.69 (m, 2H), 1.68 – 1.57 (m, 1H), 1.55 – 1.41 (m, 1H), 1.32 – 1.15 (m, 2H).

*N*⁴-((*S*)-1-(8-(allyloxy)quinolin-5-yl)-1,4,15-trioxo-20-(4-(4-oxo-4-((5-sulfamoyl-1,3,4-thiadiazol-2-yl)amino)butyl)-1*H*-1,2,3-triazol-1-yl)-2,8,11-trioxo-5,14-diazaicosan-16-yl)-*N*²-((*S*)-3-(4,4-bis(4-hydroxyphenyl)pentanamido)-3-carboxypropanoyl)-*L*-asparagine (**A40-COCH₂-QA**)

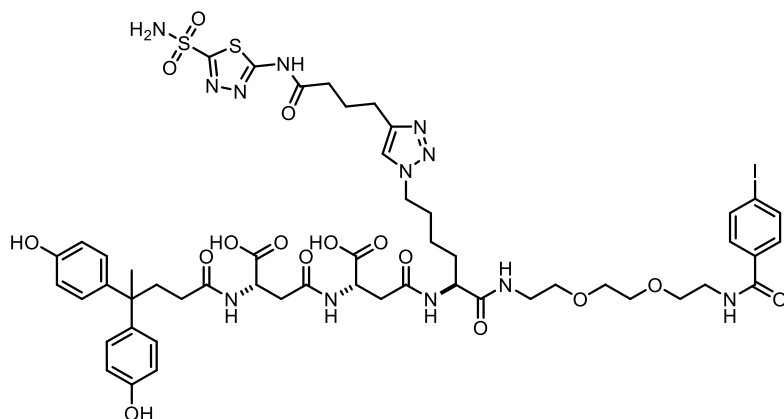


To a solution of the carboxylic acid **A7** (29 mg, 0.1 mmol) in DMF (500 μ L), HATU (34 mg, 0.09 mmol) and DIPEA (16 μ L, 0.09 mmol) were added. The mixture was stirred for 30 min and a solution of the amine **A40** (54 mg, 0.05 mmol) in DMF (200 μ L) was slowly added. The reaction mixture was stirred for 8 h, concentrated and purified by reversed-phase HPLC (90% A / 10% B to 30% A / 70% B over 30 min). After lyophilization the title compound was collected as a white powder (58 mg, 87% yield).

¹H NMR (500 MHz, DMSO-*d*₆) δ 12.98 (s, 1H), 12.57 (s, 2H), 9.32 (dd, *J* = 8.8, 1.6 Hz, 1H), 9.14 (s, 2H), 8.98 – 8.88 (m, 1H), 8.36 (d, *J* = 8.4 Hz, 1H), 8.31 (s, 2H), 8.22 (t, *J* = 5.6 Hz, 1H), 8.16 (d, *J* = 8.0

Hz, 1H), 8.04 (d, $J = 8.1$ Hz, 1H), 7.92 – 7.86 (m, 2H), 7.82 (s, 1H), 7.70 (dd, $J = 8.8, 4.1$ Hz, 1H), 7.32 (d, $J = 8.5$ Hz, 1H), 6.92 (d, $J = 8.2$ Hz, 4H), 6.64 (d, $J = 8.3$ Hz, 4H), 6.18 (ddt, $J = 17.2, 10.6, 5.3$ Hz, 1H), 5.53 (dq, $J = 17.3, 1.6$ Hz, 1H), 5.35 (dd, $J = 10.5, 1.6$ Hz, 1H), 4.88 (d, $J = 5.4$ Hz, 2H), 4.78 (s, 2H), 4.49 (ddd, $J = 13.8, 11.2, 6.9$ Hz, 2H), 4.27 – 4.12 (m, 3H), 3.56 – 3.48 (m, 4H), 3.45 (t, $J = 5.9$ Hz, 2H), 3.32 – 3.25 (m, 2H), 3.23 – 3.10 (m, 2H), 2.68 – 2.55 (m, 6H), 2.49 – 2.42 (m, 2H), 2.19 – 2.13 (m, 2H), 1.94 (p, $J = 7.4$ Hz, 2H), 1.89 – 1.81 (m, 2H), 1.78 – 1.71 (m, 2H), 1.69 – 1.58 (m, 1H), 1.48 (dt, $J = 10.1, 5.2$ Hz, 1H), 1.23 (dq, $J = 16.7, 8.9, 7.8$ Hz, 2H).

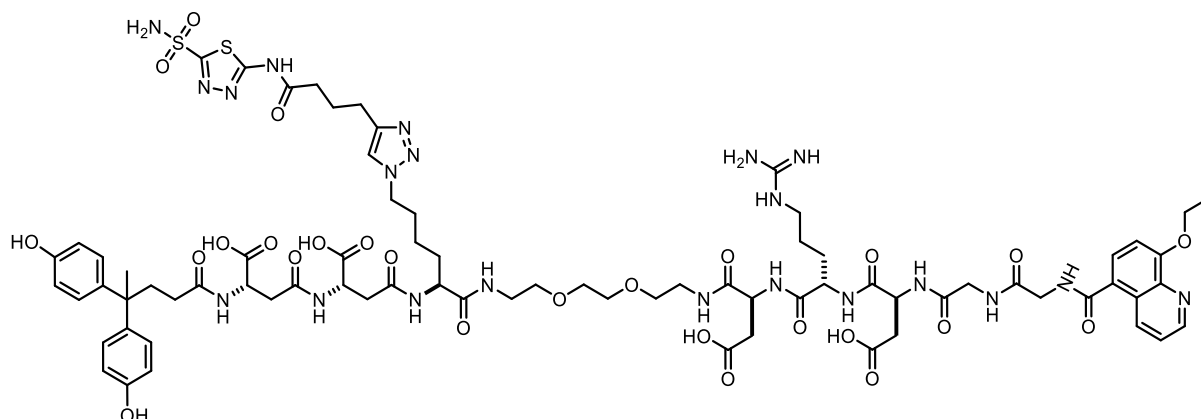
*N*²-(4,4-Bis(4-hydroxyphenyl)pentanoyl)-*N*⁴-((*S*)-1-carboxy-3-(((*S*)-1-(4-iodophenyl)-1,12-dioxo-17-(4-(4-oxo-4-((5-sulfamoyl-1,3,4-thiadiazol-2-yl)amino)butyl)-1*H*-1,2,3-triazol-1-yl)-5,8-dioxo-2,11-diazaheptadecan-13-yl)amino)-3-oxopropyl)-*L*-asparagine (**A40-p-I**)



To a solution of 4-iodobenzoic acid (6.2 mg, 0.025 mmol) in DMF (500 μ L), HATU (9.5 mg, 0.025 mmol) and DIPEA (6 μ L, 0.035 mmol) were added. The mixture was stirred for 30 min and a solution of the amine **A40** (21.5 mg, 0.02 mmol) in DMF (200 μ L) was slowly added. The reaction mixture was stirred for 72 h, concentrated and purified by reversed-phase HPLC (90% A / 10% B to 30% A / 70% B over 30 min). After lyophilization the title compound was collected as a white powder (3 mg, 9% yield).

¹H NMR (500 MHz, DMSO-*d*₆) δ 12.98 (s, 1H), 12.54 (s, 2H), 9.15 (s, 2H), 8.57 (t, $J = 5.6$ Hz, 1H), 8.31 (s, 2H), 8.16 (d, $J = 8.0$ Hz, 1H), 8.08 – 7.93 (m, 4H), 7.91 – 7.87 (m, 2H), 7.86 – 7.80 (m, 3H), 7.72 (s, 2H), 7.68 – 7.58 (m, 2H), 6.92 (d, $J = 8.4$ Hz, 4H), 6.64 (d, $J = 8.5$ Hz, 4H), 4.54 – 4.43 (m, 2H), 4.30 – 4.13 (m, 3H), 3.56 – 3.47 (m, 6H), 3.25 (q, $J = 6.2$ Hz, 2H), 3.22 – 3.13 (m, 3H), 3.05 (d, $J = 5.4$ Hz, 2H), 2.84 (q, $J = 6.0$ Hz, 2H), 2.66 – 2.55 (m, 6H), 2.21 – 2.12 (m, 2H), 1.95 (dq, $J = 15.1, 8.2, 7.7$ Hz, 2H), 1.83 (s, 2H), 1.77 – 1.70 (m, 2H), 1.68 – 1.58 (m, 1H), 1.51 – 1.42 (m, 1H), 1.33 – 1.15 (m, 4H).

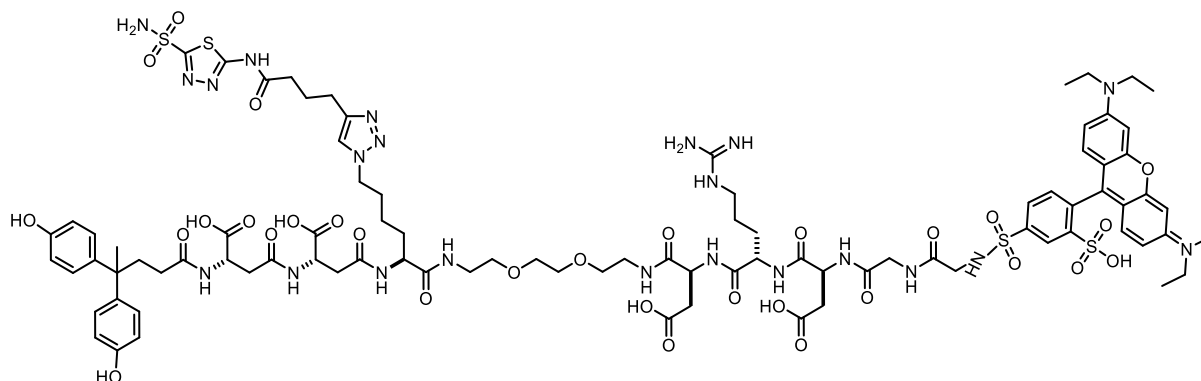
(2*S*,5*S*,8*S*,21*S*,25*S*,29*S*)-2-(2-(2-(8-(Allyloxy)quinoline-5-carboxamido)acetamido)acetamido)-8-(carboxymethyl)-5-(3-guanidinopropyl)-34,34-bis(4-hydroxyphenyl)-3,6,9,20,23,27,31-hepta-oxo-21-(4-(4-(4-oxo-4-((5-sulfamoyl-1,3,4-thiadiazol-2-yl)amino)butyl)-1*H*-1,2,3-triazol-1-yl)butyl)-13,16-dioxo-4,7,10,19,22,26,30-heptaazapentatriacontane-1,25,29-tricarboxylic acid (**A40-DRDGG-QA**)



Commercially-available pre-loaded Fmoc-Asp(OtBu)-OH on trityl resin (200 mg, 0.12 mmol) was swollen first in CH₂Cl₂ (3 × 5 min × 2 mL) and then in DMF (3 × 5 min × 2 mL). Then, it was sequentially loaded with Fmoc-Arg(Pbf)-OH, Fmoc-Asp(OtBu)-OH, Fmoc-Gly-OH, Fmoc-Gly-OH, and the carboxylic acid **A1**. The resin was treated with 20% HFIP in CH₂Cl₂, filtered, and solution was concentrated. The residue was dissolved in DMF (500 μL), HATU (34 mg, 0.09 mmol) and DIPEA (16 μL, 0.09 mmol) were added. The mixture was stirred for 30 min and a solution of the amine **A40** (54 mg, 0.05 mmol) in DMF (200 μL) was slowly added. The reaction mixture was stirred for 8 h, concentrated and purified by reversed-phase HPLC (95% A / 5% B to 20% A / 80% B over 30 min). After lyophilization, the title compound was collected as a white powder (27 mg, 30% yield).

¹H NMR (500 MHz, CH₃CN+D₂O) δ 9.56 (d, *J* = 8.3 Hz, 1H), 9.04 (d, *J* = 5.2 Hz, 1H), 8.68 (s, 2H), 8.18 – 8.07 (m, 2H), 7.68 (s, 1H), 7.51 (d, *J* = 8.4 Hz, 1H), 6.96 (d, *J* = 8.7 Hz, 4H), 6.66 (d, *J* = 8.6 Hz, 4H), 6.15 (ddt, *J* = 16.5, 11.1, 5.6 Hz, 1H), 5.49 (d, *J* = 17.4 Hz, 1H), 5.36 (d, *J* = 10.5 Hz, 1H), 4.95 (d, *J* = 5.4 Hz, 2H), 4.69 – 4.50 (m, 4H), 4.25 (t, *J* = 6.8 Hz, 2H), 3.54 – 3.41 (m, 8H), 3.24 (dd, *J* = 11.0, 6.3 Hz, 8H), 2.75 – 2.63 (m, 8H), 2.56 (t, *J* = 7.3 Hz, 2H), 2.27 – 2.18 (m, 2H), 1.76 (s, 4H), 1.64 (s, 2H), 1.57 – 1.48 (m, 4H).

(2*S*,5*S*,8*S*,21*S*,25*S*,29*S*)-8-(Carboxymethyl)-2-(2-(2-((4-(3-(diethyl-λ⁴-azaneylidene)-6-(diethylamino)-3*H*-xanthen-9-yl)-3-sulfophenyl)sulfonamido)acetamido)acetamido)-5-(3-guanidinopropyl)-34,34-bis(4-hydroxyphenyl)-3,6,9,20,23,27,31-hepta-oxo-21-(4-(4-(4-oxo-4-((5-sulfamoyl-1,3,4-thiadiazol-2-yl)amino)butyl)-1*H*-1,2,3-triazol-1-yl)butyl)-13,16-dioxo-4,7,10,19,22,26,30-heptaazapentatriacontane-1,25,29-tricarboxylic acid (**A40-DRDGG-SRB**)

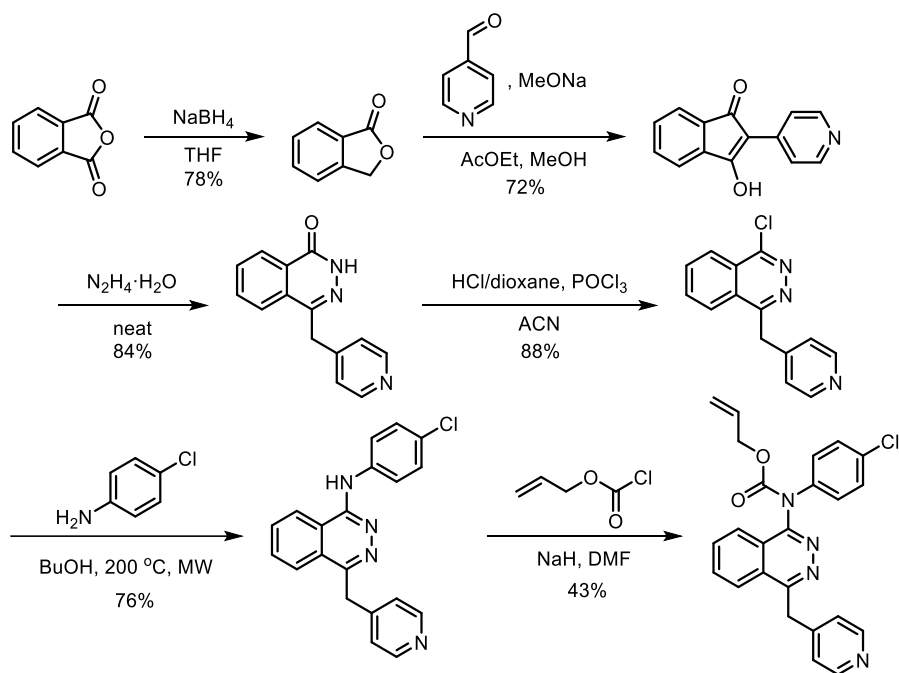


Commercially-available pre-loaded Fmoc-Asp(OtBu)-OH on trityl resin (200 mg, 0.12 mmol) was swollen first in CH₂Cl₂ (3 × 5 min × 2 mL) and then in DMF (3 × 5 min × 2 mL). Then it was sequentially loaded with Fmoc-Arg(Pbf)-OH, Fmoc-Asp(OtBu)-OH, Fmoc-Gly-OH, Fmoc-Gly-OH, and Sulforhodamine B acid chloride. One tenth of the resin was treated with 20% HFIP in CH₂Cl₂, filtered,

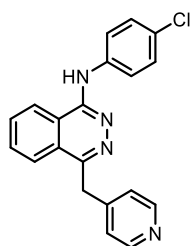
and the solution was concentrated. The residue was dissolved in DMF (100 μ L), HATU (3.4 mg, 0.009 mmol) and DIPEA (1.6 μ L, 0.009 mmol) were added. The mixture was stirred for 30 min and a solution of the amine **A40** (5.4 mg, 0.005 mmol) in DMF (100 μ L) was slowly added. The reaction mixture was stirred for 8 h, concentrated and purified by reversed-phase HPLC (95% A / 5% B to 20% A / 80% B over 30 min). After lyophilization the title compound was collected (0.3 mg, 3% yield). The product was obtained as a single peak on HPLC with the desired mass peak. $m/z = 1057.73$, calcd. 1057.86.

Drug and prodrug synthesis

Synthesis of vatalanib and Pro-Vat



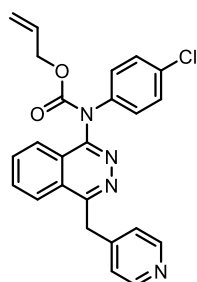
Vatalanib



Vatalanib was prepared according to a reported procedure.⁶⁶

^1H NMR (DMSO- d_6) δ 9.28 (s, 1H), 9.05 (s, 1H), 8.68 (d, 1H), 8.59 (m, 1H), 8.13 (m, 1H), 7.95 (m, 4H), 7.48 (d, 1H), 7.38 (d, 2H), 4.72 (s, 2H).

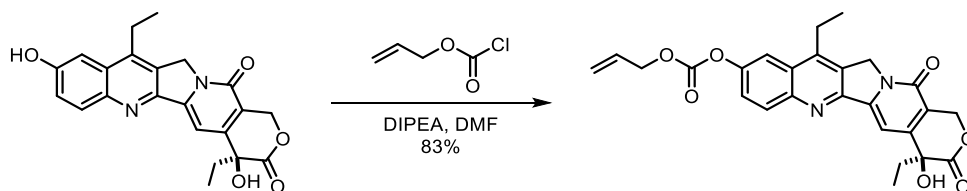
Allyl (4-chlorophenyl)(4-(pyridin-4-ylmethyl)phthalazin-1-yl)carbamate (**Pro-Vat**)



Vatalanib hydrochloride (76 mg, 0.2 mmol) was dissolved in DMF (2 mL), and NaH (60% in mineral oil, 40 mg, 1 mmol) was added at 0 °C. The reaction mixture was stirred at that temperature for 1 h, and allyl chloroformate (100 μ L, 1 mmol) was added dropwise. The reaction mixture was stirred for 16 h at room temperature and concentrated under reduced pressure. The residue was purified by silica gel column chromatography (25% EtOAc in cyclohexane) to give the carbamate **Pro-Vat** as an off-white solid (28 mg, 32%).

¹H NMR (500 MHz, DMSO-*d*₆) δ 9.19 (s, 1H), 8.52 (dd, *J* = 7.3, 2.0 Hz, 1H), 8.32 (dd, *J* = 7.4, 2.0 Hz, 1H), 8.09 – 7.89 (m, 4H), 7.78 (dd, *J* = 8.4, 2.0 Hz, 1H), 7.45 – 7.35 (m, 3H), 7.28 (dd, *J* = 8.0, 1.8 Hz, 1H), 6.54 (s, 1H), 6.33 (dd, *J* = 8.2, 2.2 Hz, 1H), 6.02 (ddt, *J* = 17.2, 10.7, 5.5 Hz, 1H), 5.42 (dq, *J* = 17.3, 1.6 Hz, 1H), 5.31 (dq, *J* = 10.6, 1.3 Hz, 1H), 4.81 (dt, *J* = 5.5, 1.4 Hz, 2H).

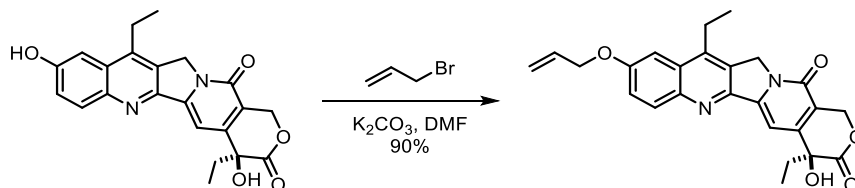
(*S*)-Allyl (4,11-diethyl-4-hydroxy-3,14-dioxo-3,4,12,14-tetrahydro-1*H*-pyrano[3',4':6,7]indolizino[1,2-*b*]quinolin-9-yl) carbonate (**Pro-SN38**)



To a stirred solution of **SN-38** (260 mg, 0.66 mmol) and DIPEA (230 μ L, 1.3 mmol) in DMF (3 mL) allyl chloroformate (140 μ L, 1.3 mmol) was added dropwise at 0 °C and the reaction mixture was stirred for 4 h. The organic solvent was removed under reduced pressure, and the residue was purified by silica gel column chromatography (100% EtOAc) to give the carbonate **Pro-SN38** as a white solid (261 mg, 83%).

¹H NMR (500 MHz, DMSO-*d*₆) δ 8.20 (d, *J* = 9.1 Hz, 1H), 8.15 (d, *J* = 2.5 Hz, 1H), 7.77 (dd, *J* = 9.1, 2.5 Hz, 1H), 7.32 (s, 1H), 6.52 (s, 1H), 6.04 (ddt, *J* = 17.2, 10.6, 5.6 Hz, 1H), 5.52 – 5.39 (m, 3H), 5.42 – 5.24 (m, 3H), 4.80 (dt, *J* = 5.6, 1.4 Hz, 2H), 3.18 (q, *J* = 7.6 Hz, 2H), 1.96 – 1.76 (m, 2H), 1.29 (t, *J* = 7.6 Hz, 3H), 0.88 (t, *J* = 7.3 Hz, 3H).

(*S*)-9-(allyloxy)-4,11-diethyl-4-hydroxy-1,12-dihydro-14*H*-pyrano[3',4':6,7]indolizino[1,2-*b*]quinoline-3,14(4*H*)-dione (**allyl-SN38**)

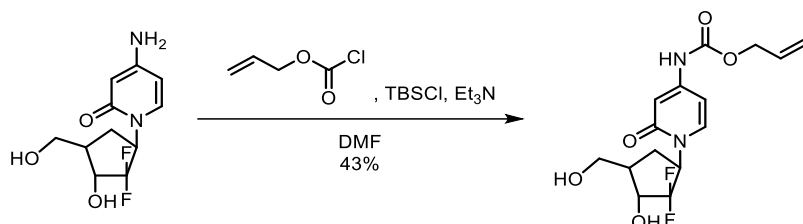


To a stirred solution of **SN-38** (80 mg, 0.2 mmol) in DMF (2 mL), K₂CO₃ (55 mg, 0.4 mmol) and allyl bromide (36 mg, 0.3 mmol) were added dropwise at 0 °C, and the reaction mixture was heated to 80 °C for 4 h. The volatiles were removed under reduced pressure, and the residue was purified by silica gel

column chromatography (100% EtOAc) to give the allylic ether **allyl-SN38** as a white solid (78 mg, 90%).

¹H NMR (500 MHz, CDCl₃) δ 8.12 (d, *J* = 9.2 Hz, 1H), 7.59 (s, 1H), 7.46 (dd, *J* = 9.2, 2.4 Hz, 1H), 7.31 (d, *J* = 2.3 Hz, 1H), 6.13 (ddt, *J* = 16.0, 10.6, 5.3 Hz, 1H), 5.73 (d, *J* = 16.2 Hz, 1H), 5.51 (d, *J* = 17.3 Hz, 1H), 5.38 (d, *J* = 10.5 Hz, 1H), 5.28 (d, *J* = 16.1 Hz, 1H), 5.21 (s, 2H), 4.72 (d, *J* = 5.2 Hz, 2H), 3.93 (s, 1H), 3.11 (q, *J* = 7.6 Hz, 2H), 1.87 (ddp, *J* = 21.1, 13.9, 6.9 Hz, 2H), 1.76 (s, 2H), 1.38 (t, *J* = 7.6 Hz, 3H), 1.02 (t, *J* = 7.3 Hz, 3H).

Allyl (1-((1*R*,3*R*,4*R*)-2,2-difluoro-3-hydroxy-4-(hydroxymethyl)cyclopentyl)-2-oxo-1,2-dihydropyridin-4-yl)carbamate (**Pro-Gem**)

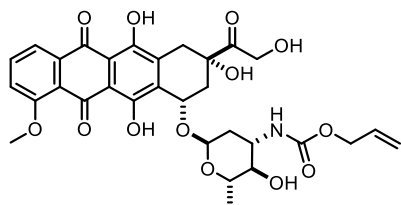


The carbamate **Pro-Gem** was synthesized according to a reported procedure.⁶⁷

¹H NMR (500 MHz, Acetone-*d*₆) δ 9.53 (s, 1H), 8.30 (d, *J* = 7.6 Hz, 1H), 7.25 (s, 1H), 6.28 (t, *J* = 7.5 Hz, 1H), 5.98 (ddt, *J* = 16.0, 10.7, 5.4 Hz, 1H), 5.51 – 5.36 (m, 2H), 5.24 (dd, *J* = 10.5, 1.3 Hz, 1H), 4.69 (d, *J* = 5.4 Hz, 2H), 4.60 (t, *J* = 4.9 Hz, 1H), 4.49 (d, *J* = 10.6 Hz, 1H), 4.12 – 3.99 (m, 3H), 3.89 (dt, *J* = 9.8, 4.4 Hz, 1H), 1.96 (s, 1H), 1.19 (t, *J* = 7.1 Hz, 1H).

¹⁹F NMR (471 MHz, Acetone-*d*₆) δ -117.99 – -119.65 (m).

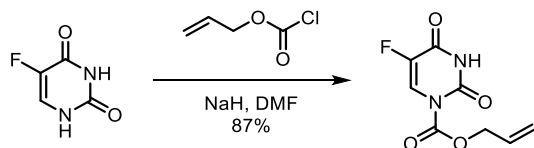
Allyl ((2*S*,3*R*,4*S*,6*R*)-3-hydroxy-2-methyl-6-(((1*S*,3*S*)-3,5,12-trihydroxy-3-(2-hydroxyacetyl)-10-methoxy-6,11-dioxo-1,2,3,4,6,11-hexahydrotetracen-1-yl)oxy)tetrahydro-2*H*-pyran-4-yl)carbamate (**Pro-Dox**)



The carbamate **Pro-Dox** was synthesized according to a reported procedure.⁶⁸

¹H NMR (500 MHz, CDCl₃): δ 13.96 (s, 1H), 13.22 (s, 1H), 8.02 (d, *J* = 7.4 Hz, 1H), 7.78 (t, *J* = 7.8 Hz, 1H), 7.39 (d, *J* = 8.3 Hz, 1H), 5.84 (m, 1H), 5.50 (s, 1H), 5.28 (m, 1H), 5.17 (m, 2H), 4.76 (s, 2H), 4.56 (s, 1H), 4.49 (d, *J* = 4.0 Hz, 2H), 4.14 (d, *J* = 5.7 Hz, 1H), 4.08 (s, 3H), 3.86 (m, 1H), 3.67 (s, 1H), 3.26 (d, *J* = 18.8 Hz, 1H), 2.99 (m, 2H), 2.33 (d, *J* = 14.6 Hz, 1H), 2.16 (d, *J* = 14.0 Hz, 1H), 2.02 (m, 1H), 1.86 (m, 2H), 1.77 (m, 1H), 1.28 (s, 3H).

Allyl 5-fluoro-2,4-dioxo-3,4-dihydropyrimidine-1(2*H*)-carboxylate (**Pro-5FU**)



5-fluoropyrimidine-2,4(1*H*,3*H*)-dione (260 mg, 2 mmol) was dissolved in DMF (3 mL), and NaH (60% in mineral oil, 100 mg, 2.5 mmol) was added in portions at 0 °C. The reaction mixture was stirred at that temperature for 1 h, and allyl chloroformate (320 μL, 3 mmol) was added dropwise. The reaction

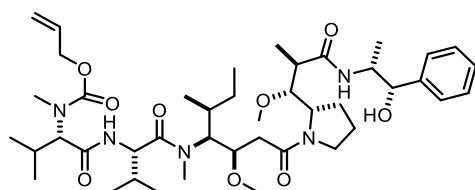
mixture was stirred for 16 h at room temperature and concentrated under reduced pressure. The residue was purified by silica gel column chromatography (30% EtOAc in cyclohexane) to give the carbamate **Pro-5FU** as a white powder (373 mg, 87%).

¹H NMR (500 MHz, DMSO-*d*₆) δ 12.02 (s, 1H), 8.22 (d, *J* = 7.3 Hz, 1H), 5.99 (ddt, *J* = 17.2, 10.6, 5.3 Hz, 1H), 5.48 (dq, *J* = 17.2, 1.6 Hz, 1H), 5.30 (dq, *J* = 10.6, 1.4 Hz, 1H), 4.83 (dt, *J* = 5.3, 1.5 Hz, 2H).

¹⁹F NMR (471 MHz, DMSO-*d*₆) δ -165.15.

¹³C NMR (126 MHz, DMSO-*d*₆) δ 157.12, 156.90, 149.41, 145.95, 141.06, 139.20, 131.25, 124.48, 124.18, 118.86, 68.74.

Allyl ((*S*)-1-(((*S*)-1-(((3*R*,4*S*,5*S*)-1-((*S*)-2-((1*R*,2*R*)-3-(((1*S*,2*R*)-1-hydroxy-1-phenylpropan-2-yl)amino)-1-methoxy-2-methyl-3-oxopropyl)pyrrolidin-1-yl)-3-methoxy-5-methyl-1-oxoheptan-4-yl)(methyl)amino)-3-methyl-1-oxobutan-2-yl)amino)-3-methyl-1-oxobutan-2-yl)(methyl)carbamate (**Alloc-MMAE**)

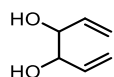


To a stirred solution of **MMAE** (36 mg, 0.05 mmol) and DIPEA (36 μL, 0.2 mmol) in DMF (1 mL) allyl chloroformate (10 μL, 0.1 mmol) was added. The reaction mixture was stirred for 4 h and then concentrated under reduced pressure. The residue was purified by reversed-phase HPLC (90% A / 10% B to 10% A / 90% B over 50 min). After lyophilization the title compound was collected as a white powder (28 mg, 70% yield).

¹H NMR (500 MHz, DMSO-*d*₆) δ 8.25 (d, *J* = 7.8 Hz, 1H), 8.02 (dd, *J* = 13.4, 8.7 Hz, 1H), 7.95 (s, 1H), 7.89 (d, *J* = 8.7 Hz, 1H), 7.63 (d, *J* = 8.5 Hz, 1H), 7.31 (d, *J* = 7.9 Hz, 4H), 7.26 (t, *J* = 7.1 Hz, 4H), 7.17 (q, *J* = 7.1 Hz, 2H), 6.00 – 5.85 (m, 2H), 5.38 (dd, *J* = 33.9, 5.0 Hz, 2H), 5.27 (t, *J* = 15.6 Hz, 2H), 5.17 (ddd, *J* = 10.5, 4.0, 1.5 Hz, 2H), 4.74 (s, 1H), 4.66 – 4.37 (m, 9H), 4.22 (dt, *J* = 24.7, 12.8 Hz, 2H), 3.98 (dtq, *J* = 27.9, 13.2, 6.6 Hz, 4H), 3.62 – 3.52 (m, 2H), 3.45 (d, *J* = 7.1 Hz, 1H), 3.23 (d, *J* = 8.6 Hz, 6H), 3.18 (d, *J* = 11.9 Hz, 6H), 3.12 (s, 3H), 3.05 (dd, *J* = 12.6, 5.5 Hz, 1H), 2.97 (s, 3H), 2.88 – 2.81 (m, 4H), 2.40 (d, *J* = 16.0 Hz, 2H), 2.27 (dd, *J* = 15.8, 9.3 Hz, 2H), 2.16 – 1.94 (m, 6H), 1.84 – 1.69 (m, 6H), 1.52 (ddt, *J* = 27.7, 14.4, 6.7 Hz, 4H), 1.27 (dq, *J* = 16.0, 6.0, 5.1 Hz, 4H), 1.08 – 0.95 (m, 12H), 0.89 – 0.73 (m, 38H).

Dimeric caging

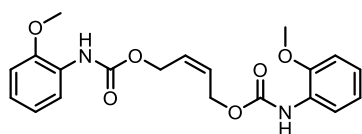
Hexa-1,5-diene-3,4-diol (**A42**)



To a stirred solution of acrolein (1 mL, 15 mmol) in THF (40 mL), a saturated solution of NH₄Cl (25 mL) was added. Then, Zn powder (2 g, 30 mmol) was added in portions at room temperature. The reaction mixture was stirred for 16 h, filtered through glass frit and extracted with ethyl acetate (2×50 mL). The combined organic phase was washed with water (30 mL) and brine (30 mL), dried over anhydrous sodium sulfate, filtered, and the organic solvent was removed under reduced pressure. The residue was purified by silica gel column chromatography (50% EtOAc in cyclohexane) to give the diol **A42** as a colourless oil (510 mg, 60%).

¹H NMR (500 MHz, CDCl₃) δ 5.98 – 5.81 (m, 4H), 5.37 (dd, *J* = 17.3, 9.0 Hz, 4H), 5.33 – 5.22 (m, 4H), 4.21 (s, 2H), 4.03 (d, *J* = 3.3 Hz, 2H), 2.29 (s, 2H), 2.07 (d, *J* = 3.4 Hz, 2H).

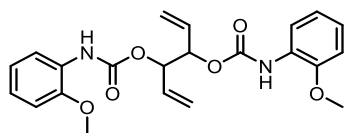
(Z)-But-2-ene-1,4-diyl bis((2-methoxyphenyl)carbamate) (**A44**)



1-Isocyanato-2-methoxybenzene (300 mg, 2 mmol), (Z)-but-2-ene-1,4-diol (79 mg, 0.9 mmol), and Et₃N (552 μ L, 4 mmol) were dissolved in THF (5 mL) and stirred at room temperature for 16 h. The volatiles were removed under reduced pressure and the residue was purified by silica gel column chromatography (25% EtOAc in cyclohexane) to give the bis(carbamate) **A44** as a colourless oil (219 mg, 63%).

¹H NMR (500 MHz, CD₂Cl₂) δ 8.03 (d, J = 7.3 Hz, 2H), 7.29 (s, 2H), 7.00 (td, J = 7.8, 1.7 Hz, 2H), 6.94 (td, J = 7.7, 1.3 Hz, 2H), 6.89 (dd, J = 8.0, 1.4 Hz, 2H), 5.84 (ddd, J = 5.1, 3.9, 1.1 Hz, 2H), 4.90 – 4.74 (m, 4H), 3.85 (s, 6H).

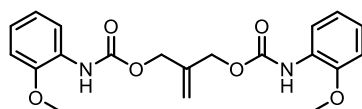
Hexa-1,5-diene-3,4-diyl bis((2-methoxyphenyl)carbamate) (**A45**)



1-Isocyanato-2-methoxybenzene (300 mg, 2 mmol), the diol **A42** (103 mg, 0.9 mmol), and pyridine (200 μ L, 2.5 mmol) were dissolved in THF (5 mL) and stirred at room temperature for 16 h. The volatiles were removed under reduced pressure, and the residue was purified by silica gel column chromatography (20% EtOAc in cyclohexane) to give the crude bis(carbamate) **A45** in an inseparable mixture containing, among others, the diol **A42** as a colourless oil (115 mg of pure product, 31%).

¹H NMR (500 MHz, CDCl₃) δ 8.09 (s, 2H), 7.36 (s, 2H), 7.01 – 6.85 (m, 6H), 5.99 – 5.90 (m, 2H), 5.48 – 5.36 (m, 4H), 3.88 (s, 6H).

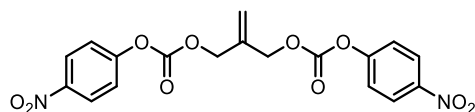
2-Methylenepropane-1,3-diyl bis((2-methoxyphenyl)carbamate) (**A46**)



1-Isocyanato-2-methoxybenzene (300 mg, 2 mmol), 2-methylenepropane-1,3-diol (79 mg, 0.9 mmol), and Et₃N (552 μ L, 4 mmol) were dissolved in THF (5 mL) and stirred at room temperature for 16 h. The volatiles were removed under reduced pressure and the residue was purified by silica gel column chromatography (25% EtOAc in cyclohexane) to give the bis(carbamate) **A46** as a colourless oil (167 mg, 48%).

¹H NMR (500 MHz, CDCl₃) δ 8.08 (s, 2H), 7.31 (s, 2H), 7.01 – 6.94 (m, 4H), 6.85 (dd, J = 8.0, 1.4 Hz, 2H), 5.37 (s, 2H), 4.76 (s, 4H), 3.85 (s, 6H).

2-Methylenepropane-1,3-diyl bis(4-nitrophenyl) bis(carbonate) (**A47**)

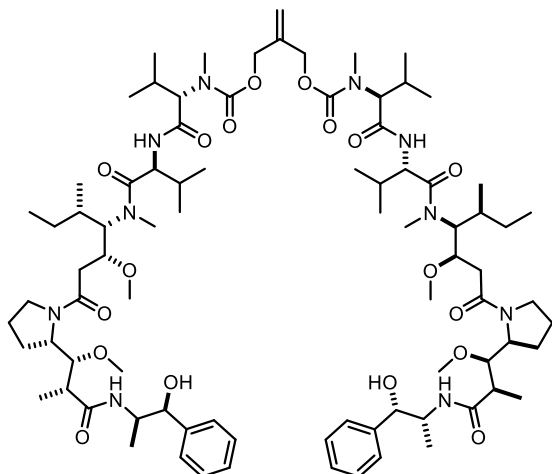


The diol **A43** (1.76 g, 20 mmol) was dissolved in pyridine (20 mL). 4-Nitrophenyl chloroformate (12.7 g, 63 mmol) was added in portions at 0 °C. The reaction mixture was stirred at 40 °C for 1 h and diluted with ethyl acetate (100 mL). The organic phase was washed with 1 M HCl (5 \times 100 mL), water (50 mL) and brine (50 mL), dried over anhydrous sodium sulfate, filtered, and the organic solvent was removed under reduced pressure. The residue was purified by silica gel column chromatography (10% EtOAc in

cyclohexane) to give the bis(carbonate) **A47** in a mixture with *p*-nitrophenol (2:3 ratio) as a yellow solid (4.82 g of pure product (calculated by NMR), 58%). The mixture was used in the next step without further purification.

^1H NMR (500 MHz, CDCl_3) δ 8.30 – 8.25 (m, 4H), 7.43 – 7.35 (m, 4H), 5.55 (s, 2H), 4.89 (s, 4H).

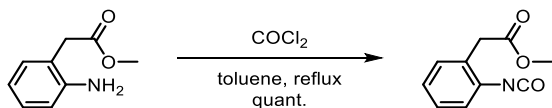
2-Methylenepropane-1,3-diyl bis(((*S*)-1-(((*S*)-1-(((3*R*,4*S*,5*S*)-1-((*S*)-2-((1*R*,2*R*)-3-(((1*S*,2*R*)-1-hydroxy-1-phenylpropan-2-yl)amino)-1-methoxy-2-methyl-3-oxopropyl)pyrrolidin-1-yl)-3-methoxy-5-methyl-1-oxoheptan-4-yl)(methyl)amino)-3-methyl-1-oxobutan-2-yl)amino)-3-methyl-1-oxobutan-2-yl)(methyl)carbamate) (**NN1**)



To a solution of **MMAE** (108 mg, 0.15 mmol) and DIPEA (178 μL , 1 mmol) in DMF (2 mL), a solution of the bis(carbonate) **A47** (21 mg, 0.05 mmol) in DMF (200 μL) was added dropwise. The reaction mixture was stirred for 16 h, concentrated and purified by reversed-phase HPLC (95% A / 5% B to 100% A / 90% B over 50 min). After lyophilization the title compound was collected as a white powder (69 mg, 88% yield).

^1H NMR (500 MHz, $\text{DMSO}-d_6$) δ 8.21 (s, 2H), 7.89 (d, $J = 8.2$ Hz, 1H), 7.62 (d, $J = 8.4$ Hz, 1H), 7.38 – 7.10 (m, 10H), 5.47 – 5.29 (m, 2H), 5.28 – 5.08 (m, 2H), 4.83 – 4.34 (m, 10H), 4.32 – 4.11 (m, 2H), 3.97 (ddt, $J = 27.9, 13.3, 6.7$ Hz, 4H), 3.56 (dt, $J = 12.2, 6.6$ Hz, 3H), 3.26 – 3.10 (m, 17H), 3.08 – 2.81 (m, 10H), 2.41 (d, $J = 15.4$ Hz, 2H), 2.26 (dd, $J = 15.3, 9.5$ Hz, 2H), 2.18 – 1.92 (m, 6H), 1.87 – 1.65 (m, 6H), 1.62 – 1.43 (m, 4H), 1.07 – 0.97 (m, 12H), 0.82 (ddt, $J = 30.2, 13.9, 7.1$ Hz, 38H).

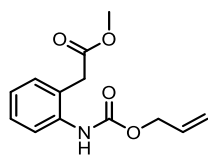
Methyl 2-(2-isocyanatophenyl)acetate (**A48**)



Toluene (30 mL) was heated to reflux, and a solution of 15 wt.% phosgene in toluene (6 mL, 8 mmol) was added. Then, a solution of methyl 2-(2-aminophenyl)acetate (201 mg, 1.22 mmol) in toluene (5 mL) was slowly added dropwise. The reaction mixture was stirred for 2 h at 110 $^{\circ}\text{C}$ and then cooled to room temperature. The volatiles were removed under reduced pressure to give the isocyanate **A48** as a colourless oil (232 mg, quant.). The crude product was used in the next step without further purification.

^1H NMR (500 MHz, CDCl_3) δ 7.29 – 7.22 (m, 2H), 7.20 – 7.11 (m, 2H), 3.72 (s, 3H), 3.69 (s, 2H).

Methyl 2-(2-(((allyloxy)carbonyl)amino)phenyl)acetate (**A49**)

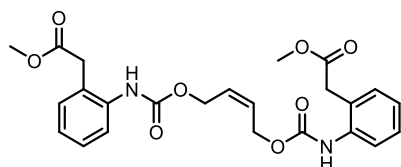


To a stirred solution of methyl 2-(2-aminophenyl)acetate (661 mg, 4 mmol) and DIPEA (1.4 mL, 8 mmol) in THF (10 mL) allyl chloroformate (640 μ L, 6 mmol) was added dropwise at 0 $^{\circ}$ C, and the reaction mixture was stirred for 4 h. The organic solvent was removed under reduced pressure, and the residue was purified by silica gel column chromatography (10% EtOAc in cyclohexane) to give the carbamate **A49** as a colourless oil (660 mg, 66%).

^1H NMR (500 MHz, CDCl_3) δ 7.93 (s, 1H), 7.78 (s, 1H), 7.40 – 7.27 (m, 1H), 7.19 (dd, J = 7.6, 1.3 Hz, 1H), 7.11 – 7.04 (m, 1H), 5.99 (ddt, J = 16.2, 10.8, 5.7 Hz, 1H), 5.44 – 5.33 (m, 1H), 5.33 – 5.22 (m, 1H), 4.68 (dt, J = 5.7, 1.3 Hz, 2H), 3.72 (s, 3H), 3.64 (s, 2H).

^{13}C NMR (126 MHz, CDCl_3) δ 172.81, 154.17, 136.93, 132.78, 130.87, 128.65, 124.83, 118.22, 66.06, 52.69, 38.56.

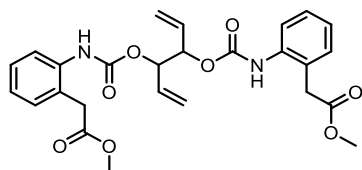
Dimethyl 2,2'-((((but-2-ene-1,4-diylbis(oxy))bis(carbonyl))bis(azanediyl))bis(2,1-phenylene))(Z)-diacetate (**A50**)



The isocyanate **A48** (200 mg, 1.05 mmol), (Z)-but-2-ene-1,4-diol (35 mg, 0.4 mmol), and DIPEA (352 μ L, 2 mmol) were dissolved in THF (5 mL) and stirred at room temperature for 16 h. The volatiles were removed under reduced pressure and the residue was purified by silica gel column chromatography (50% EtOAc in cyclohexane) to afford the bis(carbamate) **A50** as a colourless oil (104 mg, 55%).

^1H NMR (500 MHz, CDCl_3) δ 7.94 (s, 2H), 7.77 (s, 2H), 7.36 – 7.27 (m, 2H), 7.19 (dd, J = 7.6, 1.3 Hz, 2H), 7.13 – 7.04 (m, 2H), 5.97 – 5.75 (m, 2H), 4.83 (d, J = 4.9 Hz, 4H), 3.71 (s, 6H), 3.64 (s, 4H).

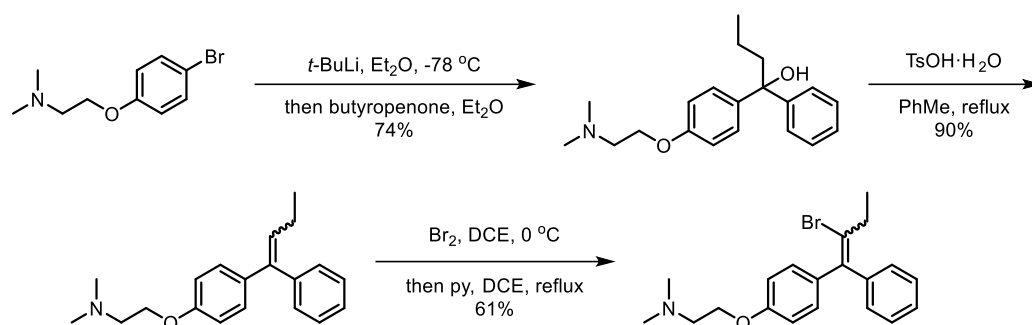
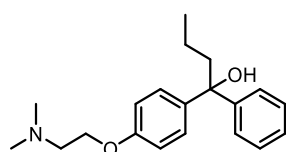
Dimethyl 2,2'-((((hexa-1,5-diene-3,4-diylbis(oxy))bis(carbonyl))bis(azanediyl))bis(2,1-phenylene))diacetate (**A51**)



The isocyanate **A48** (191 mg, 1 mmol), the diol **A42** (45 mg, 0.4 mmol), and DIPEA (352 μ L, 2 mmol) were dissolved in DMF (2 mL) and stirred at room temperature for 16 h. The volatiles were removed under reduced pressure and the residue was purified by silica gel column chromatography (50% EtOAc in cyclohexane) to give the crude bis(carbamate) **A51** in an inseparable mixture with the diol **A42** as a colourless oil (30 mg of pure product, 15%).

^1H NMR (500 MHz, CDCl_3) δ 7.97 (s, 2H), 7.75 (s, 2H), 7.31 (t, J = 7.8 Hz, 2H), 7.20 (d, J = 7.6 Hz, 2H), 7.10 (t, J = 7.4 Hz, 2H), 5.97 – 5.91 (m, 2H), 5.48 – 5.37 (m, 4H), 3.73 (s, 6H), 3.65 (s, 4H).

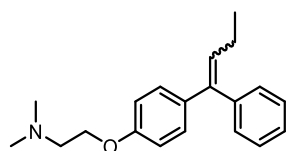
5.2. RCM Project

Substrates for the *in vivo* synthesisSynthesis of the bromoalkene **M3**1-(4-(2-(Dimethylamino)ethoxy)phenyl)-1-phenylbutan-1-ol (**M1**)

2-(4-Bromophenoxy)-*N,N*-dimethylethan-1-amine (4 g, 16.4 mmol) was dissolved in diethyl ether (125 mL) and cooled to $-78\text{ }^{\circ}\text{C}$. A solution of *tert*-BuLi (1.69M, 19.4 mL, 33 mmol) was added dropwise via cannula at that temperature. The reaction mixture was stirred at $-78\text{ }^{\circ}\text{C}$ for 1 h, and then a solution of 1-phenylbutan-1-one (2.66 g, 18 mmol) was added dropwise. The solution was warmed to room temperature and stirred for additional 4 h. A saturated solution of NH_4Cl (100 mL) was added, and the mixture was extracted with diethyl ether (3×100 mL). The combined organic phase was washed with water (100 mL) and saturated brine (100 mL), dried over anhydrous sodium sulfate, filtered, and the organic solvent was removed under reduced pressure. The crude product was purified by silica gel column chromatography (5% MeOH in CH_2Cl_2) to afford the alcohol **M1** as a colourless oil (3.8 g, 74%).

^1H NMR (500 MHz, CDCl_3) δ 7.39 (dd, $J = 8.3, 1.1$ Hz, 2H), 7.31 – 7.13 (m, 5H), 6.88 – 6.81 (m, 2H), 4.03 (t, $J = 5.8$ Hz, 2H), 2.70 (t, $J = 5.8$ Hz, 2H), 2.31 (s, 6H), 2.22 (dd, $J = 8.9, 7.5$ Hz, 2H), 1.38 – 1.18 (m, 2H), 0.92 (t, $J = 7.4$ Hz, 3H).

^{13}C NMR (126 MHz, CDCl_3) δ 157.76, 147.51, 139.79, 128.16, 127.42, 126.74, 126.15, 114.17, 78.15, 66.07, 58.45, 46.05, 44.58, 17.31, 14.59.

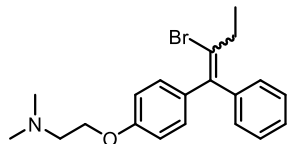
N,N-Dimethyl-2-(4-(1-phenylbut-1-en-1-yl)phenoxy)ethan-1-amine (**M2**)

The alcohol **M1** (3.8 g, 12.1 mmol) and *p*-toluenesulfonic acid monohydrate (2.85 g, 15 mmol) were mixed in toluene (100 mL) and heated to reflux for 16 h. The reaction mixture was cooled to room temperature and washed with aqueous NaOH (1M, 5×50 mL) and brine (100 mL), dried over anhydrous sodium sulfate, filtered. The organic solvent was removed under reduced pressure to give the trisubstituted alkene **M2** as a mixture of diastereomers as a colourless liquid (3.2 g, 90%). The crude product was used in the next step without further purification.

^1H NMR (500 MHz, CDCl_3) δ 7.48 – 7.06 (m, 7H), 7.00 – 6.79 (m, 2H), 6.11 – 5.86 (m, 1H), 4.07 (dt, $J = 25.5, 5.8$ Hz, 2H), 2.73 (dt, $J = 19.9, 5.8$ Hz, 2H), 2.34 (d, $J = 14.5$ Hz, 6H), 2.12 (dp, $J = 26.9, 7.5$ Hz, 2H), 1.03 (q, $J = 7.5$ Hz, 3H).

^{13}C NMR (126 MHz, CDCl_3) δ 158.04, 157.91, 143.40, 140.68, 140.65, 140.51, 135.73, 132.76, 131.66, 131.13, 130.17, 130.01, 128.34, 128.20, 128.13, 127.45, 126.88, 126.81, 114.25, 114.24, 66.13, 66.10, 58.53, 58.46, 46.10, 46.06, 23.36, 23.27, 14.75, 14.70.

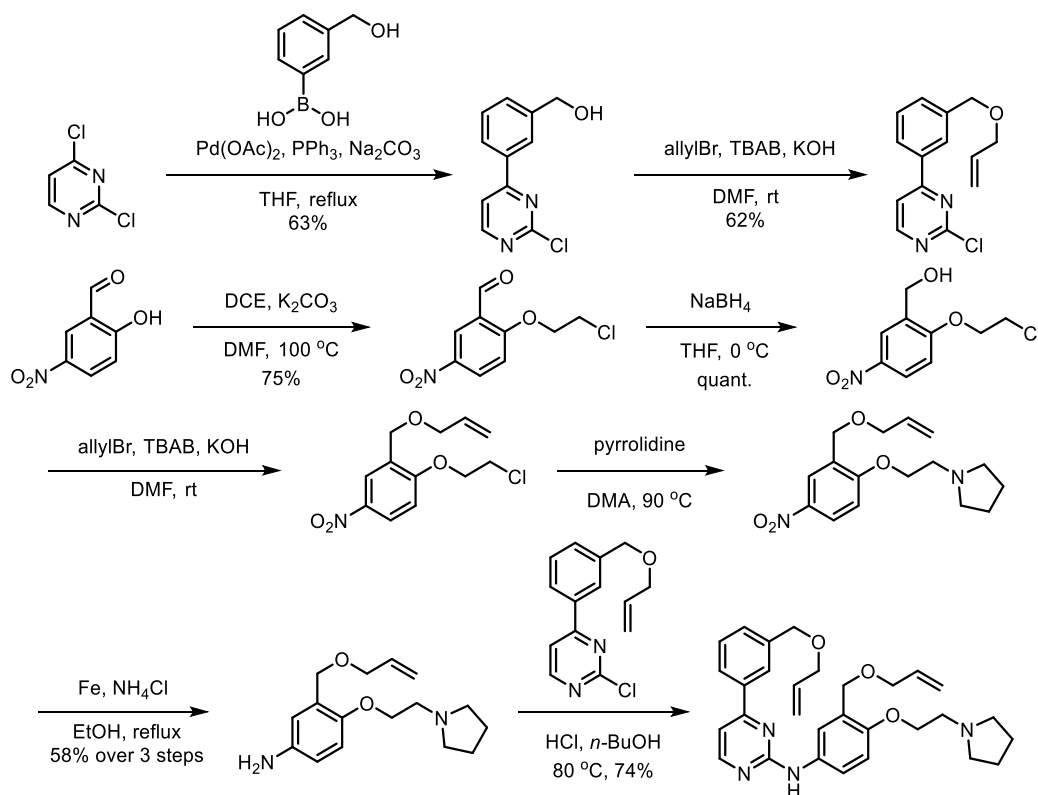
2-(4-(2-Bromo-1-phenylbut-1-en-1-yl)phenoxy)-*N,N*-dimethylethan-1-amine (**M3**)



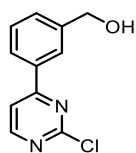
The trisubstituted alkene **M2** (3.2 g, 11 mmol) was dissolved in DCE (20 mL) and cooled to 0 °C. A solution of Br_2 (1.92 g, 12 mmol) in DCE (5 mL) was added dropwise, and the reaction mixture was stirred at room temperature for 2 h. The reaction mixture was washed with a saturated solution of Na_2SO_3 (20 mL), water (20 mL), and brine (20 mL), dried over anhydrous sodium sulfate. Following filtering, the organic solvent was removed under reduced pressure. The residue was redissolved in DCE (20 mL), and pyridine (4 mL, 50 mmol) was added at room temperature. The reaction mixture was refluxed for 16 h and cooled to room temperature. The organic phase was washed with water (2×20 mL) and brine (20 mL), dried over anhydrous sodium sulfate, filtered, and the organic solvent was removed under reduced pressure. The crude product was purified by silica gel column chromatography (3% MeOH in CH_2Cl_2) to give the bromoalkene **M3** as a mixture of diastereomers as a yellow oil (2.5 g, 61%).

^1H NMR (500 MHz, CDCl_3) δ 7.33 – 7.01 (m, 7H), 6.88 – 6.82 (m, 2H), 4.05 (td, J = 5.8, 3.3 Hz, 2H), 2.72 (t, J = 5.8 Hz, 2H), 2.56 (dq, J = 22.2, 7.3 Hz, 2H), 2.33 (s, 6H), 1.19 (dt, J = 8.7, 7.3 Hz, 3H).

Synthesis of the diolefin **M12**



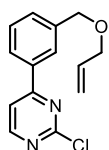
(3-(2-Chloropyrimidin-4-yl)phenyl)methanol (**M5**)



The alcohol **M5** was obtained according to a reported procedure.⁶⁹

¹H NMR (500 MHz, DMSO-*d*₆) δ 8.82 (d, *J* = 5.3 Hz, 1H), 8.21 – 8.10 (m, 2H), 8.05 (dt, *J* = 7.1, 1.7 Hz, 1H), 7.62 – 7.48 (m, 2H), 5.36 (t, *J* = 5.8 Hz, 1H), 4.61 (d, *J* = 5.7 Hz, 2H).

4-(3-((Allyloxy)methyl)phenyl)-2-chloropyrimidine (**M6**)

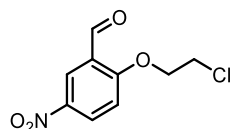


The pyrimidine **M6** was obtained according to a reported procedure.⁶⁹

¹H NMR (500 MHz, CDCl₃) δ 8.63 (d, *J* = 5.2 Hz, 1H), 8.07 (s, 1H), 8.03 – 7.98 (m, 1H), 7.66 (d, *J* = 5.2 Hz, 1H), 7.56 – 7.42 (m, 2H), 5.97 (ddt, *J* = 17.1, 10.5, 5.7 Hz, 1H), 5.33 (dq, *J* = 17.2, 1.6 Hz, 1H), 5.23 (dq, *J* = 10.4, 1.2 Hz, 1H), 4.60 (s, 2H), 4.08 (dt, *J* = 5.7, 1.4 Hz, 2H).

¹³C NMR (126 MHz, CDCl₃) δ 167.20, 161.98, 159.96, 139.69, 135.35, 134.60, 131.24, 129.36, 126.81, 126.67, 117.60, 115.38, 71.75, 71.61.

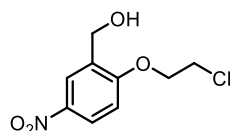
2-(2-Chloroethoxy)-5-nitrobenzaldehyde (**M7**)



The aldehyde **M7** was obtained according to a reported procedure.⁶⁹

¹H NMR (500 MHz, CDCl₃) δ 10.51 (s, 1H), 8.74 (d, *J* = 2.9 Hz, 1H), 8.45 (dd, *J* = 9.1, 2.9 Hz, 1H), 7.10 (d, *J* = 9.2 Hz, 1H), 4.49 (t, *J* = 5.5 Hz, 2H), 3.94 (t, *J* = 5.5 Hz, 2H).

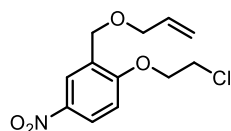
(2-(2-Chloroethoxy)-5-nitrophenyl)methanol (**M8**)



The benzylic alcohol **M8** was obtained according to a reported procedure.⁶⁹

¹H NMR (500 MHz, CDCl₃) δ 8.31 (d, *J* = 2.8 Hz, 1H), 8.20 (dd, *J* = 9.0, 2.8 Hz, 1H), 6.91 (d, *J* = 9.0 Hz, 1H), 4.78 (s, 2H), 4.41 – 4.35 (m, 2H), 3.91 – 3.86 (m, 2H).

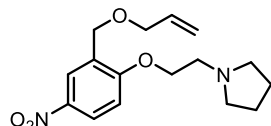
2-((Allyloxy)methyl)-1-(2-chloroethoxy)-4-nitrobenzene (**M9**)



The nitrobenzene **M9** was obtained according to a reported procedure.⁶⁹

^1H NMR (500 MHz, CDCl_3) δ 8.36 (d, J = 2.8 Hz, 1H), 8.17 (dd, J = 9.0, 2.9 Hz, 1H), 6.88 (d, J = 9.0 Hz, 1H), 5.99 (ddt, J = 17.1, 10.6, 5.6 Hz, 1H), 5.36 (dq, J = 17.2, 1.6 Hz, 1H), 5.25 (dd, J = 10.4, 1.4 Hz, 1H), 4.59 (s, 2H), 4.35 (t, J = 5.6 Hz, 2H), 4.14 (dt, J = 5.6, 1.3 Hz, 2H), 3.87 (t, J = 5.6 Hz, 2H).

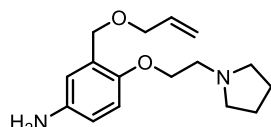
1-(2-(2-((Allyloxy)methyl)-4-nitrophenoxy)ethyl)pyrrolidine (**M10**)



The pyrrolidine **M10** was obtained according to a reported procedure.⁶⁹

^1H NMR (500 MHz, CDCl_3) δ 8.33 (d, J = 2.8 Hz, 1H), 8.16 (dd, J = 9.0, 2.9 Hz, 1H), 6.90 (d, J = 9.1 Hz, 1H), 6.07 – 5.87 (m, 1H), 5.34 (dq, J = 17.2, 1.6 Hz, 1H), 5.26 – 5.17 (m, 1H), 4.56 (s, 2H), 4.24 (t, J = 5.8 Hz, 2H), 4.18 – 4.04 (m, 2H), 2.97 (t, J = 5.9 Hz, 2H), 2.71 – 2.86 (m, 4H), 1.88 – 1.75 (m, J = 3.7, 3.0 Hz, 4H).

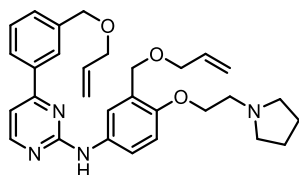
3-((Allyloxy)methyl)-4-(2-(pyrrolidin-1-yl)ethoxy)aniline (**M11**)



The aniline **M11** was obtained according to a reported procedure.⁶⁹

^1H NMR (500 MHz, CDCl_3) δ 6.78 (d, J = 2.9 Hz, 1H), 6.70 (d, J = 8.6 Hz, 1H), 6.56 (dd, J = 8.5, 2.9 Hz, 1H), 5.96 (ddt, J = 17.2, 10.6, 5.6 Hz, 1H), 5.31 (dq, J = 17.2, 1.6 Hz, 1H), 5.19 (dd, J = 10.4, 1.5 Hz, 1H), 4.51 (s, 2H), 4.12 – 3.98 (m, 4H), 3.42 (s, 1H), 2.88 (t, J = 6.0 Hz, 2H), 2.73 – 2.54 (m, 4H), 1.87 – 1.73 (m, 4H).

N-(3-((Allyloxy)methyl)-4-(2-(pyrrolidin-1-yl)ethoxy)phenyl)-4-(3-((allyloxy)methyl)phenyl)pyrimidin-2-amine (**M12**)

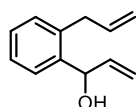


The diene **M12** was obtained according to a reported procedure.⁶⁹

^1H NMR (500 MHz, CDCl_3) δ 8.44 (d, J = 4.8 Hz, 1H), 8.08 – 7.96 (m, 2H), 7.68 – 7.57 (m, 2H), 7.52 – 7.44 (m, 2H), 7.17 – 7.08 (m, 2H), 6.93 – 6.88 (m, 1H), 6.06 – 5.88 (m, 2H), 5.41 – 5.15 (m, 4H), 4.61 (s, 2H), 4.57 (s, 2H), 4.41 (s, 2H), 4.11 – 4.03 (m, 4H), 3.31 (brs, 2H), 3.17 (brs, 4H), 2.04 (brs, 4H).

Click-to-release approach (phenols)

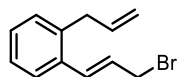
1-(2-Allylphenyl)prop-2-en-1-ol (**M13**)



The alcohol **M13** was obtained according to a reported procedure.¹²

^1H NMR (500 MHz, CDCl_3) δ 7.56 – 7.43 (m, 1H), 7.33 – 7.21 (m, 2H), 7.21 – 7.13 (m, 1H), 6.17 – 5.92 (m, 2H), 5.47 (td, J = 5.4, 4.7, 1.8 Hz, 1H), 5.35 (dt, J = 17.2, 1.5 Hz, 1H), 5.22 (dt, J = 10.4, 1.5 Hz, 1H), 5.09 (dq, J = 10.1, 1.6 Hz, 1H), 5.00 (dq, J = 17.1, 1.8 Hz, 1H), 3.50 (d, J = 6.2 Hz, 2H), 1.88 (d, J = 4.0 Hz, 1H).

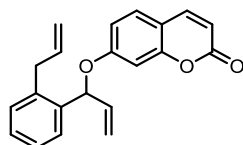
(*E*)-1-Allyl-2-(3-bromoprop-1-en-1-yl)benzene (**M14**)



To the stirred solution of the alcohol **M13** (174 mg, 1 mmol) in diethyl ether (2.5 mL), a solution of PBr_3 (135 mg, 0.5 mmol) in diethyl ether (1 mL) was added dropwise at 0 °C. The reaction mixture was stirred for 1 h, after which, a saturated solution of NaHCO_3 (1 mL) was added. The organic phase was separated, washed with brine (2 mL), dried over anhydrous sodium sulfate, filtered, and the organic solvent was removed under reduced pressure to give the allylic bromide **M14** as a pale-yellow oil (237 mg, quant.). The crude product was used in the next step without further purification.

^1H NMR (500 MHz, CDCl_3) δ 7.53 – 7.43 (m, 1H), 7.24 – 7.12 (m, 3H), 6.88 (d, J = 15.4 Hz, 1H), 6.29 (dt, J = 15.4, 7.8 Hz, 1H), 5.95 (ddt, J = 16.3, 10.1, 6.2 Hz, 1H), 5.08 (dt, J = 10.1, 1.6 Hz, 1H), 4.97 (dq, J = 17.1, 1.7 Hz, 1H), 4.17 (dd, J = 7.8, 0.9 Hz, 2H), 3.45 (d, J = 6.1 Hz, 2H).

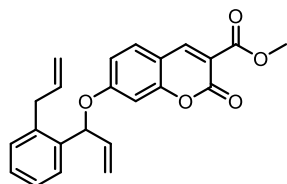
7-((1-(2-Allylphenyl)allyl)oxy)-2*H*-chromen-2-one (**M15**)



The allylic bromide **M14** (237 mg, 1 mmol), 7-hydroxy-2*H*-chromen-2-one (243 mg, 1.5 mmol), $[\text{RuCp}^*\text{Cl}_2]_2$ (60 mg, 0.1 mmol), and K_2CO_3 (350 mg, 2.5 mmol) were suspended in dry and degassed ACN (10 mL) and stirred for 3 h. The reaction mixture was centrifuged, and the supernatant was concentrated under reduced pressure. The residue was purified by silica gel column chromatography (10% EtOAc in cyclohexane) to give the coumarin **M15** as a white solid (306 mg, 96%).

^1H NMR (500 MHz, CDCl_3) δ 7.60 (d, J = 9.5 Hz, 1H), 7.44 (d, J = 7.8 Hz, 1H), 7.32 (d, J = 8.6 Hz, 1H), 7.30 – 7.21 (m, 3H), 6.87 (dd, J = 8.6, 2.4 Hz, 1H), 6.79 (d, J = 2.3 Hz, 1H), 6.23 (d, J = 9.5 Hz, 1H), 6.11 (ddd, J = 16.4, 10.5, 5.5 Hz, 1H), 5.99 (ddt, J = 16.6, 10.1, 6.3 Hz, 1H), 5.93 (d, J = 5.5 Hz, 1H), 5.38 – 5.26 (m, 2H), 5.21 – 5.13 (m, 1H), 5.06 (dd, J = 17.1, 1.6 Hz, 1H), 3.69 – 3.37 (m, 2H).

Methyl 7-((1-(2-allylphenyl)allyl)oxy)-2-oxo-2*H*-chromene-3-carboxylate (**M16**)

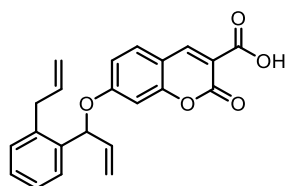


The allylic bromide **M14** (237 mg, 1 mmol), methyl 7-hydroxy-2-oxo-2*H*-chromene-3-carboxylate (330 mg, 1.5 mmol), $[\text{RuCp}^*\text{Cl}_2]_2$ (60 mg, 0.1 mmol), and K_2CO_3 (350 mg, 2.5 mmol) were suspended in dry and degassed ACN (10 mL) and stirred for 3 h. The reaction mixture was centrifuged, and the supernatant was concentrated under reduced pressure. The residue was purified by silica gel column chromatography (10% EtOAc in cyclohexane) to afford the methyl ester **M16** as a colourless oil (238 mg, 63%).

^1H NMR (500 MHz, CDCl_3) δ 8.50 (s, 1H), 7.46 (d, J = 8.7 Hz, 1H), 7.42 (d, J = 7.7 Hz, 1H), 7.35 – 7.18 (m, 3H), 6.92 (dd, J = 8.7, 2.4 Hz, 1H), 6.78 (d, J = 2.3 Hz, 1H), 6.11 (ddd, J = 17.1, 10.5, 5.5 Hz,

1H), 6.05 – 5.87 (m, 2H), 5.35 (d, $J = 10.5$ Hz, 1H), 5.31 (d, $J = 17.2$ Hz, 1H), 5.15 (dd, $J = 10.1$, 1.5 Hz, 1H), 5.06 (dd, $J = 17.1$, 1.6 Hz, 1H), 3.93 (s, 3H), 3.61 – 3.37 (m, 2H).

7-((1-(2-Allylphenyl)allyl)oxy)-2-oxo-2H-chromene-3-carboxylic acid (**M17**)

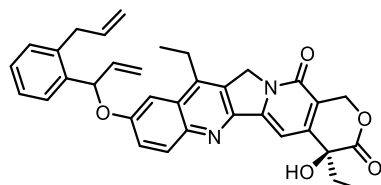


The methyl ester **M16** (200 mg, 0.53 mmol) and LiOH·H₂O (50 mg, 1.2 mmol) were mixed in a mixture of water (2 mL) and THF (2 mL) and stirred for 16 h at room temperature. A solution of HCl (0.1 M, 15 mL) was added dropwise at 0 °C, and the resulting mixture was extracted with CH₂Cl₂ (3×10 mL). The combined organic phase was washed with water (100 mL) and brine (100 mL), dried over anhydrous sodium sulfate, filtered, and the organic solvent was removed under reduced pressure. The crude product was purified by silica gel column chromatography (30% EtOAc in cyclohexane) to afford the carboxylic acid **M17** as a colourless oil that solidifies in the fridge (4 °C) (175 mg, 91%).

¹H NMR (500 MHz, CDCl₃) δ 12.02 (s, 1H), 8.82 (s, 1H), 7.59 (d, $J = 8.8$ Hz, 1H), 7.45 – 7.38 (m, 1H), 7.33 – 7.22 (m, 3H), 7.04 (dd, $J = 8.8$, 2.3 Hz, 1H), 6.89 (d, $J = 2.2$ Hz, 1H), 6.20 – 6.07 (m, 1H), 6.07 – 5.91 (m, 2H), 5.38 (d, $J = 10.5$ Hz, 1H), 5.32 (d, $J = 17.2$ Hz, 1H), 5.17 (dd, $J = 10.1$, 1.4 Hz, 1H), 5.06 (dd, $J = 17.1$, 1.6 Hz, 1H), 3.75 – 3.30 (m, 2H).

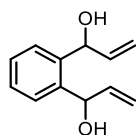
¹³C NMR (126 MHz, CDCl₃) δ 164.69, 164.62, 163.21, 156.95, 151.29, 137.14, 136.47, 135.96, 135.46, 131.75, 130.75, 128.97, 127.40, 126.99, 118.45, 117.05, 116.47, 112.56, 111.10, 103.04, 78.78, 37.06, 27.06.

(4S)-9-((1-(2-Allylphenyl)allyl)oxy)-4,11-diethyl-4-hydroxy-1,12-dihydro-14H-pyrano[3',4':6,7]indolizino[1,2-b]quinoline-3,14(4H)-dione (**M18**)



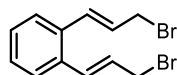
The allylic bromide **M14** (24 mg, 0.1 mmol), SN-38 (60 mg, 0.15 mmol), [RuCp*Cl₂]₂ (6 mg, 0.01 mmol), and K₂CO₃ (34.5 mg, 0.25 mmol) were suspended in dry and degassed ACN (2 mL) and stirred for 3 h. The reaction mixture was centrifuged, and the supernatant was concentrated under reduced pressure. The residue was purified by silica gel column chromatography (30% EtOAc in cyclohexane) to give the diene **M18** as a pale-yellow solid (22 mg, 40%).

¹H NMR (500 MHz, CDCl₃) δ 8.19 – 8.02 (m, 1H), 7.62 (t, $J = 3.0$ Hz, 1H), 7.55 – 7.43 (m, 2H), 7.35 – 7.20 (m, 3H), 7.16 (dd, $J = 17.1$, 2.6 Hz, 1H), 6.21 (dddd, $J = 17.5$, 10.2, 5.5, 2.6 Hz, 1H), 6.11 – 5.92 (m, 2H), 5.71 (d, $J = 16.2$ Hz, 1H), 5.40 – 5.34 (m, 2H), 5.31 – 5.10 (m, 5H), 4.23 – 4.08 (m, 2H), 3.67 – 3.50 (m, 2H), 3.08 – 2.84 (m, 2H), 1.95 – 1.78 (m, 3H), 1.14 (dt, $J = 13.3$, 7.7 Hz, 3H), 0.99 (td, $J = 7.4$, 3.0 Hz, 3H).

1,1'-(1,2-Phenylene)bis(prop-2-en-1-ol) (**M19**)

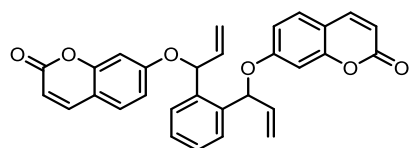
Phthalaldehyde (1.34 g, 10 mmol) was dissolved in THF (20 mL), cooled to 0 °C, and of vinylmagnesium bromide (0.7 M solution, 36 mL, 25 mmol) was added dropwise. The reaction mixture was stirred at room temperature for 1 h, and then saturated solution of NH₄Cl (20 mL) was added at room temperature. The mixture was extracted with diethyl ether (3×20 mL). The combined organic phase was washed with water (20 mL) and brine (20 mL), dried over anhydrous sodium sulfate. Following filtering, the organic solvent was removed under reduced pressure to give the diol **M19** as a mixture of diastereomers as a colourless oil (1.83 g, 96%). The crude product was used in the next step without further purification.

¹H NMR (500 MHz, CD₂Cl₂) δ 7.51 – 7.37 (m, 2H), 7.36 – 7.23 (m, 2H), 6.22 – 6.08 (m, 2H), 5.66 – 5.51 (m, 2H), 5.43 – 5.33 (m, 2H), 5.29 – 5.20 (m, 2H).

1,2-Bis((*E*)-3-bromoprop-1-en-1-yl)benzene (**M20**)

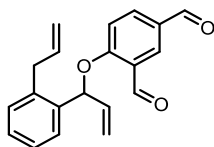
To the stirred solution of the diol **M19** (380 mg, 2 mmol) in diethyl ether (5 mL), a solution of PBr₃ (542 mg, 2 mmol) in diethyl ether (5 mL) was added dropwise at 0 °C. The reaction mixture was stirred for 1 h and then saturated solution of NaHCO₃ (10 mL) was added. The organic phase was separated, washed with brine (10 mL), dried over anhydrous sodium sulfate, filtered, and the organic solvent was removed under reduced pressure to give the dibromide **M20** as a pale-yellow oil (480 mg, 76%). The crude product was used in the next step without further purification.

¹H NMR (400 MHz, CDCl₃) δ 7.48 – 7.37 (m, 2H), 7.32 – 7.19 (m, 2H), 6.91 (d, *J* = 15.4 Hz, 2H), 6.27 (dt, *J* = 15.5, 7.8 Hz, 2H), 4.18 (dd, *J* = 7.8, 1.0 Hz, 4H).

7,7'-((1,2-Phenylenebis(prop-2-ene-1,1-diyl))bis(oxy))bis(2*H*-chromen-2-one) (**M21**)

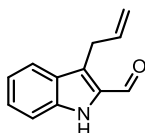
The dibromide **M20** (158 mg, 0.5 mmol), 7-hydroxy-2*H*-chromen-2-one (243 mg, 1.5 mmol), [RuCp*Cl₂]₂ (60 mg, 0.1 mmol), and K₂CO₃ (350 mg, 2.5 mmol) were suspended in dry and degassed ACN (10 mL) and stirred for 3 h. The reaction mixture was centrifuged, and the supernatant was concentrated under reduced pressure. The residue was purified by silica gel column chromatography (50% EtOAc in cyclohexane) to give the bis(coumarin) **M21** as a white solid (177 mg, 37%).

¹H NMR (500 MHz, DMSO-*d*₆) δ 8.00 – 7.49 (m, 8H), 7.42 (td, *J* = 5.9, 3.4 Hz, 2H), 7.04 – 6.89 (m, 4H), 6.82 – 6.66 (m, 2H), 6.43 (dd, *J* = 22.2, 5.7 Hz, 2H), 6.32 – 6.19 (m, 2H), 6.19 – 6.07 (m, 2H), 5.43 (dd, *J* = 22.8, 17.2 Hz, 2H), 5.32 (dd, *J* = 10.5, 6.8 Hz, 2H).

4-((1-(2-Allylphenyl)allyl)oxy)isophthalaldehyde (**M22**)

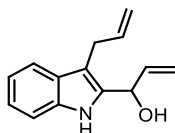
The allylic bromide **M14** (237 mg, 1 mmol), 4-hydroxyisophthalaldehyde (225 mg, 1.5 mmol), $[\text{RuCp}^*\text{Cl}_2]_2$ (60 mg, 0.1 mmol), and K_2CO_3 (350 mg, 2.5 mmol) were suspended in dry and degassed ACN (10 mL) and stirred for 3 h. The reaction mixture was centrifuged, and the supernatant was concentrated under reduced pressure. The residue was purified by silica gel column chromatography (10% EtOAc in cyclohexane) to give the dialdehyde **M22** as a colourless oil (238 mg, 78%).

^1H NMR (500 MHz, CDCl_3) δ 10.59 (s, 1H), 9.91 (s, 1H), 8.33 (d, $J = 2.1$ Hz, 1H), 7.98 (dd, $J = 8.8$, 2.2 Hz, 1H), 7.55 – 7.42 (m, 1H), 7.35 – 7.17 (m, 3H), 7.03 (d, $J = 8.8$ Hz, 1H), 6.23 – 6.06 (m, 2H), 6.06 – 5.91 (m, 1H), 5.53 – 5.28 (m, 2H), 5.13 (dd, $J = 10.1$, 1.4 Hz, 1H), 5.02 (dd, $J = 17.1$, 1.6 Hz, 1H), 3.67 – 3.39 (m, 2H).

3-Allyl-1H-indole-2-carbaldehyde (**M23**)

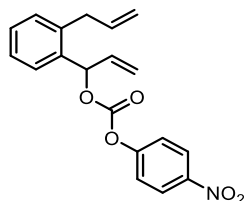
The aldehyde **M23** was synthesized according to a reported procedure.⁷⁰

^1H NMR (600 MHz, CDCl_3) δ 10.04 (s, 1H), 8.77 (s, 1H), 8.18 – 7.67 (m, 1H), 7.56 – 7.34 (m, 2H), 7.16 (ddd, $J = 8.0$, 4.7, 3.1 Hz, 1H), 6.08 (ddt, $J = 16.2$, 10.0, 6.1 Hz, 1H), 5.25 – 5.01 (m, 2H), 3.87 (dt, $J = 6.1$, 1.6 Hz, 2H).

1-(3-Allyl-1H-indol-2-yl)prop-2-en-1-ol (**M24**)

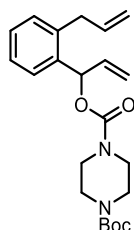
The aldehyde **M23** (200 mg, 1.1 mmol) was dissolved in THF (10 mL), cooled to 0 °C, and vinylmagnesium bromide (0.7 M solution, 1.7 mL, 1.2 mmol) was added dropwise. The reaction mixture was stirred at room temperature for 1 h, and then saturated solution of NH_4Cl (10 mL) was added at room temperature. The mixture was extracted with diethyl ether (3×10 mL). The combined organic phase was washed with water (10 mL) and brine (10 mL) successively, dried over anhydrous sodium sulfate, filtered, and the organic solvent was removed under reduced pressure to give the allylic alcohol **M24** as a pale-yellow oil (187 mg, 80%). The crude product was used in the next step without further purification.

^1H NMR (600 MHz, CDCl_3) δ 8.17 (s, 1H), 7.56 (d, $J = 7.9$ Hz, 1H), 7.33 (d, $J = 8.1$ Hz, 1H), 7.21 – 7.15 (m, 1H), 7.12 – 7.05 (m, 1H), 6.08 (ddd, $J = 17.1$, 10.4, 5.3 Hz, 1H), 6.00 (ddt, $J = 16.1$, 10.0, 6.1 Hz, 1H), 5.57 (d, $J = 4.4$ Hz, 1H), 5.45 (dt, $J = 17.1$, 1.4 Hz, 1H), 5.28 (dt, $J = 10.4$, 1.4 Hz, 1H), 5.15 – 4.98 (m, 2H), 3.53 (dt, $J = 6.1$, 1.6 Hz, 2H).

Close-to-release approach (carbamates)1-(2-Allylphenyl)allyl (4-nitrophenyl) carbonate (**M25**)

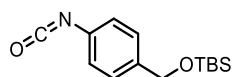
The allylic alcohol **M13** (523 mg, 3 mmol) and pyridine (400 μ L, 5 mmol) were dissolved in CH_2Cl_2 (15 mL). 4-Nitrophenyl chloroformate (666 mg, 3.3 mmol) was added portionwise at 0 $^\circ\text{C}$. The reaction mixture was stirred at that temperature for 1 h and then concentrated under reduced pressure. The residue was subjected to silica gel column chromatography (10% EtOAc in cyclohexane) to give the carbonate **M25** as a pale-yellow solid (631 mg, 62%).

^1H NMR (500 MHz, CDCl_3) δ 8.32 – 8.19 (m, 2H), 7.57 – 7.44 (m, 1H), 7.41 – 7.29 (m, 4H), 7.23 (dd, J = 6.3, 2.7 Hz, 1H), 6.44 (d, J = 5.8 Hz, 1H), 6.18 – 6.05 (m, 1H), 5.99 (ddt, J = 16.5, 10.1, 6.2 Hz, 1H), 5.42 – 5.27 (m, 2H), 5.10 (dq, J = 10.1, 1.5 Hz, 1H), 5.01 (dq, J = 17.1, 1.7 Hz, 1H), 3.58 (dd, J = 16.1, 6.4 Hz, 1H), 3.53 – 3.43 (m, 1H).

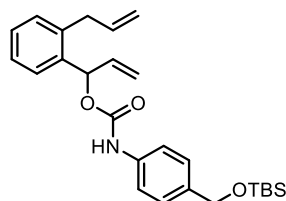
1-(1-(2-Allylphenyl)allyl) 4-(*tert*-butyl) piperazine-1,4-dicarboxylate (**M26**)

The carbonate **M25** (34 mg, 0.1 mmol) and *tert*-butyl piperazine-1-carboxylate (20 mg, 0.11 mmol) were dissolved in DMF (1 mL). Et_3N (42 μ L, 0.3 mmol) was added to the reaction mixture, and the resulting solution was stirred at room temperature for 1 h. Volatiles were removed under reduced pressure, and the residue was purified by silica gel column chromatography (10% EtOAc in cyclohexane) to give the carbamate **M26** as a pale-yellow oil (31 mg, 80%).

^1H NMR (500 MHz, CDCl_3) δ 7.37 – 7.14 (m, 4H), 6.44 (d, J = 5.2 Hz, 1H), 6.09 – 5.87 (m, 2H), 5.46 – 5.15 (m, 2H), 5.11 – 4.96 (m, 2H), 3.60 – 3.30 (m, 10H), 1.46 (s, 9H).

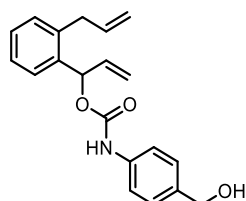
Tert-butyl((4-isocyanatobenzyl)oxy)dimethylsilane (**M27**)

The isocyanate **M27** was prepared according to a reported procedure.⁷¹

1-(2-Allylphenyl)allyl 4-(((*tert*-butyldimethylsilyl)oxy)methyl)phenyl)carbamate (**M28**)

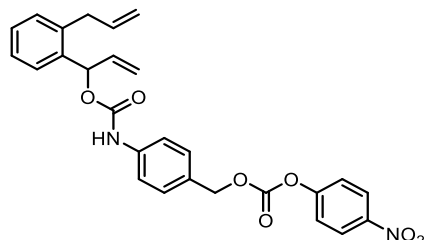
The isocyanate **M27** (1.05 g, 4 mmol), the allylic alcohol **M13** (700 mg, 4 mmol), and Et₃N (1.1 mL, 8.8 mmol) were dissolved in CH₂Cl₂ (15 mL) at 0 °C and then stirred at room temperature for 16 h. The volatiles were removed under reduced pressure and the residue was purified by silica gel column chromatography (5% EtOAc in cyclohexane) to afford the carbamate **M28** as a colourless oil (1.3 g, 74%).

¹H NMR (500 MHz, CDCl₃) δ 7.48 – 7.07 (m, 8H), 6.65 (s, 1H), 6.51 (d, *J* = 5.3 Hz, 1H), 6.18 – 5.88 (m, 2H), 5.47 – 5.19 (m, 2H), 5.16 – 4.96 (m, 2H), 4.68 (s, 2H), 3.61 (dd, *J* = 16.0, 6.5 Hz, 1H), 3.54 – 3.41 (m, 1H), 0.92 (s, 9H), 0.08 (s, 6H).

1-(2-Allylphenyl)allyl 4-(hydroxymethyl)phenyl)carbamate (**M29**)

To a solution of the carbamate **M28** (437 mg, 1 mmol) in THF (15 mL) 1 M solution of TBAF in THF (1.5 mL, 1.5 mmol) was added dropwise at 0 °C. The reaction mixture was stirred for 2 h at room temperature and then concentrated under reduced pressure. The residue was purified by silica gel column chromatography (20% EtOAc in cyclohexane) to give the alcohol **M29** as a white solid (300 mg, 93%).

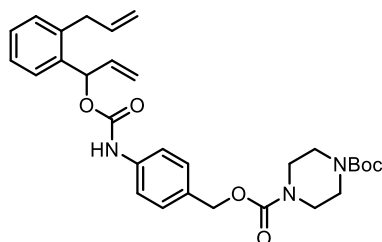
¹H NMR (500 MHz, CDCl₃) δ 7.61 – 7.03 (m, 8H), 6.70 (s, 1H), 6.50 (d, *J* = 5.3 Hz, 1H), 6.17 – 5.88 (m, 2H), 5.45 – 5.21 (m, 2H), 5.14 – 4.95 (m, 2H), 4.62 (s, 2H), 3.60 (dd, *J* = 16.0, 6.5 Hz, 1H), 3.48 (dd, *J* = 16.0, 6.0 Hz, 1H).

1-(2-Allylphenyl)allyl 4-(((4-nitrophenoxy)carbonyl)oxy)methyl)phenyl)carbamate (**M30**)

The alcohol **M29** (150 mg, 0.46 mmol) and pyridine (85 μL, 1.1 mmol) were dissolved in CH₂Cl₂ (2 mL). 4-nitrophenyl chloroformate (202 mg, 1 mmol) was added portionwise at 0 °C. The reaction mixture was stirred at that temperature for 1 h, and then concentrated under reduced pressure. The residue was directly subjected to silica gel column chromatography (10% EtOAc in cyclohexane) to give the carbonate **M30** as a pale-yellow solid (148 mg, 66%).

¹H NMR (500 MHz, CDCl₃) δ 8.29 – 8.23 (m, 2H), 7.47 – 7.30 (m, 7H), 7.30 – 7.26 (m, 2H), 7.22 (dd, *J* = 6.9, 2.1 Hz, 1H), 6.74 (s, 1H), 6.52 (d, *J* = 5.3 Hz, 1H), 6.21 – 5.92 (m, 2H), 5.36 – 5.21 (m, 4H), 5.14 – 4.98 (m, 2H), 3.61 (dd, *J* = 16.0, 6.5 Hz, 1H), 3.50 (dd, *J* = 16.0, 6.0 Hz, 1H).

1-(4-((((1-(2-allylphenyl)allyl)oxy)carbonyl)amino)benzyl) 4-(*tert*-butyl) piperazine-1,4-dicarboxylate (**M31**)

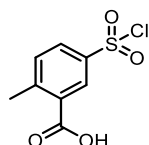


The carbonate **M30** (48 mg, 0.1 mmol) and *tert*-butyl piperazine-1-carboxylate (54 mg, 0.3 mmol) were dissolved in DMF (1 mL). DIPEA (55 μ L, 0.3 mmol) was added to the reaction mixture, and the resulting solution was stirred at room temperature for 1 h. Volatiles were removed under reduced pressure and the residue was purified by silica gel column chromatography (15% EtOAc in cyclohexane) to give the dicarbamate **M31** as a colourless oil (34 mg, 63%).

^1H NMR (500 MHz, CDCl_3) δ 7.51 – 7.14 (m, 8H), 6.87 (s, 1H), 6.50 (d, J = 5.3 Hz, 1H), 6.15 – 5.89 (m, 2H), 5.37 – 5.22 (m, 2H), 5.16 – 4.92 (m, 4H), 3.85 – 3.49 (m, 10H), 1.45 (s, 9H).

MINFLUX project

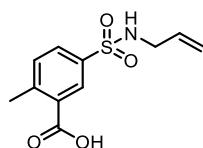
5-(Chlorosulfonyl)-2-methylbenzoic acid (**M32**)



The carboxylic acid **M32** was obtained according to a reported procedure.⁷²

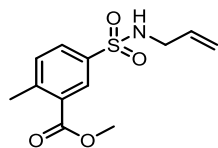
^1H NMR (500 MHz, Acetone- d_6) δ 8.55 (d, J = 2.3 Hz, 1H), 8.18 (dd, J = 8.3, 2.3 Hz, 1H), 7.77 (d, J = 8.3 Hz, 1H), 2.76 (s, 3H).

5-(*N*-Allylsulfamoyl)-2-methylbenzoic acid (**M33**)



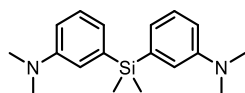
The carboxylic acid **M32** (9.4 g, 40 mmol) and pyridine (9.6 mL, 120 mmol) were dissolved in CH_2Cl_2 (120 mL). Allylamine (2.3 g, 40 mmol) was added dropwise at 0 $^\circ\text{C}$. The reaction mixture was stirred at room temperature for 4 h and then washed with 1M solution of HCl (5 \times 50 mL), water (50 mL) and brine (50 mL) successively, dried over anhydrous sodium sulfate, filtered, and the organic solvent was removed under reduced pressure to give the arylsulfonamide **M33** as a colourless oil (1 g, 10%). The crude product was used in the next step without further purification.

^1H NMR (500 MHz, Acetone- d_6) δ 8.40 (d, J = 2.1 Hz, 1H), 7.91 (dd, J = 8.0, 2.1 Hz, 1H), 7.69 – 7.49 (m, 1H), 6.75 (t, J = 5.8 Hz, 1H), 5.77 (ddt, J = 17.1, 10.3, 5.7 Hz, 1H), 5.19 (dq, J = 17.2, 1.6 Hz, 1H), 5.03 (dq, J = 10.3, 1.5 Hz, 1H), 3.58 (tt, J = 6.0, 1.6 Hz, 2H), 2.68 (s, 3H).

Methyl 5-(*N*-allylsulfamoyl)-2-methylbenzoate **M34**

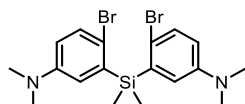
The arylsulfonamide **M33** (1.0 g, 4 mmol) was dissolved in methanol (100 mL) and sulphuric acid (200 μ L) was added. The reaction mixture was refluxed for 16 h and then concentrated under reduced pressure. The residue was dissolved in diethyl ether (50 mL) and washed with a saturated solution of NaHCO_3 (2 \times 20 mL), water (20 mL) and saturated brine (30 mL) successively, dried over anhydrous sodium sulfate, filtered, and the organic solvent was removed under reduced pressure to give the methyl ester **M34** as a colourless oil (1.05 g, quant.). The crude product was used in the next step without further purification.

^1H NMR (500 MHz, Acetone- d_6) δ 8.36 (dd, $J = 37.7, 2.1$ Hz, 1H), 7.91 (ddd, $J = 8.0, 2.0, 1.2$ Hz, 1H), 7.63 – 7.44 (m, 1H), 6.74 (s, 1H), 5.75 (ddtd, $J = 17.1, 10.4, 5.7, 4.7$ Hz, 1H), 5.18 (ddq, $J = 17.1, 3.3, 1.6$ Hz, 1H), 5.03 (dp, $J = 10.3, 1.5$ Hz, 1H), 3.75 (s, 3H), 3.63 – 3.54 (m, 2H), 2.66 (d, $J = 12.3$ Hz, 3H).

3,3'-(Dimethylsilanediyl)bis(*N,N*-dimethylaniline) (**M35**)

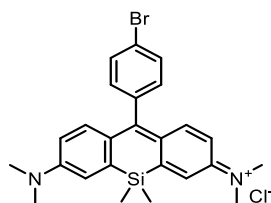
The dianiline **M35** was obtained according to a reported procedure.²³

^1H NMR (600 MHz, CDCl_3) δ 7.24 (t, $J = 7.7$ Hz, 2H), 6.98 – 6.87 (m, 4H), 6.76 (dd, $J = 8.2, 2.1$ Hz, 2H), 2.92 (s, 12H), 0.53 (s, 6H).

3,3'-(Dimethylsilanediyl)bis(4-bromo-*N,N*-dimethylaniline) (**M36**)

The dibromide **M36** was obtained according to a reported procedure.²³

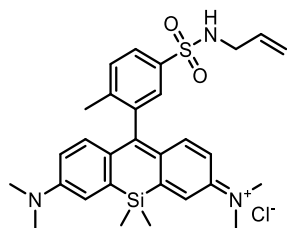
^1H NMR (600 MHz, CDCl_3) δ 7.34 (d, $J = 8.7$ Hz, 2H), 6.83 (d, $J = 3.1$ Hz, 2H), 6.59 (dd, $J = 8.8, 3.1$ Hz, 2H), 2.87 (s, 12H), 0.75 (s, 6H).

N-(10-(4-Bromophenyl)-7-(dimethylamino)-5,5-dimethyldibenzo[*b,e*]silin-3(*5H*)-ylidene)-*N*-methylnmethanaminium chloride (**M37**)

The silicorhodamine **M37** was obtained according to a reported procedure.²³

^1H NMR (400 MHz, CDCl_3) δ 7.67 (d, $J = 8.4$ Hz, 2H), 7.25 (d, $J = 2.8$ Hz, 2H), 7.17 – 7.03 (m, 4H), 6.65 (dd, $J = 9.7, 2.8$ Hz, 2H), 3.42 (s, 12H), 0.63 (s, 6H).

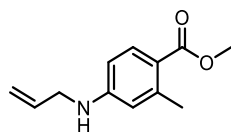
N-(10-(5-(*N*-Allylsulfamoyl)-2-methylphenyl)-7-(dimethylamino)-5,5-dimethyldibenzo[*b,e*]silin-3(5*H*)-ylidene)-*N*-methylnmethanaminium chloride (**M38**)



A solution of the dibromide **M36** (91 mg, 0.2 mmol) in THF (5 mL) was cooled to $-78\text{ }^{\circ}\text{C}$ and *sec*-BuLi (1.4 M solution, 320 μL , 0.45 mmol) was added dropwise. The reaction mixture was stirred at that temperature for 1 h, and a solution of the methyl ester **M34** (27 mg, 0.1 mmol) in THF (1 mL) was added dropwise. The reaction mixture was stirred for 1 h at $-78\text{ }^{\circ}\text{C}$ and for 16 h at room temperature. HCl (1M, 1 mL) was added, and the mixture was stirred for additional 30 min. The volatiles were removed under reduced pressure and the residue was purified by silica gel column chromatography (5% MeOH in CH_2Cl_2) to give the silicorhodamine **M38** as a blue solid (25 mg, 48%).

^1H NMR (500 MHz, CDCl_3) δ 8.01 (dd, $J = 8.1, 2.0$ Hz, 1H), 7.67 (d, $J = 1.9$ Hz, 1H), 7.48 (d, $J = 8.2$ Hz, 1H), 7.18 (d, $J = 2.8$ Hz, 2H), 7.03 (d, $J = 9.6$ Hz, 2H), 6.72 (dd, $J = 9.6, 2.8$ Hz, 2H), 6.59 (t, $J = 6.1$ Hz, 1H), 5.82 (ddt, $J = 17.0, 10.3, 5.8$ Hz, 1H), 5.18 (dq, $J = 17.1, 1.5$ Hz, 1H), 5.03 (dq, $J = 10.3, 1.3$ Hz, 1H), 3.79 – 3.62 (m, 2H), 3.40 (s, 12H), 2.09 (s, 3H).

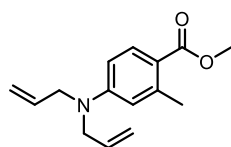
Methyl 4-(allylamino)-2-methylbenzoate (**M39**)



Methyl 4-amino-2-methylbenzoate (2.5 g, 15 mmol), allyl bromide (1.6 g, 13 mmol), and K_2CO_3 (4.14 g, 30 mmol) were heated at $60\text{ }^{\circ}\text{C}$ in DMF (50 mL) for 2 h. The reaction mixture was concentrated under reduced pressure, and the residue was dissolved in water (100 mL) and extracted with diethyl ether (3 \times 50 mL). The combined organic phase was washed with water (50 mL) and brine (50 mL) successively, dried over anhydrous sodium sulfate, filtered, and the organic solvent was removed under reduced pressure. The crude product was purified by silica gel column chromatography (5% EtOAc in cyclohexane) to give the secondary aniline **M39** as a colourless oil (1.3 g, 42%).

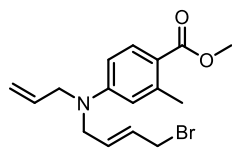
^1H NMR (500 MHz, CDCl_3) δ 7.84 (d, $J = 8.4$ Hz, 1H), 6.44 – 6.34 (m, 2H), 5.93 (ddt, $J = 17.2, 10.4, 5.3$ Hz, 1H), 5.27 (dq, $J = 17.2, 1.7$ Hz, 1H), 5.19 (dq, $J = 10.3, 1.5$ Hz, 1H), 4.14 (s, 1H), 3.90 – 3.72 (m, 5H), 2.56 (s, 3H).

Methyl 4-(diallylamino)-2-methylbenzoate (**M40**)



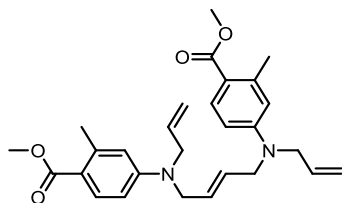
The diallyl aniline **M40** was isolated as by-product in the synthesis of the secondary aniline **M39** (840 mg, 23%).

^1H NMR (500 MHz, CDCl_3) δ 7.85 (d, $J = 8.8$ Hz, 1H), 6.56 – 6.29 (m, 2H), 5.84 (ddt, $J = 17.1, 10.3, 4.8$ Hz, 2H), 5.29 – 5.12 (m, 4H), 3.96 (dt, $J = 3.8, 1.6$ Hz, 4H), 3.81 (s, 3H), 2.57 (s, 3H).

Methyl (*E*)-4-(allyl(4-bromobut-2-en-1-yl)amino)-2-methylbenzoate (**M41**)

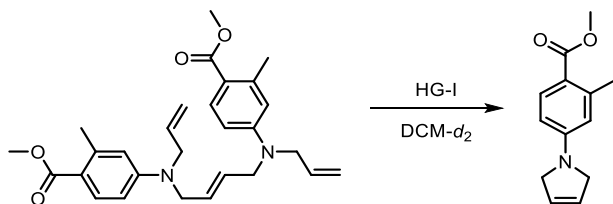
The secondary aniline **M39** (1.3 g, 6.3 mmol), (*E*)-1,4-dibromobut-2-ene (1.35 g, 6.3 mmol), and K_2CO_3 (874 mg, 6.3 mmol) were heated at 40 °C in DMF (40 mL) for 2 h. The reaction mixture was concentrated under reduced pressure. The residue was dissolved in water (100 mL) and extracted with diethyl ether (3×50 mL). The combined organic phase was washed with water (50 mL) and brine (50 mL) successively, dried over anhydrous sodium sulfate, filtered, and the organic solvent was removed under reduced pressure. The crude product was purified by silica gel column chromatography (5% EtOAc in cyclohexane) to give the aniline **M41** as a pale-yellow oil (651 mg, 31%).

1H NMR (600 MHz, $CDCl_3$) δ 7.85 (d, J = 8.8 Hz, 1H), 6.55 – 6.36 (m, 2H), 5.86 – 5.76 (m, 3H), 5.17 (dd, J = 23.2, 13.8 Hz, 2H), 4.00 – 3.91 (m, 6H), 3.82 (s, 3H), 2.57 (s, 3H).

Dimethyl 4,4'-(but-2-ene-1,4-diylbis(allylzanediyl))(*E*)-bis(2-methylbenzoate) (**M42**)

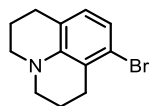
The triene **M42** was isolated as by-product in the synthesis of the aniline **M41** (212 mg, 15%).

1H NMR (600 MHz, $CDCl_3$) δ 7.84 (d, J = 8.8 Hz, 2H), 6.72 – 6.34 (m, 4H), 5.81 (ddq, J = 15.1, 9.7, 4.3 Hz, 2H), 5.58 (s, 2H), 5.29 – 5.07 (m, 4H), 4.14 – 3.89 (m, 8H), 3.82 (s, 6H), 3.49 (d, J = 5.5 Hz, 2H), 2.56 (s, 6H).

Methyl 4-(2,5-dihydro-1*H*-pyrrol-1-yl)-2-methylbenzoate

The triene **M42** (23 mg, 0.05 mmol) was dissolved in CD_2Cl_2 (400 μ L) and placed in an NMR tube. A solution of HG-I (3 mg, 0.0025 mmol) in CD_2Cl_2 (200 μ L) was added, and the reaction was monitored by 1H NMR. According to spectra, quantitative conversion of the triene **M42** to methyl 4-(2,5-dihydro-1*H*-pyrrol-1-yl)-2-methylbenzoate was achieved within 5 min.

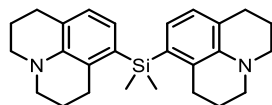
1H NMR (600 MHz, CD_2Cl_2) δ 7.78 (d, J = 8.6 Hz, 1H), 6.29 – 6.19 (m, 2H), 5.88 (s, 2H), 4.05 (s, 4H), 3.70 (s, 3H), 2.49 (s, 3H).

8-Bromo-2,3,6,7-tetrahydro-1*H*,5*H*-pyrido[3,2,1-*ij*]quinolone

8-bromo-2,3,6,7-tetrahydro-1*H*,5*H*-pyrido[3,2,1-*ij*]quinolone was obtained according to a reported procedure.⁷³

^1H NMR (600 MHz, CDCl_3) δ 6.75 (d, $J = 8.0$ Hz, 1H), 6.64 (d, $J = 8.0$ Hz, 1H), 3.12 (dt, $J = 18.1, 5.6$ Hz, 4H), 2.77 (t, $J = 6.7$ Hz, 2H), 2.70 (t, $J = 6.5$ Hz, 2H), 1.96 (dp, $J = 18.2, 6.3$ Hz, 4H).

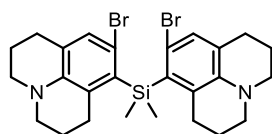
Dimethylbis(2,3,6,7-tetrahydro-1*H*,5*H*-pyrido[3,2,1-*ij*]quinolin-8-yl)silane (**M43**)



To a solution of 8-bromo-2,3,6,7-tetrahydro-1*H*,5*H*-pyrido[3,2,1-*ij*]quinoline (1 g, 4 mmol) in dry THF (25 mL), *sec*-BuLi (1.4M, 2.86 mL, 4 mmol) was added dropwise at -78°C , and the mixture was stirred 1 h at that temperature. Me_2SiCl_2 (232 mg, 1.8 mmol) was added at -78°C and the reaction mixture was allowed to warm to room temperature over 15 h. Water (10 mL) was added to the reaction and the mixture was extracted with diethyl ether (3×20 mL). The combined organic layers were washed with brine (50 mL), dried over anhydrous sodium sulfate, filtered, and the organic solvent was removed under reduced pressure. The residue was purified by silica gel column chromatography (2% EtOAc in cyclohexane) to give the silane **M43** as a pale-yellow oil (549 mg, 76%).

^1H NMR (500 MHz, CDCl_3) δ 6.77 (d, $J = 7.4$ Hz, 2H), 6.70 (d, $J = 7.4$ Hz, 2H), 3.19 – 3.10 (m, 4H), 3.10 – 3.03 (m, 4H), 2.76 (t, $J = 6.5$ Hz, 4H), 2.67 (t, $J = 6.4$ Hz, 4H), 1.96 (dt, $J = 12.0, 6.5$ Hz, 4H), 1.85 (p, $J = 6.3$ Hz, 4H), 0.51 (s, 6H).

Bis(9-bromo-2,3,6,7-tetrahydro-1*H*,5*H*-pyrido[3,2,1-*ij*]quinolin-8-yl)dimethylsilane (**M44**)

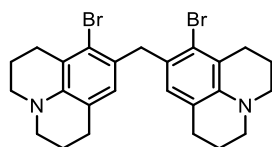


To a solution of the silane **M43** (183 mg, 0.45 mmol) in CH_2Cl_2 (5 mL), a solution of Br_2 (144 mg, 0.9 mmol) in CH_2Cl_2 (2 mL) was added at 0°C within 3 min. The reaction mixture was stirred at room temperature for 30 min and then concentrated under reduced pressure to give the dibromide **M44** as a red oil (252 mg, quant.). The crude product was used in the next step without further purification.

^1H NMR (500 MHz, CDCl_3) δ 6.93 (s, 2H), 3.48 – 3.07 (m, 4H), 3.05 (s, 4H), 2.84 – 2.54 (m, 8H), 1.99 – 1.85 (m, 4H), 1.81 (p, $J = 6.3$ Hz, 4H), 0.77 (s, 6H).

^{13}C NMR (126 MHz, CDCl_3) δ 137.69, 131.92, 129.51, 124.75, 115.48, 50.64, 49.76, 29.20, 27.85, 27.07, 22.49, 21.92, 7.71.

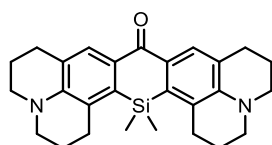
Bis(8-bromo-2,3,6,7-tetrahydro-1*H*,5*H*-pyrido[3,2,1-*ij*]quinolin-9-yl)methane (**M45**)



The dibromide **M45** was obtained according to a reported procedure.⁷⁴

^1H NMR (500 MHz, CDCl_3) δ 6.47 (s, 2H), 3.95 (s, 2H), 3.30 – 2.99 (m, 8H), 2.83 (t, $J = 6.7$ Hz, 4H), 2.64 (t, $J = 6.6$ Hz, 4H), 2.16 – 1.80 (m, 8H).

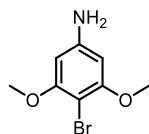
Phenone **M46**



The phenone **M46** was obtained according to a reported procedure.⁷⁵

¹H NMR (500 MHz, CDCl₃) δ 8.06 (s, 2H), 3.28 (dt, *J* = 8.8, 5.9 Hz, 8H), 3.02 – 2.86 (m, 4H), 2.82 (t, *J* = 6.3 Hz, 4H), 2.10 – 1.83 (m, 8H), 0.59 (s, 6H).

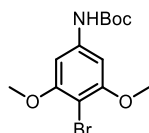
4-Bromo-3,5-dimethoxyaniline (**M47**)



The primary aniline **M47** was obtained according to a reported procedure.⁷⁶

¹H NMR (500 MHz, CDCl₃) δ 5.95 (s, 2H), 3.83 (s, 6H), 3.74 (s, 2H).

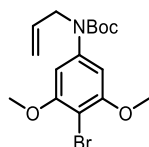
Tert-butyl (4-bromo-3,5-dimethoxyphenyl)carbamate (**M48**)



The primary aniline **M47** (635 mg, 2.7 mmol) and Boc₂O were heated in toluene at 100 °C for 16 h. The volatiles were removed under reduced pressure and the residue was purified by silica gel column chromatography (10% EtOAc in cyclohexane) to give the carbamate **M48** as a pale-yellow oil (550 mg, 61%).

¹H NMR (500 MHz, CDCl₃) δ 6.70 (s, 2H), 6.51 (s, 1H), 3.88 (s, 6H), 1.52 (s, 9H).

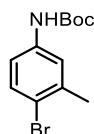
Tert-butyl allyl(4-bromo-3,5-dimethoxyphenyl)carbamate (**M49**)



The carbamate **M48** (550 mg, 1.66 mmol) was dissolved in DMF (15 mL), and 60% NaH in mineral oil (100 mg, 2.5 mmol) was added in portions. Then, allyl bromide (303 mg, 2.5 mmol) was added at 0 °C, and the reaction mixture was stirred for 16 h at room temperature. Volatiles were removed under reduced pressure and saturated solution of NH₄Cl (20 mL) was added. The mixture was extracted with CH₂Cl₂ (3×20 mL). The combined organic phase was washed with water (20 mL) and brine (20 mL) successively, dried over anhydrous sodium sulfate, filtered, and the organic solvent was removed under reduced pressure. The residue was purified by silica gel column chromatography (10% EtOAc in cyclohexane) to give the carbamate **M49** as a colourless oil (580 mg, 94%).

¹H NMR (500 MHz, CDCl₃) δ 6.50 (s, 2H), 6.05 – 5.78 (m, 1H), 5.22 – 5.08 (m, 2H), 4.40 – 4.16 (m, 2H), 3.86 (d, *J* = 1.2 Hz, 6H), 1.46 (s, 9H).

Tert-butyl (4-bromo-3-methylphenyl)carbamate (**M50**)

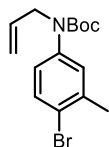


4-Bromo-3-methylaniline (4.4 g, 23.7 mmol) and Boc₂O (5.16 g, 23.7 mmol) were dissolved in toluene (40 mL) and heated at 100 °C for 40 h. The volatiles were removed under reduced pressure to give the

carbamate **M50** as a white solid (6.78 g, quant.). The crude product was used in the next step without further purification.

^1H NMR (500 MHz, CDCl_3) δ 7.40 (d, J = 8.6 Hz, 1H), 7.32 (s, 1H), 7.02 (dd, J = 8.6, 2.6 Hz, 1H), 6.42 (s, 1H), 2.36 (s, 3H), 1.51 (s, 9H).

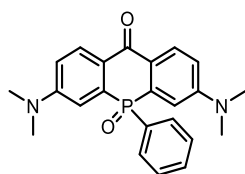
Tert-butyl allyl(4-bromo-3-methylphenyl)carbamate (**M51**)



The carbamate **M50** (6.78 g, 23.7 mmol) was dissolved in DMF (100 mL) and 60% NaH in mineral oil (1.42 g, 35.5 mmol) was added in portions. Then, allyl bromide (3.1 mL, 35.5 mmol) was added dropwise at 0 °C, and the reaction mixture was stirred for 16 h at room temperature. Volatiles were removed under reduced pressure and saturated solution of NH_4Cl (50 mL) was added. The mixture was extracted with diethyl ether (3×50 mL). The combined organic phase was washed with water (50 mL) and brine (50 mL) successively, dried over anhydrous sodium sulfate, filtered, and the organic solvent was removed under reduced pressure. The residue was purified by silica gel column chromatography (5% EtOAc in cyclohexane) to give the carbamate **M51** as a colourless oil (6.73 g, 87%).

^1H NMR (500 MHz, CDCl_3) δ 7.44 (d, J = 8.5 Hz, 1H), 7.11 (s, 1H), 6.92 (dd, J = 8.4, 2.2 Hz, 1H), 5.98 – 5.80 (m, 1H), 5.22 – 5.07 (m, 2H), 4.18 (dt, J = 5.6, 1.5 Hz, 2H), 2.36 (s, 3H), 1.44 (s, 9H).

3,7-Bis(dimethylamino)-5-phenyl-10*H*-acridophosphin-10-one 5-oxide

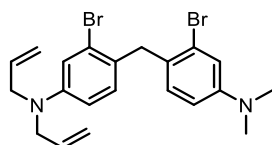


3,7-bis(dimethylamino)-5-phenyl-10*H*-acridophosphin-10-one 5-oxide was obtained according to a reported procedure.⁷⁷

^1H NMR (500 MHz, $\text{CD}_3\text{OD_SPE}$) δ 8.26 (dd, J = 9.1, 6.2 Hz, 2H), 7.63 – 7.36 (m, 5H), 7.09 (dd, J = 15.1, 2.7 Hz, 2H), 7.04 (dd, J = 9.0, 2.6 Hz, 2H), 3.09 (s, 12H).

^{31}P NMR (202 MHz, $\text{CD}_3\text{OD_SPE}$) δ 9.43.

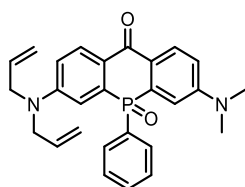
N,N-Diallyl-3-bromo-4-(2-bromo-4-(dimethylamino)benzyl)aniline (**M53**)



The dibromide **M53** was obtained according to a reported procedure.⁷⁸

^1H NMR (500 MHz, CDCl_3) δ 6.93 (d, J = 2.7 Hz, 1H), 6.90 (d, J = 2.7 Hz, 1H), 6.87 (d, J = 8.6 Hz, 1H), 6.80 (d, J = 8.6 Hz, 1H), 6.59 (dd, J = 8.6, 2.7 Hz, 1H), 6.54 (dd, J = 8.6, 2.7 Hz, 1H), 5.82 (ddt, J = 17.3, 9.8, 4.9 Hz, 2H), 5.23 – 5.11 (m, 4H), 3.98 (s, 2H), 3.87 (dt, J = 4.5, 1.5 Hz, 4H), 2.91 (s, 6H).

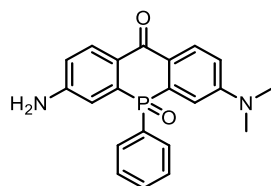
3-(Diallylamino)-7-(dimethylamino)-5-phenyl-10*H*-acridophosphin-10-one 5-oxide (**M54**)



The dibromide **M53** (2.04 g, 4.4 mmol) was dissolved in THF (15 mL) under an Ar atmosphere, and the solution was cooled to $-78\text{ }^{\circ}\text{C}$. Then, *sec*-BuLi (1.4 M, 6.6 mL, 9.28 mmol) was added dropwise, and the mixture was stirred at that temperature for 15 min. Dichlorophenylphosphine (600 μL , 4.44 mmol), dissolved in THF (5.0 mL), was added dropwise, and the mixture was stirred at the same temperature for 2 h. H_2O_2 (30% aqueous solution, 4.0 mL, 36 mmol) was added and the stirring was continued at $0\text{ }^{\circ}\text{C}$ for 2 h. The reaction mixture was diluted with H_2O and a saturated NaHCO_3 solution, extracted with EtOAc, and dried over anhydrous Na_2SO_4 . The solvent was removed under reduced pressure, and the residue was dissolved in CH_2Cl_2 (50 mL). Chloranil (1.0 g, 4.4 mmol) was added to the solution, and the mixture was stirred at room temperature for 8 h. Then, the solvent was removed under reduced pressure and the residue was purified by silica gel column chromatography (1% MeOH in CH_2Cl_2) to give the phenone **M54** as a yellow solid (660 mg, 34%).

^1H NMR (500 MHz, CDCl_3) δ 8.32 (dd, $J = 9.0, 5.9\text{ Hz}$, 1H), 8.27 (dd, $J = 9.0, 5.9\text{ Hz}$, 1H), 7.63 – 7.54 (m, 2H), 7.43 – 7.28 (m, 3H), 7.14 (td, $J = 14.5, 2.8\text{ Hz}$, 2H), 6.86 (td, $J = 8.8, 2.7\text{ Hz}$, 2H), 5.79 (ddt, $J = 17.1, 10.0, 4.8\text{ Hz}$, 2H), 5.20 – 5.02 (m, 4H), 4.05 (dd, $J = 17.3, 4.8\text{ Hz}$, 2H), 3.95 (ddt, $J = 17.4, 4.7, 1.6\text{ Hz}$, 2H), 3.08 (s, 6H).

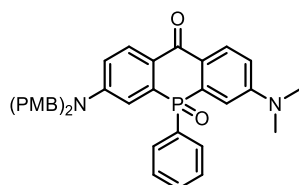
3-Amino-7-(dimethylamino)-5-phenyl-10H-acridophosphin-10-one 5-oxide (**M55**)



The phenone **M54** (500 mg, 1.13 mmol), 1,3-dimethylbarbituric acid (360 mg, 2.3 mmol), and $\text{Pd}(\text{PPh}_3)_4$ (266 mg, 0.23 mmol) were heated in DCE (20 mL) at $80\text{ }^{\circ}\text{C}$ for 5 h. The volatiles were removed under reduced pressure and the residue was purified by silica gel column chromatography (3% MeOH in CH_2Cl_2) to give the aniline **M55** as a yellow solid (280 mg, 69%).

^1H NMR (500 MHz, CDCl_3) δ 8.29 (dd, $J = 9.0, 6.1\text{ Hz}$, 1H), 8.22 (dd, $J = 8.6, 5.7\text{ Hz}$, 1H), 7.55 (ddd, $J = 12.7, 8.3, 1.3\text{ Hz}$, 2H), 7.42 – 7.29 (m, 3H), 7.14 – 7.02 (m, 2H), 6.91 – 6.72 (m, 2H), 3.06 (s, 6H).

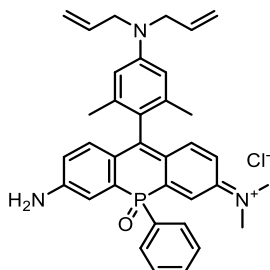
3-(bis(4-methoxybenzyl)amino)-7-(dimethylamino)-5-phenyl-10H-acridophosphin-10-one 5-oxide (**M56**)



The aniline **M55** (280 mg, 0.77 mmol) was dissolved in a mixture of CH_2Cl_2 (15 mL) and DMF (15 mL). NaH (60% in mineral oil, 462 g, 11.5 mmol) was added in portions. Then, *p*-methoxybenzyl chloride (1.2 g, 7.7 mmol) was added at $0\text{ }^{\circ}\text{C}$, and the reaction mixture was stirred for 16 h at room temperature. Volatiles were removed under reduced pressure and a saturated solution of NH_4Cl (20 mL) was added. The mixture was extracted with CH_2Cl_2 (20 mL \times 5). The combined organic phase was washed with water (50 mL) and saturated brine (50 mL) successively, dried over anhydrous sodium sulfate, filtered, and the organic solvent was removed under reduced pressure. The residue was purified by silica gel column chromatography (1% MeOH in CH_2Cl_2) to give the phenone **M56** as a yellow solid (255 mg, 55%).

^1H NMR (500 MHz, CDCl_3) δ 8.32 (dd, $J = 9.0, 5.9$ Hz, 1H), 8.23 (dd, $J = 9.0, 5.9$ Hz, 1H), 7.51 – 7.32 (m, 3H), 7.30 – 7.19 (m, 2H), 7.12 – 7.01 (m, 5H), 6.90 (ddd, $J = 16.9, 9.0, 2.7$ Hz, 2H), 6.83 – 6.63 (m, 4H), 4.74 (d, $J = 16.7$ Hz, 2H), 4.53 (d, $J = 16.7$ Hz, 2H), 3.78 (s, 6H), 3.07 (s, 6H).

N-(7-Amino-10-(4-(diallylamino)-2,6-dimethylphenyl)-5-oxido-5-phenyl-3*H*-acridophosphin-3-ylidene)-*N*-methylmethanaminium chloride (**M57**)

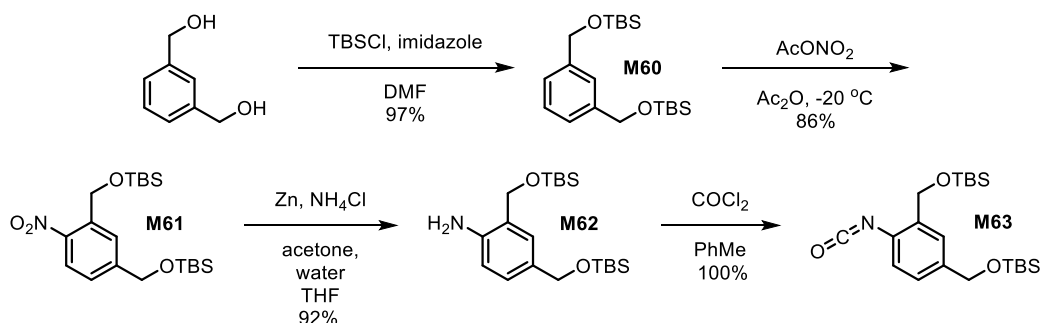


A solution of *N,N*-diallyl-4-bromo-3,5-dimethylaniline (140 mg, 0.5 mmol) in THF (5 mL) was cooled to -78°C *sec*-BuLi (1.4M, 357 μL , 0.5 mmol) was added dropwise. The reaction mixture was stirred at that temperature for 1 h, and a solution of the phenone **M56** (60 mg, 0.1 mmol) in THF (5 mL) was added dropwise. The reaction mixture was stirred for 1 h at -78°C and for 16 h at room temperature. HCl (2M, 5 mL) was added, and the mixture was stirred for an additional 30 min. The volatiles were removed under reduced pressure and the residue was purified by silica gel column chromatography (10% MeOH in CH_2Cl_2) to give the phosphonorhodamine **M57** as a turquoise solid (25 mg, 46%).

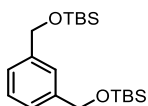
^1H NMR (500 MHz, CDCl_3) δ 7.71 – 7.35 (m, 7H), 7.04 (d, $J = 6.8$ Hz, 4H), 6.83 (s, 4H), 6.45 (s, 2H), 5.89 (s, 2H), 5.43 – 5.02 (m, 4H), 3.97 (s, 4H), 3.79 (s, 6H), 1.91 (d, $J = 25.5$ Hz, 6H).

Dendritic approach

Synthesis of **M63**



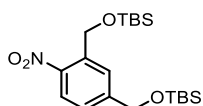
1,3-Bis(((*tert*-butyldimethylsilyl)oxy)methyl)benzene (**M60**)



The arene **M60** was obtained according to a reported procedure.⁷¹

^1H NMR (500 MHz, CDCl_3) δ 7.33 – 7.27 (m, 2H), 7.22 – 7.17 (m, 2H), 4.74 (s, 4H), 0.95 (s, 18H), 0.10 (s, 12H).

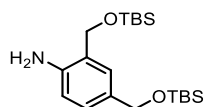
(((4-Nitro-1,3-phenylene)bis(methylene))bis(oxy))bis(*tert*-butyldimethylsilane) (**M61**)



The nitrobenzene **M61** was obtained according to a reported procedure.⁷¹

^1H NMR (500 MHz, CDCl_3) δ 8.1 (d, $J = 8.0$ Hz, 1H), 7.87 (s, 1H), 7.37 (d, $J = 8.0$ Hz, 1H), 5.11 (s, 2H), 4.82 (s, 2H), 0.94 (s, 18H), 0.13 (s, 12H).

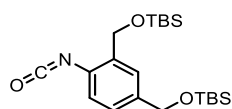
2,4-Bis(((*tert*-butyldimethylsilyl)oxy)methyl)aniline (**M62**)



The nitrobenzene **M61** (8.2 g, 20 mmol) was dissolved in a mixture of acetone (300 mL) and THF (120 mL). NH_4Cl (107 g, 2 mol) and water (200 mL) were added. Under rigorous stirring, Zn powder (65 g, 1 mol) was added in portions at room temperature. The reaction mixture was stirred for 16 h and then filtered through a glass frit. The organic solvents were removed under reduced pressure and the aqueous phase was extracted with CH_2Cl_2 (5 \times 100 mL). The combined organic phase was washed with water (200 mL) and brine (200 mL), dried over anhydrous sodium sulfate, filtered, and the organic solvent was removed under reduced pressure to give the aniline **M62** as a colourless oil (4.2 g, 55%). The crude product was used in the next step without further purification.

^1H NMR (500 MHz, CDCl_3) δ 7.05 (dd, $J = 8.0, 1.9$ Hz, 1H), 7.00 (d, $J = 1.7$ Hz, 1H), 6.63 (d, $J = 8.0$ Hz, 1H), 4.68 (s, 2H), 4.61 (s, 2H), 4.14 (s, 2H), 0.92 (s, 9H), 0.90 (s, 9H), 0.07 (d, $J = 2.0$ Hz, 12H).

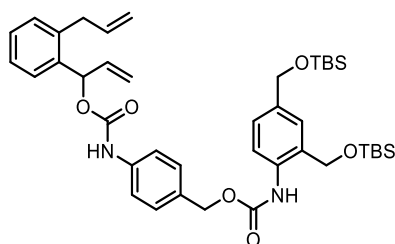
(((4-Isocyanato-1,3-phenylene)bis(methylene))bis(oxy))bis(*tert*-butyldimethylsilane) (**M63**)



Toluene (10 mL) was heated to reflux and a solution of 15 wt.% phosgene in toluene (7.5 mL, 10 mmol) was added. Then, a solution of the aniline **M62** (763 mg, 2 mmol) in toluene (5 mL) was slowly added dropwise. The reaction mixture was stirred for 2 h at 110 °C and then cooled to room temperature. The volatiles were removed under reduced pressure to give the isocyanate **M63** as a colourless oil (815 mg, quant.). The crude product was used in the next step without further purification.

^1H NMR (500 MHz, CDCl_3) δ 7.45 – 7.37 (m, 1H), 7.17 (dd, $J = 8.0, 2.0$ Hz, 1H), 7.03 (d, $J = 8.0$ Hz, 1H), 4.74 (s, 2H), 4.71 (s, 2H), 0.94 (d, $J = 2.4$ Hz, 18H), 0.11 (s, 6H), 0.09 (s, 6H).

1-(2-Allylphenyl)allyl (4-(((2,4-bis(((*tert*-butyldimethylsilyl)oxy)methyl)phenyl)carbamoyl)oxy)methyl)phenyl)carbamate (**M64**)

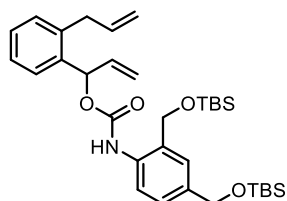


The isocyanate **M63** (80 mg, 0.2 mmol), the alcohol **M29** (49 mg, 0.15 mmol), and Et_3N (60 μL , 0.4 mmol) were dissolved in toluene (3 mL) at 0 °C and then stirred at room temperature for 16 h. The volatiles were removed under reduced pressure and the residue was purified by silica gel column chromatography (5% EtOAc in cyclohexane) to give the dicarbamate **M64** as a colourless oil (102 mg, 93%).

^1H NMR (500 MHz, CDCl_3) δ 8.33 (s, 1H), 7.97 (s, 1H), 7.44 – 7.20 (m, 9H), 7.04 (s, 1H), 6.71 (s, 1H), 6.52 (d, $J = 5.3$ Hz, 1H), 6.14 – 5.92 (m, 2H), 5.29 (dd, $J = 4.8, 1.3$ Hz, 1H), 5.26 (d, $J = 1.4$ Hz, 1H), 5.13 (s, 2H), 5.09 (dd, $J = 10.1, 1.5$ Hz, 1H), 5.03 (dd, $J = 17.1, 1.7$ Hz, 1H), 4.70 (s, 2H), 4.66 (s, 2H),

3.61 (dd, $J = 16.0, 6.5$ Hz, 1H), 3.50 (dd, $J = 16.0, 6.0$ Hz, 1H), 0.92 (s, 9H), 0.87 (s, 9H), 0.08 (s, 6H), 0.06 (s, 6H).

1-(2-Allylphenyl)allyl (2,4-bis(((*tert*-butyldimethylsilyl)oxy)methyl)phenyl)carbamate (**M65**)

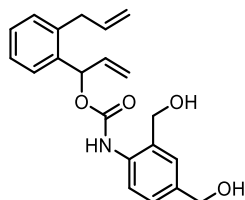


The isocyanate **M63** (1.14 g, 2.8 mmol), the allylic alcohol **M13** (348 mg, 2 mmol), and Et₃N (1 mL, 7.2 mmol) were dissolved in toluene (16 mL) at 0 °C and stirred at room temperature for 16 h. The volatiles were removed under reduced pressure and the residue was purified by silica gel column chromatography (5% EtOAc in cyclohexane) to give the carbamate **M65** as a colourless oil (890 mg, 76%).

¹H NMR (500 MHz, CDCl₃) δ 8.43 (s, 1H), 7.97 (d, $J = 7.1$ Hz, 1H), 7.44 – 7.36 (m, 1H), 7.31 – 7.15 (m, 4H), 7.04 (d, $J = 1.5$ Hz, 1H), 6.51 (dt, $J = 5.2, 1.4$ Hz, 1H), 6.12 – 5.95 (m, 2H), 5.34 – 5.20 (m, 2H), 5.12 – 4.95 (m, 2H), 4.71 (s, 2H), 4.66 (s, 2H), 3.62 (dd, $J = 16.0, 6.6$ Hz, 1H), 3.51 (ddt, $J = 15.9, 5.9, 1.5$ Hz, 1H), 0.92 (d, $J = 1.6$ Hz, 18H), 0.10 (s, 3H), 0.09 (s, 3H), 0.07 (s, 6H).

¹³C NMR (126 MHz, CDCl₃) δ 152.90, 137.72, 137.40, 137.14, 136.73, 130.02, 128.30, 127.81, 126.75, 126.69, 126.00, 116.44, 116.31, 73.33, 65.60, 64.75, 37.08, 27.06, 26.09, 25.90, 18.56, 18.23, -5.05, -5.25, -5.27.

1-(2-Allylphenyl)allyl (2,4-bis(hydroxymethyl)phenyl)carbamate (**M66**)

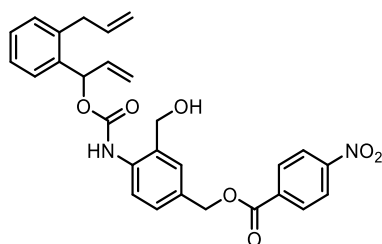


The carbamate **M65** (890 mg, 1.53 mmol) was dissolved in CH₂Cl₂ (10 mL), and Et₃N·3HF (1 mL, 6.1 mmol) was added dropwise at 0 °C. The reaction mixture was stirred for 16 h at room temperature, and then a saturated solution of NH₄Cl (10 mL) was added. The mixture was extracted with CH₂Cl₂ (3×10 mL). The combined organic phase was washed with water (20 mL) and brine (20 mL) successively, dried over anhydrous sodium sulfate, filtered, and the organic solvent was removed under reduced pressure. The residue was purified by silica gel column chromatography (50% EtOAc in cyclohexane) to give the diol **M66** as a pale-yellow solid (380 mg, 70%).

¹H NMR (500 MHz, CDCl₃) δ 8.00 – 7.81 (m, 2H), 7.46 – 7.41 (m, 1H), 7.34 – 7.24 (m, 3H), 7.24 – 7.13 (m, 2H), 6.51 (dt, $J = 5.4, 1.4$ Hz, 1H), 6.20 – 5.90 (m, 2H), 5.39 – 5.23 (m, 2H), 5.13 – 4.95 (m, 2H), 4.70 (d, $J = 5.8$ Hz, 2H), 4.63 (d, $J = 5.7$ Hz, 2H), 3.61 (dd, $J = 16.0, 6.6$ Hz, 1H), 3.55 – 3.42 (m, 1H), 1.98 (t, $J = 5.8$ Hz, 1H), 1.61 (t, $J = 5.9$ Hz, 1H).

¹³C NMR (126 MHz, CDCl₃) δ 152.95, 137.90, 137.11, 137.08, 136.44, 130.19, 128.51, 128.11, 127.87, 127.85, 126.84, 117.06, 116.33, 73.89, 64.95, 64.51, 37.08, 0.14.

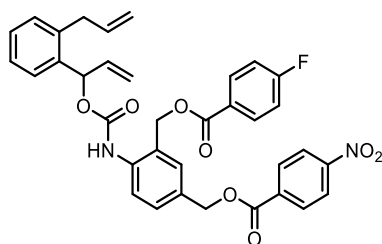
4-(((1-(2-Allylphenyl)allyl)oxy)carbonyl)amino)-3-(hydroxymethyl)benzyl 4-nitrobenzoate (**M67**)



The diol **M66** (17 mg, 0.05 mmol) and Et₃N (28 μ L, 0.2 mmol) were dissolved in CH₂Cl₂ (1 mL). A solution of 4-nitrobenzoyl chloride (9 mg, 0.05 mmol) in CH₂Cl₂ (200 μ L) was added dropwise, and the mixture was stirred for 16 h at room temperature. The reaction mixture was then concentrated under reduced pressure, and the residue was purified by silica gel column chromatography (30% EtOAc in cyclohexane) to give the alcohol 4-(((1-(2-allylphenyl)allyl)oxy)carbonyl)amino)-3-(hydroxymethyl)benzyl 4-nitrobenzoate **M67** as a white solid (10 mg, 40%).

¹H NMR (500 MHz, CDCl₃) δ 8.31 – 8.21 (m, 2H), 8.21 – 8.12 (m, 2H), 7.98 – 7.63 (m, 1H), 7.44 (d, J = 1.8 Hz, 2H), 7.36 (dd, J = 8.4, 1.9 Hz, 1H), 7.31 – 7.22 (m, 2H), 7.21 (dd, J = 7.2, 1.7 Hz, 1H), 6.53 (dt, J = 5.3, 1.3 Hz, 1H), 6.08 (ddd, J = 17.1, 10.5, 5.4 Hz, 1H), 5.99 (ddt, J = 16.7, 10.1, 6.3 Hz, 1H), 5.40 (s, 1H), 5.34 – 5.21 (m, 2H), 5.14 – 4.97 (m, 2H), 4.77 – 4.55 (m, 3H), 3.61 (dd, J = 16.0, 6.6 Hz, 1H), 3.49 (dd, J = 16.0, 6.0 Hz, 1H), 1.74 (s, 1H).

4-(((1-(2-Allylphenyl)allyl)oxy)carbonyl)amino)-3-(((4-fluorobenzoyl)oxy)methyl)benzyl 4-nitrobenzoate (**M68**)

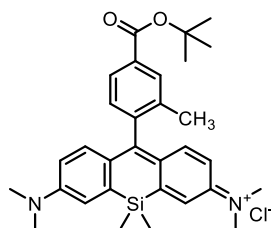


The alcohol **M67** (10 mg, 0.02 mmol) and Et₃N (28 μ L, 0.2 mmol) were dissolved in CH₂Cl₂ (3 mL). A solution of 4-fluorobenzoyl chloride (8 mg, 0.05 mmol) in CH₂Cl₂ (200 μ L) was added dropwise, and the mixture was stirred for 16 h at room temperature. The reaction mixture was then concentrated under reduced pressure, and the residue was purified by silica gel column chromatography (15% EtOAc in cyclohexane) to give the diester **M68** as a white solid (10 mg, 80%).

¹H NMR (500 MHz, CDCl₃) δ 8.28 – 8.21 (m, 2H), 8.21 – 8.15 (m, 2H), 8.10 – 8.03 (m, 2H), 7.91 (d, J = 8.2 Hz, 1H), 7.81 (s, 1H), 7.52 – 7.41 (m, 3H), 7.31 – 7.27 (m, 2H), 7.21 (dd, J = 7.2, 1.8 Hz, 1H), 7.15 – 7.06 (m, 2H), 6.53 (d, J = 5.4 Hz, 1H), 6.08 (ddd, J = 17.1, 10.5, 5.4 Hz, 1H), 5.99 (ddt, J = 16.7, 10.1, 6.3 Hz, 1H), 5.41 (s, 2H), 5.34 – 5.23 (m, 4H), 5.13 – 4.97 (m, 2H), 3.61 (dd, J = 16.0, 6.5 Hz, 1H), 3.49 (dd, J = 16.0, 6.1 Hz, 1H).

¹⁹F NMR (470 MHz, CDCl₃) δ -105.24.

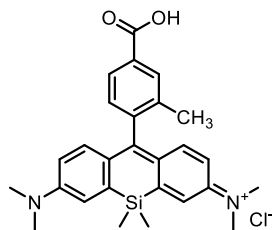
N-(10-(4-(*Tert*-butoxycarbonyl)-2-methylphenyl)-7-(dimethylamino)-5,5-dimethyldibenzo[*b,e*]silin-3(5*H*)-ylidene)-*N*-methylmethanaminium chloride (**M72**)



The silicorhodamine **M72** was obtained according to a reported procedure.²⁶

^1H NMR (500 MHz, CDCl_3) δ 8.01 (dd, $J = 8.0, 1.8$ Hz, 1H), 7.65 (d, $J = 1.8$ Hz, 1H), 7.39 (d, $J = 8.1$ Hz, 1H), 7.20 (d, $J = 2.8$ Hz, 2H), 6.98 (d, $J = 9.6$ Hz, 2H), 6.62 (dd, $J = 9.6, 2.8$ Hz, 2H), 3.39 (s, 12H), 2.06 (s, 3H), 1.56 (s, 9H), 0.61 (d, $J = 3.0$ Hz, 6H).

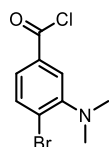
N-(10-(4-Carboxy-2-methylphenyl)-7-(dimethylamino)-5,5-dimethyldibenzo[*b,e*]silin-3(5*H*)-ylidene)-*N*-methylmethanaminium chloride (**M58**)



The carboxylic acid **M58** was obtained according to a reported procedure.²⁶

^1H NMR (500 MHz, CDCl_3) δ 8.06 (d, $J = 7.6$ Hz, 1H), 7.73 (s, 1H), 7.33 (d, $J = 7.7$ Hz, 1H), 7.14 – 7.07 (m, 2H), 7.03 (d, $J = 9.6$ Hz, 2H), 6.74 – 6.51 (m, 2H), 3.30 (s, 12H), 2.01 (s, 3H), 0.54 (d, $J = 4.4$ Hz, 6H).

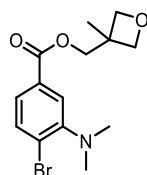
4-Bromo-3-(dimethylamino)benzoyl chloride (**M74**)



4-bromo-3-(dimethylamino)benzoic acid (1.22 g, 5 mmol) and DMF (3 drops) were dissolved in CH_2Cl_2 (60 mL). Oxalyl chloride (1.27 g, 10 mmol) was added dropwise at 0 °C. The reaction mixture was stirred for 2 h at room temperature and then concentrated under reduced pressure to give the chloroanhydride **M74** as a colourless oil (1.31 g, quant.). The crude product was used in the next step without further purification.

^1H NMR (500 MHz, $\text{DMSO}-d_6$) δ 7.70 (d, $J = 8.2$ Hz, 1H), 7.66 (d, $J = 2.0$ Hz, 1H), 7.48 (dd, $J = 8.2, 2.0$ Hz, 1H), 2.75 (s, 6H).

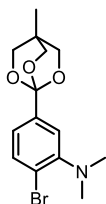
(3-Methyloxetan-3-yl)methyl 4-bromo-3-(dimethylamino)benzoate (**M75**)



(3-methyloxetan-3-yl)methanol (1.02 g, 10 mmol) and pyridine (1.18 g, 15 mmol) were dissolved in CH_2Cl_2 (25 mL). The chloroanhydride **M74** (1.31 g, 5 mmol) was added dropwise at 0 °C, and the reaction mixture was stirred for 16 h at room temperature. The organic phase was washed with 0.5 M HCl (5×20 mL), water (20 mL) and brine (20 mL) successively, dried over anhydrous sodium sulfate, filtered, and the organic solvent was removed under reduced pressure. The residue was purified by silica gel column chromatography (10% EtOAc in cyclohexane) to give the ester **M75** as a colourless oil (721 mg, 44%).

^1H NMR (500 MHz, CDCl_3) δ 7.75 (d, $J = 2.0$ Hz, 1H), 7.63 (d, $J = 8.2$ Hz, 1H), 7.54 (dd, $J = 8.2, 2.0$ Hz, 1H), 4.63 (d, $J = 6.0$ Hz, 2H), 4.46 (d, $J = 6.0$ Hz, 2H), 4.40 (s, 2H), 2.84 (s, 6H), 1.42 (s, 3H).

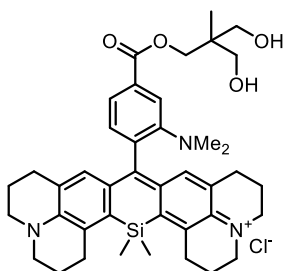
^{13}C NMR (126 MHz, CDCl_3) δ 166.27, 152.38, 134.28, 130.00, 124.99, 124.68, 121.60, 79.74, 69.35, 44.20, 39.51, 21.41.

2-Bromo-*N,N*-dimethyl-5-(4-methyl-2,6,7-trioxabicyclo[2.2.2]octan-1-yl)aniline (**M76**)

The ester **M75** (721 mg, 2.2 mmol) was dissolved in CH₂Cl₂ (15 mL) and BF₃·Et₂O (78 mg, 0.55 mmol) was added dropwise at 0 °C. The reaction mixture was stirred at room temperature for 16 h, and then Et₃N (1 mL) was added. After 10 min, the volatiles were removed and the residue was purified by silica gel column chromatography (20% EtOAc in cyclohexane) to give the orthoester **M76** as a white solid (571 mg, 79%).

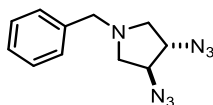
¹H NMR (500 MHz, CDCl₃) δ 7.52 (d, *J* = 8.3 Hz, 1H), 7.35 (d, *J* = 2.0 Hz, 1H), 7.14 (dd, *J* = 8.3, 2.0 Hz, 1H), 4.08 (s, 6H), 2.80 (s, 6H), 0.89 (s, 3H).

¹³C NMR (126 MHz, CDCl₃) δ 151.69, 137.76, 133.67, 121.64, 120.23, 118.17, 107.34, 73.41, 44.35, 30.65, 14.62.

Quencher **M77**

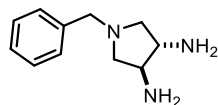
A solution of the orthoester **M76** (82 mg, 0.25 mmol) in THF (5 mL) was cooled to -78 °C and *tert*-BuLi (1.5M, 300 μL, 0.5 mmol) was added dropwise. The reaction mixture was stirred at that temperature for 1 h, and a solution of the phenome **M46** (10 mg, 0.025 mmol) in THF (1 mL) was added dropwise. The reaction mixture was stirred for 1 h at -78 °C and then for 16 h at room temperature. A solution of HCl (2 mL of a 2M solution) was added, and the mixture was stirred for an additional 30 min. The volatiles were removed under reduced pressure, and the residue was purified twice by silica gel column chromatography (10% MeOH in CH₂Cl₂) to give the silicorhodamine ester **M77** as a turquoise solid (13 mg, 77%).

¹H NMR (500 MHz, CDCl₃) δ 7.73 (d, *J* = 1.5 Hz, 1H), 7.65 (dd, *J* = 7.8, 1.5 Hz, 1H), 6.97 (d, *J* = 7.9 Hz, 1H), 6.74 (s, 2H), 4.42 (s, 2H), 3.63 – 3.49 (m, 8H), 3.36 (s, 4H), 2.98 – 2.90 (m, 4H), 2.64 (s, 6H), 2.57 – 2.46 (m, 4H), 2.17 – 2.06 (m, 4H), 1.95 (q, *J* = 6.1 Hz, 4H), 0.70 (s, 3H), 0.66 (s, 3H).

Alternative ligands(3*S*,4*S*)-3,4-Diazo-1-benzylpyrrolidine (**M78**)

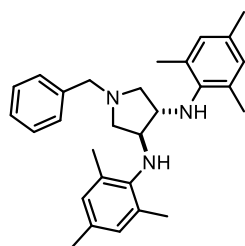
The diazide **M78** was obtained according to a reported procedure.⁷⁹

¹H NMR (500 MHz, CDCl₃) δ 7.37 – 7.24 (m, 5H), 3.90 – 3.84 (m, 2H), 3.64 (q, *J* = 13.0 Hz, 2H), 2.99 (dd, *J* = 10.0, 6.4 Hz, 2H), 2.60 (dd, *J* = 10.0, 4.7 Hz, 2H).

(3*S*,4*S*)-1-Benzylpyrrolidine-3,4-diamine (**M79**)

The diamine **M79** was obtained according to a reported procedure.⁷⁹

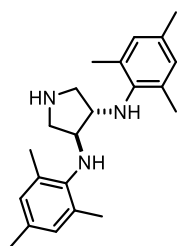
¹H NMR (500 MHz, CDCl₃) δ 7.38 – 7.17 (m, 5H), 3.69 – 3.52 (m, 2H), 3.08 – 3.00 (m, 2H), 2.94 (dt, *J* = 9.5, 4.5 Hz, 2H), 2.30 (dd, *J* = 9.5, 5.0 Hz, 2H).

(3*S*,4*S*)-1-Benzyl-*N*³,*N*⁴-dimesitylpyrrolidine-3,4-diamine (**M80**)

Under an inert atmosphere, Pd(OAc)₂ (50 mg, 0.22 mmol), BINAP (274 mg, 0.44 mmol), and sodium *tert*-butoxide (1.20 g, 12.5 mmol) were added to toluene (80 mL) and stirred for 20 min. The diamine **M79** (800 mg, 4.1 mmol) and 2-bromomesitylene (7.96 g, 8.3 mmol) were then added, and the solution was heated at 100 °C for 16 h. The solution was then cooled to room temperature and concentrated under reduced pressure. The residue was purified by silica gel column chromatography (5% EtOAc in cyclohexane) to give the bis(arylamine) **M80** as a colourless oil (1.07 g, 61%).

¹H NMR (500 MHz, CDCl₃) δ 7.39 – 7.23 (m, 5H), 6.68 (s, 4H), 3.67 (s, 2H), 3.47 (s, 2H), 3.21 (s, 2H), 2.98 (dd, *J* = 9.6, 6.0 Hz, 2H), 2.37 (d, *J* = 7.6 Hz, 2H), 2.21 (s, 6H), 1.94 (s, 12H).

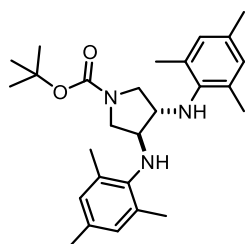
¹³C NMR (126 MHz, CDCl₃) δ 141.56, 138.89, 131.19, 129.67, 129.44, 128.90, 128.45, 127.27, 62.12, 60.18, 60.15, 27.06, 20.66, 18.44.

(3*S*,4*S*)-*N*³,*N*⁴-Dimesitylpyrrolidine-3,4-diamine (**M81**)

To a stirred suspension of 10% Pd on charcoal (400 mg, 0.38 mmol) in methanol (20 mL), a solution of the bis(arylamine) **M80** (1.07 g, 2.5 mmol) in methanol (10 mL) and ammonium formate (1.26 g, 20 mmol) were added, and the mixture was heated at reflux for 3 h. The catalyst and inorganic salts were filtered and washed with methanol. The solvent was removed under reduced pressure to give the triamine **M81** as a colourless oil (801 mg, 95%) which was used without further purification.

¹H NMR (500 MHz, CDCl₃) δ 8.52 (s, 1H), 6.72 (s, 4H), 3.70 (dd, *J* = 4.9, 2.3 Hz, 2H), 3.61 (dd, *J* = 12.0, 6.1 Hz, 2H), 3.17 (dd, *J* = 12.1, 2.7 Hz, 2H), 2.21 (s, 6H), 2.03 (s, 12H).

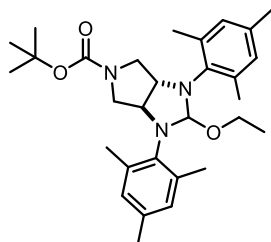
Tert-butyl (3*S*,4*S*)-3,4-bis(mesitylamino)pyrrolidine-1-carboxylate (**M82**)



The triamine **M81** (160 mg, 0.5 mmol), Et₃N (138 μ L, 1 mmol), and DMAP (6 mg, 0.05 mmol) were dissolved in CH₂Cl₂ (15 mL) and then cooled to 0 °C. Boc₂O (164 mg, 0.075 mmol) was added in portions, and the resulting mixture was stirred at 0 °C for additional 30 min and then for 3 h at room temperature. The reaction mixture was then concentrated under reduced pressure, and the residue was purified by silica gel column chromatography (10% EtOAc in cyclohexane) to afford the carbamate **M82** as a colourless oil (210 mg, 96%).

¹H NMR (500 MHz, CDCl₃) δ 6.78 (s, 4H), 3.80 – 3.52 (m, 4H), 3.43 – 3.24 (m, 2H), 3.07 (brs, 2H), 2.22 (s, 6H), 2.13 (s, 12H).

Tert-butyl (3a*S*,6a*S*)-2-ethoxy-1,3-dimesitylhaxahydropyrrolo[3,4-*d*]imidazole-5(1*H*)-carboxylate (**M83**)

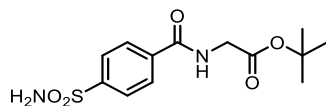


The carbamate **M82** (210 mg, 0.48 mmol) and NH₄Cl were heated to 120 °C in TEOF (2 mL) for 4 h. The volatiles were removed under reduced pressure to afford the crude imidazolidine **M83** as a pale-yellow oil (237 mg, quant.).

¹H NMR (500 MHz, CDCl₃) δ 7.94 (d, *J* = 9.2 Hz, 2H), 6.94 (s, 4H), 4.57 (d, *J* = 6.6 Hz, 1H), 4.31 (d, *J* = 6.0 Hz, 1H), 4.12 (q, *J* = 7.1 Hz, 2H), 3.84 (td, *J* = 14.5, 13.6, 7.5 Hz, 2H), 3.76 – 3.71 (m, 1H), 3.59 (d, *J* = 12.4 Hz, 1H), 2.30 (s, 6H), 2.18 (s, 3H), 2.12 (d, *J* = 2.5 Hz, 6H), 2.04 (s, 3H), 2.03 (s, 3H), 1.35 (s, 9H), 1.26 (t, *J* = 7.1 Hz, 3H).

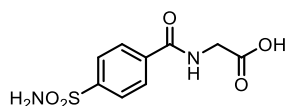
Alternative anchors

Tert-butyl (4-sulfamoylbenzoyl)glycinate



4-(aminosulfonyl)-benzoic acid (800 mg, 4 mmol), glycine *tert*-butyl ester hydrochloride (670 mg, 4.8 mmol), benzotriazol-1-ol (560 mg, 4.2 mmol), 1-ethyl-(3-(3-dimethylamino)propyl)-carbodiimide hydrochloride (800 mg, 4.2 mmol) were dissolved in ACN (125 mL), and Et₃N (1.1 mL, 8 mmol) was added. The reaction mixture was stirred at room temperature for 16 h and then concentrated under reduced pressure. Water (50 mL) was added, and the mixture was extracted with ethyl acetate (3×50 mL). The combined organic phase was washed with water (50 mL) and brine (50 mL) successively, dried over anhydrous sodium sulfate, filtered, and the organic solvent was removed under reduced pressure. The crude product was purified by silica gel column chromatography (3% MeOH in CH₂Cl₂) to give *tert*-butyl (4-sulfamoylbenzoyl)glycinate as a white solid (940 mg, 75%).

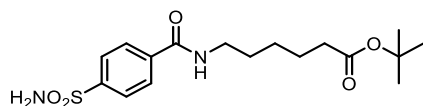
¹H NMR (500 MHz, DMSO-*d*₆) δ 9.04 (t, *J* = 5.9 Hz, 1H), 8.01 (d, *J* = 8.4 Hz, 2H), 7.92 (d, *J* = 8.4 Hz, 2H), 7.49 (s, 2H), 3.92 (d, *J* = 5.9 Hz, 2H), 1.43 (s, 9H).

(4-Sulfamoylbenzoyl)glycine (**M84**)

Tert-butyl (4-sulfamoylbenzoyl)glycinate (940 mg, 3 mmol) was dissolved in CH₂Cl₂ (80 mL) and trifluoroacetic acid (10 mL) was added dropwise at 0 °C. The reaction mixture was stirred at that temperature for 2 h, and then volatiles were removed under reduced pressure to give the carboxylic acid **M84** as a white crystalline powder (772 mg, quant.). The crude product was used in the next step without further purification.

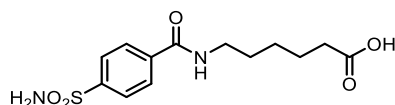
¹H NMR (500 MHz, DMSO-*d*₆) δ 12.67 (s, 1H), 9.02 (t, *J* = 5.4 Hz, 1H), 8.02 (d, *J* = 8.1 Hz, 2H), 7.92 (d, *J* = 8.1 Hz, 2H), 7.49 (s, 2H), 3.94 (d, *J* = 5.6 Hz, 2H).

¹³C NMR (126 MHz, DMSO-*d*₆) δ 171.08, 165.46, 146.45, 136.69, 127.91, 125.71, 41.29.

Tert-butyl 6-(4-sulfamoylbenzamido)hexanoate

4-(aminosulfonyl)-benzoic acid (1.52 g, 7.5 mmol), *tert*-butyl 6-aminohexanoate (1.42 g, 7.5 mmol), benzotriazol-1-ol (1.06 g, 7.9 mmol), 1-ethyl-(3-(3-dimethylamino)propyl)-carbodiimide hydrochloride (1.52 g, 7.9 mmol) were dissolved in ACN (200 mL), and Et₃N (2.1 mL, 15.4 mmol) was added. The reaction mixture was stirred at room temperature for 16 h and then concentrated under reduced pressure. Water (100 mL) was added, and the mixture was extracted with CH₂Cl₂ (3×100 mL). The combined organic phase was washed with water (100 mL) and brine (100 mL) successively, dried over anhydrous sodium sulfate, filtered, and the organic solvent was removed under reduced pressure. The crude product was purified by silica gel column chromatography (3% MeOH in CH₂Cl₂) to give *tert*-butyl 6-(4-sulfamoylbenzamido)hexanoate as a white solid (1.51 g, 54%).

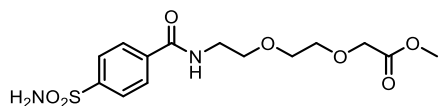
¹H NMR (500 MHz, DMSO-*d*₆) δ 8.62 (t, *J* = 5.5 Hz, 1H), 7.98 (d, *J* = 8.4 Hz, 2H), 7.89 (d, *J* = 8.5 Hz, 2H), 7.47 (s, 2H), 3.26 (q, *J* = 6.7 Hz, 2H), 2.19 (t, *J* = 7.3 Hz, 2H), 1.57 – 1.47 (m, 6H), 1.38 (s, 9H), 1.33 – 1.24 (m, 2H).

6-(4-Sulfamoylbenzamido)hexanoic acid (**M85**)

Tert-butyl 6-(4-sulfamoylbenzamido)hexanoate (1.51 g, 4.1 mmol) was dissolved in CH₂Cl₂ (60 mL) and trifluoroacetic acid (20 mL) was added dropwise at 0 °C. The reaction mixture was stirred at that temperature for 2 h, and the volatiles were removed under reduced pressure to give the carboxylic acid **M85** as a white solid (1.28 g, quant.). The crude product was used in the next step without further purification.

¹H NMR (500 MHz, DMSO-*d*₆) δ 8.62 (t, *J* = 5.5 Hz, 1H), 7.97 (d, *J* = 8.5 Hz, 2H), 7.88 (d, *J* = 8.4 Hz, 2H), 7.46 (s, 2H), 3.26 (q, *J* = 6.8 Hz, 2H), 2.21 (t, *J* = 7.3 Hz, 2H), 1.57 – 1.44 (m, 4H), 1.36 – 1.28 (m, 2H).

Methyl 2-(2-(2-(4-sulfamoylbenzamido)ethoxy)ethoxy)acetate

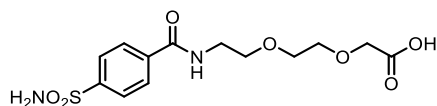


4-(aminosulfonyl)-benzoic acid (606 mg, 3 mmol), methyl 2-(2-(2-aminoethoxy)ethoxy)acetate (531 mg, 3 mmol) (obtained in 5 steps from triethyleneglycol),⁸⁰ benzotriazol-1-ol (424 mg, 3.1 mmol), 1-ethyl-(3-(3-dimethylamino)propyl)-carbodiimide hydrochloride (600 mg, 3.1 mmol) were dissolved in ACN (80 mL), and Et₃N (840 μ L, 6.2 mmol) was added. The reaction mixture was stirred at room temperature for 16 h and then concentrated under reduced pressure. Water (50 mL) was added, and the mixture was extracted with ethyl acetate (6 \times 50 mL). The combined organic phase was washed with brine (50 mL), dried over anhydrous sodium sulfate, filtered, and the organic solvent was removed under reduced pressure. The crude product was purified by silica gel column chromatography (5% MeOH in CH₂Cl₂) to give methyl 2-(2-(2-(4-sulfamoylbenzamido)ethoxy)ethoxy)acetate as a colourless oil (390 mg, 36%).

¹H NMR (500 MHz, DMSO-*d*₆) δ 8.70 (t, *J* = 5.5 Hz, 1H), 8.04 – 7.97 (m, 2H), 7.93 – 7.87 (m, 2H), 7.48 (s, 2H), 4.13 (s, 2H), 3.63 (s, 3H), 3.62 – 3.53 (m, 6H), 3.44 (q, *J* = 5.8 Hz, 2H).

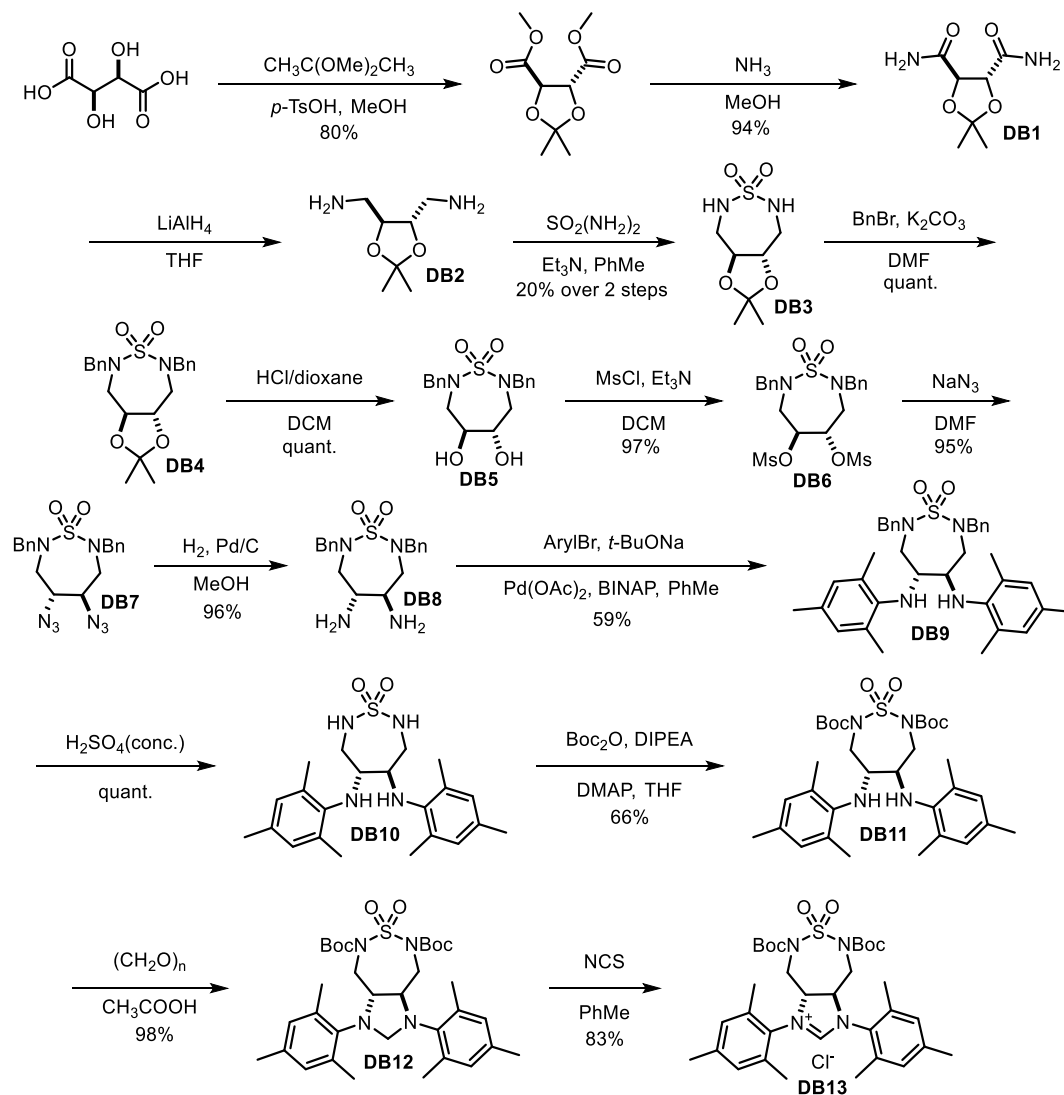
¹³C NMR (126 MHz, DMSO-*d*₆) δ 170.63, 165.34, 146.23, 137.33, 127.88, 125.63, 69.99, 69.59, 68.75, 67.65, 51.36.

2-(2-(2-(4-Sulfamoylbenzamido)ethoxy)ethoxy)acetic acid (**M86**)

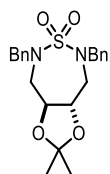


Methyl 2-(2-(2-(4-sulfamoylbenzamido)ethoxy)ethoxy)acetate (130 mg, 0.36 mmol) and LiOH·H₂O (100 mg, 2.4 mmol) were dissolved in mixture of methanol (5 mL), THF (7.5 mL), and water (7.5 mL). The reaction mixture was stirred at room temperature for 4 h and then was concentrated under reduced pressure. Water (5 mL) was added, and the mixture was extracted with CH₂Cl₂ (10 \times 10 mL). The combined organic phase was washed with brine (5 mL), dried over anhydrous sodium sulfate, filtered, and the organic solvent was removed under reduced pressure to give the carboxylic acid **M86** as a white solid (114 mg, 92%). The crude product was used in the next step without further purification.

¹H NMR (500 MHz, DMSO-*d*₆) δ 8.70 (t, *J* = 5.5 Hz, 1H), 7.99 (d, *J* = 8.5 Hz, 2H), 7.89 (d, *J* = 8.5 Hz, 2H), 7.47 (s, 2H), 4.02 (s, 2H), 3.64 – 3.52 (m, 6H), 3.43 (q, *J* = 5.8 Hz, 2H).

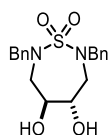
5.3. *De Novo* ArMs ProjectSynthesis of NHC precursor **DB13**

(3*aS*,8*aS*)-5,7-Dibenzyl-2,2-dimethylhexahydro-[1,3]dioxolo[4,5-*d*][1,2,7]thiadiazepine 6,6-dioxide (**DB4**)



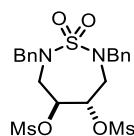
The sulfamide **DB4** was obtained according to known procedure.⁵³

^1H NMR (500 MHz, CDCl_3) δ 7.40 – 7.28 (m, 10H), 4.47 (d, J = 14.5 Hz, 2H), 4.36 (d, J = 14.5 Hz, 2H), 4.25 – 4.12 (m, 2H), 3.44 (dd, J = 12.9, 4.2 Hz, 2H), 3.05 – 2.94 (m, 2H), 1.35 (s, 6H).

(4*S*,5*S*)-2,7-Dibenzyl-4,5-dihydroxy-1,2,7-thiadiazepane 1,1-dioxide (**DB5**)

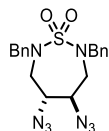
The diol **DB5** was obtained according to known procedure.⁵³

¹H NMR (500 MHz, CDCl₃) δ 7.47 – 7.28 (m, 10H), 4.65 (d, *J* = 15.3 Hz, 2H), 4.46 (d, *J* = 15.3 Hz, 2H), 3.58 – 3.45 (m, 2H), 3.38 (dd, *J* = 15.1, 8.8 Hz, 2H), 3.16 (dd, *J* = 15.1, 2.6 Hz, 2H), 2.08 (d, *J* = 3.7 Hz, 2H).

(4*S*,5*S*)-2,7-Dibenzyl-1,1-dioxido-1,2,7-thiadiazepane-4,5-diyl dimethanesulfonate (**DB6**)

The crude diol **DB5** (7.25 g, 20 mmol) was dissolved in anhydrous CH₂Cl₂ (150 mL). Triethylamine (11.05 mL, 80 mmol) was added dropwise, and then methanesulfonyl chloride (3.5 mL, 45 mmol) was added dropwise to the reaction at 0 °C. After completion of the dropwise addition, the mixture was stirred at room temperature for 12 h. After completion of the reaction as revealed by TLC, the mixture was washed with water, saturated sodium bicarbonate and saturated brine, dried over anhydrous sodium sulfate, and filtered. The volatiles were removed under reduced pressure to give the sulfamide **DB6** as a yellow foam (10.05 g, 97%). The crude product was used in the next step without further purification.

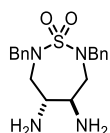
¹H NMR (500 MHz, CDCl₃) δ 7.48 – 7.31 (m, 10H), 4.59 (d, *J* = 15.1 Hz, 2H), 4.52 (d, *J* = 15.1 Hz, 2H), 4.47 – 4.39 (m, 2H), 3.60 (dt, *J* = 14.7, 7.3 Hz, 2H), 3.43 (dd, *J* = 15.6, 2.9 Hz, 2H), 2.93 (s, 6H).

(4*R*,5*R*)-4,5-Diazo-2,7-dibenzyl-1,2,7-thiadiazepane 1,1-dioxide (**DB7**)

The sulfamide **DB6** (5 g, 9.6 mmol) was dissolved in DMF (80 mL), then sodium azide (2.5 g, 38.5 mmol) was added, then reaction mixture was heated to 80 °C and stirred for 16 h. 200 mL of water was added, and mixture was extracted with ethyl acetate (150 mL×3). The combined organic phase was washed with water (200 mL×2) and saturated brine (200 mL), dried over anhydrous sodium sulfate, filtered, and the organic solvent was removed under reduced pressure. The crude product was purified by silica gel column chromatography (3-5% EtOAc in cyclohexane) to give the diazide **DB7** as a pale-yellow oil (3.76 g, 95%).

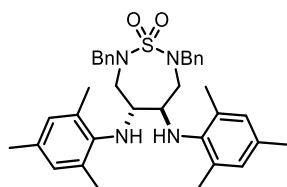
¹H NMR (500 MHz, CDCl₃) δ 7.45 – 7.33 (m, 10H), 4.56 (d, *J* = 15.0 Hz, 2H), 4.51 (d, *J* = 15.0 Hz, 2H), 3.47 (dt, *J* = 16.3, 8.2 Hz, 2H), 3.10 (dd, *J* = 15.5, 2.7 Hz, 2H), 3.00 – 2.92 (m, 2H).

¹³C NMR (126 MHz, CDCl₃) δ 135.73, 129.32, 128.74, 128.72, 62.77, 52.69, 46.96.

(4*R*,5*R*)-4,5-Diamino-2,7-dibenzyl-1,2,7-thiadiazepane 1,1-dioxide (**DB8**)

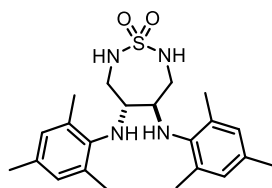
To a stirred suspension of 10% Pd on charcoal (1.65 g, 0.14 eq.) in methanol (100 mL) the solution of the diazide **DB7** (4.5 g, 10.9 mmol) in methanol (50 mL) was added and the mixture was hydrogenated at atmospheric pressure at r.t. for 6 h. The catalyst was filtered off and washed with methanol. The solvent was removed under reduced pressure to give the diamine **DB8** as a colourless oil (3.76 g, 96%), which was used in the next step without further purification.

¹H NMR (500 MHz, CDCl₃) δ 7.43 – 7.28 (m, 10H), 4.73 (d, *J* = 15.5 Hz, 2H), 4.37 (d, *J* = 15.5 Hz, 2H), 3.40 (dt, *J* = 15.3, 7.2 Hz, 2H), 2.88 (dd, *J* = 15.3, 2.4 Hz, 2H), 2.46 – 2.37 (m, 2H).

(4*R*,5*R*)-2,7-Dibenzyl-4,5-bis(mesitylamino)-1,2,7-thiadiazepane 1,1-dioxide (**DB9**)

Under inert atmosphere, Pd₂dba₃ (1.40 g, 1.5 mmol), BINAP (1.86 g, 3 mmol), and sodium *tert*-butoxide (4.20 g, 43.7 mmol) were added to toluene (300 mL) and stirred for 20 min. The diamine **DB8** (3.61 g, 10 mmol) and 2-bromomesitylene (7.96 g, 40 mmol) were then added and the solution was heated to 100 °C for 16 h. The solution was then cooled to room temperature and concentrated under reduced pressure. The residue was purified by silica gel column chromatography (10% EtOAc in cyclohexane) to afford the bis(arylamine) **DB9** as a white foam (3.53 g, 59%).

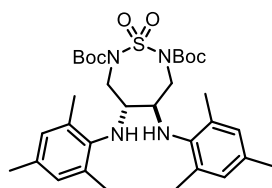
¹H NMR (500 MHz, CDCl₃) δ 7.29 – 7.23 (m, 2H), 7.20 (t, *J* = 7.4 Hz, 4H), 6.99 (d, *J* = 7.2 Hz, 4H), 6.79 (s, 4H), 4.32 (d, *J* = 14.6 Hz, 2H), 4.24 (d, *J* = 14.6 Hz, 2H), 3.36 (dt, *J* = 15.4, 7.6 Hz, 2H), 3.03 (s, 2H), 2.83 (d, *J* = 15.1 Hz, 2H), 2.78 (d, *J* = 8.6 Hz, 2H), 2.28 (s, 6H), 2.06 (s, 12H).

(4*R*,5*R*)-4,5-Bis(mesitylamino)-1,2,7-thiadiazepane 1,1-dioxide (**DB10**)

The bis(arylamine) **DB9** (3.53 g, 5.9 mmol) was crushed and mixed with concentrated H₂SO₄ (40 mL). The reaction mixture was vigorously stirred for 1 h and then crushed ice (200 g) was added at 0 °C. Then, 2M NaOH was added dropwise to pH = 8. The mixture was extracted with CH₂Cl₂ (100 mL×6). The combined organic phase was washed with water (100 mL) and saturated brine (200 mL) successively, dried over anhydrous sodium sulfate, filtered, and the organic solvent was removed under reduced pressure to give the sulfamide **DB10** as an off-white solid (2.43 g, quant.). The crude product was used in the next step without further purification.

¹H NMR (500 MHz, CDCl₃) δ 6.80 (s, 4H), 4.63 (t, *J* = 6.2 Hz, 2H), 3.52 (dd, *J* = 15.2, 6.3 Hz, 2H), 3.25 – 3.18 (m, 2H), 3.14 (d, *J* = 5.4 Hz, 2H), 2.22 (s, 6H), 2.13 (s, 12H).

Di-*tert*-butyl (4*R*,5*R*)-4,5-bis(mesitylamino)-1,2,7-thiadiazepane-2,7-dicarboxylate 1,1-dioxide (**DB11**)

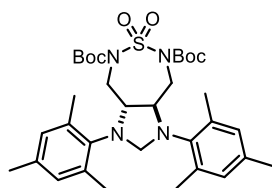


The sulfamide **DB10** (2.43 g, 5.9 mmol), Et₃N (5.0 mL, 36 mmol), and DMAP (216 mg, 1.77 mmol) were dissolved in chloroform (250 mL) and then cooled to 0 °C. Boc₂O (3.86 g, 17.7 mmol) was added portionwise and the resulting mixture was stirred at 0 °C for additional 30 min and for 3 h at room temperature. The reaction mixture was concentrated under reduced pressure and purified by silica gel column chromatography (15% EtOAc in cyclohexane) to give the bis(arylamine) **DB11** as a white foam (2.4 g, 66%).

¹H NMR (500 MHz, CDCl₃) δ 6.82 (s, 4H), 3.99 (d, *J* = 15.4 Hz, 2H), 3.70 (dd, *J* = 15.1, 7.8 Hz, 2H), 3.39 (m, 4H), 2.22 (s, 18H), 1.39 (s, 18H).

¹³C NMR (126 MHz, CDCl₃) δ 150.33, 139.70, 133.00, 131.86, 129.97, 85.29, 60.41, 48.25, 27.86, 20.70, 19.06.

Di-*tert*-butyl (3*aR*,8*aR*)-1,3-dimesitylhexahydro-1*H*-imidazo[4,5-*d*][1,2,7]thiadiazepine-5,7 dicarboxylate 6,6-dioxide (**DB12**)

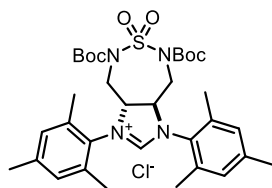


The bis(arylamine) **DB11** (2.4 g, 3.9 mmol) was dissolved in acetic acid (100 mL) and paraformaldehyde (0.40 g, 13.3 mmol) was added. The reaction was stirred until the paraformaldehyde had dissolved. Acetic acid was removed under reduced pressure and the resulting crude material was purified by column chromatography on SiO₂ (10% EtOAc in cyclohexane) to afford the imidazolidine **DB12** as a white foam (2.41 g, 98%).

¹H NMR (500 MHz, CDCl₃) δ 6.88 (s, 2H), 6.84 (s, 2H), 4.38 (s, 2H), 4.11 – 4.03 (m, 2H), 3.82 (dd, *J* = 14.0, 2.8 Hz, 2H), 3.61 (dt, *J* = 14.0, 7.3 Hz, 2H), 2.40 (s, 6H), 2.33 (s, 6H), 2.25 (s, 6H), 1.43 (s, 18H).

¹³C NMR (126 MHz, CDCl₃) δ 150.78, 139.84, 137.35, 137.24, 136.48, 130.98, 129.32, 84.77, 70.94, 66.32, 48.69, 27.92, 27.06, 20.92, 19.16, 19.16.

(3*aR*,8*aR*)-5,7-Bis(*tert*-butoxycarbonyl)-1,3-dimesityl-3*a*,4,5,7,8,8*a*-hexahydro-1*H*-imidazo[4,5-*d*][1,2,7]thiadiazepin-3-ium 6,6-dioxide chloride (**DB13**).



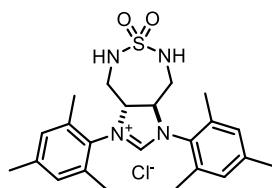
The imidazolidine **DB12** (200 mg, 0.32 mmol) was dissolved in toluene (20 mL). *N*-Chlorosuccinimide (45 mg, 0.34 mmol) was added, and the reaction mixture was stirred at room temperature for 5 h (depending on the quality of NCS, the reaction time may be extended to achieve full conversion). After reaction completion, toluene was removed under reduced pressure and the resulting foam was dissolved in minimal amount of CH₂Cl₂. This solution was added dropwise to a vigorously stirred mixture of

hexane (20 mL) and diethyl ether (20 mL) to separate product from succinimide. Solids were collected by vac-filtration, washed with hexane-ether mixture, and dried to give the imidazoline **DB13** as a white powder (176 mg, 83%).

^1H NMR (500 MHz, CDCl_3) δ 10.92 (s, 1H), 7.01 (s, 2H), 6.98 (s, 2H), 4.81 (s, 2H), 4.01 (d, J = 14.1 Hz, 2H), 3.97 – 3.89 (m, 2H), 2.46 (s, 6H), 2.37 (s, 6H), 2.29 (s, 6H), 1.46 (s, 18H).

^{13}C NMR (126 MHz, CDCl_3) δ 162.07, 149.87, 141.45, 135.98, 134.72, 130.95, 130.68, 127.82, 87.02, 67.73, 45.09, 27.84, 21.20, 19.42, 18.60.

(3*aR*,8*aR*)-1,3-Dimesityl-3*a*,4,5,7,8,8*a*-hexahydro-1*H*-imidazo[4,5-*d*][1,2,7]thiadiazepin-3-ium 6,6-dioxide chloride (**DB14**)

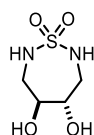


The imidazolidine **DB13** (20 mg, 0.03 mmol) was dissolved in CH_2Cl_2 (5 mL) and HCl gas was purged through the solution for 3 h at room temperature. The gaseous HCl was generated by dropwise addition of concentrated H_2SO_4 to solid NH_4Cl . The solution was stirred for an additional 1 h at room temperature. Upon completion of the reaction as revealed by ^1H NMR, the solvent was evaporated under reduced pressure to give the imidazoline **DB14** as a white solid (13.9 mg, quant.). This compound was used without further purification.

^1H NMR (500 MHz, CDCl_3) δ 7.82 (s, 1H), 7.03 (s, 2H), 7.01 (s, 2H), 5.36 (s, 2H), 3.64 (s, 2H), 3.39 (s, 4H), 2.32 (s, 18H).

Alternative routes' products

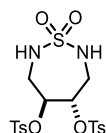
(4*S*,5*S*)-4,5-Dihydroxy-1,2,7-thiadiazepane 1,1-dioxide (**DB4A**)



To a solution of the sulfamide **DB3** (1 g, 4.5 mmol) in CH_2Cl_2 (5 mL), 2 M HCl in dioxane (1 mL) were added. Then, the reaction mixture was stirred for 3 h. and then concentrated. The diol **DB4A** was obtained as a brownish solid (819 mg, quant.) and used in the next step without further purification.

^1H NMR (500 MHz, Acetone- d_6) δ 5.86 (s, 2H), 4.44 (s, 2H), 3.71 (d, J = 4.2 Hz, 2H), 3.34 (dd, J = 15.5, 7.6 Hz, 2H), 3.02 (ddd, J = 15.3, 7.4, 5.0 Hz, 2H).

(4*S*,5*S*)-1,1-Dioxido-1,2,7-thiadiazepane-4,5-diyl bis(4-methylbenzenesulfonate) (**DB5A**)

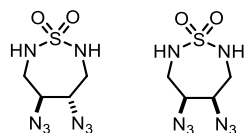


The diol **DB4A** (182 mg, 1 mmol) and 4-toluenesulfonyl chloride (572 mg, 3 mmol) were dissolved in pyridine (5 mL) at room temperature. The reaction mixture was stirred overnight at that temperature and then was diluted with distilled water (20 mL) and 1M HCl solution (100 mL) was added dropwise at 0 °C. Water phase was extracted with ethyl acetate (50 mL×3). The combined organic phase was washed with water (50 mL×2) and saturated brine (50 mL), dried over anhydrous sodium sulfate, filtered, and the organic solvent was removed under reduced pressure. The crude product was purified by silica gel

column chromatography (15% EtOAc in cyclohexane) to afford the sulfamide **DB5A** as a yellowish solid (294 mg, 60%).

^1H NMR (500 MHz, Acetone- d_6) δ 7.77 (d, J = 8.4 Hz, 4H), 7.50 (d, J = 8.0 Hz, 4H), 6.72 (t, J = 6.3 Hz, 2H), 4.54 – 4.49 (m, 2H), 3.55 – 3.46 (m, 2H), 3.15 – 3.08 (m, 2H), 2.49 (s, 6H).

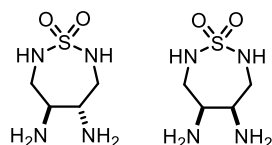
Meso- and rac-4,5-diazido-1,2,7-thiadiazepane 1,1-dioxide (**DB6A**)



The sulfamide **DB5A** (294 mg, 0.6 mmol) was dissolved in DMF (10 mL), then sodium azide (260 mg, 4 mmol) was added. The resulting reaction mixture was heated to 80 °C and stirred for 16 h. Water (20 mL) was added, and mixture was extracted with ethyl acetate (10 mL \times 3). The combined organic phase was washed with water (10 mL \times 2) and saturated brine (20 mL), dried over anhydrous sodium sulfate, filtered, and the organic solvent was removed under reduced pressure. The crude product was purified by silica gel column chromatography (10% EtOAc in cyclohexane) to give the mixture of the meso- and rac-diazide **DB6A** as a pale-yellow oil (105 mg, 75%).

^1H NMR (500 MHz, Acetone- d_6) δ 6.42 (s, 2H), 6.06 (m, 2H), 3.89 – 3.72 (m, 6H), 3.70 – 3.51 (m, 3H), 3.51 – 3.41 (m, 3H), 3.33 – 3.21 (m, 2H).

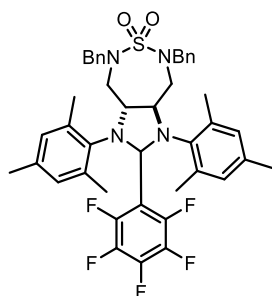
Meso- and rac-4,5-diamino-1,2,7-thiadiazepane 1,1-dioxide (**DB7A**)



To a stirred suspension of 10% Pd on charcoal (100 mg) in ethanol (50 mL), a solution of the diazide **DB6A** (100 mg, 0.43 mmol) in ethanol (5 mL), was added and the mixture was hydrogenated at atmospheric pressure and room temperature for 6 h. The catalyst was filtered off and washed with methanol. The solvent was removed under reduced pressure to give the mixture of the meso- and rac-diamine **DB7A** as a colourless oil (77 mg, quant.).

^1H NMR (500 MHz, CD $_3$ OD) δ 3.36 (dd, J = 13.9, 4.6 Hz, 2H), 3.30 – 3.28 (m, 2H), 3.20 (dd, J = 13.9, 10.0 Hz, 2H), 3.08 (dd, J = 13.4, 3.9 Hz, 2H), 2.81 (dd, J = 13.5, 8.6 Hz, 2H), 2.61 (td, J = 9.7, 4.6 Hz, 2H).

(3a*R*,8a*R*)-5,7-Dibenzyl-1,3-dimesityl-2-(perfluorophenyl)octahydro-1*H*-imidazo[4,5-*d*][1,2,7]thiadiazepine 6,6-dioxide (**DB9-PFP**)



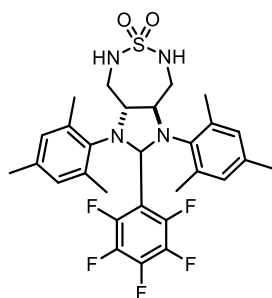
The bis(arylamine) **DB9** (100 mg, 0.17 mmol) was dissolved in acetic acid (2 mL) and 2,3,4,5,6-pentafluorobenzaldehyde (36 mg, 0.18 mmol) was added. The reaction was stirred for 16 h and acetic acid was removed under reduced pressure. The resulting crude material was purified by column

chromatography (0.5% MeOH in CH₂Cl₂) to give the imidazolidine **DB9-PFP** as a white solid (96 mg, 73%).

¹H NMR (500 MHz, CDCl₃) δ 7.34 – 7.20 (m, 8H), 7.14 – 7.08 (m, 2H), 6.89 (s, 1H), 6.74 (s, 1H), 6.67 (s, 1H), 6.51 (s, 1H), 6.16 (s, 1H), 4.79 (brs, 1H), 4.42 (dd, *J* = 14.3, 7.6 Hz, 2H), 4.31 (m, 2H), 4.20 (d, *J* = 13.9 Hz, 1H), 3.36 (dd, *J* = 13.2, 9.7 Hz, 1H), 3.06 (dd, *J* = 12.9, 4.4 Hz, 1H), 2.94 (dd, *J* = 13.3, 3.7 Hz, 1H), 2.84 (dd, *J* = 12.8, 9.6 Hz, 1H), 2.57 (s, 3H), 2.33 (s, 3H), 2.23 (s, 3H), 2.14 (s, 3H), 2.01 (s, 3H), 1.86 (s, 3H).

¹⁹F NMR (471 MHz, CDCl₃) δ -134.49 (dd, *J* = 22.9, 8.4 Hz), -147.47 (dd, *J* = 22.8, 7.9 Hz), -154.45 (t, *J* = 20.8 Hz), -161.91 – -162.07 (m), -162.35 – -162.51 (m).

(3*aR*,8*aR*)-1,3-Dimesityl-2-(perfluorophenyl)octahydro-1*H*-imidazo[4,5-*d*][1,2,7]thiadiazepine 6,6-dioxide (**DB10-PFP**)



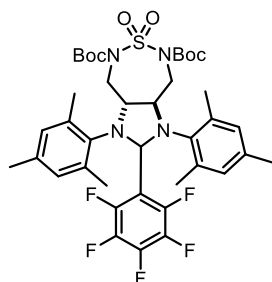
The sulfamide **DB10** (21 mg, 0.05 mmol) was dissolved in acetic acid (1 mL) and 2,3,4,5,6-pentafluorobenzaldehyde (11 mg, 0.055 mmol) was added. The reaction was stirred for 16 h and acetic acid was removed under reduced pressure. The resulting crude material was purified by column chromatography (1% MeOH in CH₂Cl₂) to give the imidazolidine **DB10-PFP** as a white solid (24 mg, 81%).

¹H NMR (500 MHz, CDCl₃) δ 6.90 (s, 1H), 6.81 (s, 1H), 6.77 (s, 1H), 6.64 (s, 1H), 6.22 (s, 1H), 4.82 (brs, 1H), 4.49 (dd, *J* = 6.8, 3.9 Hz, 1H), 4.39 (dd, *J* = 7.5, 4.0 Hz, 1H), 4.18 (t, *J* = 7.4 Hz, 1H), 3.56 – 3.47 (m, 1H), 3.19 (dt, *J* = 13.1, 4.2 Hz, 1H), 3.13 (dt, *J* = 13.1, 3.8 Hz, 1H), 2.91 (ddd, *J* = 13.1, 10.1, 7.0 Hz, 1H), 2.61 (s, 3H), 2.43 (s, 3H), 2.23 (s, 3H), 2.19 (s, 3H), 2.18 (s, 3H), 2.04 (s, 3H).

¹⁹F NMR (471 MHz, CDCl₃) δ -134.49 (dd, *J* = 23.1, 8.2 Hz), -147.48 (dd, *J* = 23.2, 8.1 Hz), -154.12 (t, *J* = 20.9 Hz), -161.78 (td, *J* = 21.0, 7.3 Hz), -162.21 (td, *J* = 21.7, 21.1, 7.1 Hz).

¹³C NMR (126 MHz, CDCl₃) δ 139.77, 137.80, 137.52, 137.28, 137.05, 135.80, 135.55, 134.37, 131.60, 131.26, 130.44, 129.93, 69.02, 64.60, 45.69, 45.15, 20.93, 20.92, 20.84, 20.64, 19.35, 18.69.

Di-*tert*-butyl (3*aR*,8*aR*)-1,3-dimesityl-2-(perfluorophenyl)hexahydro-1*H*-imidazo[4,5-*d*][1,2,7]thiadiazepine-5,7-dicarboxylate 6,6-dioxide (**DB11-PFP**)



The imidazolidine **DB10-PFP** (62 mg, 0.1 mmol), DIPEA (100 μL, 0.6 mmol), and DMAP (5 mg, 0.04 mmol) were dissolved in THF (5 mL) and then cooled to 0 °C. Boc₂O (87.3 g, 0.4 mmol) was added, and the resulting mixture was stirred at 0 °C for an additional 30 min, and for 3 h at room temperature. The reaction mixture was concentrated under reduced pressure and purified by silica gel column

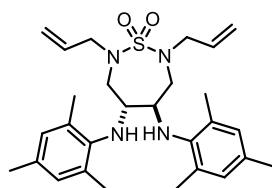
chromatography (5% EtOAc in cyclohexane) to give the imidazolidine **DB11-PFP** as a white foam (66 mg, 80%).

^1H NMR (500 MHz, CDCl_3) δ 6.87 (s, 1H), 6.82 (s, 1H), 6.77 (s, 1H), 6.66 (s, 1H), 6.31 (s, 1H), 4.59 (brs, 1H), 4.18 – 4.07 (m, 1H), 3.97 (dd, J = 14.2, 3.9 Hz, 1H), 3.91 – 3.80 (m, 2H), 3.51 (dd, J = 14.2, 9.6 Hz, 1H), 2.59 (s, 3H), 2.45 (s, 3H), 2.21 (s, 3H), 2.18 (s, 3H), 2.16 (s, 3H), 2.09 (s, 3H), 1.51 (s, 9H), 1.39 (s, 9H).

^{19}F NMR (471 MHz, CDCl_3) δ -133.39 (dd, J = 23.2, 8.1 Hz), -147.37 (dd, J = 23.2, 8.6 Hz), -154.08 (t, J = 20.5 Hz), -161.82 (td, J = 22.2, 7.9 Hz), -162.12 – -162.66 (m).

^{13}C NMR (126 MHz, CDCl_3) δ 150.77, 150.34, 140.05, 137.49, 137.10, 136.98, 136.51, 136.33, 135.48, 134.02, 131.51, 131.00, 130.18, 129.86, 85.13, 84.63, 68.04, 48.36, 20.90, 20.66, 20.55, 19.39, 18.56.

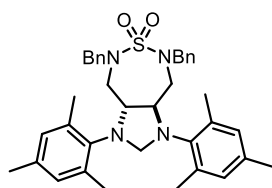
(4*R*,5*R*)-2,7-Diallyl-4,5-bis(mesitylamino)-1,2,7-thiadiazepane 1,1-dioxide (**DB11A**)



The sulfamide **DB10** (84 mg, 0.2 mmol) and K_2CO_3 (77 mg, 0.56 mmol) were stirred in DMF (2 mL) at room temperature and allylbromide (48 mg, 0.4 mmol) was added. The reaction mixture was stirred at room temperature for 16 h and then was concentrated under reduced pressure. The crude material was purified by silica gel column chromatography (5% EtOAc in cyclohexane) to give the bis(arylamine) **DB11A** (91.4 mg, 92%) as a white foam.

^1H NMR (500 MHz, CDCl_3) δ 6.82 (s, 4H), 5.73 (ddt, J = 16.7, 10.1, 6.6 Hz, 2H), 5.02 (d, J = 10.0 Hz, 2H), 4.89 (d, J = 17.0 Hz, 2H), 3.82 (dd, J = 15.2, 6.6 Hz, 2H), 3.71 (dd, J = 15.2, 6.6 Hz, 2H), 3.33 (dd, J = 14.9, 8.7 Hz, 4H), 3.15 (d, J = 7.9 Hz, 2H), 3.05 (d, J = 14.9 Hz, 2H), 2.24 (s, 6H), 2.22 (s, 12H).

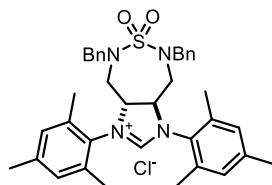
(3*aR*,8*aR*)-5,7-Dibenzyl-1,3-dimesityloctahydro-1*H*-imidazo[4,5-*d*][1,2,7]thiadiazepine 6,6-dioxide (**DB12A**)



The bis(arylamine) **DB9** (1.2 g, 2 mmol) was dissolved in a mixture of acetic acid (10 mL) and methanol (100 mL) and paraformaldehyde (240 mg, 8 mmol) was added. The reaction was stirred until the paraformaldehyde had dissolved. Acetic acid was removed under reduced pressure and the resulting crude material was purified by column chromatography on silica gel (10% EtOAc in cyclohexane) to give the imidazolidine **DB12A** as a white foam (1.26 g, quant.).

^1H NMR (500 MHz, CDCl_3) δ 7.25 (d, J = 9.7 Hz, 6H), 7.16 (dd, J = 6.3, 3.0 Hz, 4H), 6.83 (s, 2H), 6.80 (s, 2H), 4.42 (d, J = 14.3 Hz, 2H), 4.33 – 4.23 (m, 4H), 4.19 (d, J = 14.2 Hz, 2H), 3.06 (dd, J = 13.1, 8.9 Hz, 2H), 2.93 (dd, J = 13.0, 3.5 Hz, 2H), 2.39 (s, 6H), 2.24 (s, 6H), 2.18 (s, 6H).

(3*aR*,8*aR*)-5,7-Dibenzyl-1,3-dimesityl-3*a*,4,5,7,8,8*a*-hexahydro-1*H*-imidazo[4,5-*d*][1,2,7]thiadiazepin-3-ium 6,6-dioxide (**DB13A**)

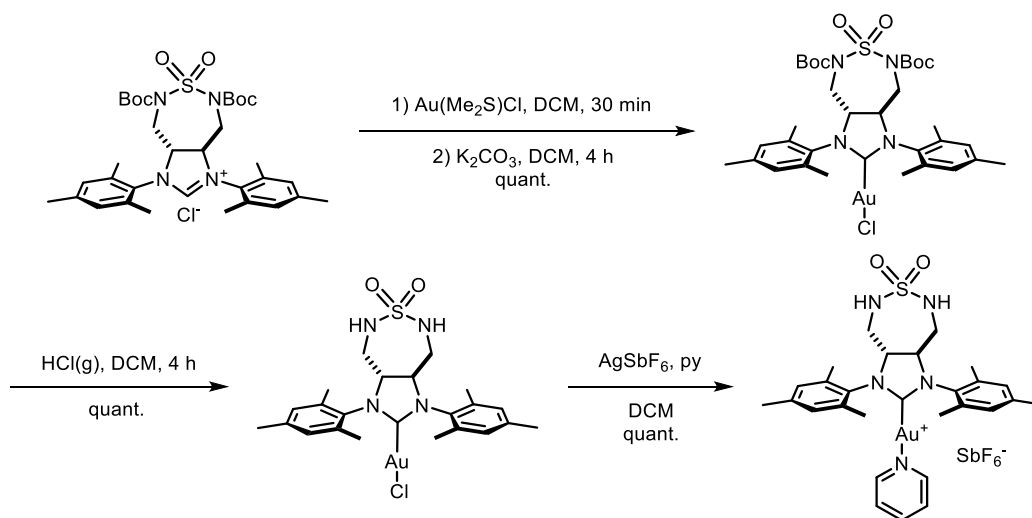


The imidazolidine **DB12A** (609 mg, 1 mmol) was dissolved in toluene (150 mL). *N*-Chlorosuccinimide (536 mg, 4 mmol) was added, and the reaction mixture was stirred at room temperature for 5 h. After reaction completion, toluene was removed under reduced pressure and the resulting foam was dissolved in a minimal amount of CH₂Cl₂. This solution was added dropwise to vigorously stirring mixture of hexane (40 mL) and diethyl ether (40 mL) to separate the product from succinimide and *N*-chlorosuccinimide. The solids were collected by vacuum-filtration, washed with hexane-ether mixture, and dried to give the imidazoline **DB13A** as a white solid (353 mg, 55%).

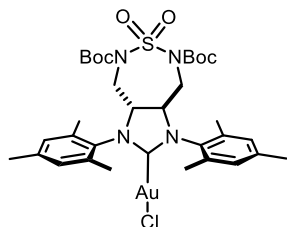
¹H NMR (500 MHz, CDCl₃) δ 9.78 (s, 1H), 7.31 – 7.19 (m, 10H), 6.90 (s, 2H), 6.87 (s, 2H), 5.44 – 5.25 (m, 2H), 4.69 (d, *J* = 14.3 Hz, 2H), 4.45 (d, *J* = 14.3 Hz, 2H), 3.52 – 3.44 (m, 2H), 3.06 (d, *J* = 13.0 Hz, 2H), 2.35 (s, 6H), 2.26 (s, 12H).

Gold cofactors

Synthesis of **DBAu-Cl** and **DBAu-py-SbF₆**



((3*aR*,8*aR*)-5,7-Bis(*tert*-butoxycarbonyl)-1,3-dimesityl-6,6-dioxidoctahydro-2*H*-imidazo[4,5-*d*][1,2,7]thiadiazepin-2-ylidene)gold(I) chloride (**DBBoc2-Au-Cl**)

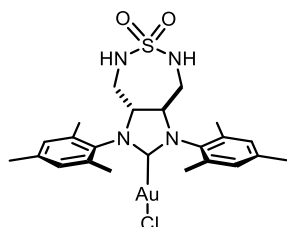


The imidazoline **DB13** (44 mg, 0.066 mmol) was dissolved in CH₂Cl₂ (3 mL) in a small vial. Chloro(dimethylsulfide)gold(I) (21 mg, 0.07 mmol) was added, the vial was wrapped with aluminium foil, and the reaction mixture was stirred at room temperature for 30 min. K₂CO₃ (97 mg, 0.7 mmol) was added, and mixture was stirred at room temperature overnight. After reaction completion, the reaction mixture was filtered through small pad of celite, and the solvent was removed under reduced

pressure to give the complex **DBBoc2-Au-Cl** as an off-white solid (56 mg, quant.). The crude product was used in the next step without further purification.

^1H NMR (500 MHz, CD_2Cl_2) δ 7.08 (s, 2H), 7.04 (s, 2H), 4.54 – 4.47 (m, 2H), 3.98 – 3.80 (m, 4H), 2.37 (s, 6H), 2.35 (s, 6H), 2.31 (s, 6H), 1.44 (s, 18H). ^{13}C NMR (126 MHz, CD_2Cl_2) δ 198.42, 150.55, 140.55, 137.07, 135.92, 132.94, 130.96, 130.56, 86.71, 68.05, 46.74, 28.09, 21.43, 19.40, 18.62.

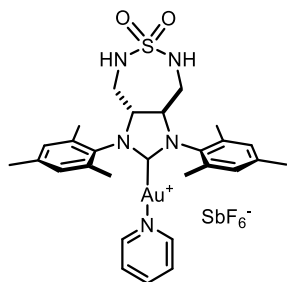
((3*a*,8*aR*)-1,3-Dimesityl-6,6-dioxidoctahydro-2*H*-imidazo[4,5-*d*][1,2,7]thiadiazepin-2-ylidene) gold(I) chloride (**DBAu-Cl**)



The complex **DBBoc2-Au-Cl** (56 mg, 0.066 mmol) was dissolved in CH_2Cl_2 (5 mL) in Schlenk tube, wrapped with aluminium foil, and HCl gas was purged through the solution for 3 h at room temperature. The gaseous HCl was generated by dropwise addition of concentrated H_2SO_4 to solid NH_4Cl . The solution was stirred for an additional 1 h at room temperature. Upon completion of the reaction as revealed by ^1H NMR, the solvent was evaporated under reduced pressure to give the cofactor **DBAu-Cl** as a white solid (42.8 mg, quant.). The crude product was used in the next step without further purification.

^1H NMR (500 MHz, CDCl_3) δ 6.97 (s, 2H), 6.95 (s, 2H), 4.73 – 4.60 (m, 2H), 4.56 – 4.47 (m, 2H), 3.38 – 3.18 (m, 4H), 2.32 (s, 6H), 2.31 (s, 6H), 2.30 (s, 6H).

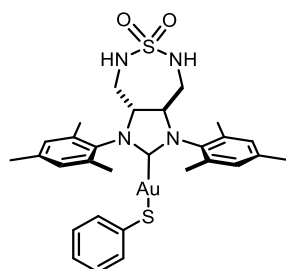
((3*a*,8*aR*)-1,3-Dimesityl-6,6-dioxidoctahydro-2*H*-imidazo[4,5-*d*][1,2,7]thiadiazepin-2-ylidene) (pyridine)gold(I) hexafluoroantimonate (**DBAu-py-SbF6**)



The complex **DBAu-Cl** (42.8 mg, 0.065 mmol) and pyridine (80 μL , 1 mmol) were dissolved in CH_2Cl_2 (3 mL). AgSbF_6 (23 mg, 0.067 mmol) was added, and reaction mixture was stirred overnight. After reaction completion, the resulting suspension was filtered through small pad of celite, and the organic solvent was removed under reduced pressure. The solids were dissolved in a minimal amount of CH_2Cl_2 . This solution was added dropwise to vigorously stirred diethyl ether (5 mL). The suspension was centrifuged (4000 rpm, 5 min) and the supernatant was discarded. Precipitation was repeated twice, and the resulting solid was dried in vacuo to give the cofactor **DBAu-py-SbF6** as a yellowish powder (57 mg, 94%).

^1H NMR (500 MHz, CD_2Cl_2) δ 8.02 – 7.92 (m, 1H), 7.87 (d, J = 4.9 Hz, 2H), 7.48 (t, J = 6.7 Hz, 2H), 7.03 (s, 4H), 5.55 (dd, J = 8.7, 4.4 Hz, 2H), 5.10 – 5.04 (m, 2H), 3.39 – 3.29 (m, 2H), 3.25 (dt, J = 13.3, 4.2 Hz, 2H), 2.42 (s, 6H), 2.39 (s, 6H), 2.32 (s, 6H).

((3*aR*,8*aR*)-1,3-Dimesityl-6,6-dioxidoctahydro-2*H*-imidazo[4,5-*d*][1,2,7]thiadiazepin-2-ylidene) (phenylthio)gold(I) (**DBAu-SPh**)

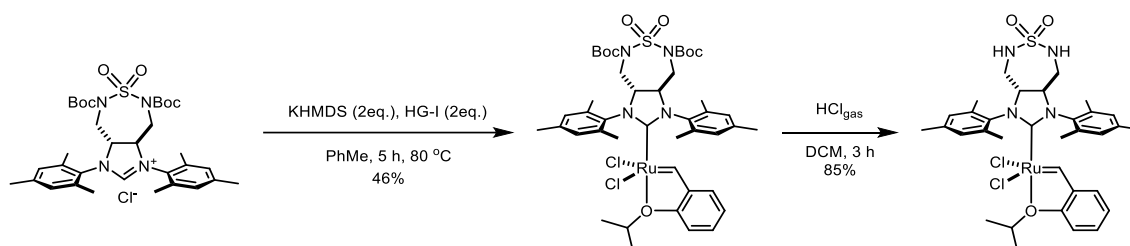


The complex **DBAu-Cl** (42.8 mg, 0.065 mmol) and thiophenol (35.7 g, 33 μ L, 0.325 mmol) were dissolved in CH_2Cl_2 (3 mL). K_2CO_3 (90 mg, 0.65 mmol) was added, and reaction mixture was stirred overnight. After reaction completion, the suspension was filtered through a small pad of celite, and the organic solvent was removed under reduced pressure. The solids were dissolved in minimal amount of CH_2Cl_2 . This solution was added dropwise to vigorously stirred diethyl ether (5 mL). The resulting suspension was filtered, washed with diethyl ether, and dried in vacuo to give the phenylthiol complex **DBAu-SPh** as a yellowish powder (57 mg, 94%).

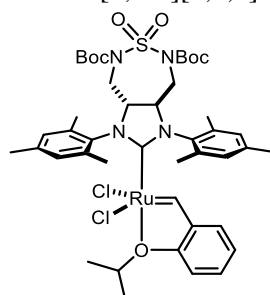
^1H NMR (500 MHz, CD_2Cl_2) δ 7.05 (s, 2H), 7.03 (s, 2H), 6.80 – 6.68 (m, 5H), 4.80 – 4.54 (m, 4H), 3.26 (dd, J = 4.9, 2.2 Hz, 4H), 2.36 (s, 12H), 2.35 (s, 6H).

Ru-cofactors

Synthesis of cofactor **DBRu1**



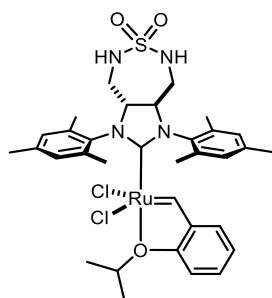
Dichloro((3*aR*,8*aR*)-5,7-bis(*tert*-butoxycarbonyl)-1,3-dimesityl-6,6-dioxidoctahydro-2*H*-imidazo[4,5-*d*][1,2,7]thiadiazepin-2-ylidene)(2-isopropoxybenzylidene)ruthenium(II) (**DBBoc2-Ru**)



The imidazoline **DB13** (40 mg, 0.06 mmol), KHMDS (24 mg, 0.12 mmol), and the Hoveyda-Grubbs 1st generation catalyst (72 mg, 0.12 mmol) were suspended in dry and degassed toluene (10 mL). The reaction mixture was heated to 80 $^\circ\text{C}$ for 5 h. The solvent was evaporated, and the crude material was purified by column chromatography (10% EtOAc in cyclohexane) to afford the complex **DBBoc2-Ru** as a green solid (26 mg, 46%).

^1H NMR (500 MHz, CD_2Cl_2) δ 16.20 (d, J = 0.8 Hz, 1H), 7.56 (dt, J = 8.4, 4.5 Hz, 1H), 7.13 (s, 2H), 7.08 (s, 2H), 6.92 (d, J = 4.3 Hz, 2H), 6.85 (d, J = 8.3 Hz, 1H), 4.89 (hept, J = 6.1 Hz, 1H), 4.71 (brs, 2H), 4.09 – 3.77 (m, 4H), 2.42 (brs, 18H), 1.43 (s, 18H), 1.20 (dd, J = 6.1, 3.0 Hz, 6H).

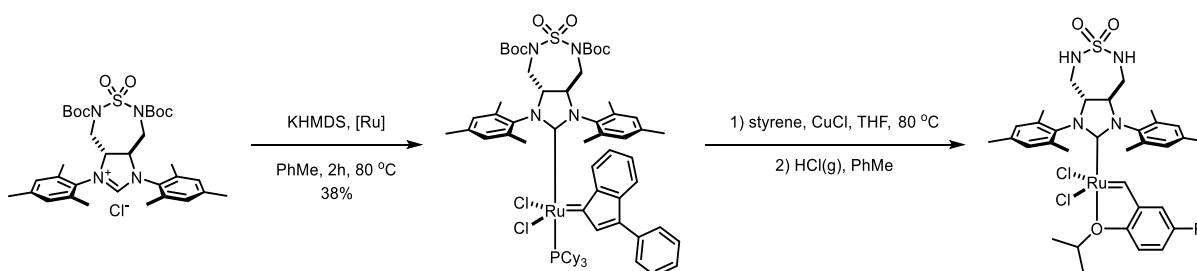
Dichloro((3*aR*,8*aR*)-1,3-dimesityl-6,6-dioxidoctahydro-2*H*-imidazo[4,5-*d*][1,2,7]thiadiazepin-2-ylidene)(2-isopropoxybenzylidene)ruthenium(II) (**DBRu1**)



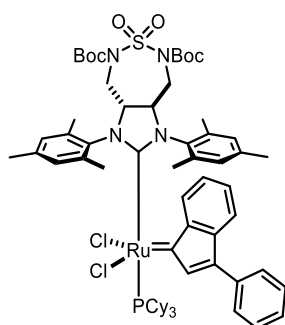
The complex **DBBoc2-Ru** (26 mg, 0.027 mmol) was dissolved in CH₂Cl₂ (5 mL) in a Schlenk tube, and HCl gas was purged through the solution for 3 h at room temperature. The gaseous HCl was generated by dropwise addition of concentrated H₂SO₄ to solid NH₄Cl. The solution was stirred for an additional 1 h at room temperature. Upon completion of the reaction as revealed by TLC (30% EtOAc in cyclohexane), the solvent was evaporated under reduced pressure, and the crude material was purified by column chromatography (30% EtOAc in cyclohexane) to give the cofactor **DBRu1** as a green solid (17.4 mg, 85%).

¹H NMR (500 MHz, CD₂Cl₂) δ 16.23 (d, *J* = 0.8 Hz, 1H), 7.56 (ddd, *J* = 8.4, 5.5, 3.6 Hz, 1H), 7.11 (s, 2H), 7.08 (s, 2H), 6.94 – 6.87 (m, 2H), 6.84 (d, *J* = 8.3 Hz, 1H), 4.89 (hept, *J* = 6.1 Hz, 1H), 4.87 – 4.80 (m, 2H), 4.60 (t, *J* = 5.5 Hz, 2H), 3.32 (s, 4H), 2.41 (brs, 18H), 1.19 (dd, *J* = 6.1, 3.5 Hz, 6H).

Synthesis of the intermediate **DBRu0** and derivatized cofactors **DBRu-*m*-XX**



Dichloro((3*aR*,8*aR*)-5,7-bis(*tert*-butoxycarbonyl)-1,3-dimesityl-6,6-dioxidoctahydro-2*H*-imidazo[4,5-*d*][1,2,7]thiadiazepin-2-ylidene)(3-phenyl-1*H*-inden-1-ylidene)ruthenium(II) (**DBRu0**)

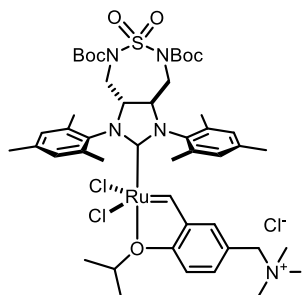


The imidazoline **DB13** (20 mg, 0.03 mmol), KHMDS (9 mg, 0.045 mmol), and dichloro(3-phenyl-1*H*-inden-1-ylidene)bis(tricyclohexylphosphine)ruthenium(II) (41.5 mg, 0.045 mmol) were suspended in dry and degassed toluene (10 mL). The reaction mixture was heated to 80 °C for 5 h. The solvent was evaporated, and the crude material was purified by column chromatography (5% EtOAc in cyclohexane) to afford the complex **DBRu0** as a red-brown solid (14.5 mg, 38%).

¹H NMR (500 MHz, CD₂Cl₂) δ 8.57 (ddd, *J* = 21.4, 7.5, 0.9 Hz, 1H), 7.75 – 7.66 (m, 2H), 7.55 – 7.39 (m, 4H), 7.29 – 7.14 (m, 3H), 7.13 – 7.01 (m, 3H), 6.44 (d, *J* = 6.1 Hz, 1H), 6.03 – 5.98 (m, 1H), 4.58 – 4.37 (m, 2H), 3.91 – 3.65 (m, 2H), 3.64 – 3.40 (m, 2H), 2.71 (d, *J* = 3.9 Hz, 3H), 2.60 (d, *J* = 7.8 Hz,

3H), 2.35 (s, 3H), 2.22 (d, $J = 22.6$ Hz, 3H), 2.17 – 2.02 (m, 6H), 1.86 (d, $J = 11.7$ Hz, 3H), 1.41 – 1.34 (m, 12H), 1.12 – 0.91 (m, 18H).

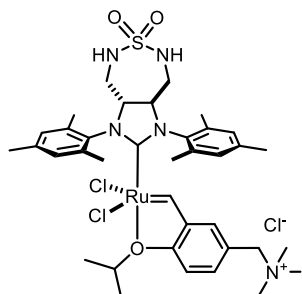
Dichloro((3*aR*,8*aR*)-5,7-bis(*tert*-butoxycarbonyl)-1,3-dimesityl-6,6-dioxidoctahydro-2*H*-imidazo[4,5-*d*][1,2,7]thiadiazepin-2-ylidene)(2-isopropoxy-5-((trimethylammonio)methyl)benzylidene)ruthenium(II) chloride (**DBBoc2-Ru-*m*-N⁺**).



The complex **DBRu0** (18 mg, 0.014 mmol), the styrene **DBS-*m*-N⁺** (3.2 mg, 0.012 mmol), and CuCl (4.5 mg, 0.045 mmol) were suspended in THF (3 mL) and stirred at 60 °C for 1 h. The solvent was evaporated, and the crude material was purified twice by column chromatography (neutral Al₂O₃, 10% MeOH in CH₂Cl₂) to give the complex **DBBoc2-Ru-*m*-N⁺** as a green solid (11.5 mg, 78%).

¹H NMR (500 MHz, CD₂Cl₂) δ 16.20 (s, 1H), 8.06 (d, $J = 8.7$ Hz, 1H), 7.14 (s, 2H), 7.09 (s, 2H), 6.99 (d, $J = 8.4$ Hz, 1H), 6.97 (s, 1H), 5.01 – 4.88 (m, 3H), 4.80 – 4.60 (m, 2H), 4.16 – 3.75 (m, 4H), 3.28 (s, 9H), 2.43 (s, 18H), 1.45 (s, 18H), 1.21 (dd, $J = 6.0, 3.5$ Hz, 6H).

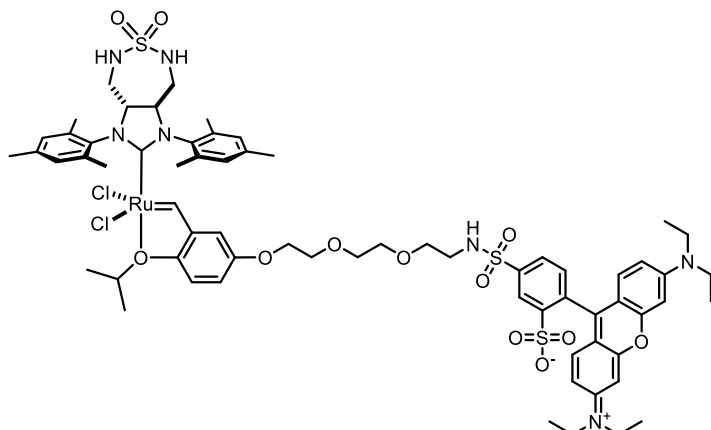
Dichloro((3*aR*,8*aR*)-1,3-dimesityl-6,6-dioxidoctahydro-2*H*-imidazo[4,5-*d*][1,2,7]thiadiazepin-2-ylidene)(2-isopropoxy-5-((trimethylammonio)methyl)benzylidene)ruthenium(II) chloride (**DBRu-*m*-N⁺**)



The complex **DBBoc2-Ru-*m*-N⁺** (11.5 mg, 0.011 mmol) was dissolved in toluene (5 mL) in a Schlenk tube, and HCl gas was purged through the solution for 3 h at room temperature. The gaseous HCl was generated by dropwise addition of concentrated H₂SO₄ to solid NH₄Cl. The solution was stirred for an additional 1 h at room temperature. Upon completion of the reaction as revealed by TLC (neutral Al₂O₃, 10% MeOH in CH₂Cl₂), the solvent was evaporated under reduced pressure, and the crude material was purified by column chromatography (neutral Al₂O₃, 10% MeOH in CH₂Cl₂) to give the cofactor **DBRu-*m*-N⁺** as a green solid (8.1 mg, 86%).

¹H NMR (500 MHz, CD₃OD) δ 16.48 (s, 1H), 7.79 (dd, $J = 8.5, 2.2$ Hz, 1H), 7.25 – 7.04 (m, 6H), 7.01 (d, $J = 2.2$ Hz, 1H), 5.05 – 4.97 (m, 1H), 4.55 (s, 2H), 3.25 – 3.13 (m, 4H), 3.07 (s, 9H), 2.44 (s, 18H), 1.21 (t, $J = 5.8$ Hz, 6H).

Dichloro(5-(2-(2-(2-((4-(6-(diethylamino)-3-(diethyliminio)-3*H*-xanthen-9-yl)-3-sulfonatophenyl)sulfonamido)ethoxy)ethoxy)ethoxy)-2-isopropoxybenzylidene)((3*aR*,8*aR*)-1,3-dimesityl-6,6-dioxidoctahydro-2*H*-imidazo[4,5-*d*][1,2,7]thiadiazepin-2-ylidene)ruthenium(II) (**DBRu-*m*-SRB**)

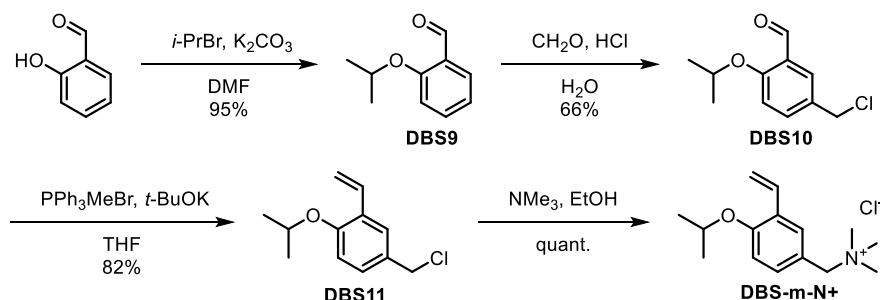


The styrene **DBS-*m*-SRB** (12.75 mg, 0.015 mmol), complex **DBRu0** (9 mg, 0.007 mmol), and CuCl (5 mg, 0.05 mmol) were suspended in THF (3 mL) and stirred at 60 °C for 1 h. The solvent was evaporated, and the crude material was purified by column chromatography (8% MeOH in CH₂Cl₂) to give the semipure complex **DBBoc2Ru-*m*-SRB** as a pink solid (9.26 mg, 84%).

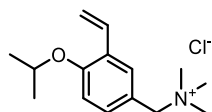
The crude complex **DBBoc2Ru-*m*-SRB** (9.26 mg, 0.006 mmol) was dissolved in CH₂Cl₂ (5 mL) in Schlenk tube, and HCl gas was purged through the solution for 3 h at room temperature. The gaseous HCl was generated by dropwise addition of concentrated H₂SO₄ to NH₄Cl. The solution was stirred for an additional 1 h at room temperature. Upon completion of the reaction as revealed by TLC (10% MeOH in CH₂Cl₂), the solvent was evaporated under reduced pressure, and crude material was purified by column chromatography (10% MeOH in CH₂Cl₂) to give the complex **DBRu-*m*-SRB** as a pink solid (7.6 mg, 90%).

¹H NMR (500 MHz, CD₂Cl₂) δ 16.09 (s, 1H), 8.65 (d, *J* = 1.8 Hz, 1H), 7.90 (dd, *J* = 7.9, 1.9 Hz, 1H), 7.25 – 7.17 (m, 4H), 7.16 – 7.01 (m, 4H), 6.86 – 6.80 (m, 2H), 6.76 – 6.70 (m, 3H), 6.45 (d, *J* = 3.0 Hz, 1H), 5.45 (t, *J* = 6.0 Hz, 0H), 4.85 – 4.53 (m, 3H), 4.11 – 4.04 (m, 2H), 3.96 – 3.77 (m, 6H), 3.73 – 3.67 (m, 2H), 3.67 – 3.50 (m, 12H), 3.25 (q, *J* = 5.7 Hz, 2H), 2.40 (brs, 18H), 1.44 (s, 18H), 1.37 – 1.20 (m, 12H), 1.14 (dd, *J* = 6.1, 2.3 Hz, 6H).

Synthesis of the intermediate **DBS-*m*-N⁺**



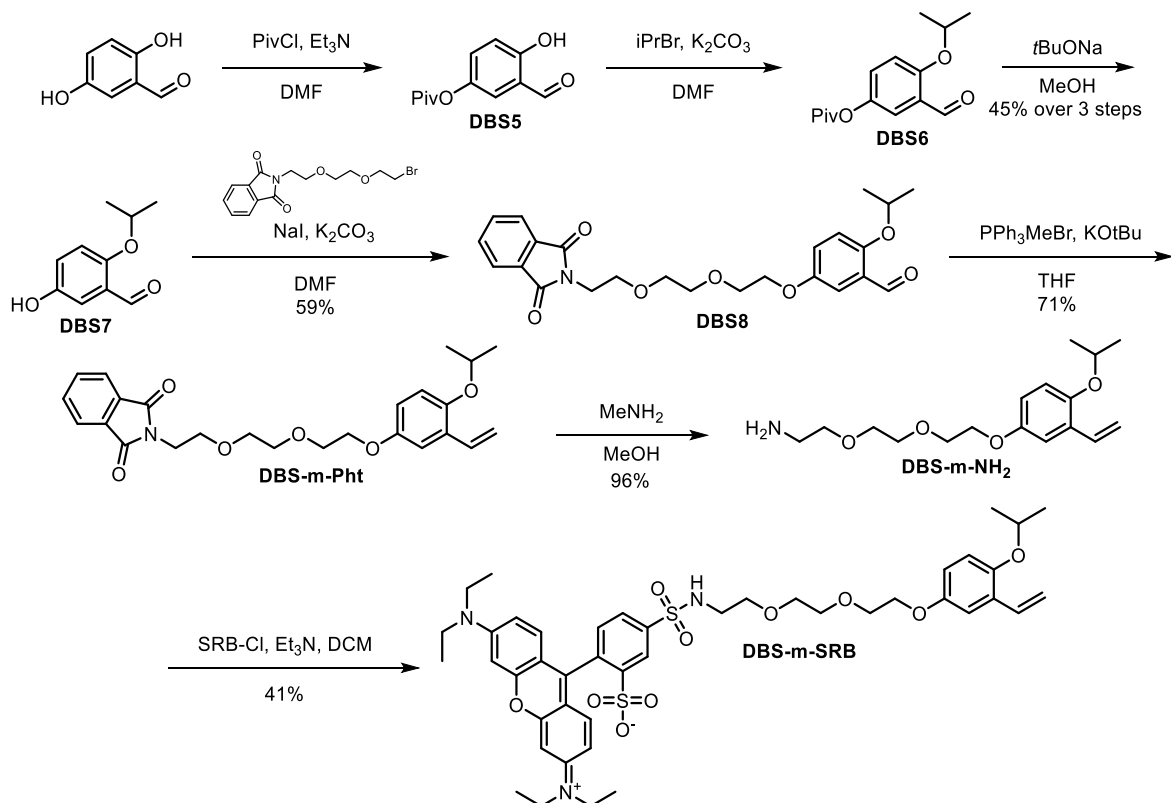
1-(4-Isopropoxy-3-vinylphenyl)-*N,N,N*-trimethylmethanaminium chloride (**DBS-*m*-N⁺**)



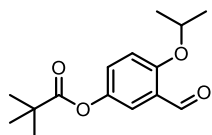
The styrene **DBS-*m*-N⁺** was obtained according to literature procedure.⁸¹

^1H NMR (500 MHz, CDCl_3) δ 7.60 (d, J = 1.9 Hz, 1H), 7.51 (dd, J = 8.4, 1.9 Hz, 1H), 6.97 (dd, J = 17.8, 11.2 Hz, 1H), 6.89 (d, J = 8.5 Hz, 1H), 5.80 (d, J = 17.7 Hz, 1H), 5.29 (d, J = 11.3 Hz, 1H), 4.87 (s, 2H), 4.58 (p, J = 6.0 Hz, 1H), 3.37 (s, 9H), 1.35 (d, J = 6.0 Hz, 6H).

Synthesis of styrenes **DBS-*m*-SRB** and **DBS-*m*-BODIPY**



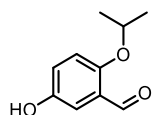
3-Formyl-4-isopropoxyphenyl pivalate (**DBS6**)



The aldehyde **DBS6** was obtained according to known procedure.⁸²

^1H NMR (500 MHz, CDCl_3) δ 10.03 (s, 1H), 7.28 – 7.23 (m, 1H), 7.06 (dd, J = 8.8, 3.1 Hz, 1H), 6.97 (d, J = 8.8 Hz, 1H), 1.40 (s, 9H).

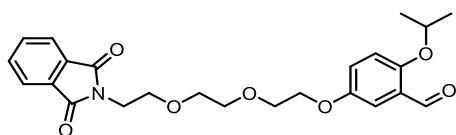
5-Hydroxy-2-isopropoxybenzaldehyde (**DBS7**)



The aldehyde **DBS6** (3.83 g, 14.5 mmol) was dissolved in methanol (100 mL), cooled to 0 °C, and sodium *tert*-butoxide (6.96 g, 72.5 mmol) was added portionwise. The reaction mixture was warmed to room temperature and stirred for additional 16 h. A concentrated solution of NH_4Cl (100 mL) was added and the mixture was extracted with ethyl acetate (100 mL \times 2). The combined organic phase was washed with water (100 mL \times 2) and saturated brine (100 mL) successively, dried over anhydrous sodium sulfate, filtered, and the organic solvent was removed under reduced pressure. The crude product was purified by silica gel column chromatography (30% EtOAc in cyclohexane) to give the phenol **DBS7** as a colourless oil (2.02 g, 77%).

^1H NMR (500 MHz, CDCl_3) δ 10.40 (s, 1H), 7.35 (d, $J = 3.2$ Hz, 1H), 7.10 (dd, $J = 9.0, 3.2$ Hz, 1H), 6.92 (d, $J = 9.0$ Hz, 1H), 6.00 (brs, 1H), 4.55 (hept, $J = 6.1$ Hz, 1H), 1.41 – 1.33 (m, 6H).

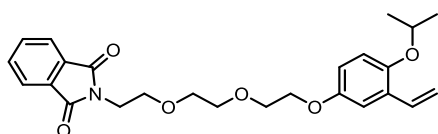
5-(2-(2-(2-(1,3-Dioxoisindolin-2-yl)ethoxy)ethoxy)ethoxy)-2-isopropoxybenzaldehyde (**DBS8**)



The phenol **DBS7** (810 mg, 4.5 mmol), 2-(2-(2-(2-bromoethoxy)ethoxy)ethyl)isindoline-1,3-dione (1.56 g, 4.5 mmol), NaI (150 mg, 1 mmol), and K_2CO_3 (828 mg, 6 mmol) were suspended in DMF (25 mL). The reaction mixture was heated at 80 °C overnight. 50 mL of water was added, and mixture was extracted with ethyl acetate (25 mL \times 3), and the combined organic phase was washed with water (50 mL \times 2) and saturated brine (50 mL) successively, dried over anhydrous sodium sulfate, filtered, and the organic solvent was removed under reduced pressure. The crude product was purified by silica gel column chromatography (50% EtOAc in cyclohexane) to give the aldehyde **DBS8** as a viscous colourless oil that solidifies in fridge (4 °C) (1.05 g, 59%).

^1H NMR (500 MHz, CDCl_3) δ 10.43 (s, 1H), 7.83 (dt, $J = 7.2, 3.6$ Hz, 4H), 7.74 – 7.66 (m, 4H), 7.26 (d, $J = 3.9$ Hz, 1H), 7.12 (dd, $J = 9.1, 3.3$ Hz, 1H), 6.93 (d, $J = 9.1$ Hz, 1H), 4.56 (hept, $J = 6.1$ Hz, 1H), 4.03 – 3.98 (m, 2H), 3.91 (t, $J = 5.8$ Hz, 2H), 3.84 (t, $J = 5.8$ Hz, 2H), 3.79 – 3.71 (m, 4H), 3.70 – 3.64 (m, 6H), 3.59 (s, 2H), 1.37 (d, $J = 6.1$ Hz, 6H).

2-(2-(2-(2-(4-Isopropoxy-3-vinylphenoxy)ethoxy)ethoxy)ethyl)isindoline-1,3-dione (**DBS-*m*-Pht**)

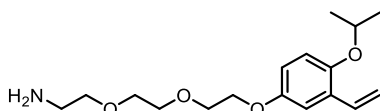


Methyltriphenylphosphonium bromide (1.07 g, 3 mmol) was suspended in THF (10 mL). The 0.5M solution of KHMDS (6.4 mL, 3.2 mmol) was added dropwise at 0 °C. After 30 min solution of the aldehyde **DBS8** (1.0 g, 2.26 mmol) in THF (5 mL) was added dropwise at 0 °C. The reaction mixture was stirred at room temperature overnight. A concentrated solution of NH_4Cl (20 mL) was added and the mixture was extracted with ethyl acetate (25 mL \times 3). The combined organic phase was washed with water (50 mL \times 2) and saturated brine (50 mL) successively, dried over anhydrous sodium sulfate, filtered, and the organic solvent was removed under reduced pressure. The crude product was purified by silica gel column chromatography (25% EtOAc in cyclohexane) to give the styrene **DBS-*m*-Pht** as a viscous colourless oil that solidifies in fridge (4 °C) (705 mg, 71%).

^1H NMR (500 MHz, CDCl_3) δ 7.82 (dt, $J = 7.0, 3.5$ Hz, 2H), 7.72 – 7.64 (m, 2H), 7.05 – 6.96 (m, 2H), 6.80 (d, $J = 8.9$ Hz, 1H), 6.74 (dd, $J = 8.9, 3.0$ Hz, 1H), 5.69 (dd, $J = 17.8, 1.2$ Hz, 1H), 5.23 (dd, $J = 11.1, 1.1$ Hz, 1H), 4.37 (hept, $J = 6.1$ Hz, 1H), 4.04 – 3.99 (m, 2H), 3.91 (t, $J = 5.8$ Hz, 2H), 3.76 (dt, $J = 9.2, 5.5$ Hz, 4H), 3.67 (s, 4H), 1.31 (d, $J = 6.1$ Hz, 6H).

^{13}C NMR (126 MHz, CDCl_3) δ 168.42, 153.25, 149.72, 134.04, 132.29, 131.95, 129.39, 123.36, 117.04, 115.10, 114.28, 112.35, 72.42, 70.87, 70.34, 70.01, 68.11, 68.04, 37.43, 27.06, 22.38.

2-(2-(2-(2-(4-Isopropoxy-3-vinylphenoxy)ethoxy)ethoxy)ethoxy)ethan-1-amine (**DBS-*m*-NH2**)

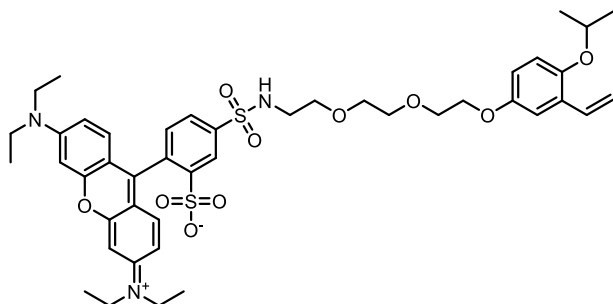


The styrene **DBS-*m*-Pht** (100 mg, 0.22 mmol) was dissolved in ethanol (3 mL). A 33% solution of methylamine in water (3 mL) was added dropwise, and the resulting mixture was heated to 60 °C for 3 h. The solvents were evaporated under reduced pressure and residue was sonicated with chloroform. The resulting suspension was filtered, and the solvent was removed under reduced pressure to give the

crude amine **DBS-*m*-NH₂** as a colourless oil (65 mg, 96%). The crude product was used in the next step without further purification.

¹H NMR (500 MHz, CDCl₃) δ 7.11 – 6.97 (m, 2H), 6.82 (d, *J* = 8.9 Hz, 1H), 6.77 (dd, *J* = 8.9, 3.0 Hz, 1H), 5.69 (dd, *J* = 17.8, 1.4 Hz, 1H), 5.23 (dd, *J* = 11.1, 1.4 Hz, 1H), 4.37 (hept, *J* = 6.1 Hz, 1H), 4.11 (dd, *J* = 5.4, 4.4 Hz, 2H), 3.84 (dd, *J* = 5.5, 4.3 Hz, 2H), 3.69 – 3.60 (m, 2H), 3.55 – 3.49 (m, 2H), 2.87 (t, *J* = 5.2 Hz, 2H), 1.30 (d, *J* = 6.1 Hz, 6H).

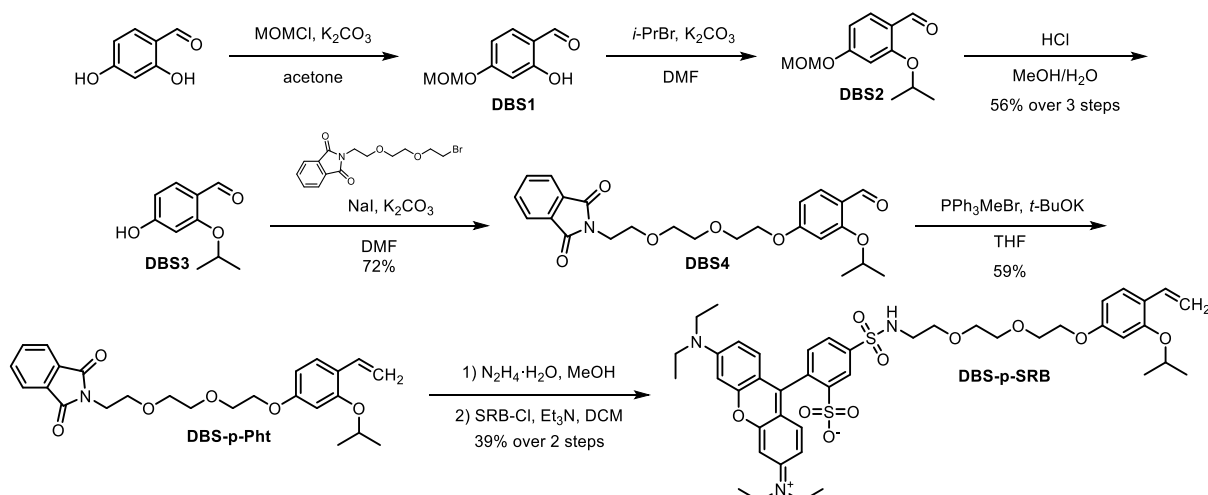
2-(6-(Diethylamino)-3-(diethyliminio)-3*H*-xanthen-9-yl)-5-(*N*-(2-(2-(2-(4-isopropoxy-3-vinylphenoxy)ethoxy)ethoxy)ethyl)sulfamoyl)benzenesulfonate (**DBS-*m*-SRB**)



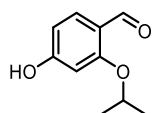
The crude amine **DBS-*m*-NH₂** (65 mg, 0.21 mmol), Et₃N (138 μL, 1 mmol) were dissolved in CH₂Cl₂ (8 mL). Sulforhodamine B acid chloride (144 mg, 0.25 mmol) was added portionwise at 0 °C. The reaction mixture was stirred at room temperature overnight and then concentrated under reduced pressure. The crude mixture was purified by column chromatography (5% MeOH in CH₂Cl₂) to give the styrene **DBS-*m*-SRB** as a pink solid (73.2 mg, 41%).

¹H NMR (500 MHz, CDCl₃) δ 8.86 (d, *J* = 1.8 Hz, 1H), 7.95 (dd, *J* = 7.9, 1.9 Hz, 1H), 7.17 (d, *J* = 8.0 Hz, 1H), 7.08 – 6.95 (m, 2H), 6.81 – 6.75 (m, 4H), 6.66 (d, *J* = 2.5 Hz, 2H), 5.69 (dd, *J* = 17.8, 1.4 Hz, 1H), 5.45 (t, *J* = 6.0 Hz, 1H), 5.20 (dd, *J* = 11.1, 1.4 Hz, 1H), 4.36 (hept, *J* = 6.1 Hz, 1H), 4.18 – 4.12 (m, 2H), 3.91 – 3.86 (m, 2H), 3.75 (dd, *J* = 5.6, 3.3 Hz, 2H), 3.72 – 3.62 (m, 4H), 3.54 (hept, *J* = 7.4 Hz, 8H), 3.31 (q, *J* = 5.6 Hz, 2H), 1.32 – 1.27 (m, 18H).

Alternative routes' products



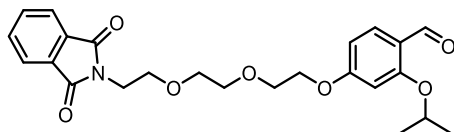
4-Hydroxy-2-isopropoxybenzaldehyde (**DBS3**)



The phenol **DBS3** was obtained according to a reported procedure.⁸³

^1H NMR (500 MHz, CDCl_3) δ 10.29 (s, 1H), 7.80 – 7.72 (m, 1H), 6.54 – 6.36 (m, 2H), 4.61 (hept, J = 6.2 Hz, 1H), 1.40 (d, J = 6.1 Hz, 6H).

4-(2-(2-(2-(1,3-Dioxoisindolin-2-yl)ethoxy)ethoxy)ethoxy)-2-isopropoxybenzaldehyde (**DBS4**)

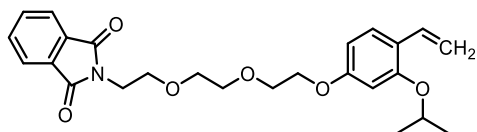


The phenol **DBS3** (900 mg, 5 mmol), 2-(2-(2-(2-bromoethoxy)ethoxy)ethyl)isoindoline-1,3-dione (1.5 g, 4.4 mmol), NaI (150 mg, 1 mmol), and K_2CO_3 (828 mg, 6 mmol) were suspended in DMF (25 mL). The reaction mixture was heated at 80 °C overnight. Water (50 mL) was added, and the mixture was extracted with ethyl acetate (25 mL \times 3). The combined organic phase was washed with water (50 mL \times 2) and saturated brine (50 mL) successively, dried over anhydrous sodium sulfate, filtered, and the organic solvent was removed under reduced pressure. The crude product was purified by silica gel column chromatography (50% EtOAc in cyclohexane) to give the aldehyde **DBS4** as a viscous colourless oil that solidifies in the fridge (4 °C) (1.4 g, 72%).

^1H NMR (500 MHz, CDCl_3) δ 10.30 (s, 1H), 7.88 – 7.75 (m, 3H), 7.69 (dt, J = 5.4, 3.5 Hz, 3H), 6.50 – 6.43 (m, 3H), 4.61 (hept, J = 6.1 Hz, 1H), 4.10 – 4.07 (m, 3H), 3.90 (t, J = 5.8 Hz, 2H), 3.82 – 3.78 (m, 3H), 3.75 (t, J = 5.8 Hz, 2H), 3.67 (s, 5H), 1.38 (d, J = 6.1 Hz, 6H).

^{13}C NMR (126 MHz, CDCl_3) δ 188.87, 168.40, 165.34, 162.39, 134.08, 132.25, 130.33, 123.35, 120.12, 106.33, 100.74, 71.26, 70.92, 70.33, 69.61, 68.13, 67.77, 37.41, 22.10.

2-(2-(2-(2-(3-Isopropoxy-4-vinylphenoxy)ethoxy)ethoxy)ethyl)isoindoline-1,3-dione (**DBS-*p*-Pht**)

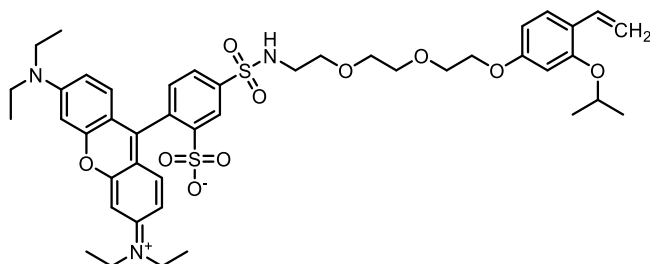


Methyltriphenylphosphonium bromide (1.22 g, 3.4 mmol) was suspended in THF (10 mL). A 1.6 M solution of *n*-BuLi (2 mL, 3.2 mmol) was added dropwise at 0 °C. After 30 min, the solution of the aldehyde **DBS4** (1.4 g, 3.2 mmol) in THF (5 mL) was added dropwise at 0 °C. The reaction mixture was stirred at room temperature overnight. The concentrated solution of NH_4Cl (20 mL) was added, and the mixture was extracted with ethyl acetate (25 mL \times 3). The combined organic phase was washed with water (50 mL \times 2) and saturated brine (50 mL) successively, dried over anhydrous sodium sulfate, filtered, and the organic solvent was removed under reduced pressure. The crude product was purified by silica gel column chromatography (25% EtOAc in cyclohexane) to give the styrene **DBS-*p*-Pht** as a viscous colourless oil that solidifies in the fridge (4 °C) (830 mg, 59%).

^1H NMR (500 MHz, CDCl_3) δ 7.82 (dd, J = 5.4, 3.0 Hz, 2H), 7.72 – 7.65 (m, 2H), 7.36 (d, J = 8.5 Hz, 1H), 6.95 (dd, J = 17.8, 11.2 Hz, 1H), 6.45 (d, J = 2.4 Hz, 1H), 6.42 (dd, J = 8.5, 2.4 Hz, 1H), 5.61 (dd, J = 17.8, 1.6 Hz, 1H), 5.10 (dd, J = 11.2, 1.6 Hz, 1H), 4.49 (hept, J = 6.1 Hz, 1H), 4.06 – 4.00 (m, 2H), 3.91 (t, J = 5.8 Hz, 2H), 3.80 – 3.77 (m, 2H), 3.75 (t, J = 5.8 Hz, 2H), 3.67 (s, 4H), 1.34 (d, J = 6.1 Hz, 6H).

^{13}C NMR (126 MHz, CDCl_3) δ 168.43, 159.69, 156.31, 134.06, 132.28, 131.73, 127.27, 123.37, 121.23, 111.90, 105.93, 101.94, 70.95, 70.89, 70.32, 69.88, 68.13, 67.52, 37.42, 22.32.

2-(6-(Diethylamino)-3-(diethyliminio)-3*H*-xanthen-9-yl)-5-(*N*-(2-(2-(2-(3-isopropoxy-4-vinylphenoxy)ethoxy)ethoxy)ethyl)sulfamoyl)benzenesulfonate (**DBS-*p*-SRB**)



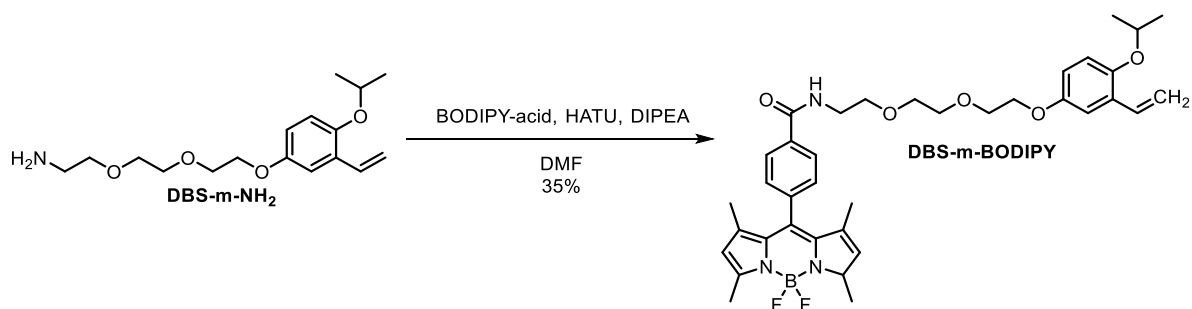
The styrene **DBS-*p*-Ph** (100 mg, 0.22 mmol) was dissolved in methanol (10 mL). Hydrazine hydrate (200 μ L, 6.25 mmol) was added dropwise, and the resulting mixture was stirred at room temperature for 16 h. The solvents were evaporated under reduced pressure and the residue was sonicated with chloroform. The resulting suspension was filtered and the solvent was removed under reduced pressure to give the crude amine **DBS-*p*-NH₂** as a colourless oil (65 mg, 96%).

The crude amine **DBS-*p*-NH₂** (65 mg, 0.21 mmol) and Et₃N (100 μ L, 0.72 mmol) were dissolved in CH₂Cl₂ (25 mL). Sulforhodamine B acid chloride (144 mg, 0.25 mmol) was added portionwise at 0 °C. The reaction mixture was stirred at room temperature overnight and then concentrated under reduced pressure. The crude mixture was purified by silica gel column chromatography (6% MeOH in CH₂Cl₂) to give the styrene **DBS-*p*-SRB** as a pink solid (73.2 mg, 41%).

¹H NMR (500 MHz, CDCl₃) δ 8.83 (s, 1H), 7.96 (dd, *J* = 7.9, 1.6 Hz, 1H), 7.34 (d, *J* = 8.4 Hz, 1H), 7.30 – 7.22 (m, 3H), 7.18 (d, *J* = 7.9 Hz, 1H), 7.00 – 6.88 (m, 1H), 6.79 (dd, *J* = 9.5, 2.2 Hz, 2H), 6.66 (d, *J* = 1.8 Hz, 2H), 6.51 – 6.36 (m, 2H), 5.81 – 5.72 (m, 1H), 5.58 (d, *J* = 17.8 Hz, 1H), 5.07 (d, *J* = 11.2 Hz, 1H), 4.50 (hept, *J* = 5.9 Hz, 1H), 4.19 – 4.11 (m, 2H), 3.88 (q, *J* = 7.8, 6.3 Hz, 2H), 3.73 (dd, *J* = 5.6, 3.0 Hz, 2H), 3.70 – 3.61 (m, 4H), 3.60 – 3.47 (m, *J* = 7.3 Hz, 8H), 3.28 (q, *J* = 5.3 Hz, 2H), 1.32 (d, *J* = 6.1 Hz, 6H), 1.28 (t, *J* = 7.1 Hz, 12H).

¹³C NMR (126 MHz, CDCl₃) δ 159.71, 159.18, 158.04, 156.49, 156.29, 155.65, 148.41, 141.93, 133.78, 133.61, 131.74, 129.86, 129.22, 127.56, 127.26, 127.06, 126.37, 121.08, 114.51, 113.63, 111.74, 106.17, 104.95, 101.86, 101.47, 95.73, 70.93, 70.84, 70.59, 69.95, 69.89, 69.69, 67.62, 50.94, 45.96, 43.35, 22.93, 22.31, 22.29, 14.57, 12.71.

4-(5,5-Difluoro-1,3,7,9-tetramethyl-3*H*,5*H*-5 λ^4 -dipyrrolo[1,2-*c*:2',1'-*f*][1,3,2]diazaborinin-10-yl)-*N*-(2-(2-(4-isopropoxy-3-vinylphenoxy)ethoxy)ethoxy)ethyl)benzamide (**DBS-*m*-BODIPY**)

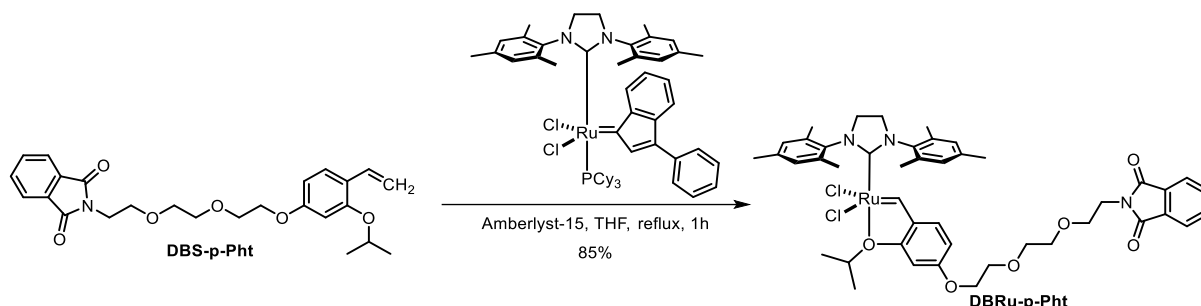


4,4-Difluoro-8-(4'-carboxyphenyl)-1,3,5,7-tetramethyl-4-bora-3*a*,4*a*,-diazas-indacene (60 mg, 0.163 mmol), HATU (114 mg, 0.3 mmol), and DIPEA (107 μ L, 0.6 mmol) were stirred in DMF (3 mL) for 30 min. The solution of the crude amine **DBS-*m*-NH₂** (70 mg, 0.23 mmol) in DMF (1 mL) was added, and the mixture was stirred at room temperature for an additional 16 h. The organic solvent was removed under reduced pressure, and the crude material was purified by column chromatography (5% MeOH in CH₂Cl₂) to give the styrene **DBS-*m*-BODIPY** as brown solid (42 mg, 35%).

¹H NMR (500 MHz, CDCl₃) δ 7.94 (d, *J* = 8.2 Hz, 2H), 7.34 (d, *J* = 8.2 Hz, 2H), 7.05 – 6.92 (m, 3H), 6.80 – 6.68 (m, 2H), 5.97 (s, 2H), 5.65 (dd, *J* = 17.8, 1.2 Hz, 1H), 5.21 (dd, *J* = 11.1, 1.2 Hz, 1H), 4.34

(hept, $J = 5.8$ Hz, 1H), 4.12 – 4.05 (m, 2H), 3.85 (q, $J = 5.0$ Hz, 2H), 3.81 – 3.67 (m, 8H), 2.55 (s, 6H), 1.33 (s, 6H), 1.28 (d, $J = 6.1$ Hz, 6H).

Dichloro[1,3-dimesitylimidazolidin-2-ylidene](4-(2-(2-(2-(1,3-dioxoisindolin-2-yl)ethoxy)ethoxy)ethoxy)-2-isopropoxybenzylidene)ruthenium(II) (**DBRu-*p*-Pht**)

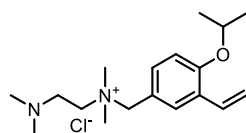


Dichloro[1,3-bis(2,4,6-trimethylphenyl)-2-imidazolidinylidene](3-phenyl-1*H*-inden-1-ylidene)(tricyclohexylphosphine)ruthenium(II) (30 mg, 0.032 mmol), the styrene **DBS-*p*-Pht** (18 mg, 0.041 mmol), and Amberlyst-15A (40 mg) were suspended in THF (3 mL) and stirred at 60 °C for 1 h. The solvent was evaporated, and the crude material was purified twice by column chromatography (15% EtOAc in cyclohexane) to afford the complex **DBRu-*p*-Pht** as a green solid (24.6 mg, 85%).

^1H NMR (600 MHz, CD_2Cl_2) δ 7.80 – 7.75 (m, 2H), 7.68 (dd, $J = 5.0, 3.2$ Hz, 2H), 7.06 (s, 4H), 6.83 (d, $J = 8.5$ Hz, 1H), 6.40 (d, $J = 8.5$ Hz, 1H), 6.38 (s, 1H), 4.81 (hept, $J = 5.9$ Hz, 1H), 4.15 (s, 4H), 4.01 – 3.95 (m, 2H), 3.84 (t, $J = 5.7$ Hz, 2H), 3.70 (dt, $J = 15.1, 5.2$ Hz, 4H), 3.58 (s, 4H), 2.42 (d, $J = 20.7$ Hz, 18H), 1.22 (d, $J = 6.1$ Hz, 6H).

^{13}C NMR (151 MHz, CD_2Cl_2) δ 212.06, 168.12, 160.69, 153.93, 140.83, 138.74, 133.91, 132.04, 129.17, 123.20, 122.94, 106.65, 101.04, 75.28, 70.54, 70.17, 69.27, 67.88, 67.81, 37.37, 26.87, 20.80.

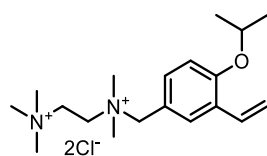
2-(Dimethylamino)-*N*-(4-isopropoxy-3-vinylbenzyl)-*N,N*-dimethylethan-1-aminium chloride (**DBS12**)



The styrene **DBS12** was obtained according to a reported procedure.⁸¹

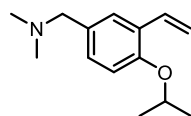
^1H NMR (500 MHz, CDCl_3) δ 7.60 (d, $J = 2.3$ Hz, 1H), 7.53 (dd, $J = 8.5, 2.3$ Hz, 1H), 6.97 (dd, $J = 17.8, 11.3$ Hz, 1H), 6.89 (d, $J = 8.6$ Hz, 1H), 5.80 (dd, $J = 17.8, 1.2$ Hz, 1H), 5.29 (dd, $J = 11.2, 1.2$ Hz, 1H), 4.92 (s, 2H), 4.58 (hept, $J = 6.0$ Hz, 1H), 3.82 – 3.79 (m, 2H), 3.28 (s, 6H), 2.80 (t, $J = 5.6$ Hz, 2H), 2.27 (s, 6H), 1.36 (d, $J = 6.1$ Hz, 6H).

*N*¹-(4-Isopropoxy-3-vinylbenzyl)-*N*¹,*N*¹,*N*²,*N*²,*N*²-pentamethylethane-1,2-diaminium dichloride (**DBS-*m*-NN++**)



The styrene **DBS-*m*-NN++** was obtained according to a reported procedure.⁸¹

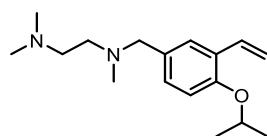
^1H NMR (500 MHz, $\text{DMSO}-d_6$) δ 7.71 (d, $J = 2.3$ Hz, 1H), 7.47 (dd, $J = 8.6, 2.3$ Hz, 1H), 7.17 (d, $J = 8.8$ Hz, 1H), 6.96 (dd, $J = 17.8, 11.3$ Hz, 1H), 5.86 (dd, $J = 17.8, 1.5$ Hz, 1H), 5.35 (dd, $J = 11.2, 1.5$ Hz, 1H), 4.73 (hept, $J = 5.9$ Hz, 1H), 4.52 (s, 2H), 3.98 (dd, $J = 10.2, 5.9$ Hz, 2H), 3.84 (dd, $J = 10.2, 6.0$ Hz, 2H), 3.19 (s, 9H), 3.02 (s, 6H), 1.32 (d, $J = 6.0$ Hz, 6H).

1-(4-Isopropoxy-3-vinylphenyl)-*N,N*-dimethylmethanamine (**DBS-*m*-N**)

The chloride **DBS11** (633 mg, 3 mmol) was dissolved in ethanol (20 mL). Me₂NH (40 wt % solution in water 3.375 g, 30 mmol) was added quickly at room temperature. The mixture was stirred for 1 h, and the organic solvent was removed under reduced pressure. The residue was dissolved in 0.1M NaOH (50 mL), extracted with diethyl ether (25 mL×3). The combined organic phase was washed with water (20 mL) and saturated brine (20 mL), dried over anhydrous sodium sulfate, filtered. After removal of the organic solvent under reduced pressure, the amine **DBS-*m*-N** was obtained as a yellow oil (657 mg, quant.) which was used without further purification.

¹H NMR (500 MHz, CDCl₃) δ 7.40 (d, *J* = 2.2 Hz, 1H), 7.13 (dd, *J* = 8.4, 2.2 Hz, 1H), 7.04 (dd, *J* = 17.8, 11.2 Hz, 1H), 6.83 (d, *J* = 8.4 Hz, 1H), 5.76 (dd, *J* = 17.8, 1.6 Hz, 1H), 5.22 (dd, *J* = 11.2, 1.6 Hz, 1H), 4.52 (hept, *J* = 6.1 Hz, 1H), 3.35 (s, 2H), 2.23 (s, 6H), 1.34 (d, *J* = 6.1 Hz, 6H).

¹³C NMR (126 MHz, CDCl₃) δ 154.47, 132.07, 130.99, 129.58, 127.66, 127.46, 114.20, 114.12, 71.05, 64.05, 45.43, 22.35.

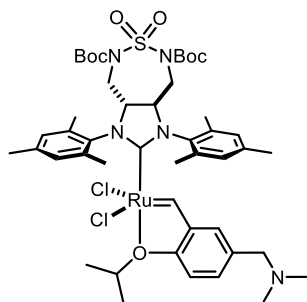
*N*¹-(4-Isopropoxy-3-vinylbenzyl)-*N*¹,*N*²,*N*²-trimethylethane-1,2-diamine (**DBS-*m*-NN**)

The chloride **DBS11** (211 mg, 1 mmol) was dissolved in ACN (20 mL). TBAI (37 mg, 0.1 mmol), K₂CO₃ (276 mg, 2 mmol) and *N,N,N'*-Trimethylethylenediamine (204 mg, 2 mmol) were added to the solution in that order. The mixture was stirred for 16 h, and the organic solvent was removed under reduced pressure. The residue was dissolved in 0.1M NaOH (20 mL), extracted with diethyl ether (15 mL×5), and the combined organic phase was washed with water (20 mL) and saturated brine (20 mL), dried over anhydrous sodium sulfate, filtered, and the organic solvent was removed under reduced pressure to give the diamine **DBS-*m*-NN** as a yellow oil (232 mg, 84%).

¹H NMR (500 MHz, CDCl₃) δ 7.41 (d, *J* = 2.2 Hz, 1H), 7.17 (dd, *J* = 8.4, 2.2 Hz, 1H), 7.03 (dd, *J* = 17.8, 11.2 Hz, 1H), 6.84 (d, *J* = 8.4 Hz, 1H), 5.75 (dd, *J* = 17.8, 1.5 Hz, 1H), 5.23 (dd, *J* = 11.2, 1.5 Hz, 1H), 4.52 (hept, *J* = 6.0 Hz, 1H), 3.51 (s, 2H), 2.65 (s, 4H), 2.39 (s, 6H), 2.29 (s, 3H), 1.34 (d, *J* = 6.1 Hz, 6H).

¹³C NMR (126 MHz, CDCl₃) δ 154.67, 131.96, 129.78, 127.78, 127.62, 114.31, 71.11, 62.34, 45.04, 42.36, 22.33.

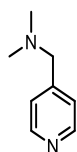
Dichloro((3a*R*,8a*R*)-5,7-bis(*tert*-butoxycarbonyl)-1,3-dimesityl-6,6-dioxidoctahydro-2*H*-imidazo[4,5-*d*][1,2,7]thiadiazepin-2-ylidene)(5-((dimethylamino)methyl)-2-isopropoxybenzylidene)ruthenium(II) (**DBSRu-*m*-N**)



The complex **DBRu0** (5 mg, 0.004 mmol), CuCl (2 mg, 0.02 mmol), and the styrene **DBS-*m*-N** (2.2 mg, 0.01 mmol) were stirred in toluene (2 mL) at 80 °C for 3 h. The organic solvent was removed under reduced pressure and the residue was purified by silica gel column chromatography (25% EtOAc in cyclohexane) to give the complex **DBSRu-*m*-N** as a green solid (2.3 mg, 57%).

¹H NMR (500 MHz, CD₂Cl₂) δ 16.14 (s, 1H), 7.60 (d, *J* = 7.1 Hz, 1H), 7.13 (s, 2H), 7.09 (s, 2H), 6.83 (d, *J* = 6.9 Hz, 2H), 4.88 (hept, *J* = 6.1 Hz, 1H), 4.72 (brs, 2H), 4.15 – 3.75 (m, 4H), 3.60 (brs, 2H), 2.65 – 2.19 (m, 24H), 1.45 (s, 18H), 1.19 (dd, *J* = 6.1, 3.1 Hz, 6H).

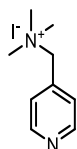
N,N-Dimethyl-1-(pyridin-4-yl)methanamine (**DBP-N**)



4-Picolylchloride hydrochloride (1.64 mg, 10 mmol) was suspended in ethanol (20 mL). Me₂NH (40 wt% solution in water, 11.25 g, 100 mmol) was quickly added at room temperature. The mixture was stirred for 1 h, and the organic solvent was removed under reduced pressure. The residue was dissolved in 0.1M NaOH (100 mL), extracted with diethyl ether (50 mL×3), and the combined organic phase was washed with water (100 mL) and saturated brine (100 mL), dried over anhydrous sodium sulfate, filtered, and the organic solvent was removed under reduced pressure to give the amine **DBP-N** as a colourless oil (1.36 g, quant.). The crude product was used in the next step without further purification.

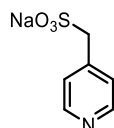
¹H NMR (500 MHz, CDCl₃) δ 8.56 – 8.51 (m, 2H), 7.26 – 7.23 (m, 2H), 3.42 (s, 2H), 2.24 (s, 6H).

N,N,N-Trimethyl-1-(pyridin-4-yl)methanaminium iodide (**DBP-N⁺**)



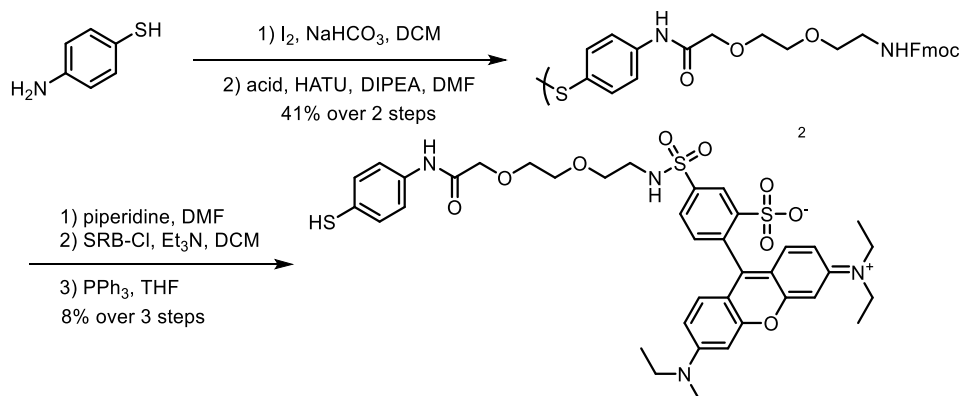
The amine **DBP-N** (1.36 g, 10 mmol) was dissolved in THF (30 mL). A solution of methyl iodide (1.28 g, 9 mmol) in THF (10 mL) was added dropwise. The reaction mixture was stirred for an additional 1 h and the solid residue was filtered, washed with THF and dried in vacuo to afford the pyridine **DBP-N⁺** as a white solid (2.33 g, 93%).

¹H NMR (500 MHz, CDCl₃) δ 8.75 – 8.69 (m, 2H), 7.66 – 7.61 (m, 2H), 5.09 (s, 2H), 3.34 (s, 9H).

Sodium pyridin-4-ylmethanesulfonate (**DBP-S-**)

4-picolylchloride hydrochloride (164 mg, 1 mmol), Na₂SO₃ (300 mg, 2.4 mmol), and sodium iodide (50 mg, 0.33 mmol) were dissolved in a mixture of water (10 mL) and ethanol (5 mL). The reaction mixture was stirred at 60 °C for 3 h. The solution was concentrated under reduced pressure to afford a white solid which was dissolved in water (1.5 mL) and adjusted to pH 9 with 2M sodium hydroxide. The resulting white suspension was filtered, and the filtrate was evaporated under reduced pressure to give the pyridine **DBP-S-** as a white solid (121 mg, 62%).

¹H NMR (500 MHz, DMSO-*d*₆) δ 8.43 (dd, *J* = 4.5, 1.4 Hz, 2H), 7.30 (d, *J* = 5.9 Hz, 2H), 3.75 (s, 2H).

2-(6-(diethylamino)-3-(diethyliminio)-3*H*-xanthen-9-yl)-5-(*N*-(2-(2-((4-mercaptophenyl)amino)-2-oxoethoxy)ethoxy)ethyl)sulfamoyl)benzenesulfonate (**DBHS-SRB**)

4-aminothiophenol (2.5 g, 20 mmol) and NaHCO₃ (2.1 g, 25 mmol) were suspended in CH₂Cl₂ (150 mL). After 15 min, iodine (7.62 g, 30 mmol) was added portionwise at 0 °C and the mixture was stirred for an additional 30 min. Then, a saturated solution of sodium thiosulfate was added dropwise at 0 °C until the solution became colourless. The two phases were separated, and the organic phase was washed with water (100 mL) and saturated brine (100 mL), dried over anhydrous sodium sulfate, filtered, and the organic solvent was removed under reduced pressure to give crude 4,4'-disulfanediyl dianiline (2 g, 81%) as dark green solid.

1-(9*H*-fluoren-9-yl)-3-oxo-2,7,10-trioxa-4-azadodecan-12-oic acid (1.7 g, 4.4 mmol), HATU (1.7 g, 4.44 mmol), and DIPEA (870 µL, 5 mmol) were dissolved in DMF (20 mL) and stirred for 30 min at room temperature. The solution of crude 4,4'-disulfanediyl dianiline (500 mg, 2 mmol) in DMF (5 mL) was added, and the reaction mixture was stirred for additional 16 h. The organic solvent was removed under reduced pressure and residue was purified by flash column chromatography (3% MeOH in CH₂Cl₂) to give crude bis((9*H*-fluoren-9-yl)methyl) (((((((disulfanediylbis(4,1-phenylene))bis(azanediyl))bis(2-oxoethane-2,1-diyl))bis(oxy))bis(ethane-2,1-diyl))bis(oxy))bis(ethane-2,1-diyl))dicarbamate as brown semi-solid (982 mg, 50%).

bis((9*H*-fluoren-9-yl)methyl) (((((((disulfanediylbis(4,1-phenylene))bis(azanediyl))bis(2-oxoethane-2,1-diyl))bis(oxy))bis(ethane-2,1-diyl))bis(oxy))bis(ethane-2,1-diyl))dicarbamate as brown semi-solid (491 mg, 0.5 mmol) was dissolved in DMF (10 mL) and piperidine (425 mg, 5 mmol) was added at room temperature. The reaction mixture was stirred for 16 h and concentrated under reduced pressure. The residue was co-evaporated with toluene three times to remove excess of piperidine, and the residue was subjected to acid-base extraction to afford *N,N'*-(disulfanediylbis(4,1-phenylene))bis(2-(2-(2-aminoethoxy)ethoxy)acetamide) as colourless oil (164 mg, 60%).

The crude *N,N'*-(disulfanediylbis(4,1-phenylene))bis(2-(2-(2-aminoethoxy)ethoxy)acetamide) and Et₃N were dissolved in CH₂Cl₂ (15 mL) and Sulforhodamine B acid chloride (300 mg, 0.6 mmol) was added.

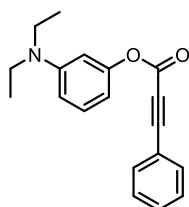
The reaction mixture was stirred at room temperature overnight and then was concentrated under reduced pressure. The crude mixture was purified by silica gel column chromatography (10% MeOH in CH₂Cl₂) to give 2-(6-(diethylamino)-3-(diethyliminio)-3*H*-xanthen-9-yl)-5-(*N*-(2-(2-(2-((4-(2-(2-(2-((4-(6-(diethylamino)-3-(diethyliminio)-3*H*-xanthen-9-yl)-3-sulfonatophenyl)sulfonamido)ethoxy)ethoxy)acetamido)phenyl)disulfaneyl)phenyl)amino)-2-oxoethoxy)ethoxy)ethyl)sulfamoyl)benzenesulfonate as pink solid (83 mg, 17%).

The disulfide (16 mg, 0.01 mmol) and triphenylphosphine (8 mg, 0.03 mmol) were dissolved in THF (2 mL) and stirred for 2 days at room temperature. The reaction mixture was concentrated under reduced pressure and the residue was purified by silica gel column chromatography (7% MeOH in CH₂Cl₂) to give the thiol **DBHS-SRB** as a pink solid (12 mg, 74%).

¹H NMR (500 MHz, CDCl₃) δ 9.12 (s, 1H), 8.88 (d, *J* = 1.8 Hz, 1H), 8.01 (dd, *J* = 7.9, 1.9 Hz, 1H), 7.51 – 7.45 (m, 2H), 7.25 – 7.21 (m, 2H), 7.16 – 7.10 (m, 2H), 6.75 (dd, *J* = 9.5, 2.5 Hz, 2H), 6.63 (d, *J* = 2.5 Hz, 2H), 5.46 (t, *J* = 5.8 Hz, 1H), 4.16 (s, 2H), 3.79 (dd, *J* = 5.5, 3.4 Hz, 2H), 3.69 (dd, *J* = 5.5, 3.4 Hz, 2H), 3.64 (t, *J* = 5.1 Hz, 2H), 3.59 – 3.45 (m, 10H), 3.39 (s, 1H), 3.34 (q, *J* = 5.5 Hz, 2H), 1.28 (t, *J* = 7.1 Hz, 12H).

Substrates and products for catalytic assays

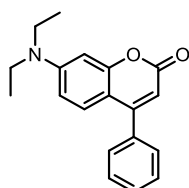
3-(Diethylamino)phenyl 3-phenylpropiolate (**DBSb1**)



The alkyne **DBSb1** was obtained according to a reported procedure.⁸⁴

¹H NMR (400 MHz, CDCl₃) δ 7.62 (dd, *J* = 8.3, 1.3 Hz, 2H), 7.52 – 7.44 (m, 1H), 7.44 – 7.35 (m, 2H), 7.21 (t, *J* = 8.2 Hz, 1H), 6.56 (dd, *J* = 8.4, 2.2 Hz, 1H), 6.48 – 6.39 (m, 2H), 3.34 (q, *J* = 7.1 Hz, 4H), 1.16 (t, *J* = 7.1 Hz, 6H).

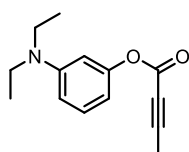
7-(Diethylamino)-4-phenyl-2*H*-chromen-2-one (**DBPr1**)



The coumarin **DBPr1** was obtained according to known procedure.⁸⁴

¹H NMR (500 MHz, CDCl₃) δ 7.38 (d, *J* = 8.9 Hz, 1H), 7.25 (d, *J* = 9.0 Hz, 1H), 6.58 (dd, *J* = 9.0, 2.6 Hz, 1H), 6.50 (d, *J* = 2.6 Hz, 1H), 5.96 – 5.92 (m, 1H), 3.41 (q, *J* = 7.1 Hz, 4H), 1.21 (t, *J* = 7.1 Hz, 6H).

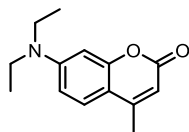
3-(Diethylamino)phenyl but-2-ynoate (**DBSb2**)



The alkyne **DBSb2** was obtained according to a reported procedure.⁸⁵

^1H NMR (500 MHz, CDCl_3) δ 7.17 – 7.11 (m, 1H), 6.55 – 6.50 (m, 1H), 6.33 – 6.29 (m, 2H), 3.35 (q, J = 7.1 Hz, 4H), 2.52 (s, 3H), 1.18 (t, J = 7.1 Hz, 6H).

7-(Diethylamino)-4-methyl-2*H*-chromen-2-one (**DBPr2**)



The coumarin **DBPr2** was obtained according to a reported procedure.⁸⁵

^1H NMR (500 MHz, CDCl_3) δ 7.38 (d, J = 8.9 Hz, 1H), 6.58 (dd, J = 9.0, 2.6 Hz, 1H), 6.50 (d, J = 2.6 Hz, 1H), 5.96 – 5.92 (m, 1H), 3.41 (q, J = 7.1 Hz, 4H), 2.34 (d, J = 1.1 Hz, 3H), 1.21 (t, J = 7.1 Hz, 6H).

6. Index of Abbreviations

°C	degree <i>Celsius</i>
Å	Ångstrom, 10^{-10} m
AAZ	acetazolamide
Ac	acetyl
ACN	acetonitrile
ADC	antibody-drug conjugate
alloc	allyloxycarbonyl
Ar	aryl
ArM	artificial metalloenzyme
BINAP	2,2'-bis(diphenylphosphino)-1,1'-binaphthyl
Bn	benzyl
Boc	<i>tert</i> -butyloxycarbonyl
BODIPY	4,4-difluoro-4-bora-3a,4a-diaza- <i>s</i> -indacene
Bu	butyl
CD	circular dichroism
CDI	1,1'-carbonyldiimidazole
cod	1,5-cyclooctadiene
Cp	cyclopentadienyl
Cp*	1,2,3,4,5-pentamethylcyclopentadienyl
δ	chemical shift
DAPI	4',6-diamidino-2-phenylindole
dba	dibenzylideneacetone
DCE	1,2-dichloroethane
DCM	dichloromethane
DDQ	2,3-dichloro-5,6-dicyano-1,4-benzoquinone
DIPEA	<i>N,N</i> -Diisopropylethylamine
DMAP	4-dimethylaminopyridine
DMF	<i>N,N</i> -dimethylformamide
DMSO	dimethyl sulfoxide
EDC·HCl	1-ethyl-3-carbodiimide hydrochloride
eq.	equivalent
<i>e.g.</i>	lat. <i>exempli gratia</i> , for example
e.r.	enantiomeric ratio

Index of Abbreviations

et al.	lat. <i>et alia</i> , and others
Et	ethyl
FACS	fluorescence-activated cell sorting
FDA	Food and Drug Administration
FITC	fluorescein isothiocyanate
Fmoc	fluorenylmethyloxycarbonyl
FRET	Förster or fluorescence resonance energy transfer
g	gram
G-I	1 st generation Grubbs' catalysts
GSH	glutathione
h	hours
HATU	hexafluorophosphate azabenzotriazole tetramethyl uronium
HBTU	hexafluorophosphate benzotriazole tetramethyl uronium
hCA	human carbonic anhydrase
HCTU	hexafluorophosphate 6-Cl-benzotriazole tetramethyl uranium
HFIP	1,1,1,3,3,3-hexafluoro-2-propanol
HG	Hoveyda-Grubbs catalyst
HOBt·H ₂ O	1-hydroxybenzotriazole monohydrate
HRMS	high-resolution mass spectrometry
HPLC	high performance liquid chromatography
HSA	human serum albumin
Hz	hertz
IC ₅₀	half maximal inhibitory concentration
ICP-MS	inductively coupled plasma mass spectrometry
ITC	isothermal titration calorimetry
<i>k</i>	reaction rate
K	kelvin
K _d	dissociation constant
KHMDS	potassium bis(trimethylsilyl)amide
L	liter
LC	liquid chromatography
LG	leaving group
μL	microliter
μmol	micromol

Index of Abbreviations

M	metal
M	molarity, mol
Me	methyl
Ms	methanesulfonyl
MS	mass spectrometry
min	minutes
MINFLUX	maximally informative luminescence excitation probing
mL	milliliter
MMAE	monomethyl auristatin E
mmol	millimole
MOF	metal-organic framework
NBA	<i>N</i> -bromoacetamide,
N(B/C/H/I)S	<i>N</i> -(bromo/chloro/hydroxy/iodo)succinimide
nM	nanomol
NMR	nuclear magnetic resonance
NP	nanoparticle
PAB	<i>p</i> -aminobenzyl alcohol
PBS	phosphate-buffered saline
PFP	2,3,4,5,6-pentafluoromethylphenyl
PG	protecting group
pH	lat. <i>pondus hydrogenii</i> , negative base 10 logarithm of the activity of the hydrogen ion in a solution
Piv	pivaloyl
Ph	phenyl
Pht	phthalimide
PMB	<i>p</i> -methoxybenzyl
PNP	<i>p</i> -nitrophenyl
ppm	parts per million, 10 ⁻⁶
Pr	propyl
py	pyridine
RCM	ring-closing metathesis
rt	room temperature
SRB	sulforhodamine B
TBAB, TBAI	tetrabutylammonium bromide, tetrabutylammonium iodide

Index of Abbreviations

TBS	<i>tert</i> -butyldimethylsilyl
TEOF	triethyl ortoformate
TFA	trifluoroacetic acid
THF	tetrahydrofuran
TLC	thin-layer chromatography
TON	turnover number
TRP	tandem repeat protein
Ts	<i>p</i> -toluenesulfonyl
UPLC	ultra-high performance liquid chromatography
UV	ultraviolet

7. Literature References

1. Rebelein, J. G. & Ward, T. R. *In Vivo* Catalyzed New-to-Nature Reactions. *Curr Opin Biotechnol* **53**, 106–114 (2018).
2. Bray, T. L. *et al.* Bright Insights into Palladium-Triggered Local Chemotherapy. *Chem Sci* **9**, 7354–7361 (2018).
3. Ortega-Liebana, M. C. *et al.* Truly-Biocompatible Gold Catalysis Enables Vivo-Orthogonal Intra-CNS Release of Anxiolytics. *Angew Chem Int Ed* **61**, e202111461, 1–5 (2022).
4. Adam, C. *et al.* A 5-FU Precursor Designed to Evade Anabolic and Catabolic Drug Pathways and Activated by Pd Chemistry *in Vitro* and *in Vivo*. *J Med Chem* **65**, 552–561 (2022).
5. Dudutiene, V. *et al.* Functionalization of Fluorinated Benzenesulfonamides and Their Inhibitory Properties Toward Carbonic Anhydrases. *ChemMedChem* **10**, 662–687 (2015).
6. Wichert, M. *et al.* Dual-Display of Small Molecules Enables the Discovery of Ligand Pairs and Facilitates Affinity Maturation. *Nat Chem* **7**, 241–249 (2015).
7. Pérez-López, A. M. *et al.* Bioorthogonal Uncaging of Cytotoxic Paclitaxel through Pd Nanosheet-Hydrogel Frameworks. *J Med Chem* **63**, 9650–9659 (2020).
8. Chen, Z. *et al.* Bioorthogonal Catalytic Patch. *Nat Nanotechnol* **16**, 933–941 (2021).
9. Sabatino, V. & Ward, T. R. Aqueous Olefin Metathesis: Recent Developments and Applications. *Beilstein J Org Chem* **15**, 445–468 (2019).
10. Toussaint, S. N. W., Calkins, R. T., Lee, S. & Michel, B. W. Olefin Metathesis-Based Fluorescent Probes for the Selective Detection of Ethylene in Live Cells. *J Am Chem Soc* **140**, 13151–13155 (2018).
11. Sabatino, V., Staub, D. & Ward, T. R. Synthesis of *N*-Substituted Indoles via Aqueous Ring-Closing Metathesis. *Catal Lett* **151**, 1–7 (2021).
12. Sabatino, V., Rebelein, J. G. & Ward, T. R. ‘Close-to-Release’: Spontaneous Bioorthogonal Uncaging Resulting from Ring-Closing Metathesis. *J Am Chem Soc* **141**, 17048–17052 (2019).
13. Van Otterlo, W. A. L. & de Koning, C. B. Metathesis in the Synthesis of Aromatic Compounds. *Chem Rev* **109**, 3743–3782 (2009).
14. Lozhkin, B. & Ward, T. R. A Close-to-Aromatize Approach for the Late-Stage Functionalization through Ring Closing Metathesis. *Helv Chim Acta* **104**, e2100024 (2021).
15. World Health Organization Model List of Essential Medicines. (2021). <https://www.who.int/publications/i/item/WHO-MHP-HPS-EML-2021.02>
16. William, A. D. & Lee, A. C. H. Acid Mediated Ring Closing Metathesis: A Powerful Synthetic Tool Enabling the Synthesis of Clinical Stage Kinase Inhibitors. *Chimia (Aarau)* **69**, 142–145 (2015).
17. Hartwig, J., Shu, C., Ohmura, T., Kiener, C. & Lopez, F. G. Enantioselective Amination and Etherification. *WO2004024684A2* (2004).
18. Brancatelli, G. *et al.* Basicity and Bulkiness Effects of 1,8-Diaminonaphthalene, 8-Aminoquinoline and Their Alkylated Derivatives on the Different Efficiencies of $\eta^5\text{-C}_5\text{H}_5$ and $\eta^5\text{-C}_5\text{Me}_5$ Ruthenium Precatalysts in Allylic Etherification Reactions. *New J Chem* **34**, 2853–2860 (2010).

19. Siddappa, R. K. G., Chang, C. W. & Chein, R. J. From Precursor to Catalyst: The Involvement of $[\text{Ru}(\eta^5\text{-Cp}^*)\text{Cl}_2]_2$ in Highly Branch Selective Allylic Etherification of Cinnamyl Chlorides. *Tetrahedron Lett* **55**, 1031–1035 (2014).
20. Egger, L. *et al.* Regio- and Enantioselective Allylation of Phenols via Decarboxylative Allylic Etherification of Allyl Aryl Carbonates Catalyzed by (Cyclopentadienyl)ruthenium(II) Complexes and Pyridine-Hydrazone Ligands. *Adv Synth Catal* **357**, 3325–3331 (2015).
21. Schmidt, R. *et al.* MINFLUX Nanometer-Scale 3D Imaging and Microsecond-Range Tracking on a Common Fluorescence Microscope. *Nat Commun* **12**, 1478–1489 (2021).
22. Reuter, R. & Ward, T. R. Profluorescent Substrates for the Screening of Olefin Metathesis Catalysts. *Beilstein J Org Chem* **11**, 1886–1892 (2015).
23. Fischer, C. & Sparr, C. Direct Transformation of Esters into Heterocyclic Fluorophores. *Angew Chem Int Ed* **57**, 2436–2440 (2018).
24. Amir, R. J., Pessah, N., Shamis, M. & Shabat, D. Self-Immolative Dendrimers. *Angew Chem Int Ed* **42**, 4494–4499 (2003).
25. Sagi, A., Segal, E., Satchi-Fainaro, R. & Shabat, D. Remarkable Drug-Release Enhancement with an Elimination-Based AB_3 Self-Immolative Dendritic Amplifier. *Bioorg Med Chem* **15**, 3720–3727 (2007).
26. Sato, R. *et al.* Intracellular Protein-Labeling Probes for Multicolor Single-Molecule Imaging of Immune Receptor-Adaptor Molecular Dynamics. *J Am Chem Soc* **139**, 17397–17404 (2017).
27. Scholl, M., Ding, S., Lee, C. W. & Grubbs, R. H. Synthesis and Activity of a New Generation of Ruthenium-Based Olefin Metathesis Catalysts Coordinated with 1,3-Dimesityl-4,5-dihydroimidazol-2-ylidene Ligands. *Org Lett* **1**, 953–956 (1999).
28. Schwizer, F. *et al.* Artificial Metalloenzymes: Reaction Scope and Optimization Strategies. *Chem Rev* **118**, 142–231 (2018).
29. Davis, H. J. & Ward, T. R. Artificial Metalloenzymes: Challenges and Opportunities. *ACS Cent Sci* **5**, 1120–1136 (2019).
30. Yamamura, K. & Kaiser, E.T. Studies on the Oxidase Activity of Copper(II) Carboxypeptidase A. *J. Chem. Soc., Chem. Commun* 830–831 (1976).
31. Wilson, M. E. & Whitesides, G. M. Conversion of a Protein to a Homogeneous Asymmetric Hydrogenation Catalyst by Site-Specific Modification with a Diphosphinerhodium(I) Moiety. *J Am Chem Soc* **100**, 306–307 (1978).
32. Jeong, W. J., Yu, J. & Song, W. J. Proteins as Diverse, Efficient, and Evolvable Scaffolds for Artificial Metalloenzymes. *Chem Commun* **56**, 9586–9599 (2020).
33. Basler, S. *et al.* Efficient Lewis Acid Catalysis of an Abiological Reaction in a *De Novo* Protein Scaffold. *Nat Chem* **13**, 231–235 (2021).
34. Upp, D. M. *et al.* Engineering Dirhodium Artificial Metalloenzymes for Diazo Coupling Cascade Reactions. *Angew Chem Int Ed* **60**, 23672–23677 (2021).
35. Chordia, S., Narasimhan, S., Paioni, A. L., Baldus, M. & Roelfes, G. *In Vivo* Assembly of Artificial Metalloenzymes and Application in Whole-Cell Biocatalysis. *Angew Chem Int Ed* **60**, 5913–5920 (2021).

Literature References

36. Goldberg, N. W., Knight, A. M., Zhang, R. K. & Arnold, F. H. Nitrene Transfer Catalyzed by a Non-Heme Iron Enzyme and Enhanced by Non-Native Small-Molecule Ligands. *J Am Chem Soc* **141**, 19585–19588 (2019).
37. Hao, J. *et al.* Enantioselective Olefin Cyclopropanation with G-Quadruplex DNA-Based Biocatalysts. *ACS Catal* **10**, 6561–6567 (2020).
38. Jiang, L. *et al.* *De Novo* Computational Design of Retro-Aldol Enzymes. *Science* **319**, 1387–1391 (2008).
39. Jumper, J. *et al.* Highly Accurate Protein Structure Prediction with AlphaFold. *Nature* **596**, 583–589 (2021).
40. Cao, L. *et al.* Design of Protein-Binding Proteins from the Target Structure Alone. *Nature* **605**, 551–560 (2022).
41. Case, J. B. *et al.* Ultrapotent Miniproteins Targeting the SARS-CoV-2 Receptor-Binding Domain Protect Against Infection and Disease. *Cell Host Microbe* **29**, 1151–1161 (2021).
42. Lovelock, S. L. *et al.* The Road to Fully Programmable Protein Catalysis. *Nature* **606**, 49–58 (2022).
43. Richter, F. *et al.* Computational Design of Catalytic Dyads and Oxyanion Holes for Ester Hydrolysis. *J Am Chem Soc* **134**, 16197–16206 (2012).
44. Studer, S. *et al.* Evolution of a Highly Active and Enantiospecific Metalloenzyme from Short Peptides. *Science* **362**, 1285–1288 (2022).
45. Preiswerk, N. *et al.* Impact of Scaffold Rigidity on the Design and Evolution of an Artificial Diels-Alderase. *PNAS* **111**, 8013–8018 (2014).
46. Obexer, R. *et al.* Emergence of a Catalytic Tetrad during Evolution of a Highly Active Artificial Aldolase. *Nat Chem* **9**, 50–56 (2017).
47. Salgado, E. N. *et al.* Metal Templated Design of Protein Interfaces. *PNAS* **107**, 1827–1832 (2010).
48. Churchfield, L. A., Medina-Morales, A., Brodin, J. D., Perez, A. & Tezcan, F. A. *De Novo* Design of an Allosteric Metalloprotein Assembly with Strained Disulfide Bonds. *J Am Chem Soc* **138**, 13163–13166 (2016).
49. Song, W. J. & Tezcan, F. A. A Designed Supramolecular Protein Assembly with *In Vivo* Enzymatic Activity. *Science* **346**, 1525–1528 (2014).
50. Chino, M. *et al.* A *De Novo* Heterodimeric Duet Ferri Protein Minimizes the Release of Reactive Intermediates in Dioxygen-Dependent Oxidation. *Angew Chem Int Ed* **129**, 15580–15583 (2017).
51. Brunette, T. J. *et al.* Exploring the Repeat Protein Universe Through Computational Protein Design. *Nature* **528**, 580–584 (2015).
52. Doyle, L. *et al.* Rational Design of α -Helical Tandem Repeat Proteins with Closed Architectures. *Nature* **528**, 585–588 (2015).
53. Ax, A. *et al.* Cyclic Sulfamide HIV-1 Protease Inhibitors, with Sidechains Spanning From P2/P2' to P1/P1'. *Bioorg Med Chem* **13**, 755–764 (2005).
54. Bock, M. *et al.* Cyclic Urea Derivatives as Androgen Receptor Antagonists. *WO2013084138A* (2013).

Literature References

55. Nyce, G. W., Csihony, S., Waymouth, R. M. & Hedrick, J. L. A General and Versatile Approach to Thermally Generated *N*-Heterocyclic Carbenes. *Chem Eur J* **10**, 4073–4079 (2004).
56. Denk, M. K., Gupta, S., Brownie, J., Tajammul, S. & Lough, A. J. C-H Activation with Elemental Sulfur: Synthesis of Cyclic Thioureas from Formaldehyde Aminals and S₈. *Chem Eur J* **7**, 4477–4486 (2001).
57. Salerno, A., Caterina, C. & Perillo, I. A. Synthesis of Substituted 1*H*-4,5-Dihydroimidazolium Salts by Dehydrogenation of Imidazolidines. *Synth Commun* **30**, 3369–3382 (2000).
58. Egert, M., Walther, S. & Plenio, H. Synthesis of Substituted Imidazolidines: Base-Stable Precursors of 4,5-Dihydro-1*H*-imidazol-3-ium Salts and *N*-Heterocyclic Carbenes. *Eur J Org Chem* **2014**, 4362–4369 (2014).
59. Jordan, J. P. & Grubbs, R. H. Small-Molecule *N*-Heterocyclic-Carbene-Containing Olefin-Metathesis Catalysts for Use in Water. *Angew Chem Int Ed* **46**, 5152–5155 (2007).
60. Xiong, T. M. *et al.* Enzyme-Like Catalysis by Single Chain Nanoparticles that Use Transition Metal Cofactors. *Chem Commun* **58**, 985–988 (2022).
61. Völker, T., Dempwolff, F., Graumann, P. L. & Meggers, E. Progress Towards Bioorthogonal Catalysis with Organometallic Compounds. *Angew Chem Int Ed* **53**, 10536–10540 (2014).
62. Dudutiene, V. *et al.* 4-Substituted-2,3,5,6-tetrafluorobenzenesulfonamides as Inhibitors of carbonic anhydrases I, II, VII, XII, and XIII. *Bioorg Med Chem* **21**, 2093–2106 (2013).
63. Krchová, T. *et al.* Lanthanide(III) Complexes of Aminoethyl-DO3A as PARACEST Contrast Agents Based on Decoordination of the Weakly Bound Amino Group. *Dalton Trans* **42**, 15735–15747 (2013).
64. Yeo, W. S., Min, D. H., Hsieh, R. W., Greene, G. L. & Mrksich, M. Label-Free Detection of Protein-Protein Interactions on Biochips. *Angew Chem Int Ed* **44**, 5480–5483 (2005).
65. Dudutiene, V. *et al.* Discovery and Characterization of Novel Selective Inhibitors of Carbonic Anhydrase IX. *J Med Chem* **57**, 9435–9446 (2014).
66. Bold, G. *et al.* New Anilinophthalazines as Potent and Orally Well Absorbed Inhibitors of the VEGF Receptor Tyrosine Kinases Useful as Antagonists of Tumor-Driven Angiogenesis. *J Med Chem* **43**, 2310–2323 (2000).
67. Weiss, J. T. *et al.* Development and Bioorthogonal Activation of Palladium-Labile Prodrugs of Gemcitabine. *J Med Chem* **57**, 5395–5404 (2014).
68. Singh, N. *et al.* Iridium-Triggered Allylcarbamate Uncaging in Living Cells. *Inorg Chem* **60**, 12644–12650 (2021).
69. William, A. D. *et al.* Discovery of the Macrocycle 11-(2-Pyrrolidin-1-yl-ethoxy)-14,19-dioxo-5,7,26-triaza-tetracyclo[19.3.1.1(2,6).1(8,12)]heptacos-1(25),2(26),3,5,8,10,12(27),16,21,23-decaene (SB1518), a Potent Janus Kinase 2/Fms-like Tyrosine Kinase-3 (JAK2/FLT3) Inhibitor for the Treatment of Myelofibrosis and Lymphoma. *J Med Chem* **54**, 4638–4658 (2011).
70. Dethe, D. H. & Boda, R. A Novel Pd-Catalysed Annulation Reaction for the Syntheses of Pyrroloindoles and Pyrroloquinolines. *Chem Eur J* **22**, 106–110 (2016).
71. Erez, R. & Shabat, D. The Azaquinone-Methide Elimination: Comparison Study of 1,6- and 1,4-Eliminations under Physiological Conditions. *Org Biomol Chem* **6**, 2669–2672 (2008).
72. Yang, Y. L. *et al.* Chemoselective Synthesis of Aryl Carboxamido Sulfonic Acid Derivatives. *Tetrahedron* **69**, 2640–2646 (2013).

73. Roth, A., Li, H., Anorma, C. & Chan, J. A Reaction-Based Fluorescent Probe for Imaging of Formaldehyde in Living Cells. *J Am Chem Soc* **137**, 10890–10893 (2015).
74. Zhou, X., Lai, R., Beck, J. R., Li, H. & Stains, C. I. Nebraska Red: A Phosphinate-Based Near-Infrared Fluorophore Scaffold for Chemical Biology Applications. *Chem Commun* **52**, 12290–12293 (2016).
75. Wei, L. *et al.* Super-Multiplex Vibrational Imaging. *Nature* **544**, 465–470 (2017).
76. Zhao, H. Y., Yang, X. Y., Lei, H., Xin, M. & Zhang, S. Q. Cu-Mediated Selective Bromination of Aniline Derivatives and Preliminary Mechanism Study. *Synth Commun* **49**, 1406–1415 (2019).
77. Takahashi, S. *et al.* Rational Design of a Near-infrared Fluorescence Probe for Ca²⁺ Based on Phosphorus-Substituted Rhodamines Utilizing Photoinduced Electron Transfer. *Chem Asian J* **15**, 524–530 (2020).
78. Fujioka, H. *et al.* Multicolor Activatable Raman Probes for Simultaneous Detection of Plural Enzyme Activities. *J Am Chem Soc* **142**, 20701–20707 (2020).
79. Hui, A., Zhang, J. & Wang, Z. Asymmetric Addition of Diethylzinc to Ketones Promoted by Tartaric Acid Derivatives. *Synth Commun* **38**, 2374–2384 (2008).
80. Clavé, G. *et al.* A Novel Heterotrifunctional Peptide-Based Cross-Linking Reagent for Facile Access to Bioconjugates. Applications to Peptide Fluorescent Labelling and Immobilisation. *Org Biomol Chem* **6**, 3065–3078 (2008).
81. Jordan, J. P. & Grubbs, R. H. Small-Molecule *N*-Heterocyclic-Carbene-Containing Olefin-Metathesis Catalysts for Use in Water. *Angew Chem Int Ed* **46**, 5152–5155 (2007).
82. Chen, S. W., Kim, J. H., Song, C. E. & Lee, S. G. Self-Supported Oligomeric Grubbs/Hoveyda-Type Ru-Carbene Complexes for Ring-Closing Metathesis. *Org Lett* **9**, 3845–3848 (2007).
83. Tangdenpaisal, K., Sualek, S., Ruchirawat, S. & Ploypradith, P. Factors Affecting Orthogonality in the Deprotection of 2,4-Di-Protected Aromatic Ethers Employing Solid-Supported Acids. *Tetrahedron* **65**, 4316–4325 (2009).
84. Do, J. H., Kim, H. N., Yoon, J., Kim, J. S. & Kim, H. J. A Rationally Designed Fluorescence Turn-On Probe for the Gold(III) Ion. *Org Lett* **12**, 932–934 (2010).
85. Zhu, X. *et al.* Permethylated NHC-Capped α - and β -Cyclodextrins (ICyDMe) Regioselective and Enantioselective Gold-Catalysis in Pure Water. *Chem Eur J* **26**, 15901–15909 (2020).

8. Reprint Permissions

Elsevier

The manuscript published in *Bioorganic & Medicinal Chemistry* (Open Access) was reproduced with permission from the Elsevier. A reprint of the manuscript can be found in chapter 1.2.

Bibliographic data of the publication:

Bioorthogonal strategies for the *in vivo* synthesis or release of drugs

Boris Lozhkin^a and Thomas R. Ward^{*a}

^a Department of Chemistry, University of Basel, BPR 1096, Mattenstrasse 24a, Biopark Rosental, 4058 Basel, Switzerland

*Corresponding Author: thomas.ward@unibas.ch

Originally published in *Bioorganic & medicinal chemistry* **2021**, 45, 116310.

DOI: 10.1016/j.bmc.2021.116310

URL: <https://www.sciencedirect.com/science/article/pii/S0968089621003187>

Wiley Online Library

The manuscript published in *Helvetica Chimica Acta* (Open Access) was reproduced with permission from the John Wiley and Sons. A reprint of the manuscript can be found in chapter 3.2.

Bibliographic data of the publication:

A Close-to-Aromatize Approach for the Late-Stage Functionalization through Ring Closing Metathesis

Boris Lozhkin^a and Thomas R. Ward^{*a}

^a Department of Chemistry, University of Basel, Building 1096, Mattenstrasse 24a, Biopark Rosental, CH-4058 Basel, Switzerland

*Corresponding Author: thomas.ward@unibas.ch

Originally published in *Helvetica Chimica Acta* **2021**, 104(5), e2100024.

DOI: 10.1002/hlca.202100024

URL: <https://onlinelibrary.wiley.com/doi/10.1002/hlca.202100024>

A1

Chemical structure: C=CCOC1=CC=C2C(=C1)C(=O)O=C2N

¹H NMR spectrum (CDCl₃) showing peaks and integration values:

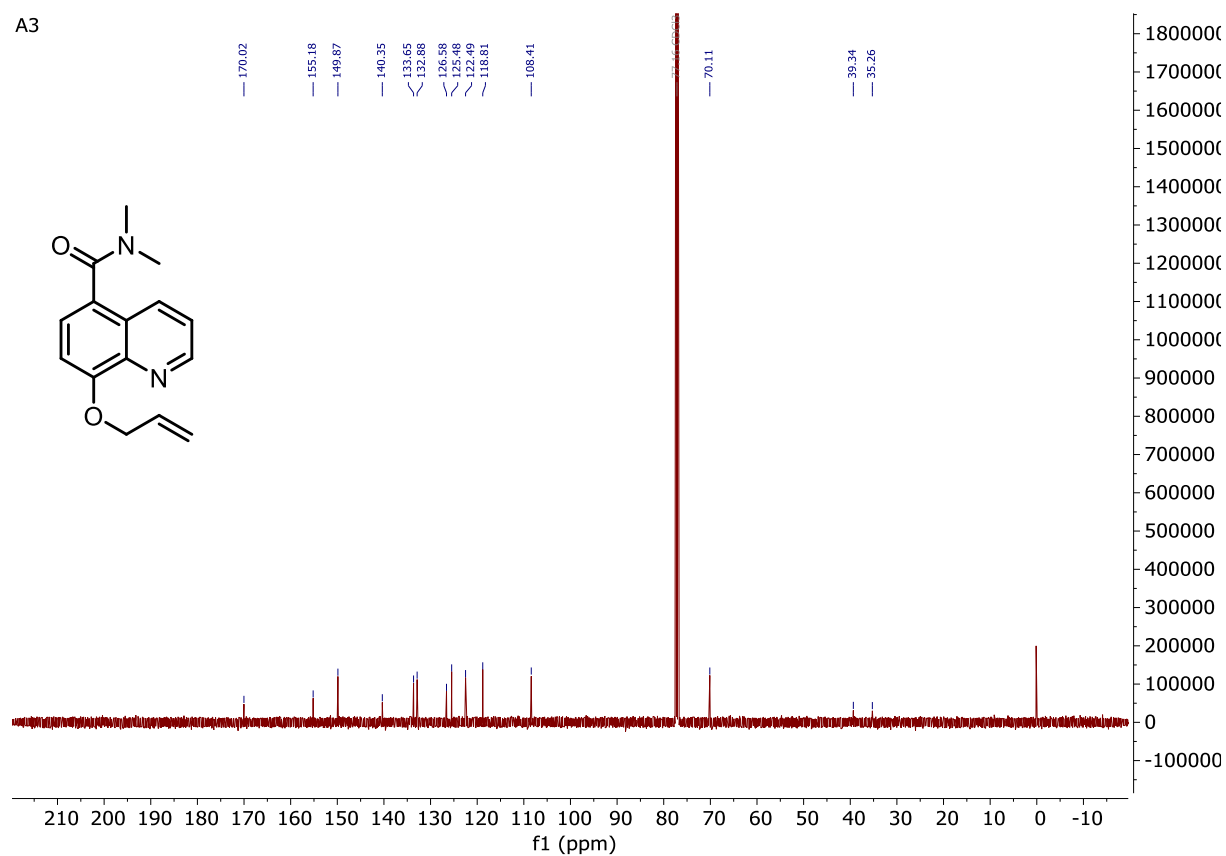
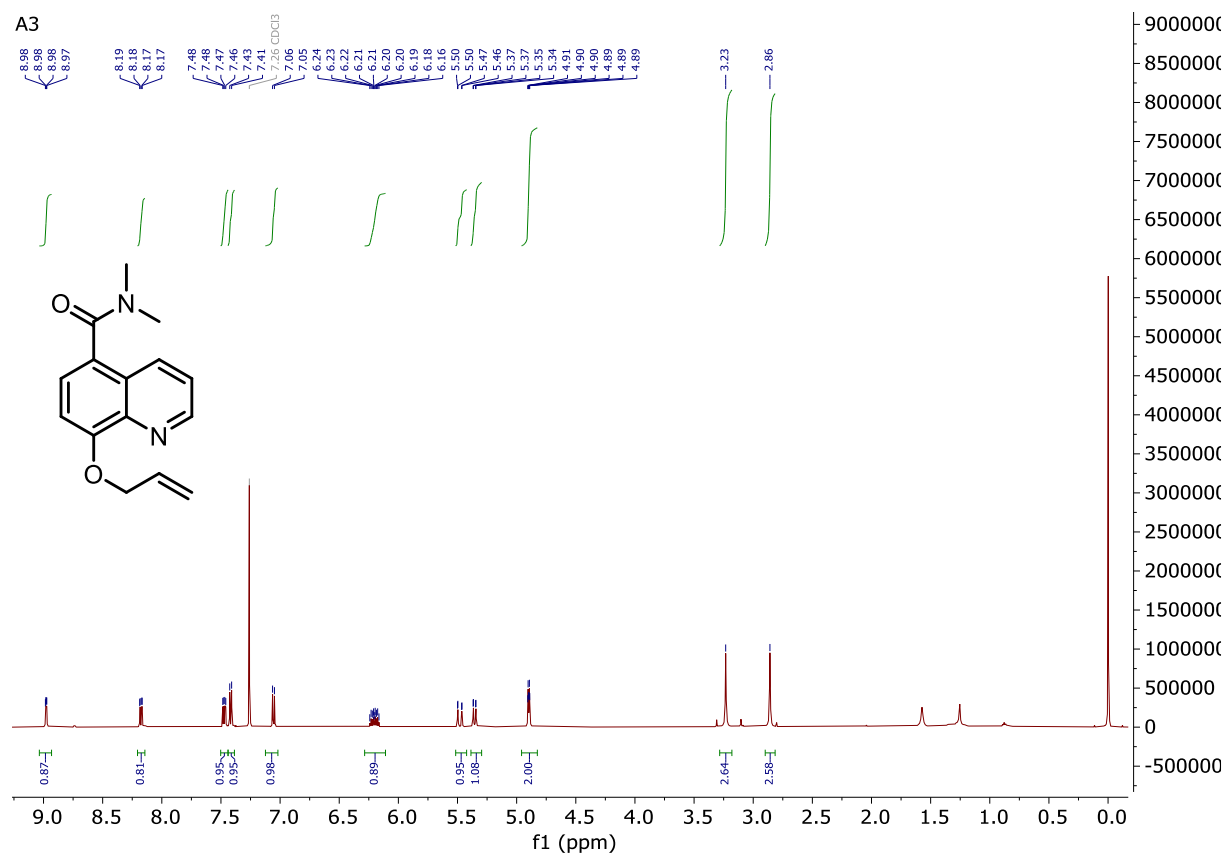
Chemical Shift (ppm)	Integration
9.24, 9.22, 9.05	1.00
8.52, 8.50	0.99
7.70, 7.69	0.99
7.76, 7.09, 7.08	1.00
6.22, 6.21, 6.20, 6.18, 6.17	1.00
5.54, 5.50, 5.43, 5.41	1.02, 1.02
4.99, 4.98	2.00

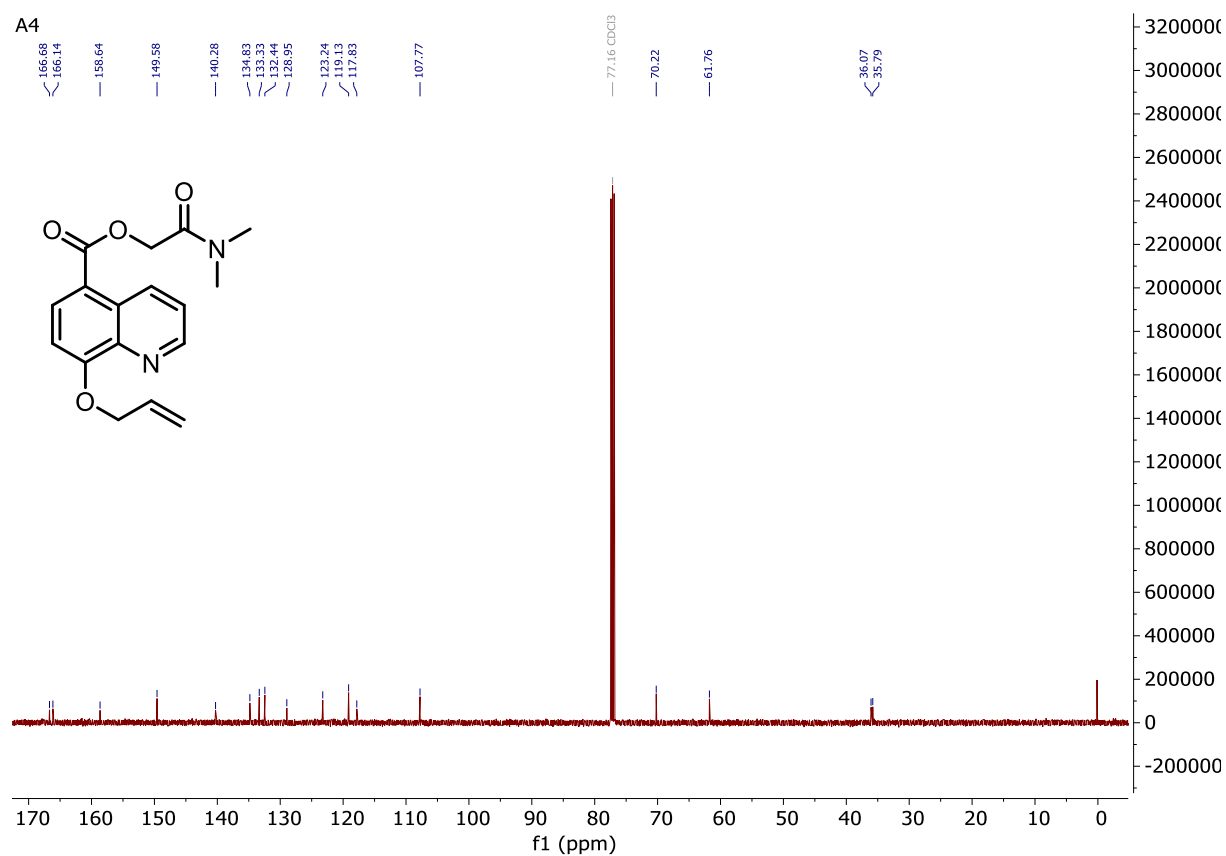
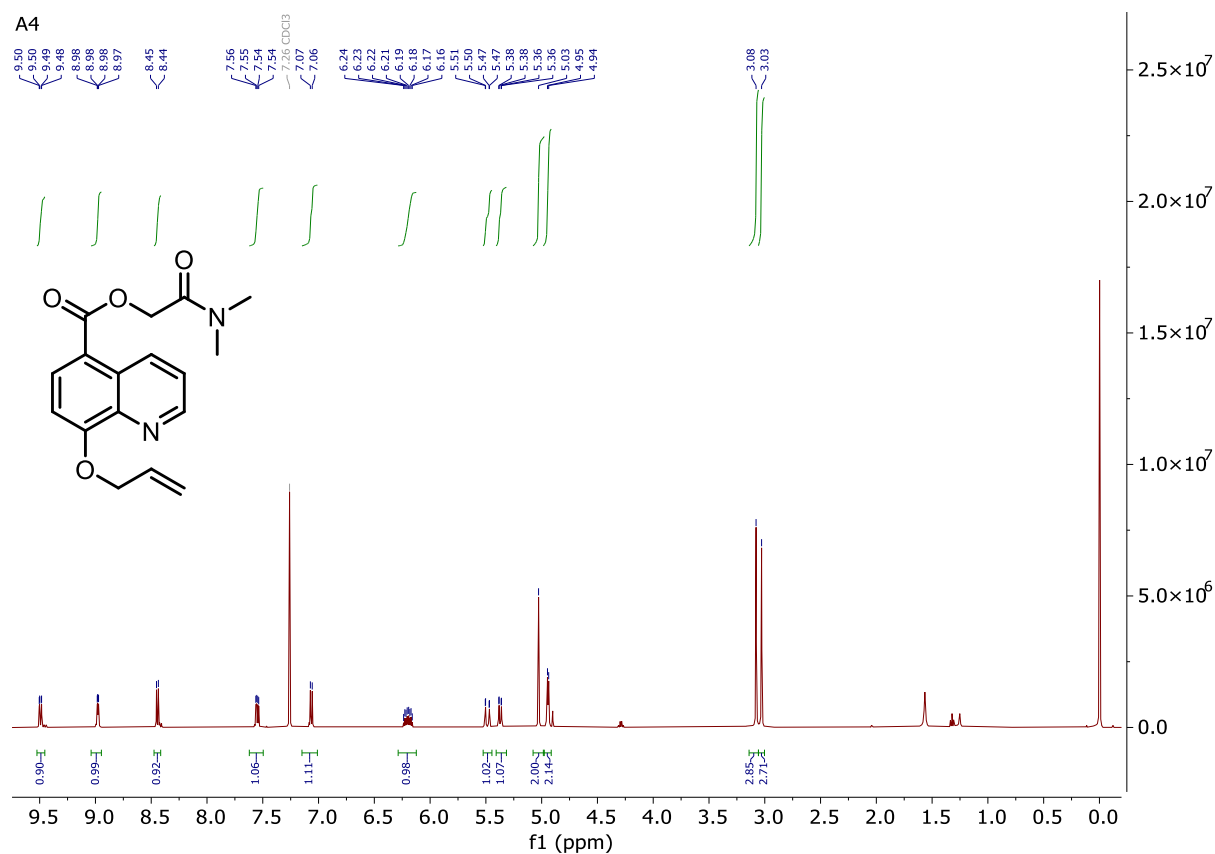
A2

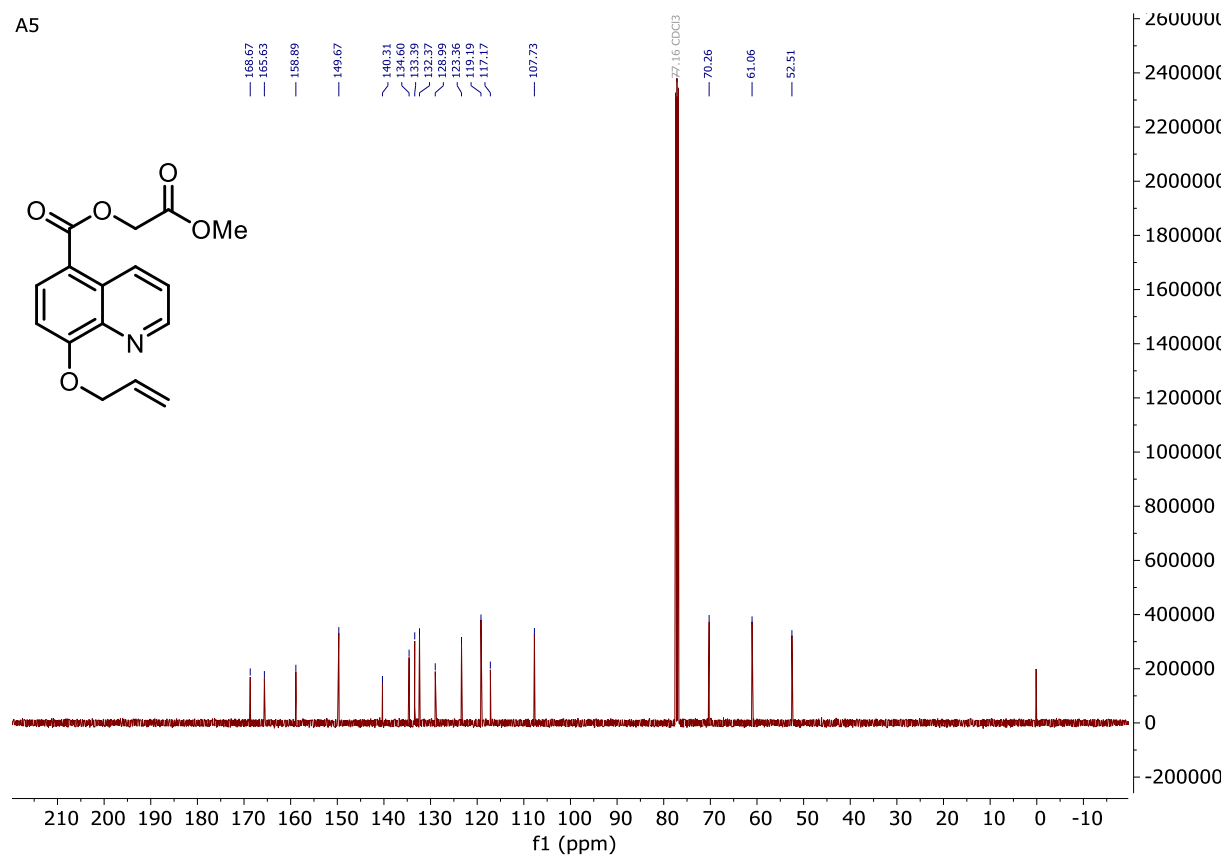
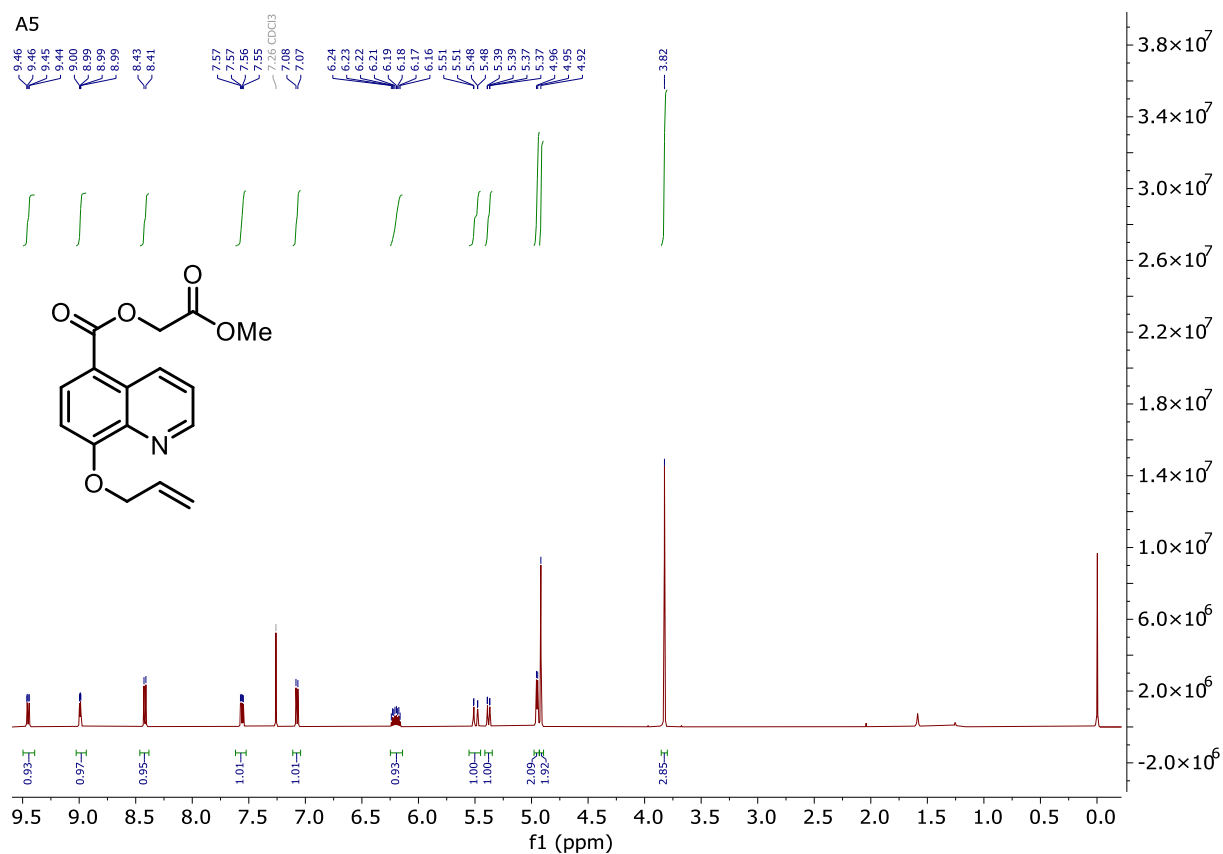
Chemical structure: COc1ccc2c(c1)ccc(OC/C=C/C)cn2

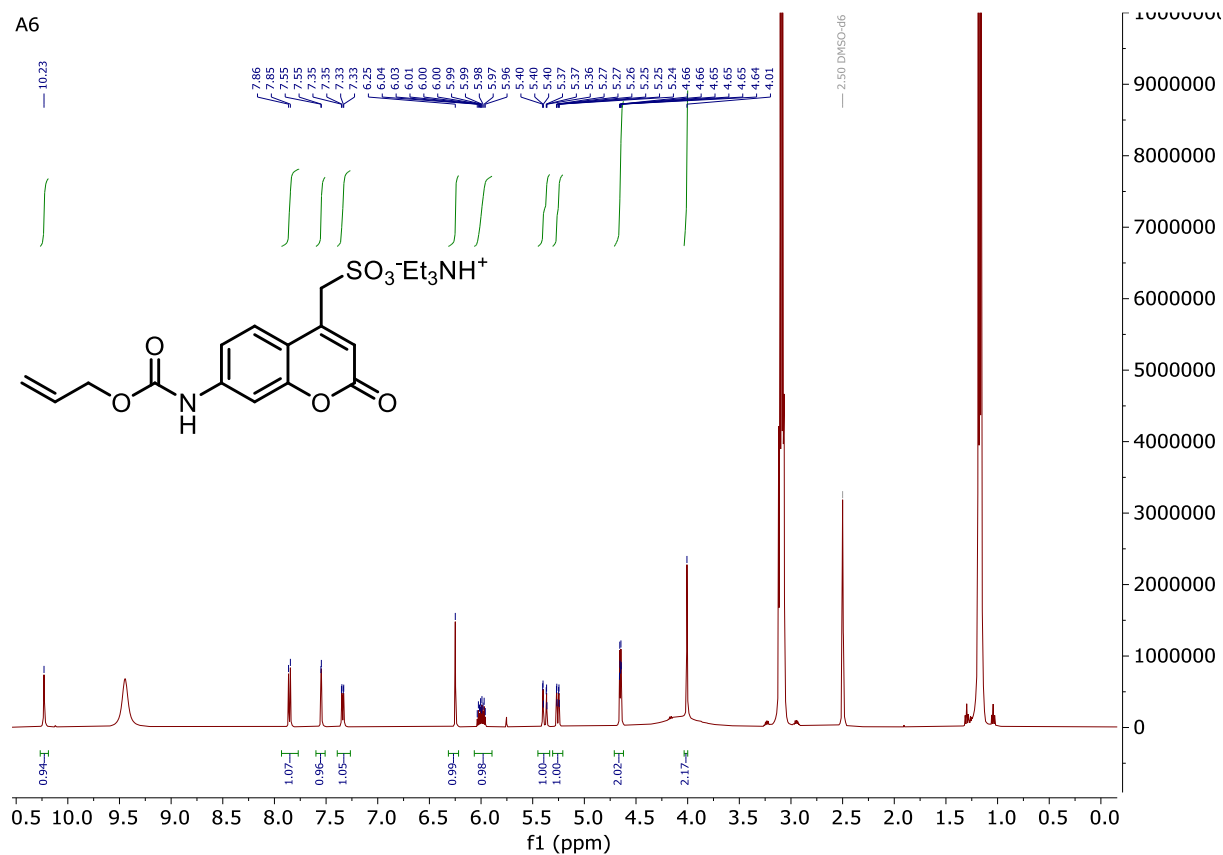
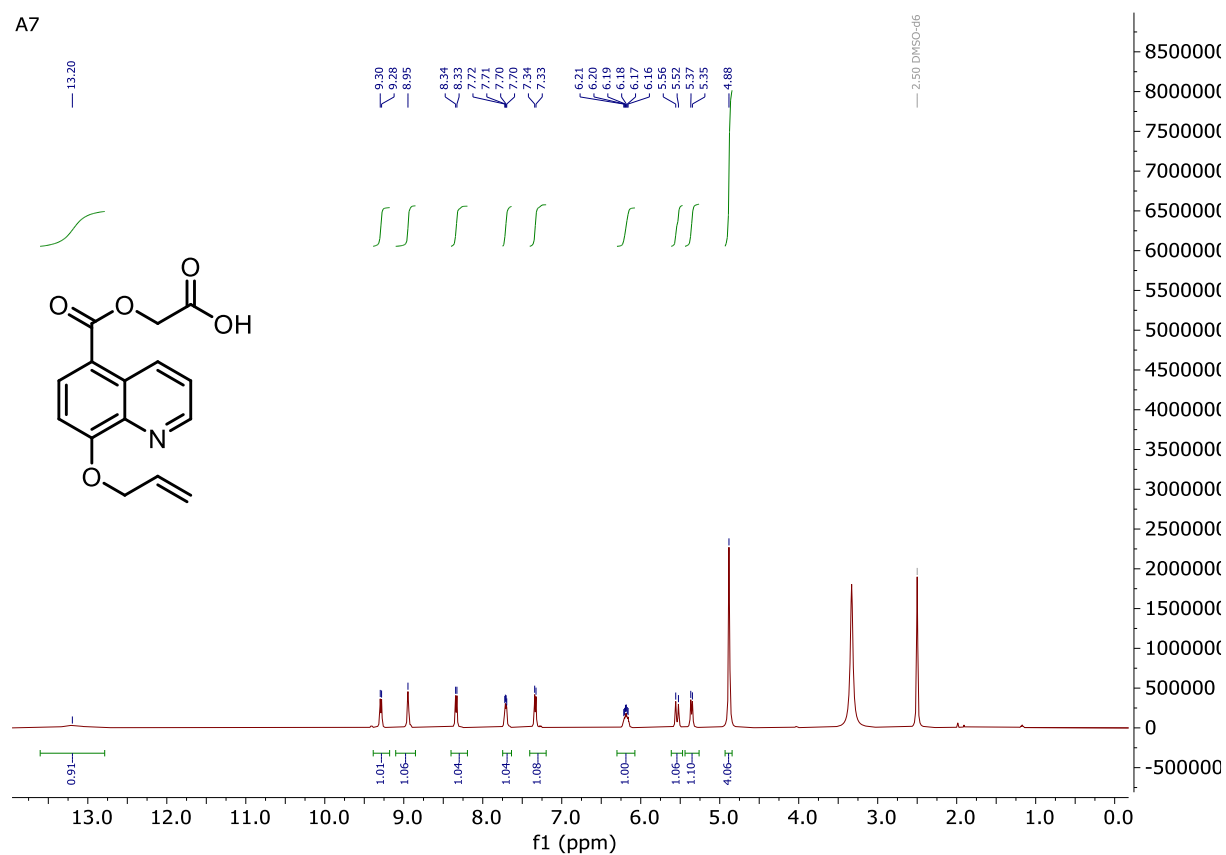
¹H NMR spectrum (CDCl₃) showing peaks and integration values:

Chemical Shift (ppm)	Integration
9.47, 9.46, 9.45, 8.99, 8.98	0.89
8.31, 8.30	0.90
7.57, 7.56, 7.55, 7.54	0.91
7.26 (CDCl ₃), 7.06, 7.05, 6.24, 6.22, 6.21, 6.20, 6.19, 6.17	0.96
5.51, 5.51, 5.51, 5.50, 5.48, 5.46, 5.47, 5.39, 5.38, 5.37, 5.36, 5.35, 4.95, 4.94, 4.93, 4.93	0.98
3.97	2.88

8-(Allyloxy)-N,N-dimethylquinoline-5-carboxamide (**A3**)

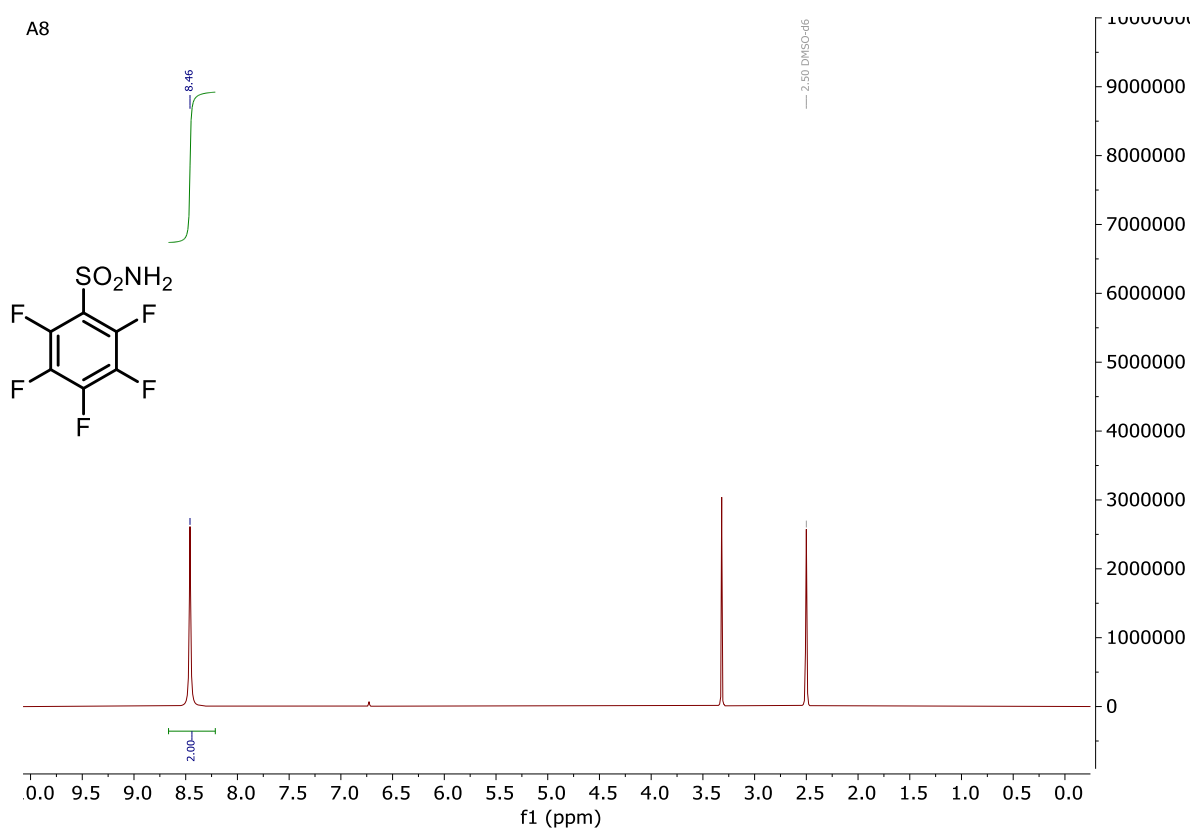
2-(Dimethylamino)-2-oxoethyl 8-(allyloxy)quinoline-5-carboxylate (**A4**)

2-Methoxy-2-oxoethyl 8-(allyloxy)quinoline-5-carboxylate (**A5**)

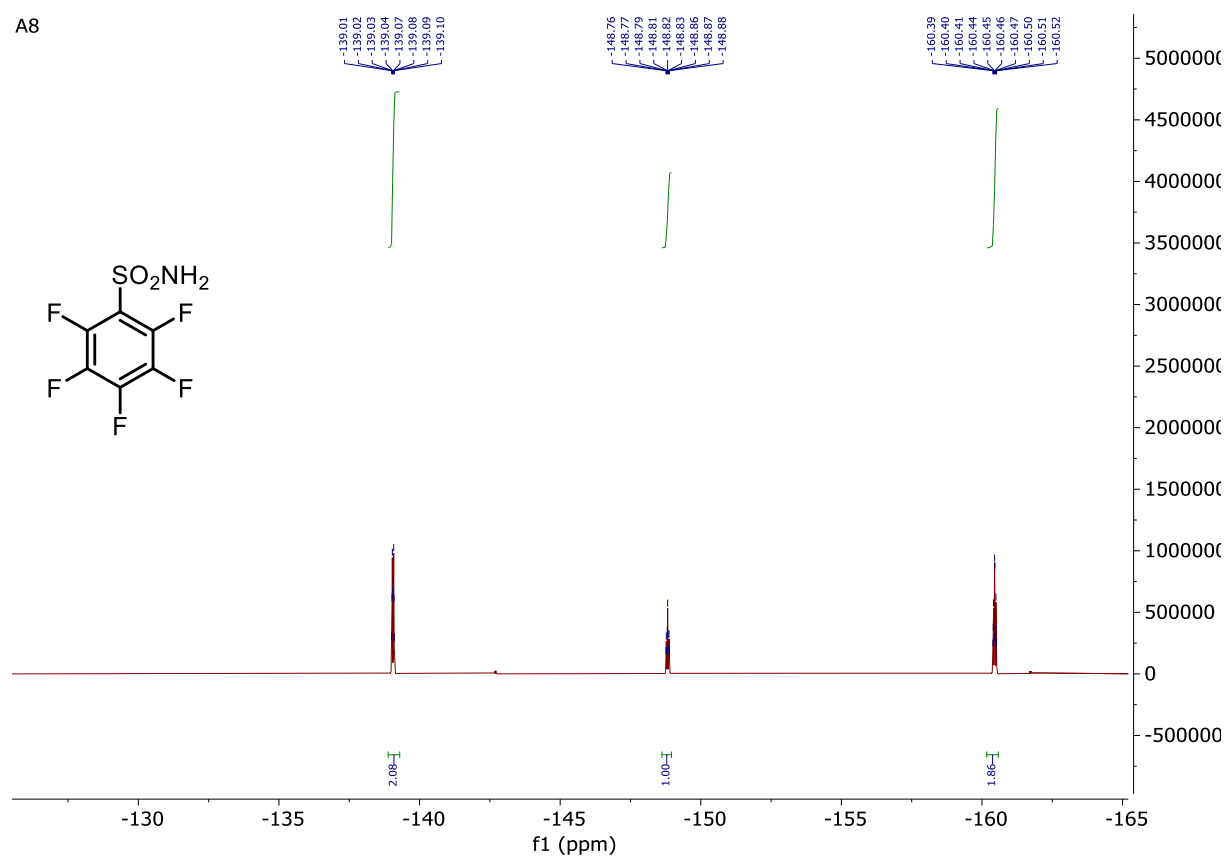
(7-(((Allyloxy)carbonyl)amino)-2-oxo-2*H*-chromen-4-yl)methanesulfonic acid triethylammonium salt (**A6**)2-((8-(Allyloxy)quinoline-5-carbonyl)oxy)acetic acid (**A7**)

2,3,4,5,6-Pentafluorobenzenesulfonamide (**A8**)

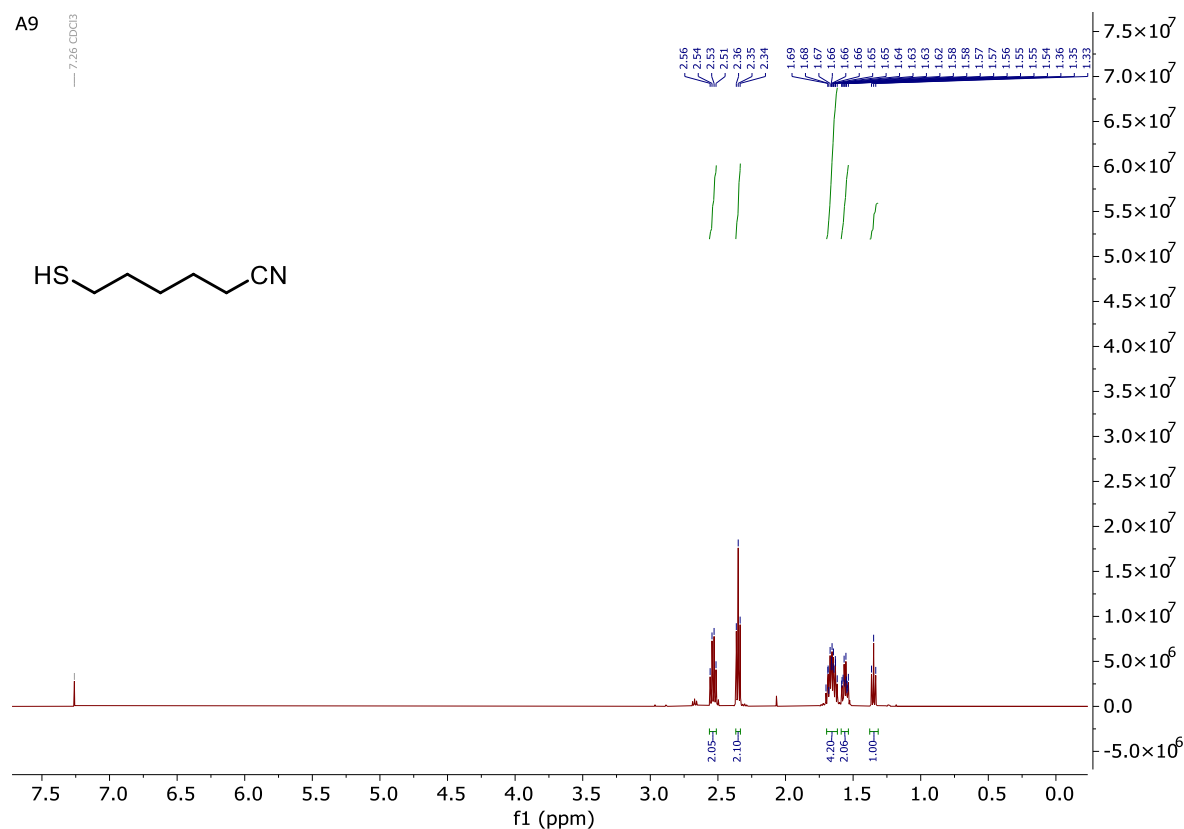
A8



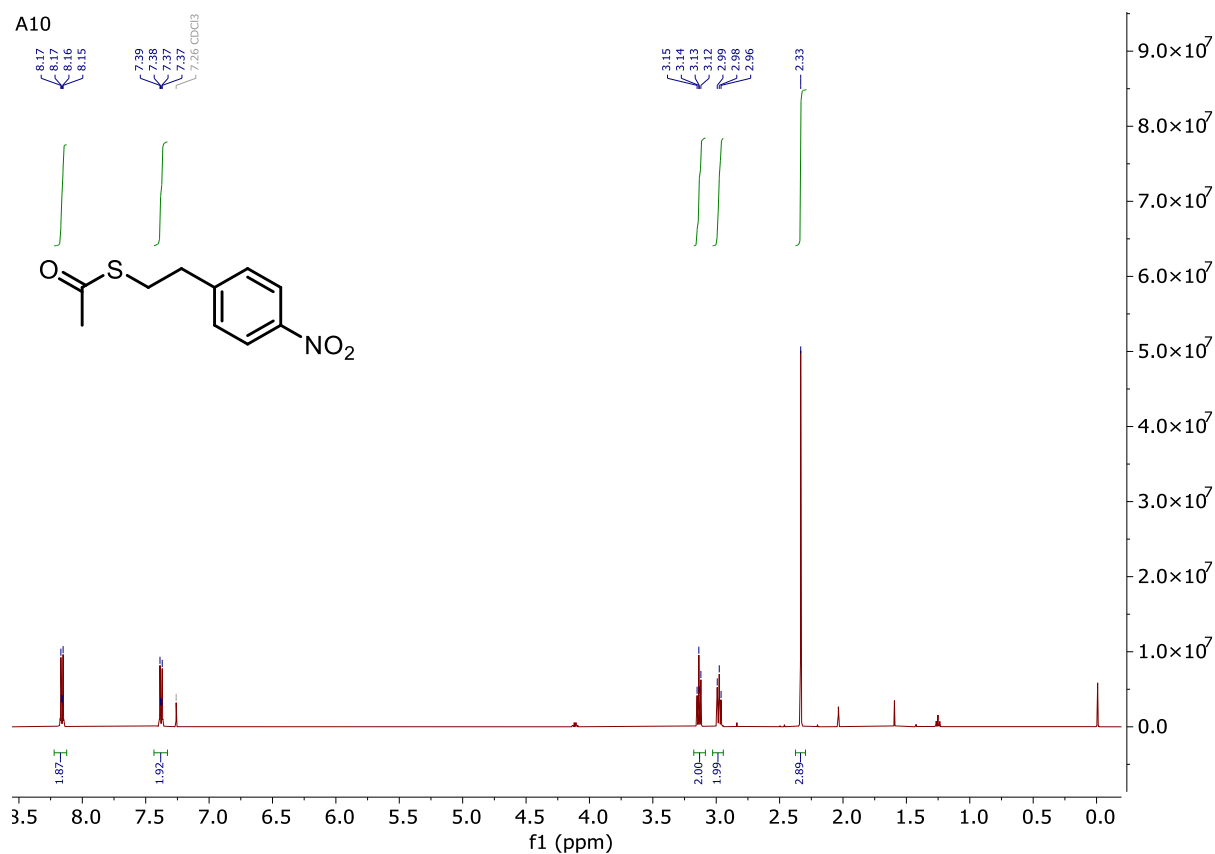
A8



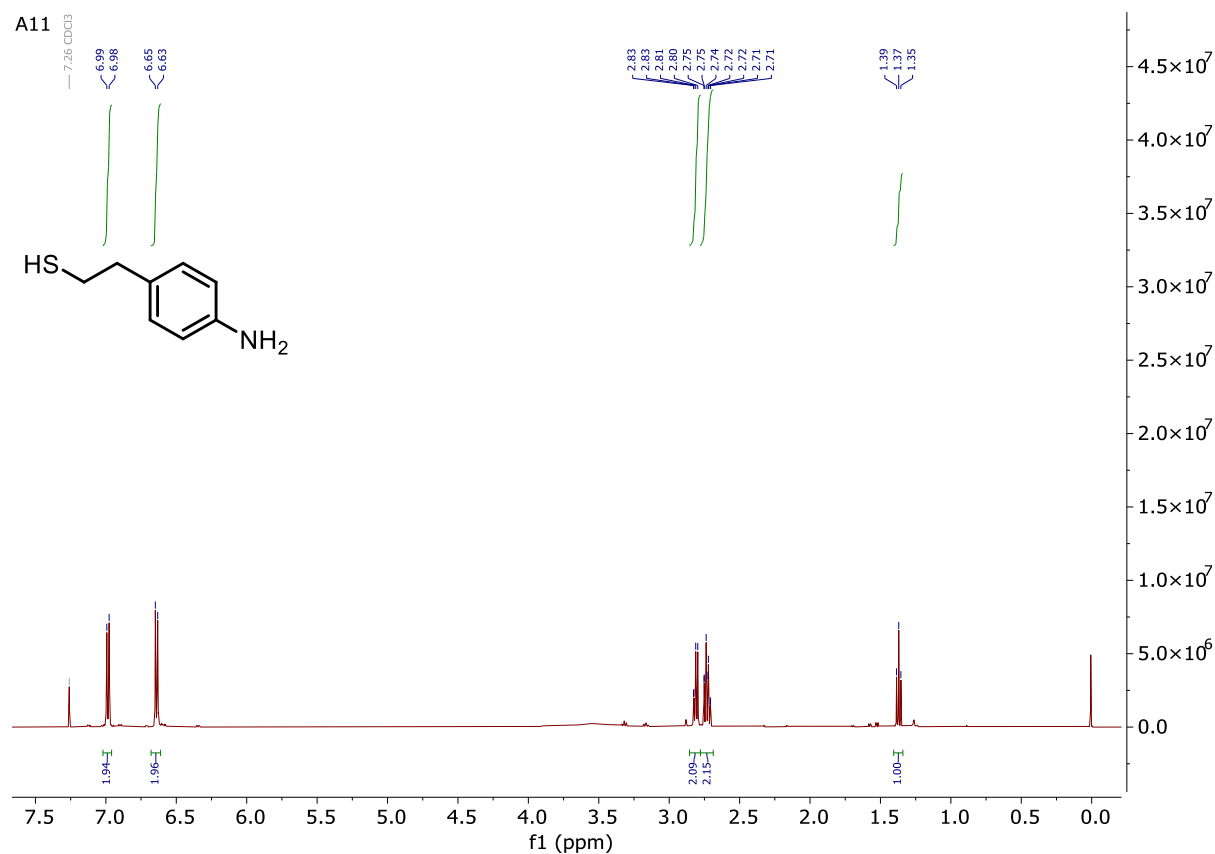
6-Mercaptohexanenitrile (A9)



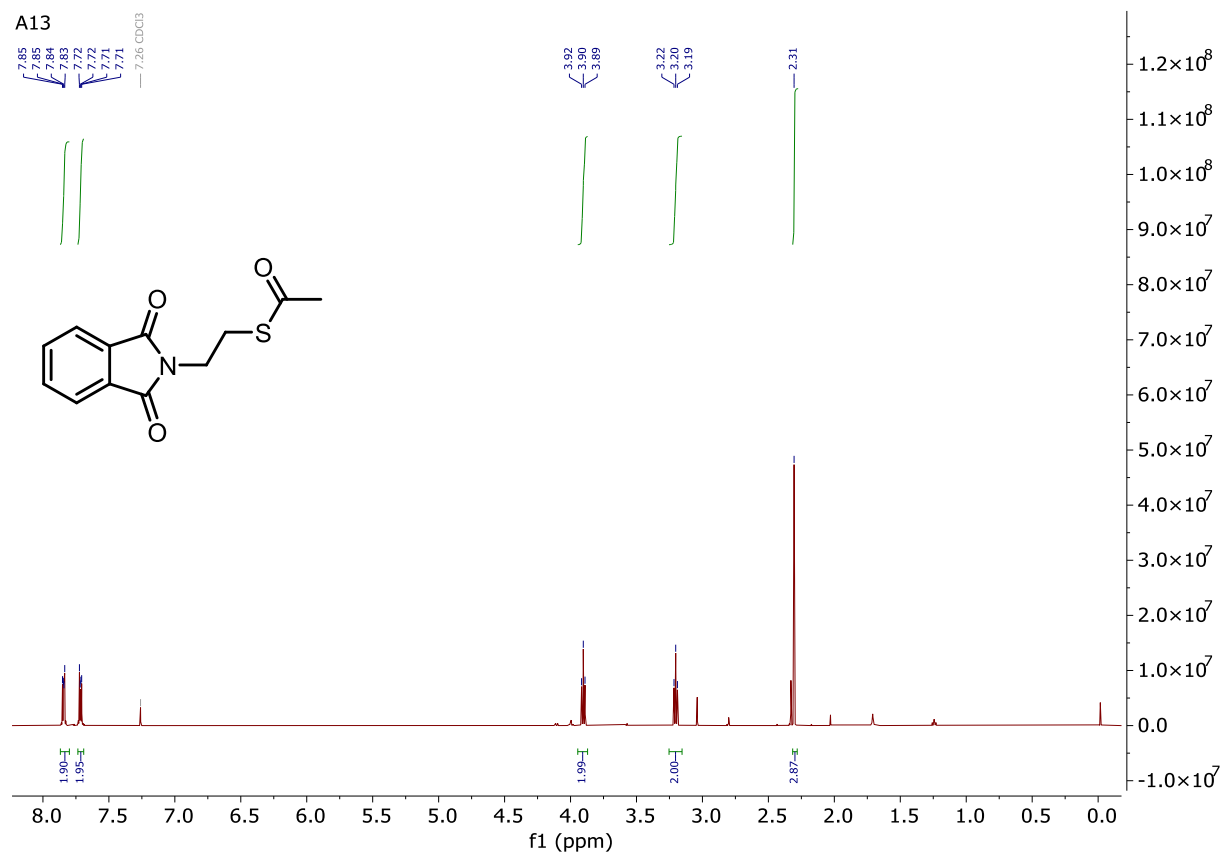
S-(4-Nitrophenethyl) ethanethioate (A10)

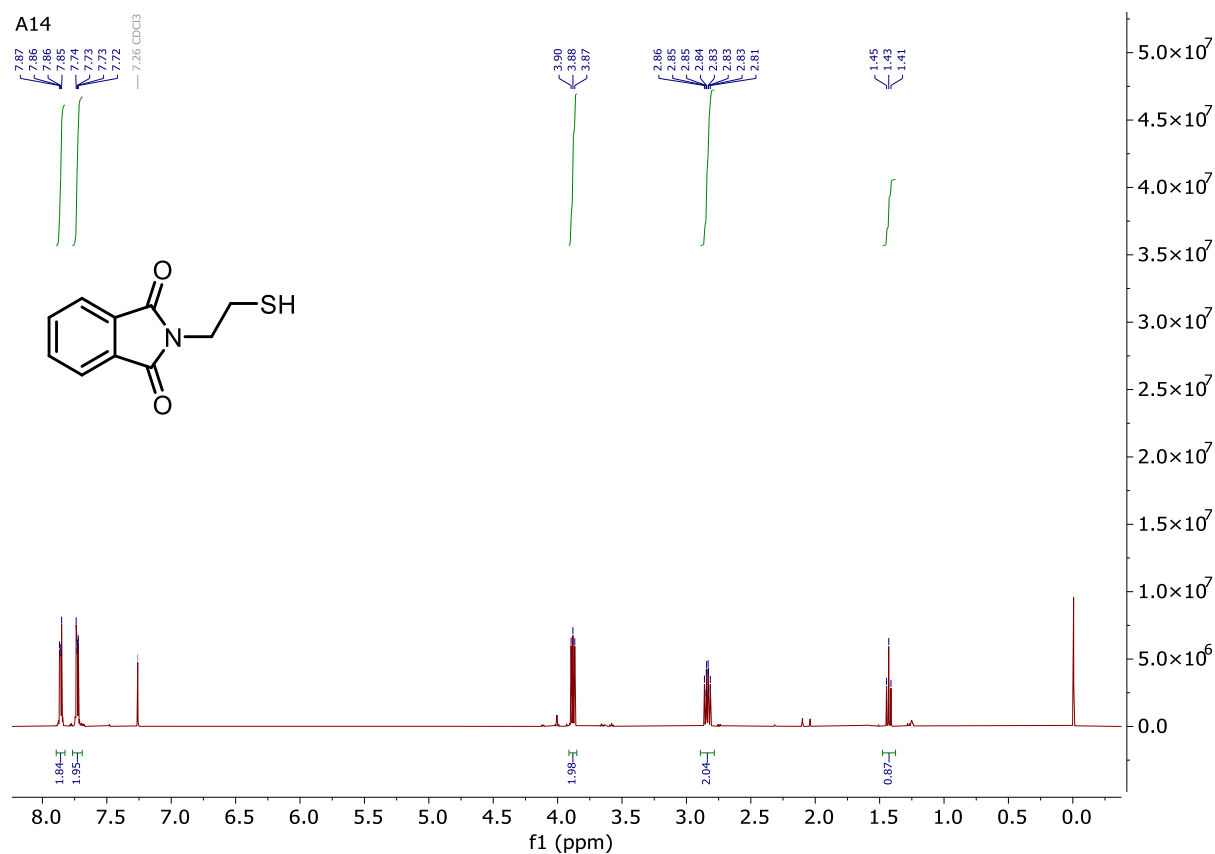
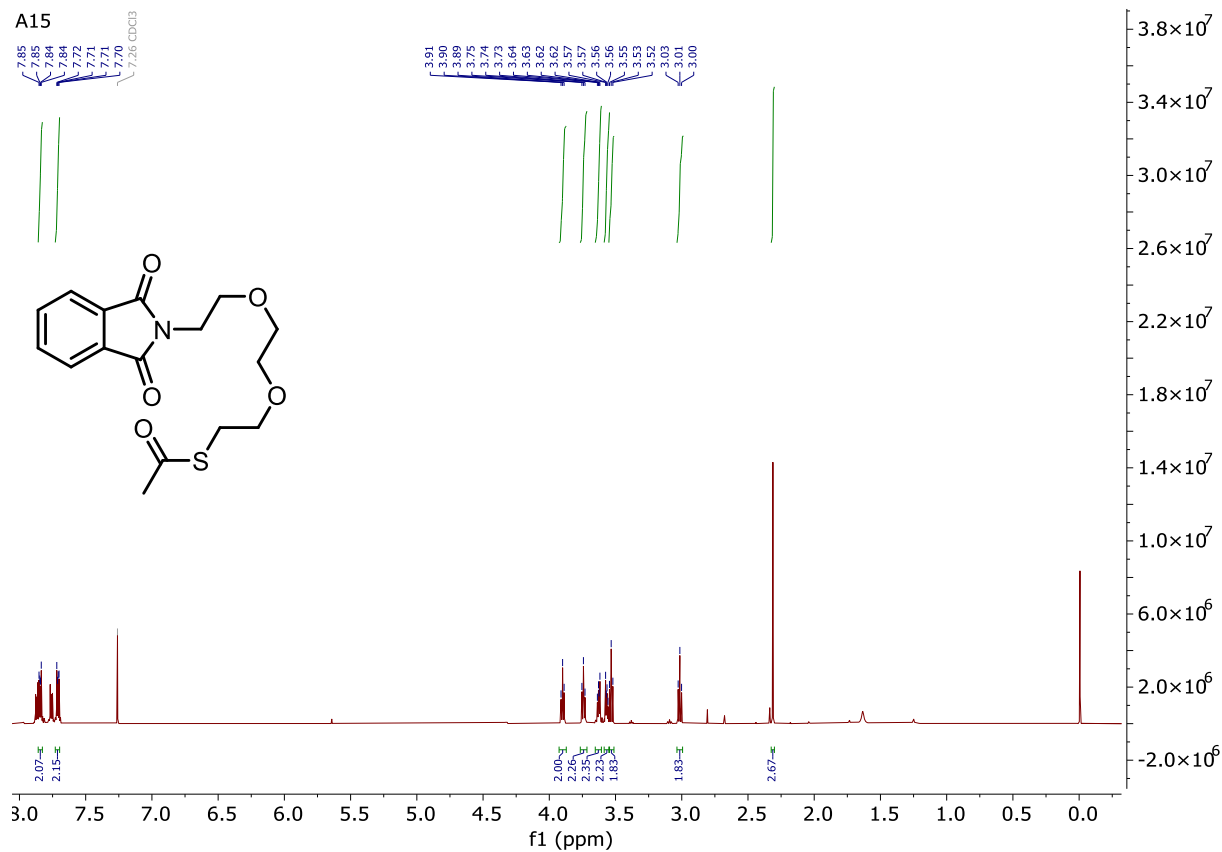


2-(4-Aminophenyl)ethane-1-thiol (**A11**)

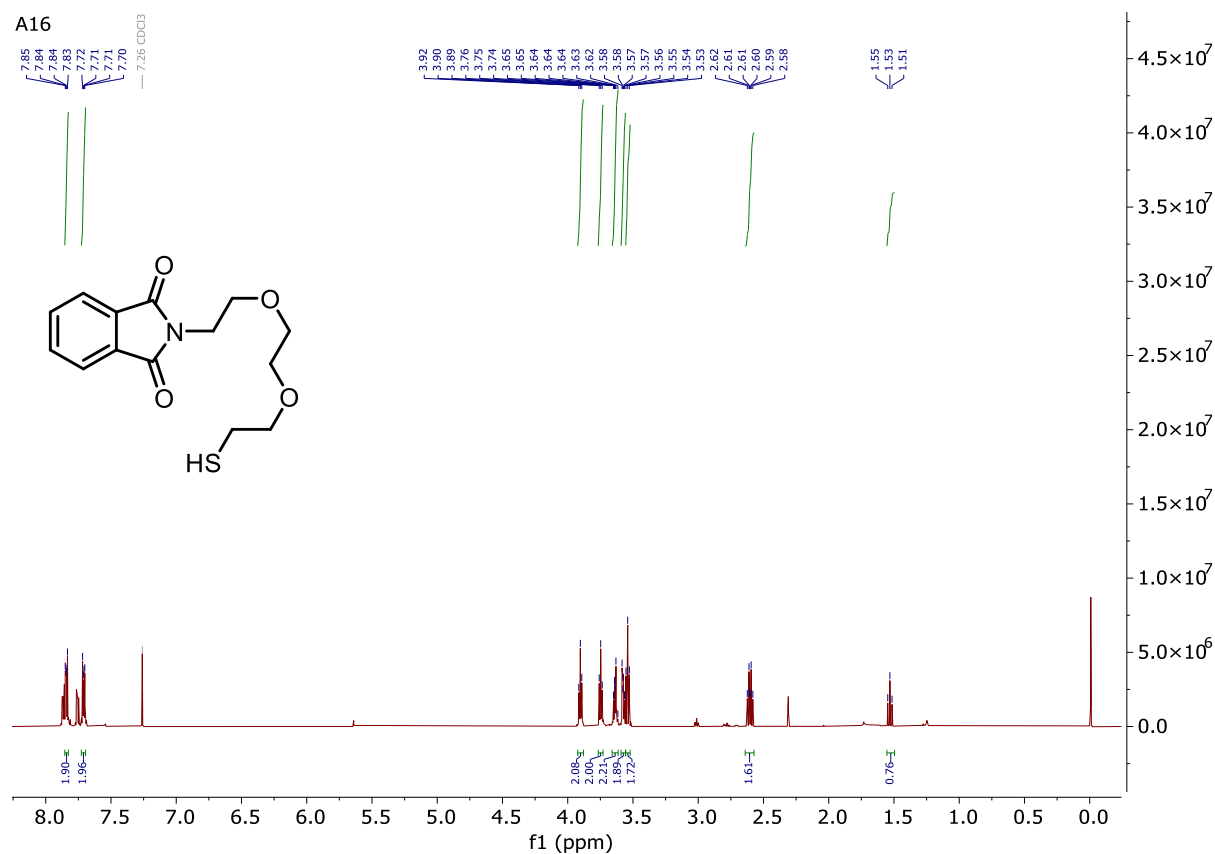


S-(2-(1,3-Dioxisoindolin-2-yl)ethyl) ethanethioate (**A13**)

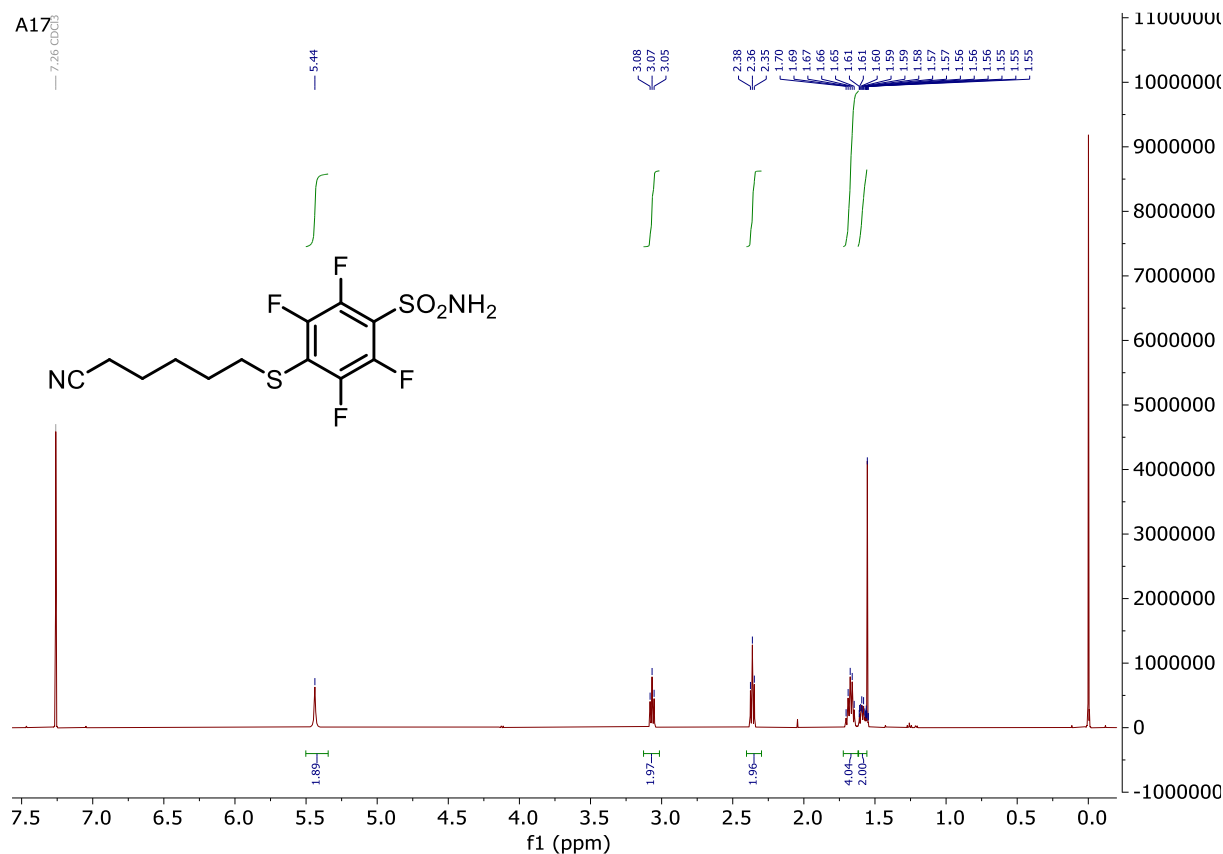


2-(2-Mercaptoethyl)isoindoline-1,3-dione (**A14**)S-(2-(2-(2-(1,3-Dioxoisindolin-2-yl)ethoxy)ethoxy)ethyl) ethanethioate (**A15**)

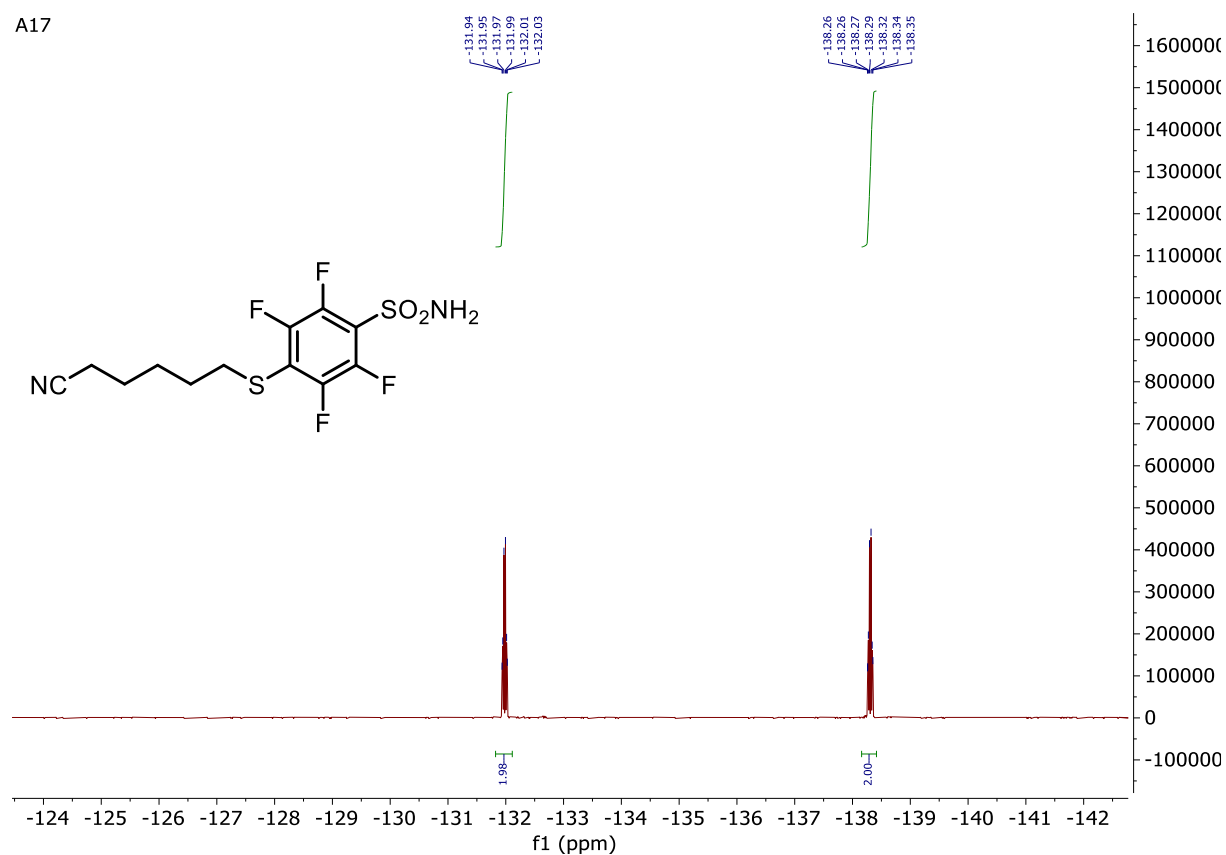
2-(2-(2-(2-Mercaptoethoxy)ethoxy)ethyl)isoindoline-1,3-dione (**A16**)



4-((5-Cyanopentyl)thio)-2,3,5,6-tetrafluorobenzenesulfonamide (**A17**)

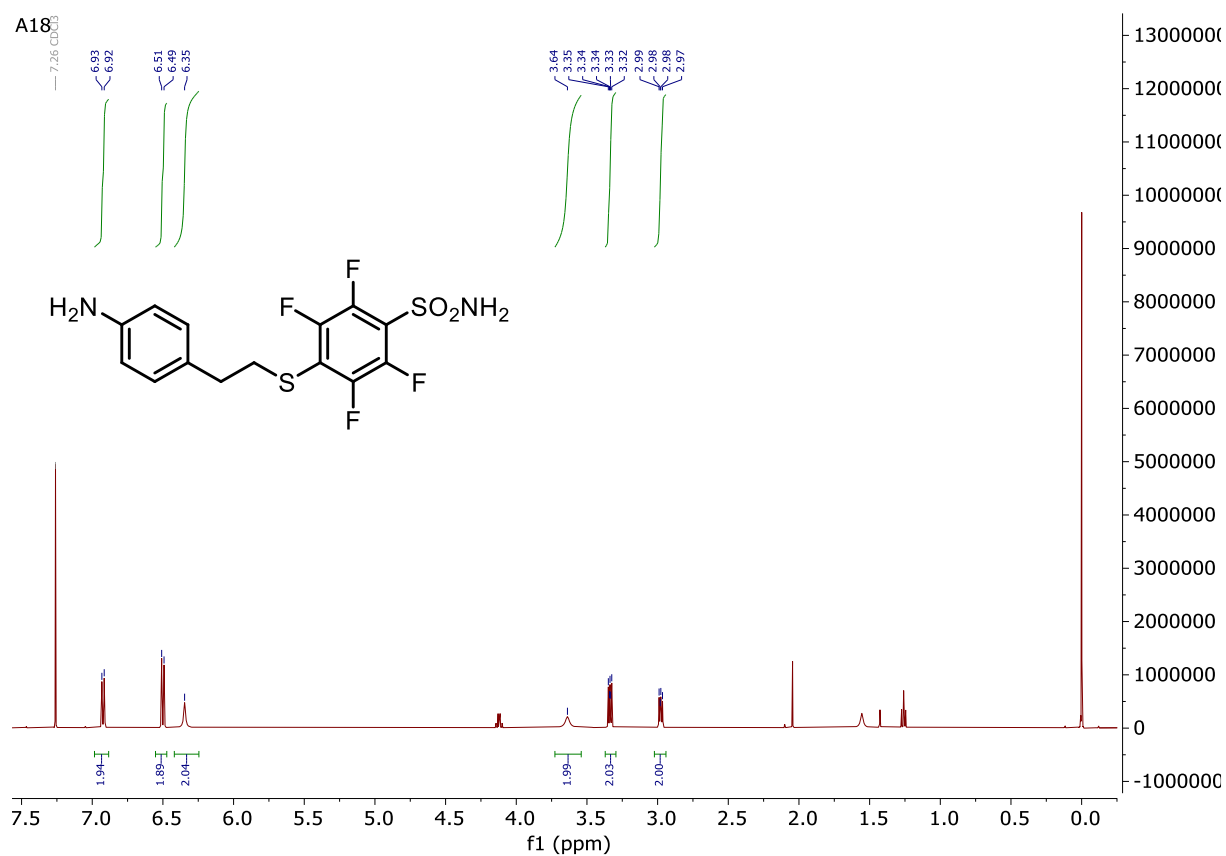


A17

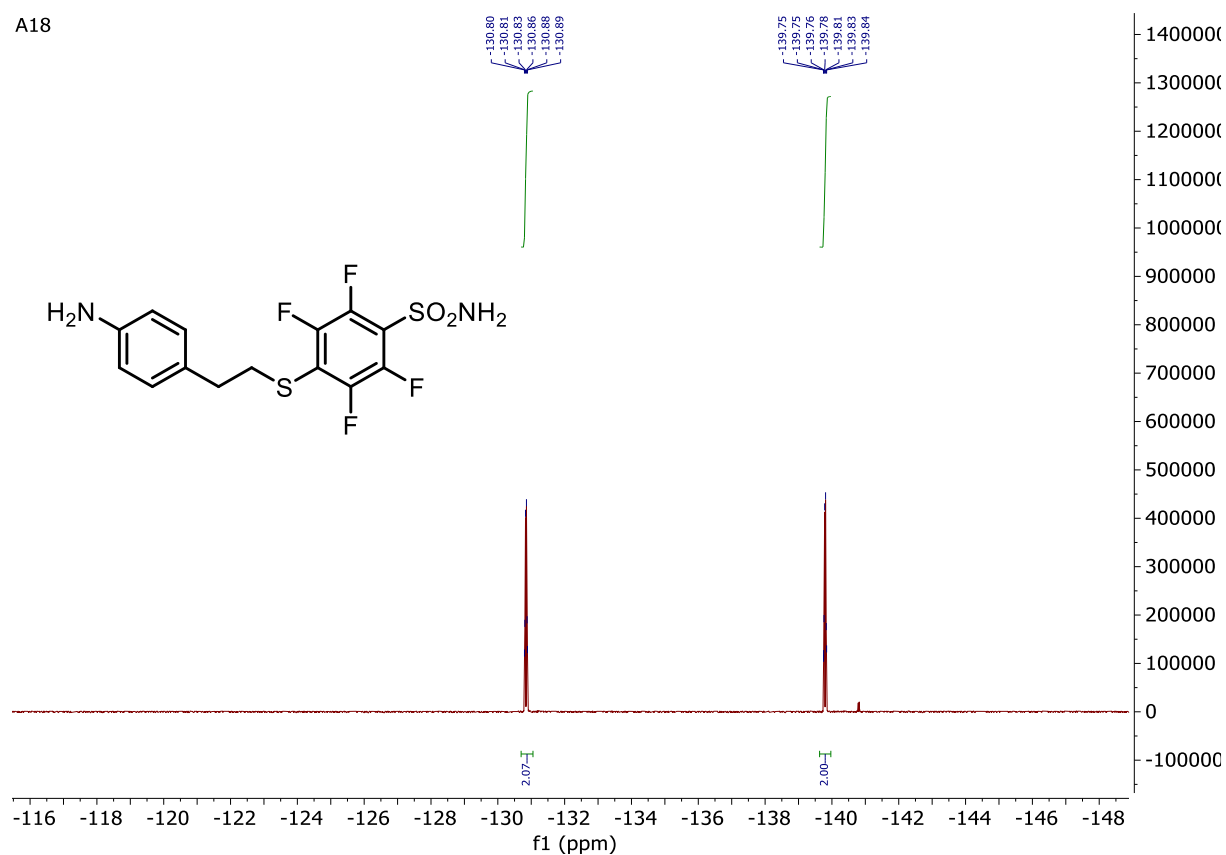


4-((4-Aminophenethyl)thio)-2,3,5,6-tetrafluorobenzenesulfonamide (A18)

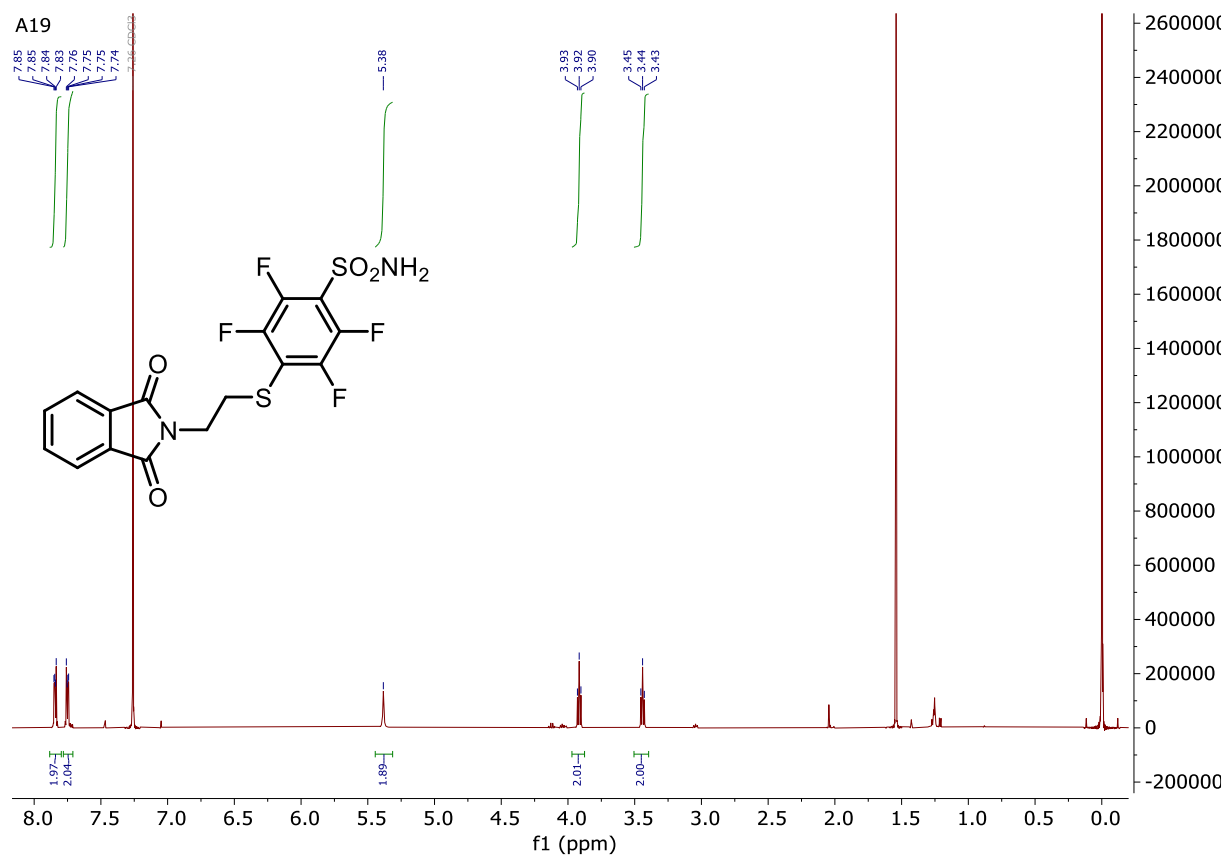
A18



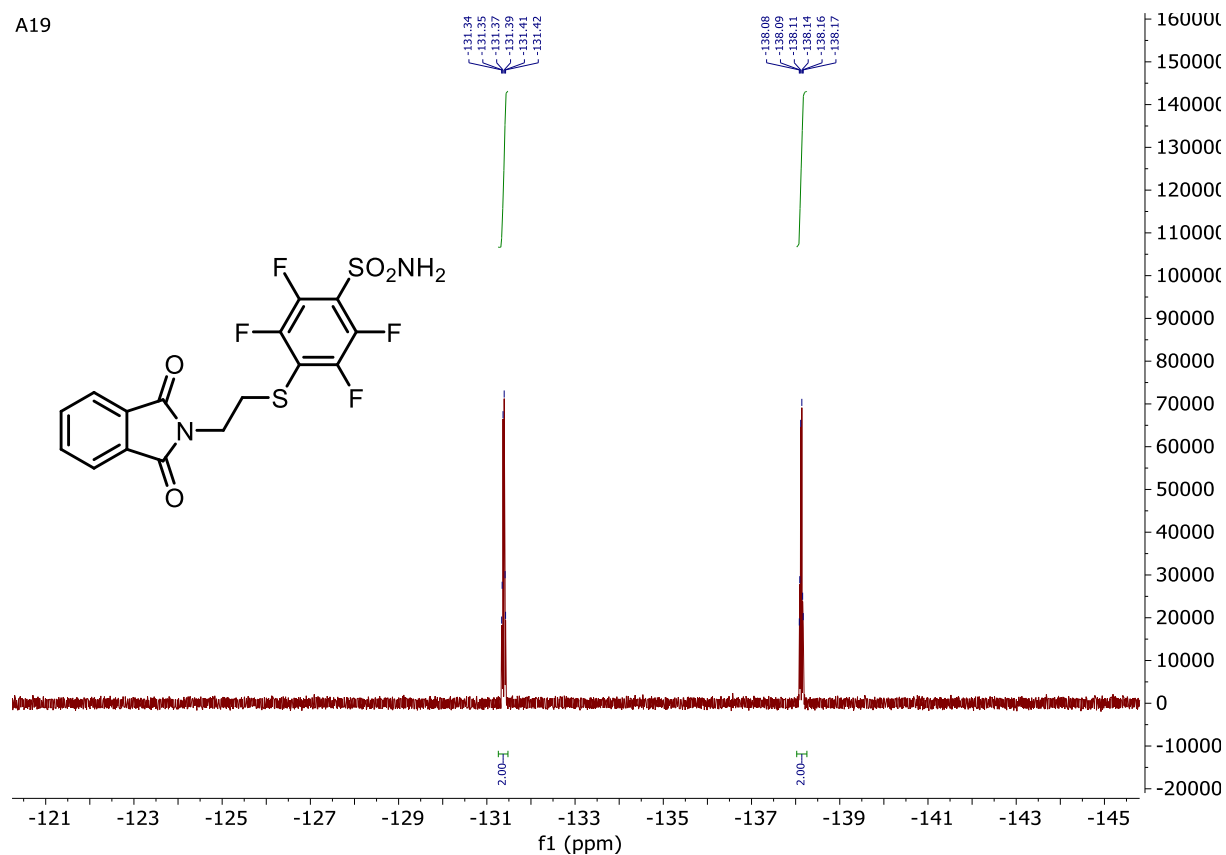
A18

4-((2-(1,3-Dioxisoindolin-2-yl)ethyl)thio)-2,3,5,6-tetrafluorobenzenesulfonamide (**A19**)

A19

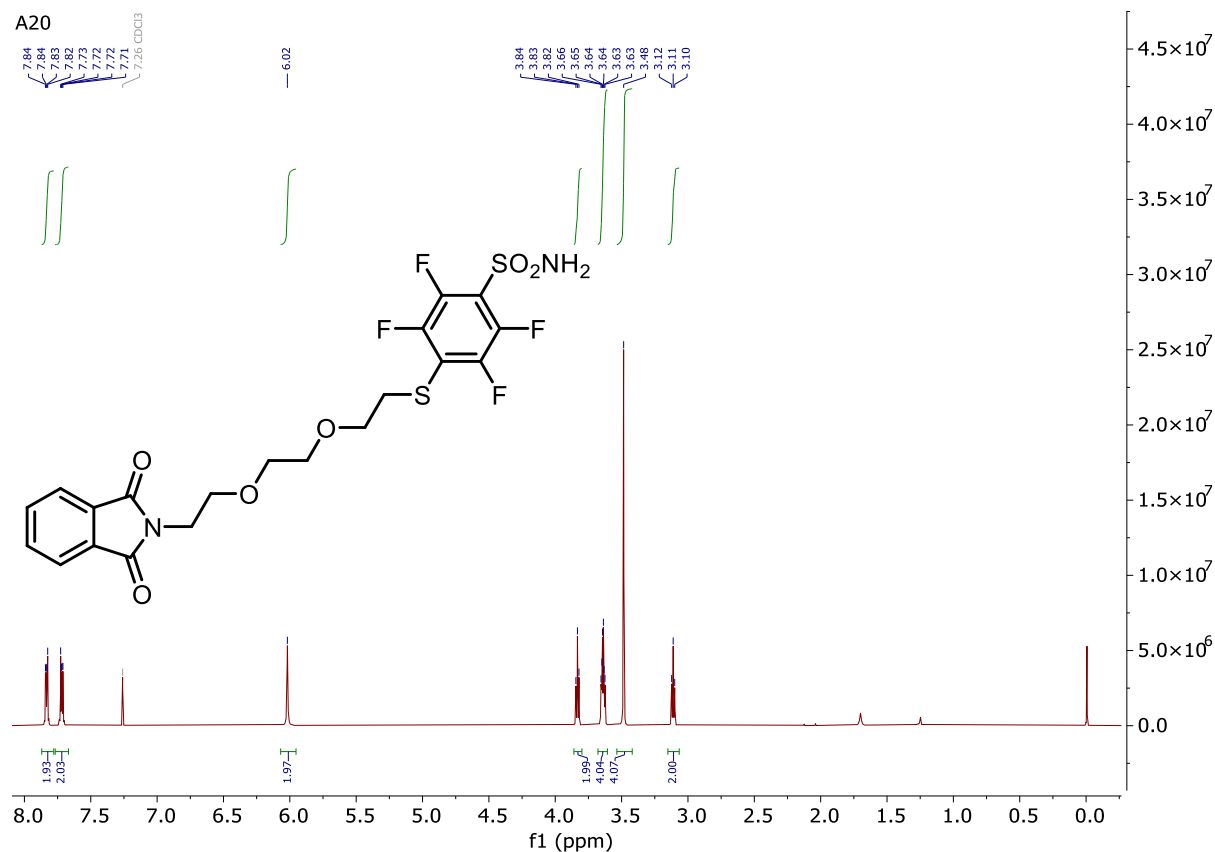


A19



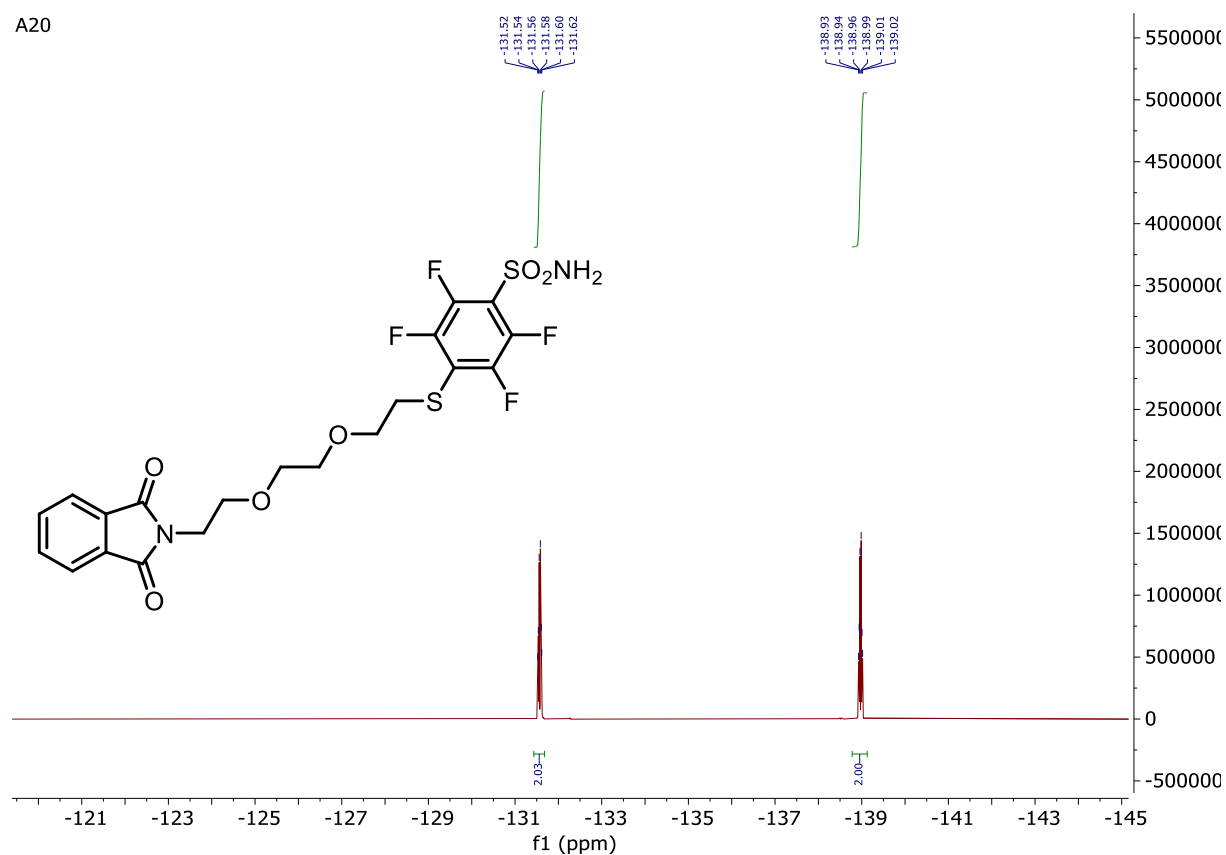
4-((2-(2-(2-(1,3-dioxoisindolin-2-yl)ethoxy)ethoxy)ethylthio)-2,3,5,6-tetrafluorobenzenesulfonamide (A20)

A20

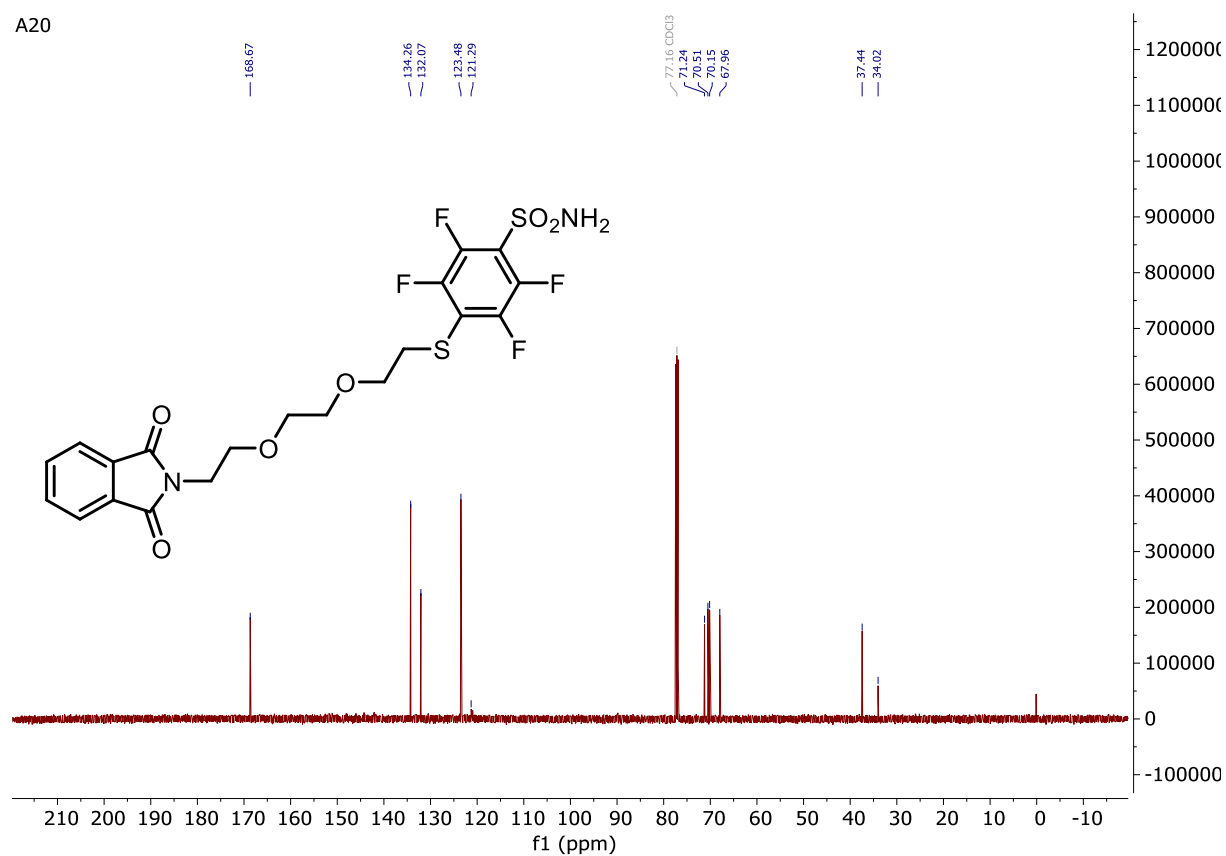


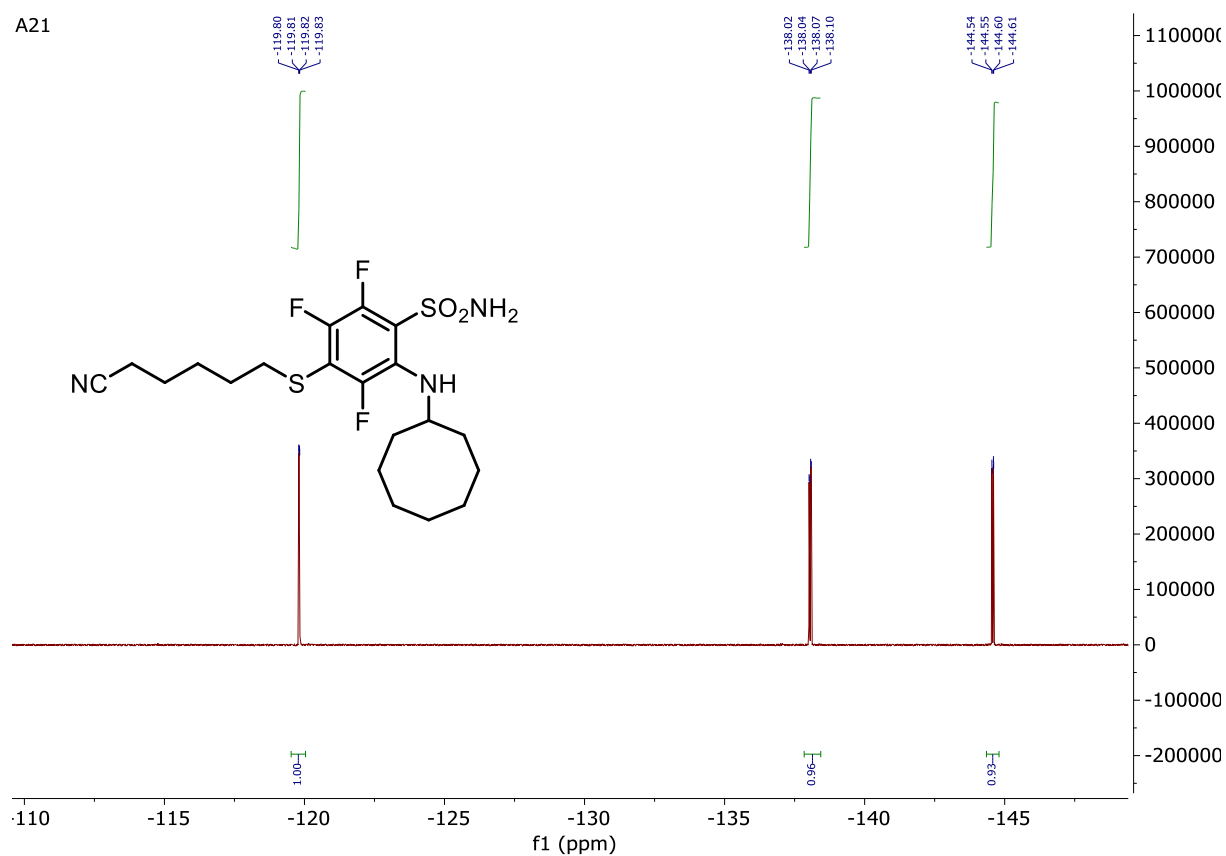
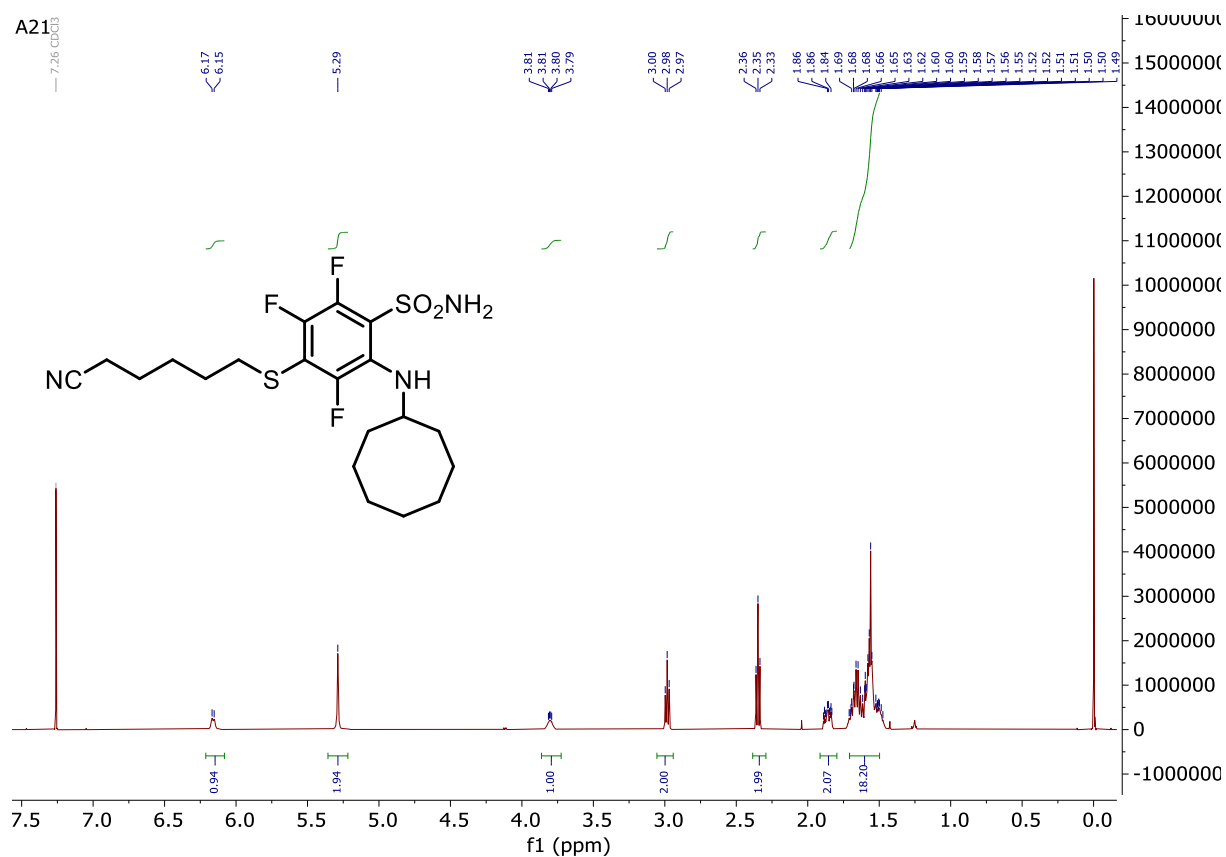
Appendix

A20

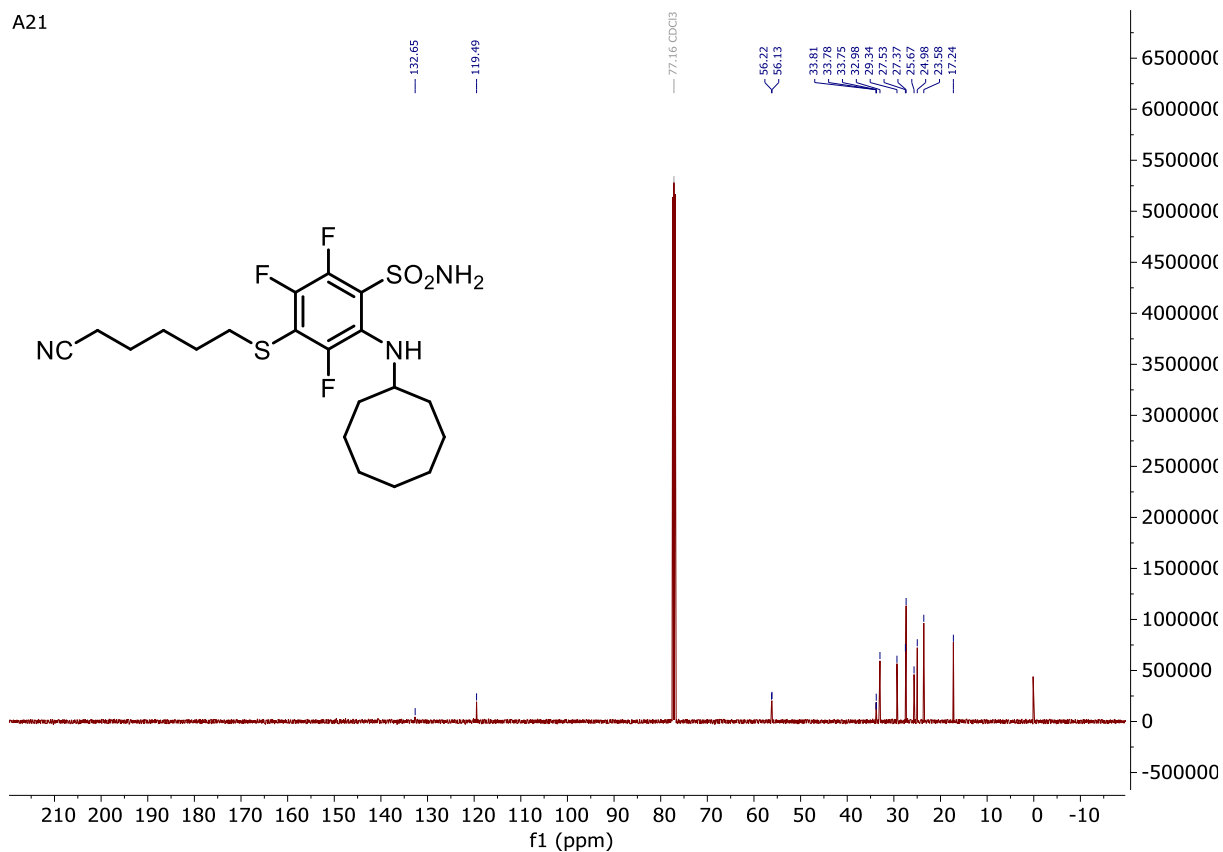


A20



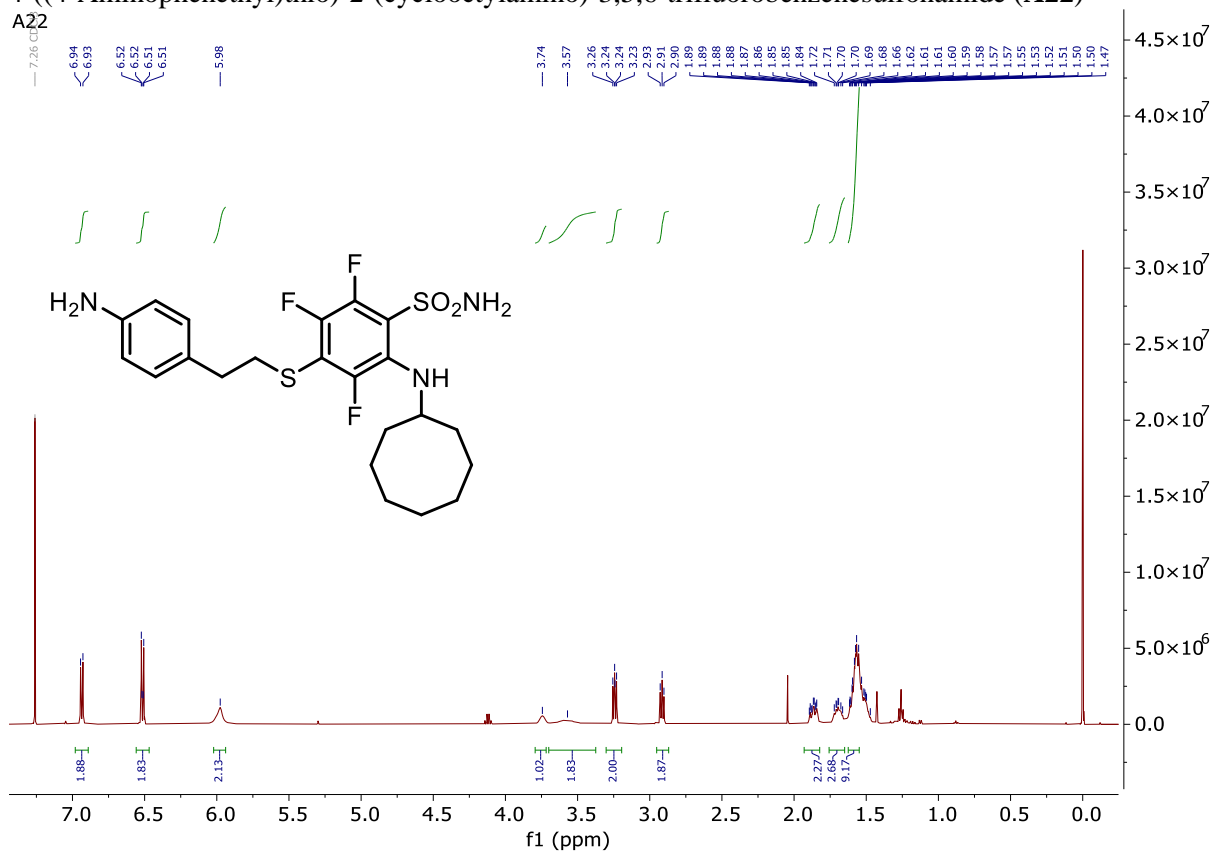
4-((5-Cyanopentyl)thio)-2-(cyclooctylamino)-3,5,6-trifluorobenzenesulfonamide (**A21**)

A21

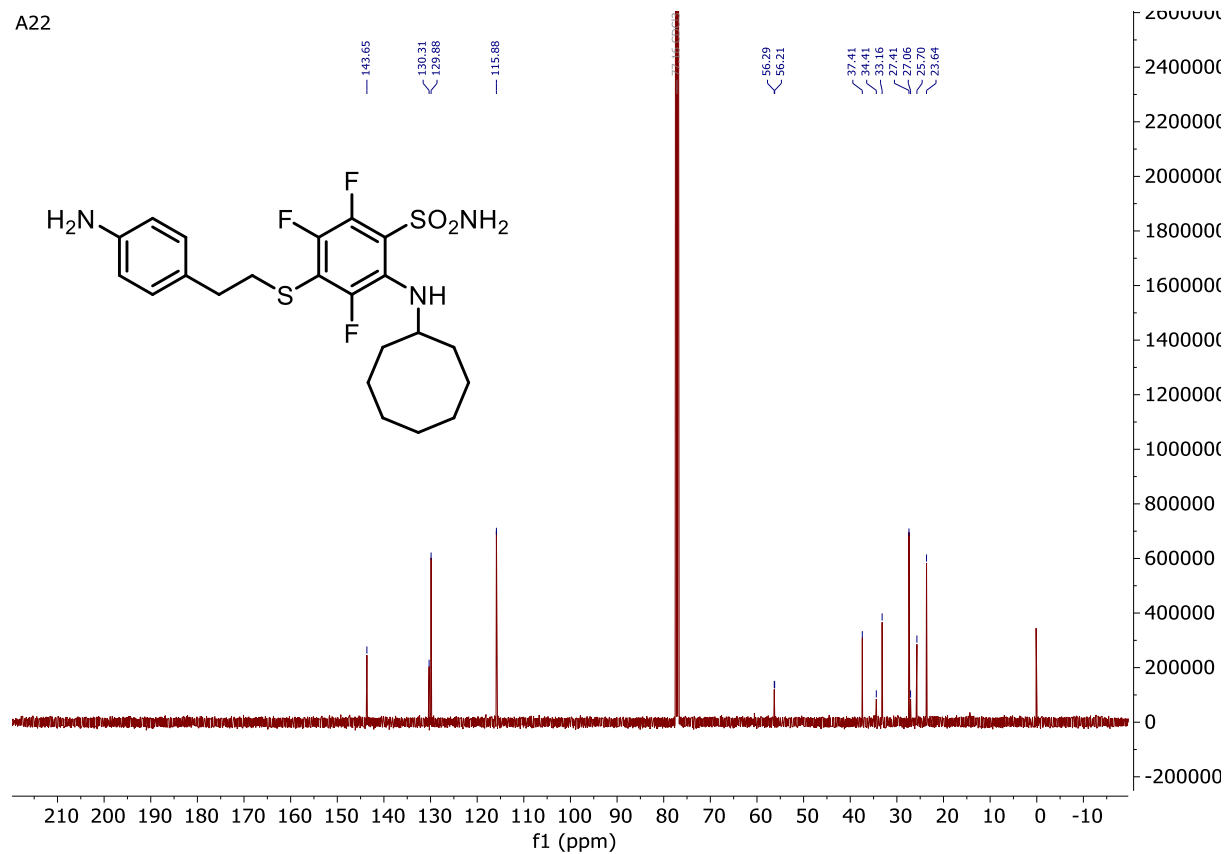
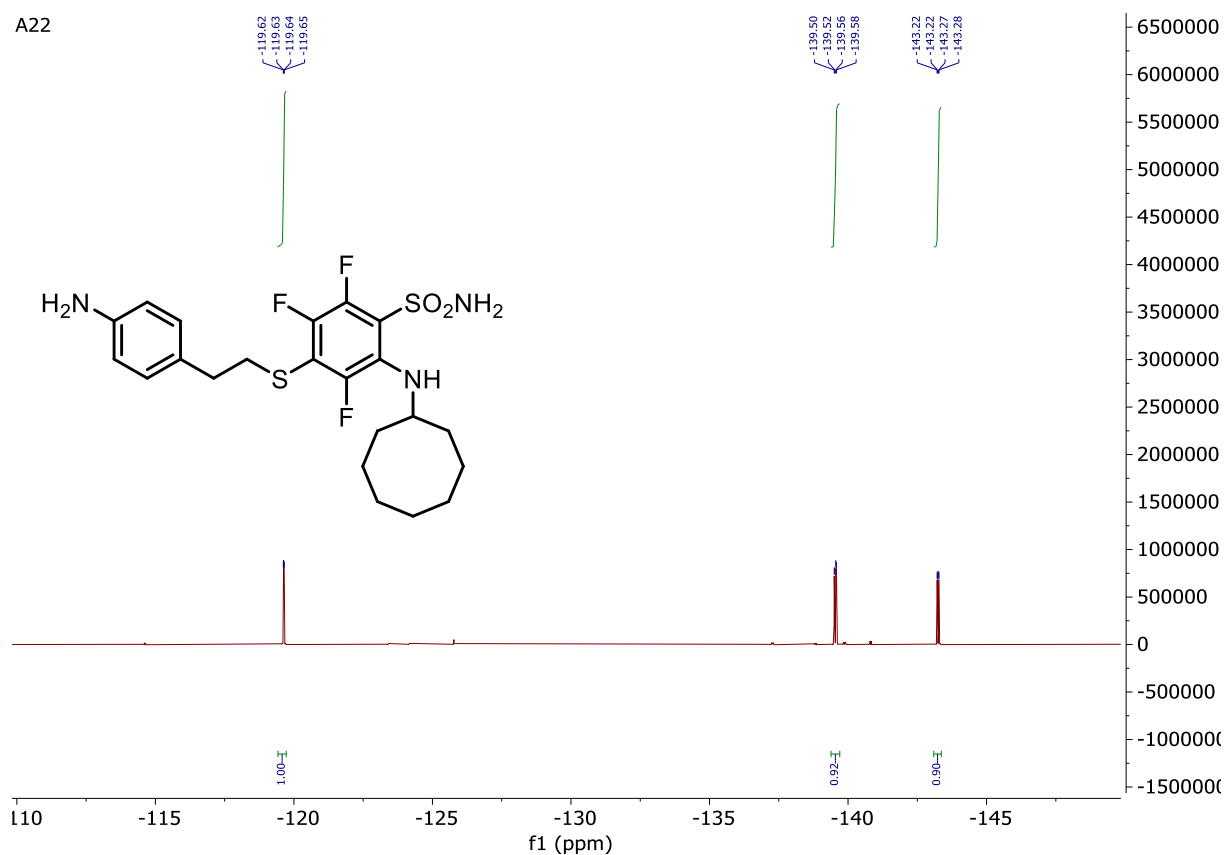


4-((4-Aminophenethyl)thio)-2-(cyclooctylamino)-3,5,6-trifluorobenzenesulfonamide (A22)

A22

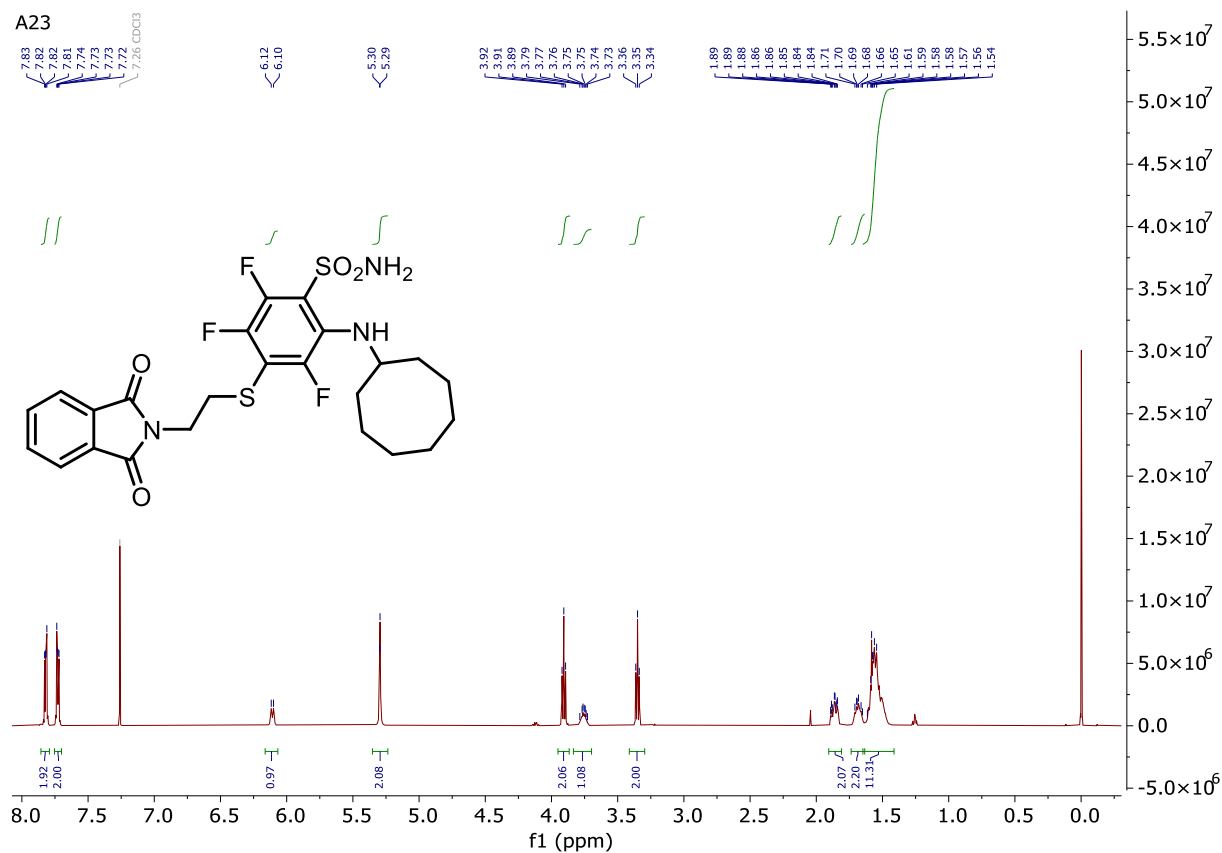


Appendix

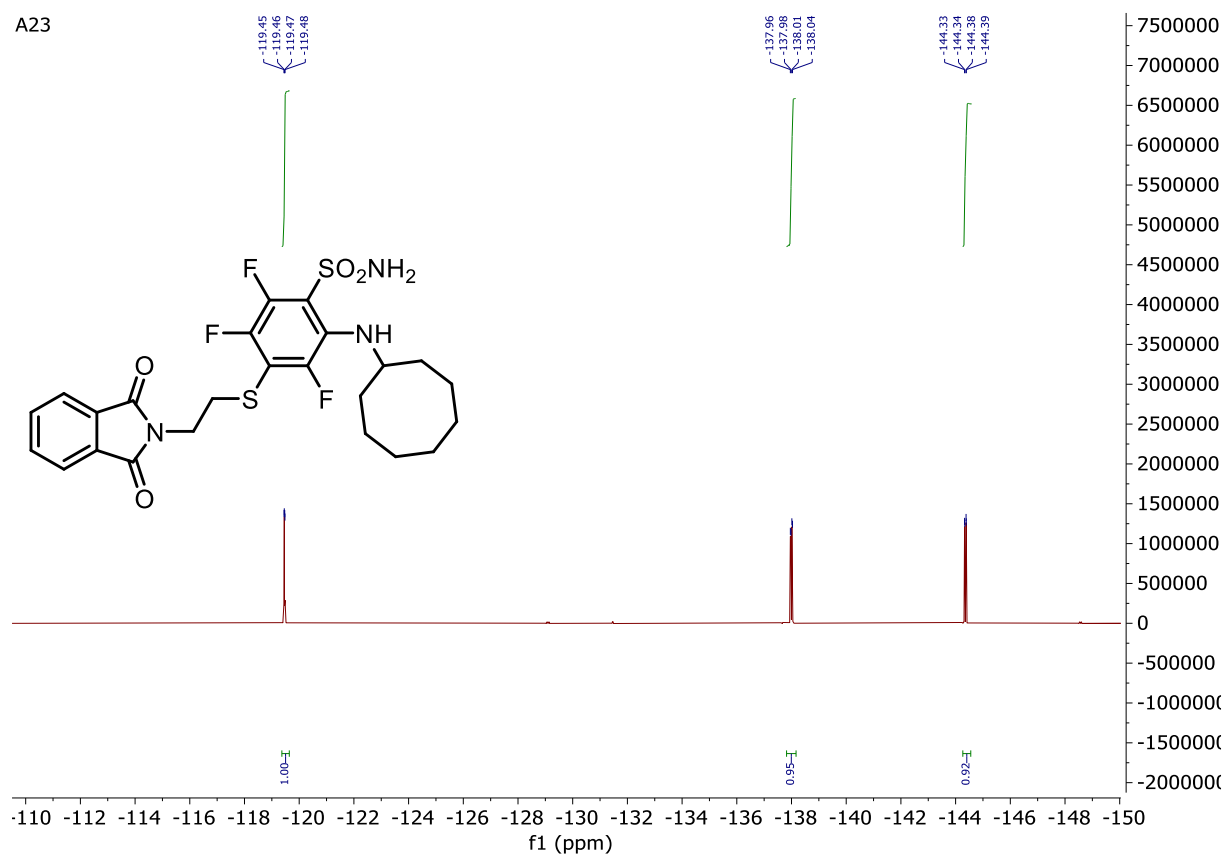


2-(Cyclooctylamino)-4-((2-(1,3-dioxisoindolin-2-yl)ethyl)thio)-3,5,6-trifluorobenzenesulfonamide (A23)

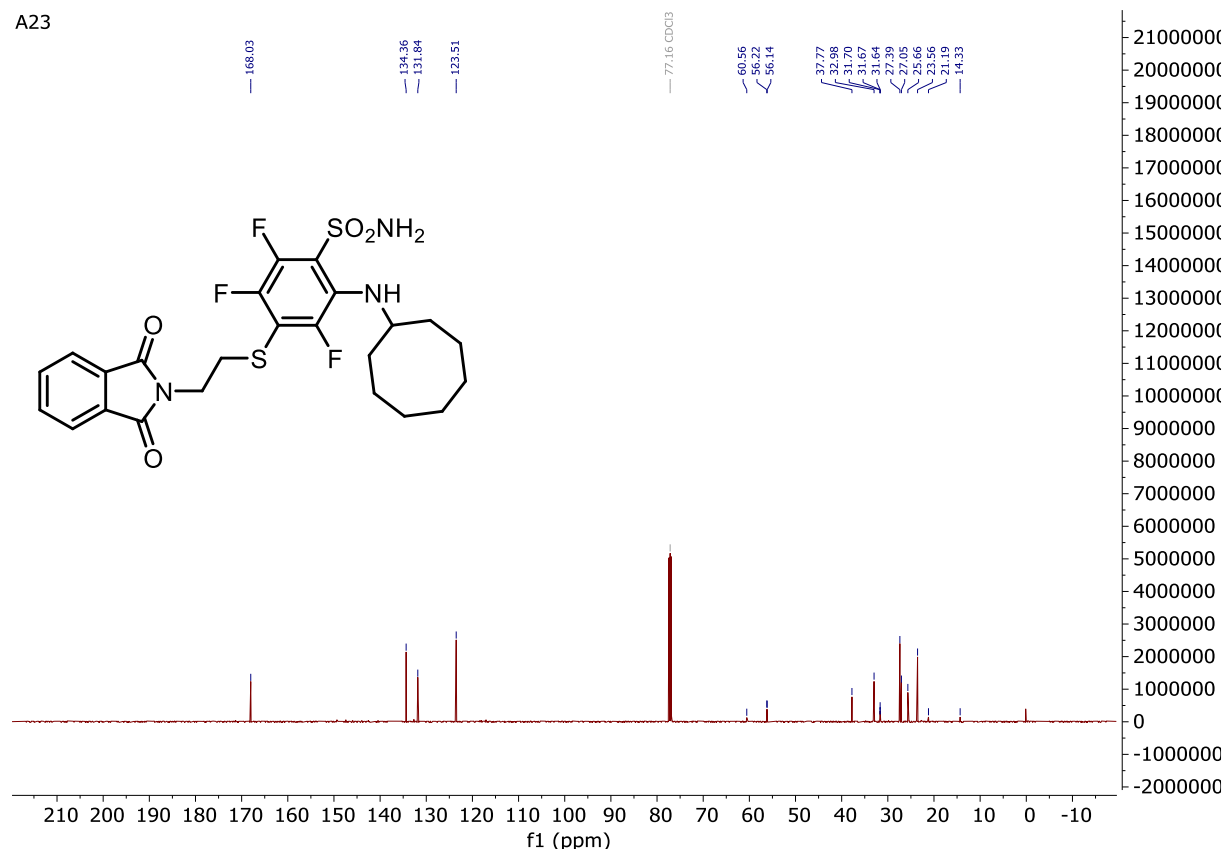
A23



A23

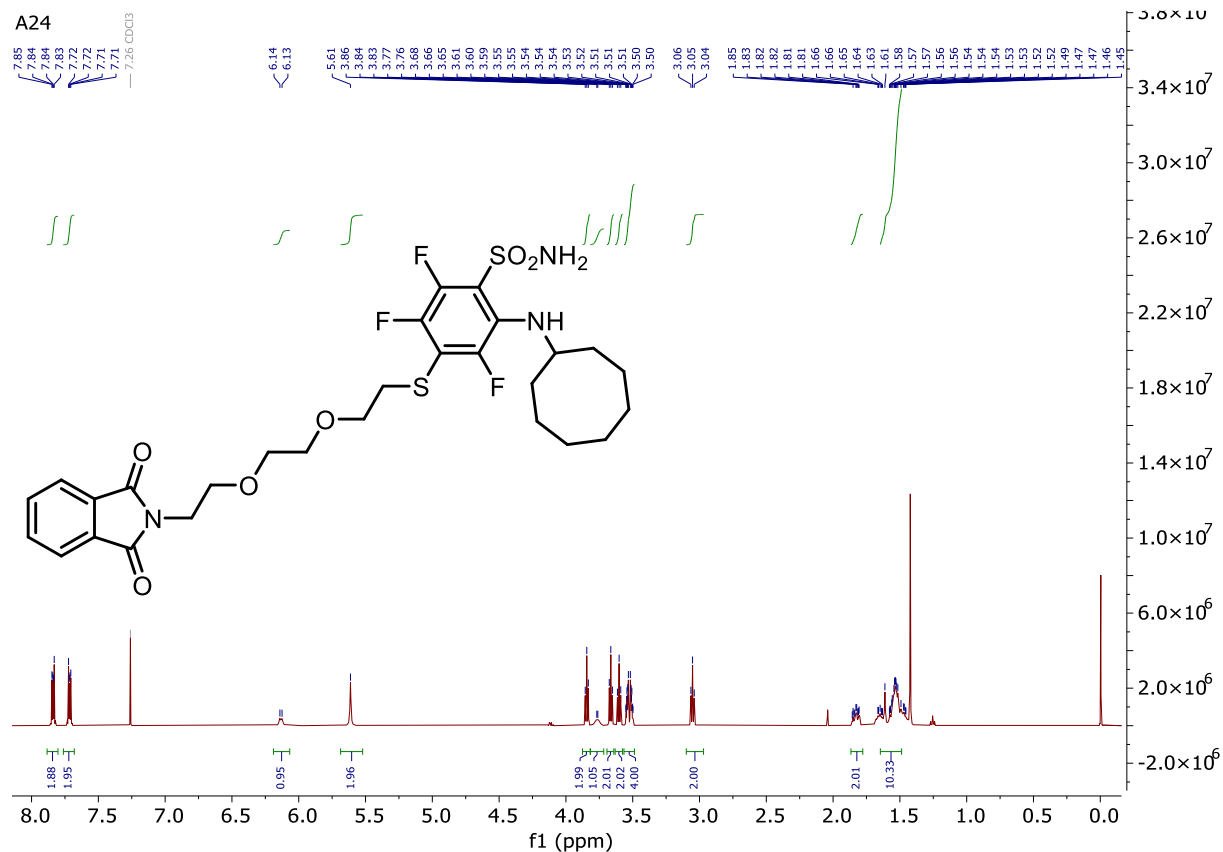


A23



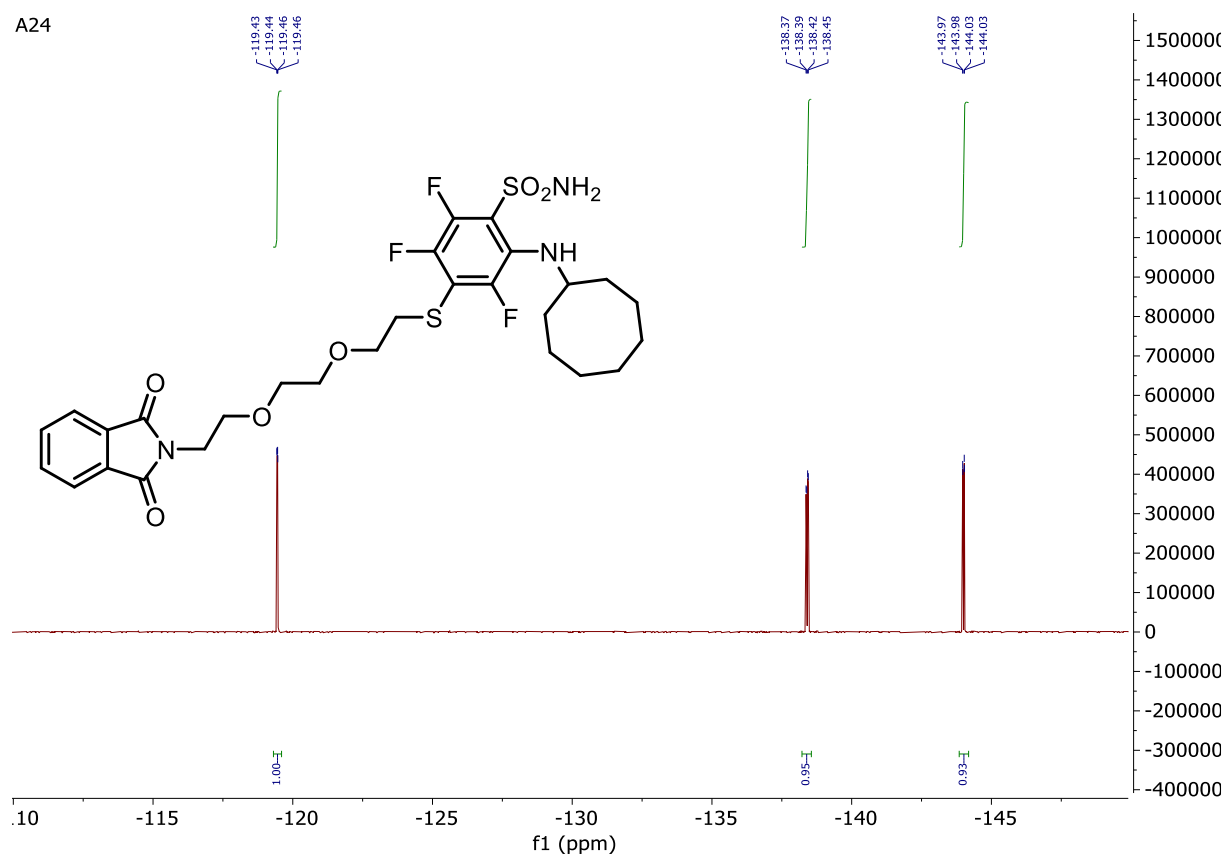
2-(Cyclooctylamino)-4-((2-(2-(1,3-dioxoisindolin-2-yl)ethoxy)ethoxy)ethylthio)-3,5,6-trifluorobenzenesulfonamide (**A24**)

A24

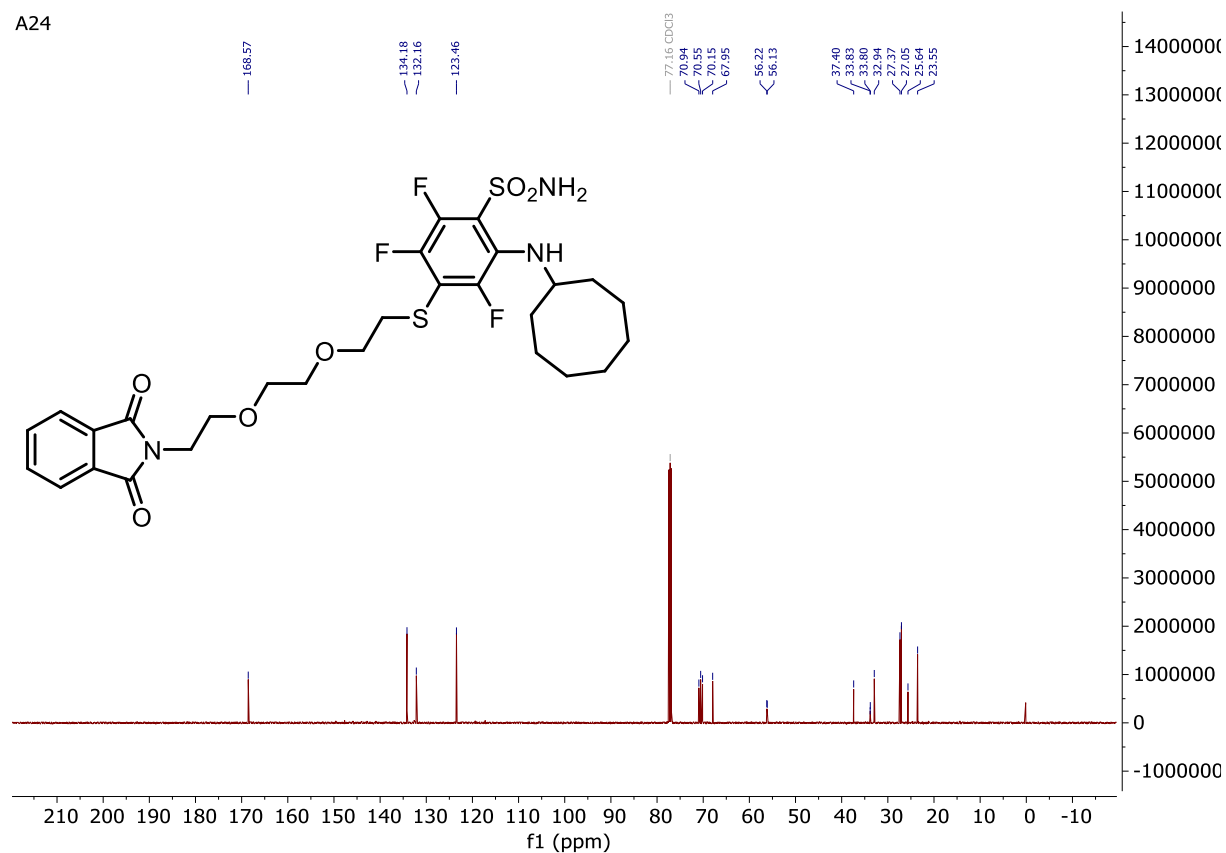


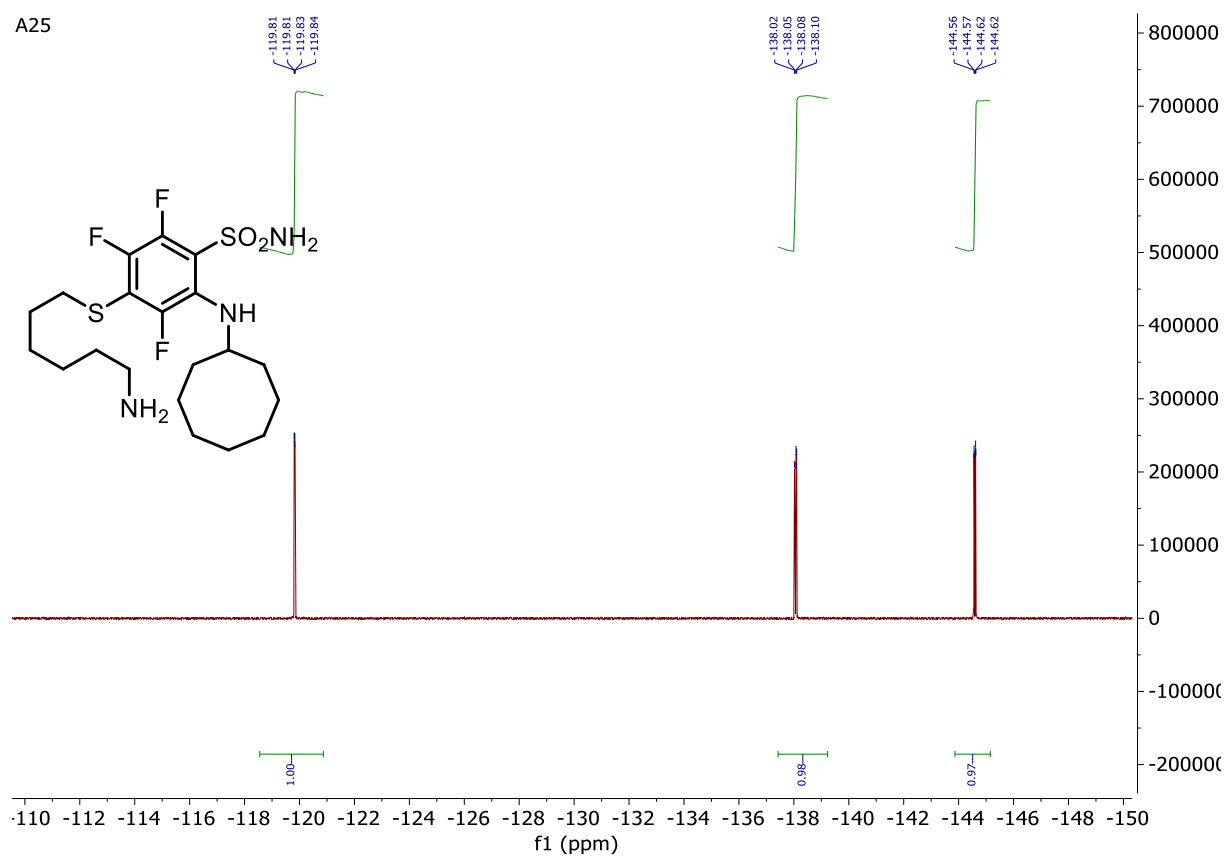
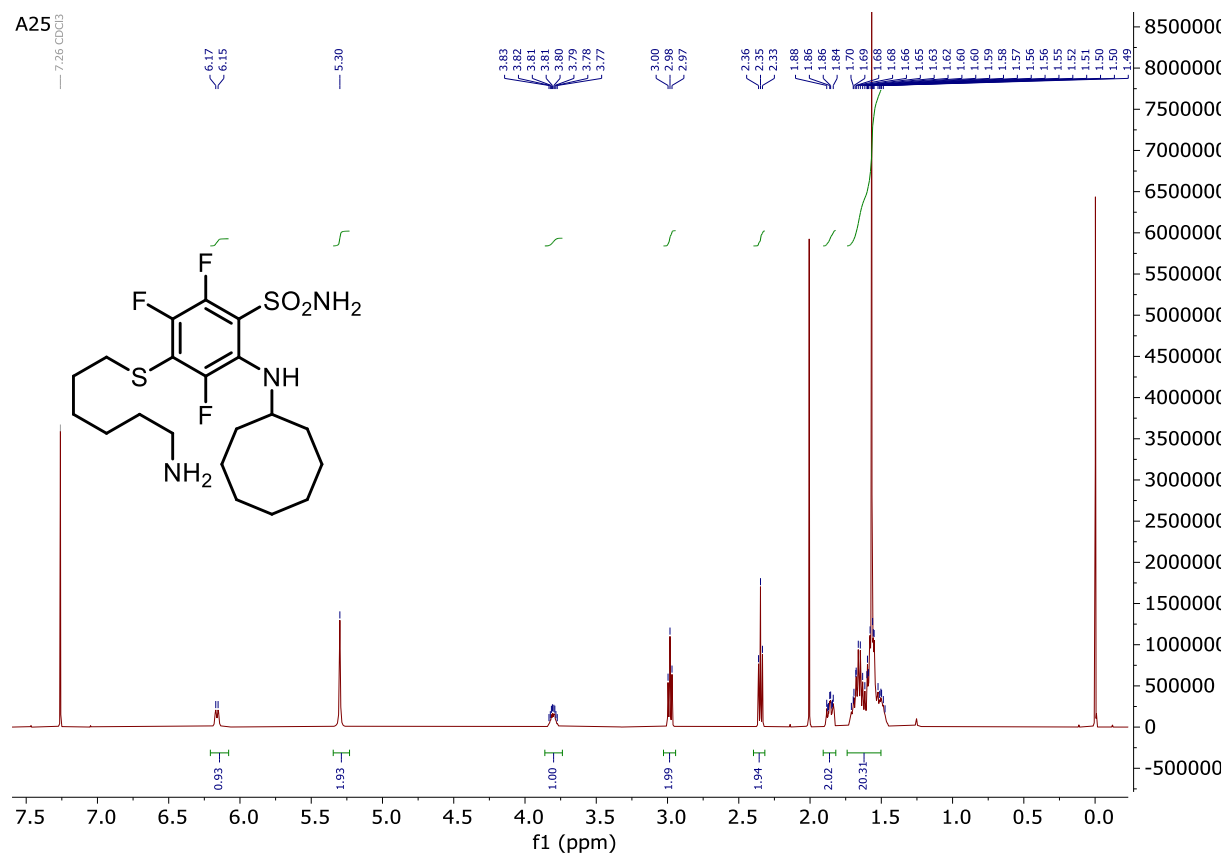
Appendix

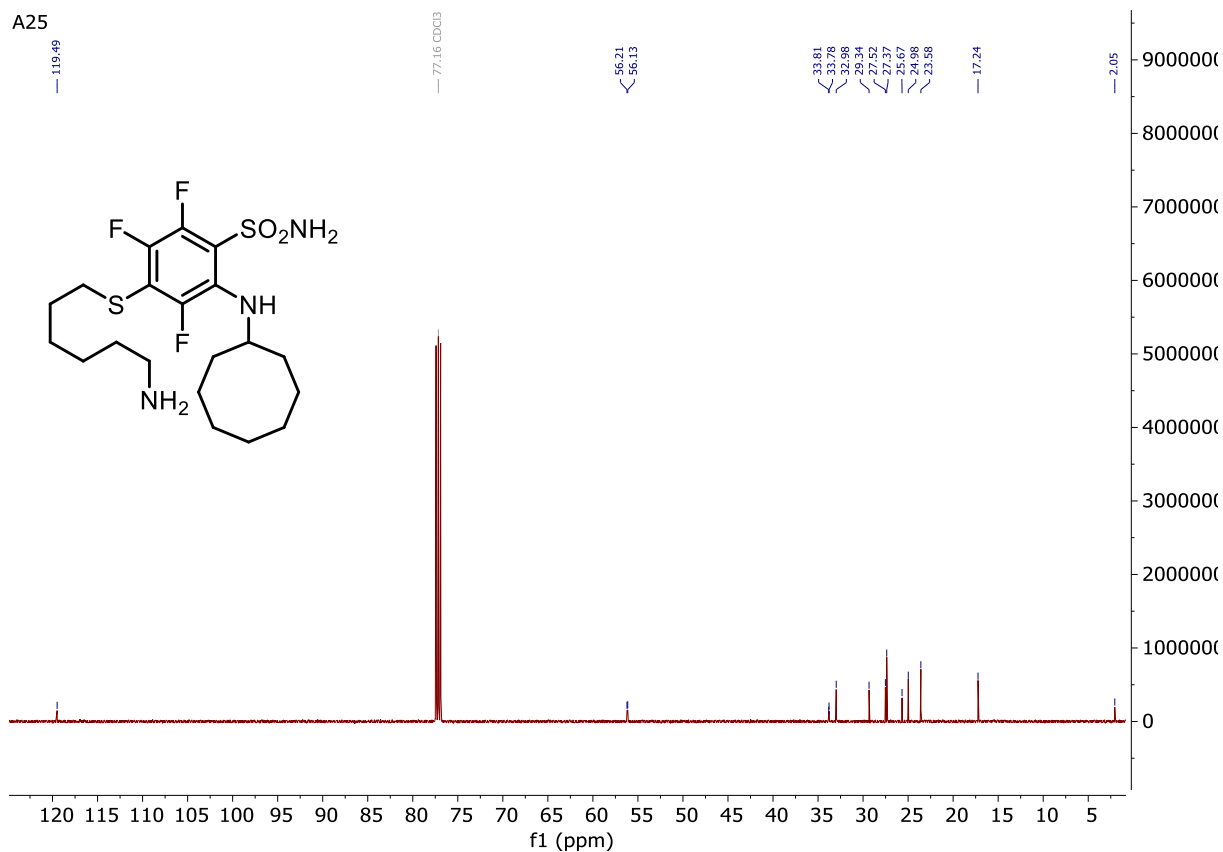
A24



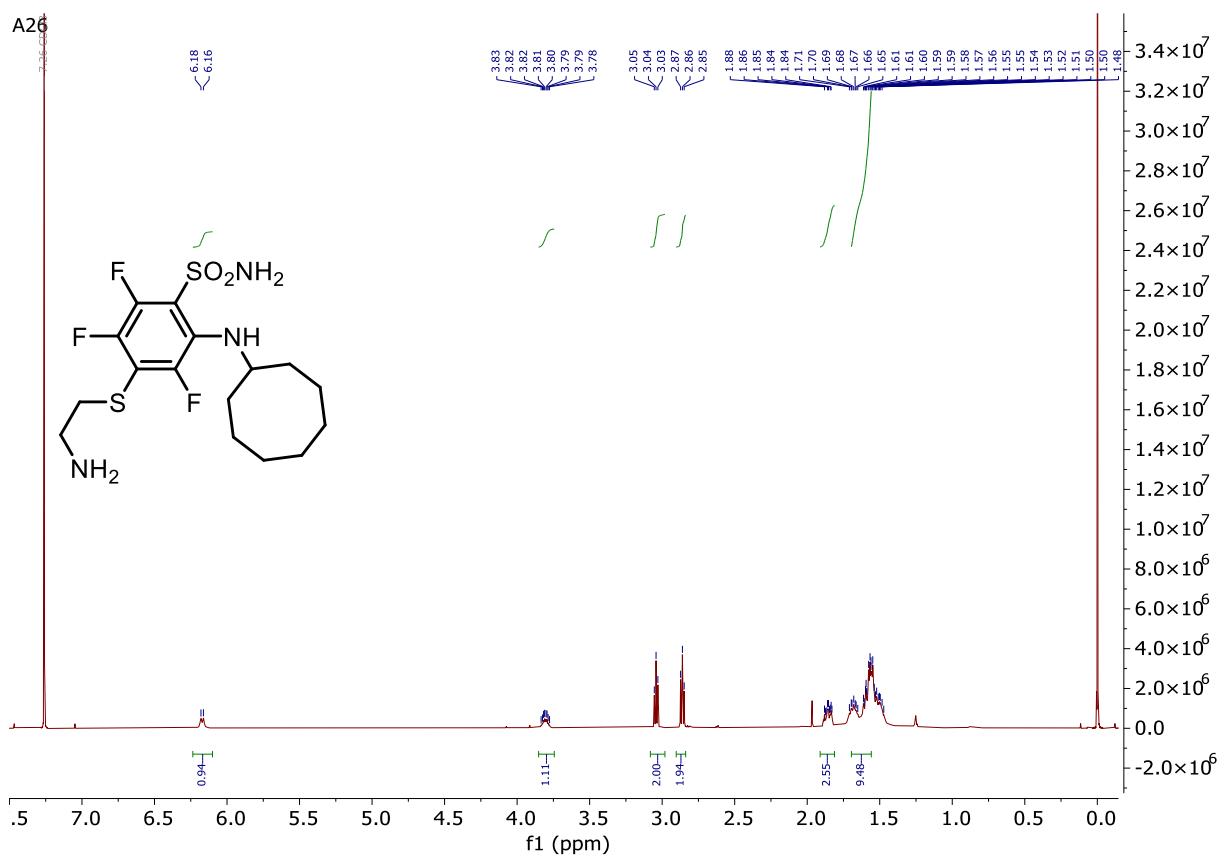
A24

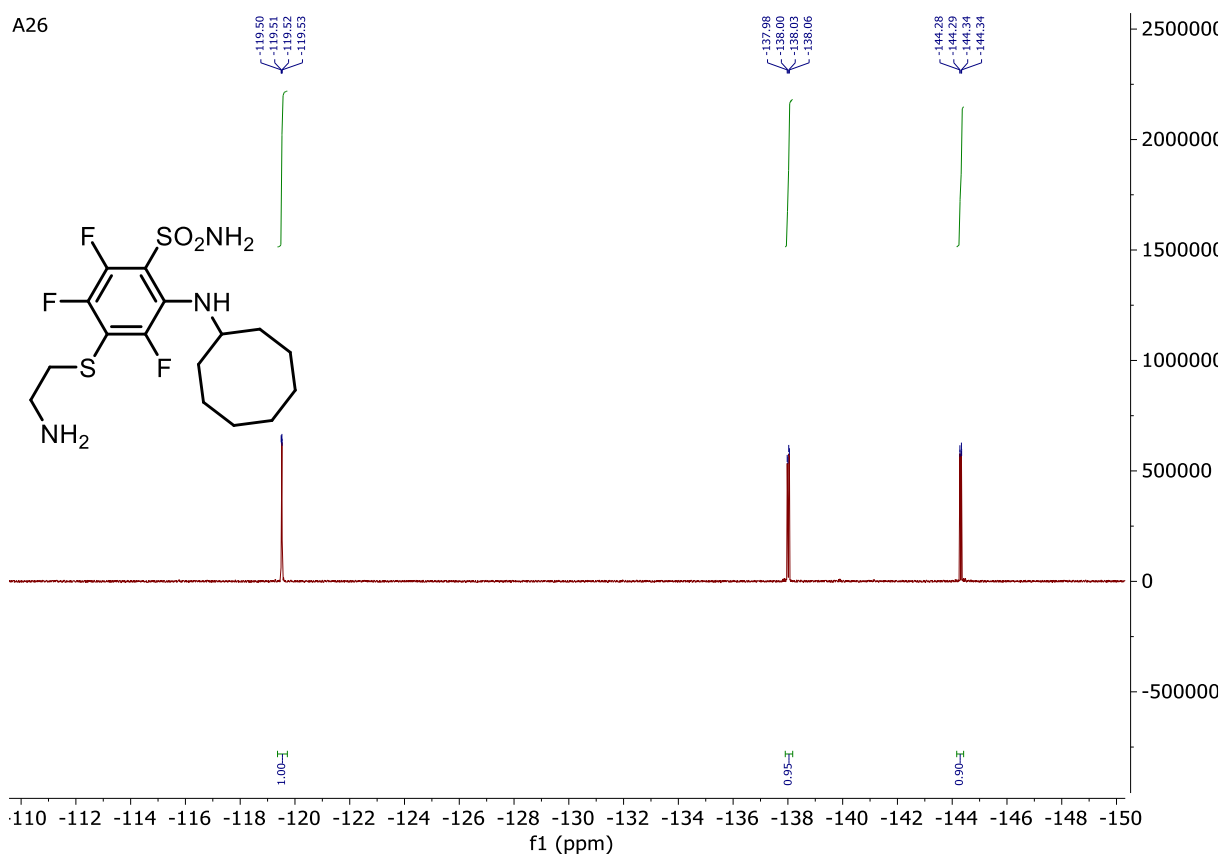


4-((6-Aminoethyl)thio)-2-(cyclooctylamino)-3,5,6-trifluorobenzenesulfonamide (**A25**)

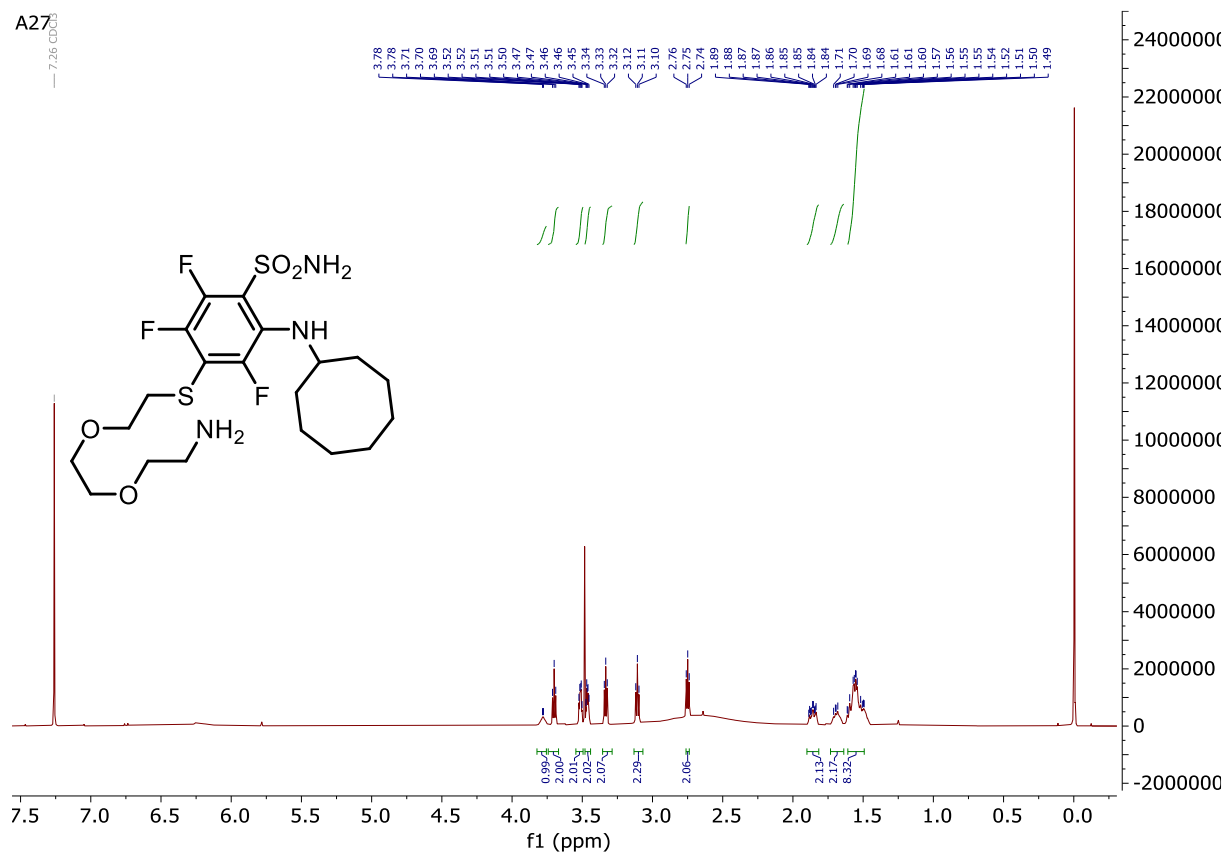


4-((2-Aminoethyl)thio)-2-(cyclooctylamino)-3,5,6-trifluorobenzenesulfonamide (A26)



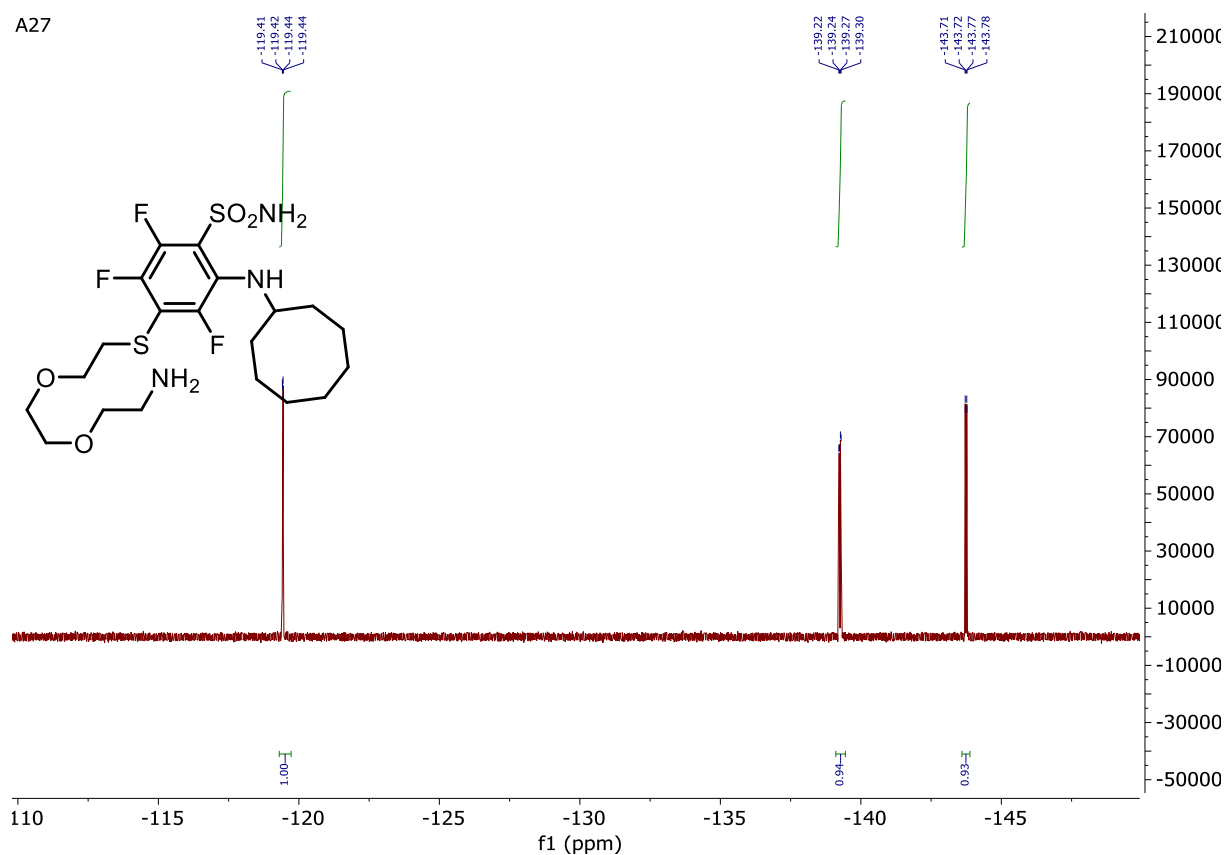


4-((2-(2-(2-Aminoethoxy)ethoxy)ethyl)thio)-2-(cyclooctylamino)-3,5,6-trifluorobenzenesulfonamide (A27)

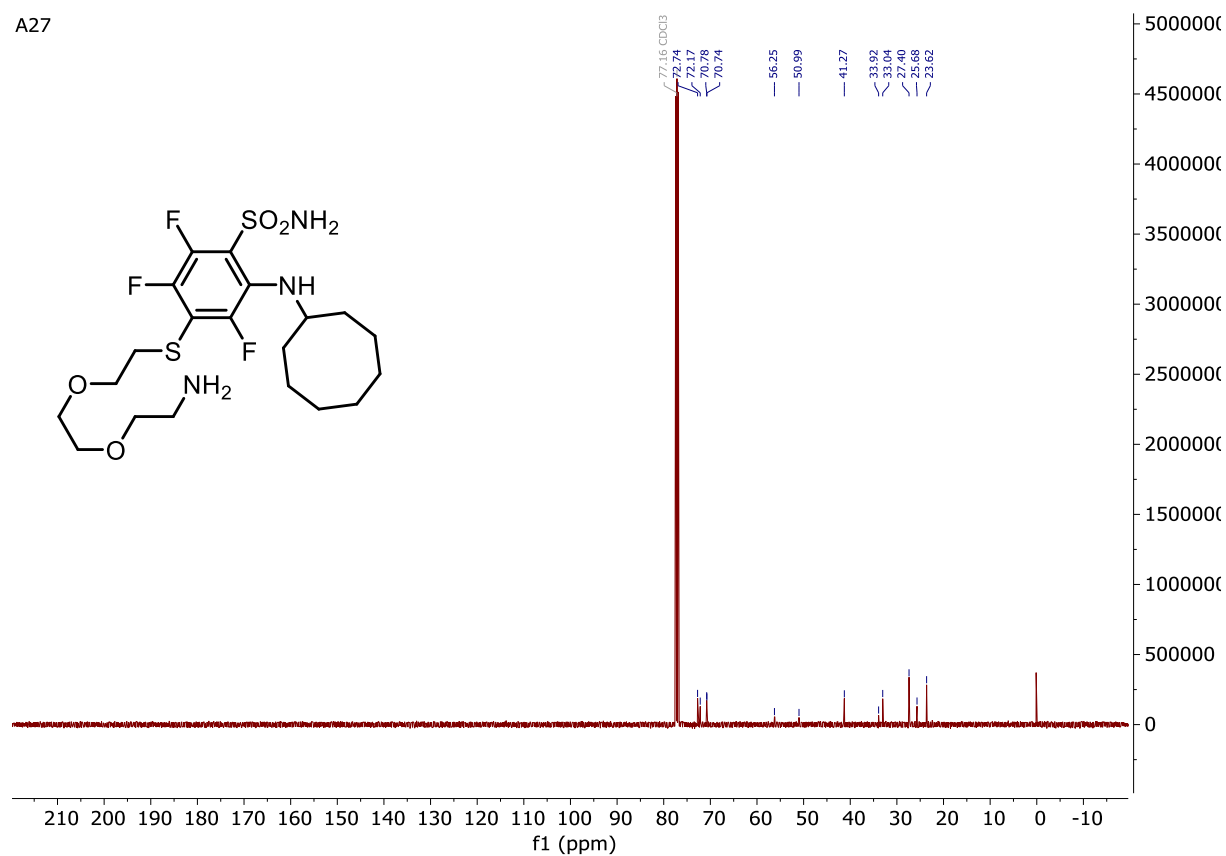


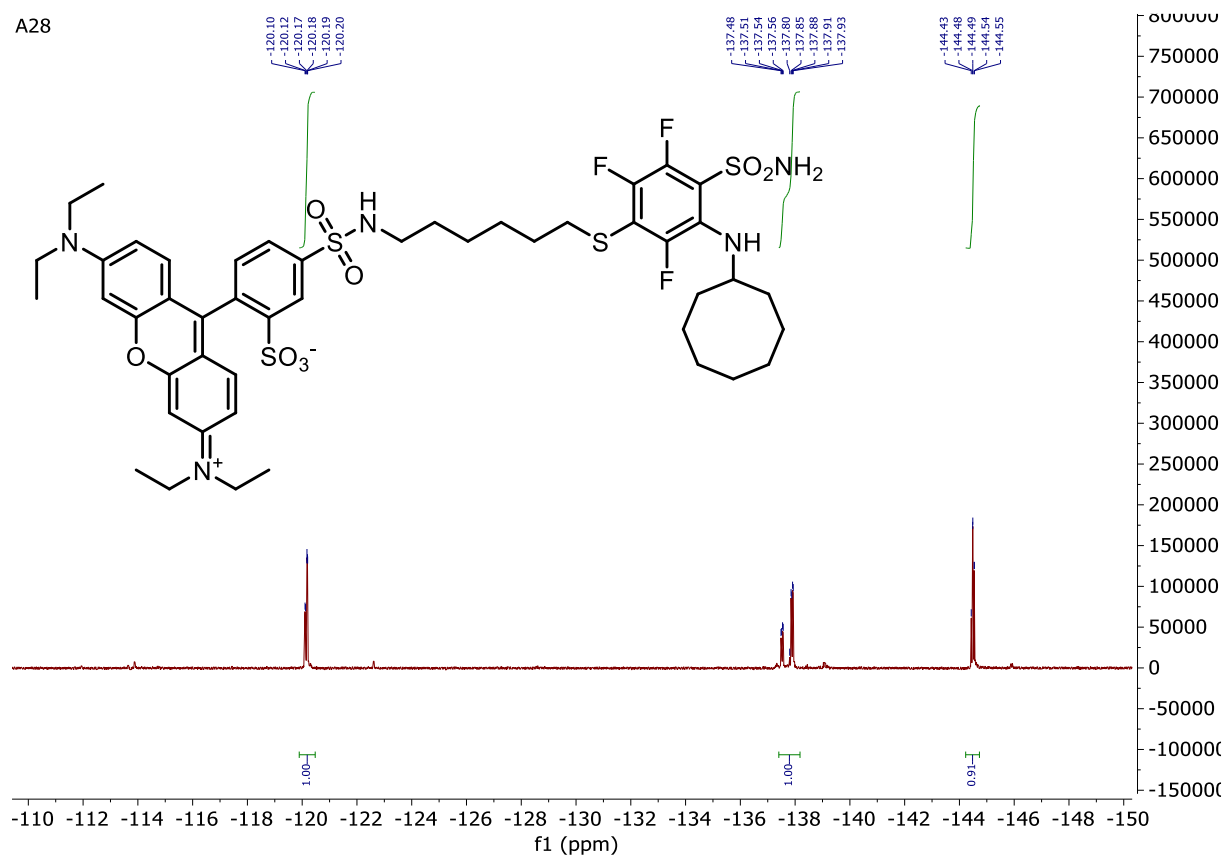
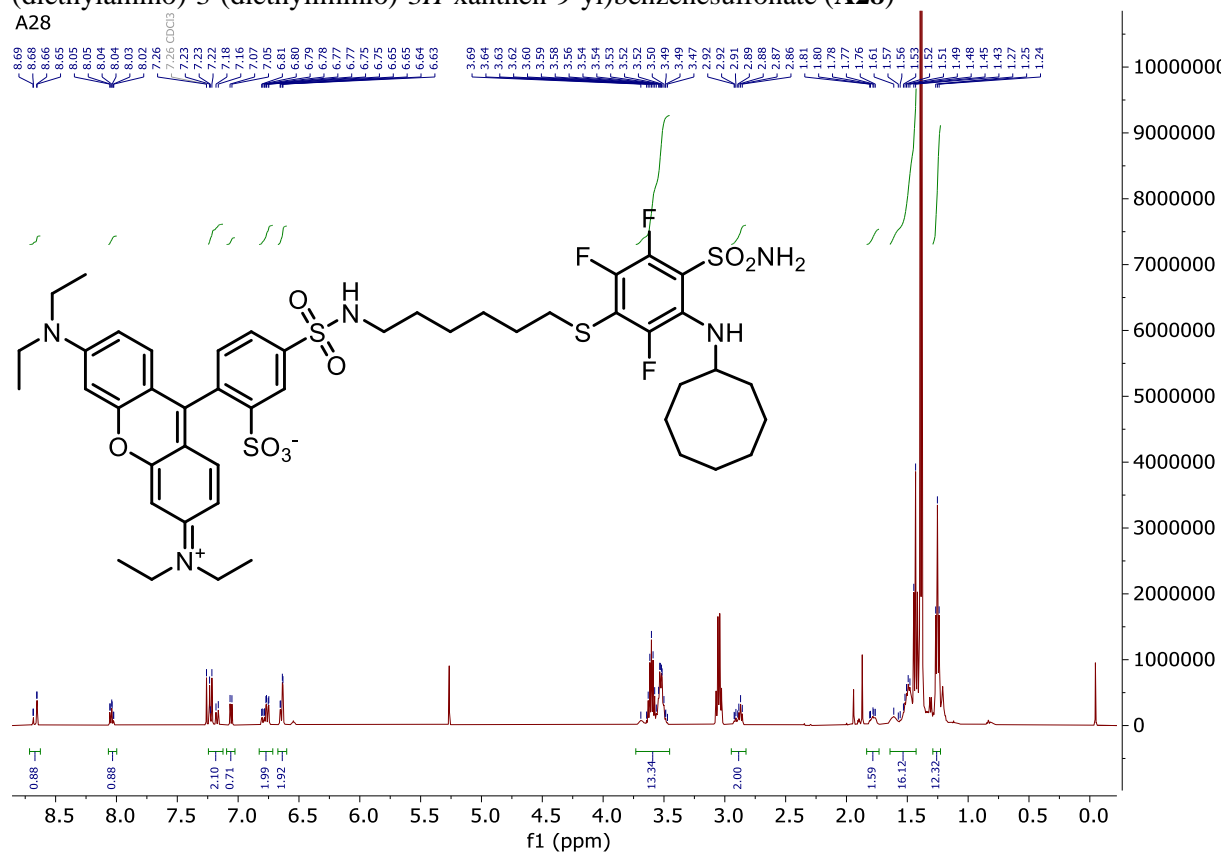
Appendix

A27



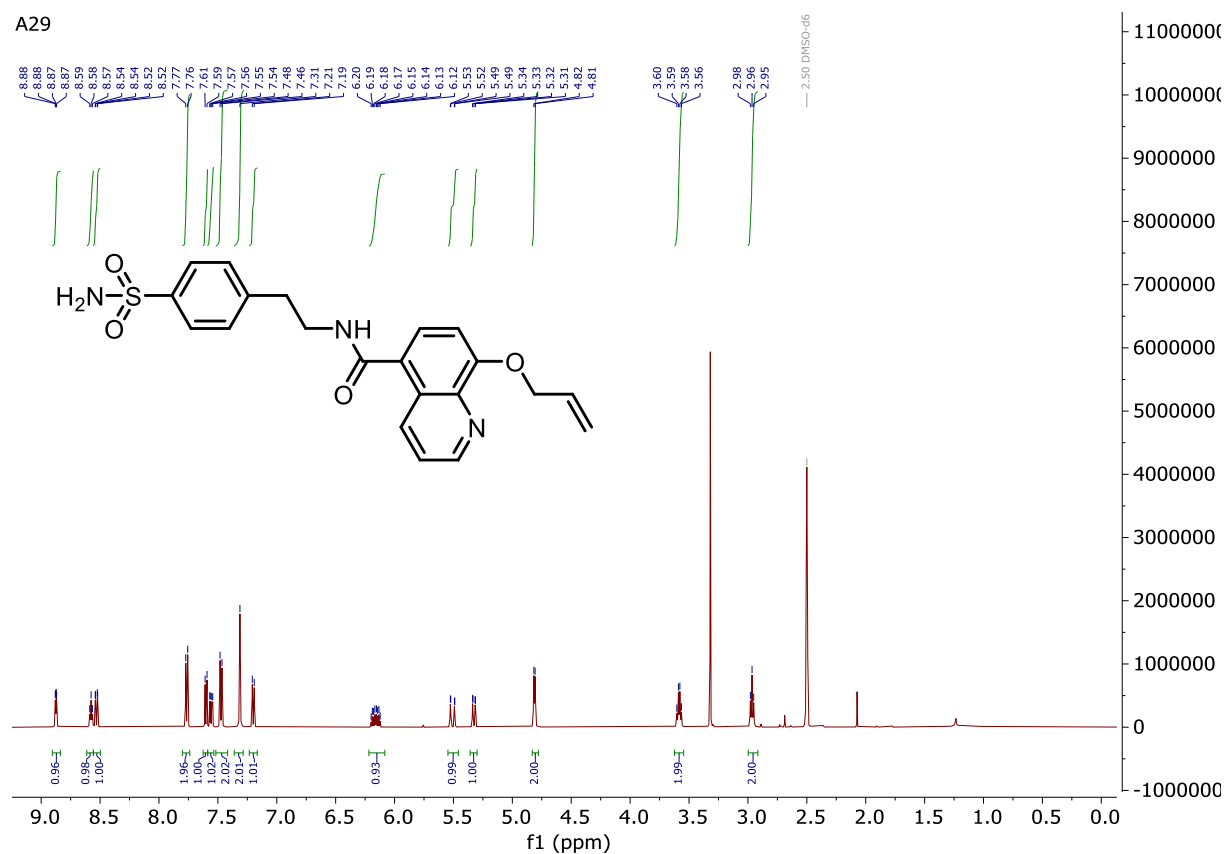
A27



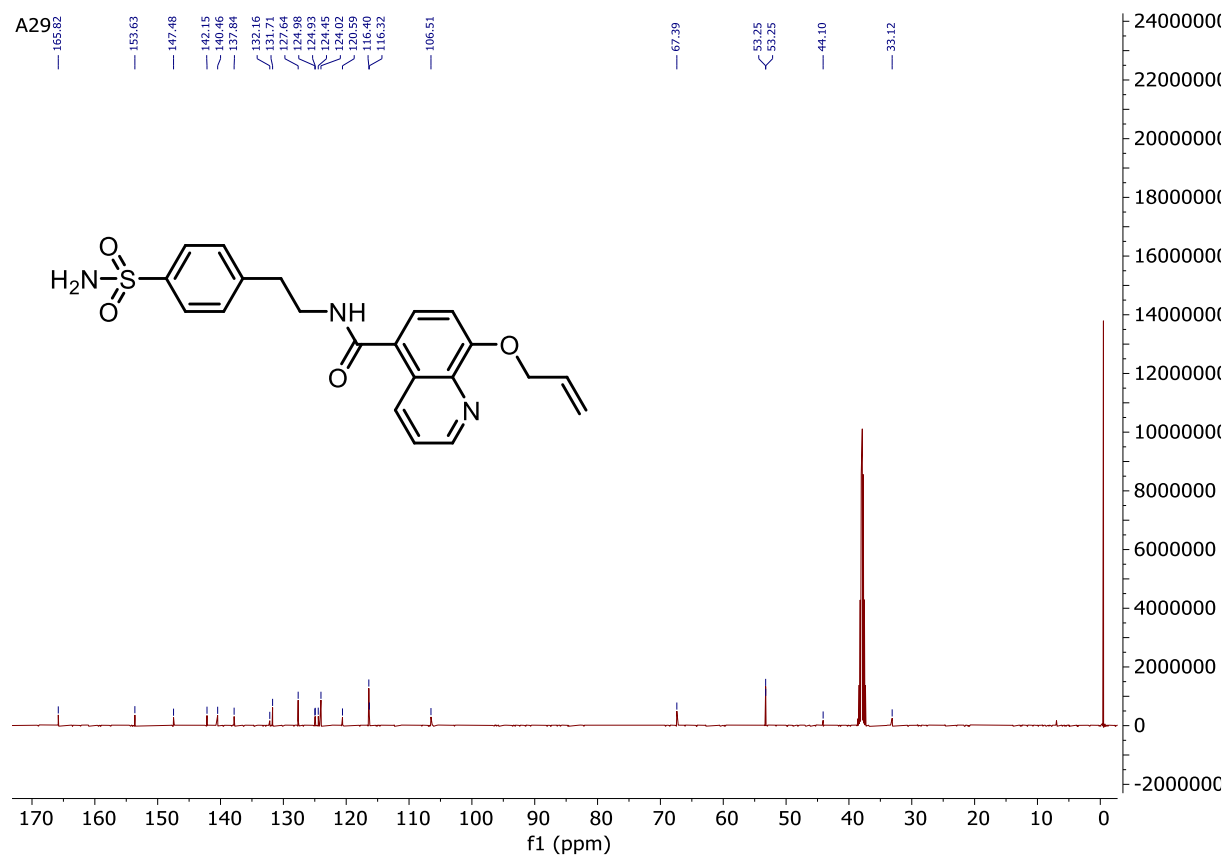
5-(*N*-(6-((3-(cyclooctylamino)-2,5,6-trifluoro-4-sulfamoylphenyl)thio)hexyl)sulfamoyl)-2-(6-(diethylamino)-3-(diethyliminio)-3*H*-xanthen-9-yl)benzenesulfonate (**A28**)

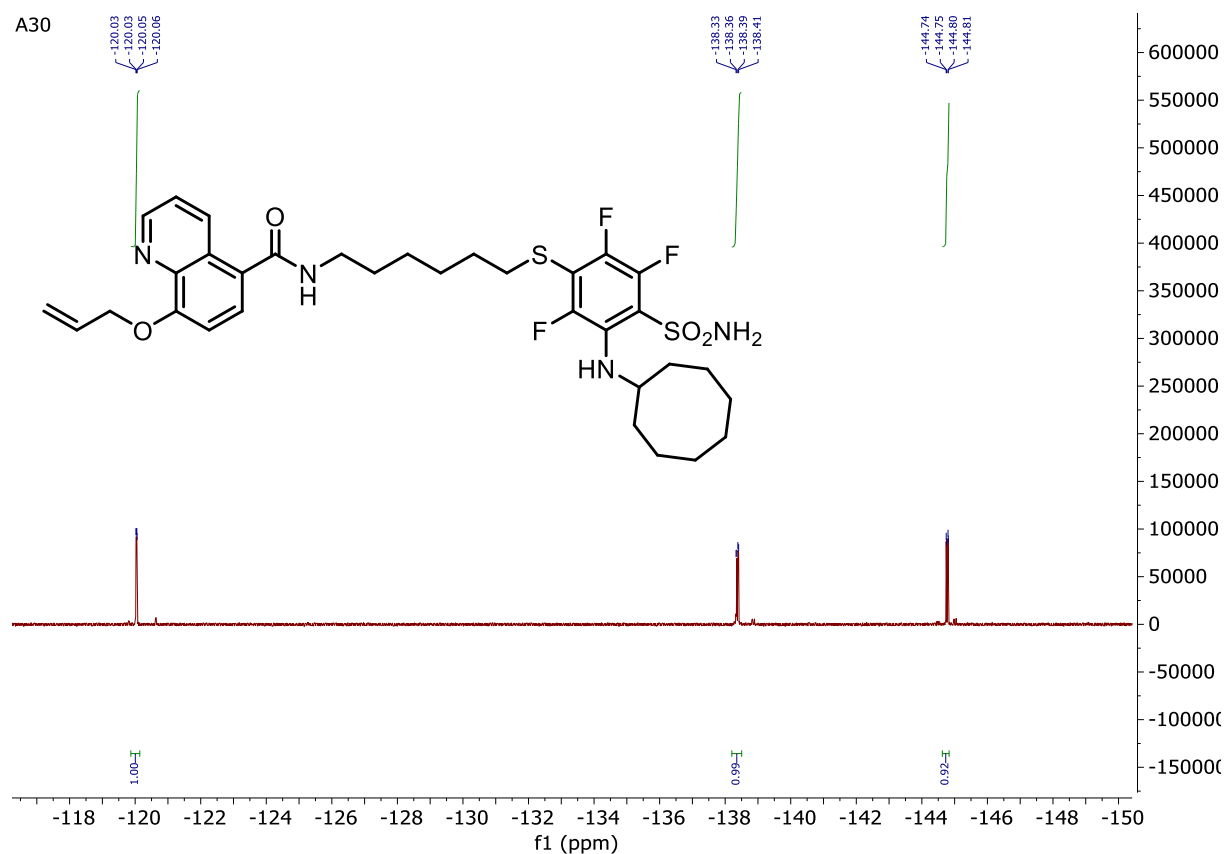
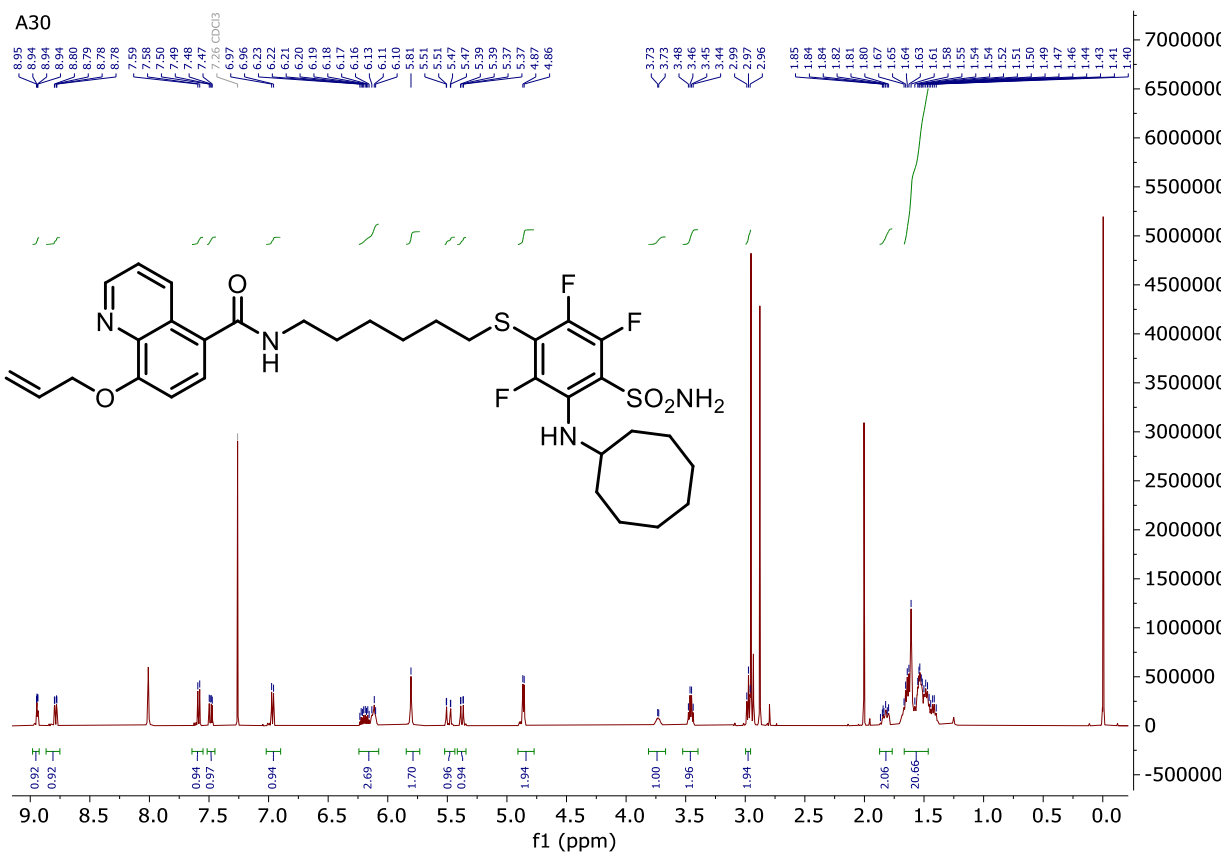
8-(Allyloxy)-*N*-(4-sulfamoylphenethyl)quinoline-5-carboxamide (**A29**)

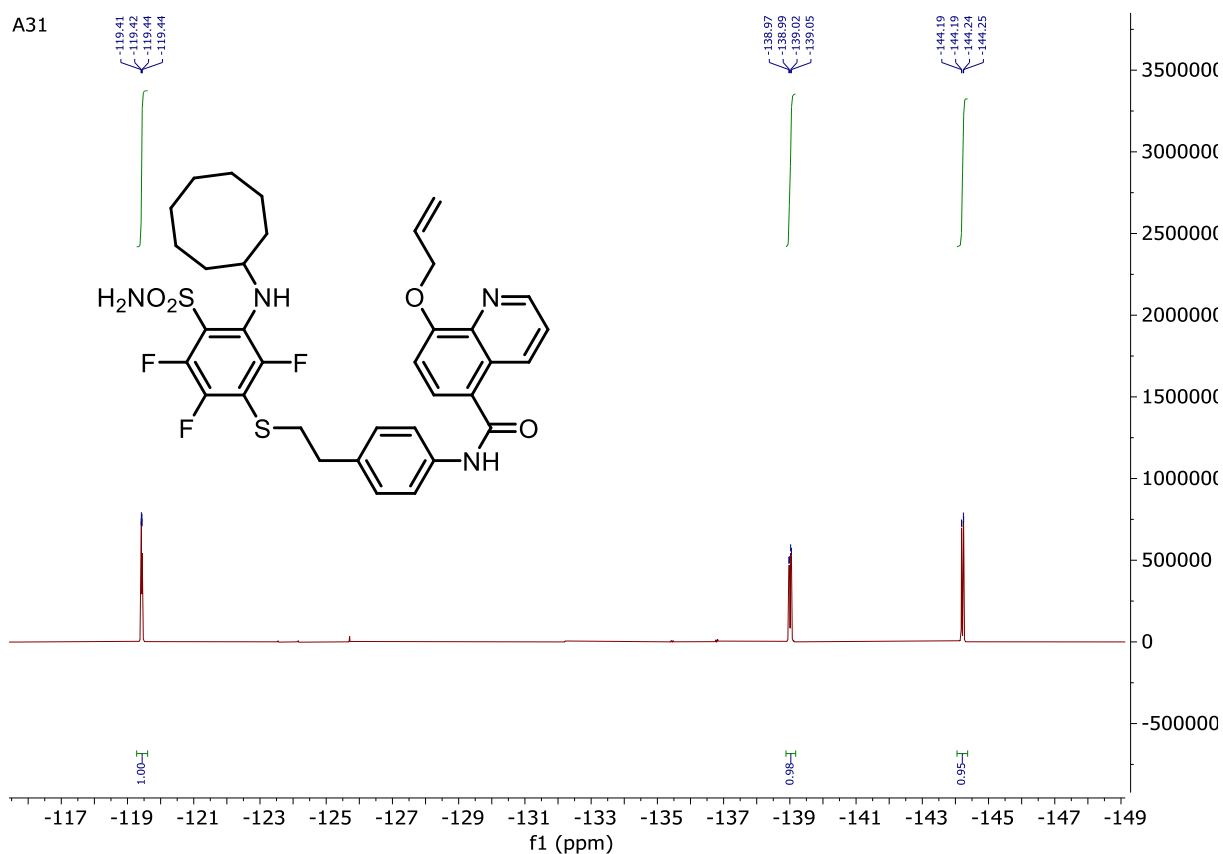
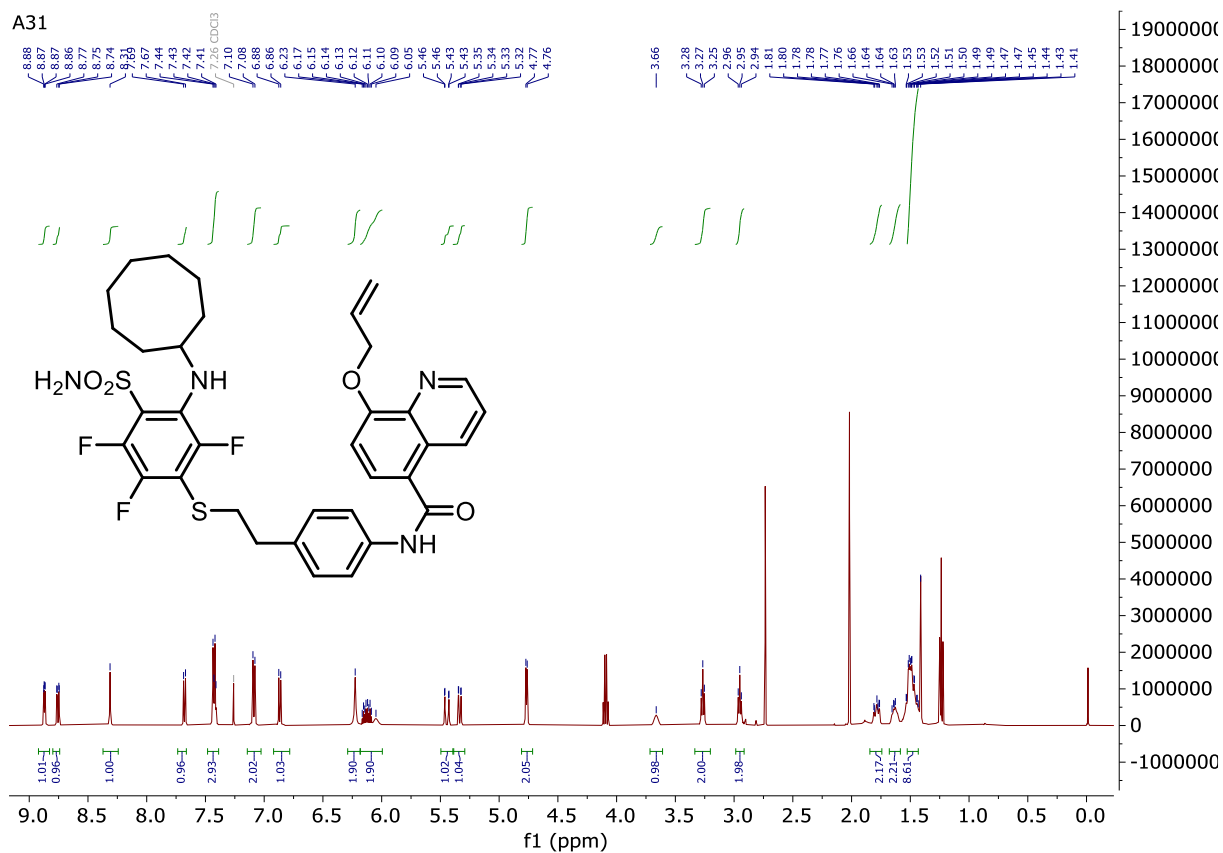
A29

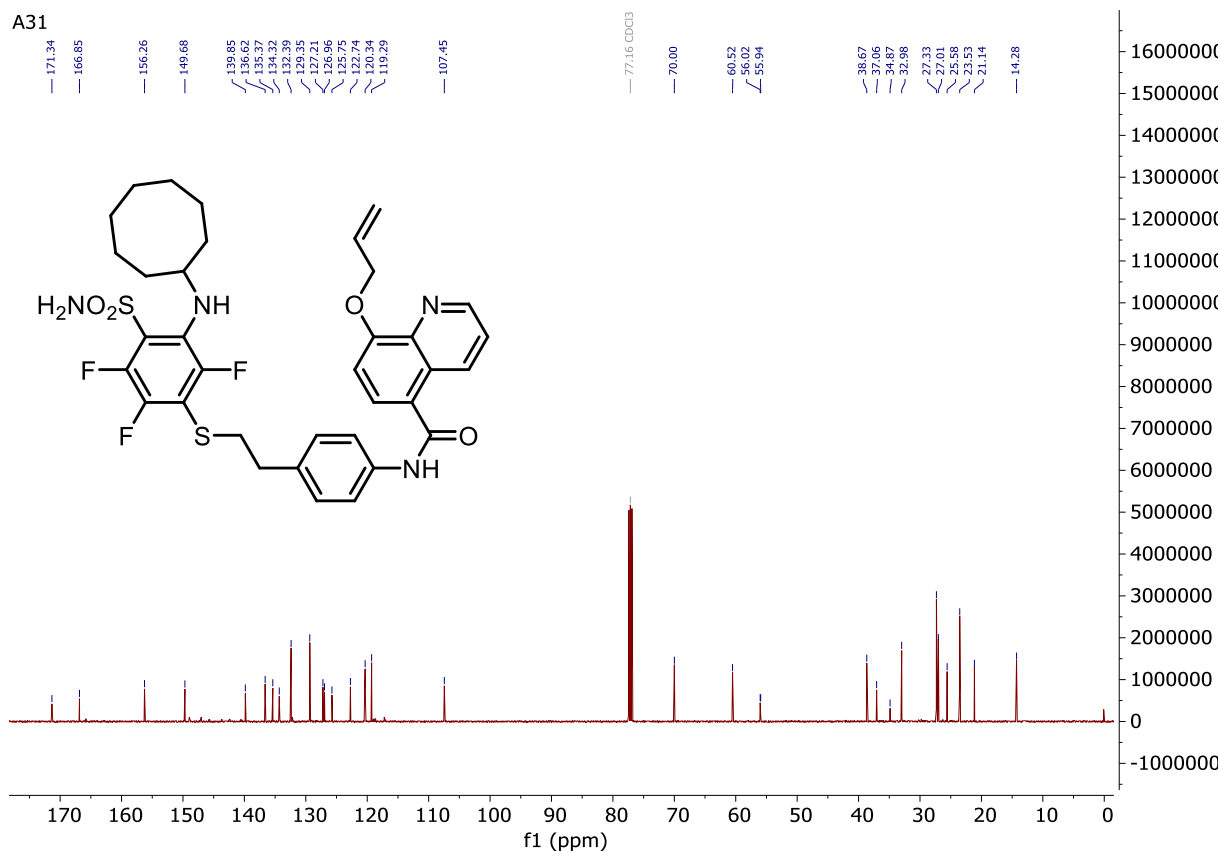


A29

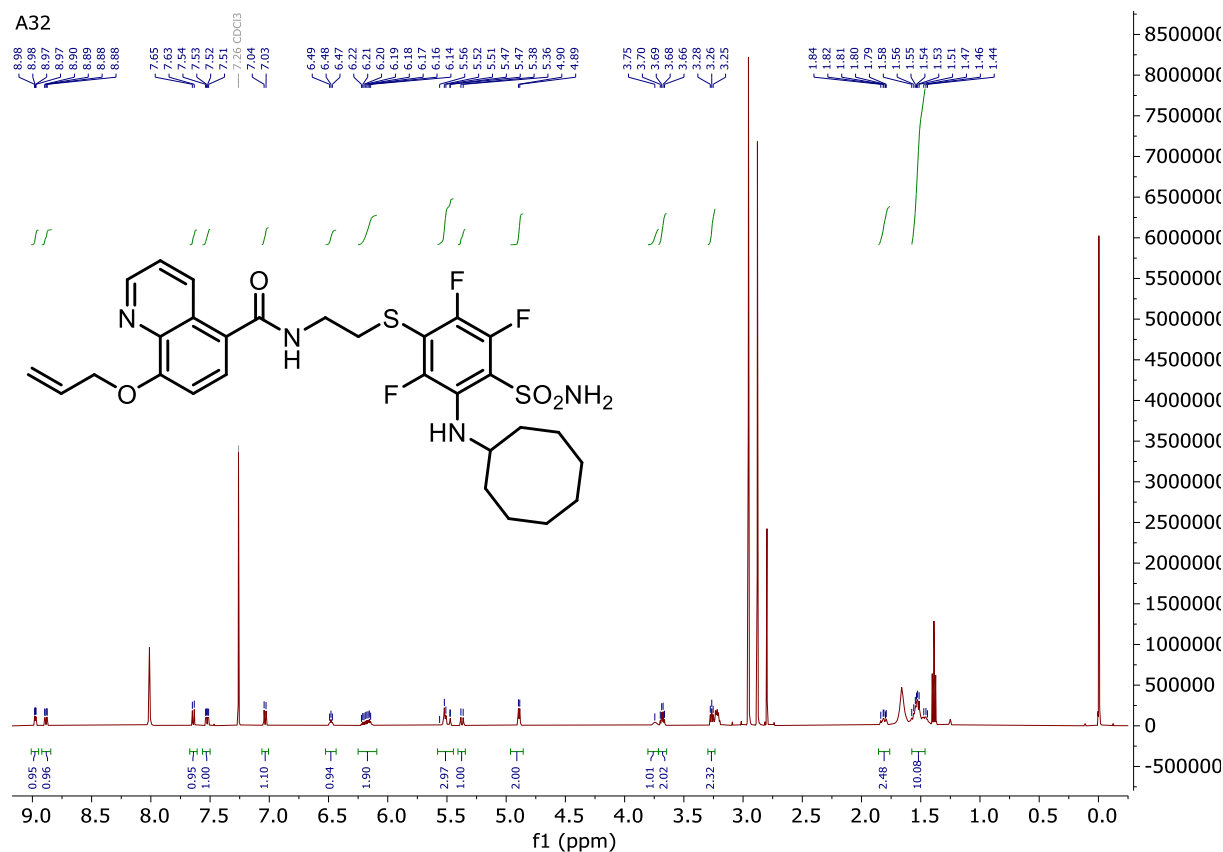


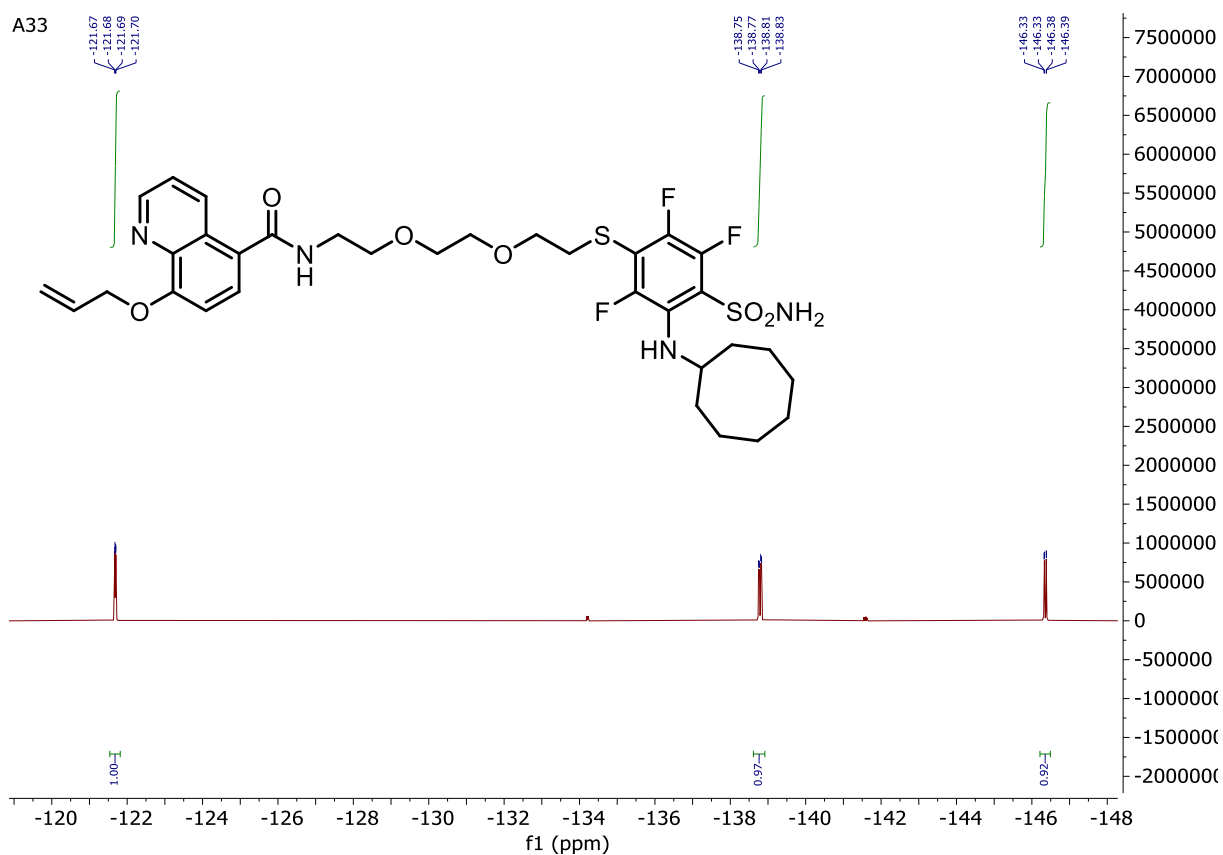
8-(Allyloxy)-*N*-(6-((3-(cyclooctylamino)-2,5,6-trifluoro-4-sulfamoylphenyl)thio)hexyl)quinoline-5-carboxamide (**A30**)

8-(Allyloxy)-*N*-(4-(2-((3-(cyclooctylamino)-2,5,6-trifluoro-4-sulfamoylphenyl)thio)ethyl)phenyl)quinoline-5-carboxamide (**A31**)

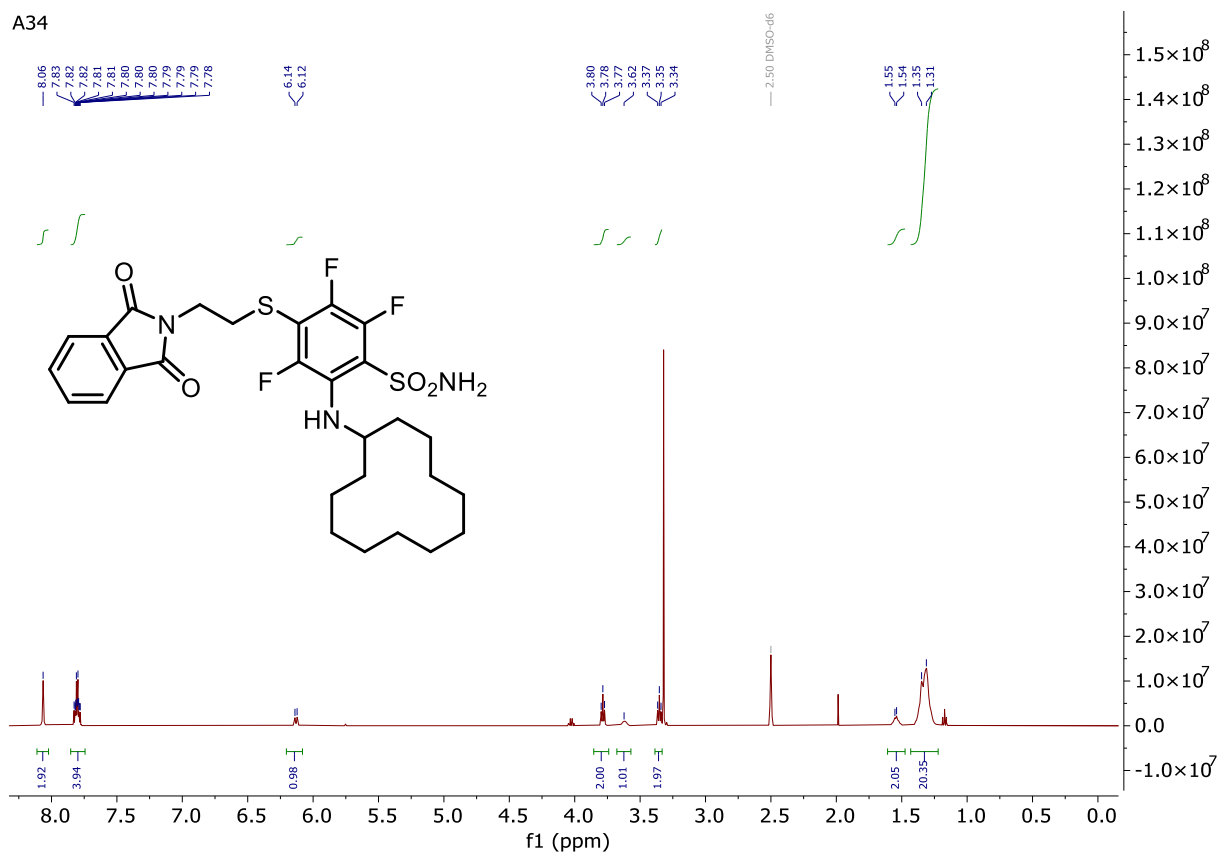


8-(Allyloxy)-*N*-(2-((3-(cyclooctylamino)-2,5,6-trifluoro-4-sulfamoylphenyl)thio)ethyl)quinoline-5-carboxamide (**A32**)



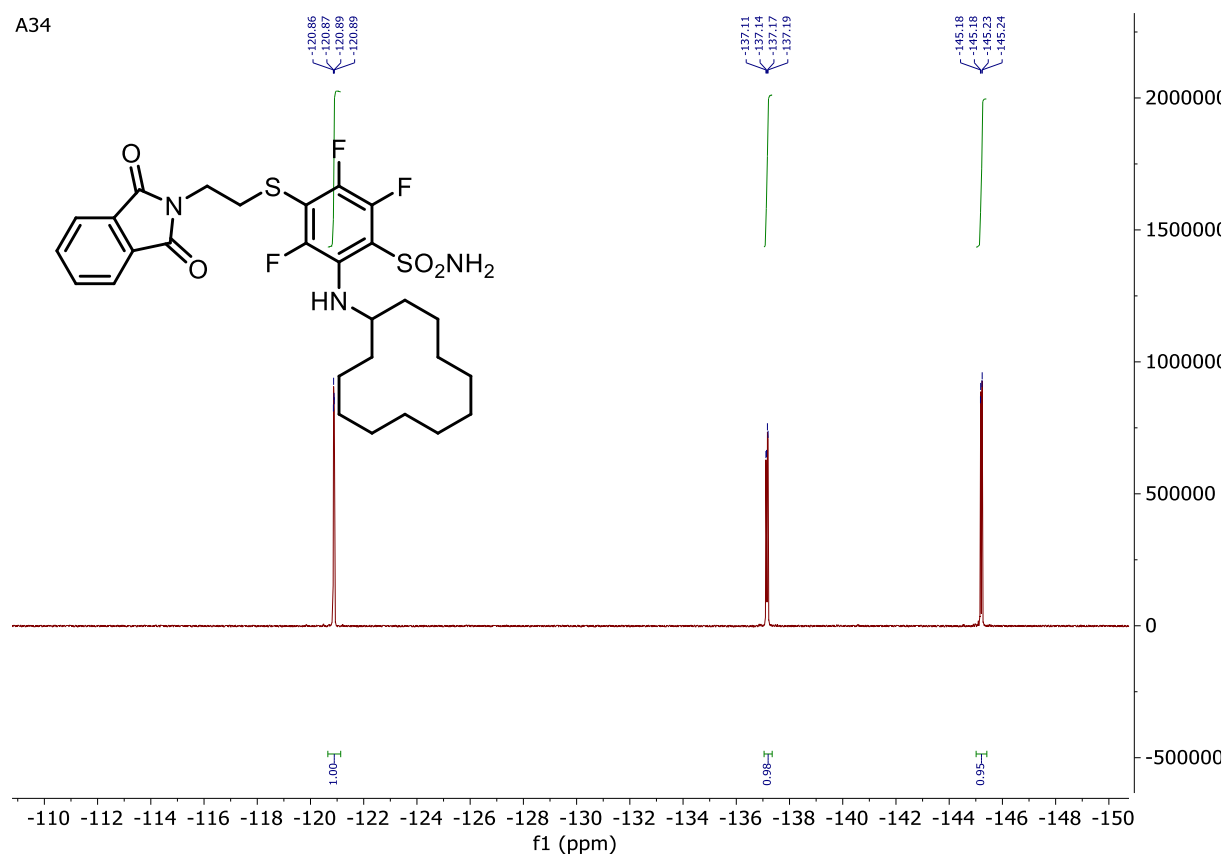


2-(Cyclododecylamino)-4-((2-(1,3-dioxoisindolin-2-yl)ethyl)thio)-3,5,6-trifluorobenzenesulfonamide (A34)

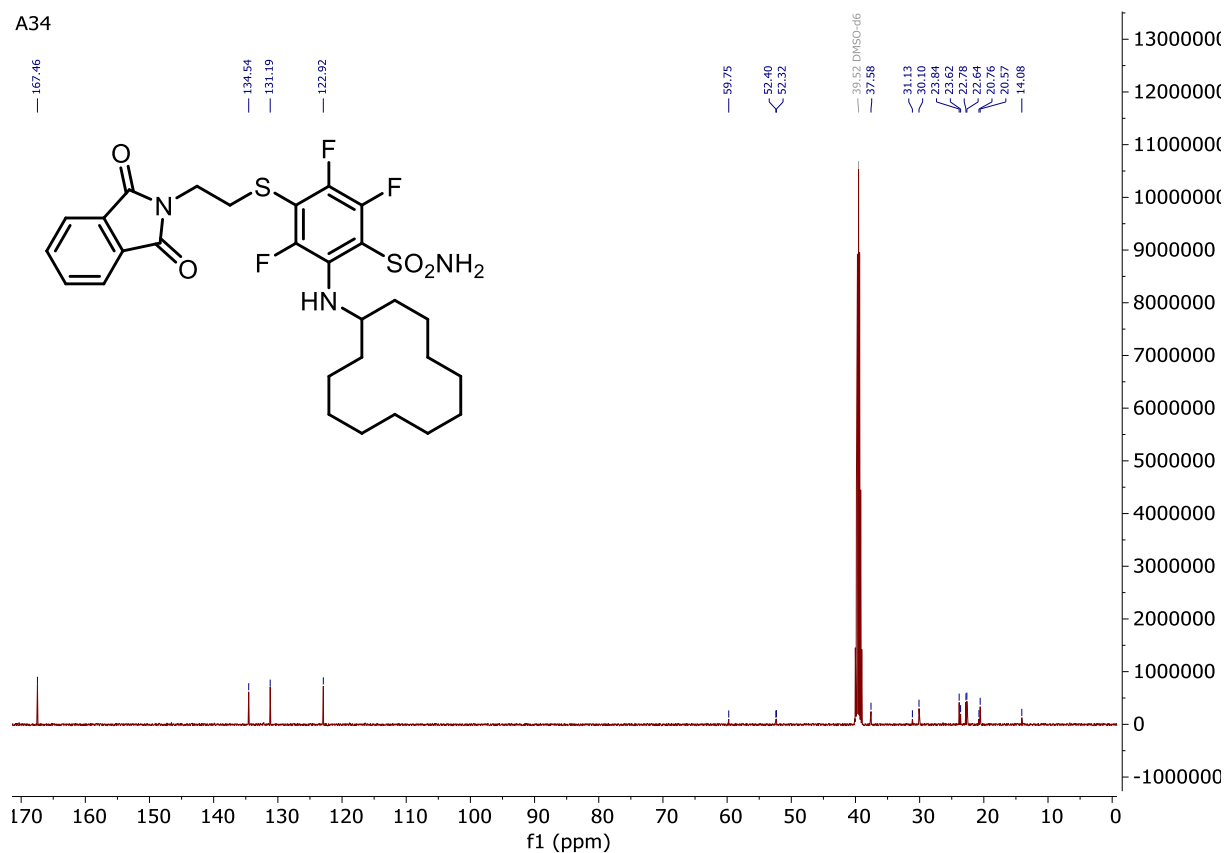


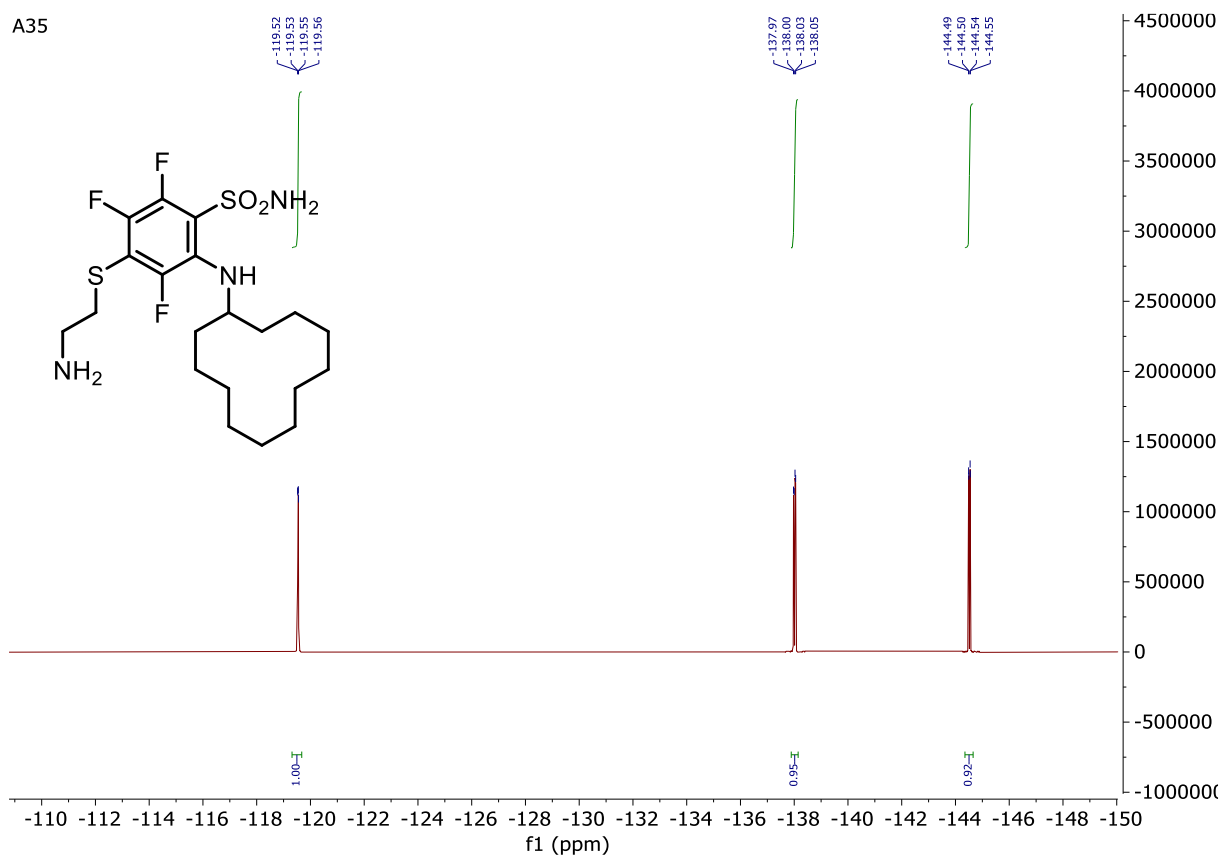
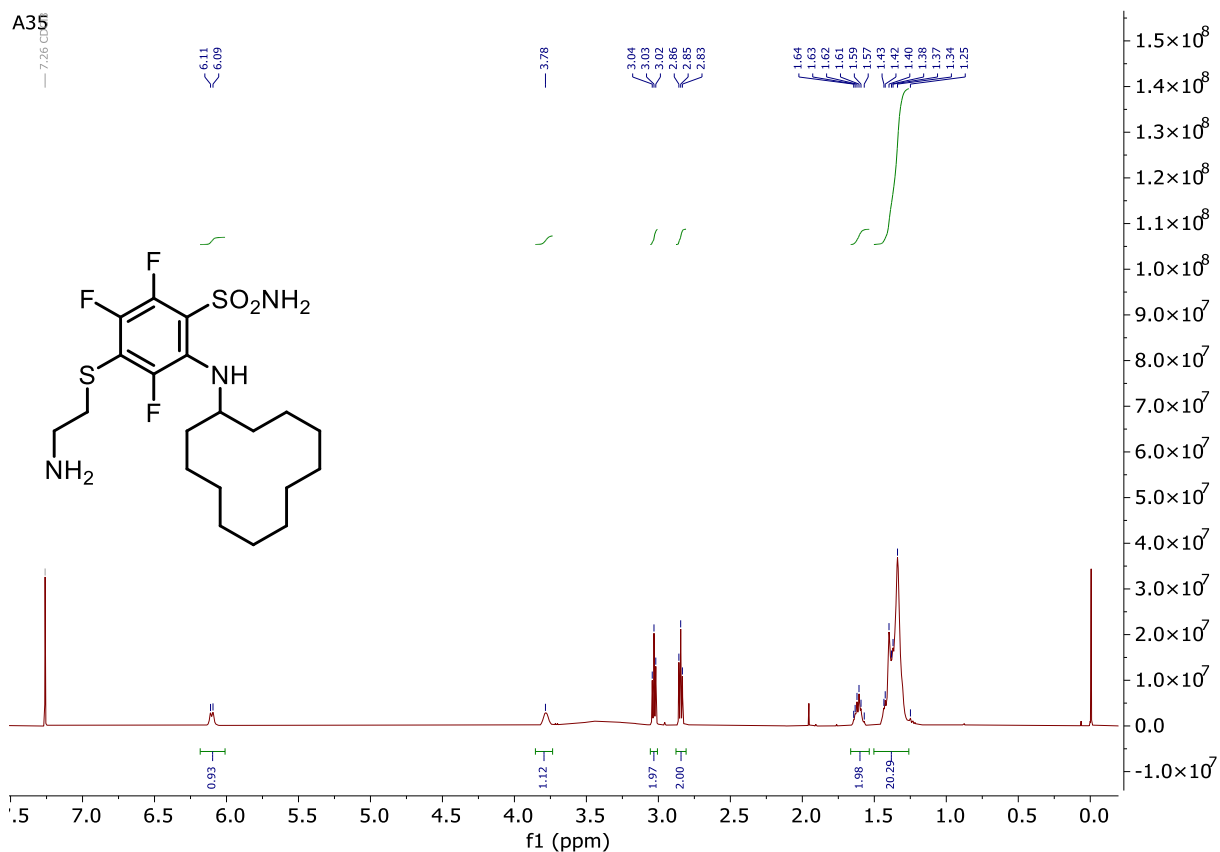
Appendix

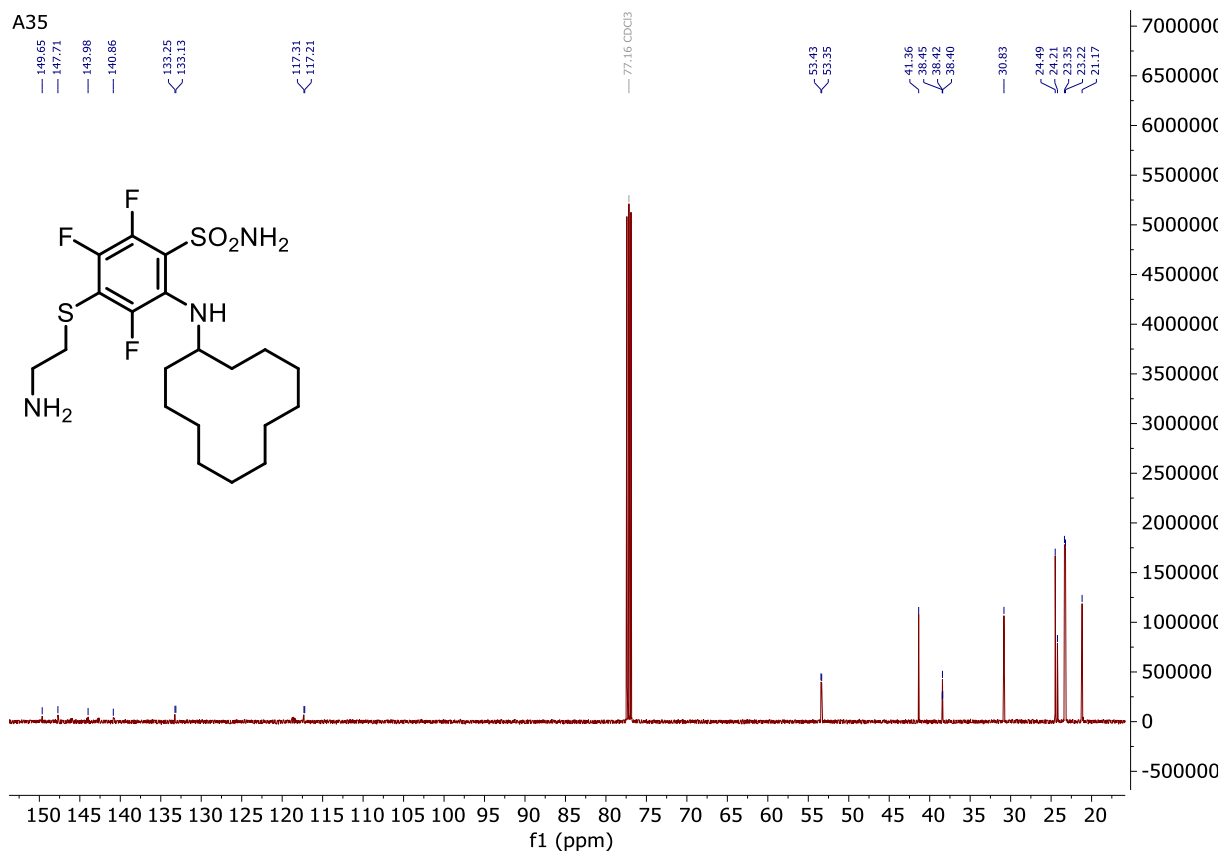
A34



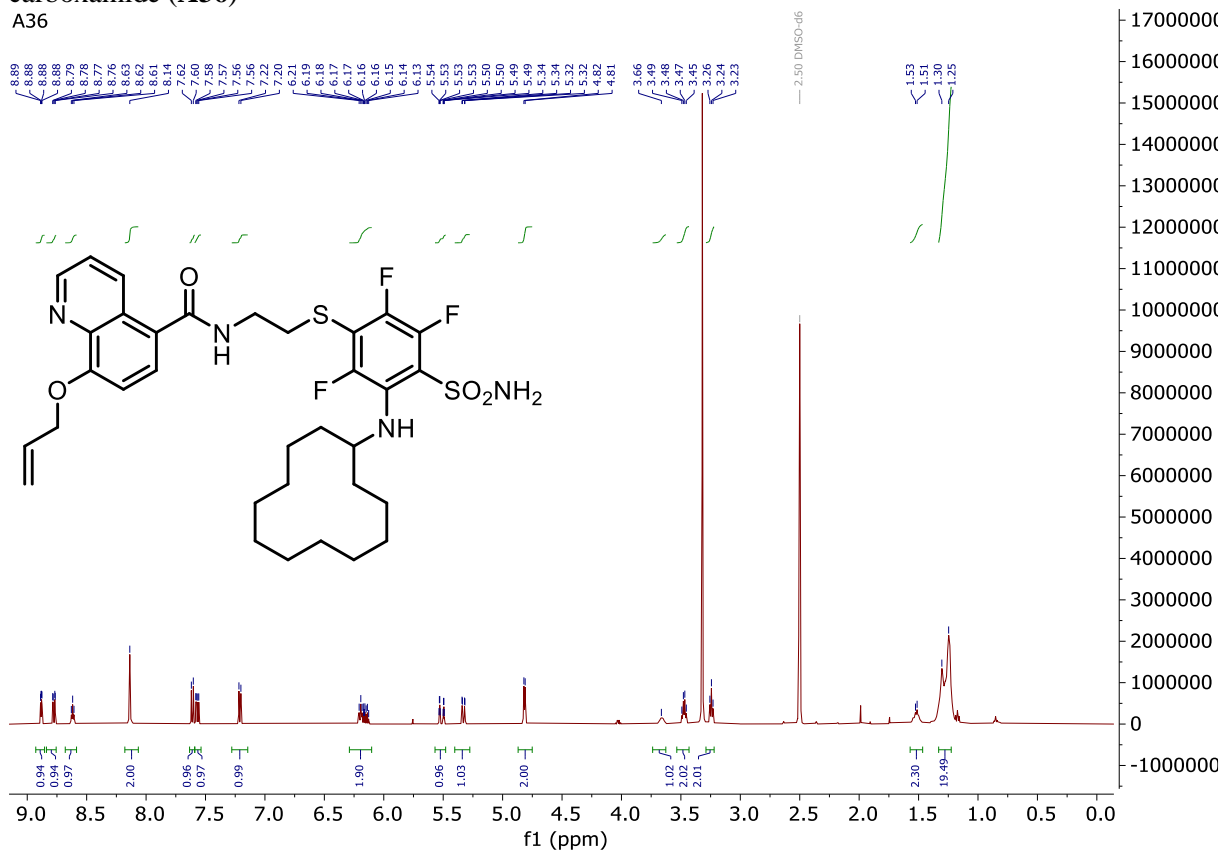
A34

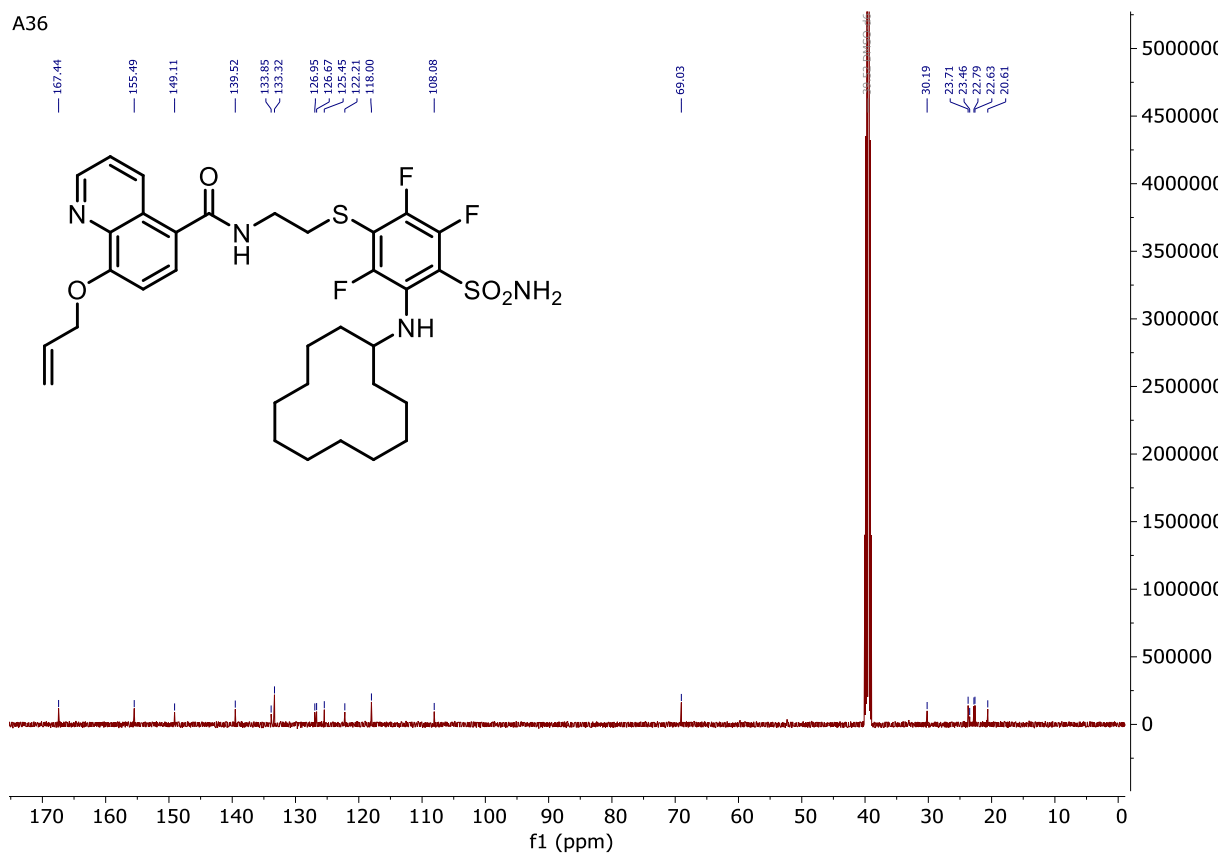
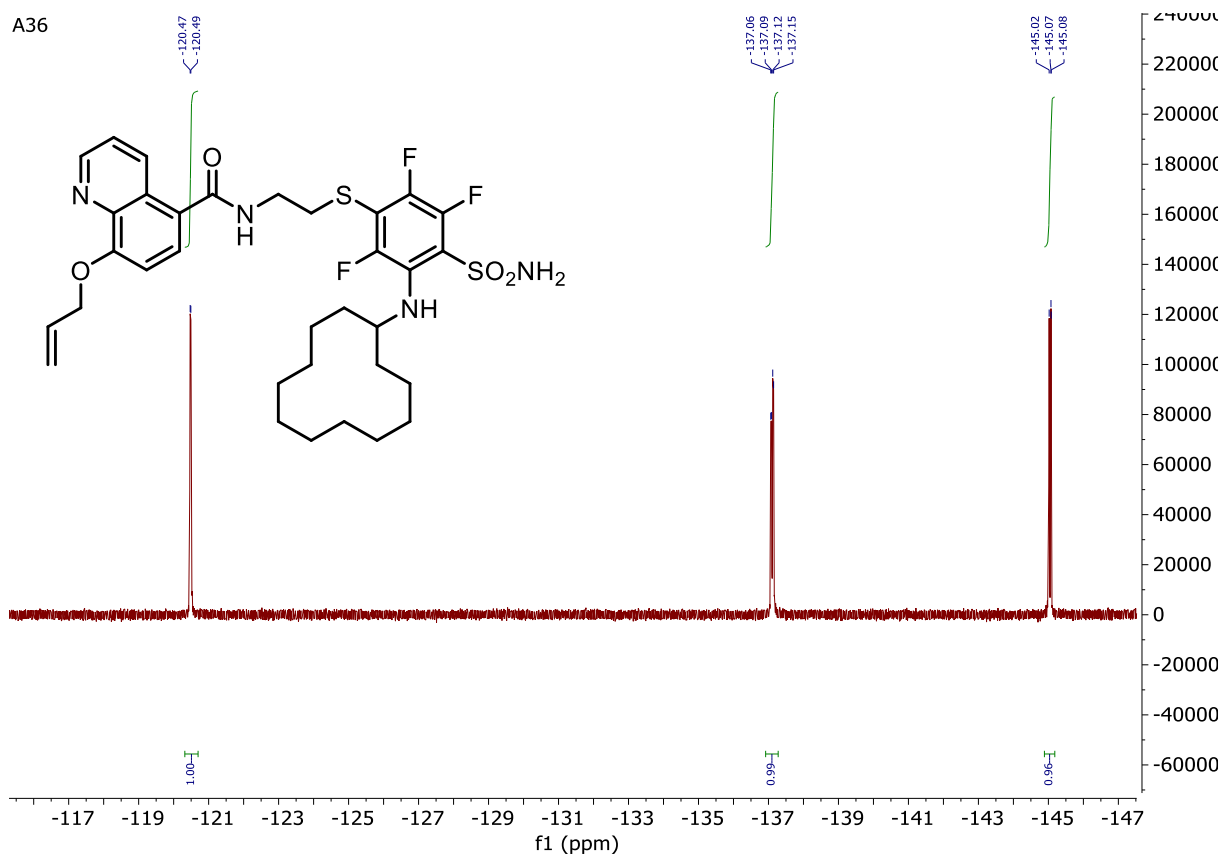


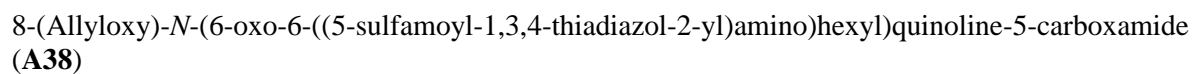
4-((2-Aminoethyl)thio)-2-(cyclododecylamino)-3,5,6-trifluorobenzenesulfonamide (**A35**)



8-(Allyloxy)-*N*-(2-((3-(cyclododecylamino)-2,5,6-trifluoro-4-sulfamoylphenyl)thio)ethyl)quinoline-5-carboxamide (**A36**)

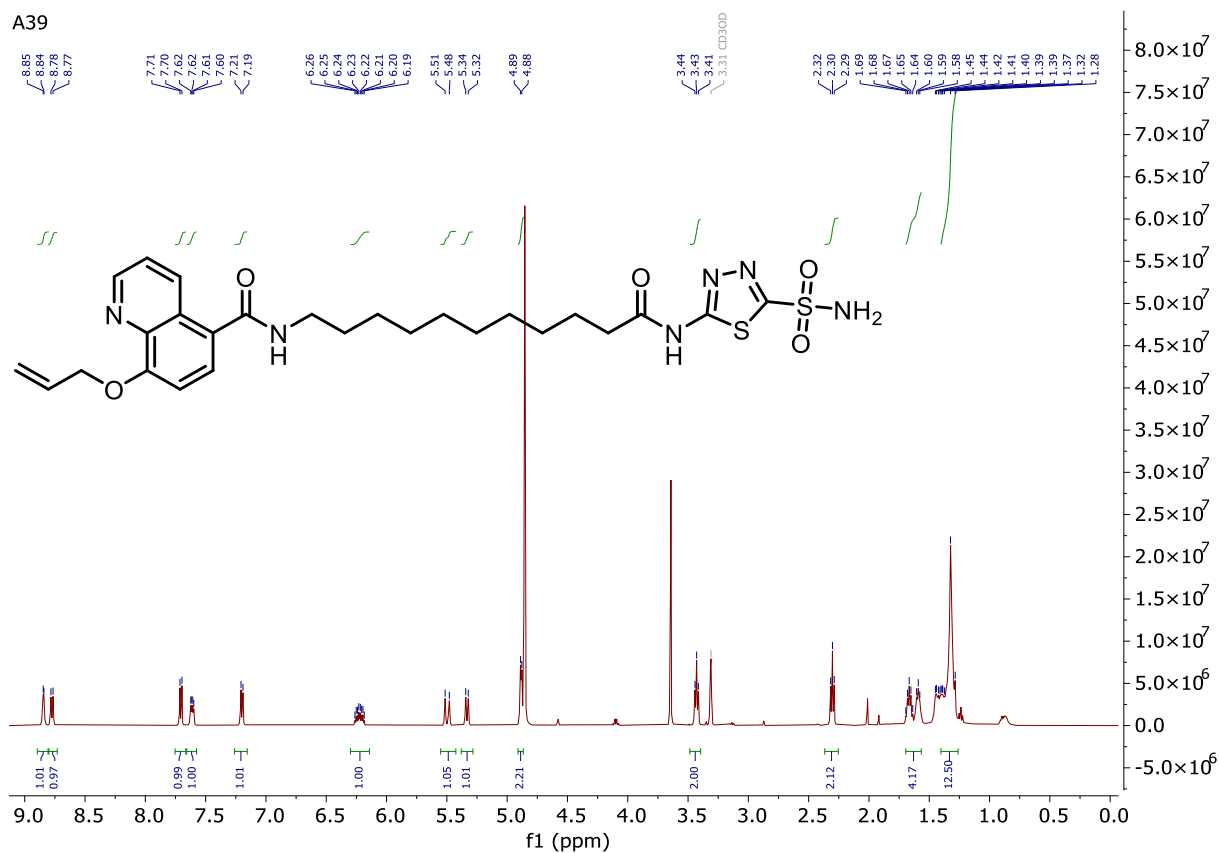




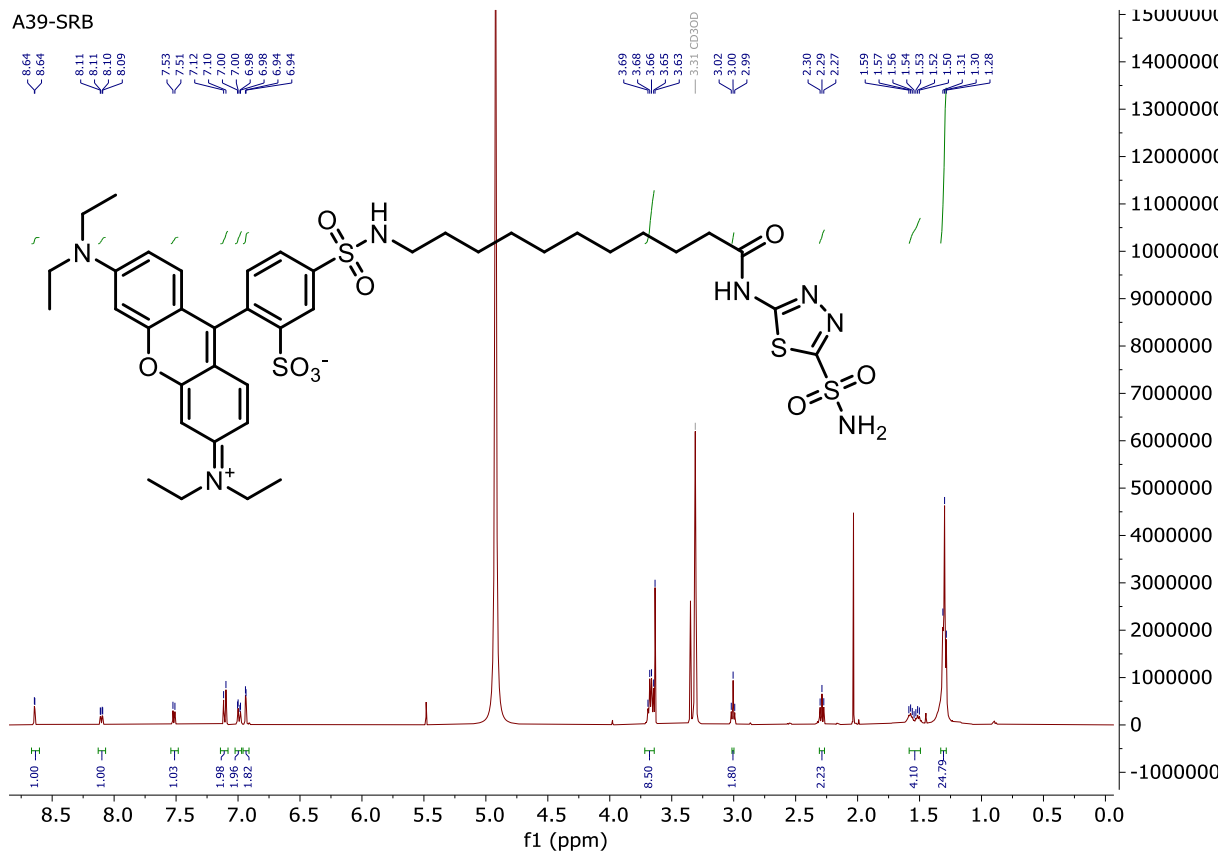


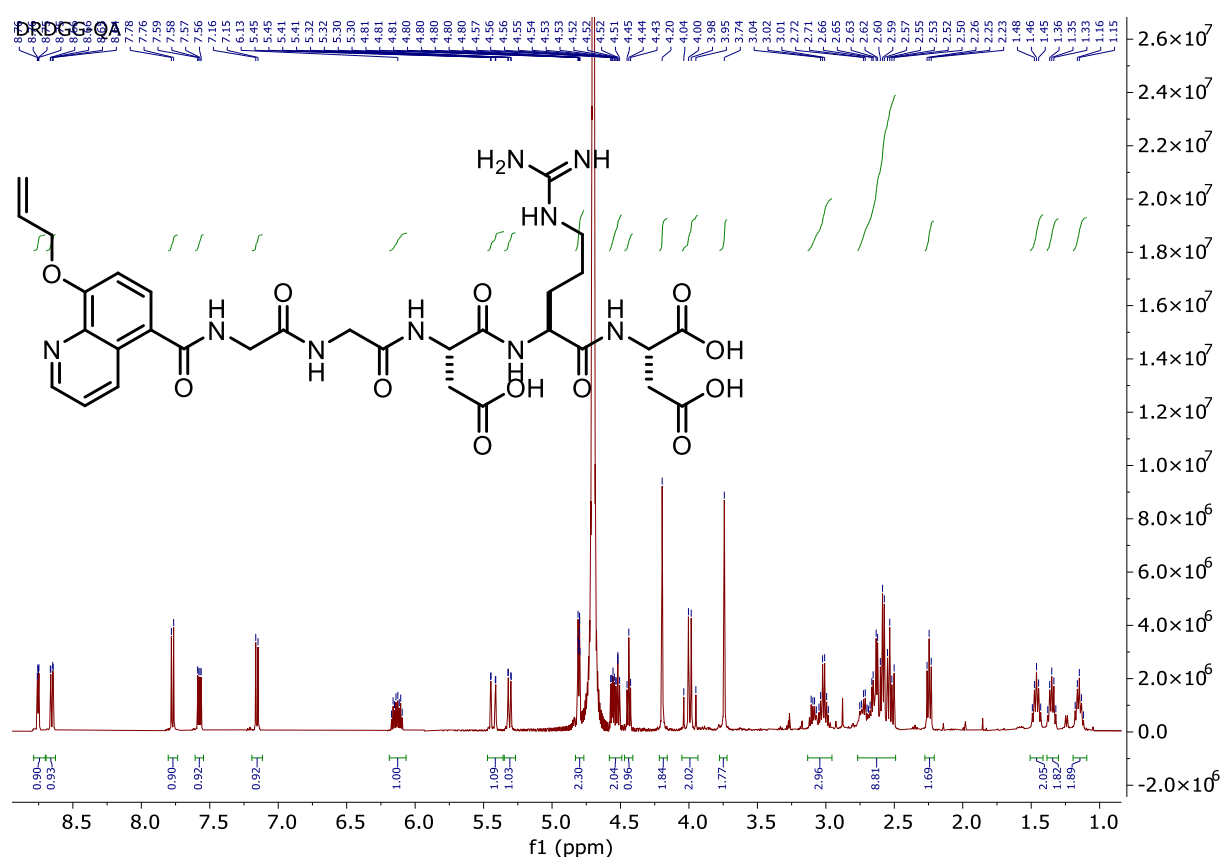
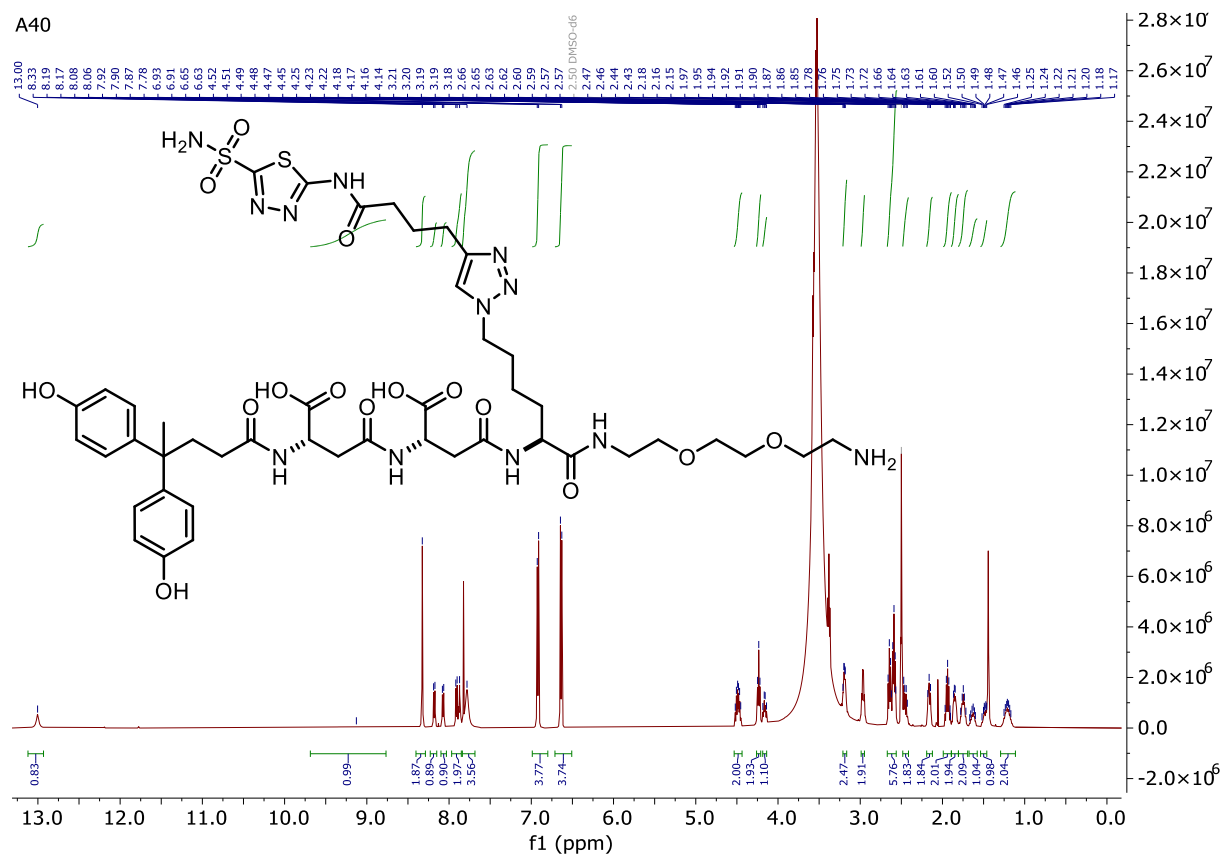
8-(Allyloxy)-*N*-(11-oxo-11-((5-sulfamoyl-1,3,4-thiadiazol-2-yl)amino)undecyl)quinoline-5-carboxamide (**A39**)

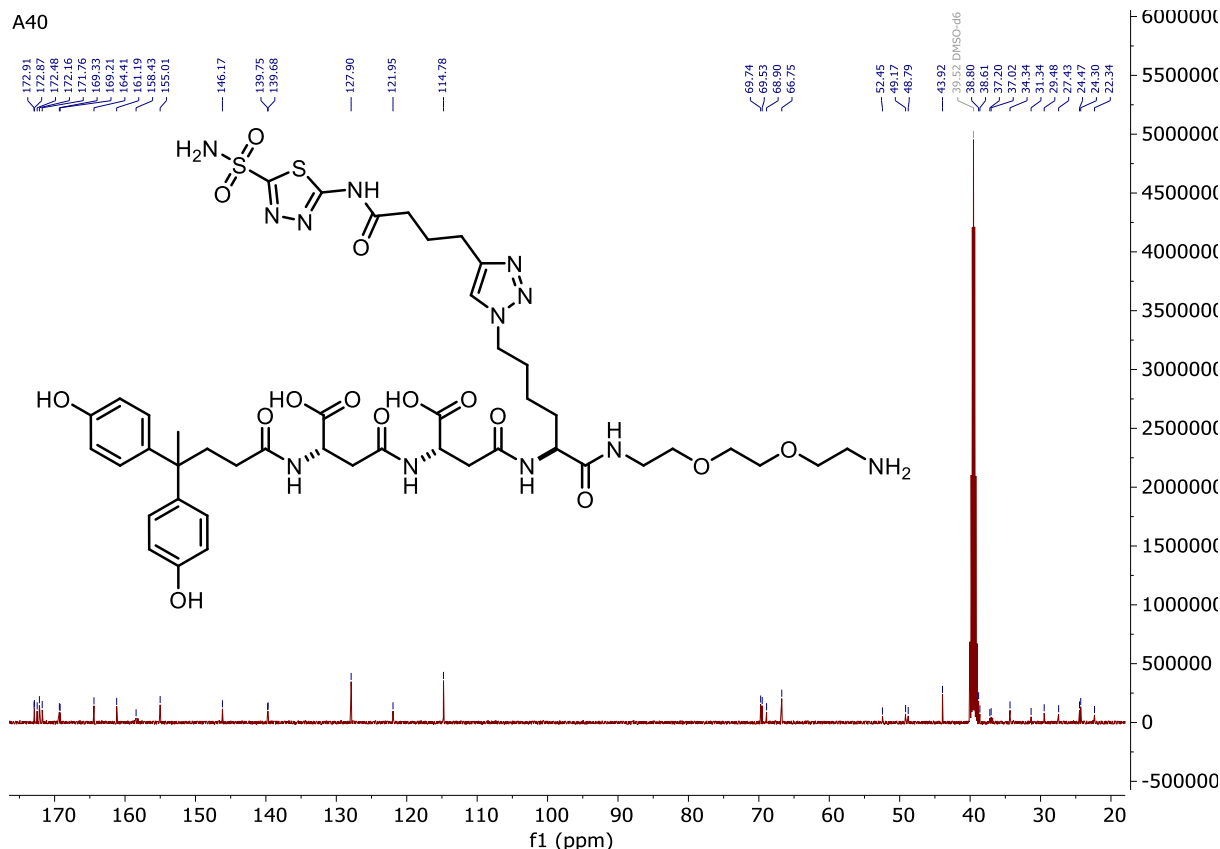
A39

2-(6-(Diethylamino)-3-(diethyliminio)-3*H*-xanthen-9-yl)-5-(*N*-(11-oxo-11-((5-sulfamoyl-1,3,4-thiadiazol-2-yl)amino)undecyl)sulfamoyl)benzenesulfonate (**A39-SRB**)

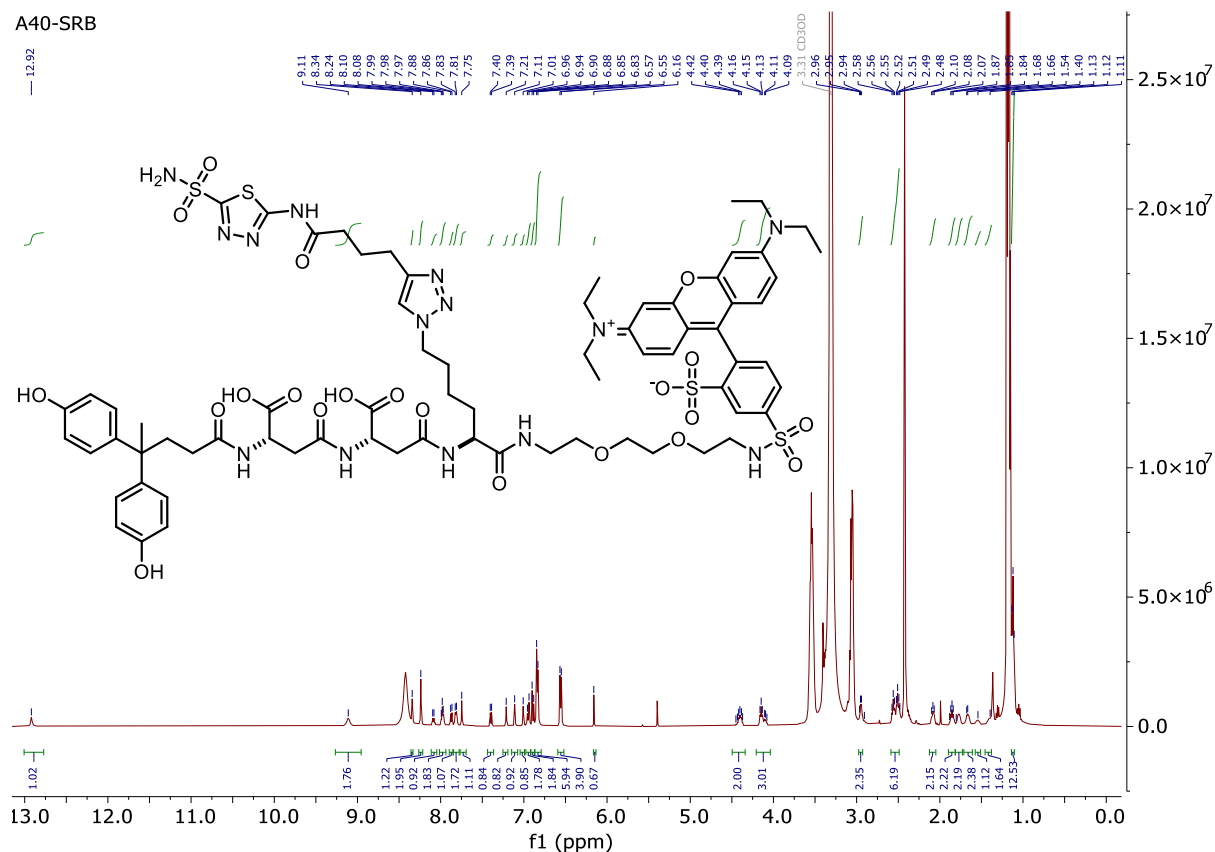
A39-SRB



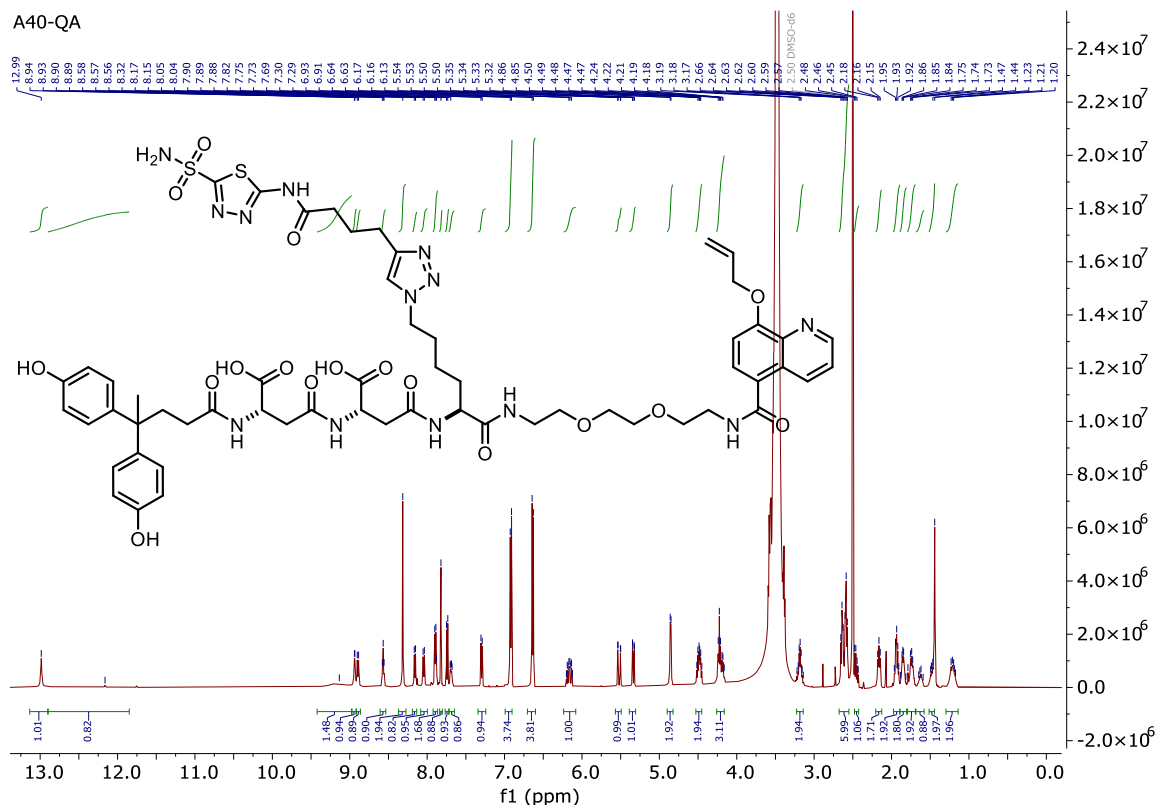
(8-Allyloxy)quinoline-5-carbonyl)glycylglycyl-*L*-aspartyl-*L*-arginyl-*L*-aspartic acid (**DRDGG-QA**)*N*⁴-((*S*)-1-((2-(2-(2-aminoethoxy)ethoxy)ethyl)amino)-1-oxo-6-(4-(4-oxo-4-((5-sulfamoyl-1,3,4-thiadiazol-2-yl)amino)butyl)-1*H*-1,2,3-triazol-1-yl)hexan-2-yl)-*N*²-((*S*)-3-(4,4-bis(4-hydroxyphenyl)pentanamido)-3-carboxypropanoyl)-*L*-asparagine (**A40**)



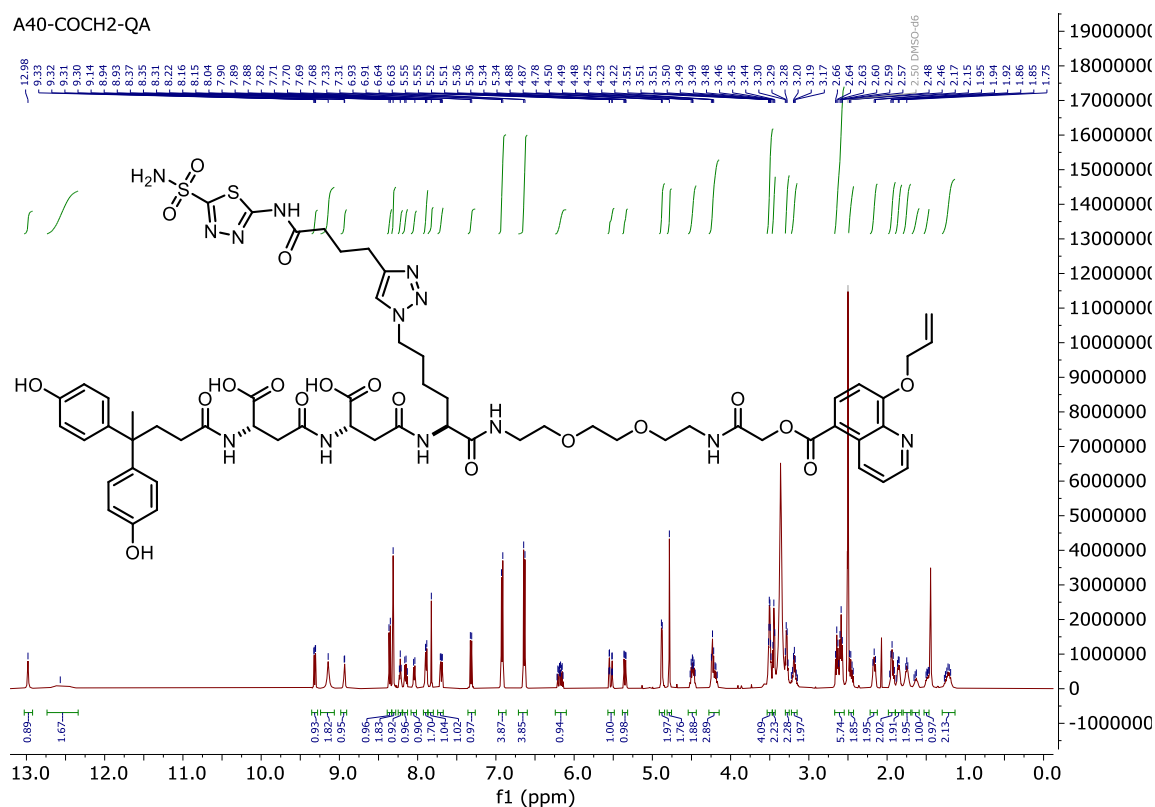
5-(*N*-((1*S*,15*S*,19*S*)-15,19-Dicarboxy-24,24-bis(4-hydroxyphenyl)-10,13,17,21-tetraoxo-11-(4-(4-oxo-4-((5-sulfamoyl-1,3,4-thiadiazol-2-yl)amino)butyl)-1*H*-1,2,3-triazol-1-yl)butyl)-3,6-dioxo-9,12,16,20-tetraazapentacosyl)sulfamoyl)-2-(6-(diethylamino)-3-(diethyliminio)-3*H*-xanthen-9-yl)benzenesulfonate (**A40-SRB**)



N^4 -((*S*)-1-(8-(Allyloxy)quinolin-5-yl)-1,12-dioxo-17-(4-(4-oxo-4-((5-sulfamoyl-1,3,4-thiadiazol-2-yl)amino)butyl)-1*H*-1,2,3-triazol-1-yl)-5,8-dioxo-2,11-diazaheptadecan-13-yl)- N^2 -((*S*)-3-(4,4-bis(4-hydroxyphenyl)pentanamido)-3-carboxypropanoyl)-*L*-asparagine (**A40-QA**)

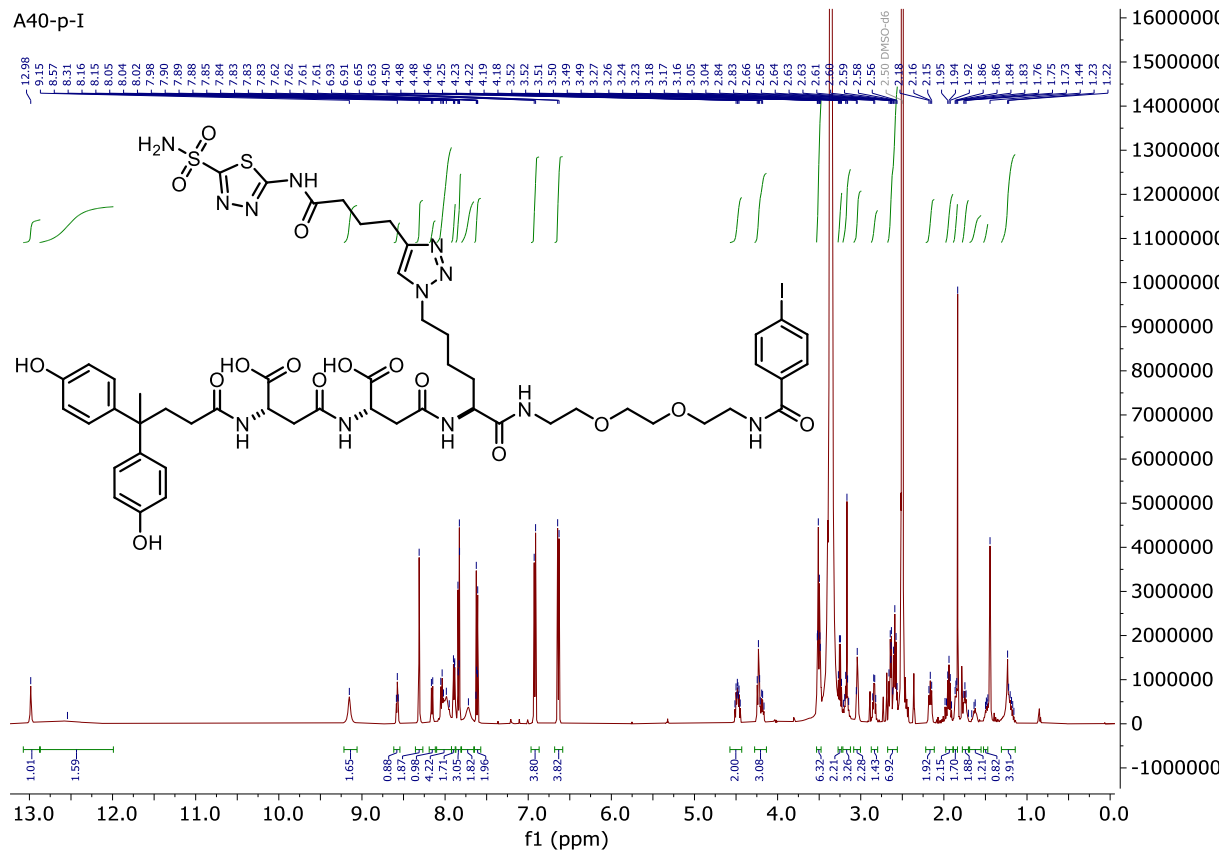


N^4 -((*S*)-1-(8-(allyloxy)quinolin-5-yl)-1,4,15-trioxo-20-(4-(4-oxo-4-((5-sulfamoyl-1,3,4-thiadiazol-2-yl)amino)butyl)-1*H*-1,2,3-triazol-1-yl)-2,8,11-trioxo-5,14-diazaicosan-16-yl)- N^2 -((*S*)-3-(4,4-bis(4-hydroxyphenyl)pentanamido)-3-carboxypropanoyl)-*L*-asparagine (**A40-COCH₂-QA**)

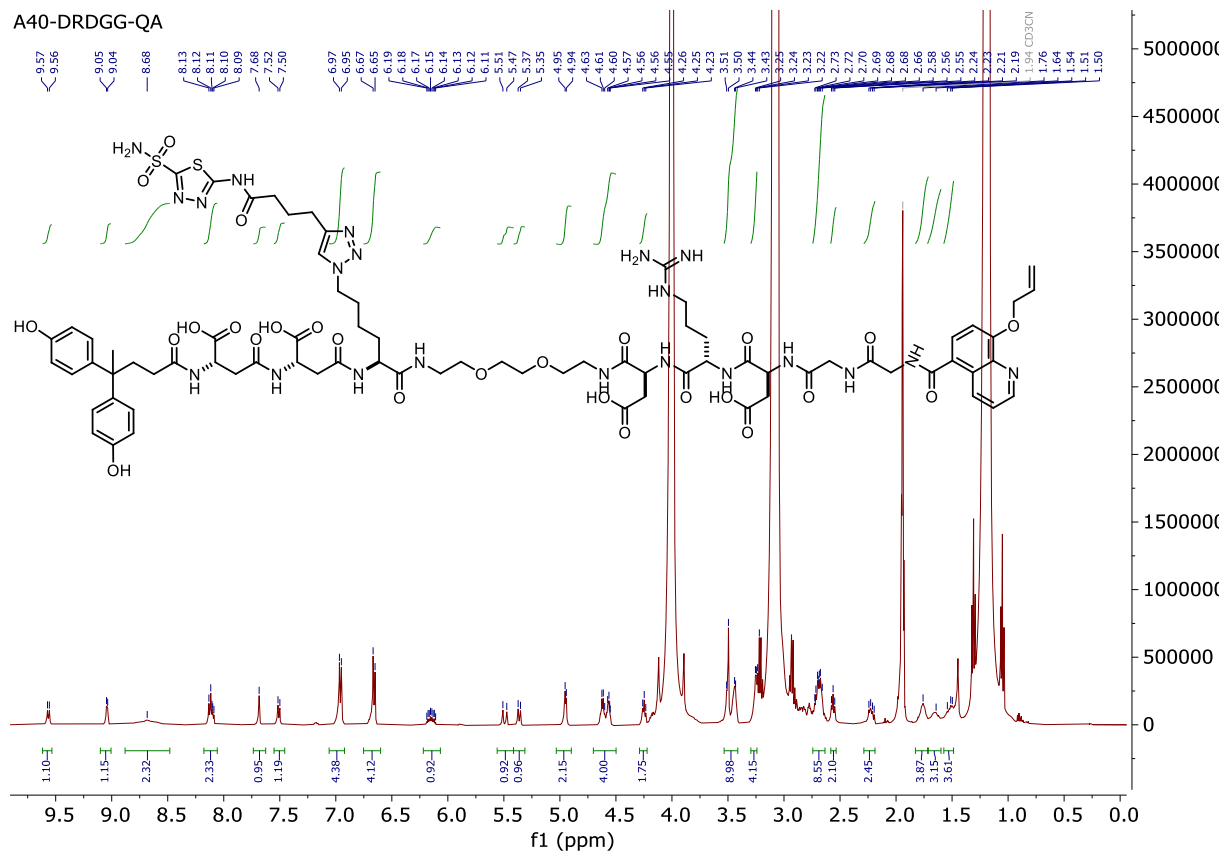


Appendix

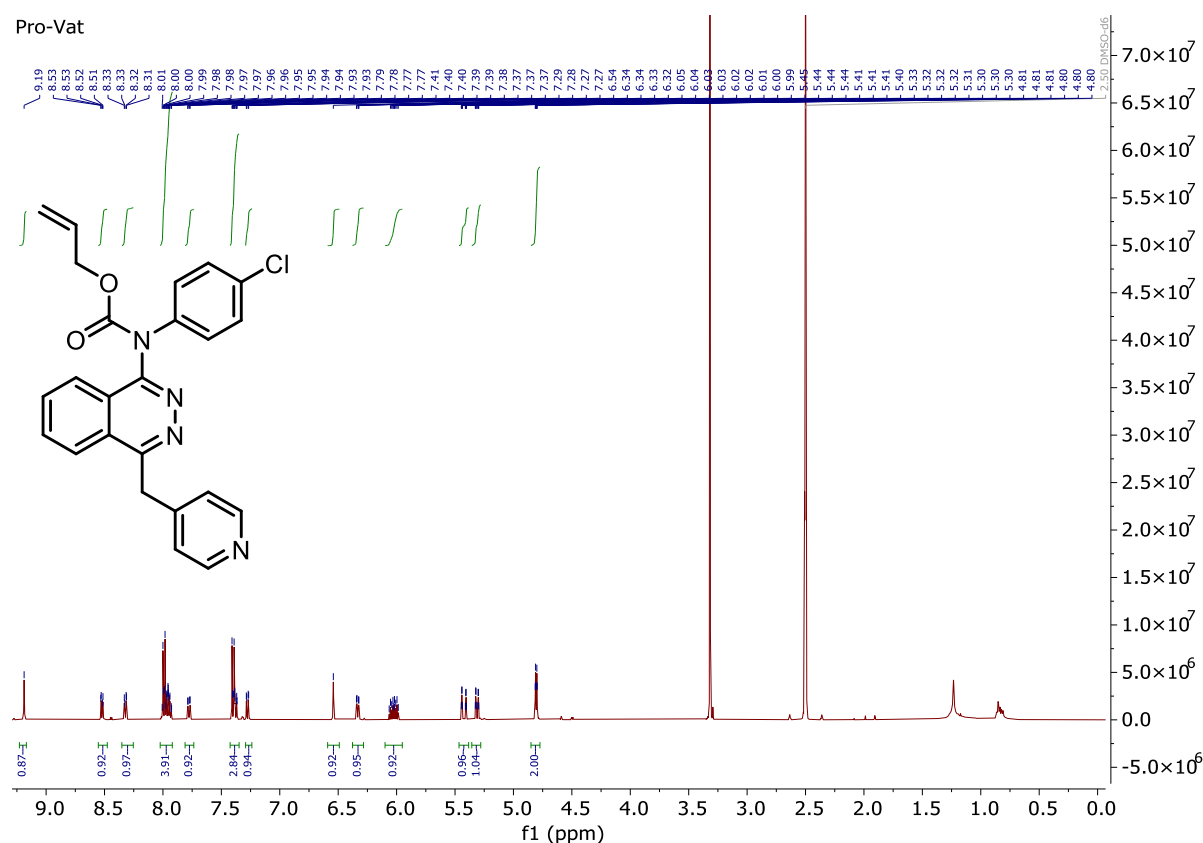
*N*²-(4,4-Bis(4-hydroxyphenyl)pentanoyl)-*N*⁴-((*S*)-1-carboxy-3-(((*S*)-1-(4-iodophenyl)-1,12-dioxo-17-(4-(4-oxo-4-((5-sulfamoyl-1,3,4-thiadiazol-2-yl)amino)butyl)-1*H*-1,2,3-triazol-1-yl)-5,8-dioxa-2,11-diazaheptadecan-13-yl)amino)-3-oxopropyl)-*L*-asparagine (**A40-p-I**)



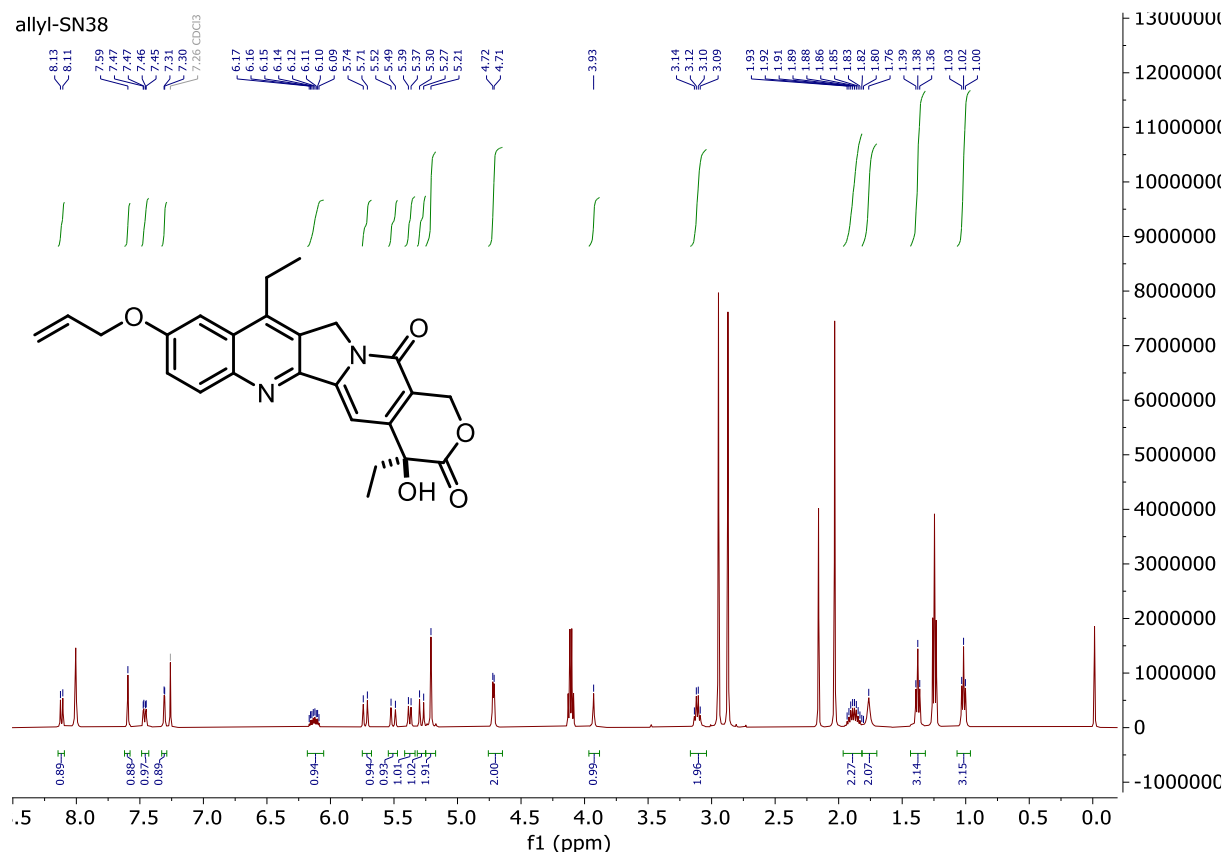
A40-DRDGG-QA



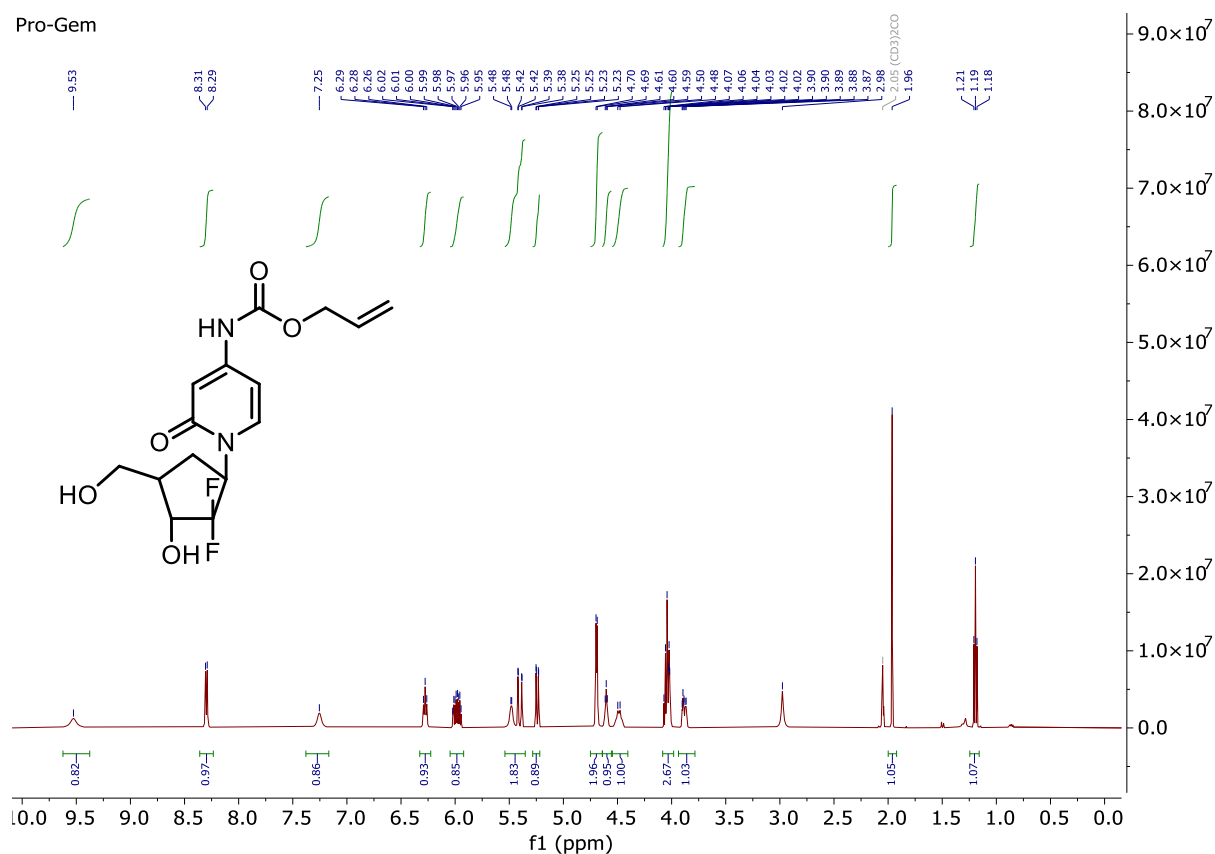
Allyl (4-chlorophenyl)(4-(pyridin-4-ylmethyl)phthalazin-1-yl)carbamate (**Pro-Vat**)



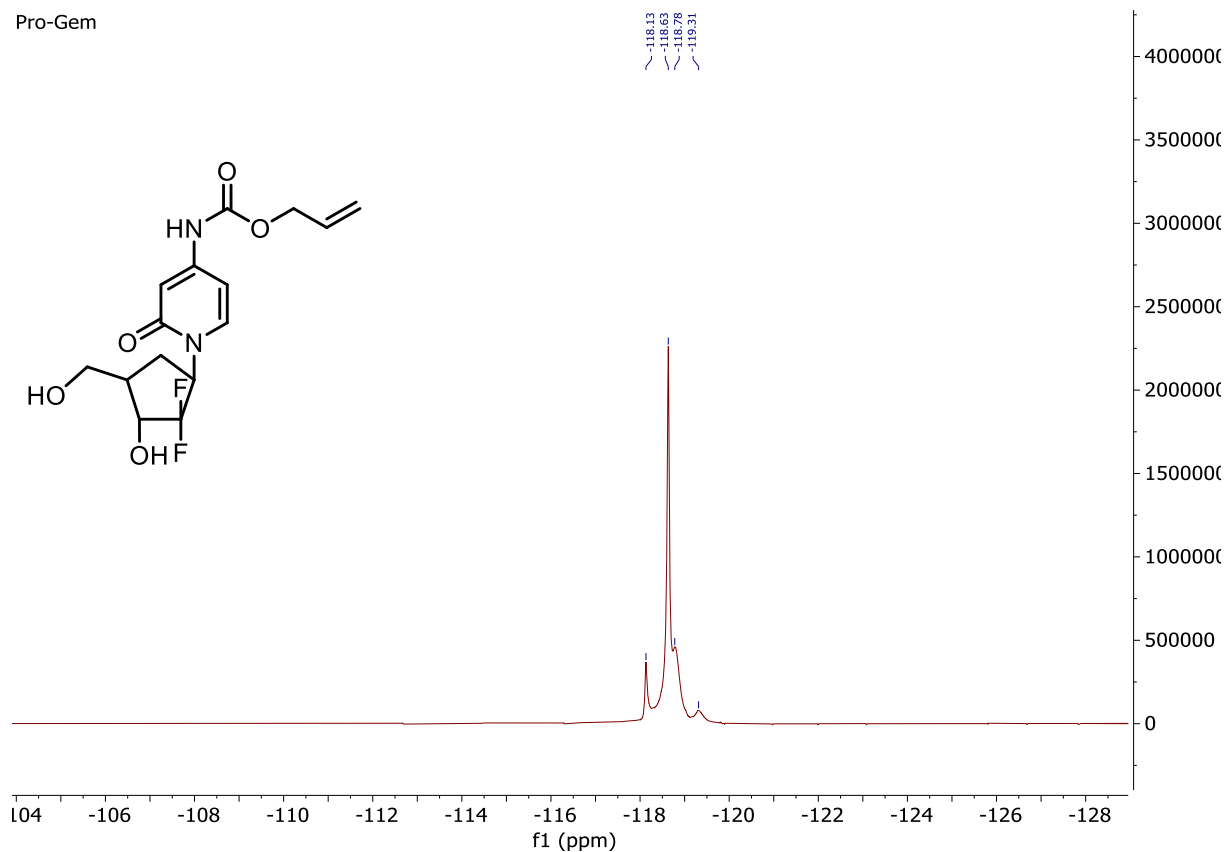
(*S*)-9-(allyloxy)-4,11-diethyl-4-hydroxy-1,12-dihydro-14*H*-pyrano[3',4':6,7]indolizino[1,2-*b*]quinoline-3,14(4*H*)-dione (**allyl-SN38**)



Allyl (1-((1*R*,3*R*,4*R*)-2,2-difluoro-3-hydroxy-4-(hydroxymethyl)cyclopentyl)-2-oxo-1,2-dihydropyridin-4-yl)carbamate (**Pro-Gem**)

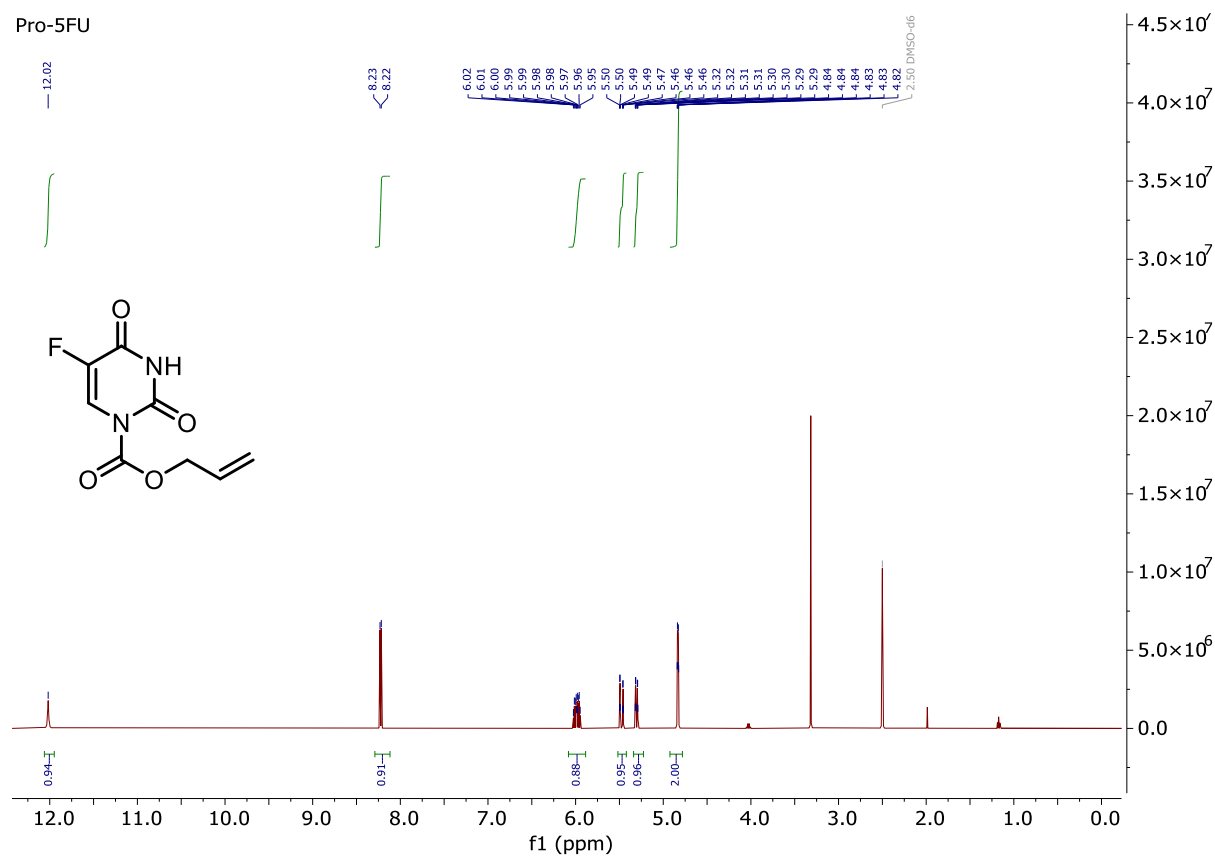


Pro-Gem



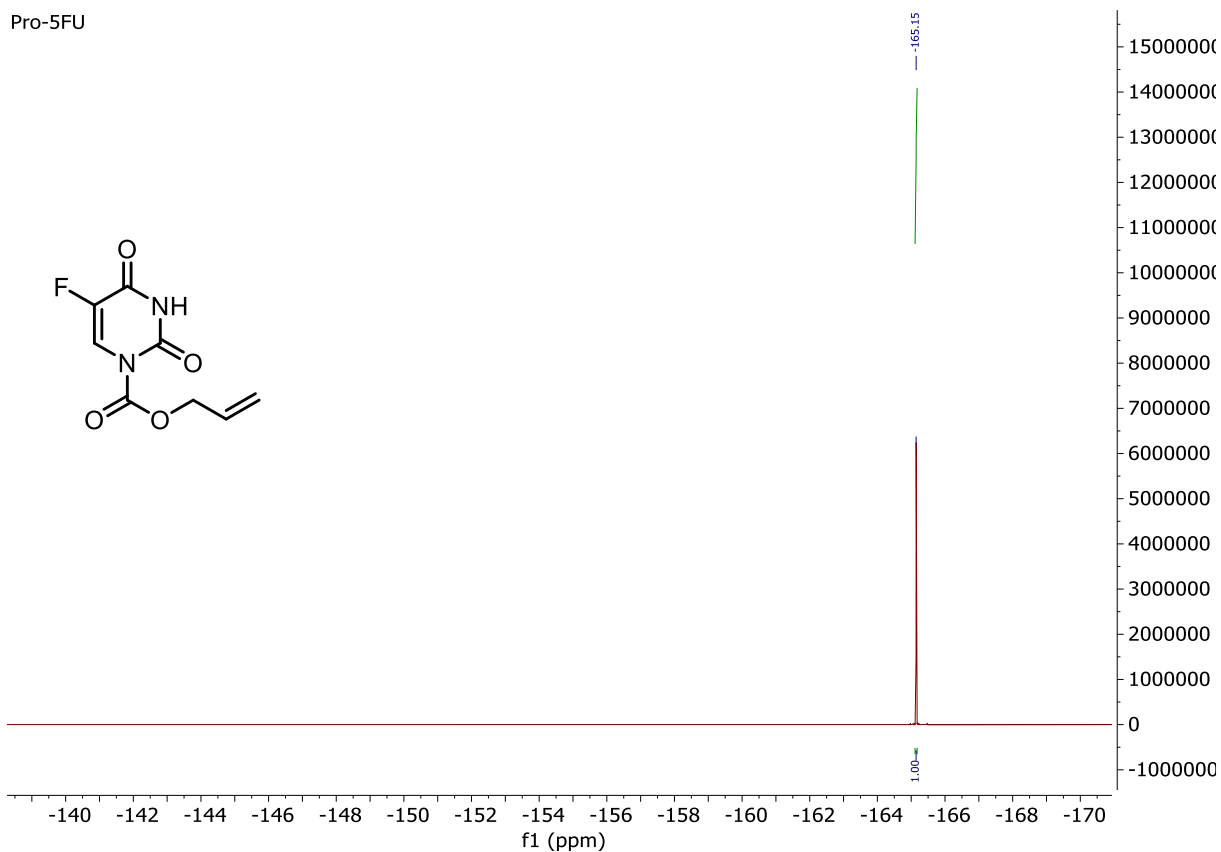
Allyl 5-fluoro-2,4-dioxo-3,4-dihydropyrimidine-1(2H)-carboxylate (**Pro-5FU**)

Pro-5FU

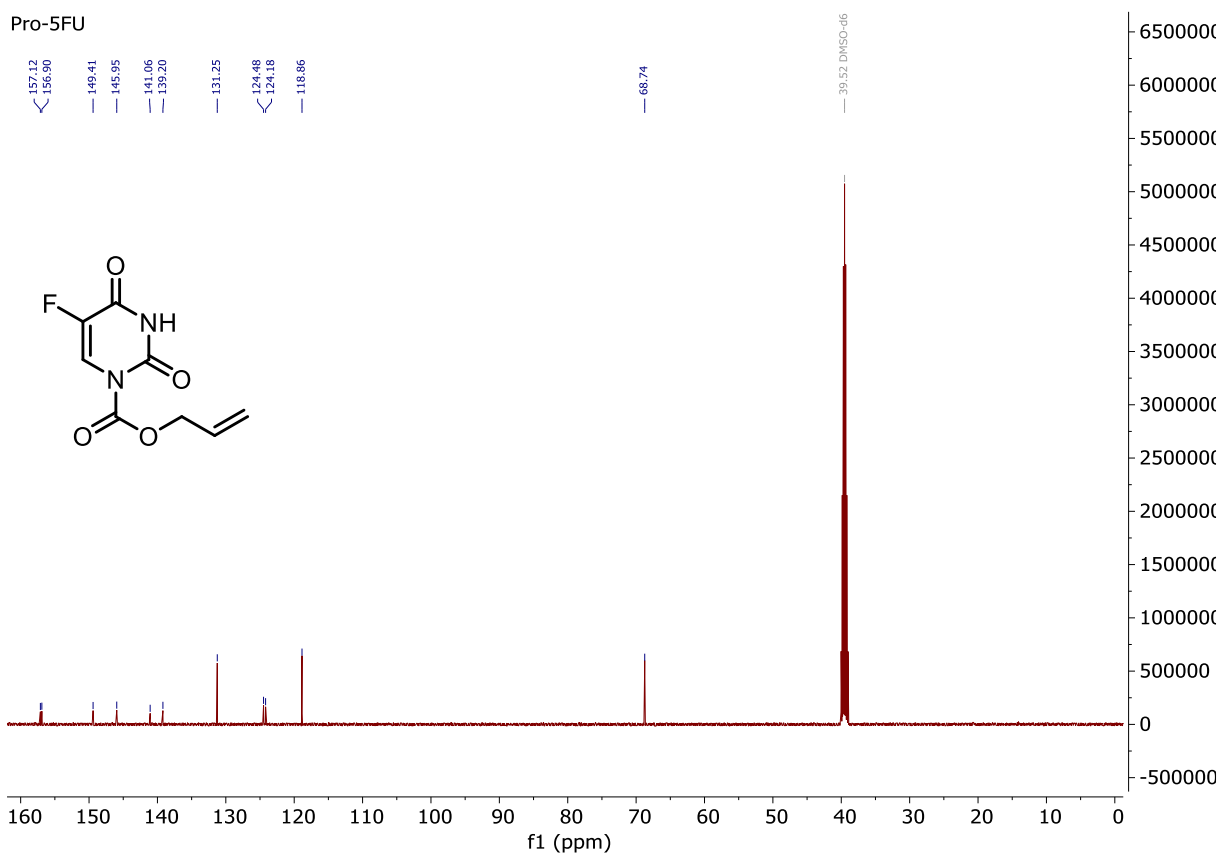


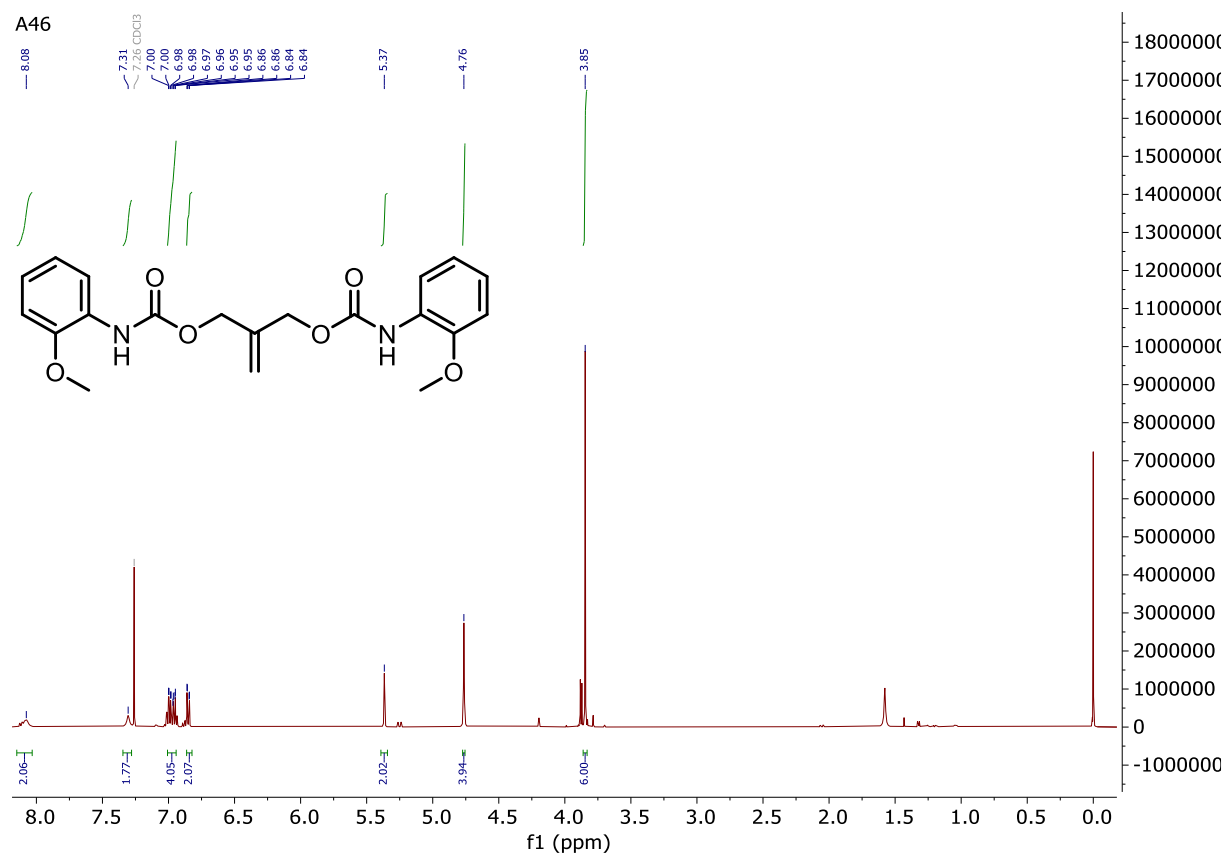
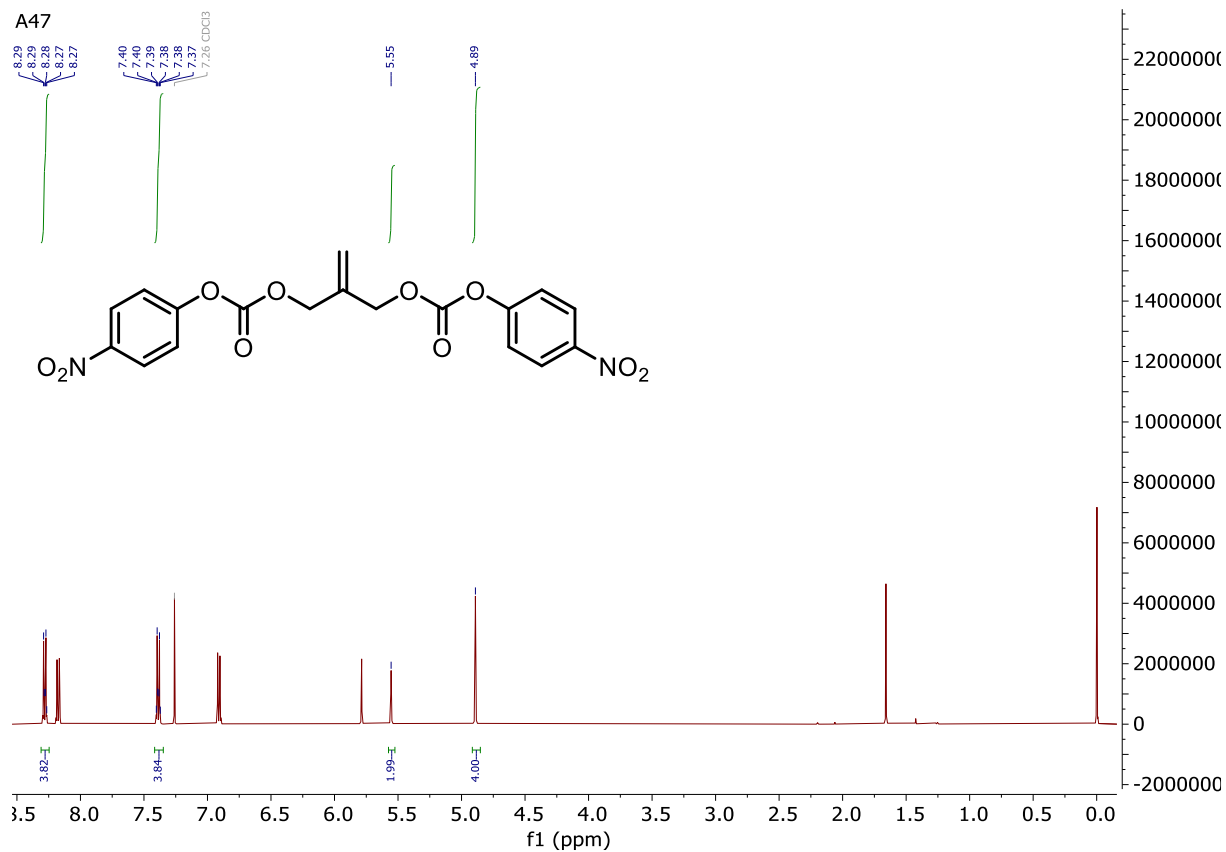
Appendix

Pro-5FU

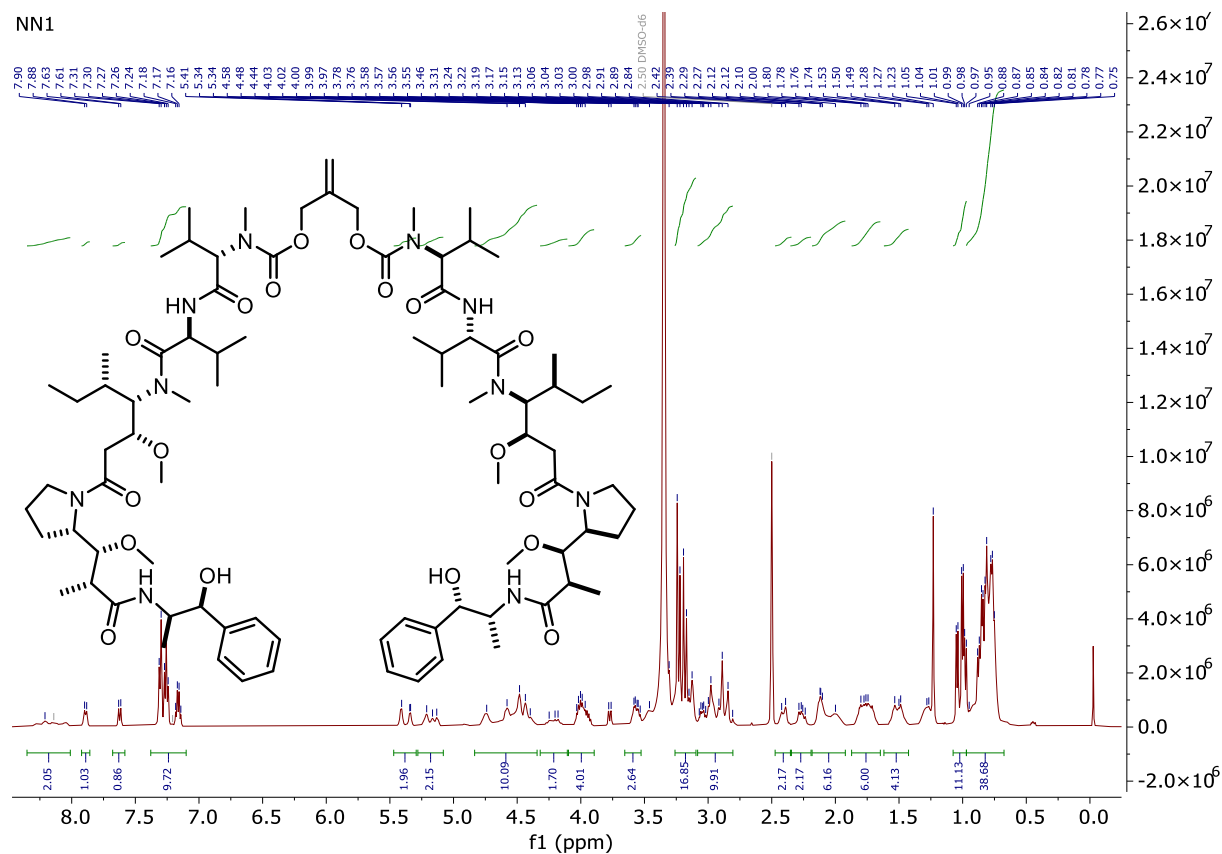


Pro-5FU

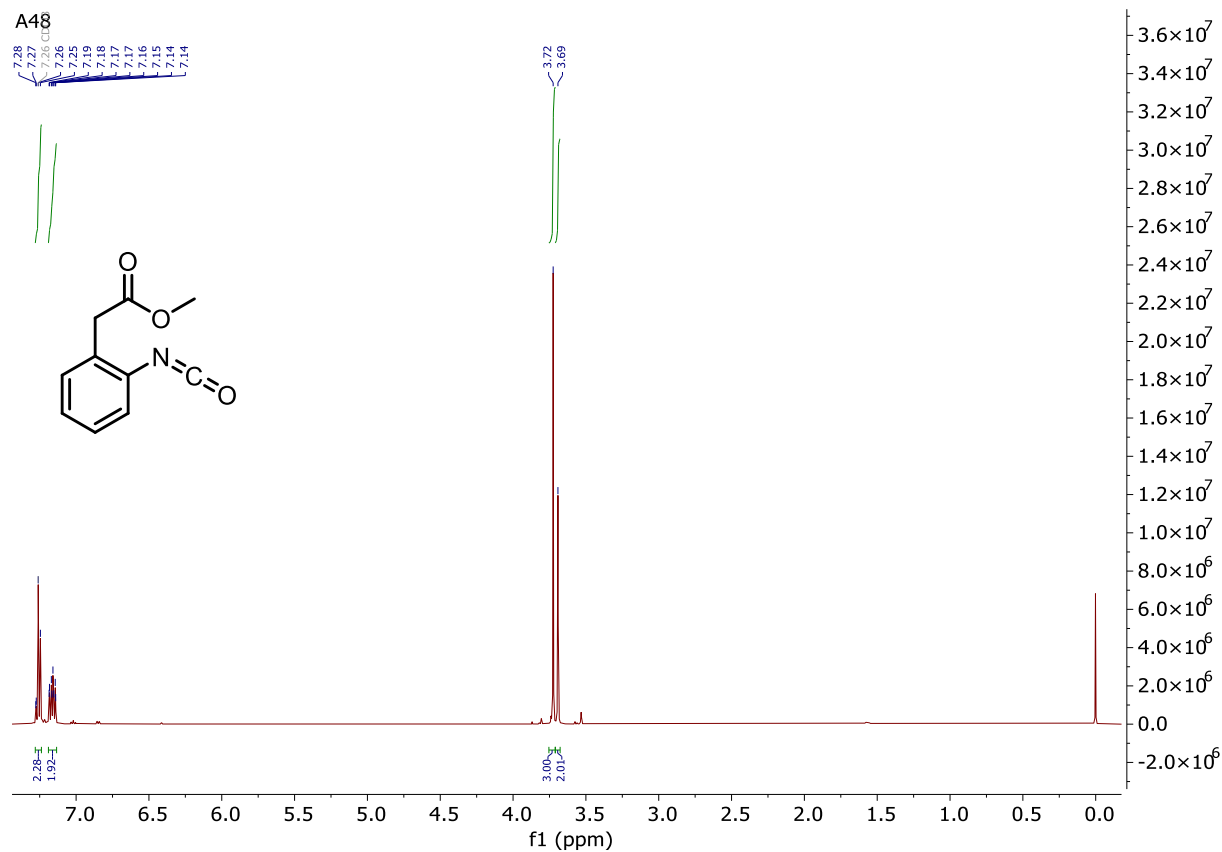


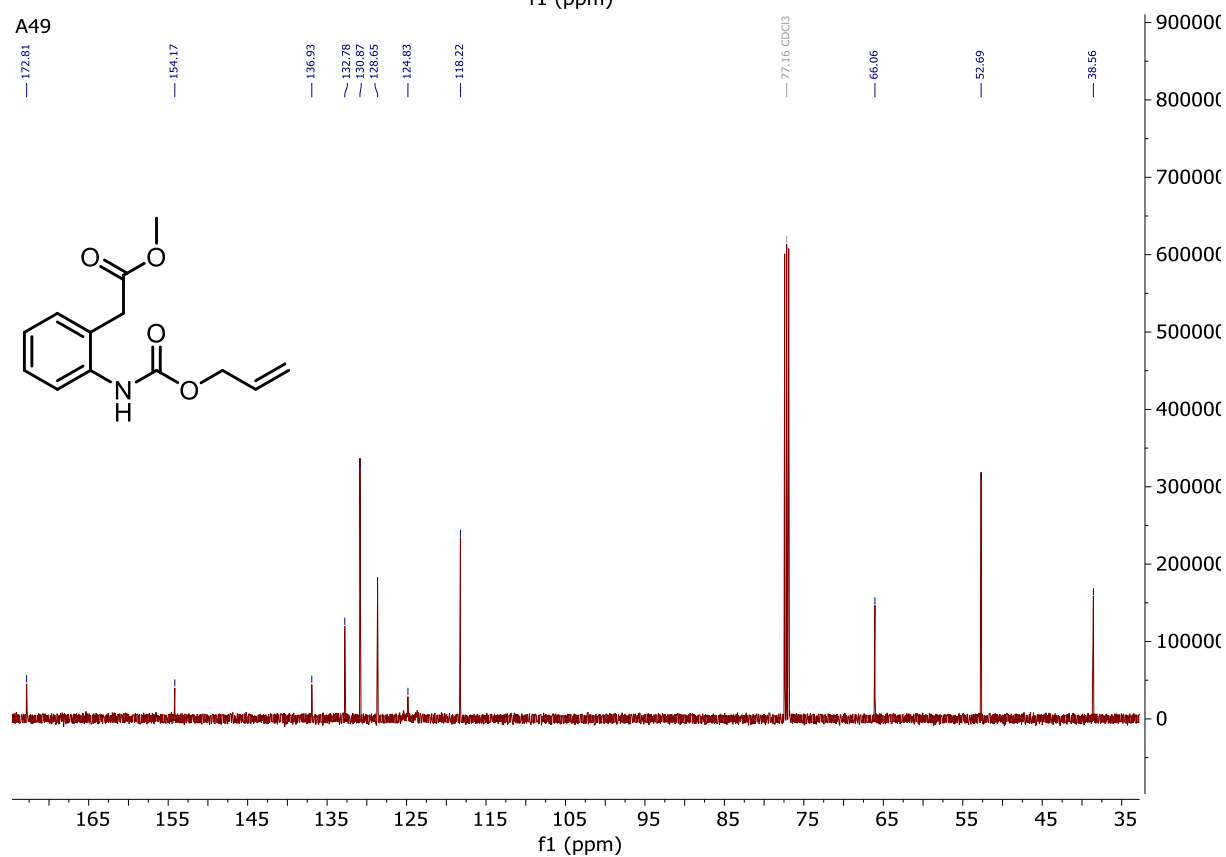
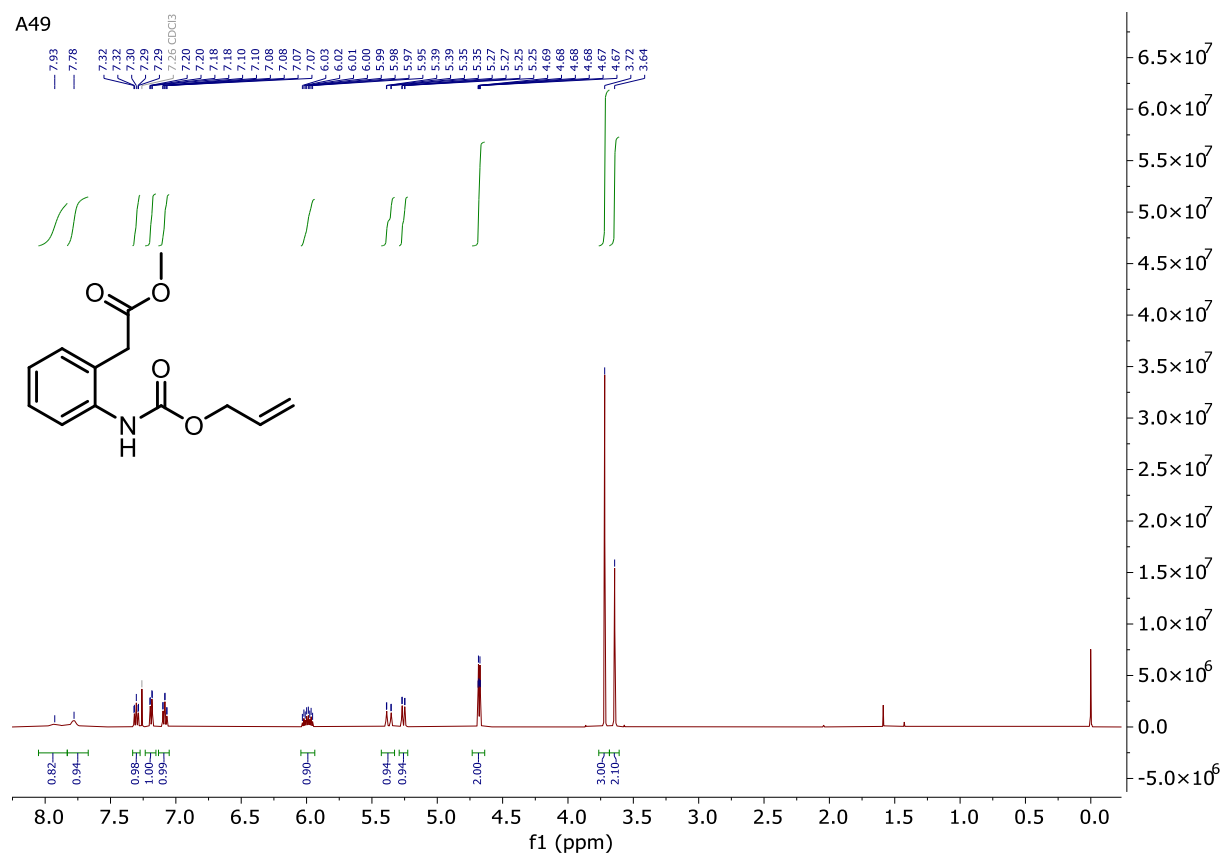
2-Methylenepropane-1,3-diyl bis((2-methoxyphenyl)carbamate) (**A46**)2-Methylenepropane-1,3-diyl bis(4-nitrophenyl) bis(carbonate) (**A47**)

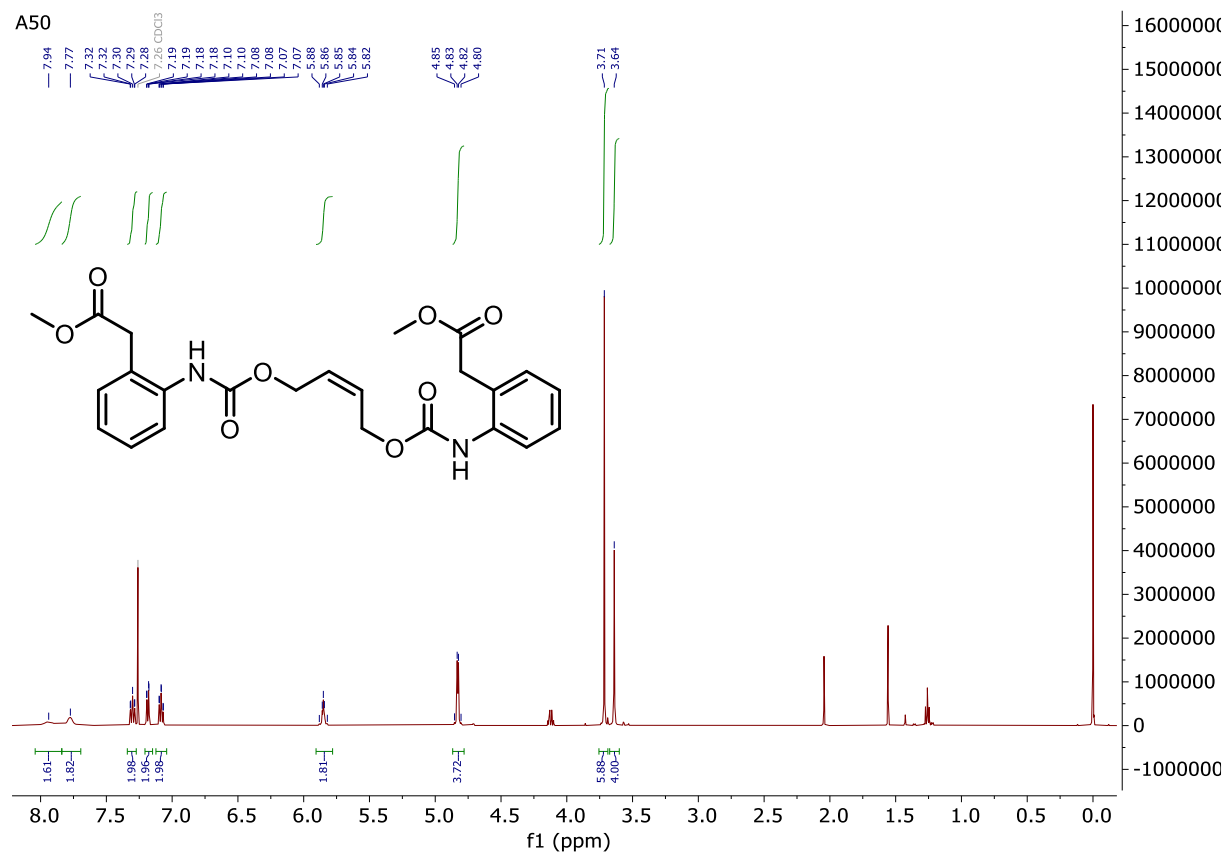
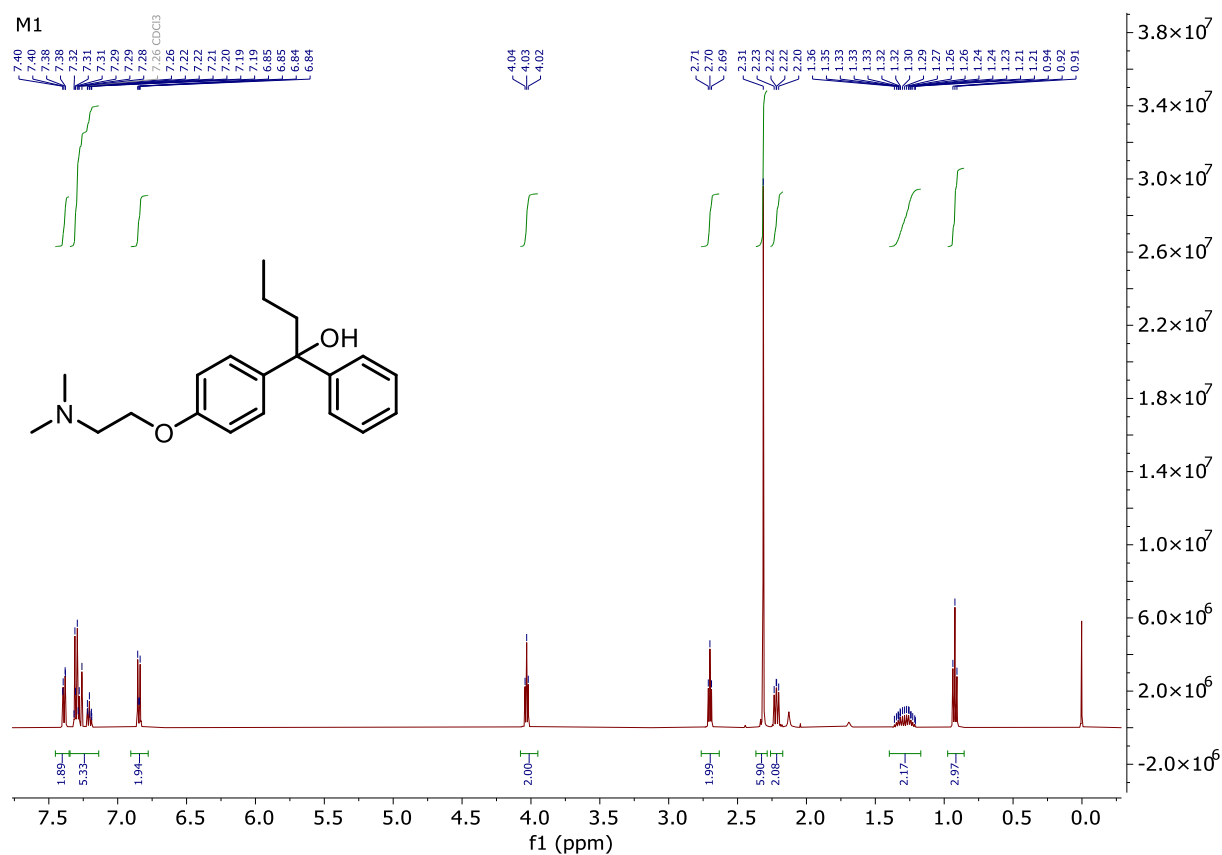
NN1

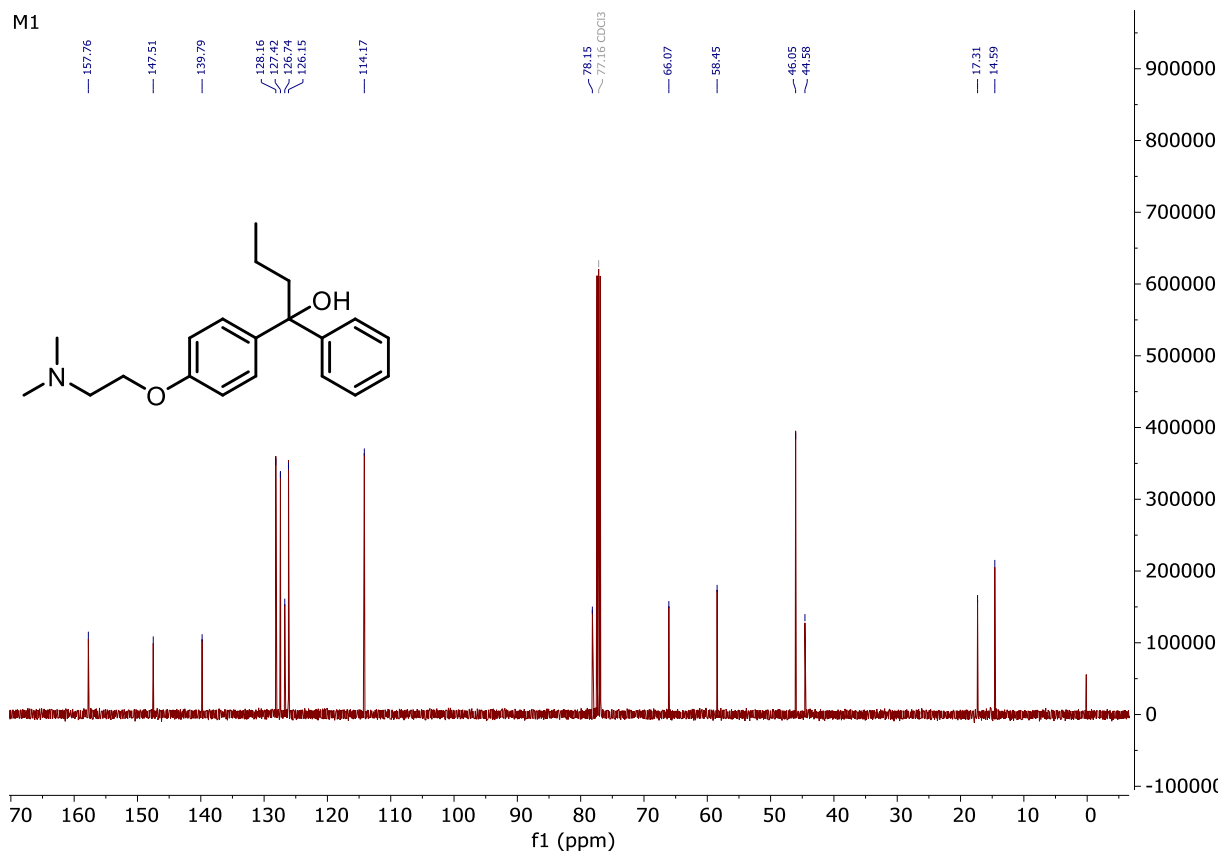


Methyl 2-(2-isocyanatophenyl)acetate (A48)

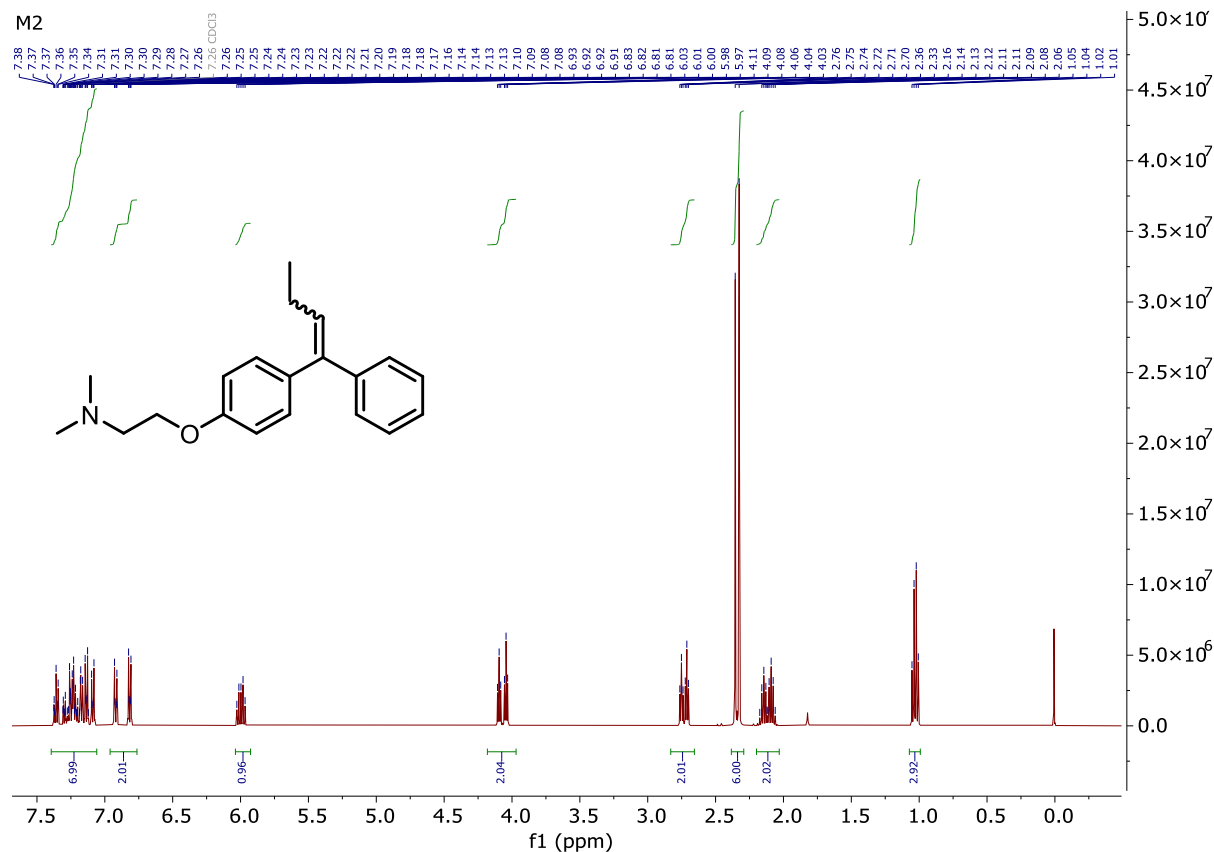


Methyl 2-(2-(((allyloxy)carbonyl)amino)phenyl)acetate (**A49**)

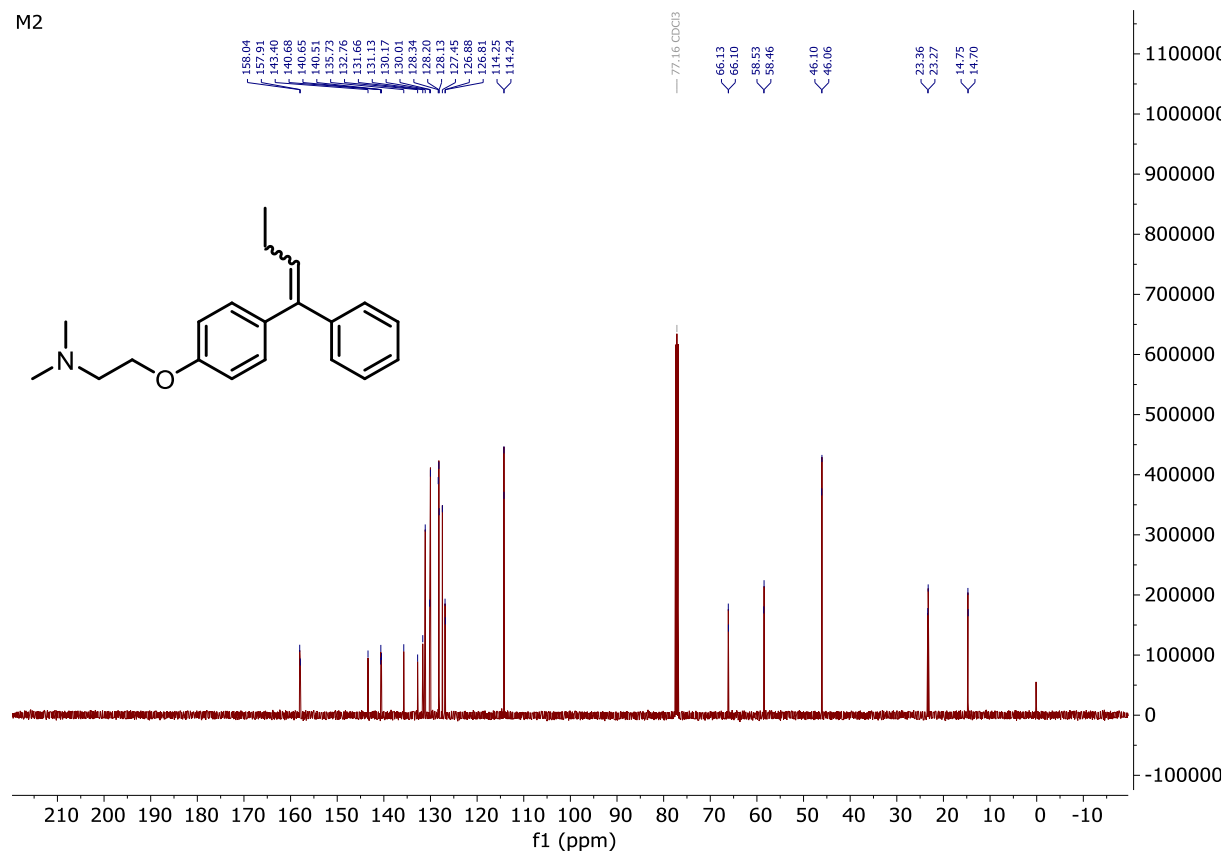
Dimethyl 2,2'-((((but-2-ene-1,4-diylbis(oxy)))bis(carbonyl))bis(azanediy))bis(2,1-phenylene))(Z)-diacetate (**A50**)1-(4-(2-(Dimethylamino)ethoxy)phenyl)-1-phenylbutan-1-ol (**M1**)



N,N-Dimethyl-2-(4-(1-phenylbut-1-en-1-yl)phenoxy)ethan-1-amine (M2)

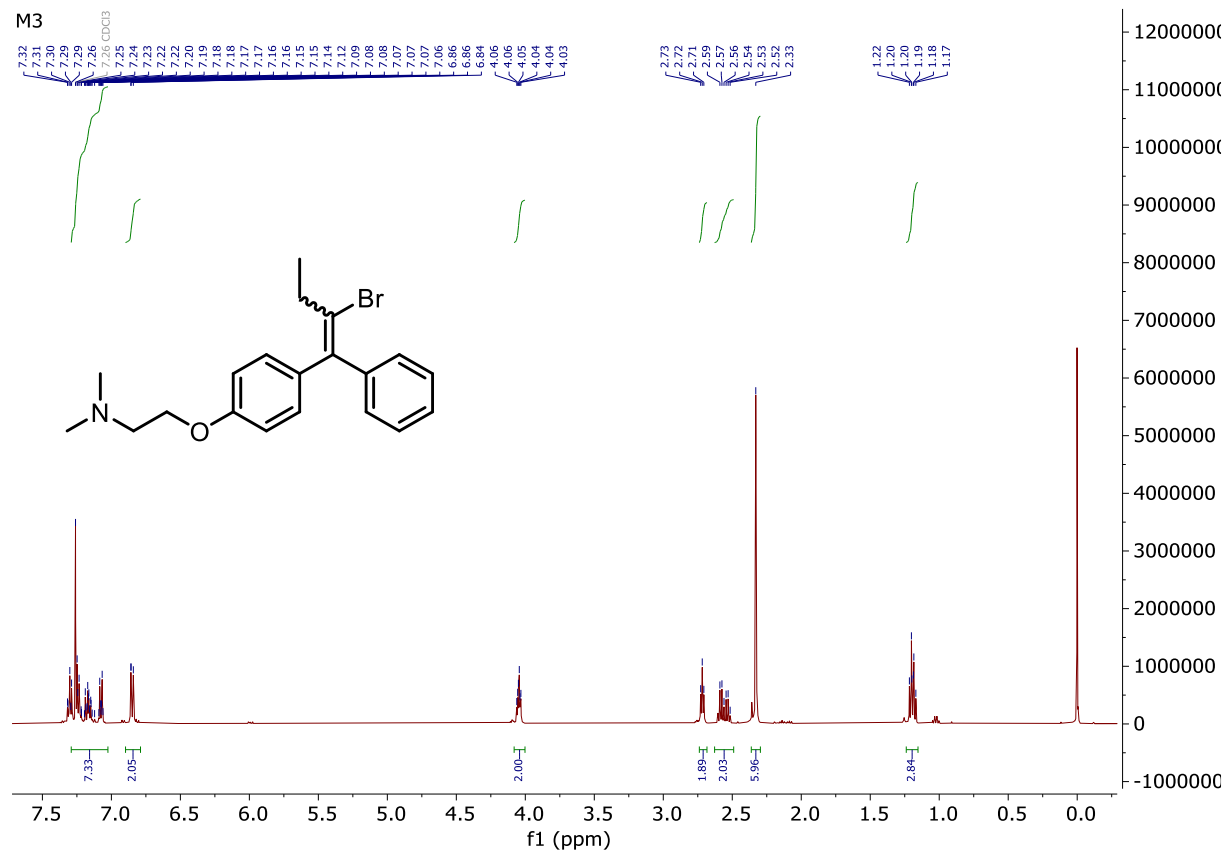


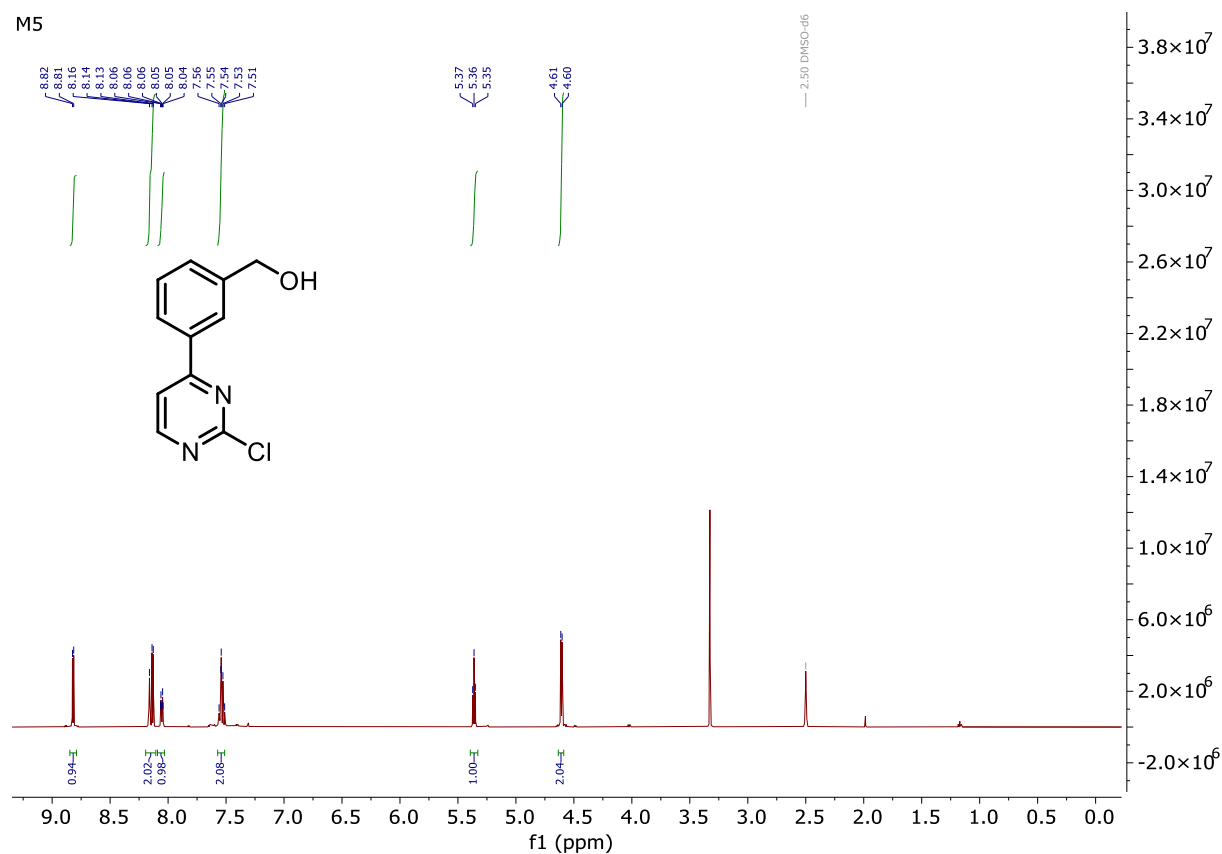
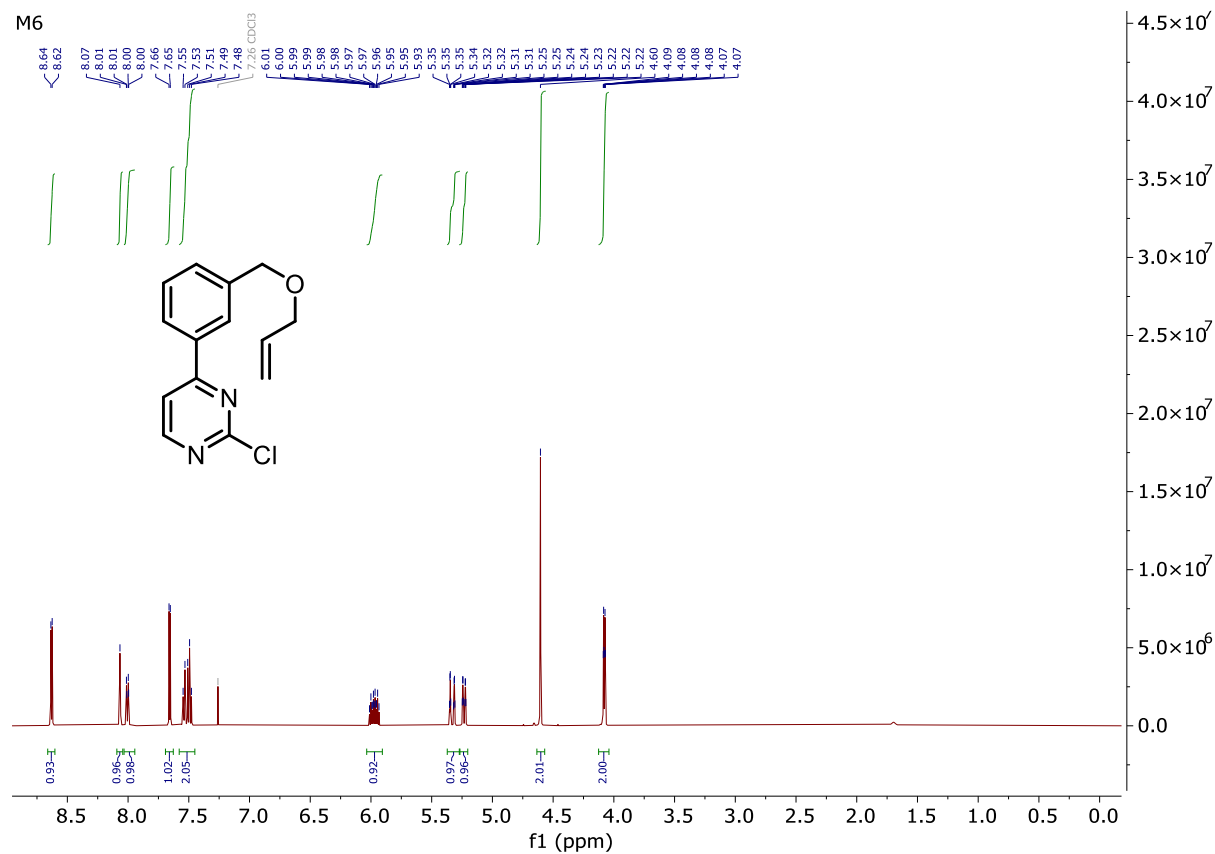
M2

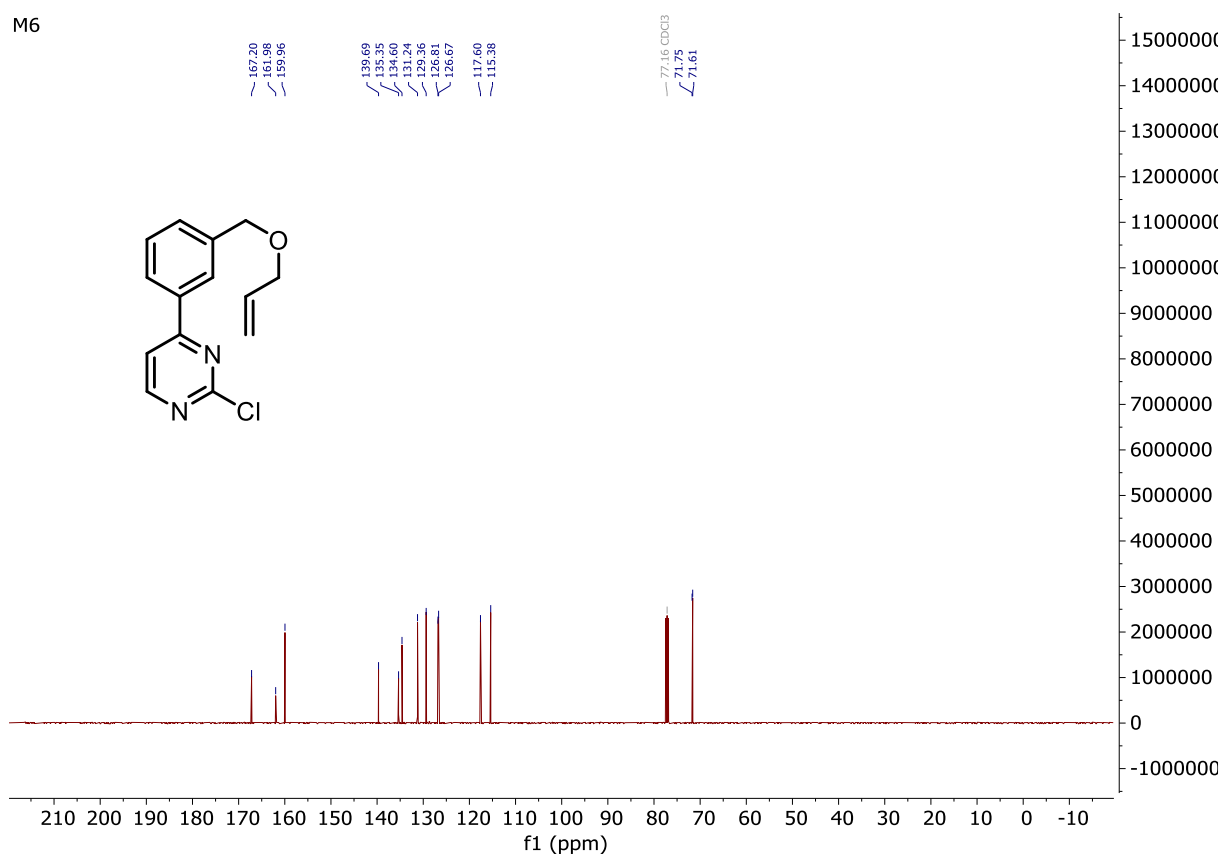


2-(4-(2-Bromo-1-phenylbut-1-en-1-yl)phenoxy)-*N,N*-dimethylethan-1-amine (M3)

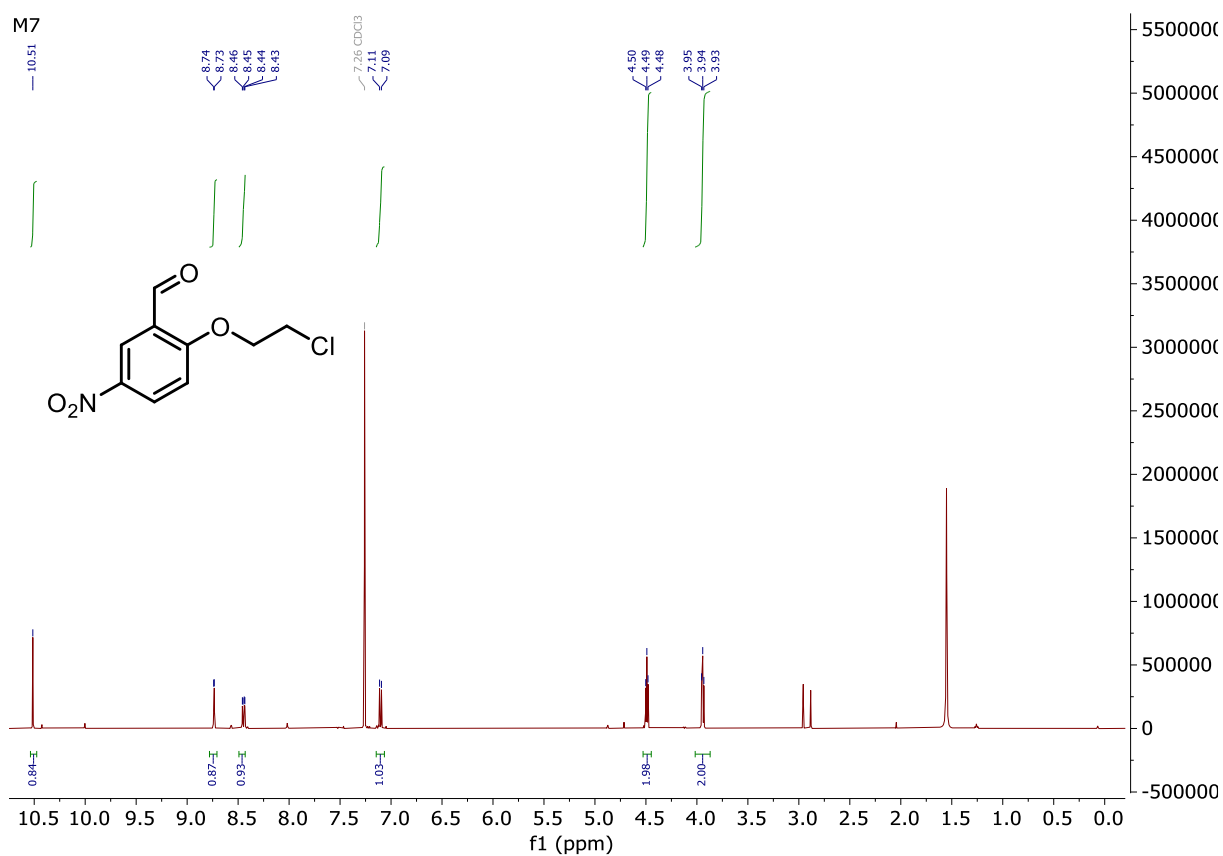
M3

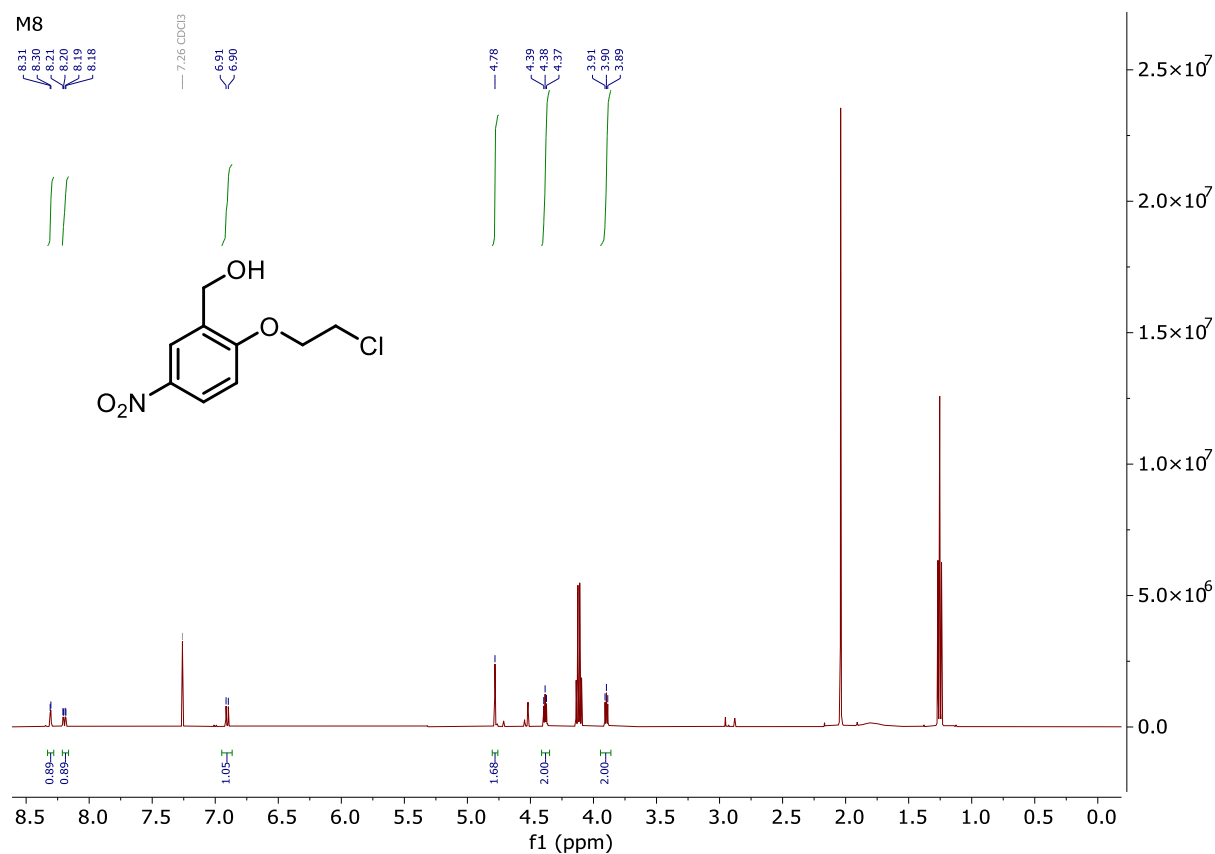
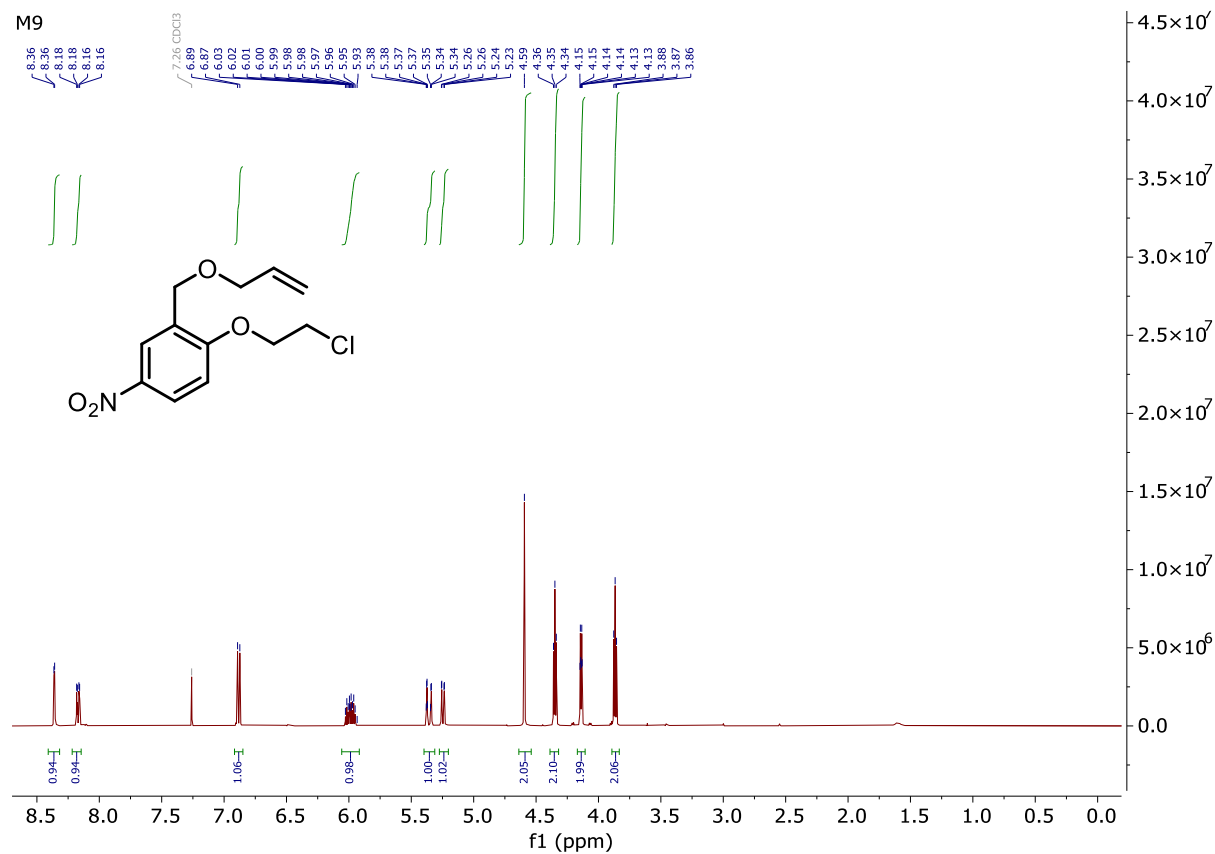


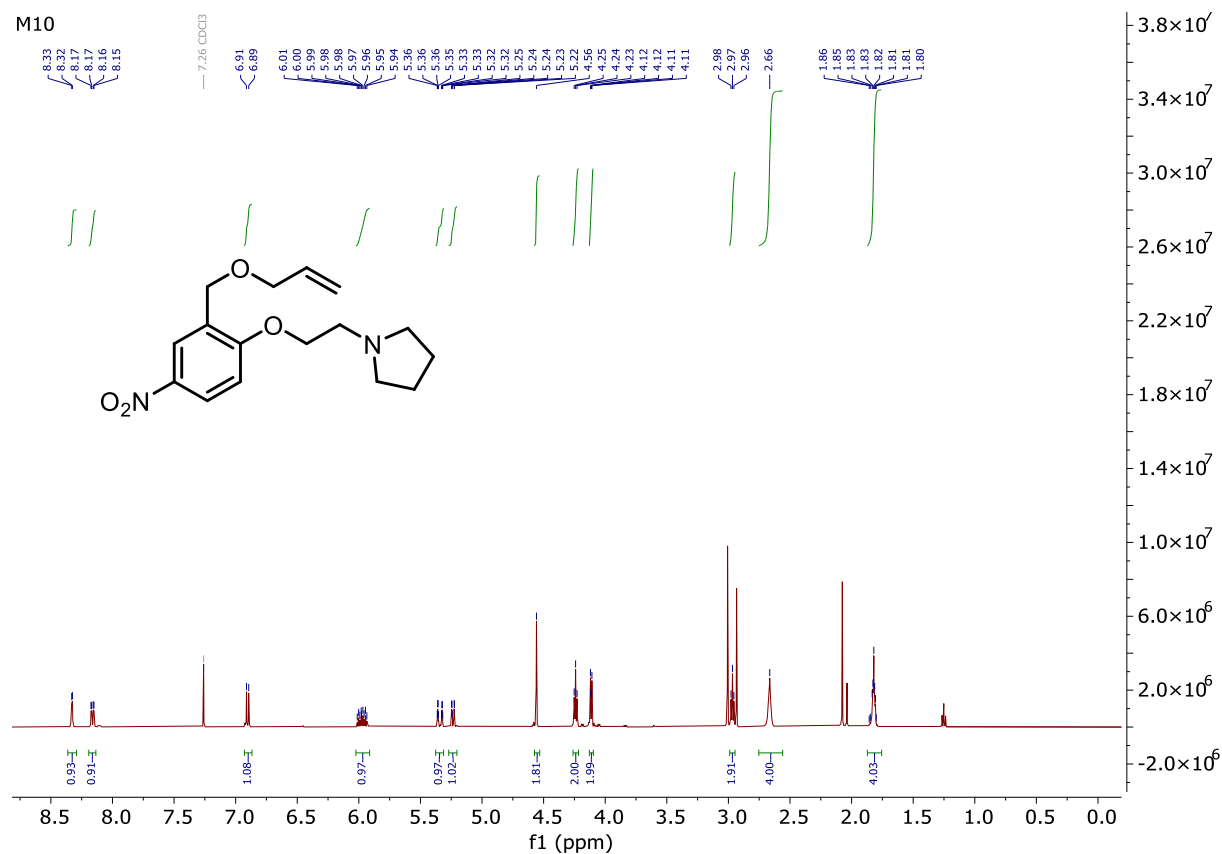
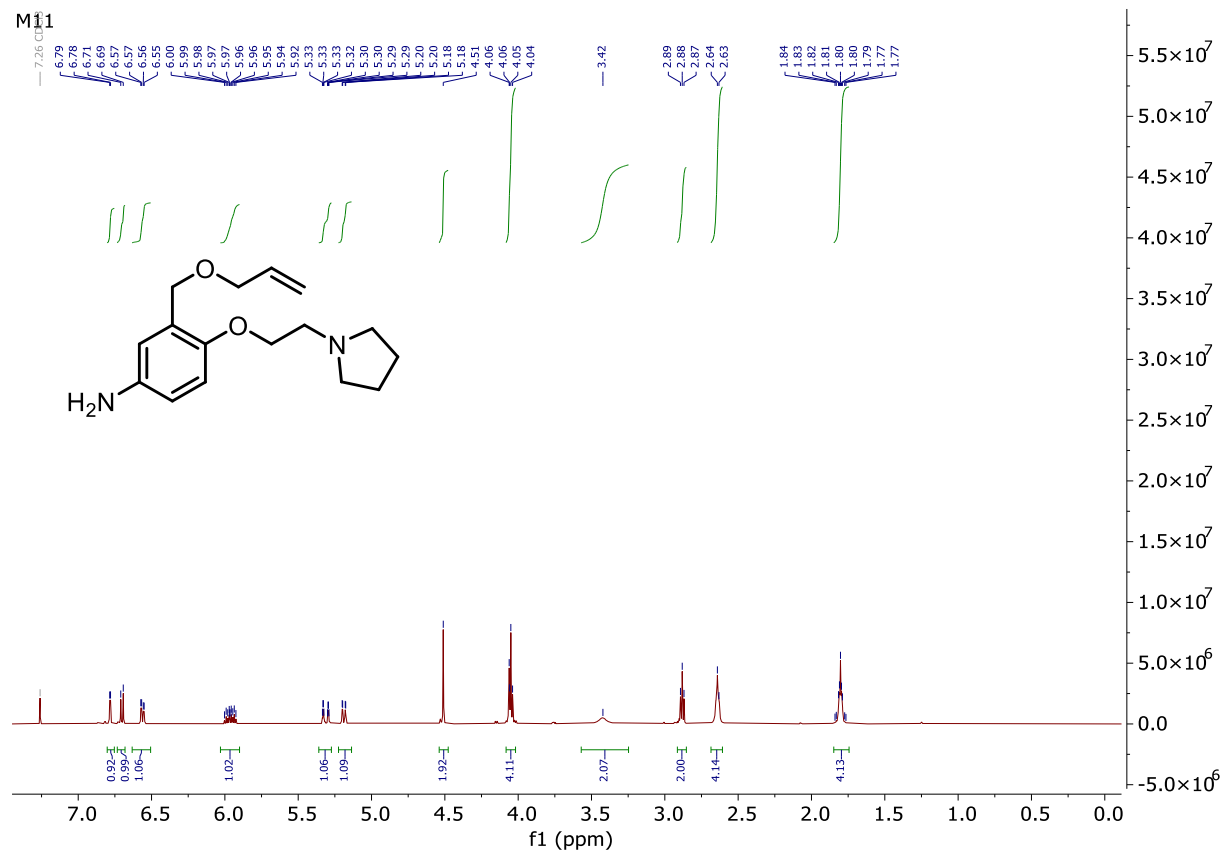
(3-(2-Chloropyrimidin-4-yl)phenyl)methanol (**M5**)4-(3-((Allyloxy)methyl)phenyl)-2-chloropyrimidine (**M6**)



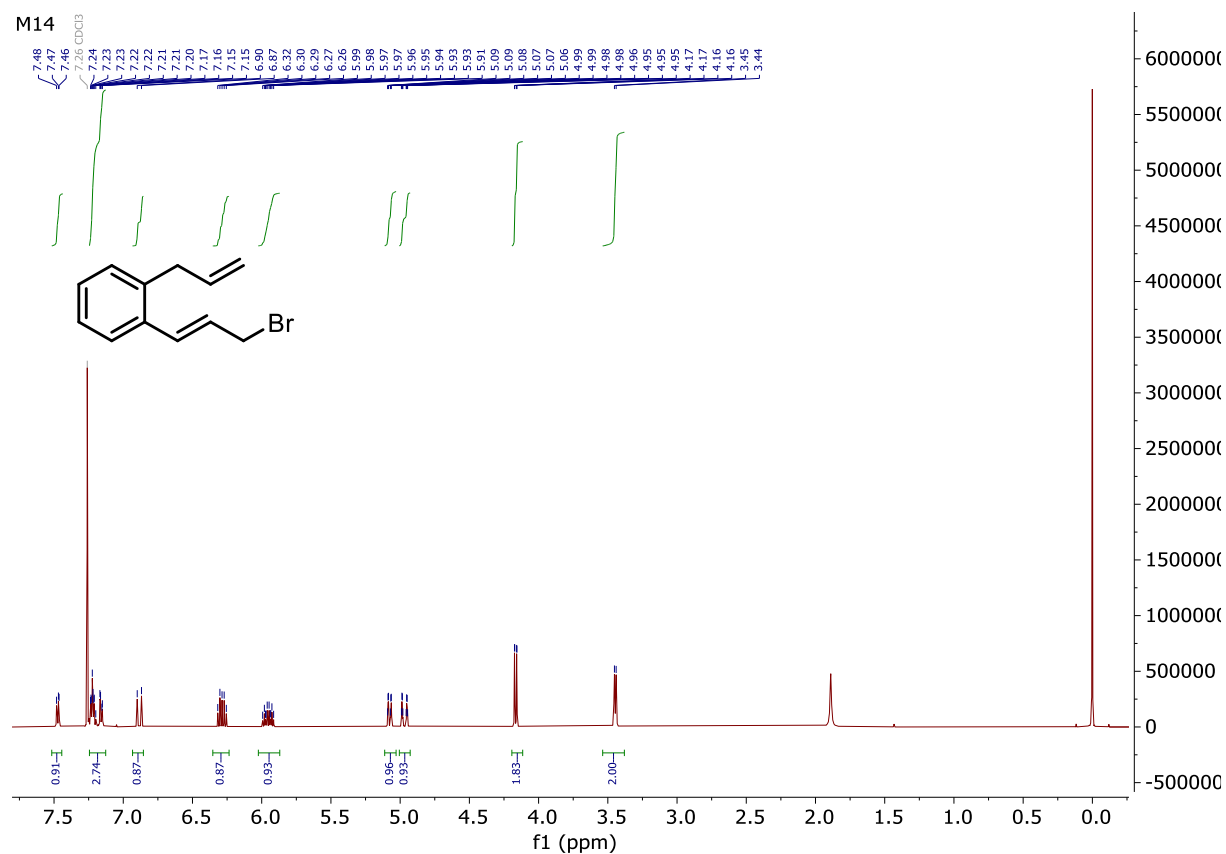
2-(2-Chloroethoxy)-5-nitrobenzaldehyde (M7)



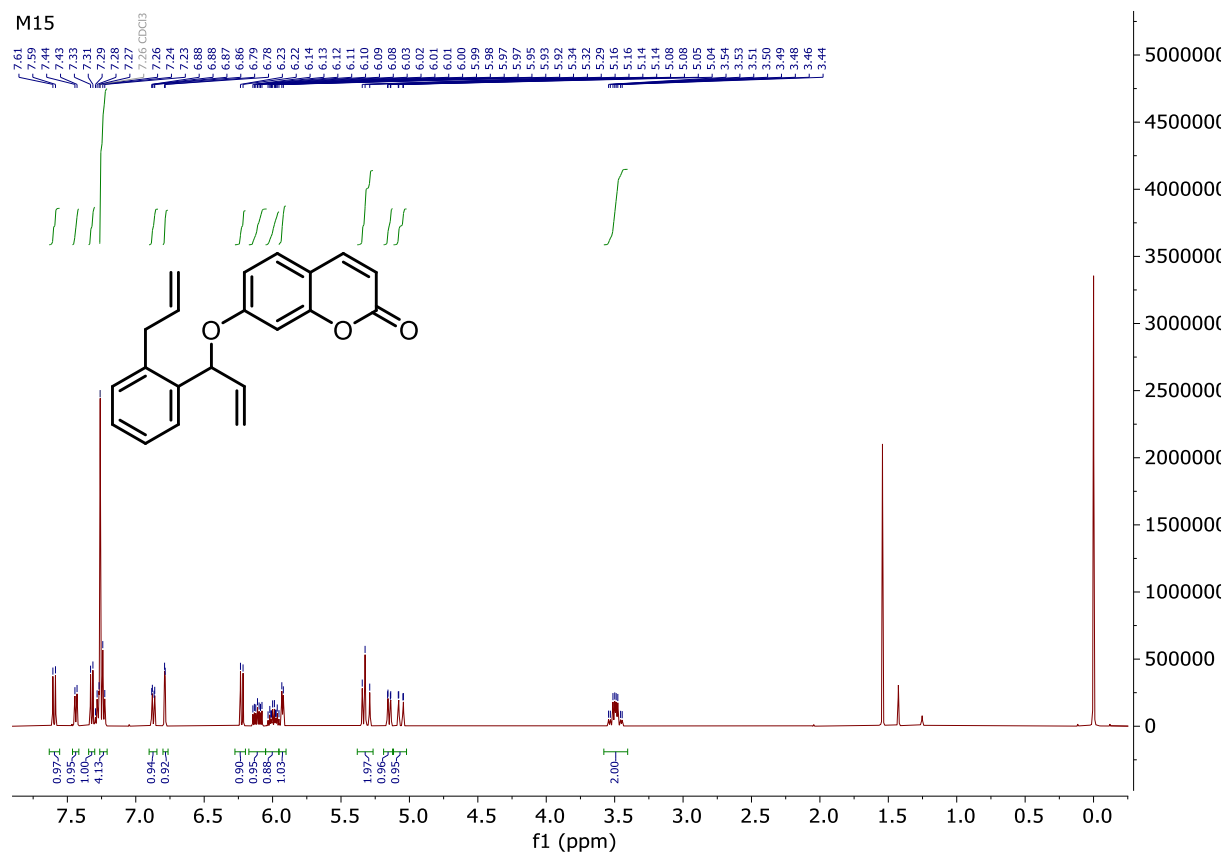
(2-(2-Chloroethoxy)-5-nitrophenyl)methanol (**M8**)2-((Allyloxy)methyl)-1-(2-chloroethoxy)-4-nitrobenzene (**M9**)

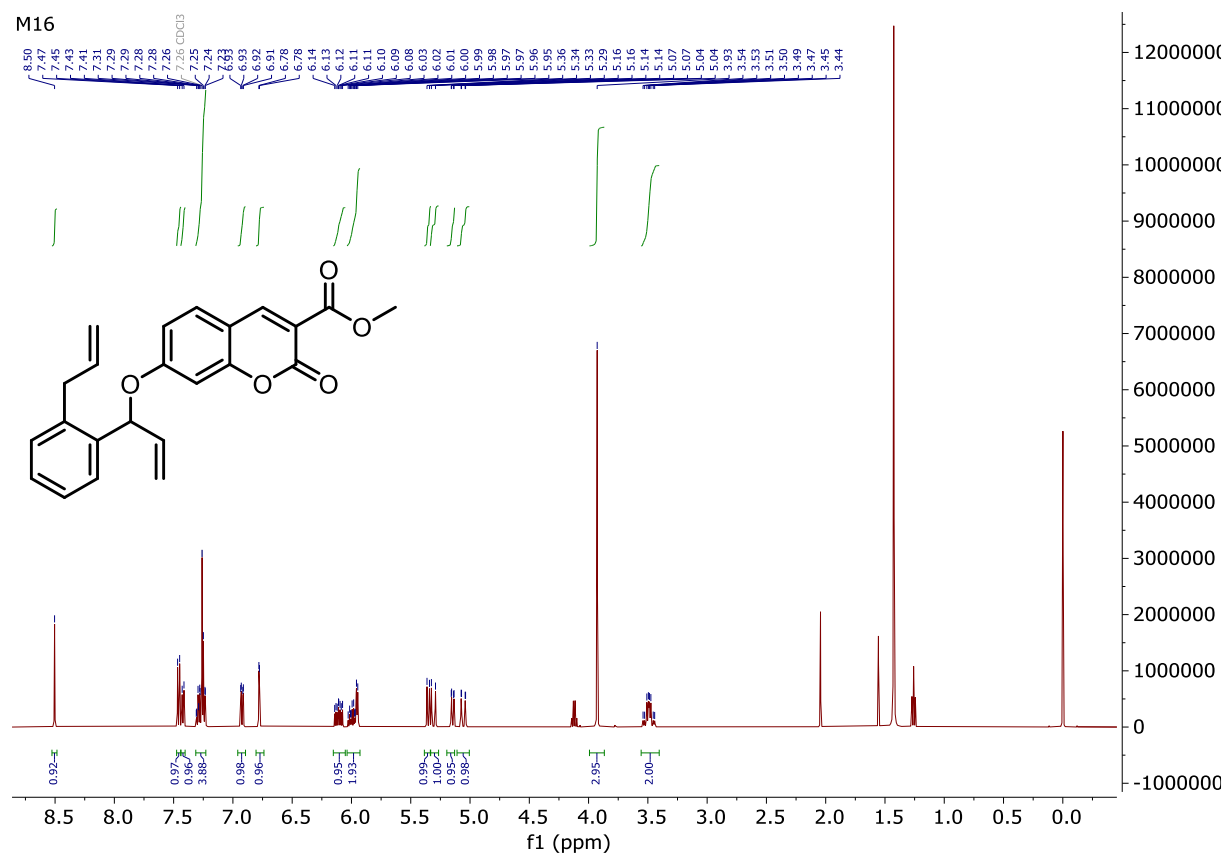
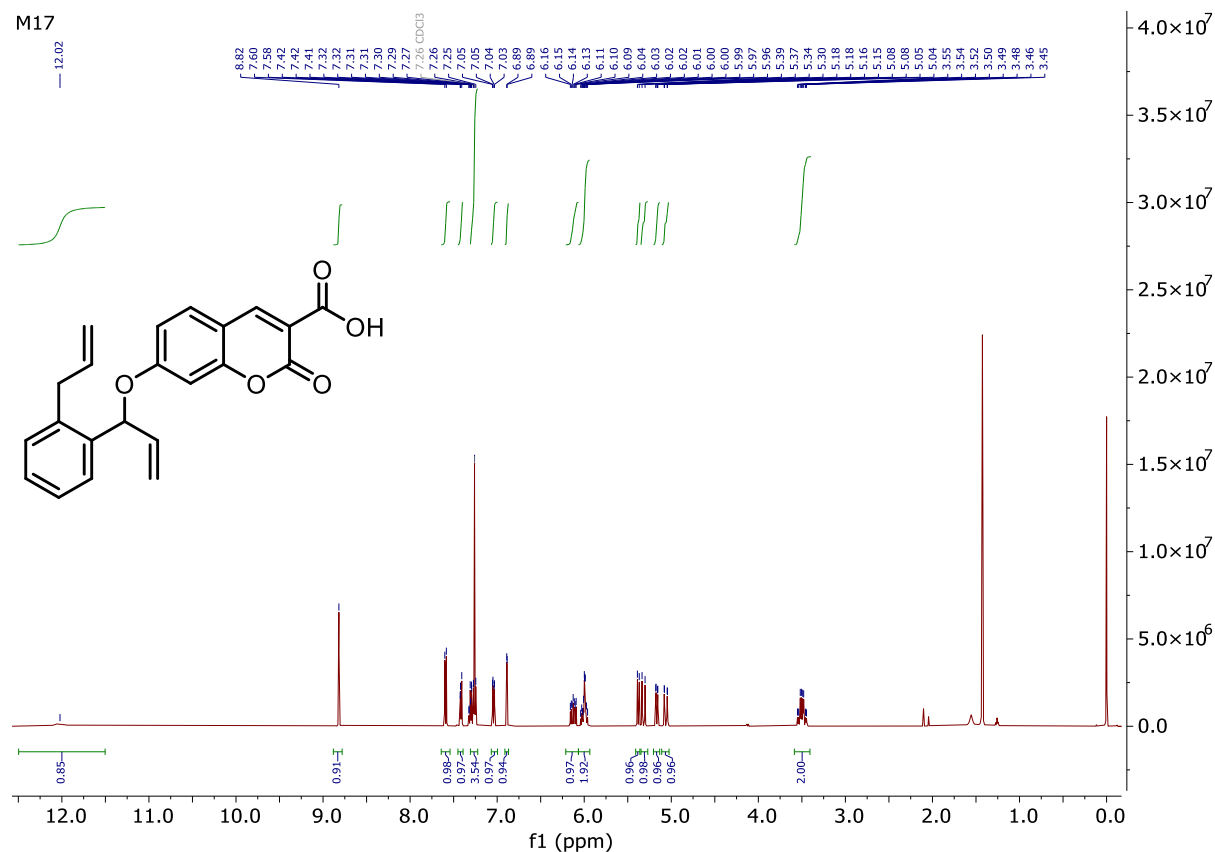
1-(2-(2-((Allyloxy)methyl)-4-nitrophenoxy)ethyl)pyrrolidine (**M10**)3-((Allyloxy)methyl)-4-(2-(pyrrolidin-1-yl)ethoxy)aniline (**M11**)

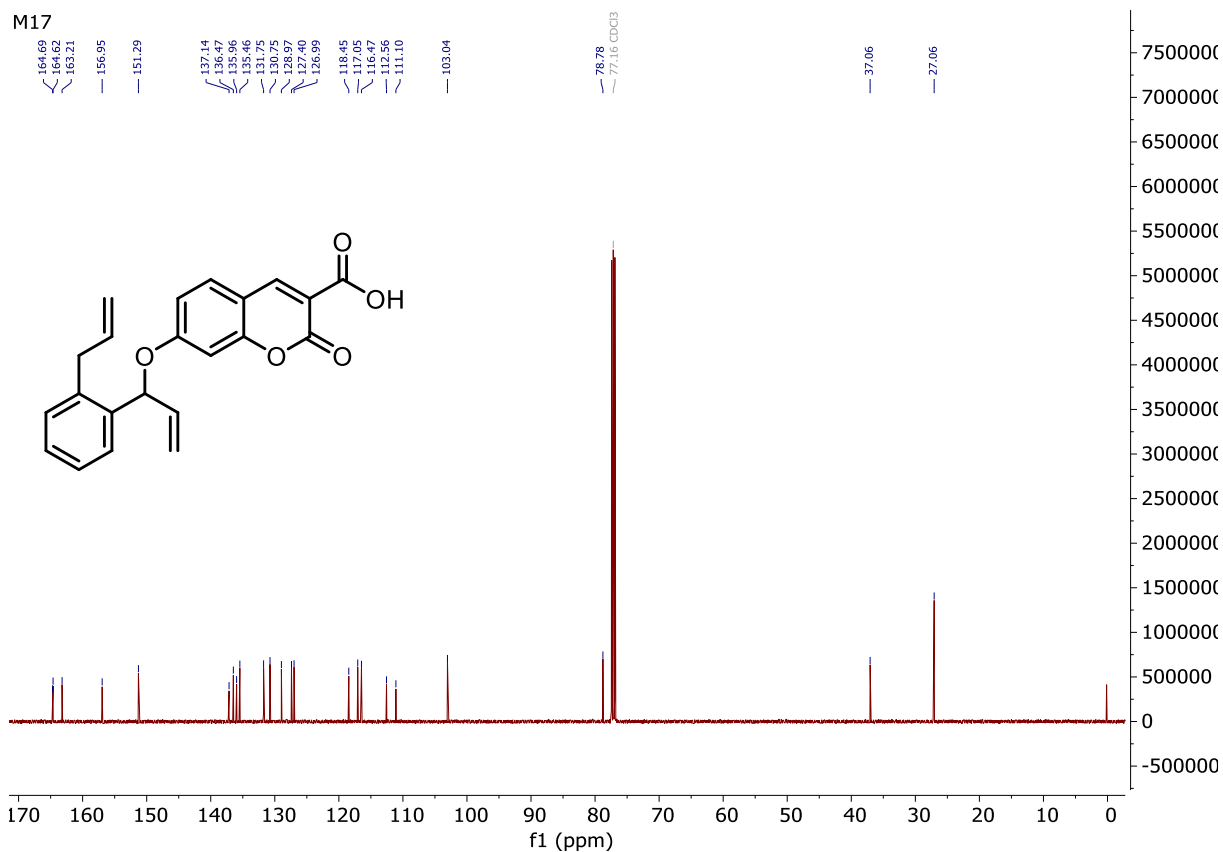
(*E*)-1-Allyl-2-(3-bromoprop-1-en-1-yl)benzene (M14)



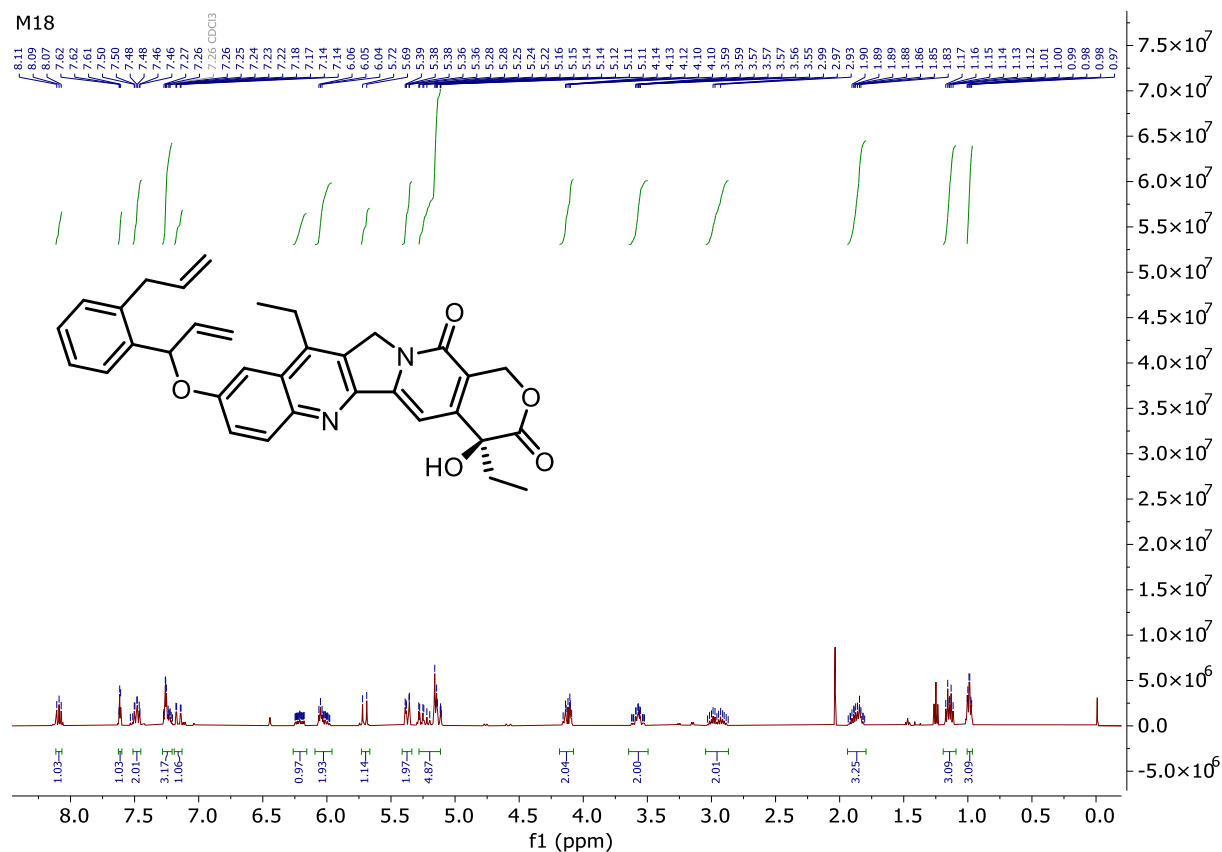
7-((1-(2-Allylphenyl)allyl)oxy)-2*H*-chromen-2-one (M15)



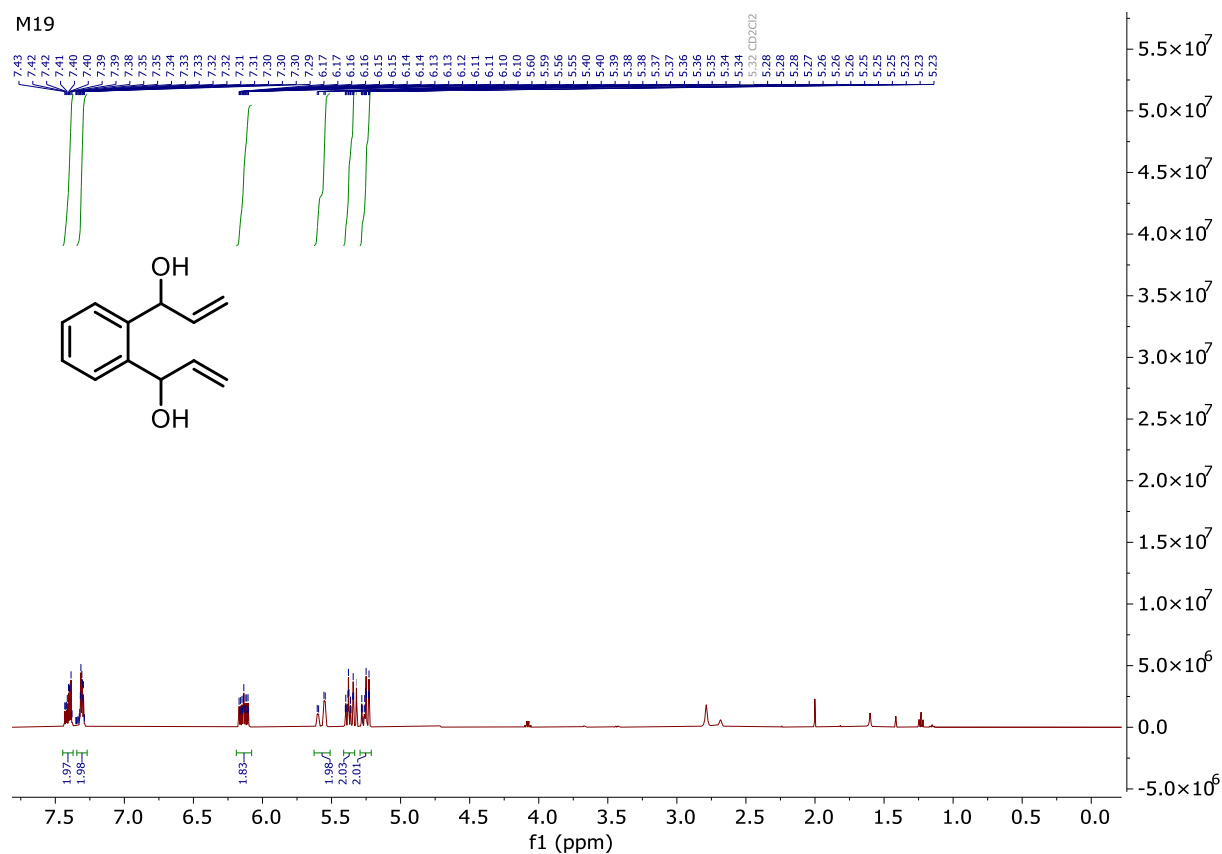
Methyl 7-((1-(2-allylphenyl)allyl)oxy)-2-oxo-2H-chromene-3-carboxylate (**M16**)7-((1-(2-Allylphenyl)allyl)oxy)-2-oxo-2H-chromene-3-carboxylic acid (**M17**)



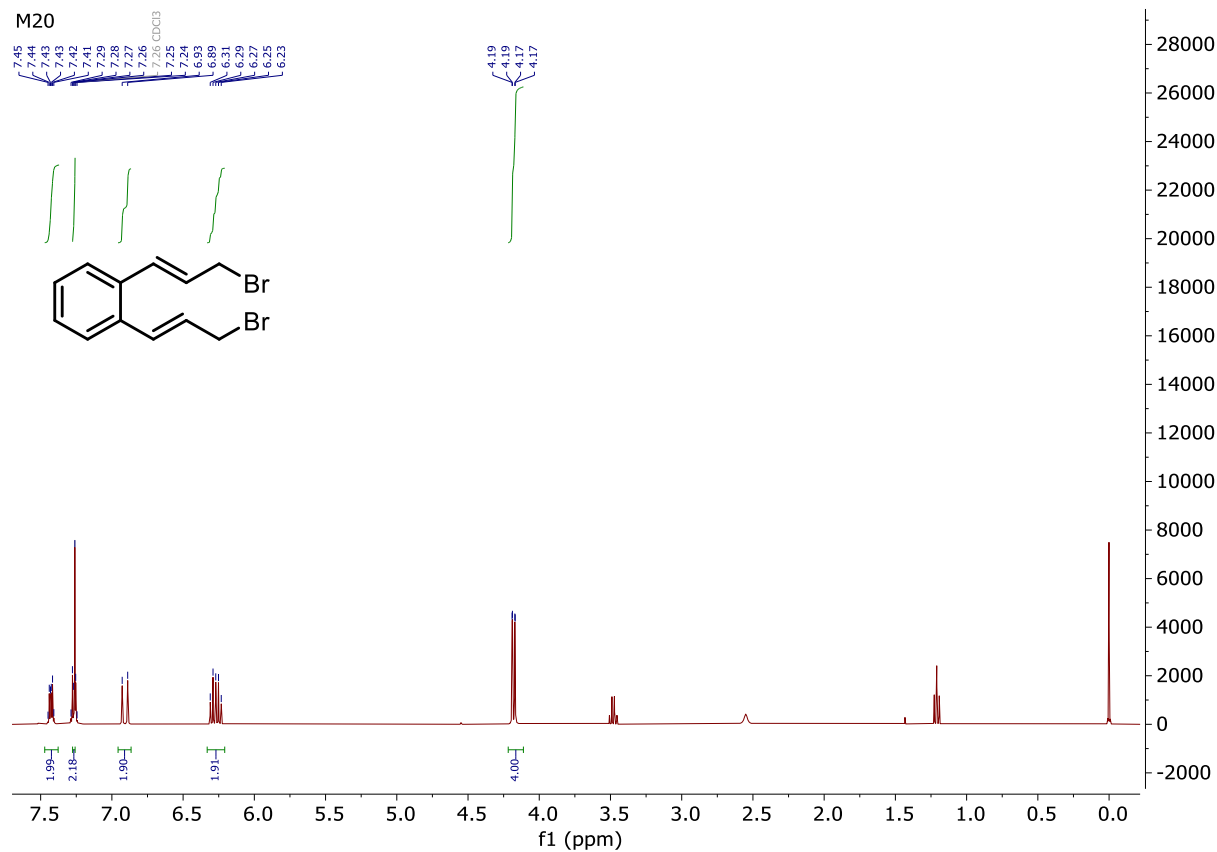
(4S)-9-((1-(2-Allylphenyl)allyl)oxy)-4,11-diethyl-4-hydroxy-1,12-dihydro-14H-pyrano[3',4':6,7]indolizino[1,2-b]quinoline-3,14(4H)-dione (**M18**)

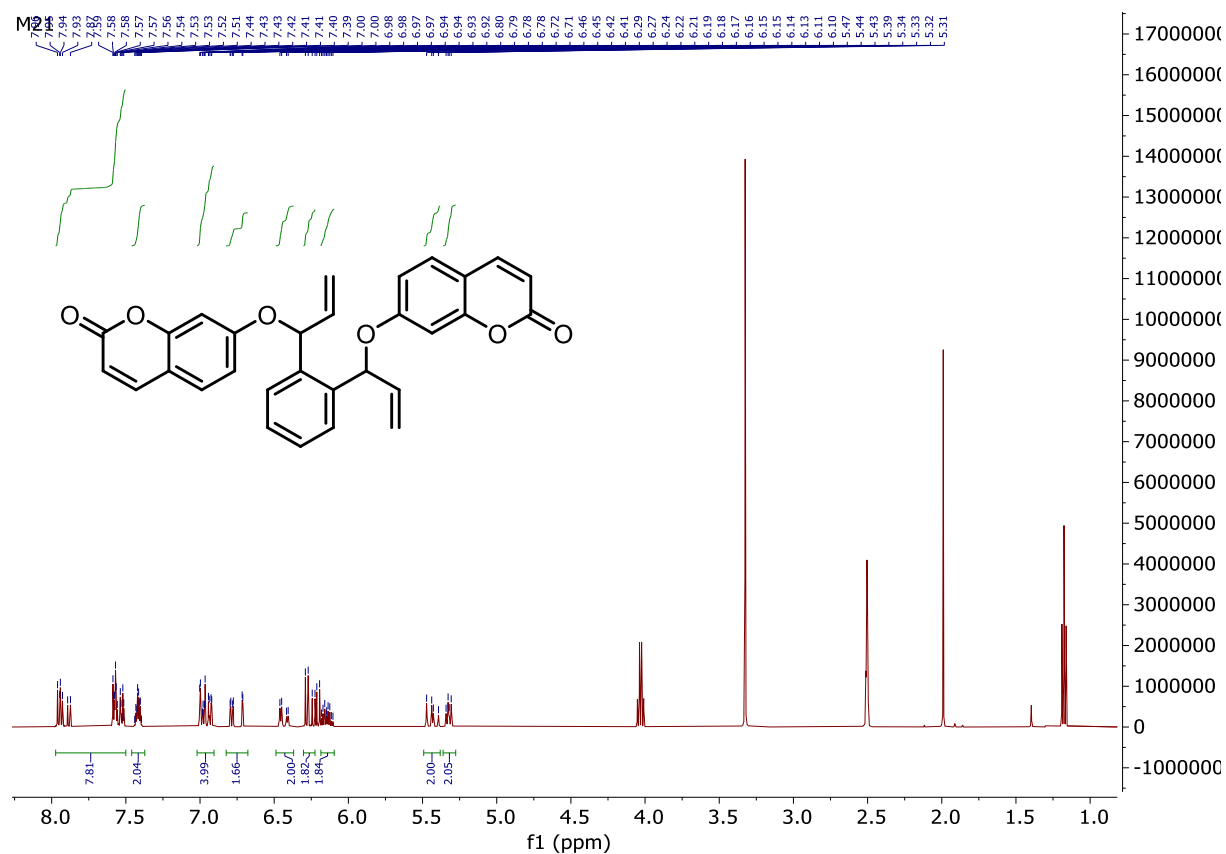
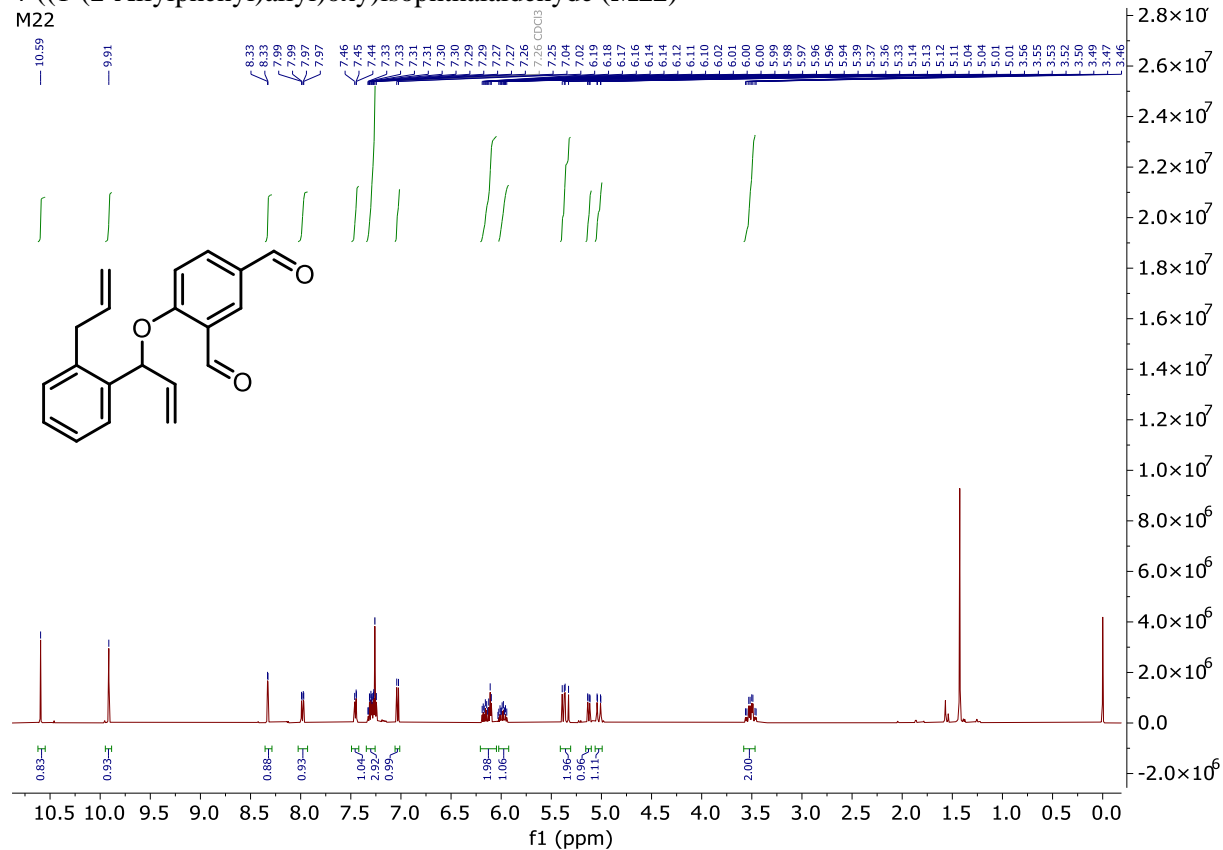


1,1'-(1,2-Phenylene)bis(prop-2-en-1-ol) (M19)

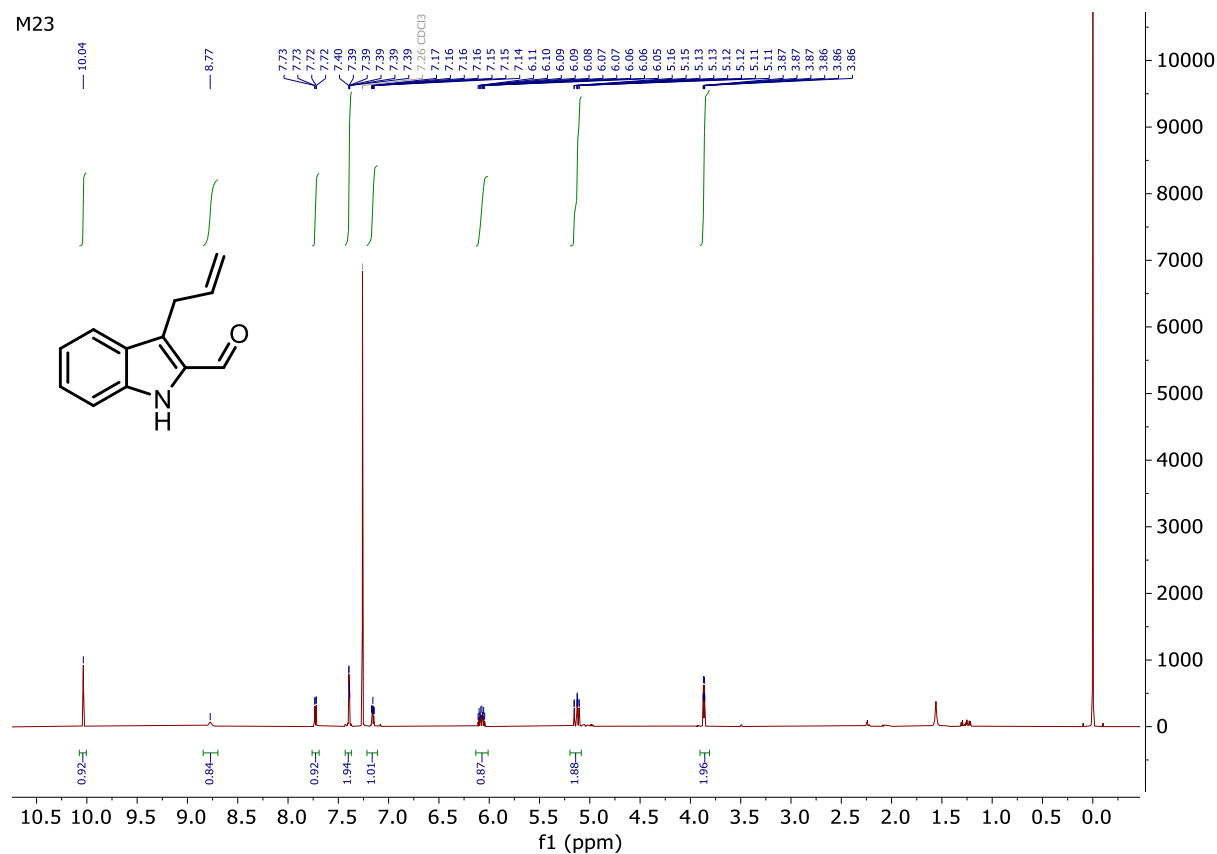


1,2-Bis((E)-3-bromoprop-1-en-1-yl)benzene (M20)

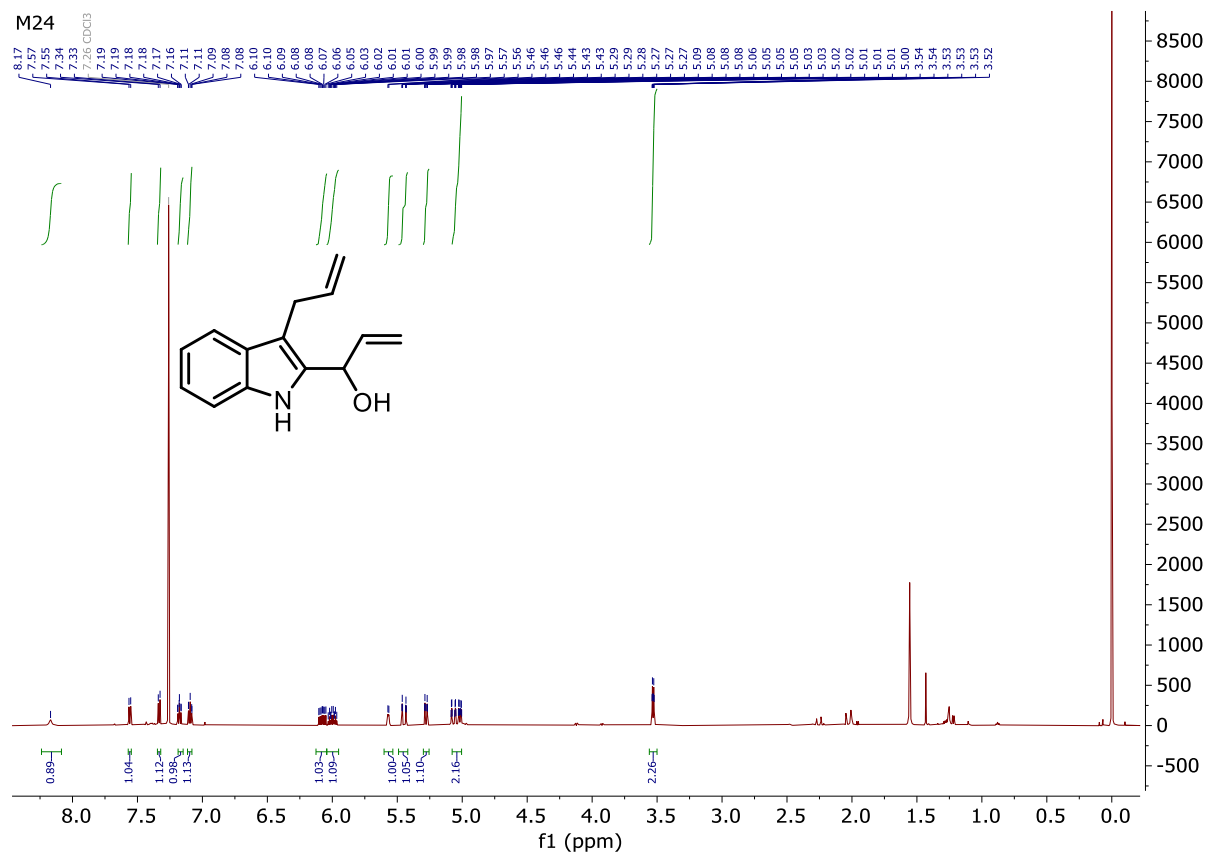


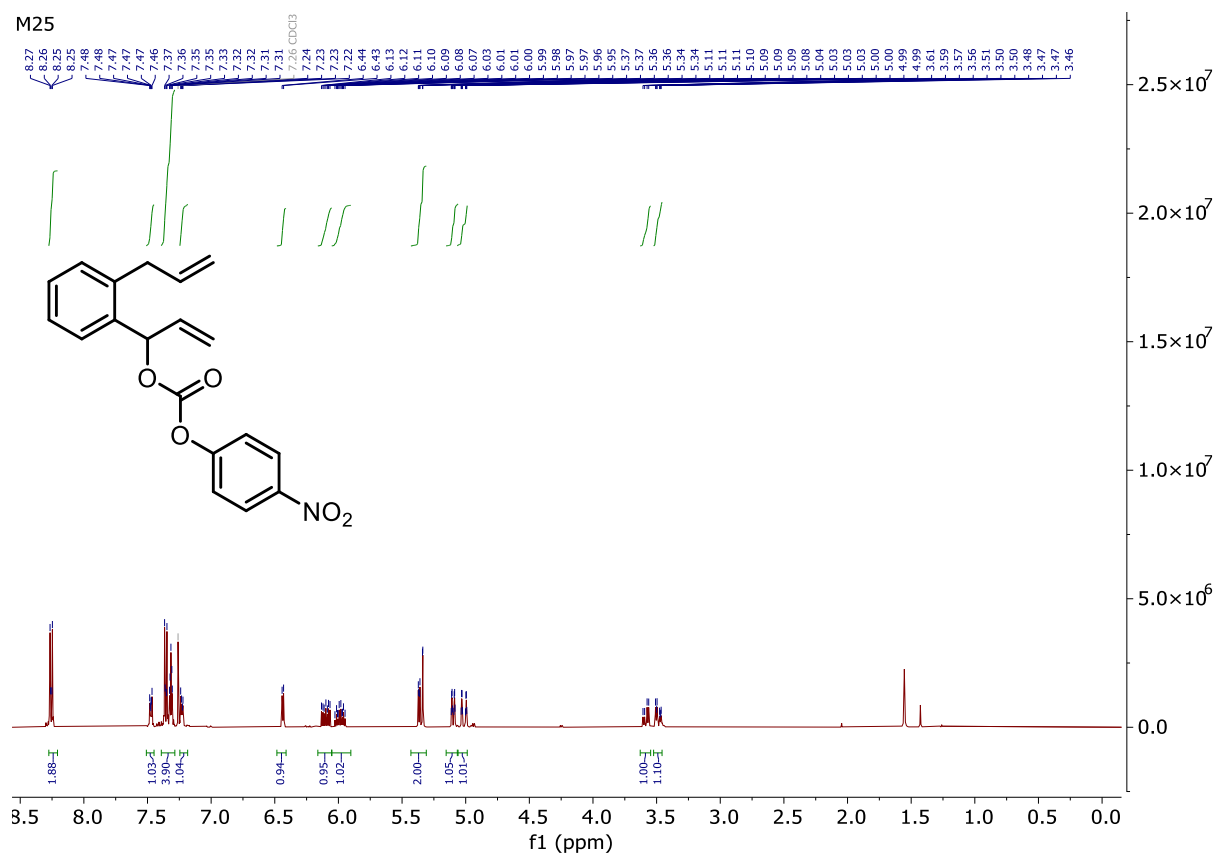
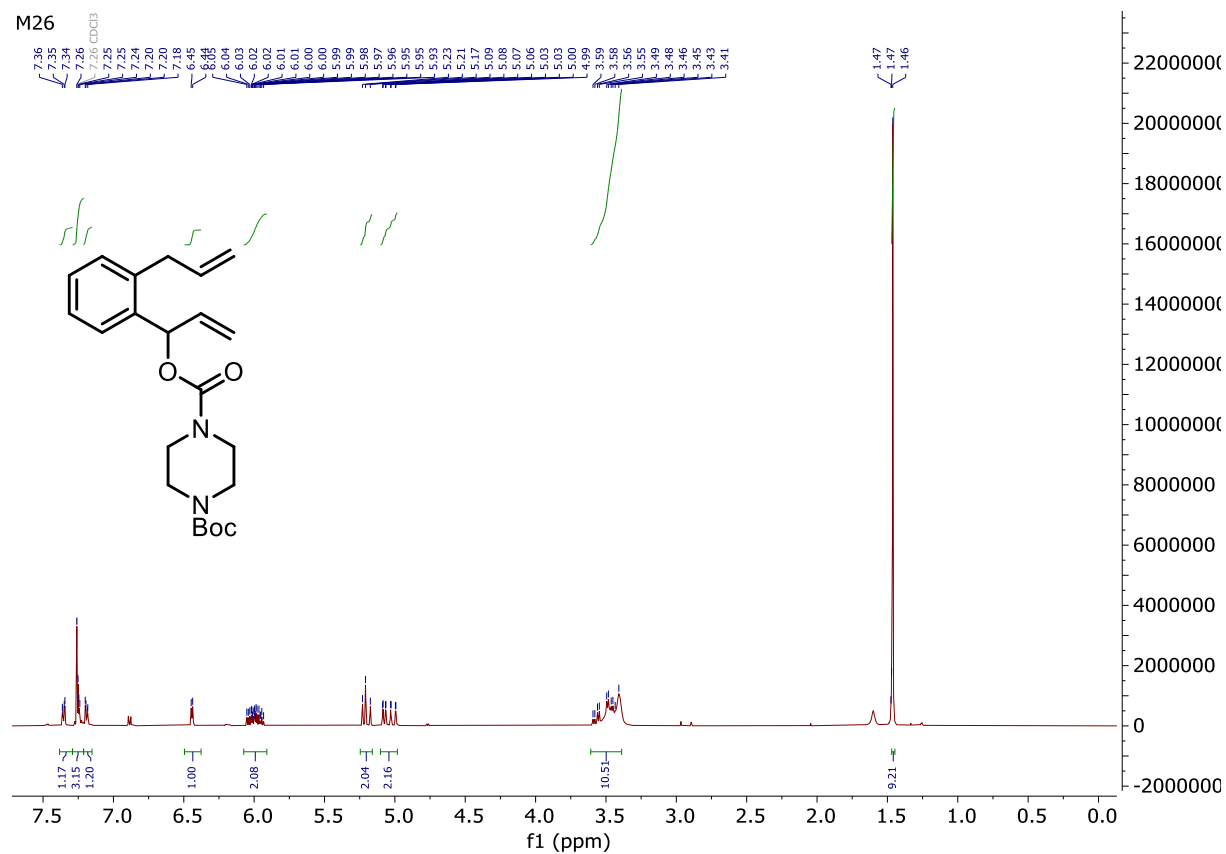
7,7'-((1,2-Phenylenebis(prop-2-ene-1,1-diyl))bis(oxy))bis(2*H*-chromen-2-one) (**M21**)4-((1-(2-Allylphenyl)allyl)oxy)isophthalaldehyde (**M22**)

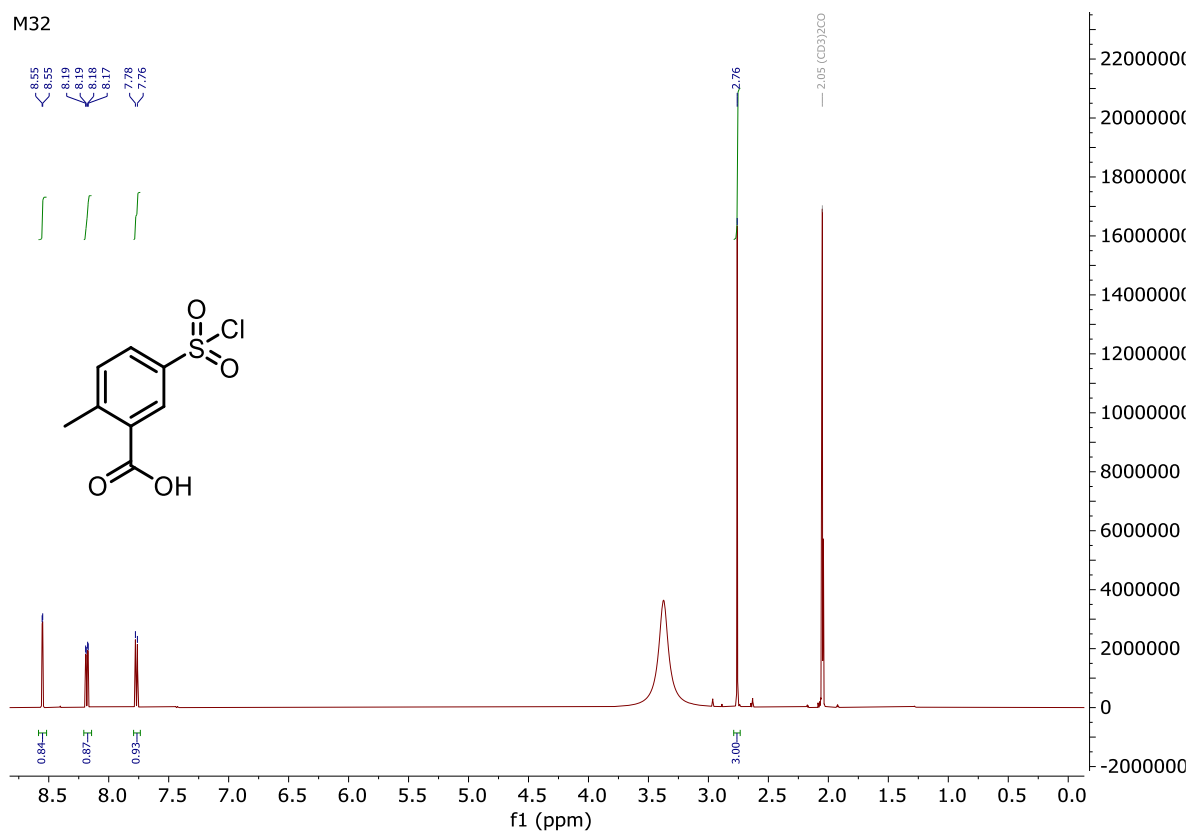
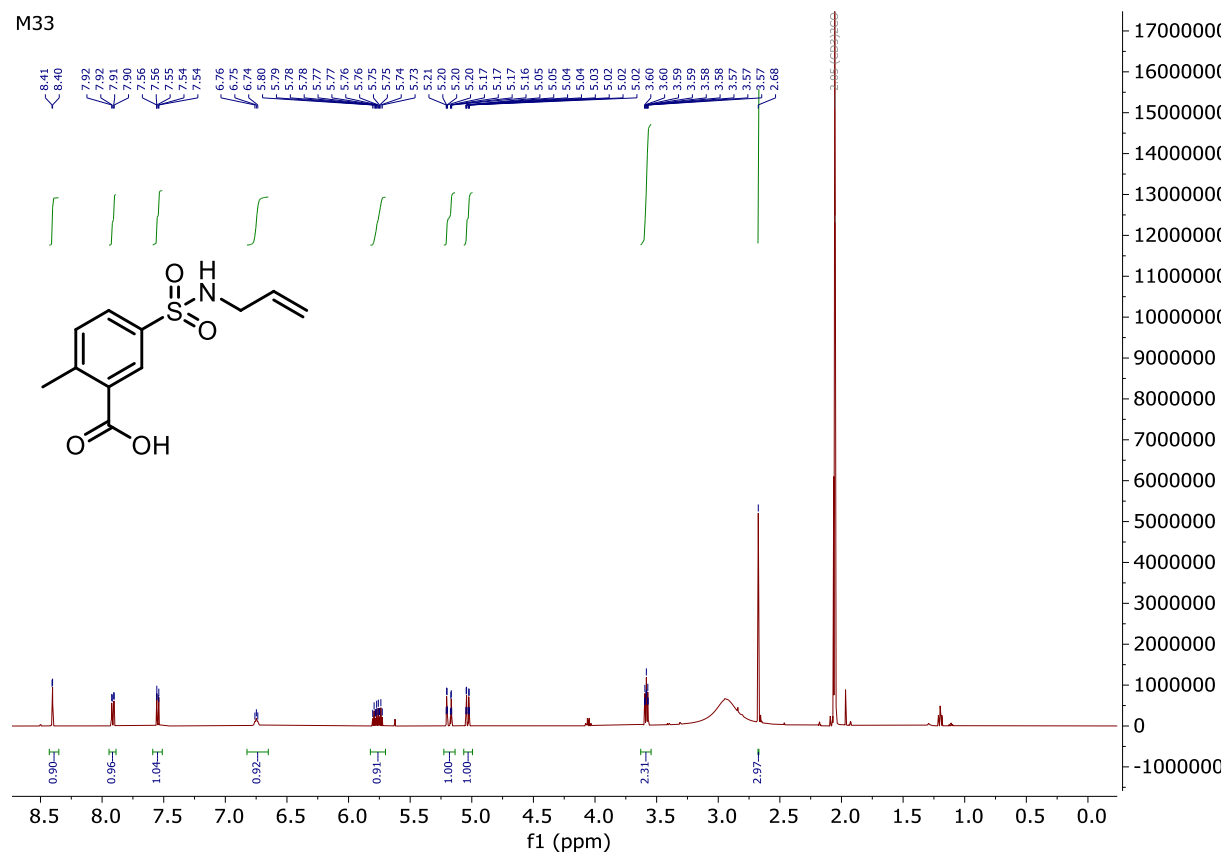
3-Allyl-1H-indole-2-carbaldehyde (M23)

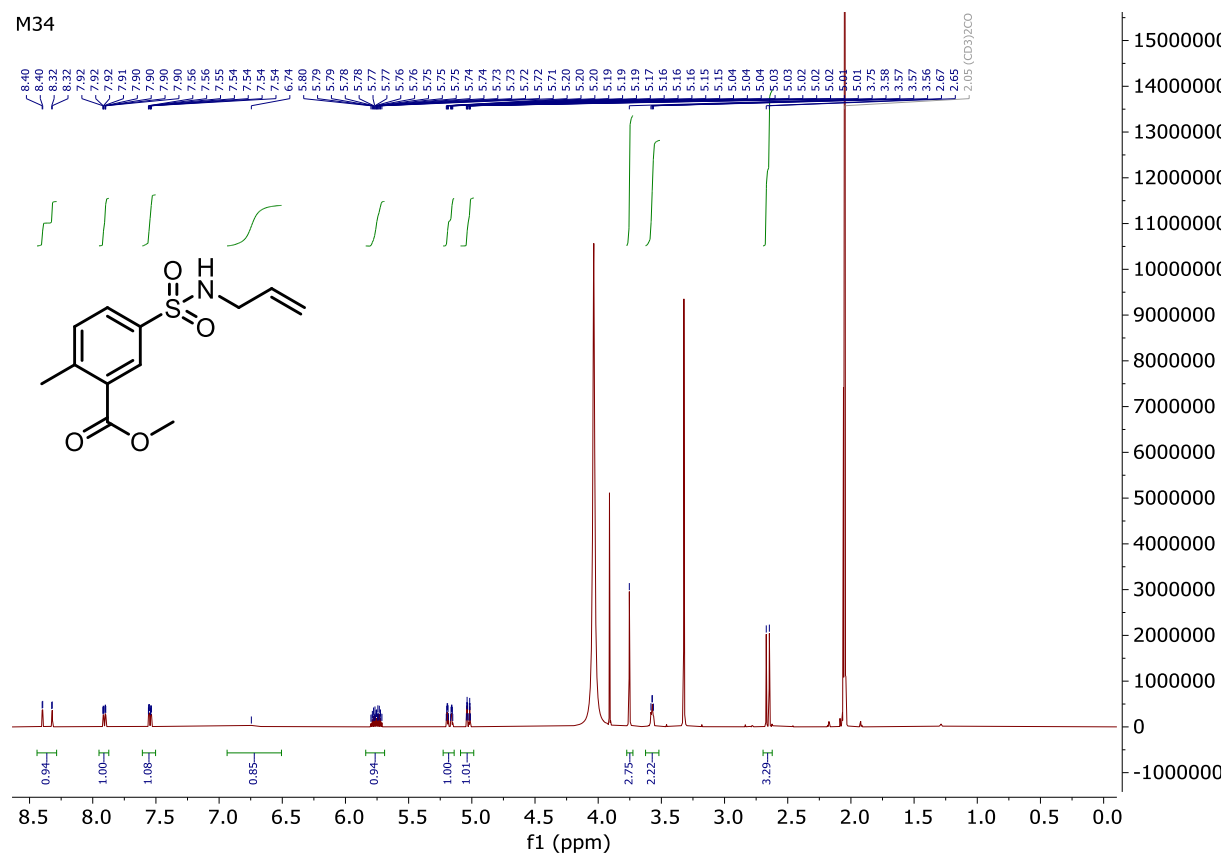
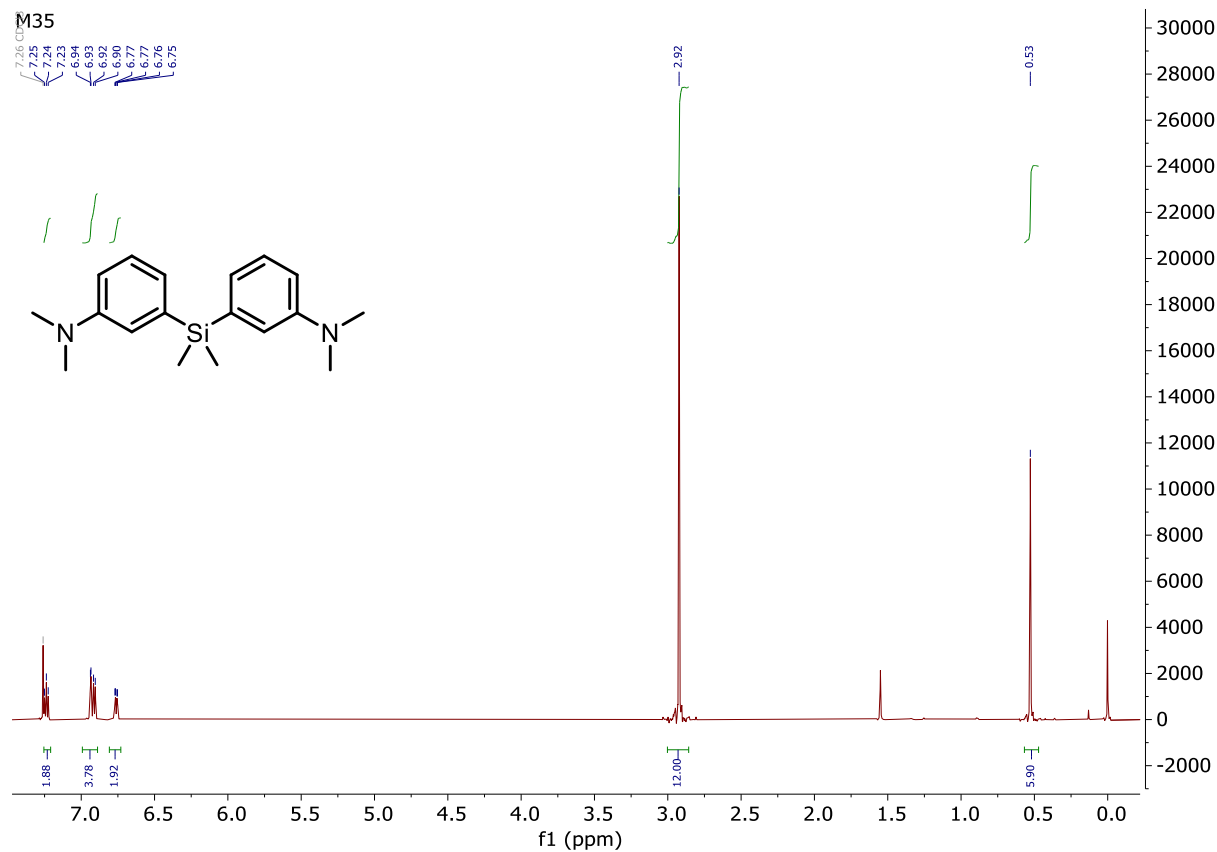


1-(3-Allyl-1H-indol-2-yl)prop-2-en-1-ol (M24)

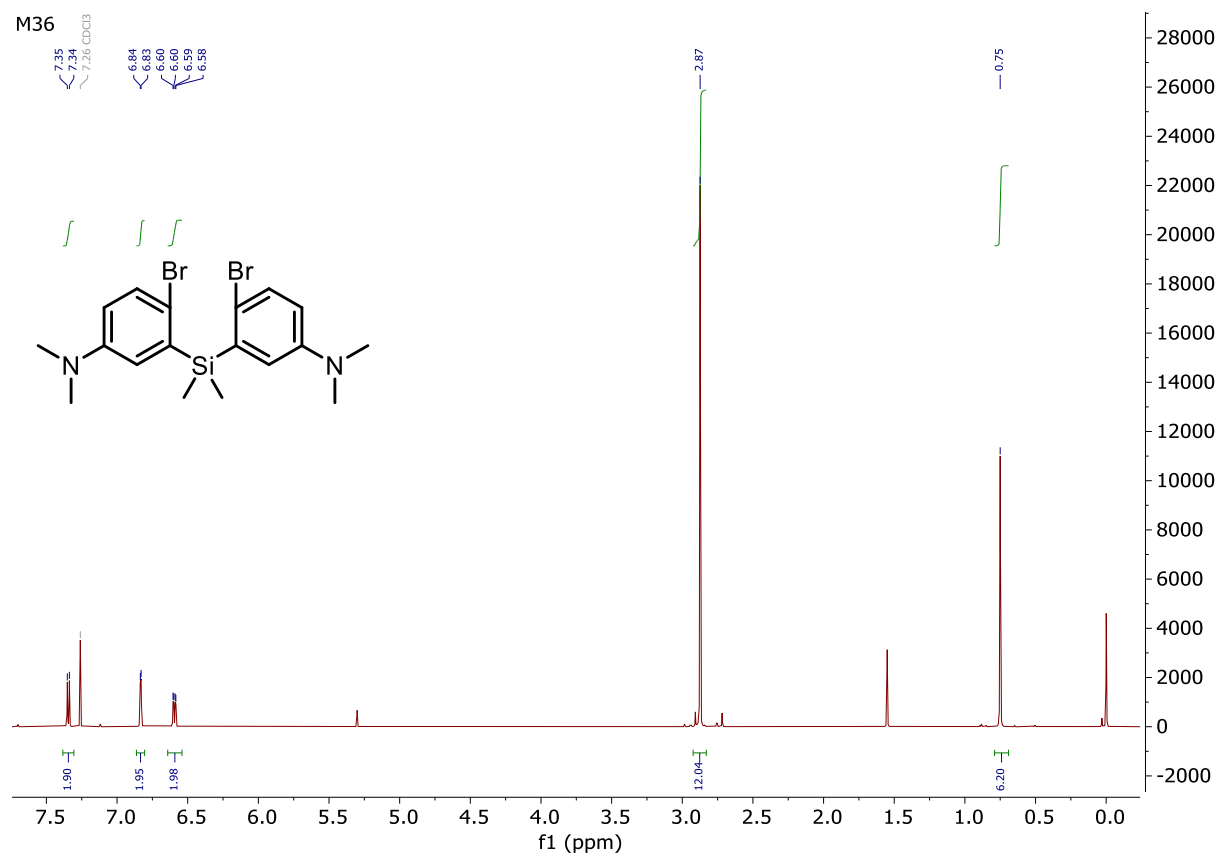


1-(2-Allylphenyl)allyl (4-nitrophenyl) carbonate (**M25**)1-(1-(2-Allylphenyl)allyl) 4-(*tert*-butyl) piperazine-1,4-dicarboxylate (**M26**)

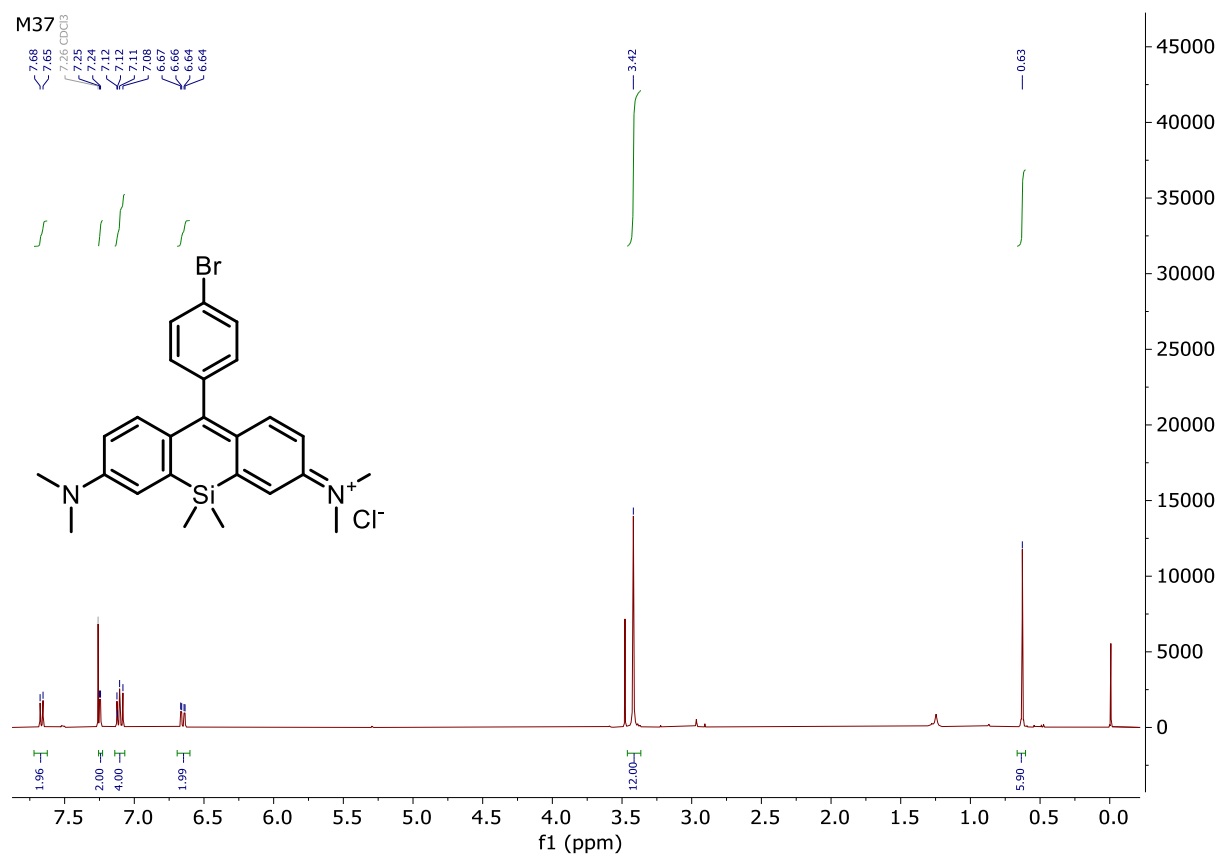
5-(Chlorosulfonyl)-2-methylbenzoic acid (**M32**)5-(*N*-Allylsulfamoyl)-2-methylbenzoic acid (**M33**)

Methyl 5-(*N*-allylsulfamoyl)-2-methylbenzoate **M34**3,3'-(Dimethylsilanediyl)bis(*N,N*-dimethylaniline) (**M35**)

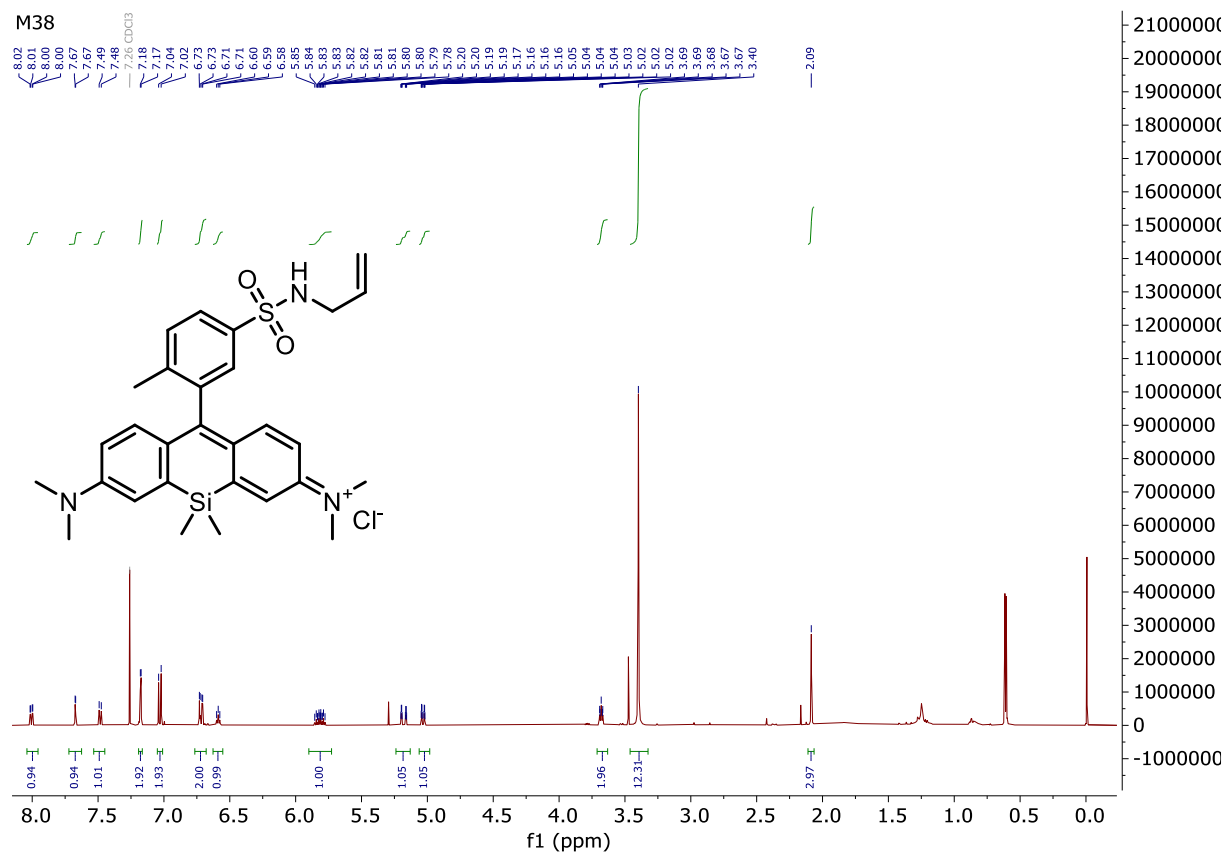
3,3'-(Dimethylsilanediyl)bis(4-bromo-*N,N*-dimethylaniline) (**M36**)



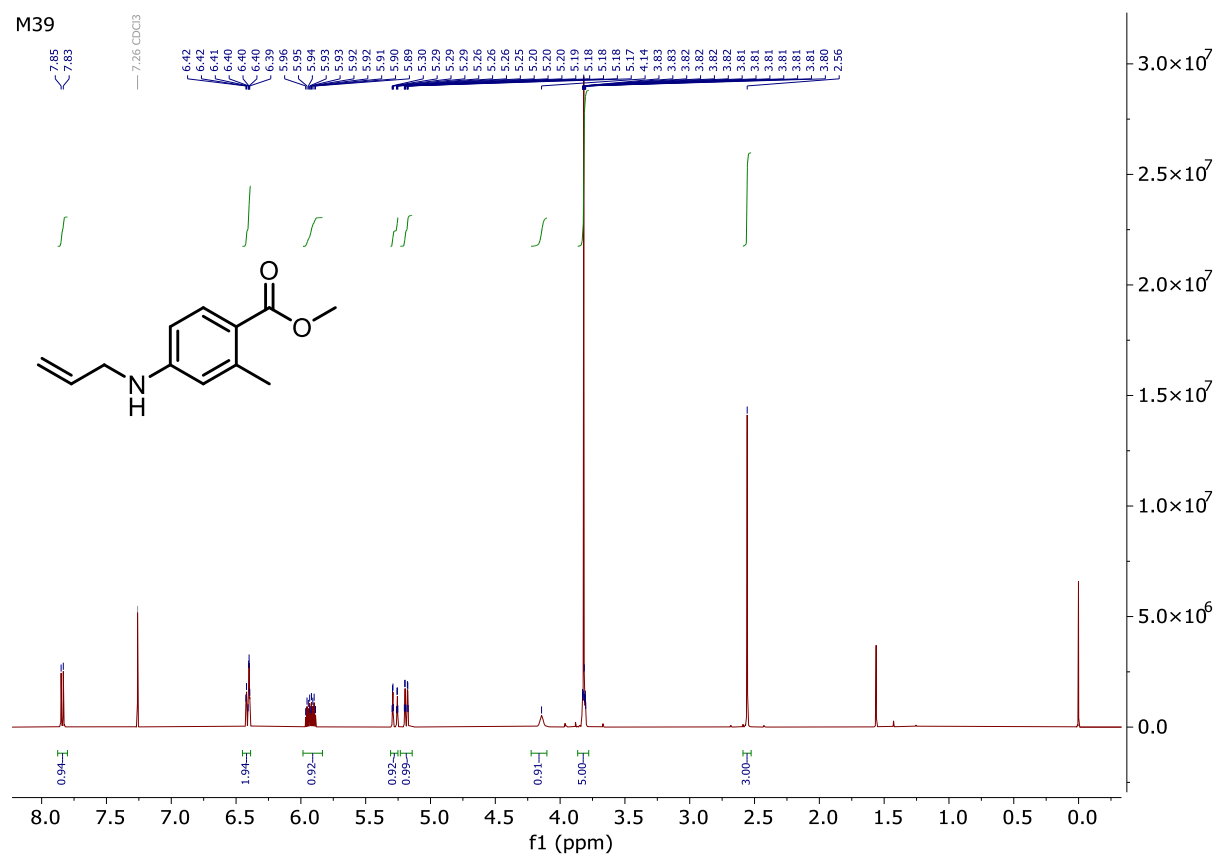
N-(10-(4-Bromophenyl)-7-(dimethylamino)-5,5-dimethyldibenzo[*b,e*]silin-3(*5H*)-ylidene)-*N*-methylmethanaminium chloride (**M37**)

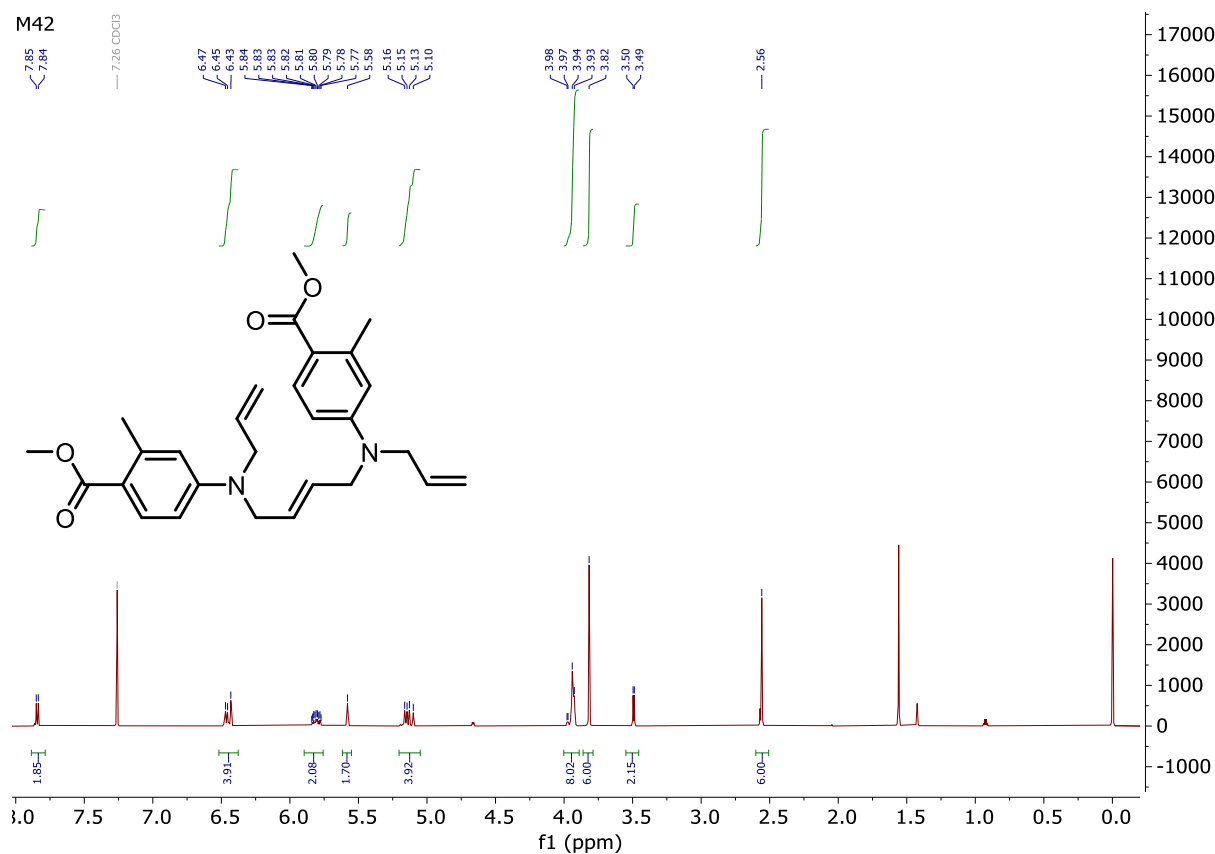


N-(10-(5-(*N*-Allylsulfamoyl)-2-methylphenyl)-7-(dimethylamino)-5,5-dimethyldibenzo[*b,e*]silin-3(5*H*)-ylidene)-*N*-methylmethanaminium chloride (**M38**)

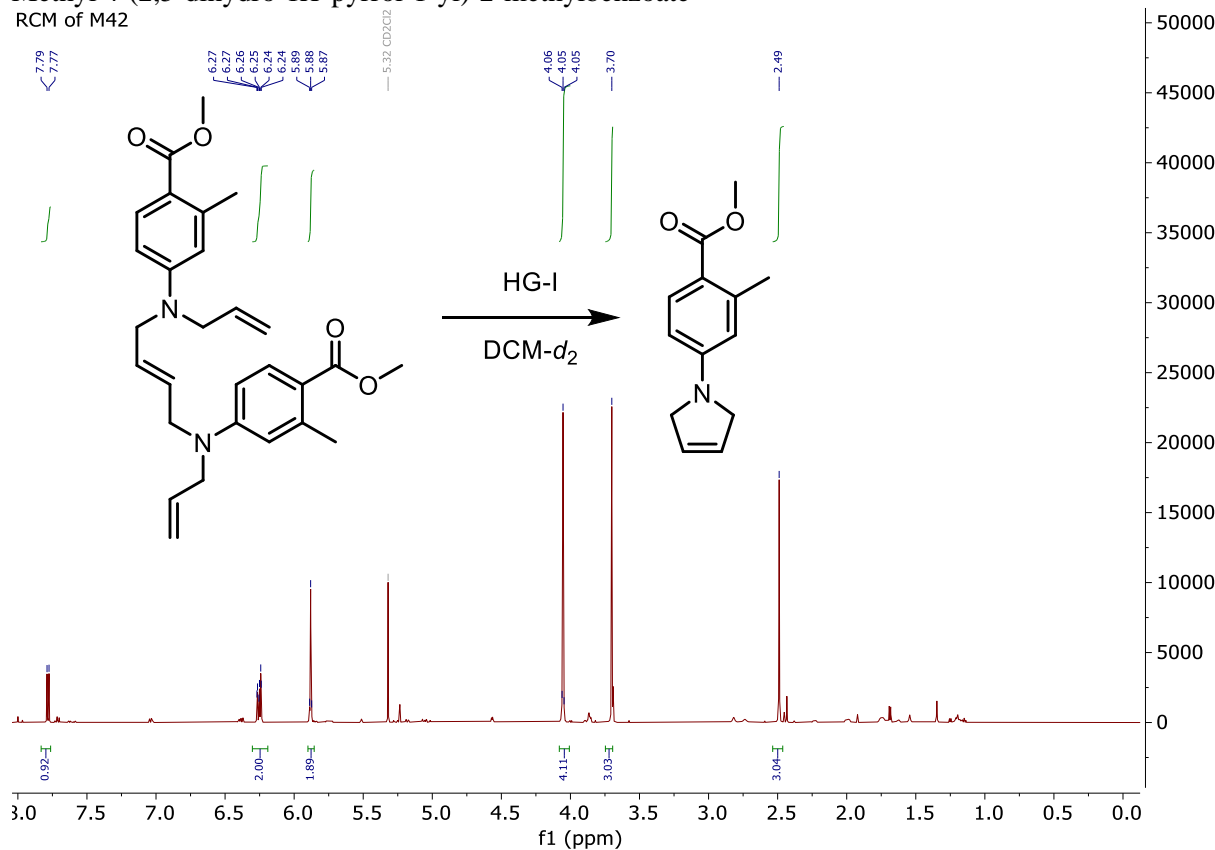


Methyl 4-(allylamino)-2-methylbenzoate (**M39**)



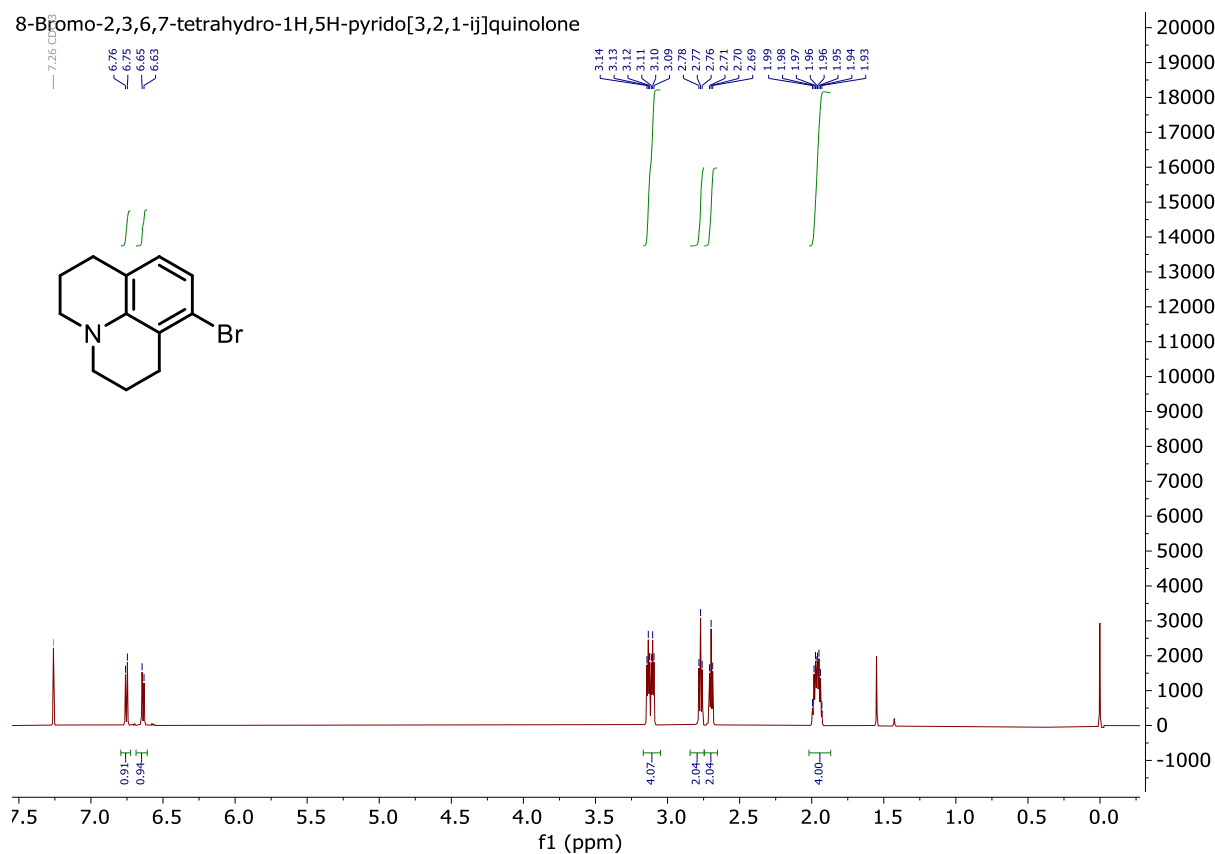
Dimethyl 4,4'-(but-2-ene-1,4-diylbis(allylzanediyl))(E)-bis(2-methylbenzoate) (**M42**)

Methyl 4-(2,5-dihydro-1H-pyrrol-1-yl)-2-methylbenzoate

RCM of **M42**

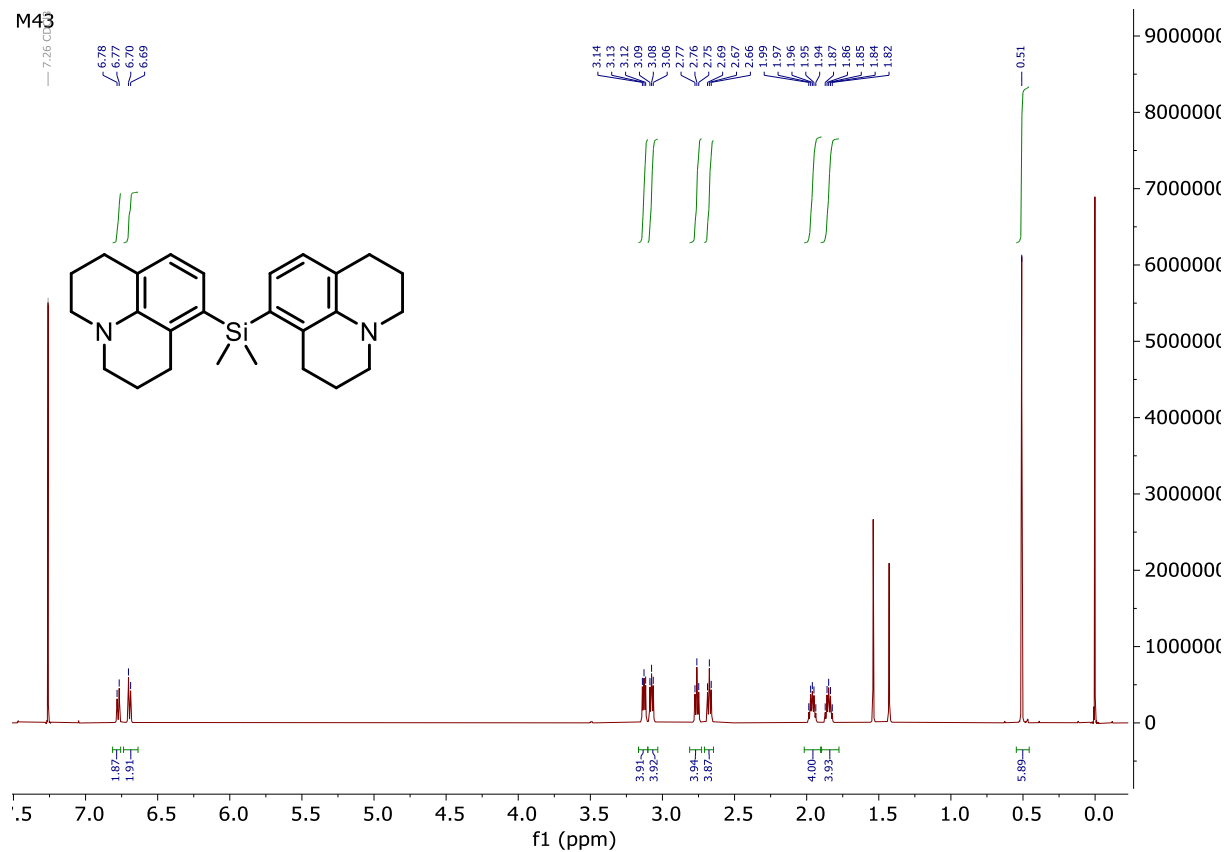
8-Bromo-2,3,6,7-tetrahydro-1*H*,5*H*-pyrido[3,2,1-*ij*]quinolone

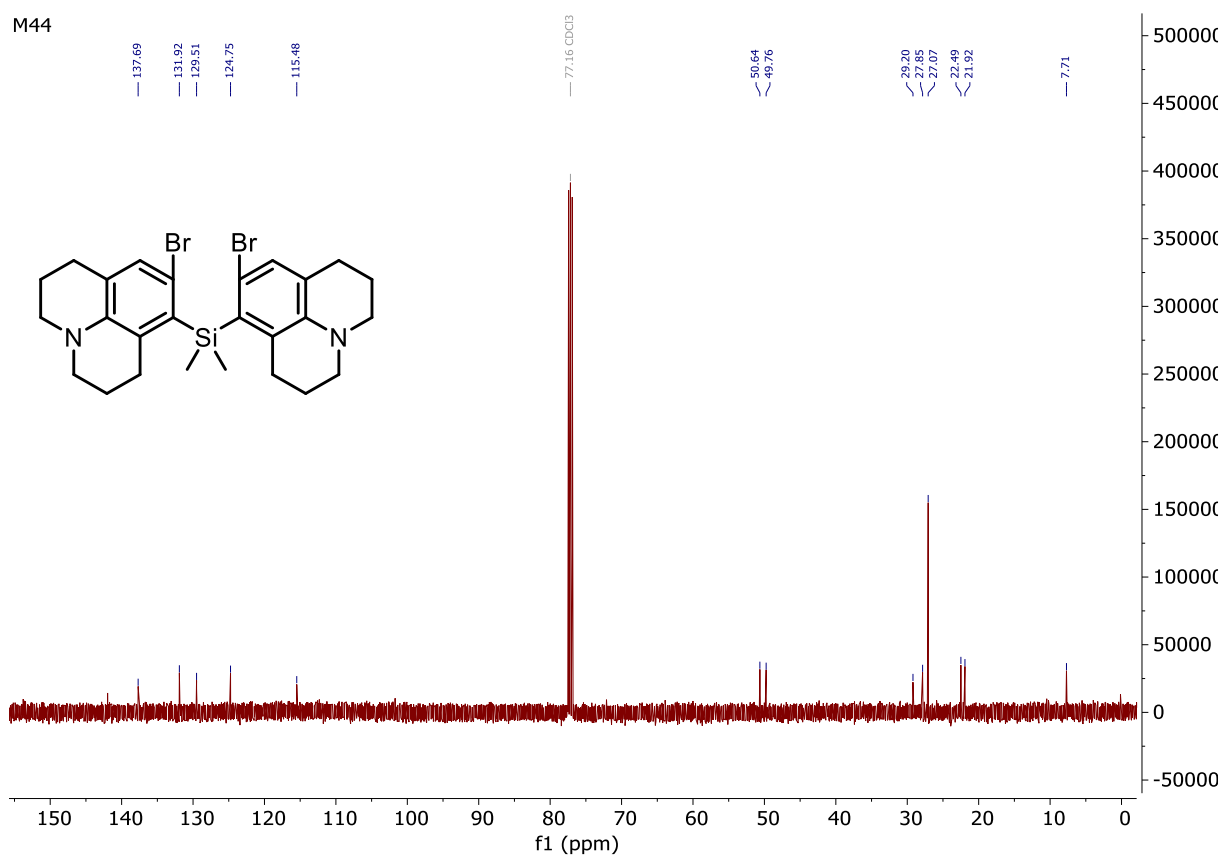
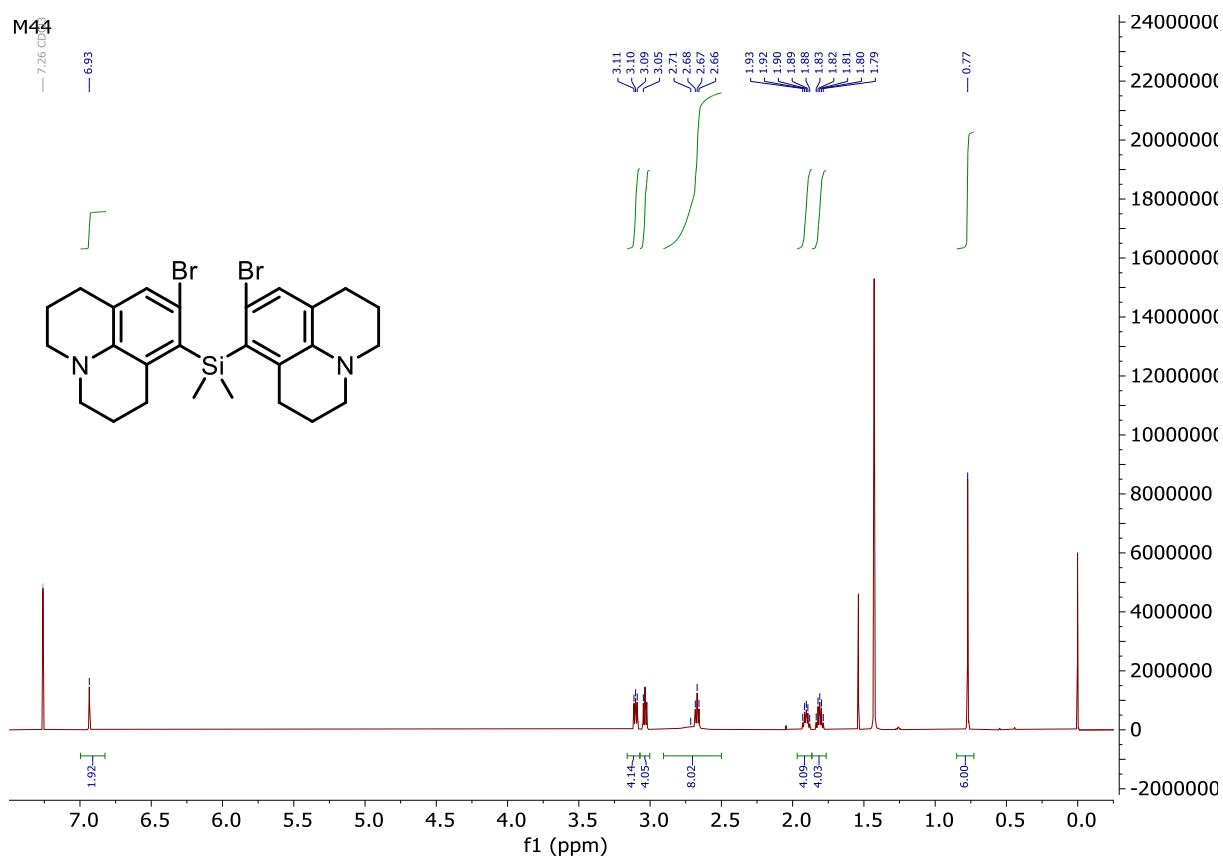
8-Bromo-2,3,6,7-tetrahydro-1*H*,5*H*-pyrido[3,2,1-*ij*]quinolone

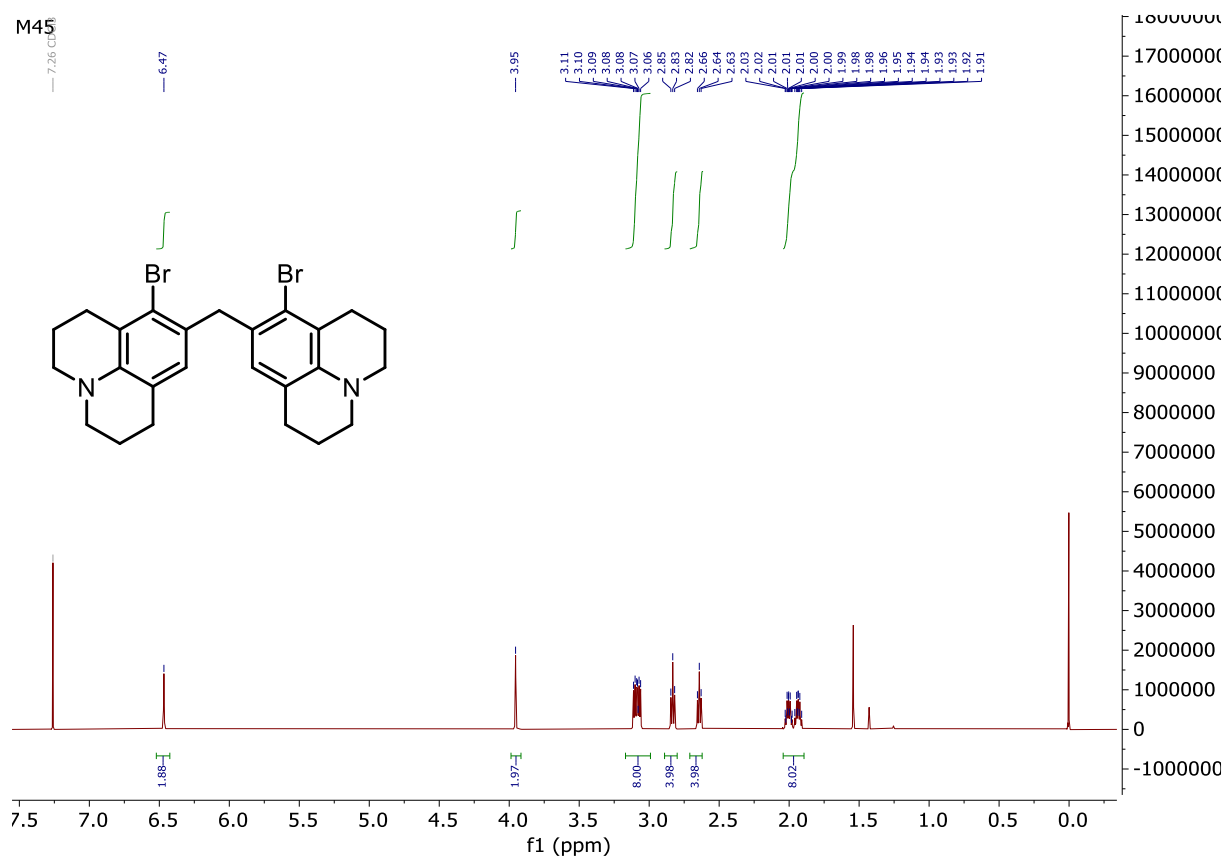
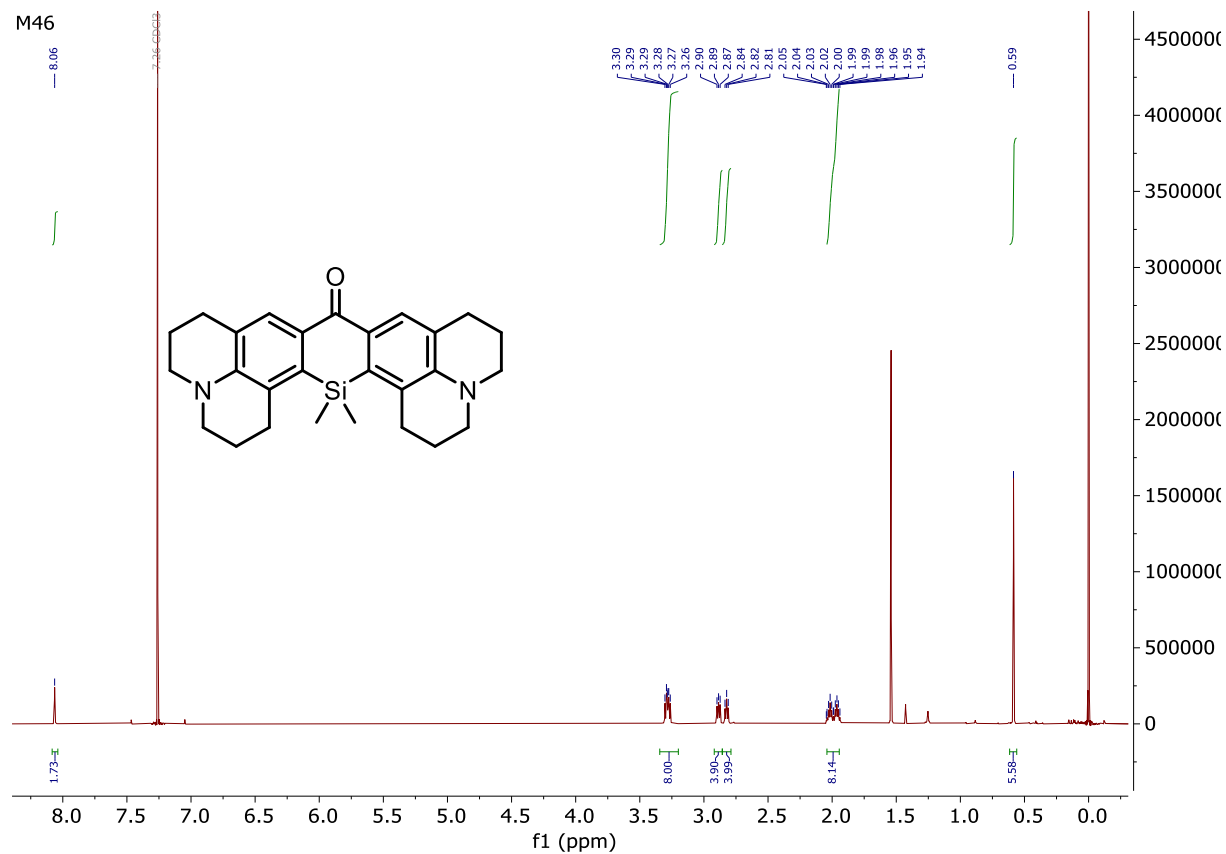


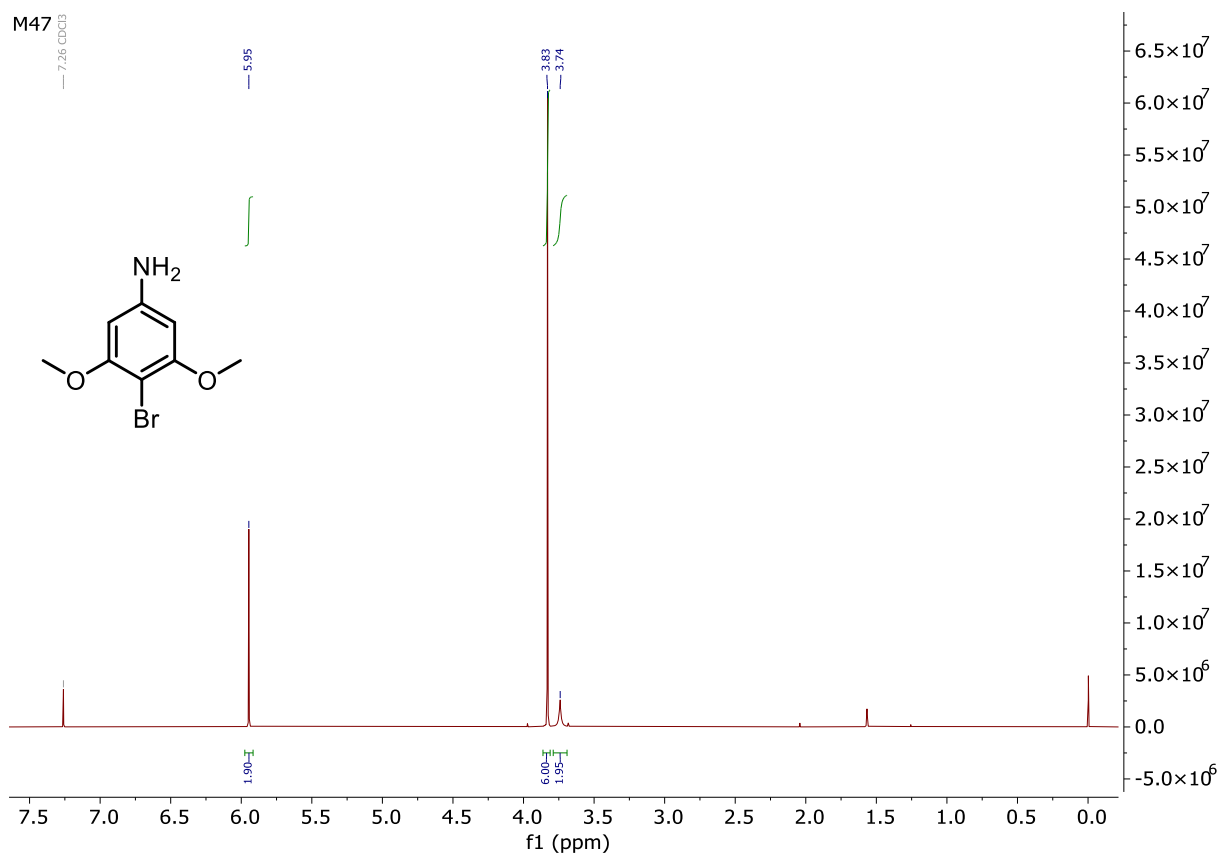
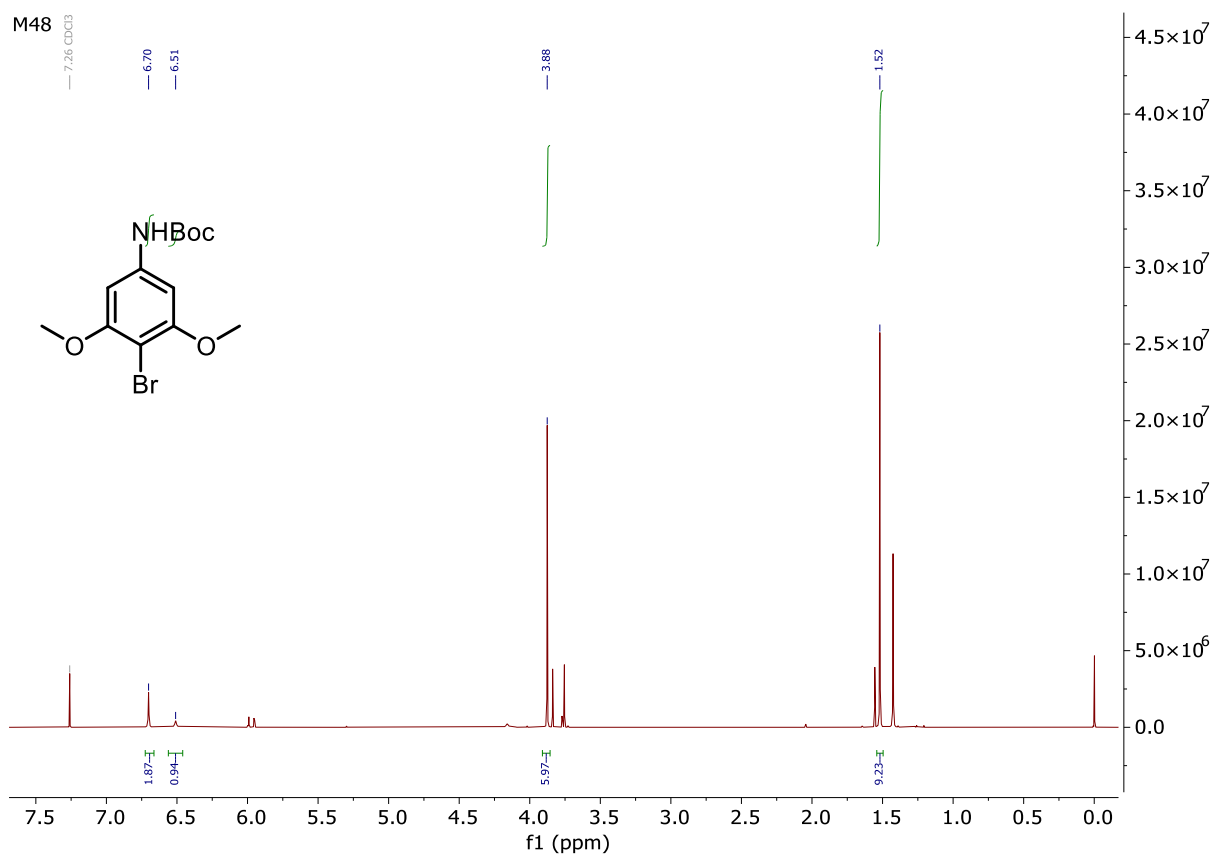
Dimethylbis(2,3,6,7-tetrahydro-1*H*,5*H*-pyrido[3,2,1-*ij*]quinolin-8-yl)silane (**M43**)

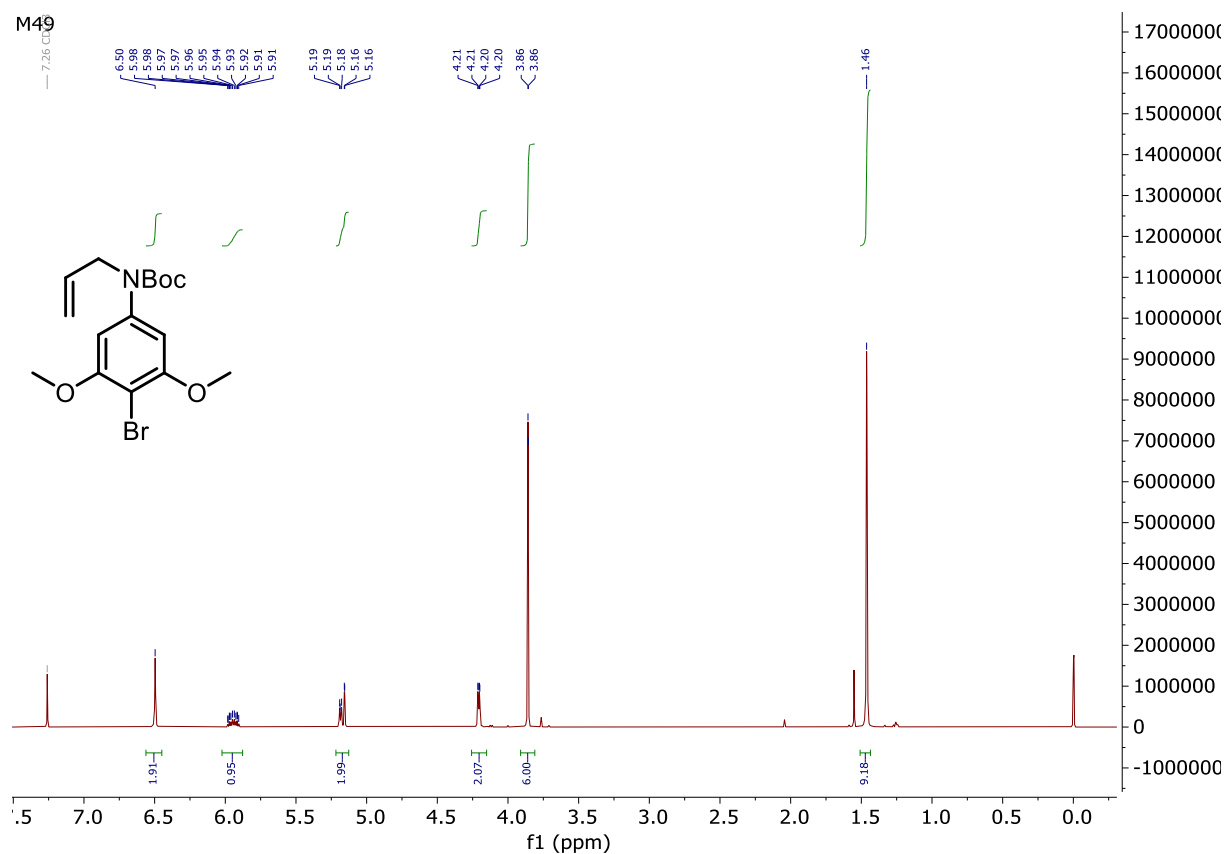
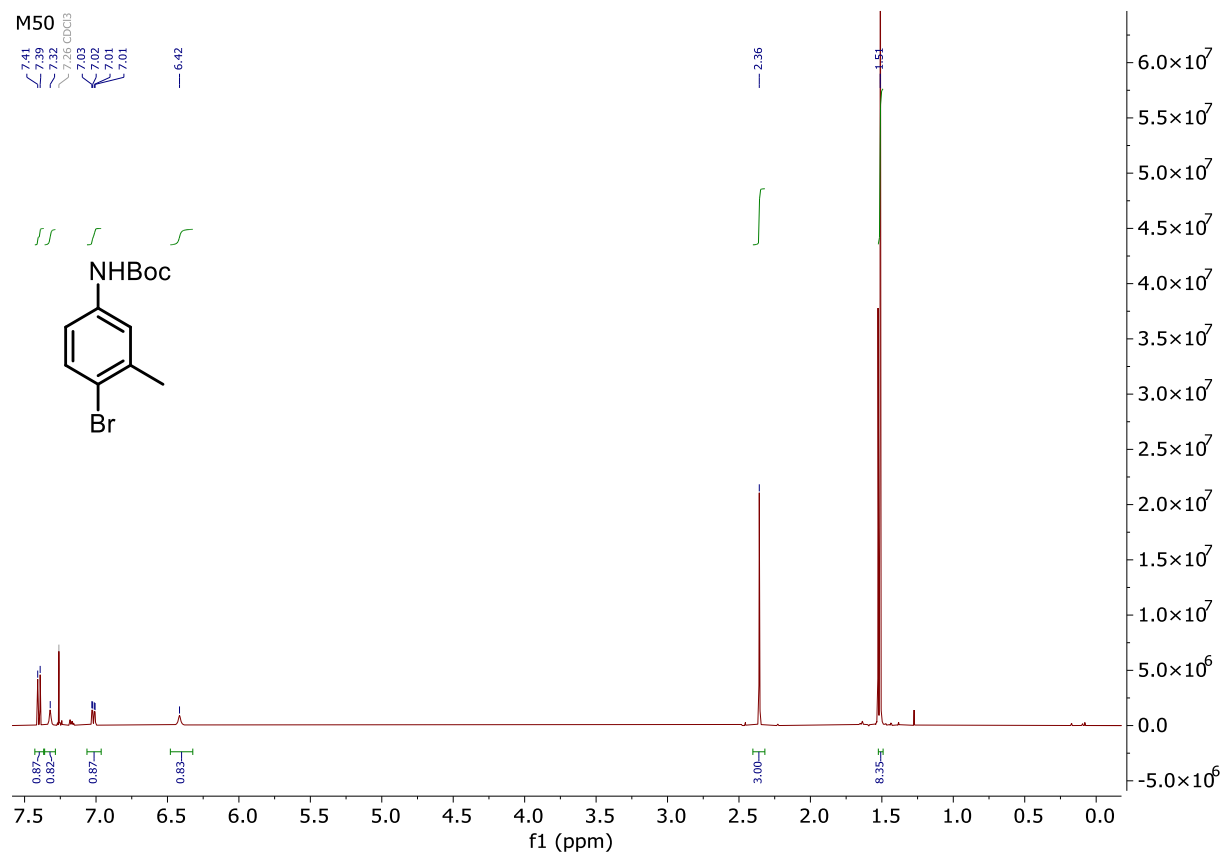
M43

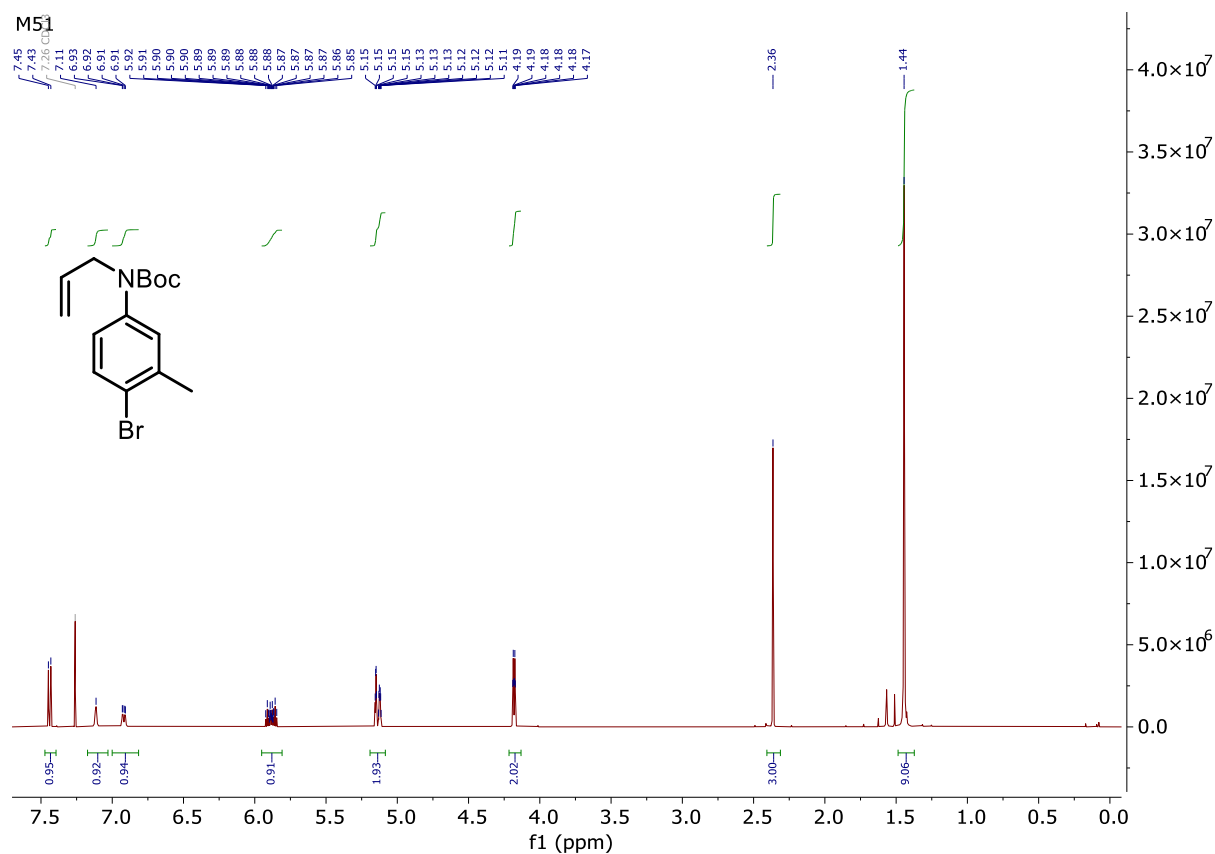
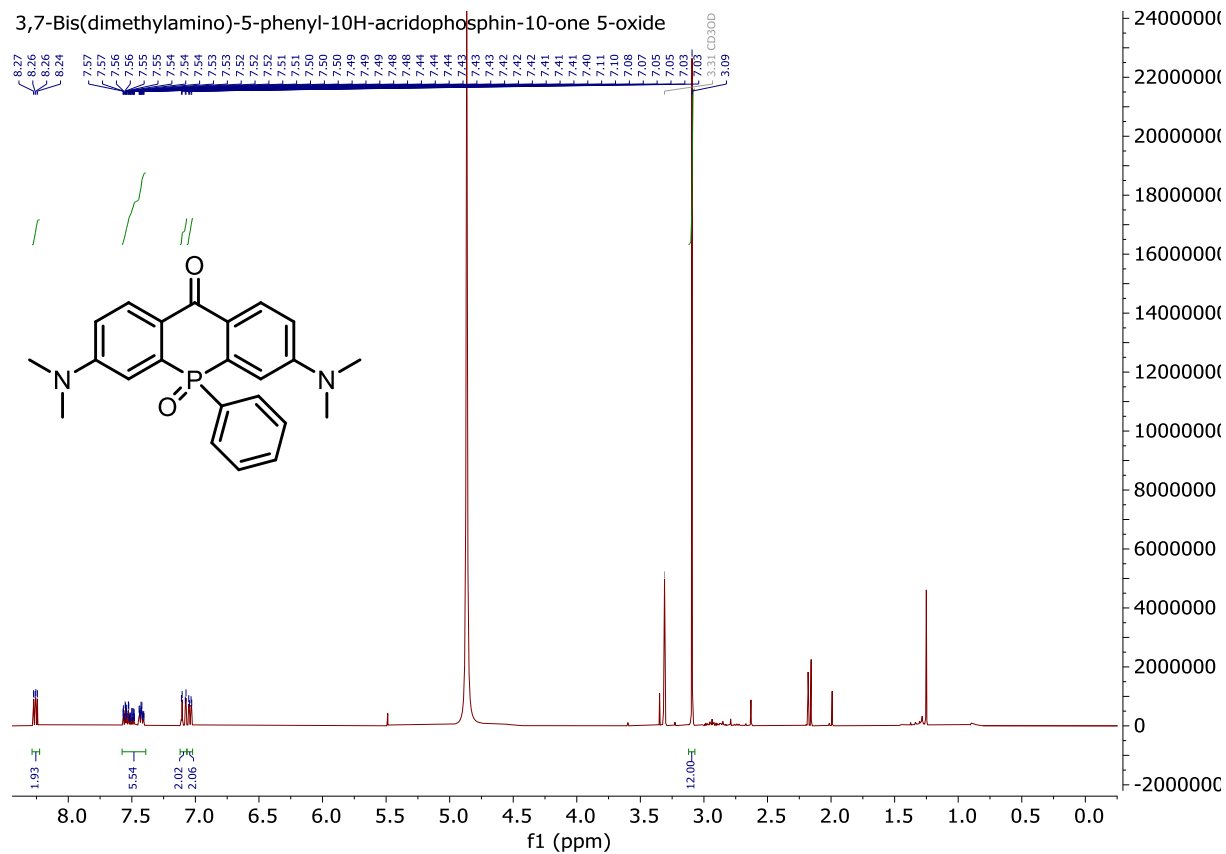


Bis(9-bromo-2,3,6,7-tetrahydro-1*H*,5*H*-pyrido[3,2-*ij*]quinolin-8-yl)dimethylsilane (**M44**)

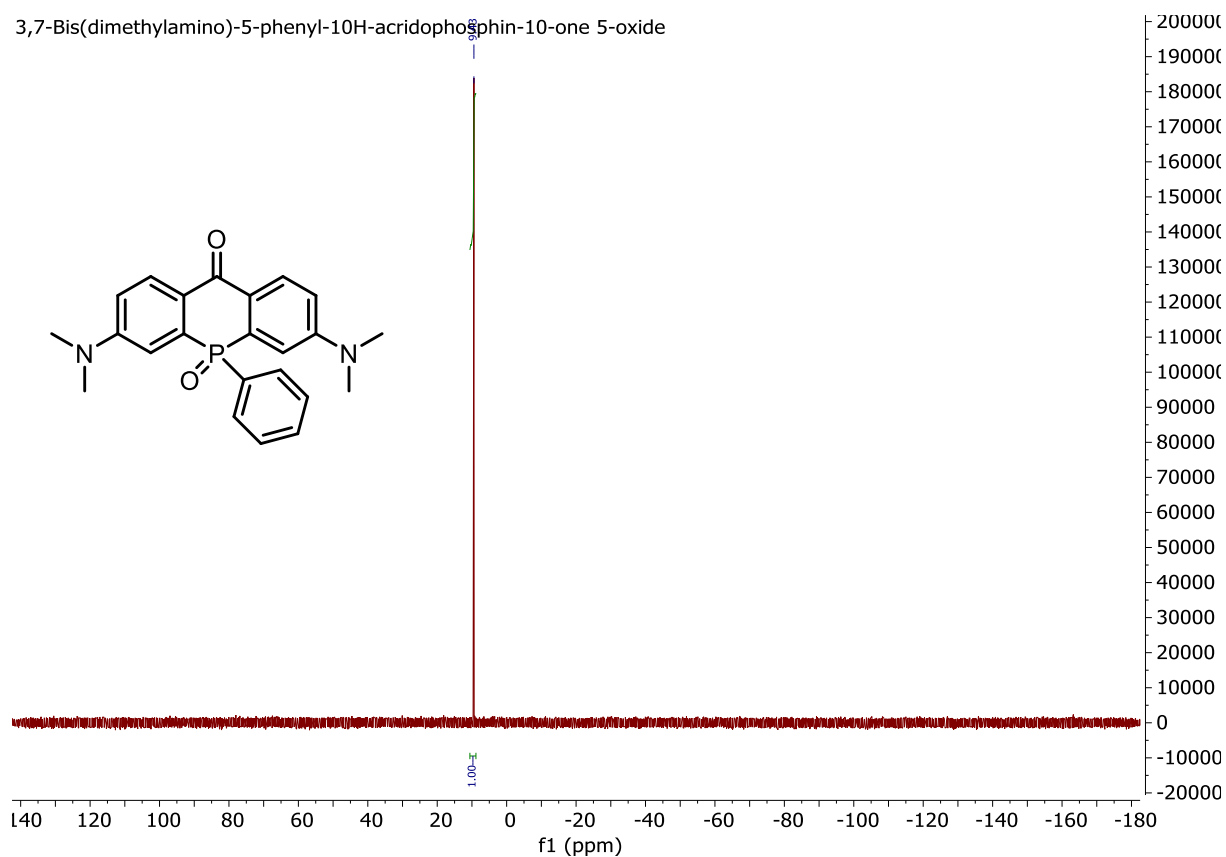
Bis(8-bromo-2,3,6,7-tetrahydro-1*H*,5*H*-pyrido[3,2-*ij*]quinolin-9-yl)methane (**M45**)Phenone **M46**

4-Bromo-3,5-dimethoxyaniline (**M47**)*Tert*-butyl (4-bromo-3,5-dimethoxyphenyl)carbamate (**M48**)

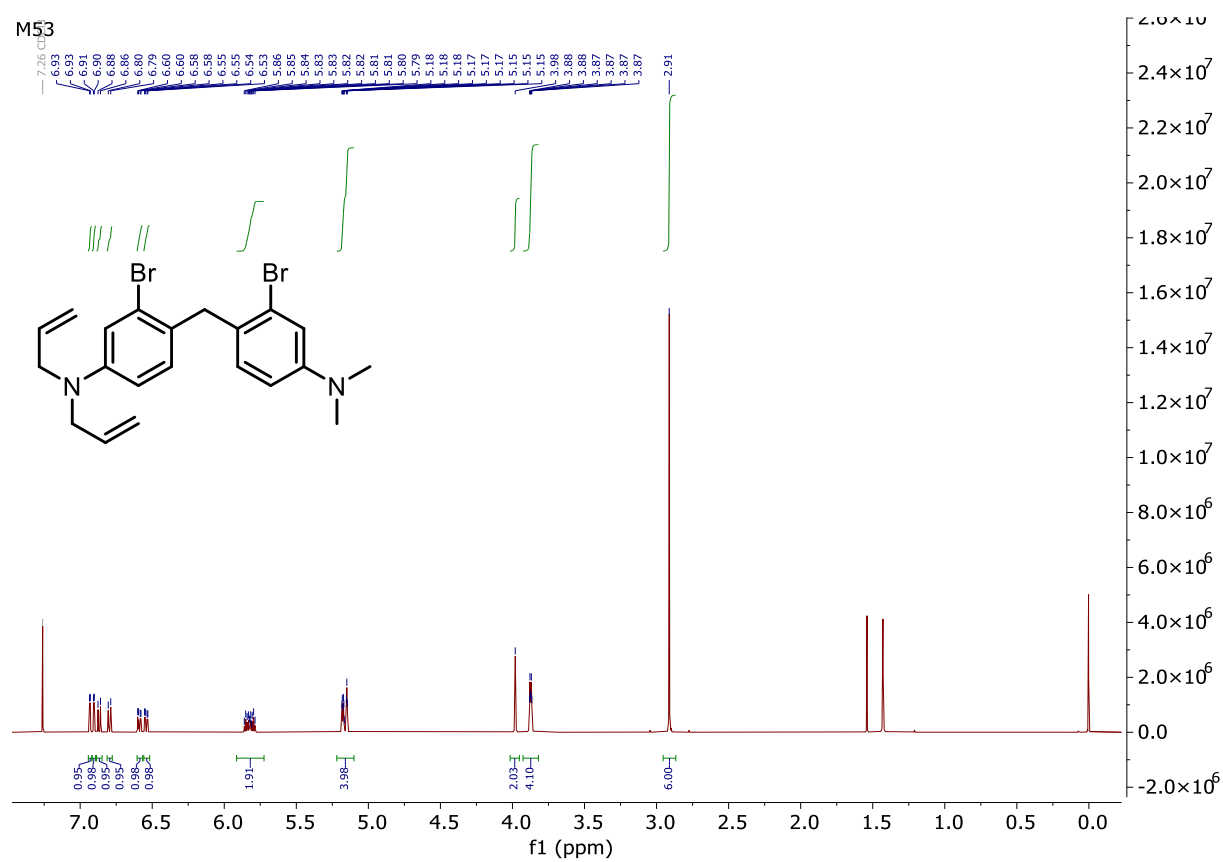
Tert-butyl allyl(4-bromo-3,5-dimethoxyphenyl)carbamate (**M49**)*Tert*-butyl (4-bromo-3-methylphenyl)carbamate (**M50**)

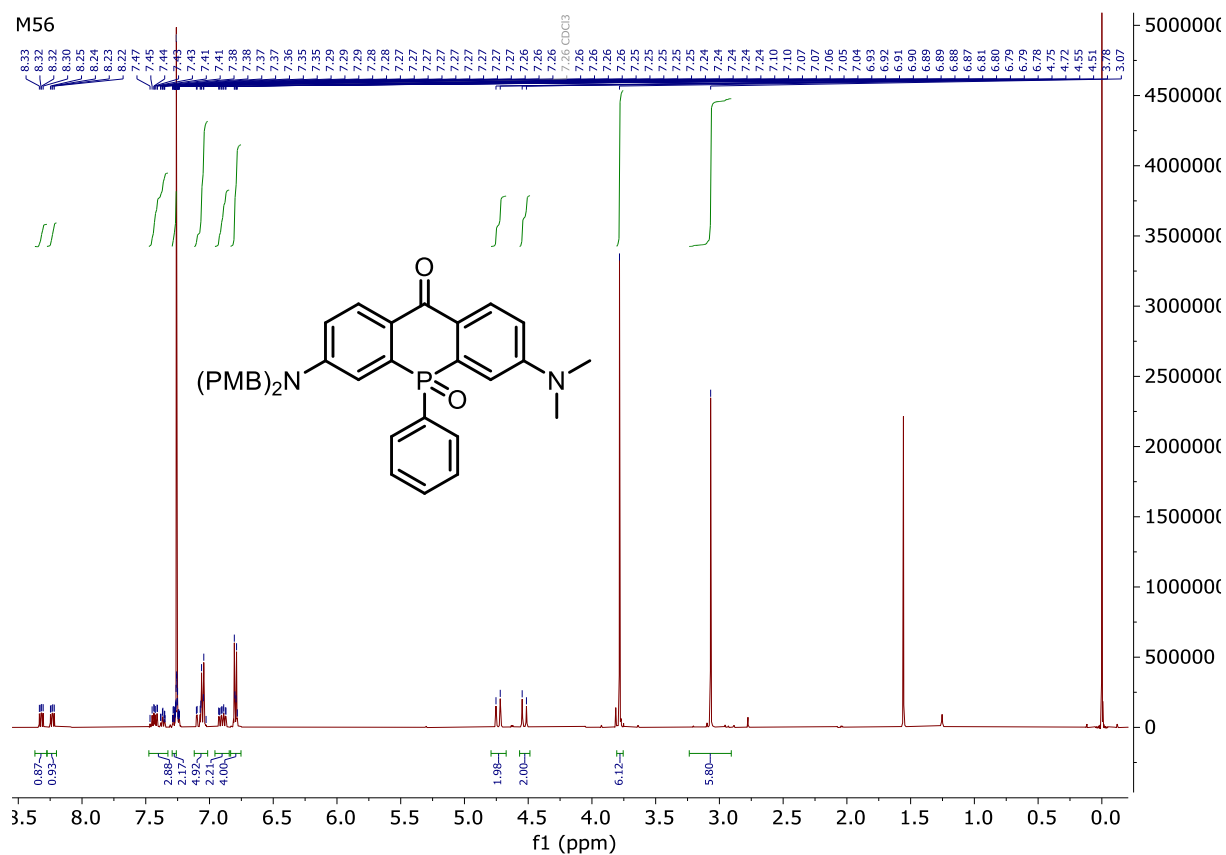
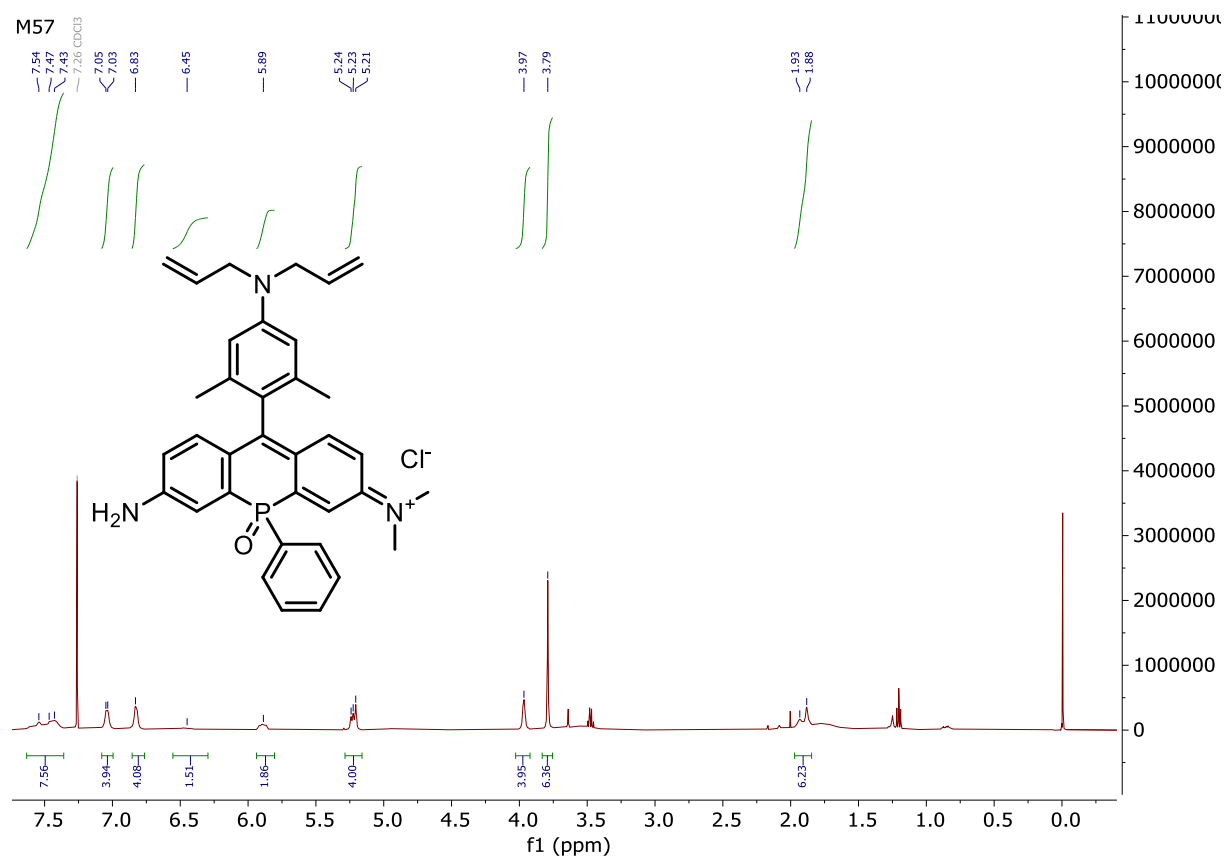
Tert-butyl allyl(4-bromo-3-methylphenyl)carbamate (**M51**)3,7-Bis(dimethylamino)-5-phenyl-10*H*-acridophosphin-10-one 5-oxide

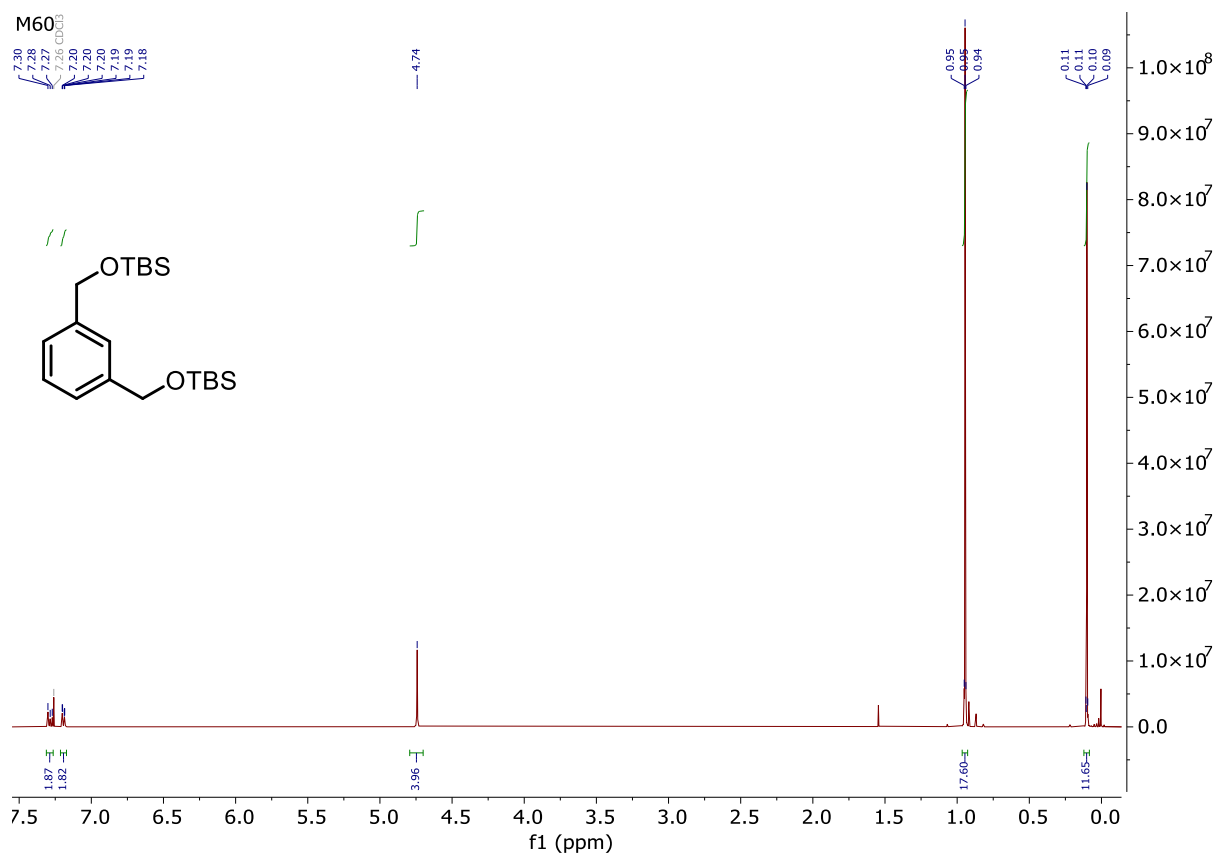
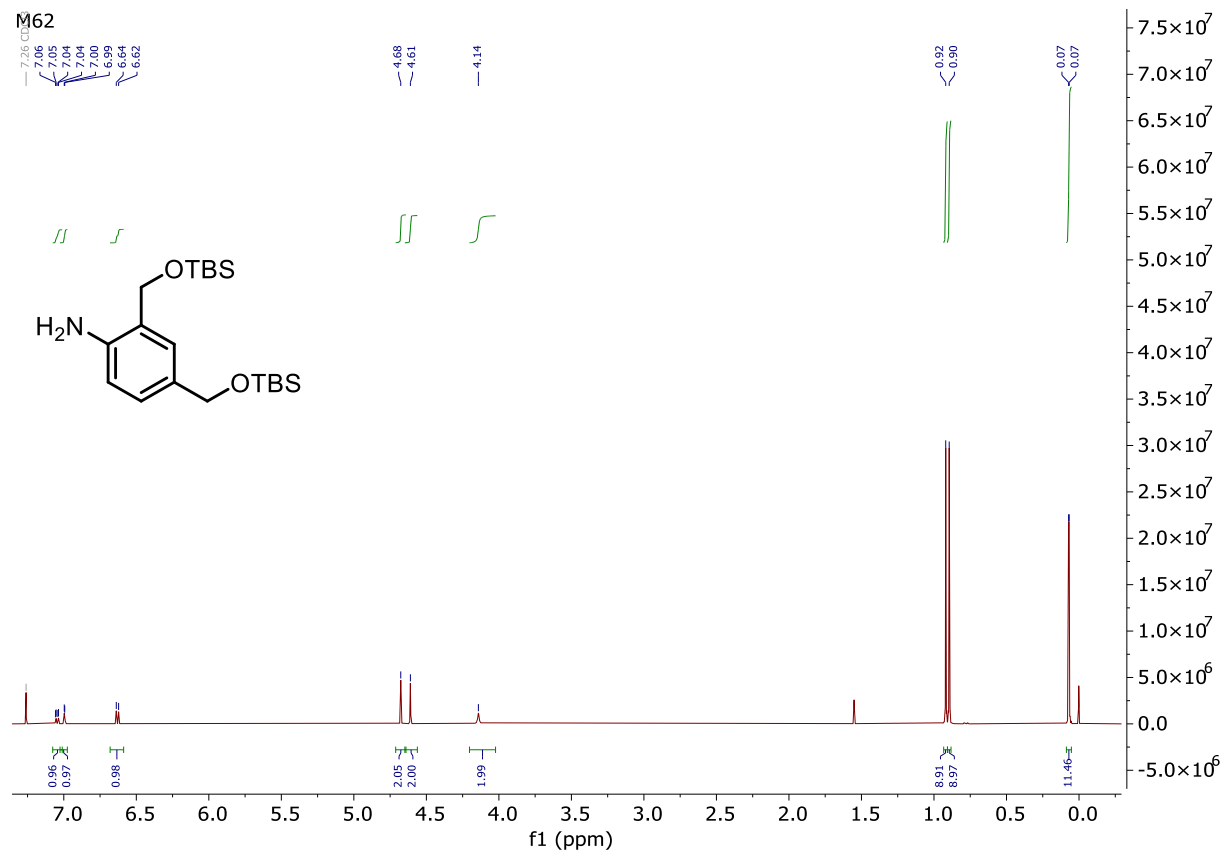
3,7-Bis(dimethylamino)-5-phenyl-10H-acridophosphin-10-one 5-oxide

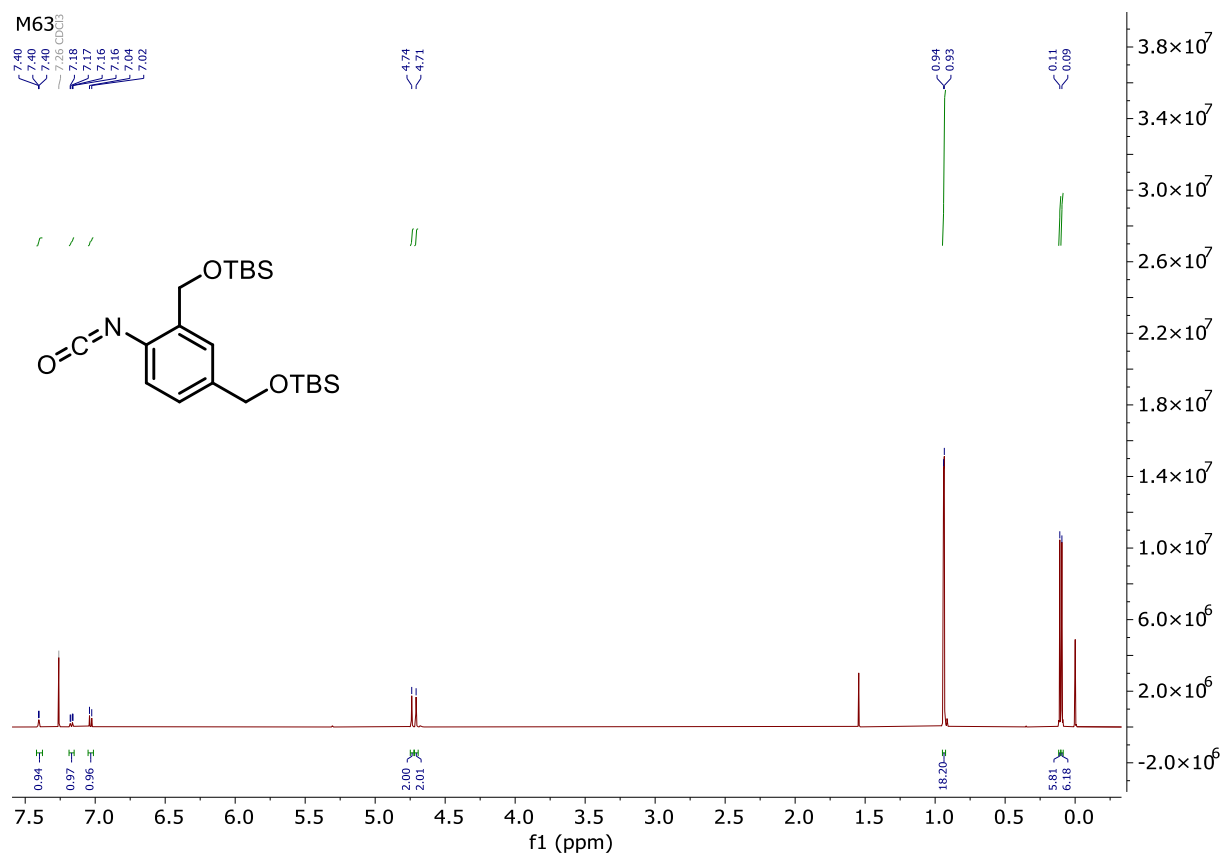
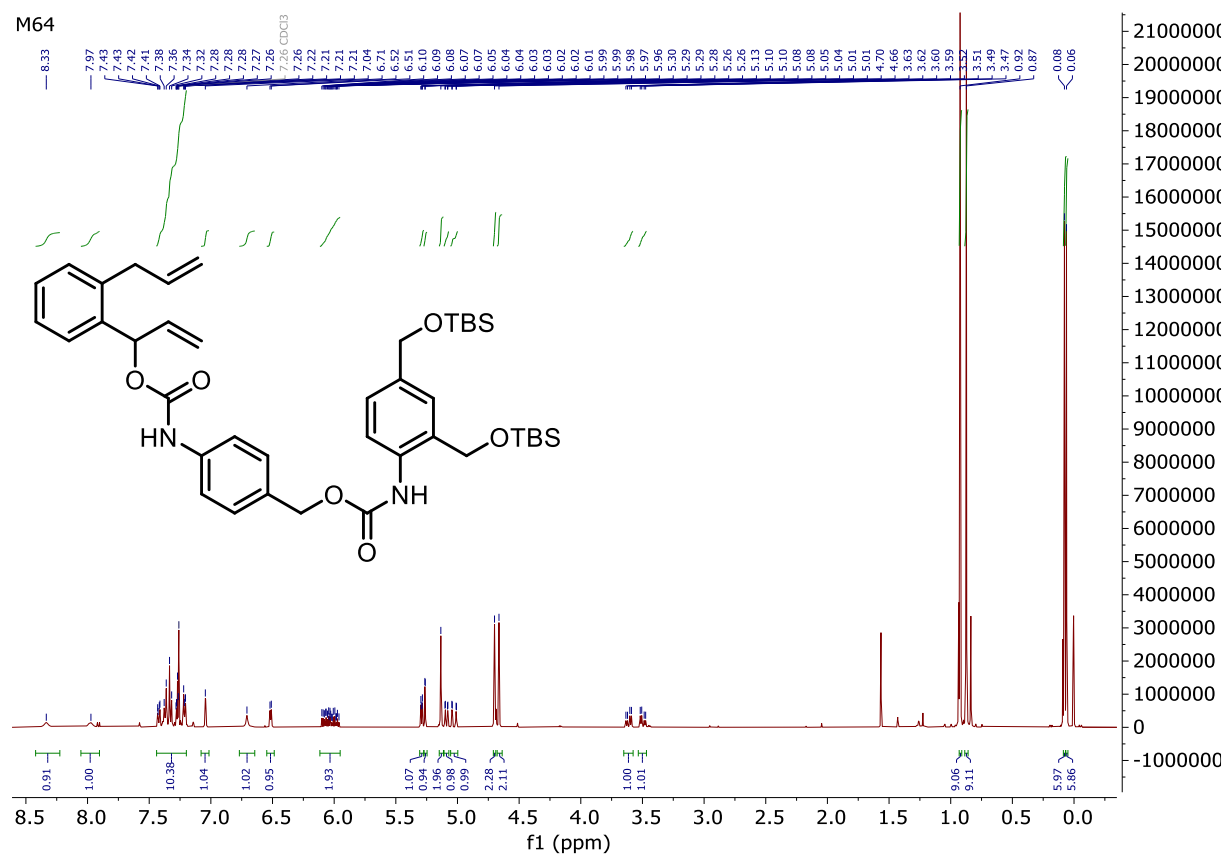


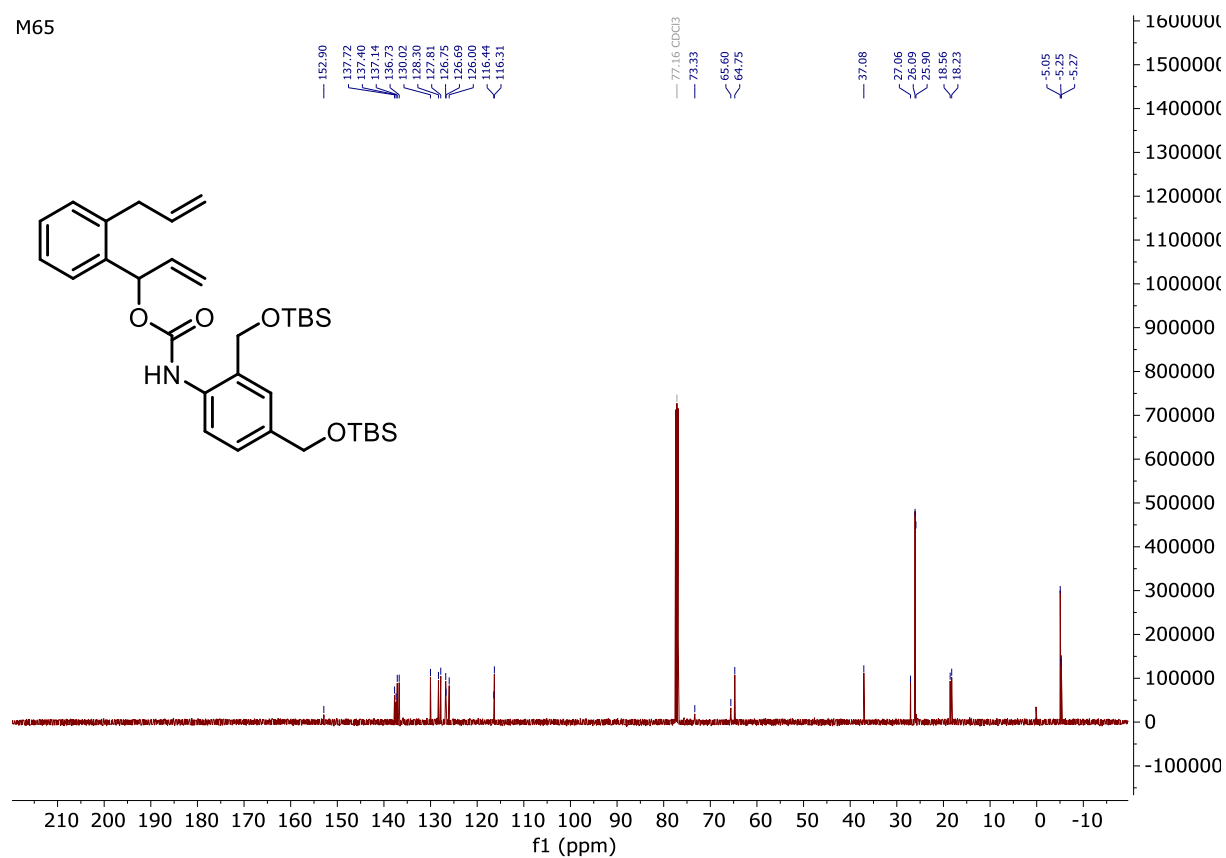
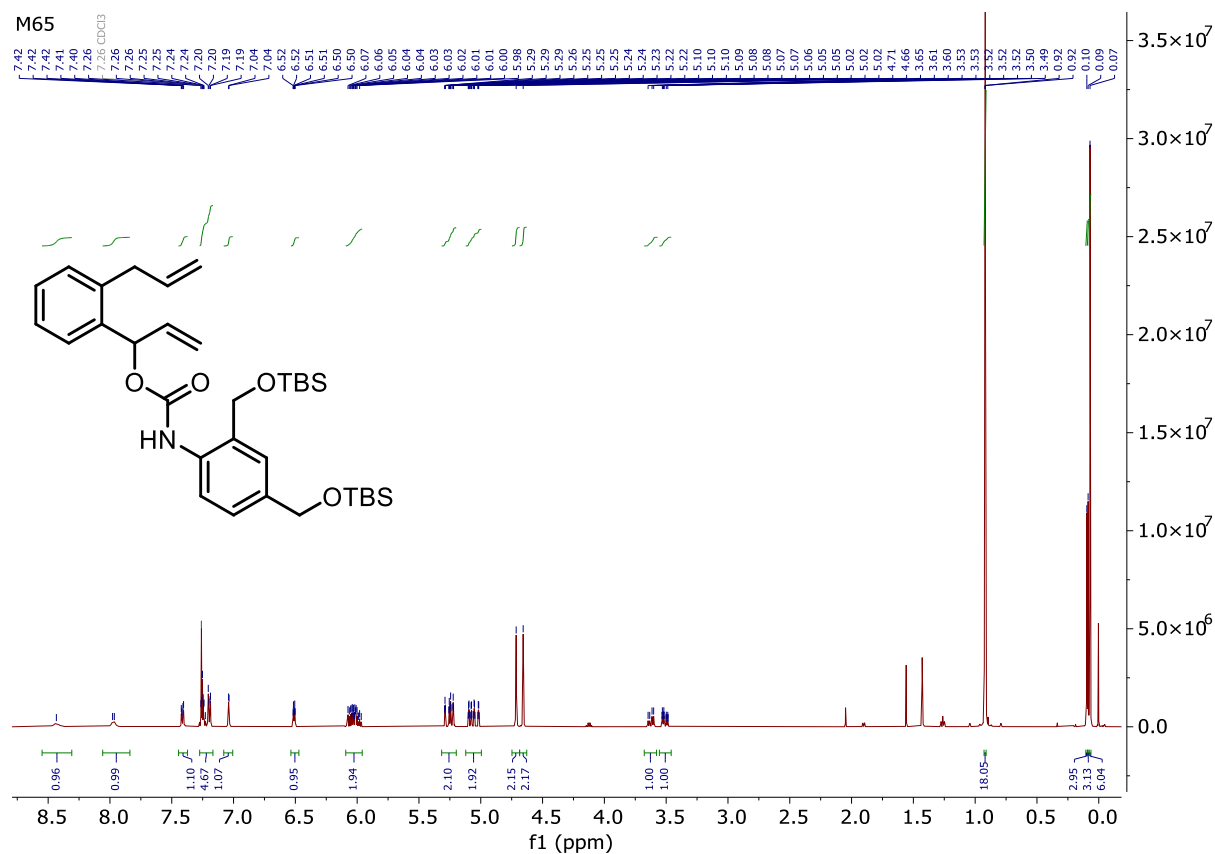
N,N-Diallyl-3-bromo-4-(2-bromo-4-(dimethylamino)benzyl)aniline (**M53**)



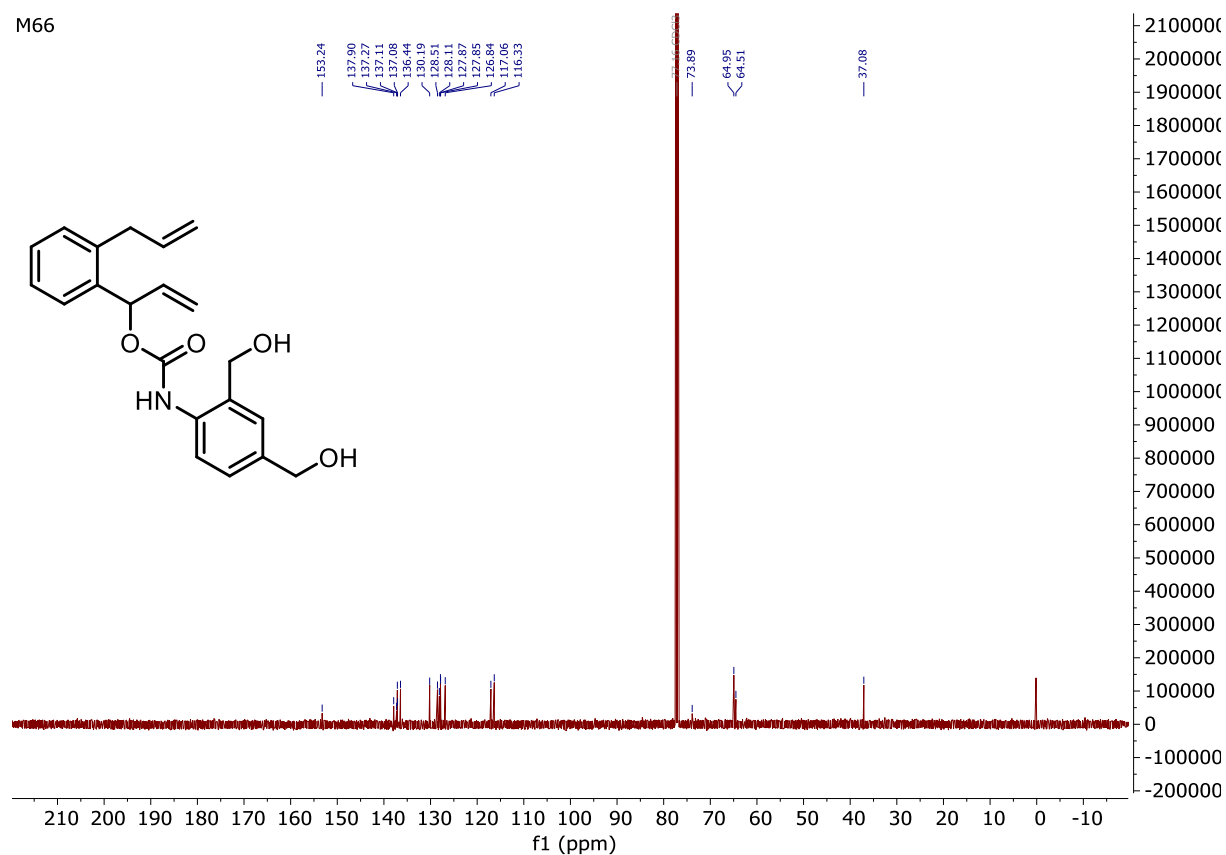
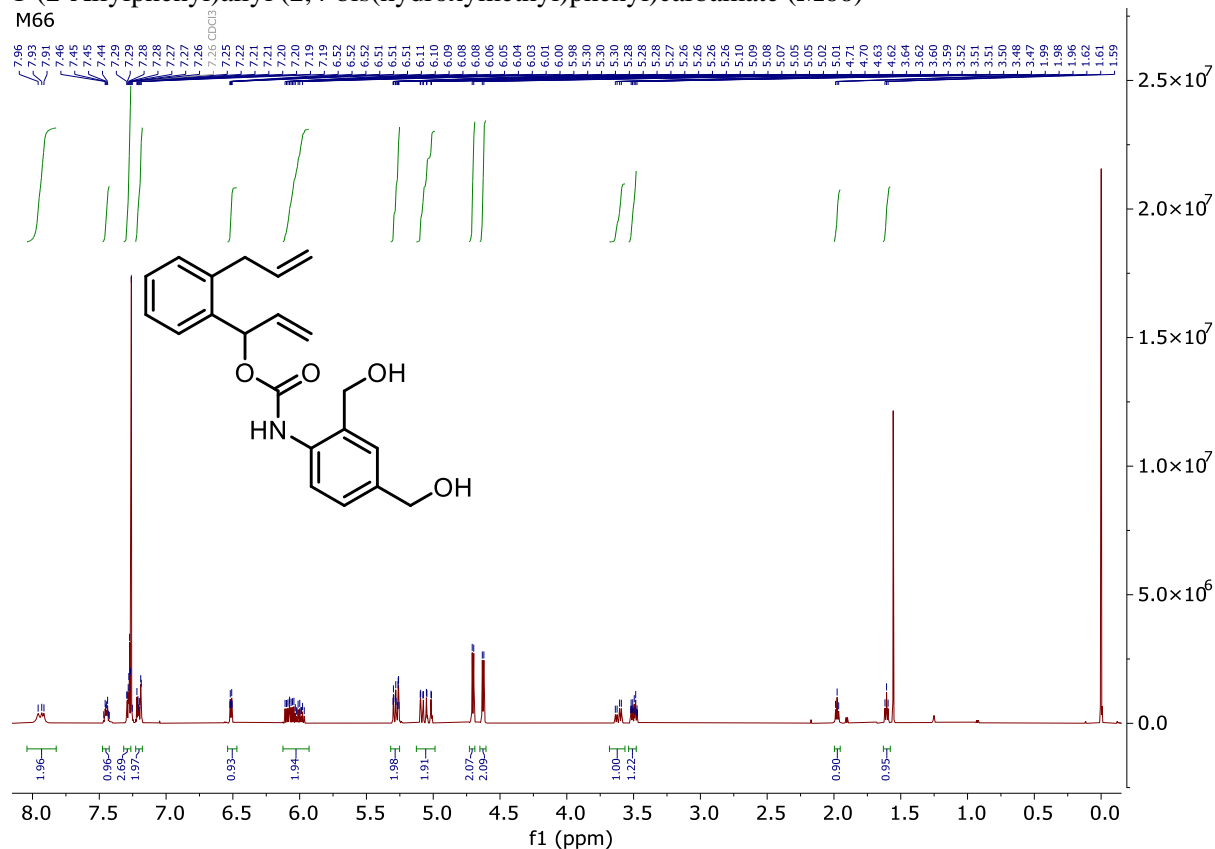
3-(bis(4-methoxybenzyl)amino)-7-(dimethylamino)-5-phenyl-10*H*-acridophosphin-10-one 5-oxide (M56)*N*-(7-Amino-10-(4-(diallylamino)-2,6-dimethylphenyl)-5-oxido-5-phenyl-3*H*-acridophosphin-3-ylidene)-*N*-methylmethanaminium chloride (M57)

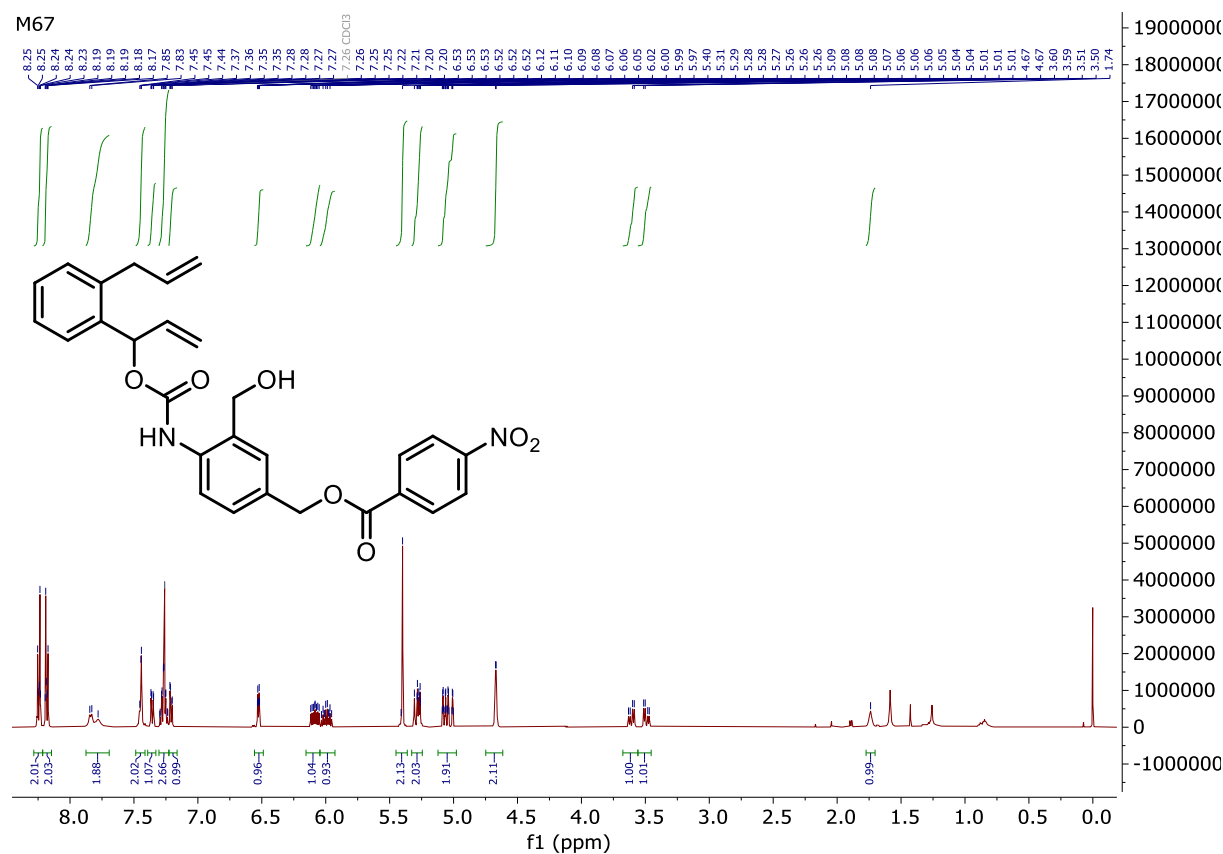
1,3-Bis(((*tert*-butyldimethylsilyl)oxy)methyl)benzene (**M60**)2,4-Bis(((*tert*-butyldimethylsilyl)oxy)methyl)aniline (**M62**)

(((4-Isocyanato-1,3-phenylene)bis(methylene))bis(oxy))bis(*tert*-butyldimethylsilane) (**M63**)1-(2-Allylphenyl)allyl (4-(((2,4-bis(((*tert*-butyldimethylsilyl)oxy)methyl)phenyl)carbamoyl)oxy)methyl)phenyl)carbamate (**M64**)

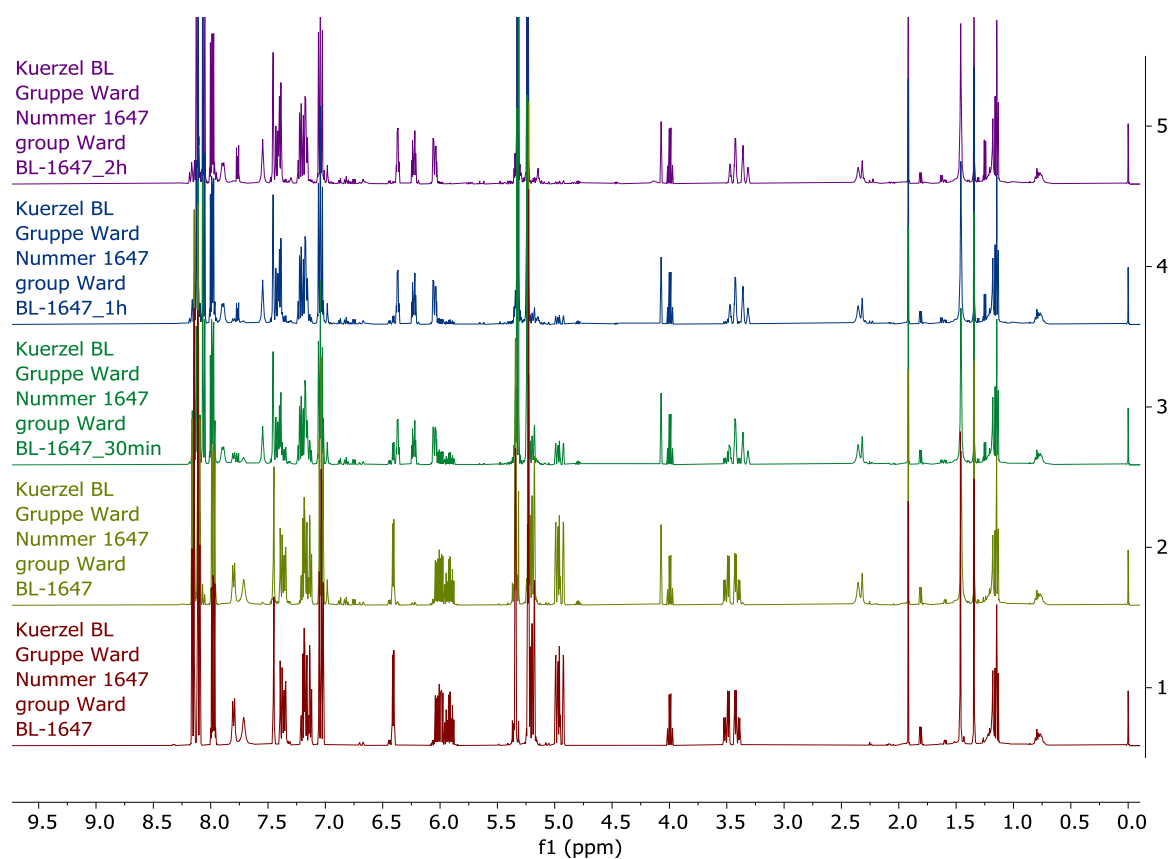
1-(2-Allylphenyl)allyl (2,4-bis(((*tert*-butyldimethylsilyl)oxy)methyl)phenyl)carbamate (**M65**)

1-(2-Allylphenyl)allyl (2,4-bis(hydroxymethyl)phenyl)carbamate (**M66**)

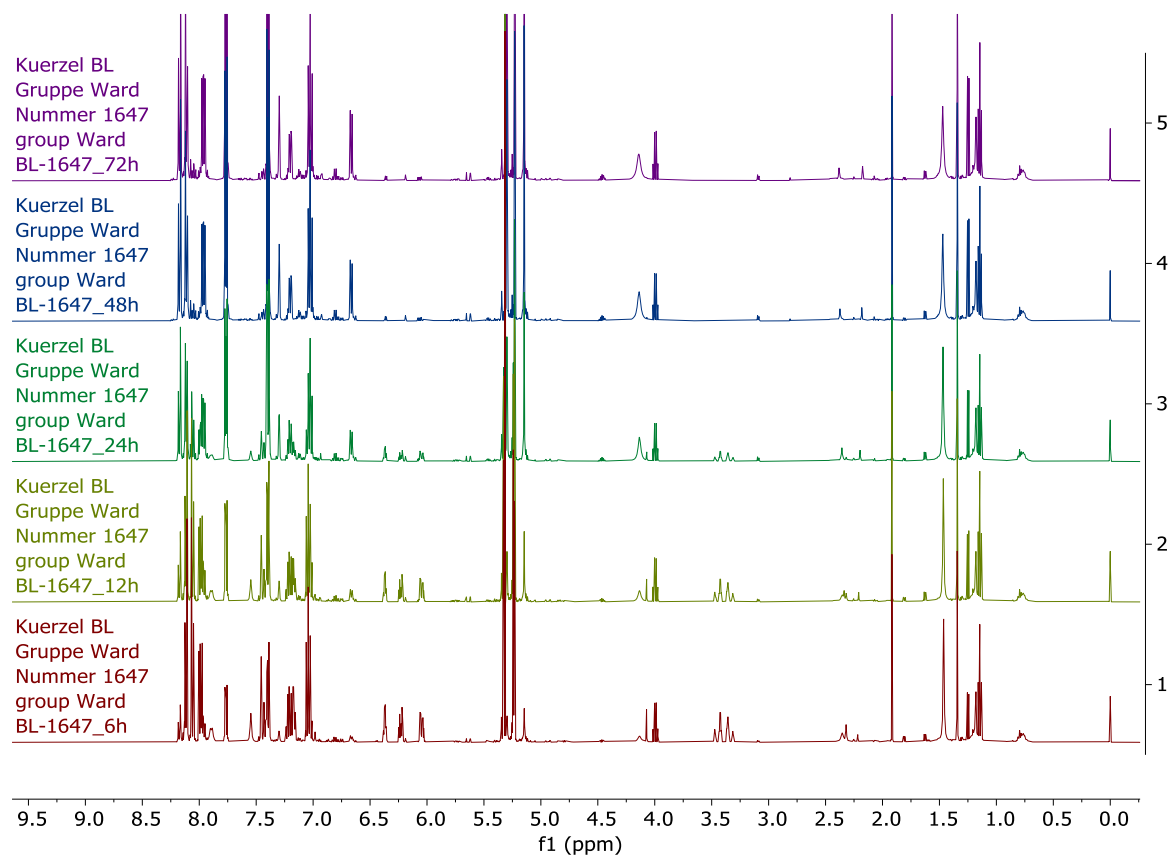


4-(((1-(2-Allylphenyl)allyl)oxy)carbonyl)amino)-3-(hydroxymethyl)benzyl 4-nitrobenzoate (**M67**)

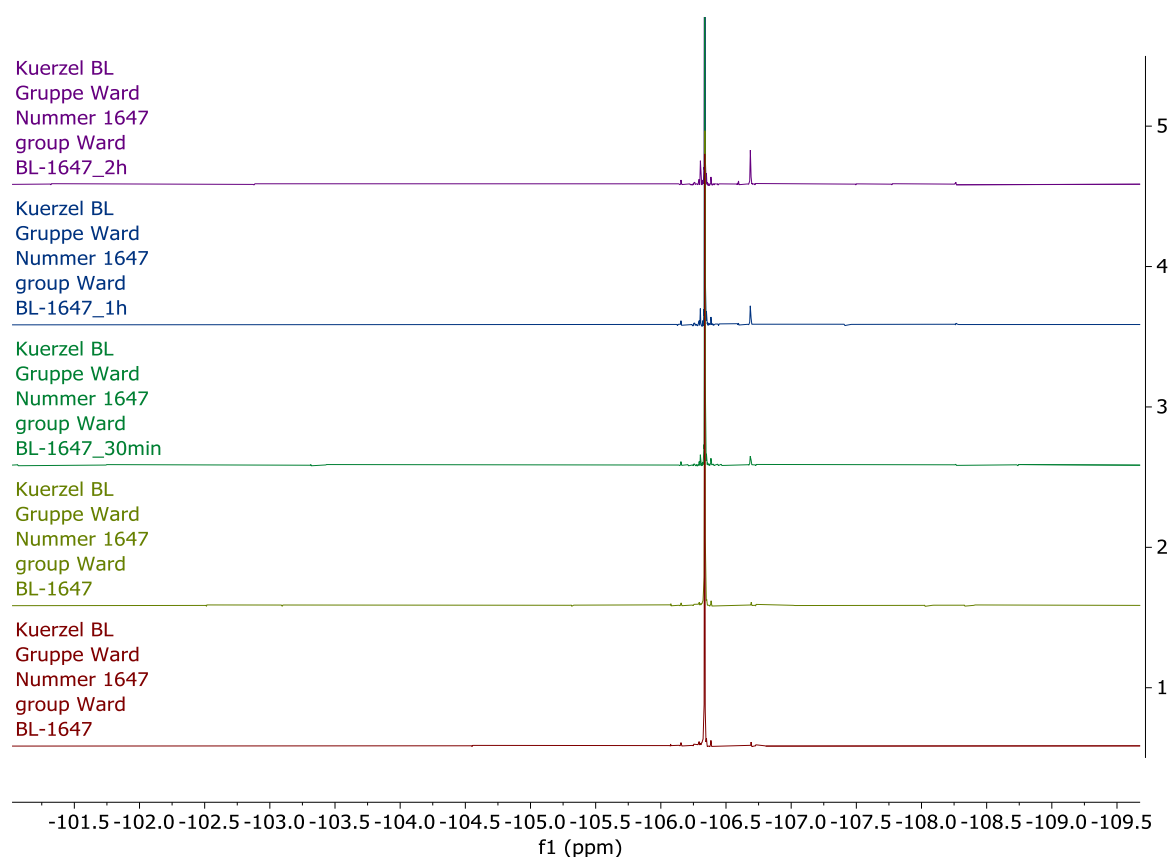
^1H NMR. RCM of **M68** in DCM (0–2h).



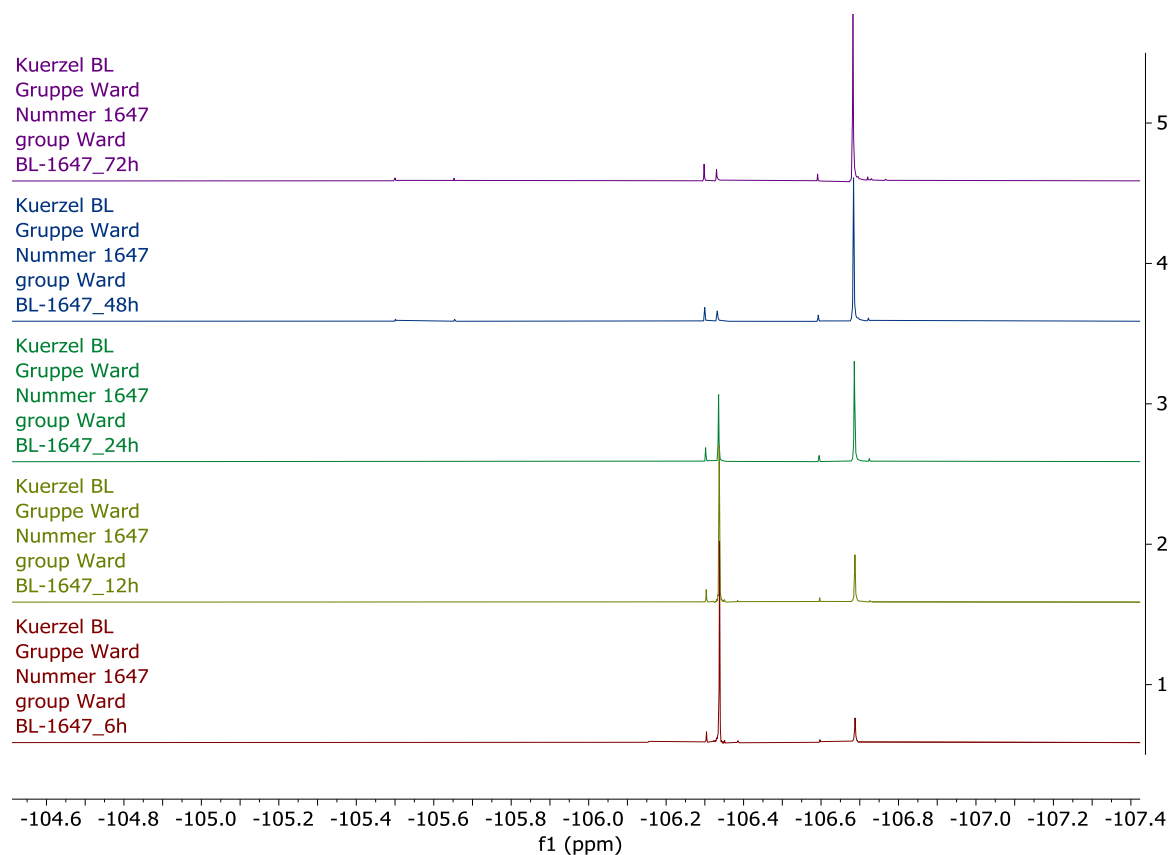
^1H NMR. RCM of **M68** in DCM (6–72h).



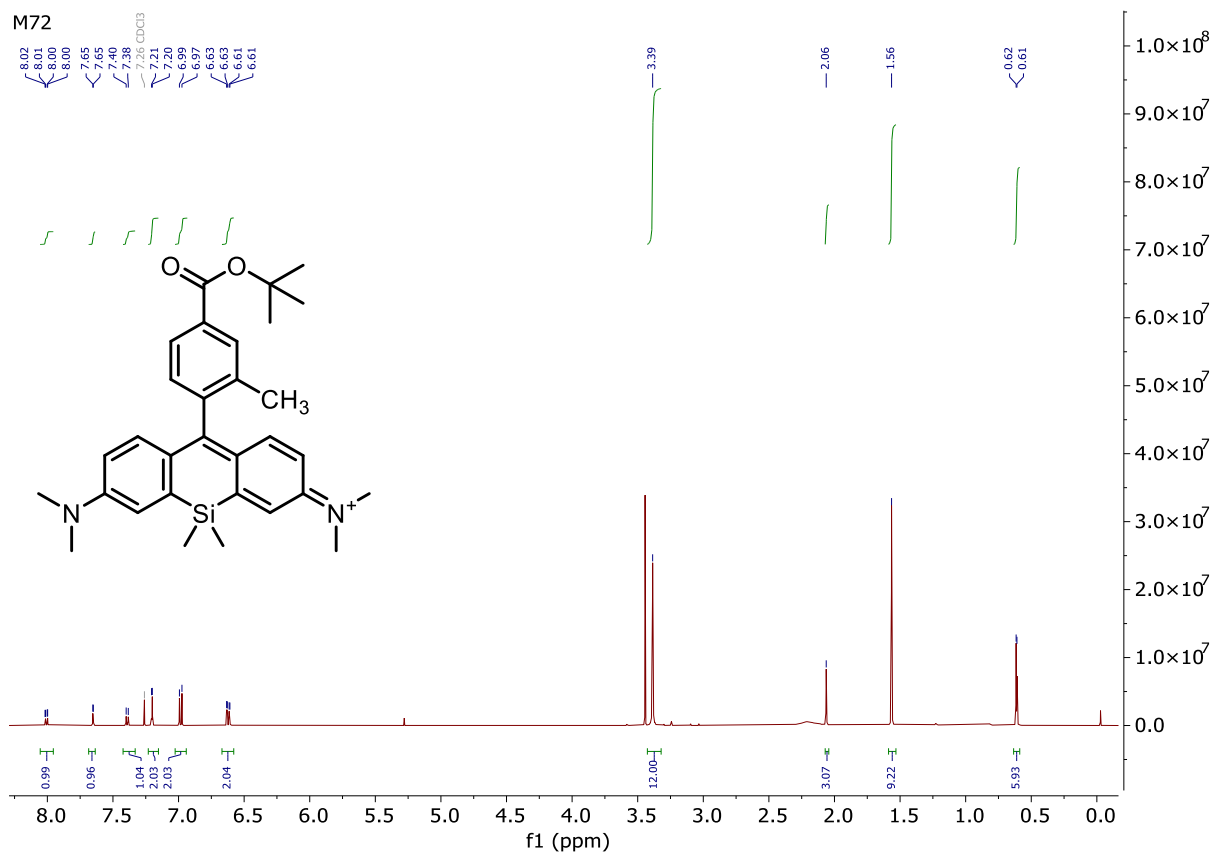
^{19}F NMR. RCM of **M68** in DCM (0–2h).



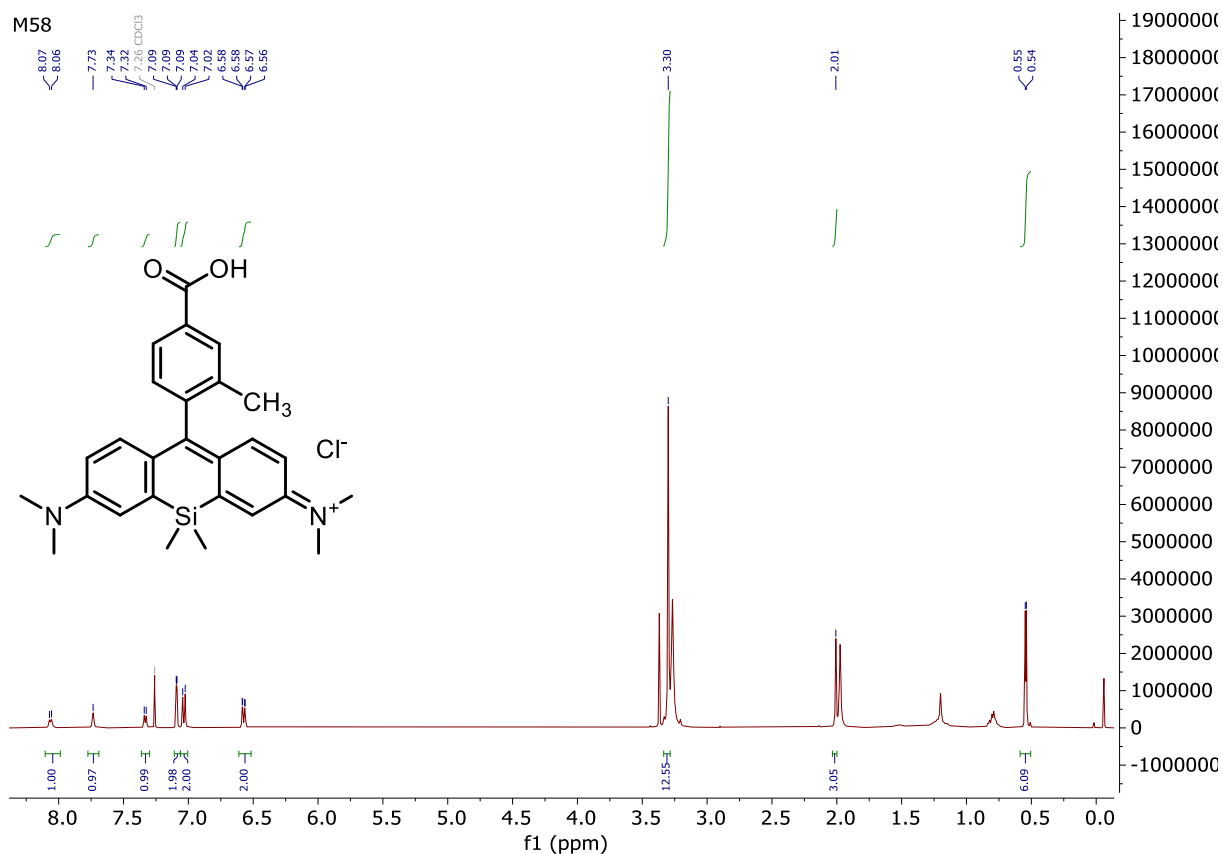
^{19}F NMR. RCM of **M68** in DCM (6–72h).



N-(10-(4-(*Tert*-butoxycarbonyl)-2-methylphenyl)-7-(dimethylamino)-5,5-dimethyldibenzo[*b,e*]silin-3(5*H*)-ylidene)-*N*-methylmethanaminium chloride (**M72**)

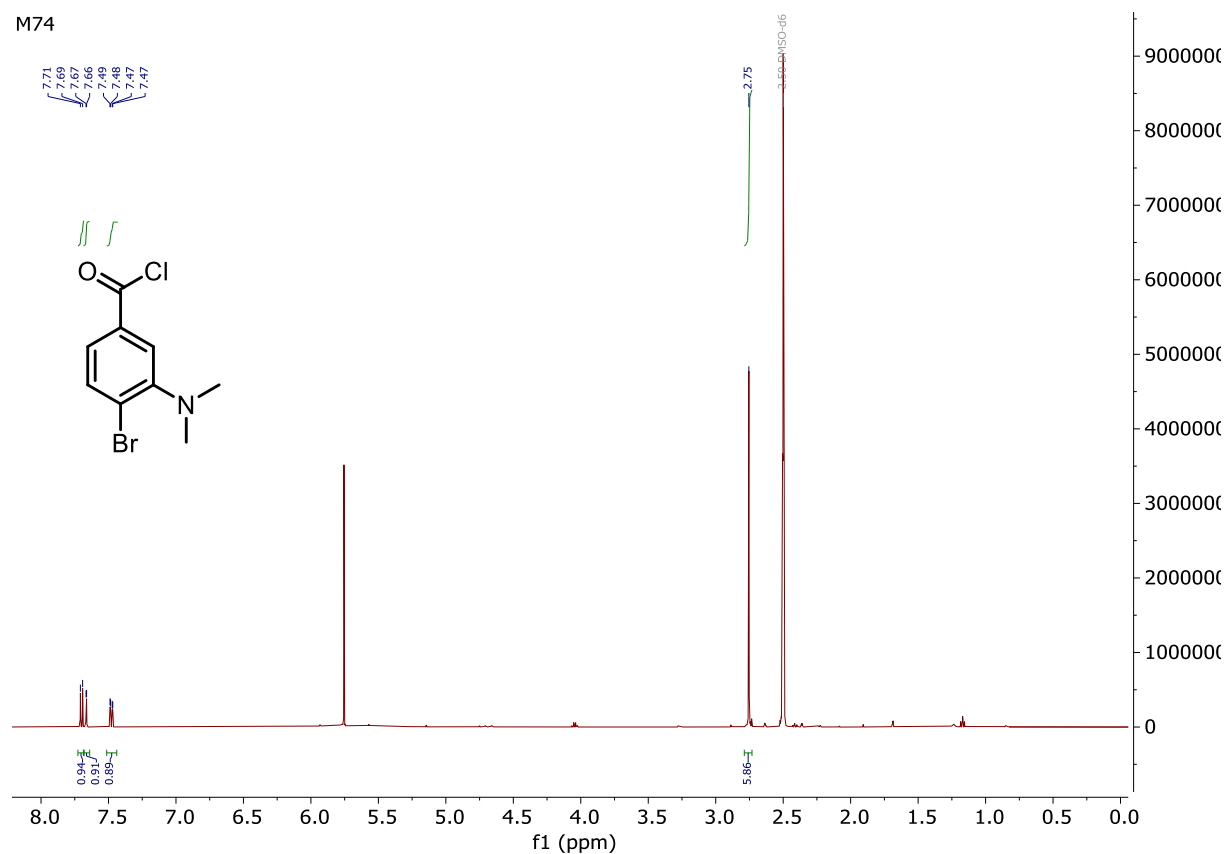


N-(10-(4-Carboxy-2-methylphenyl)-7-(dimethylamino)-5,5-dimethyldibenzo[*b,e*]silin-3(5*H*)-ylidene)-*N*-methylmethanaminium chloride (**M58**)

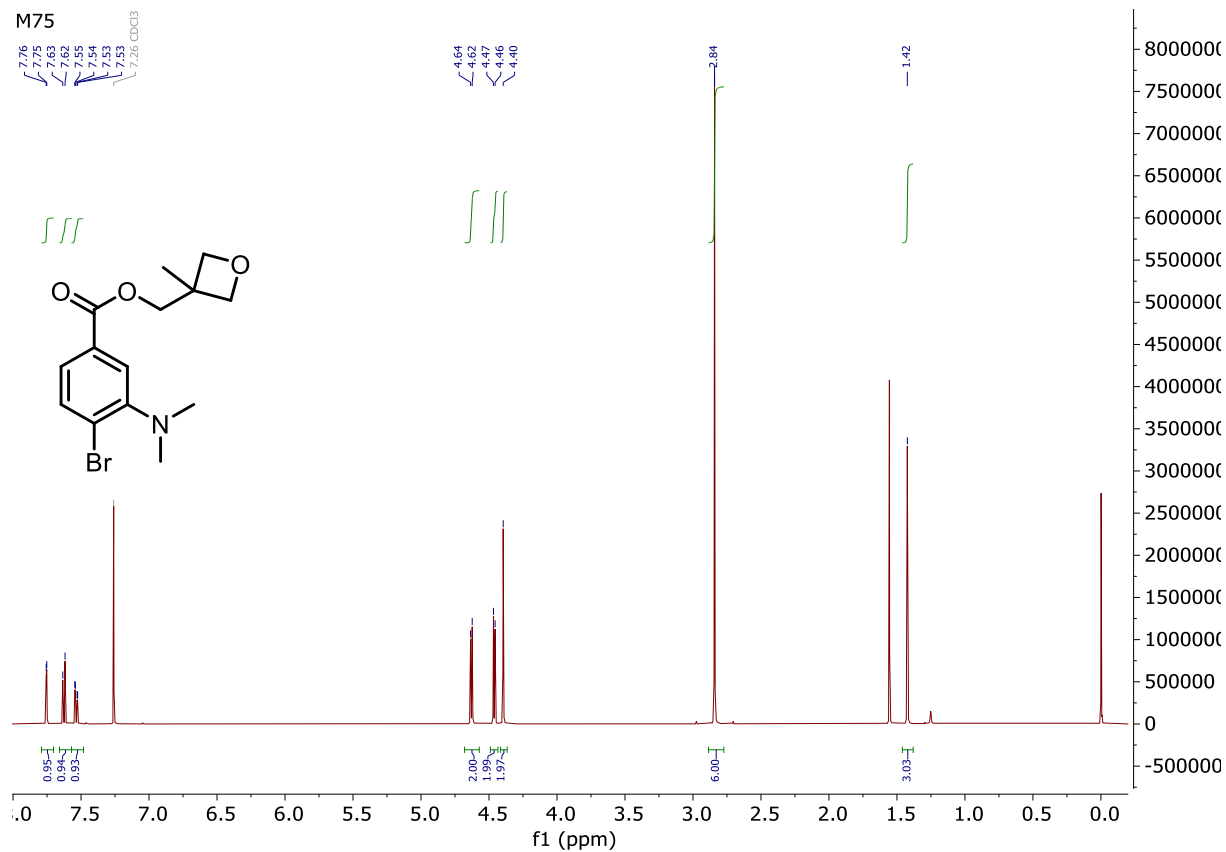


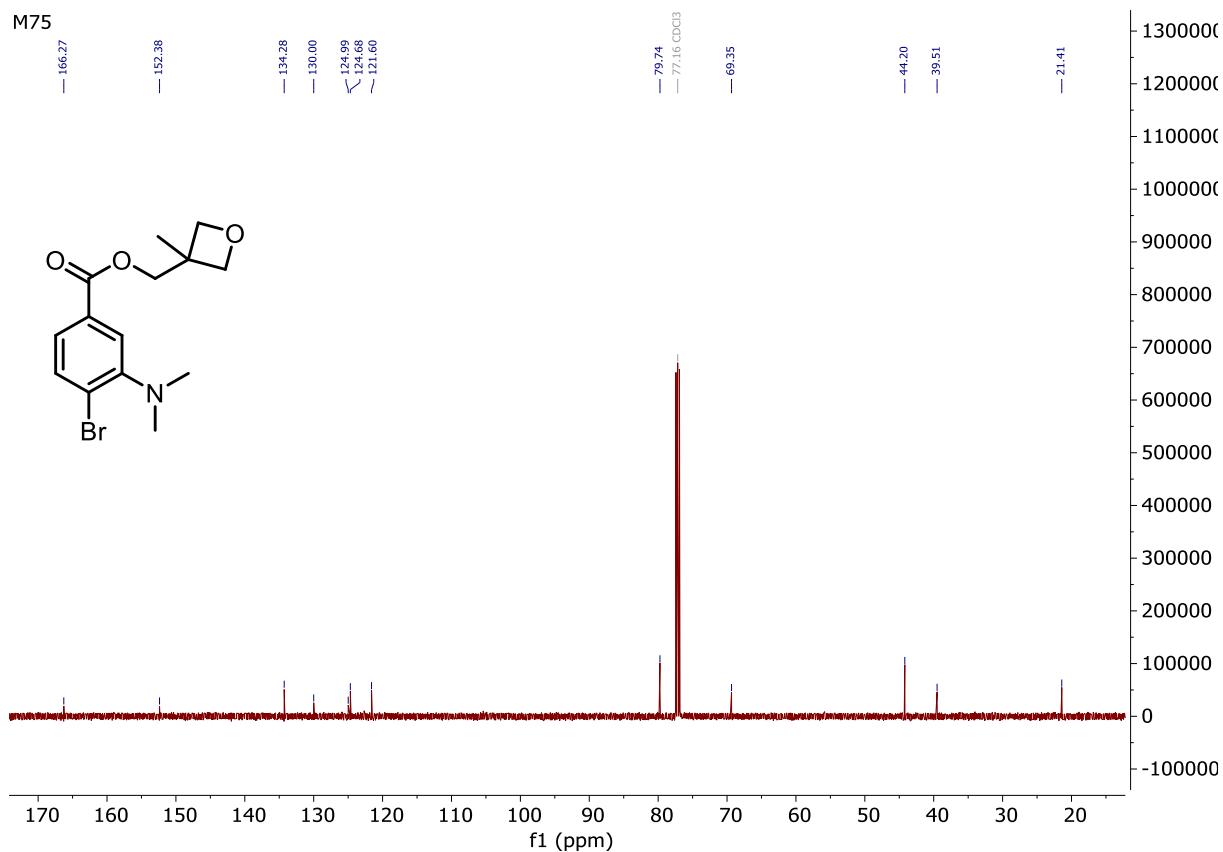
4-Bromo-3-(dimethylamino)benzoyl chloride (**M74**)

M74

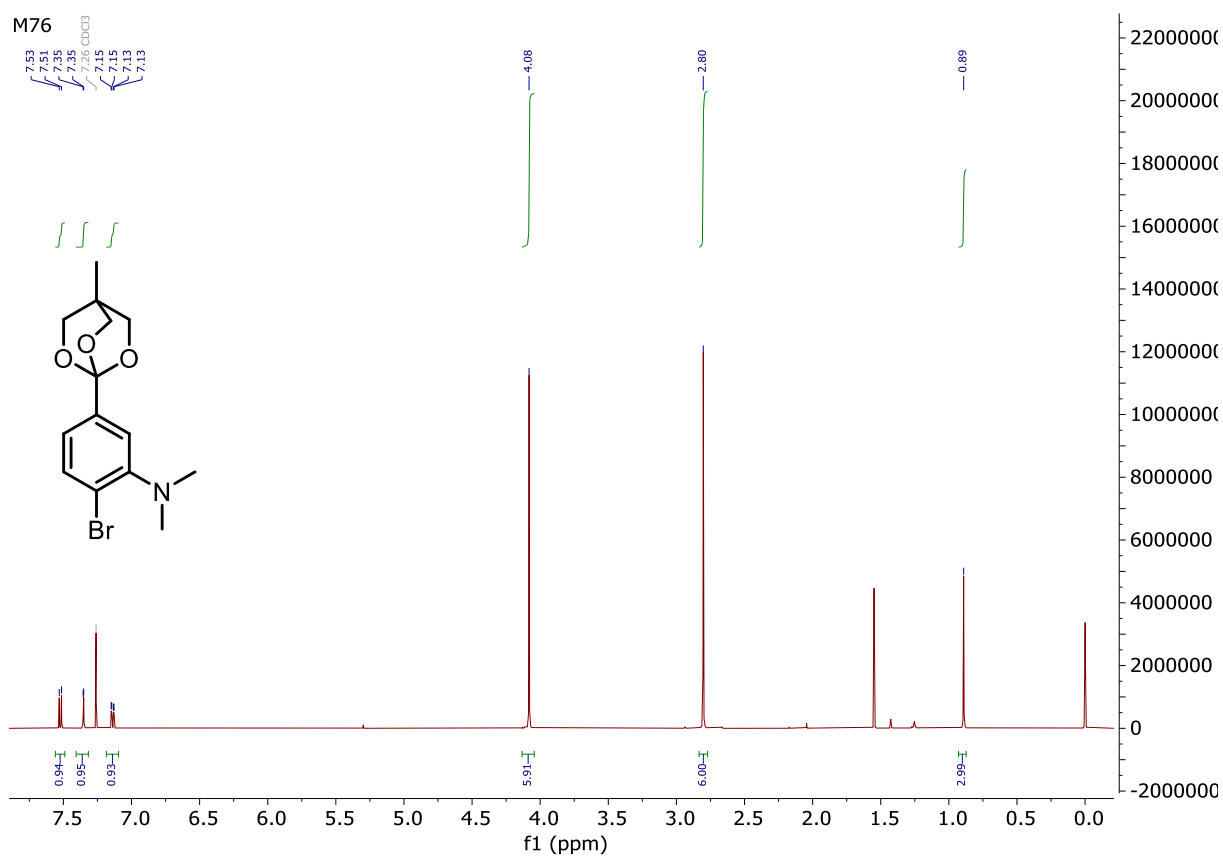
(3-Methyloxetan-3-yl)methyl 4-bromo-3-(dimethylamino)benzoate (**M75**)

M75



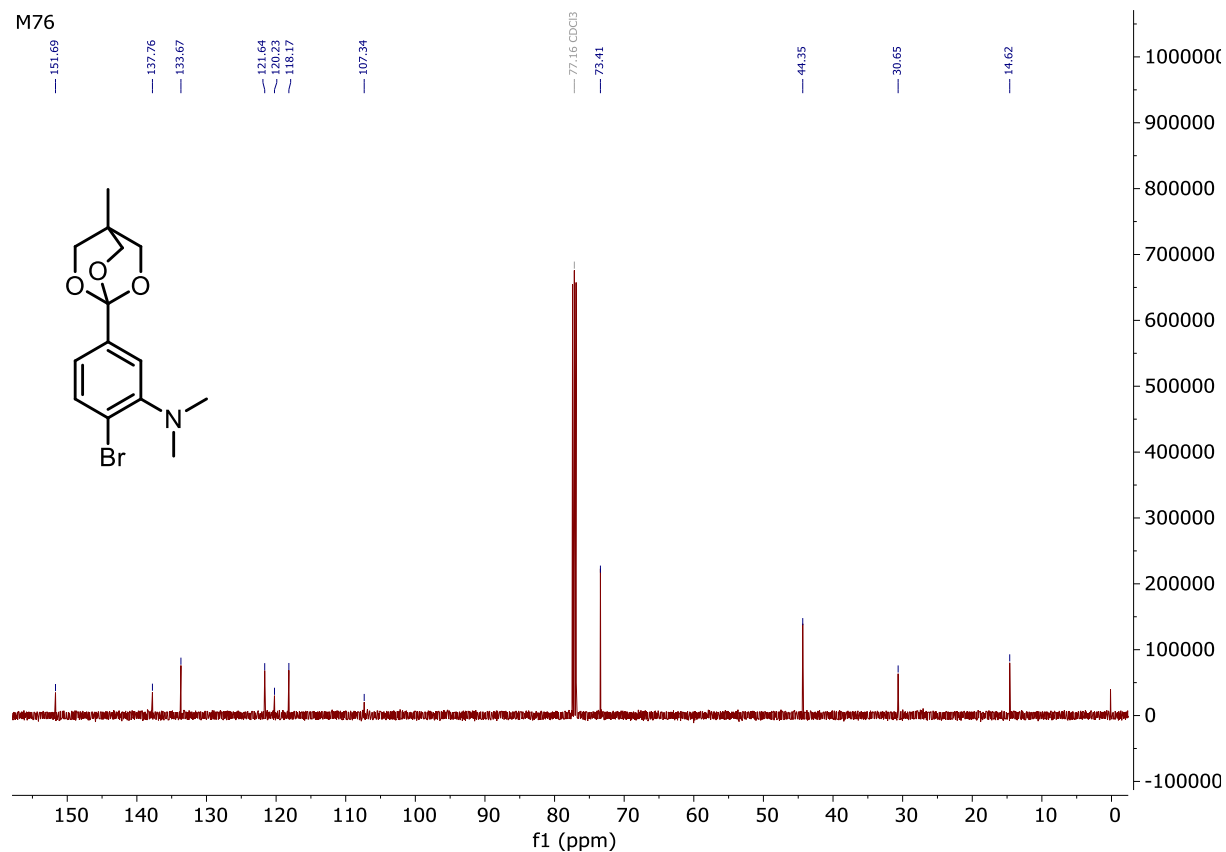


2-Bromo-*N,N*-dimethyl-5-(4-methyl-2,6,7-trioxabicyclo[2.2.2]octan-1-yl)aniline (**M76**)



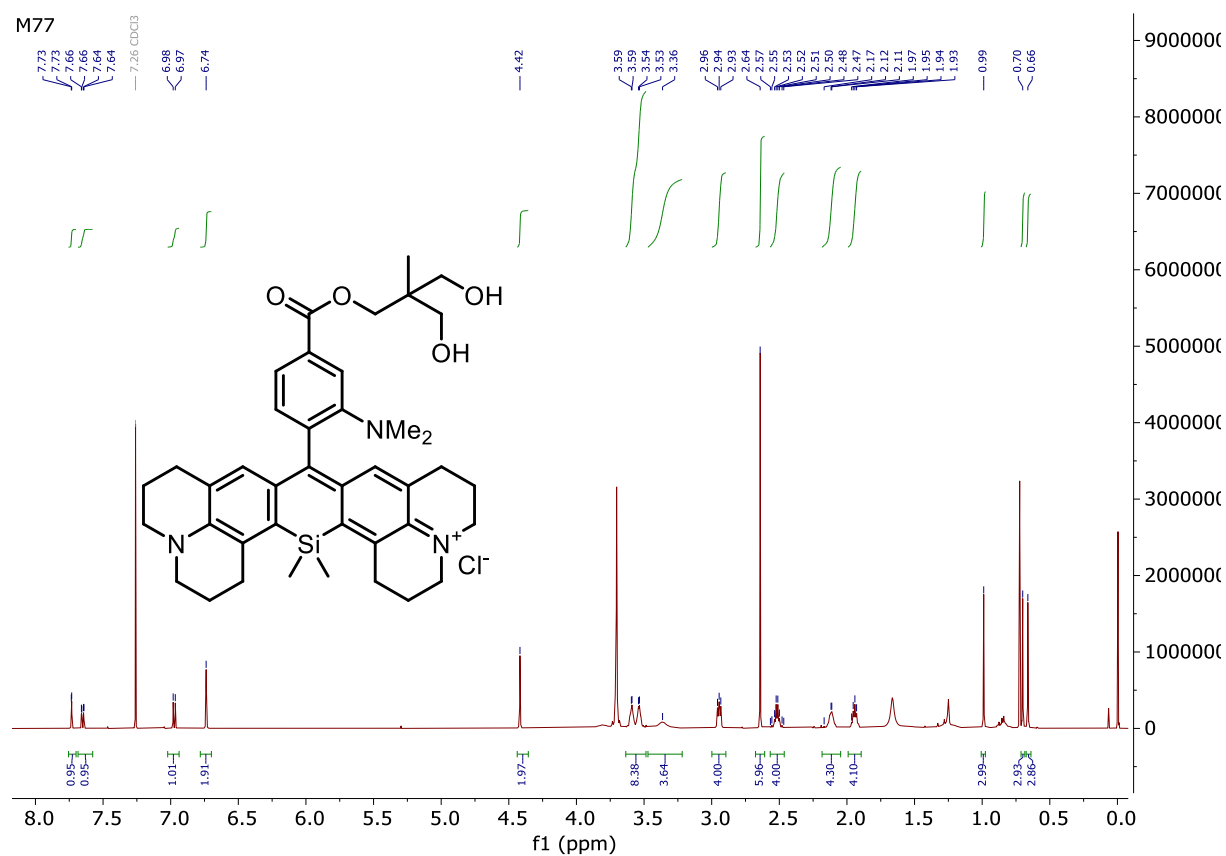
Appendix

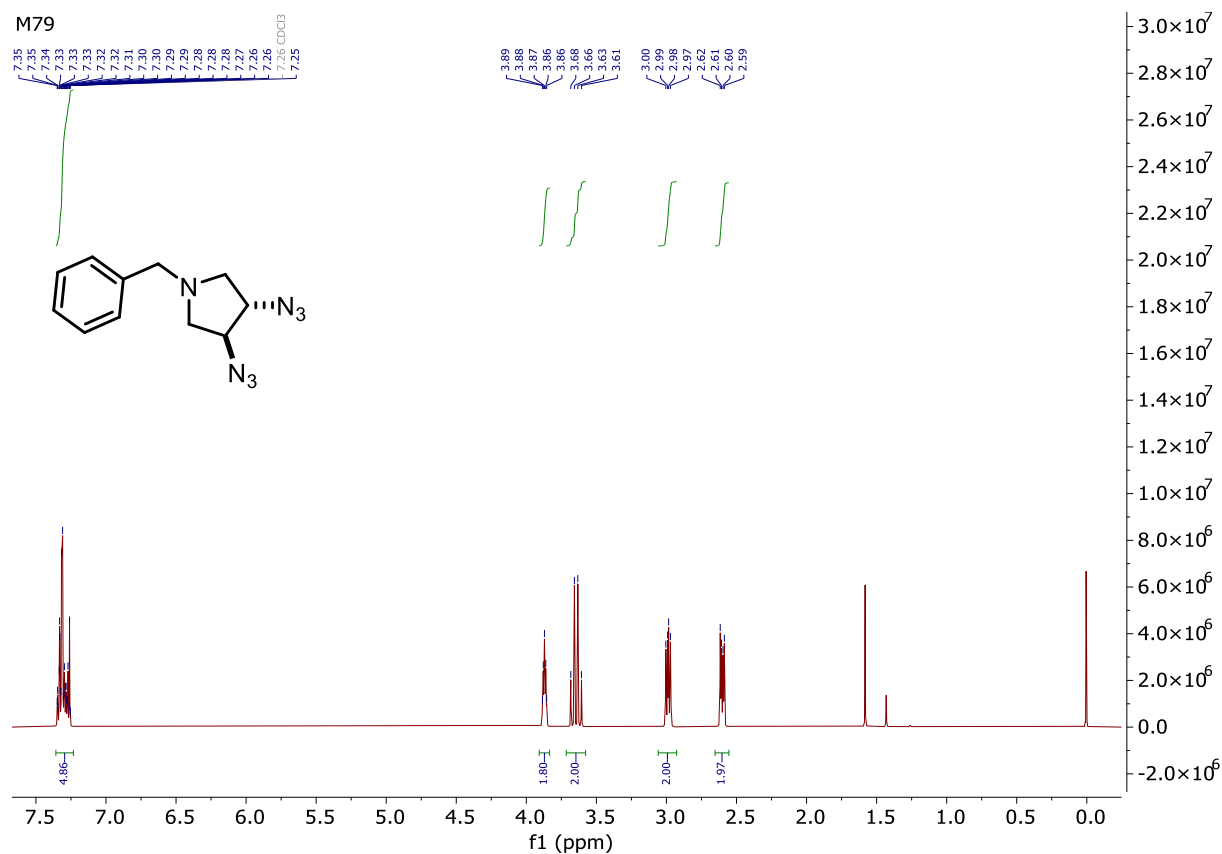
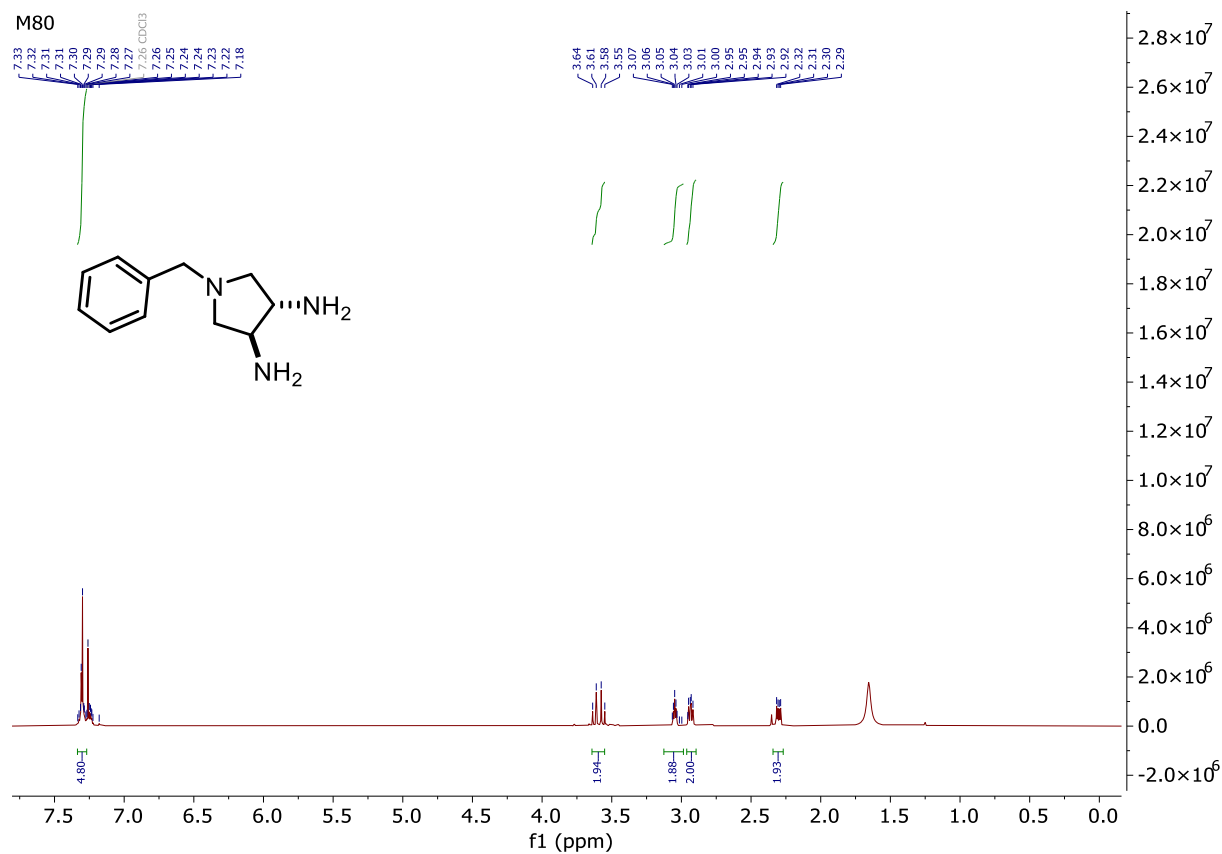
M76



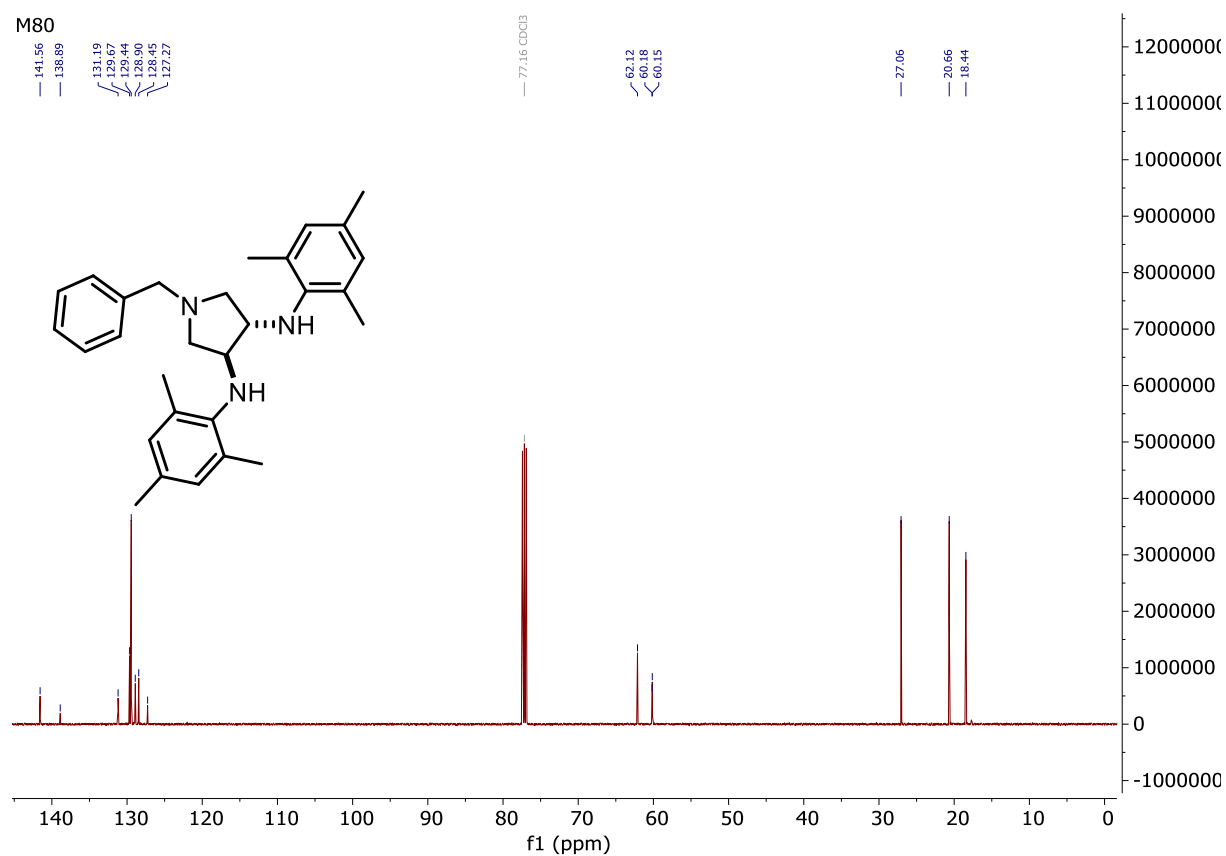
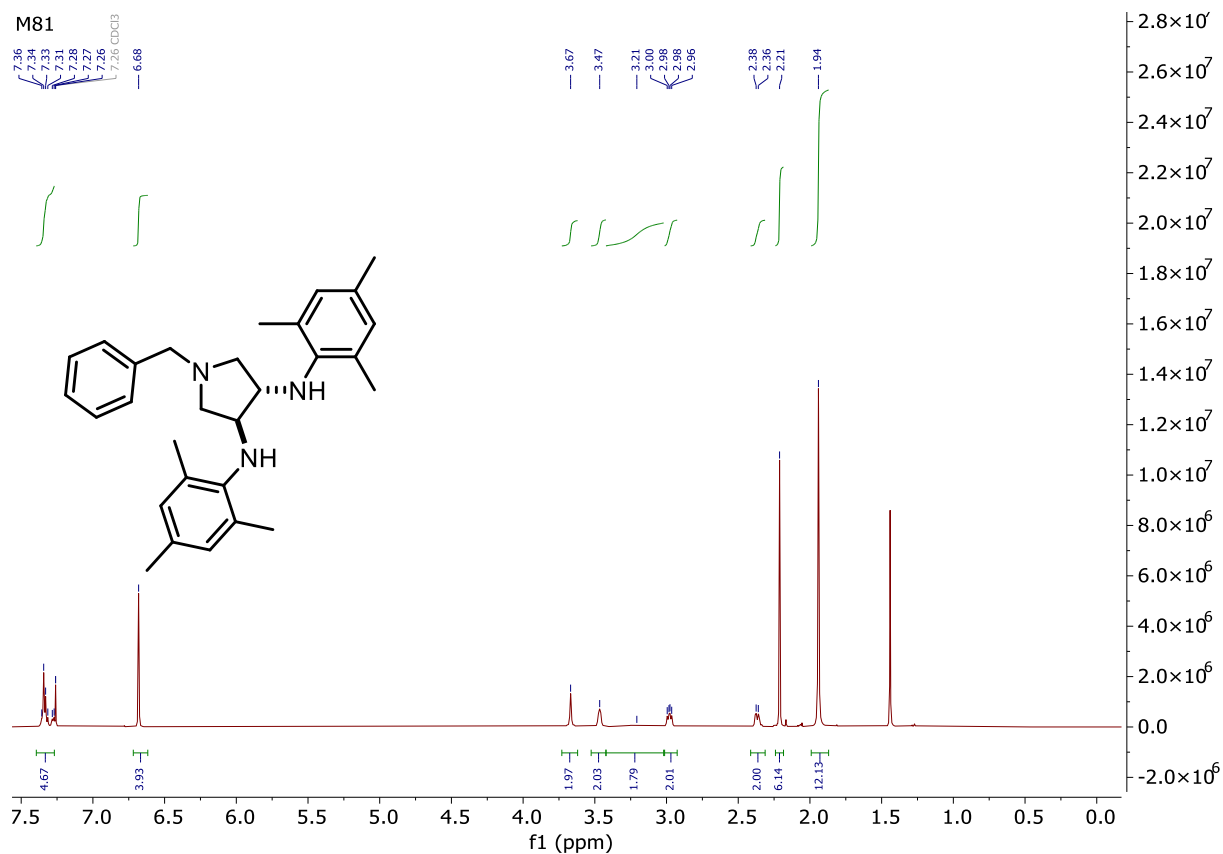
Quencher **M77**

M77

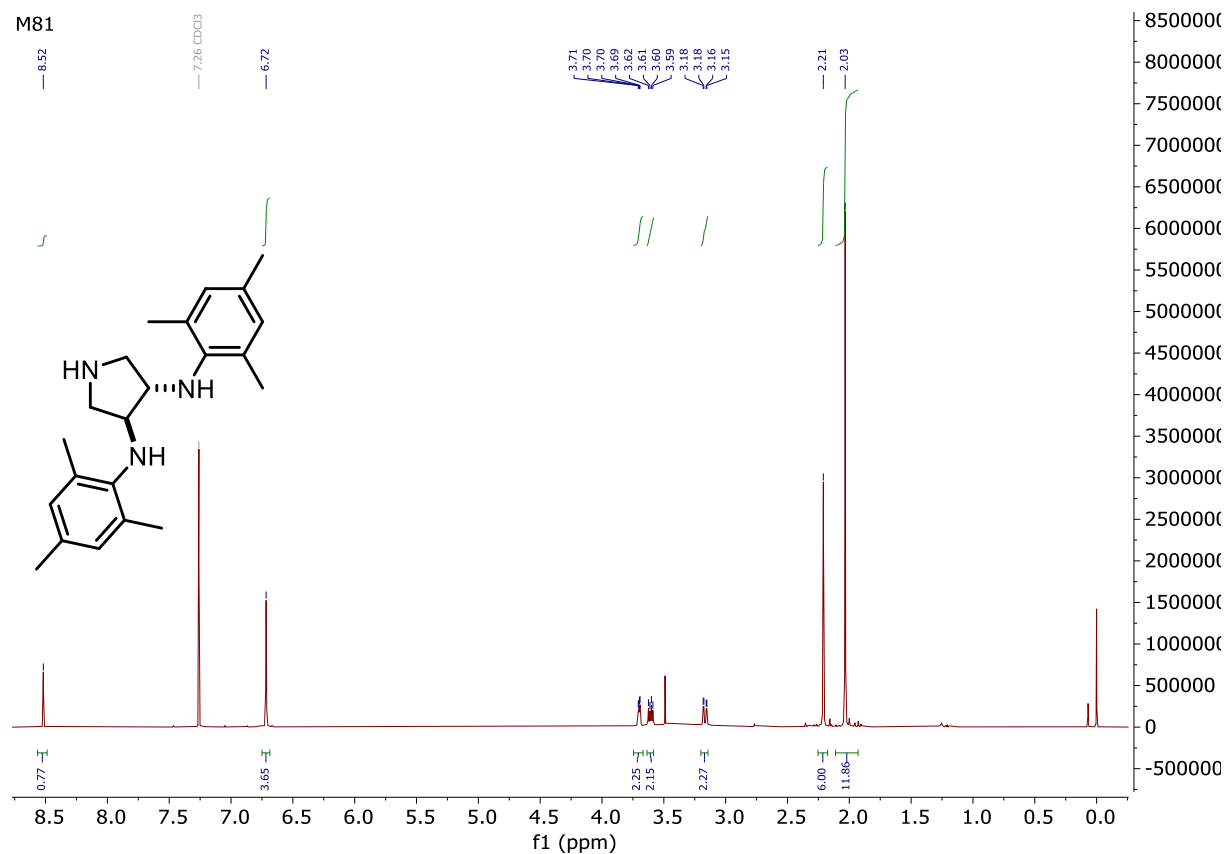


(3*S*,4*S*)-3,4-Diazido-1-benzylpyrrolidine (**M78**)(3*S*,4*S*)-1-Benzylpyrrolidine-3,4-diamine (**M79**)

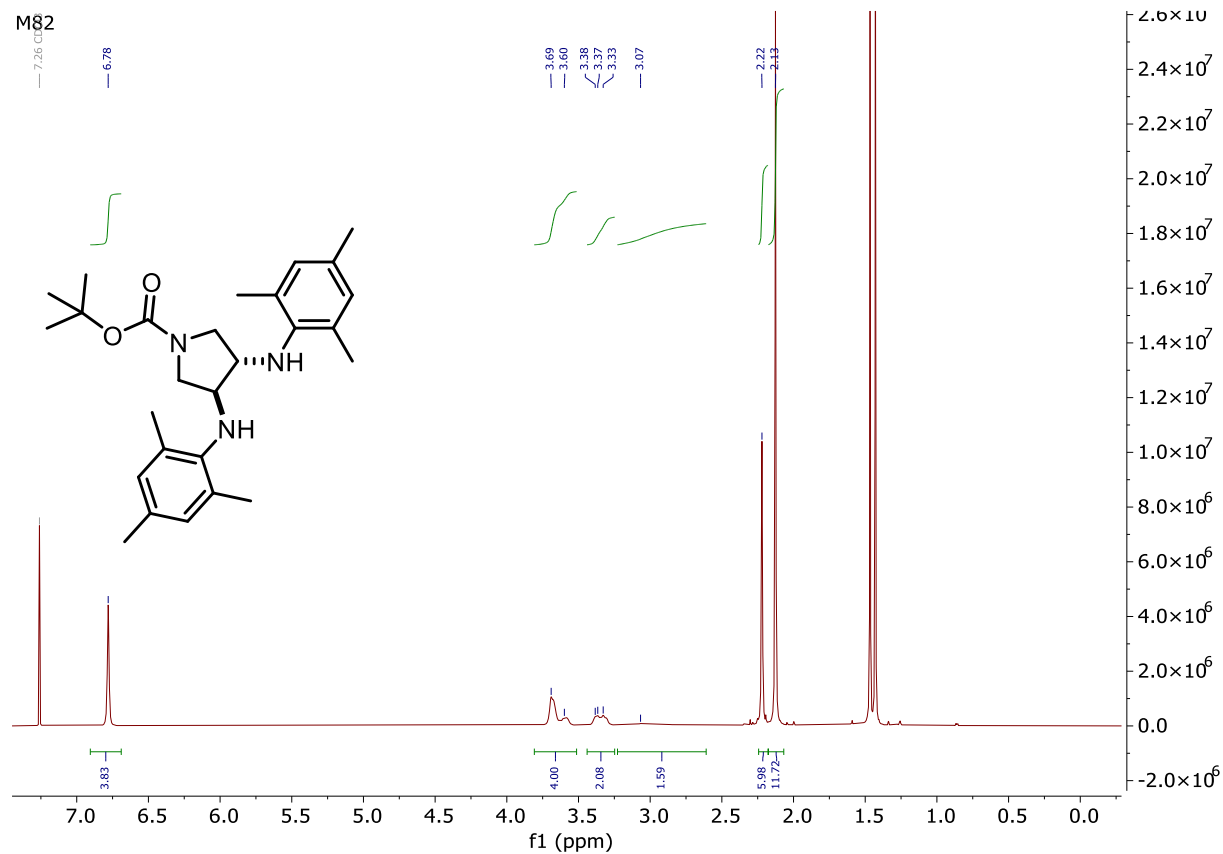
(3*S*,4*S*)-1-Benzyl-*N*³,*N*⁴-dimesitylpyrrolidine-3,4-diamine (**M80**)

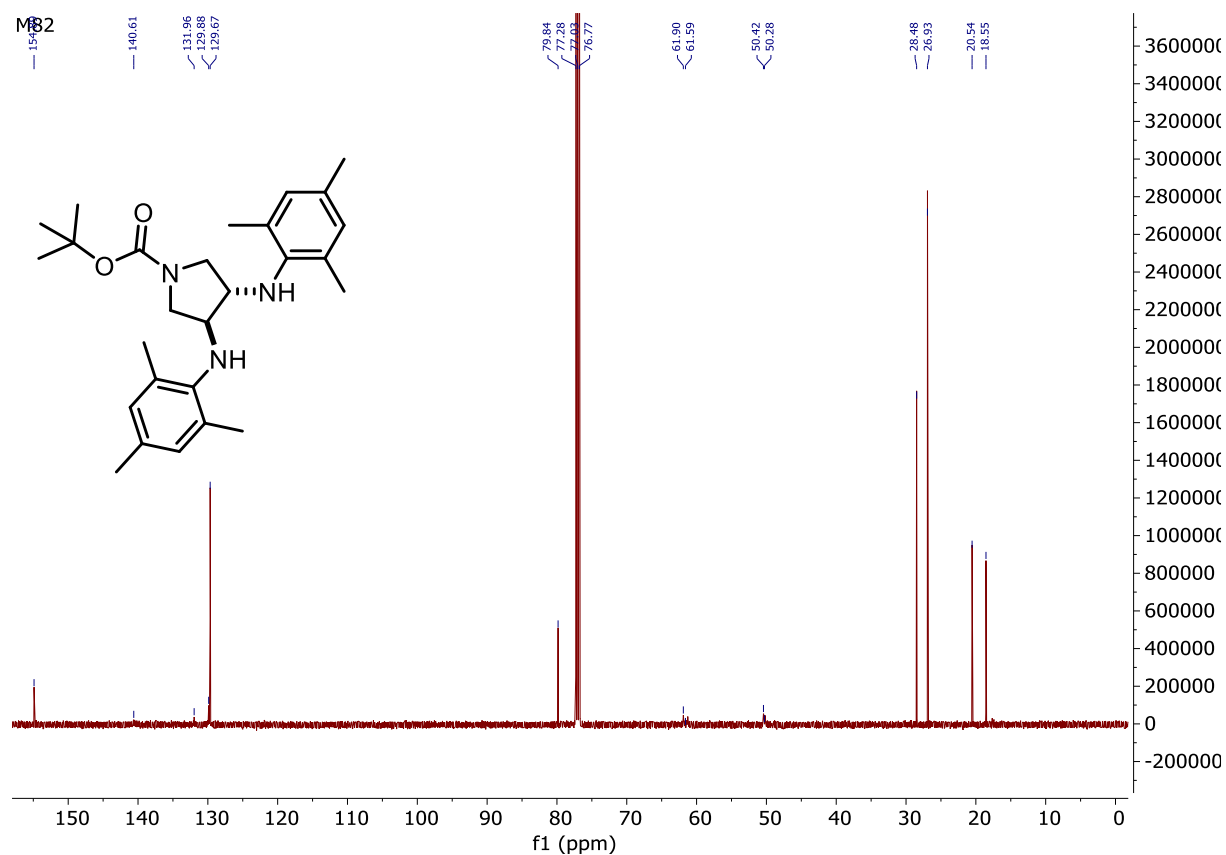


(3*S*,4*S*)-*N*³,*N*⁴-Dimesitylpyrrolidine-3,4-diamine (**M81**)

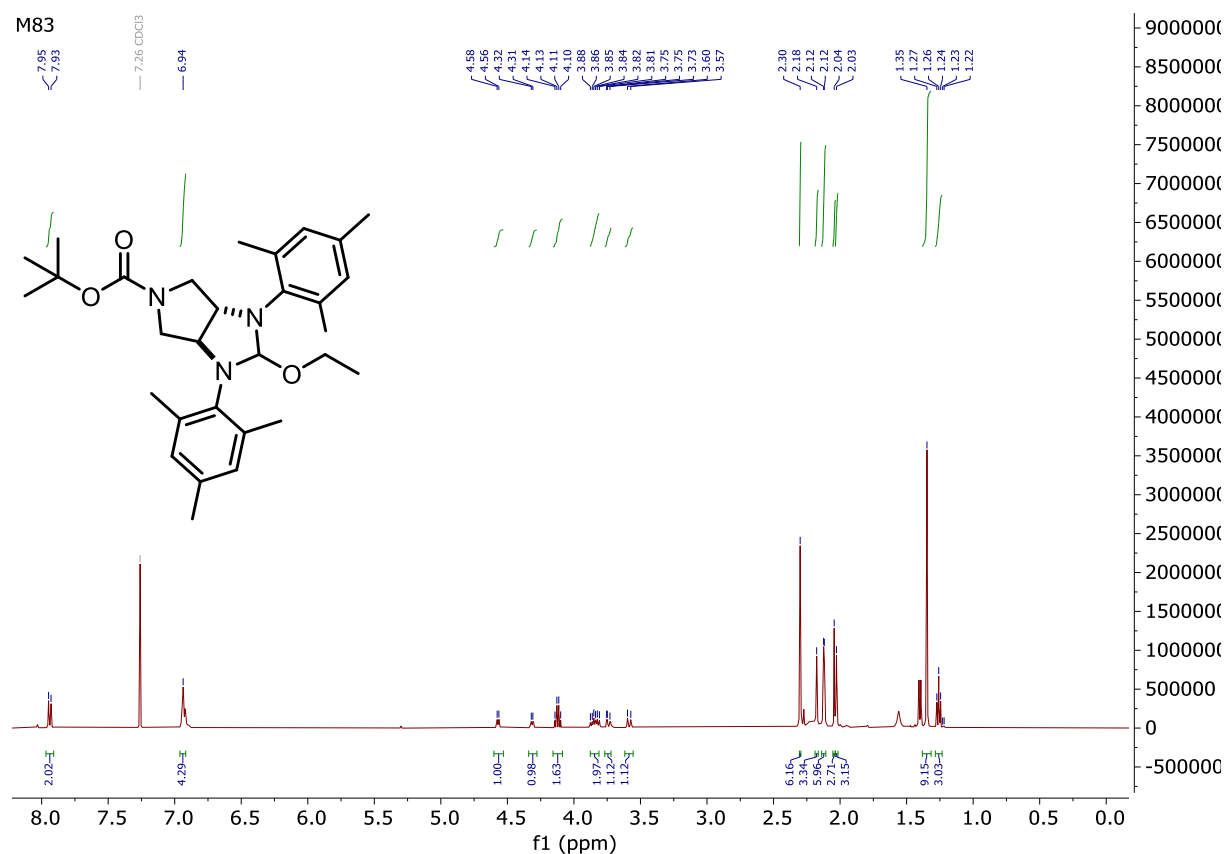


Tert-butyl (3*S*,4*S*)-3,4-bis(mesitylamino)pyrrolidine-1-carboxylate (**M82**)



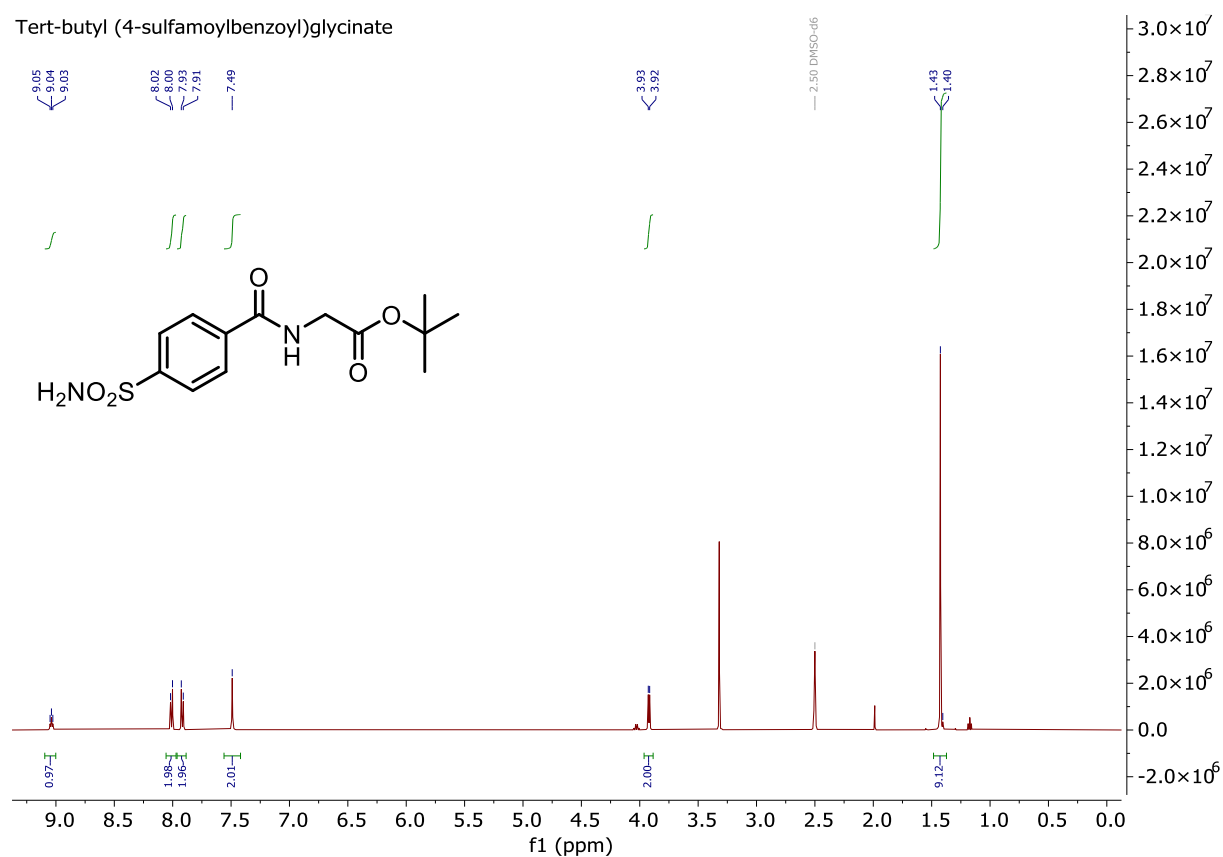


Tert-butyl (3a*S*,6a*S*)-2-ethoxy-1,3-dimesitylhexahydropyrrolo[3,4-*d*]imidazole-5(1*H*)-carboxylate (**M83**)

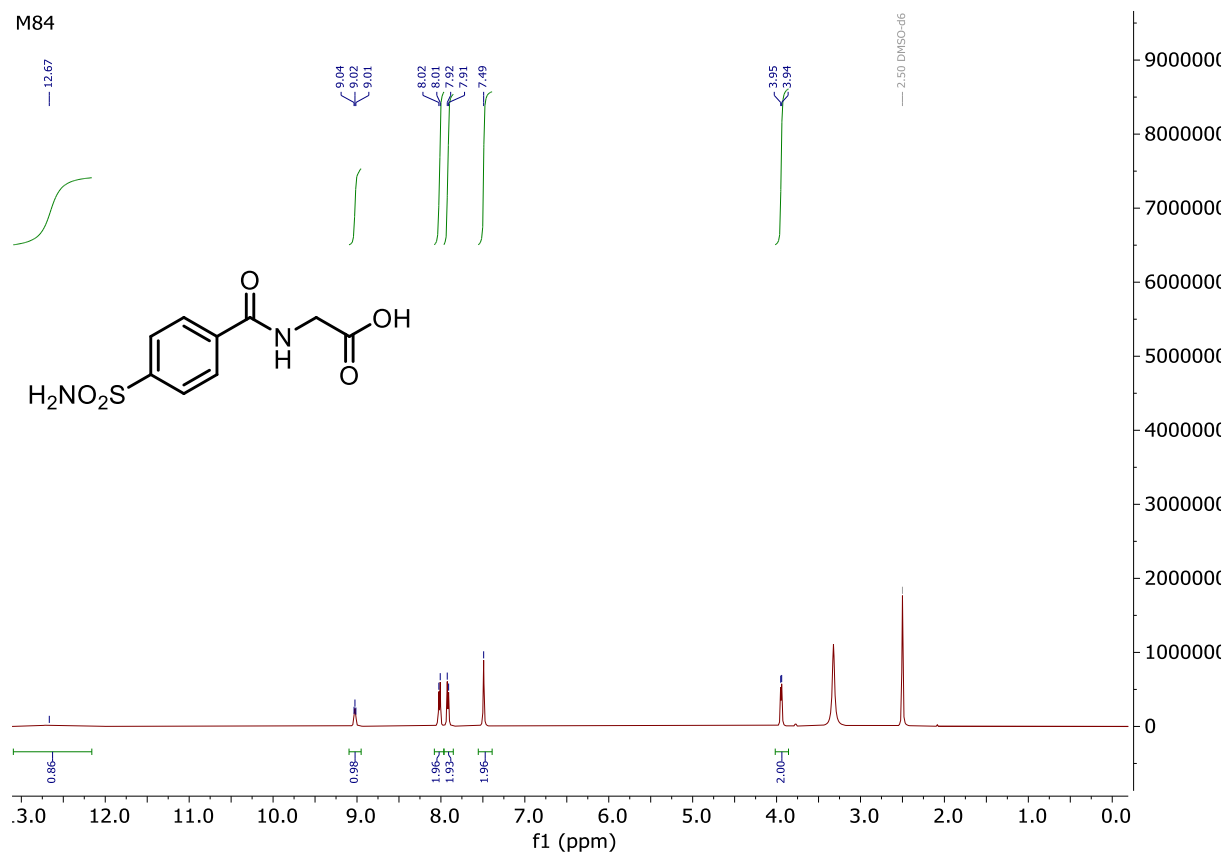


Tert-butyl (4-sulfamoylbenzoyl)glycinate

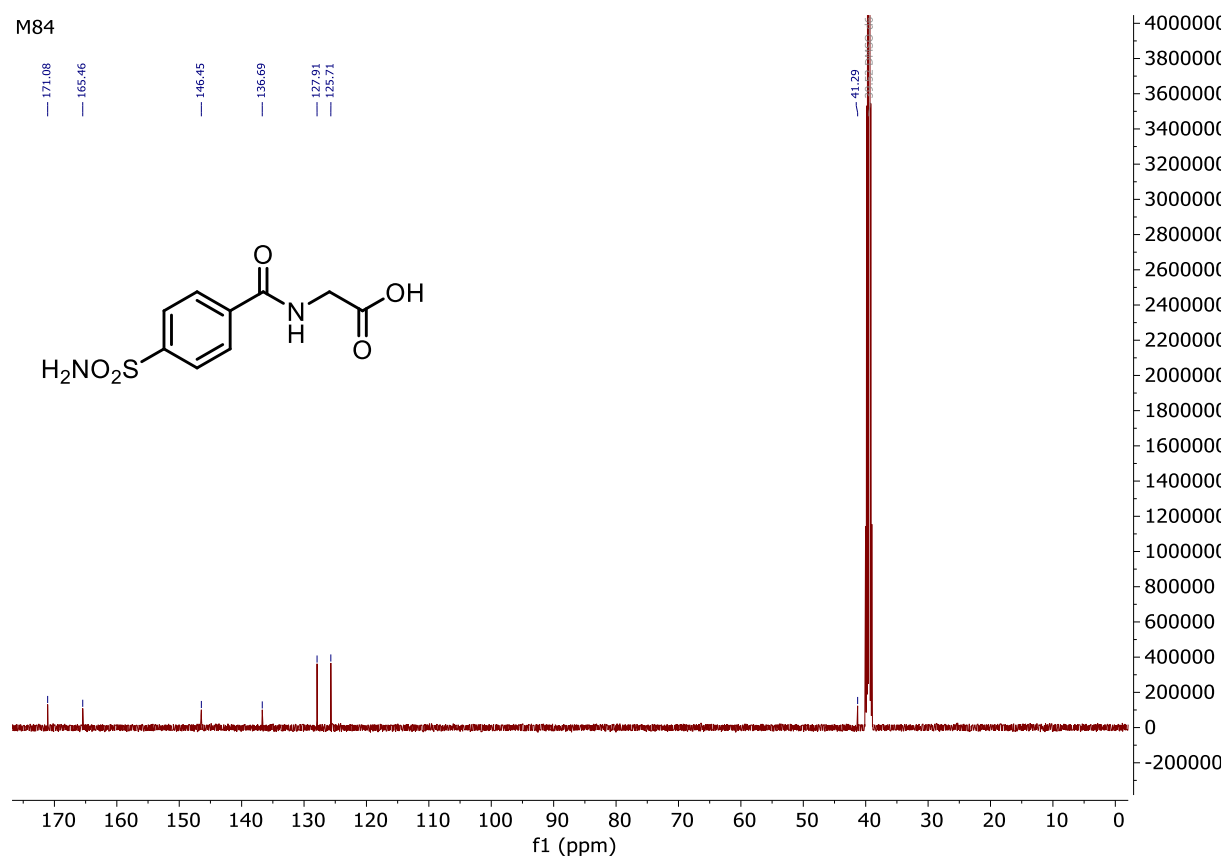
Tert-butyl (4-sulfamoylbenzoyl)glycinate

(4-Sulfamoylbenzoyl)glycine (**M84**)

M84

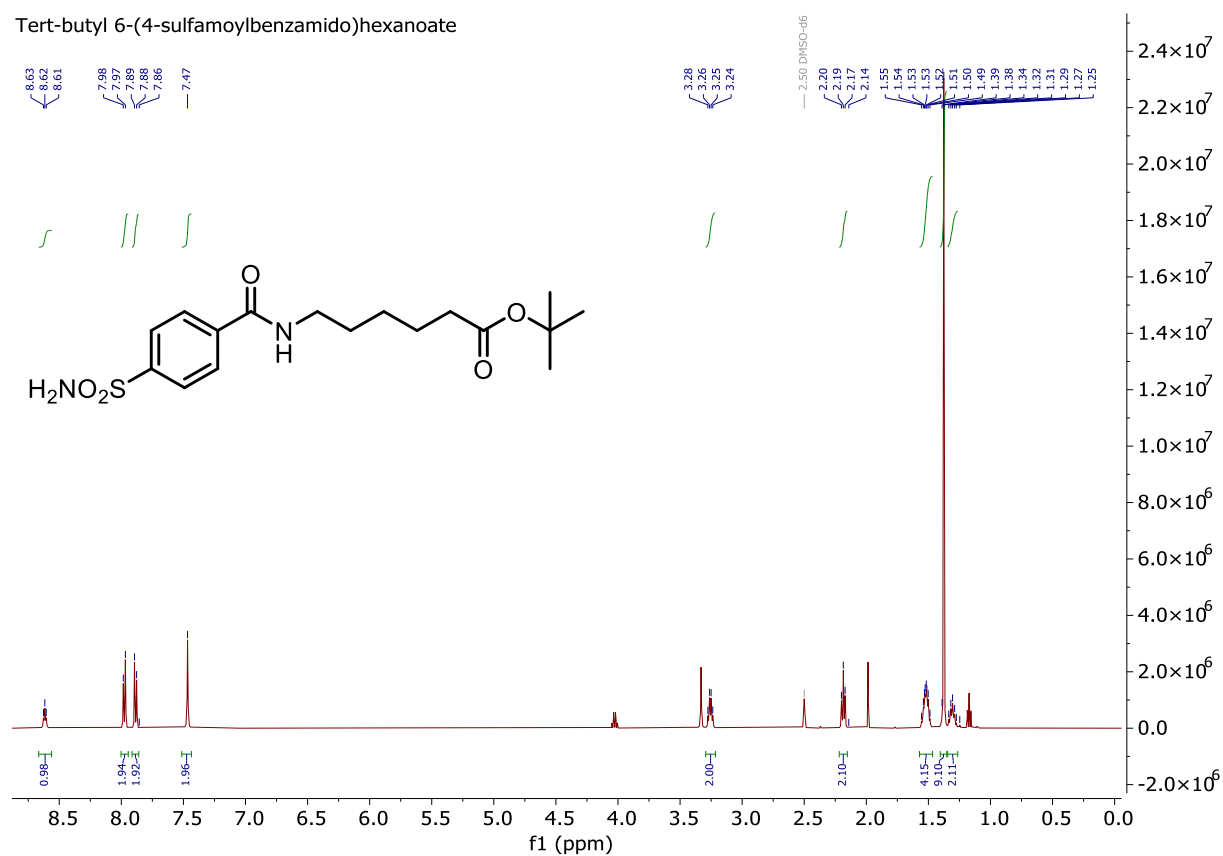


M84



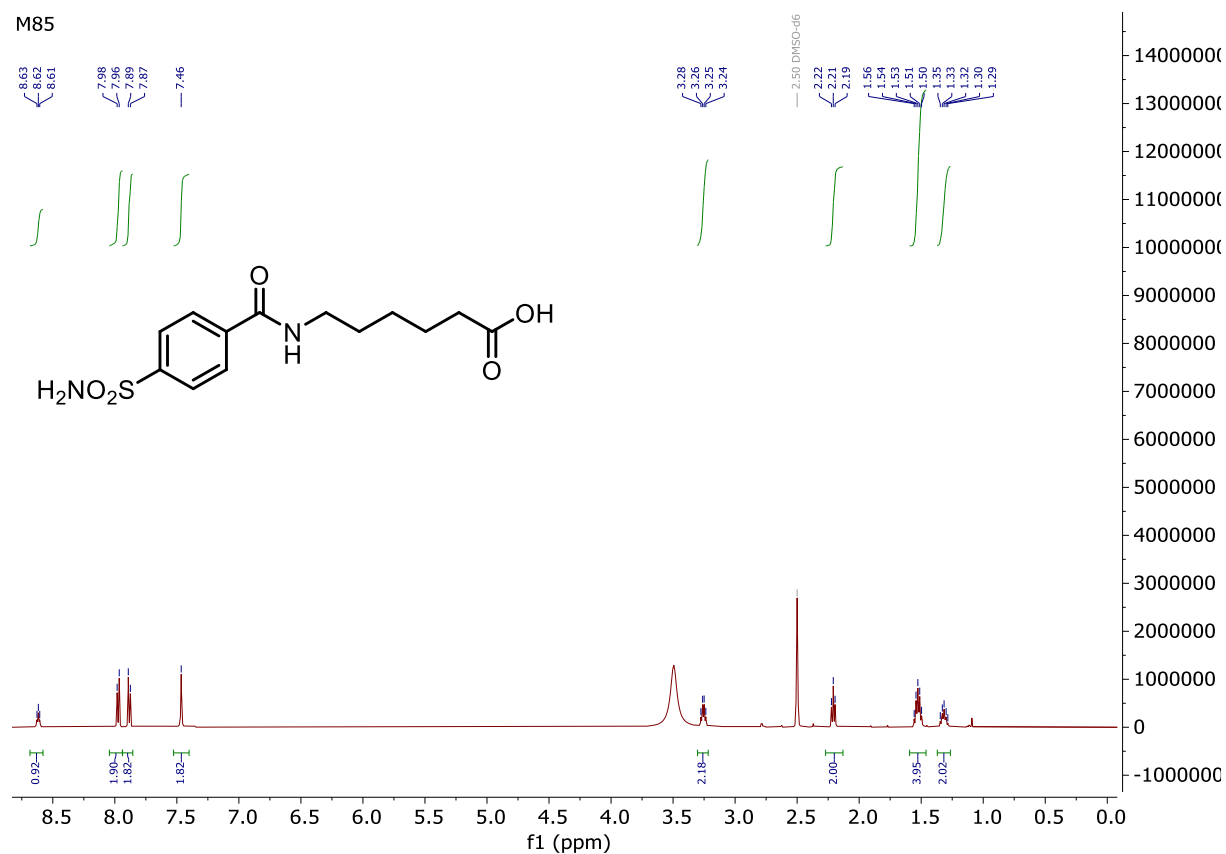
Tert-butyl 6-(4-sulfamoylbenzamido)hexanoate

Tert-butyl 6-(4-sulfamoylbenzamido)hexanoate

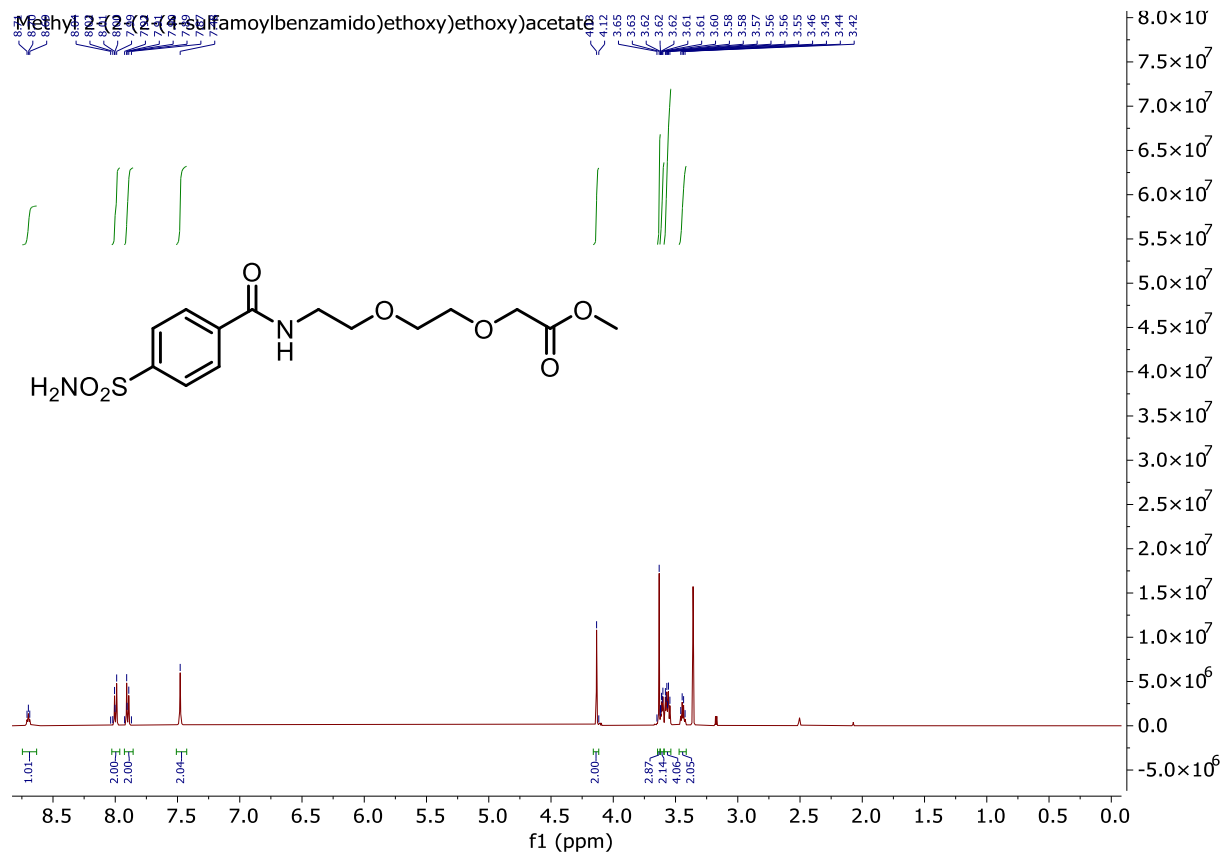


6-(4-Sulfamoylbenzamido)hexanoic acid (**M85**)

M85

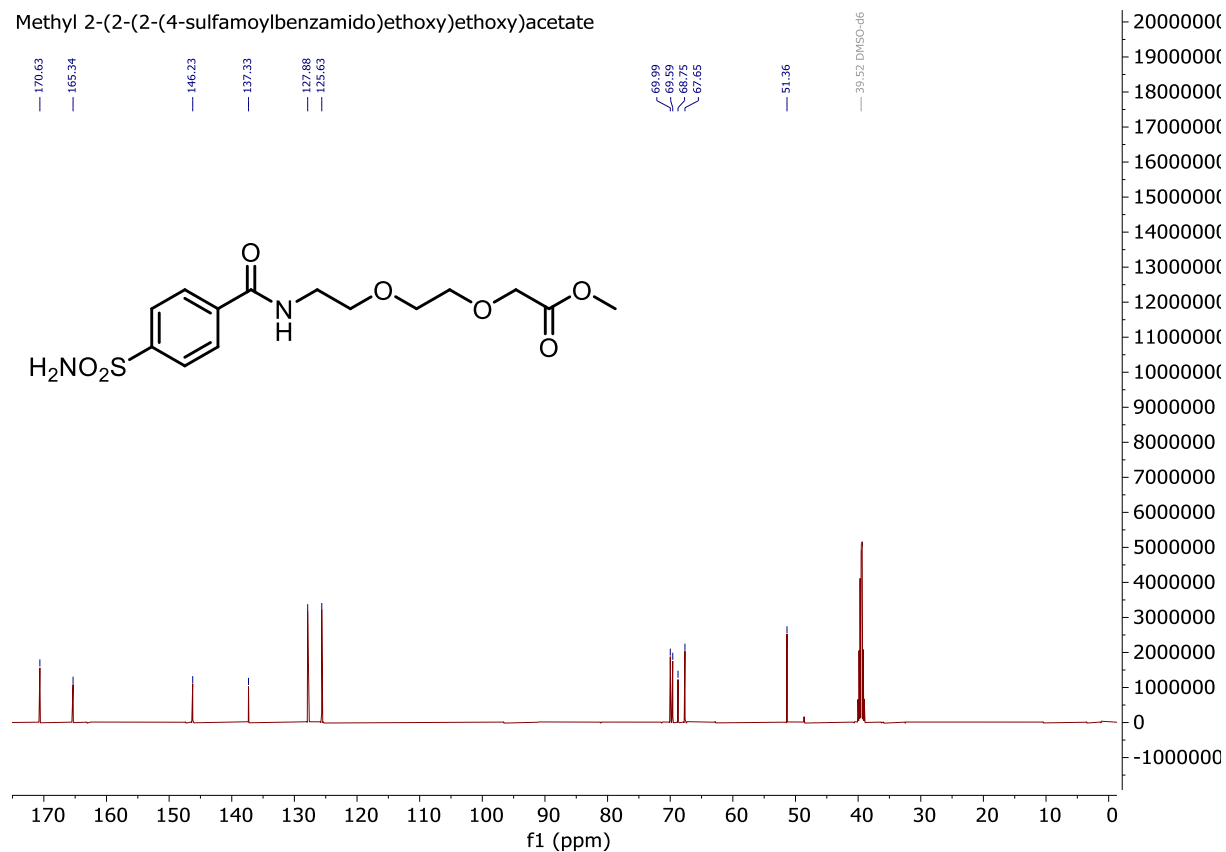


Methyl 2-(2-(2-(4-sulfamoylbenzamido)ethoxy)ethoxy)acetate



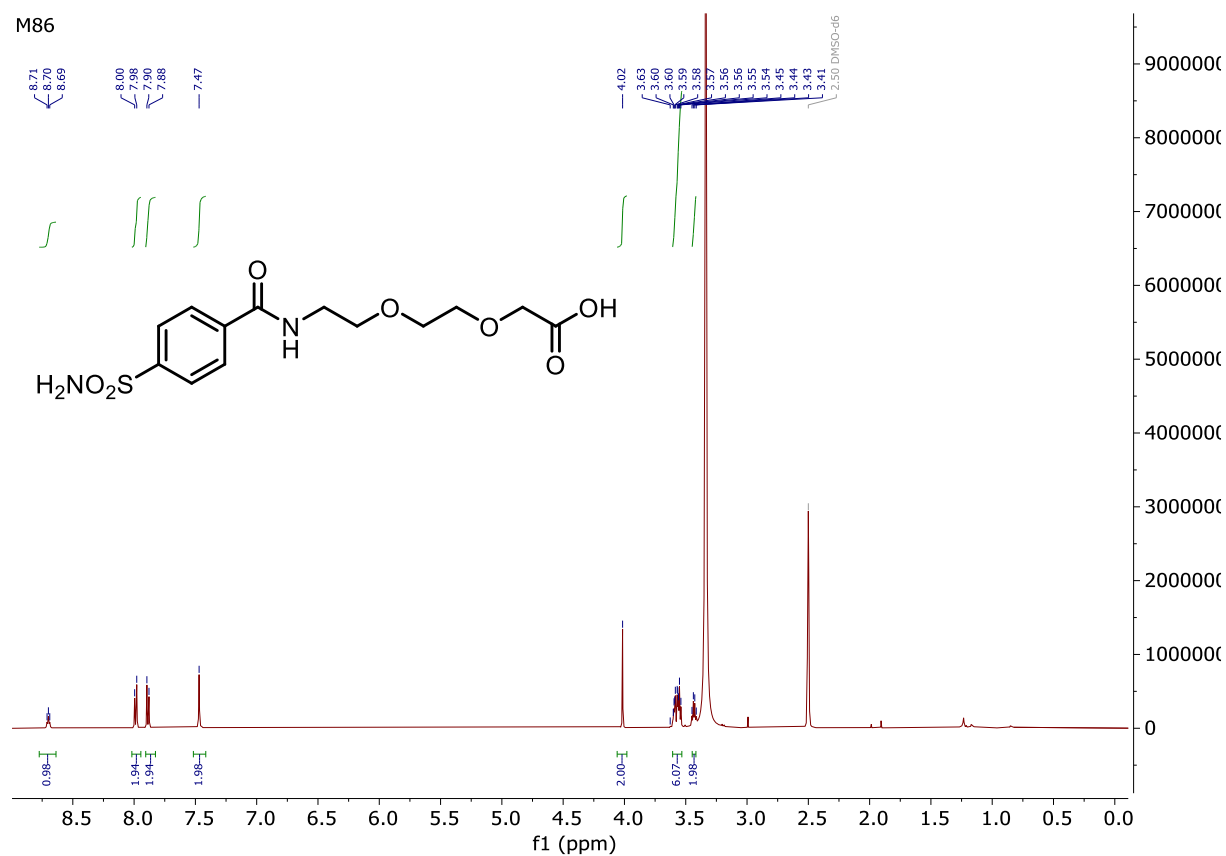
Appendix

Methyl 2-(2-(2-(4-sulfamoylbenzamido)ethoxy)ethoxy)acetate

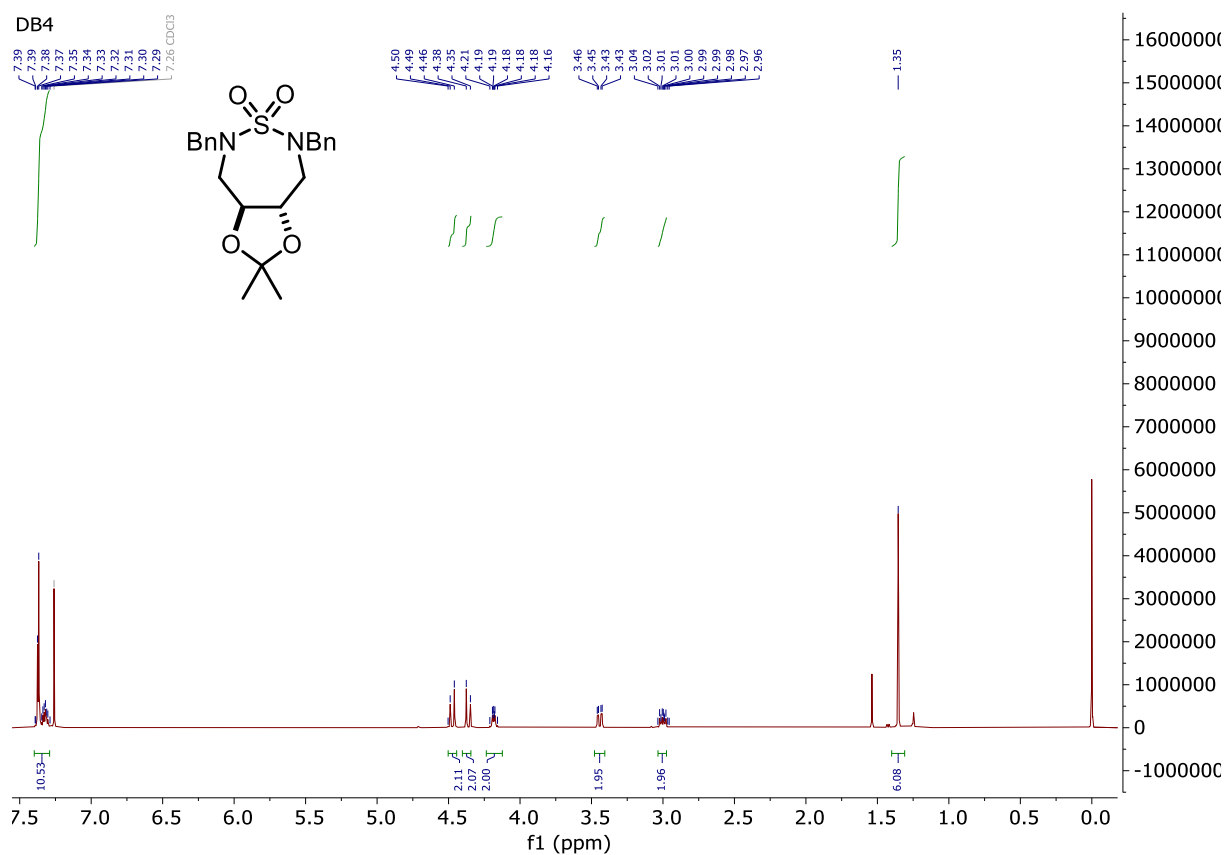


2-(2-(2-(4-Sulfamoylbenzamido)ethoxy)ethoxy)acetic acid (M86)

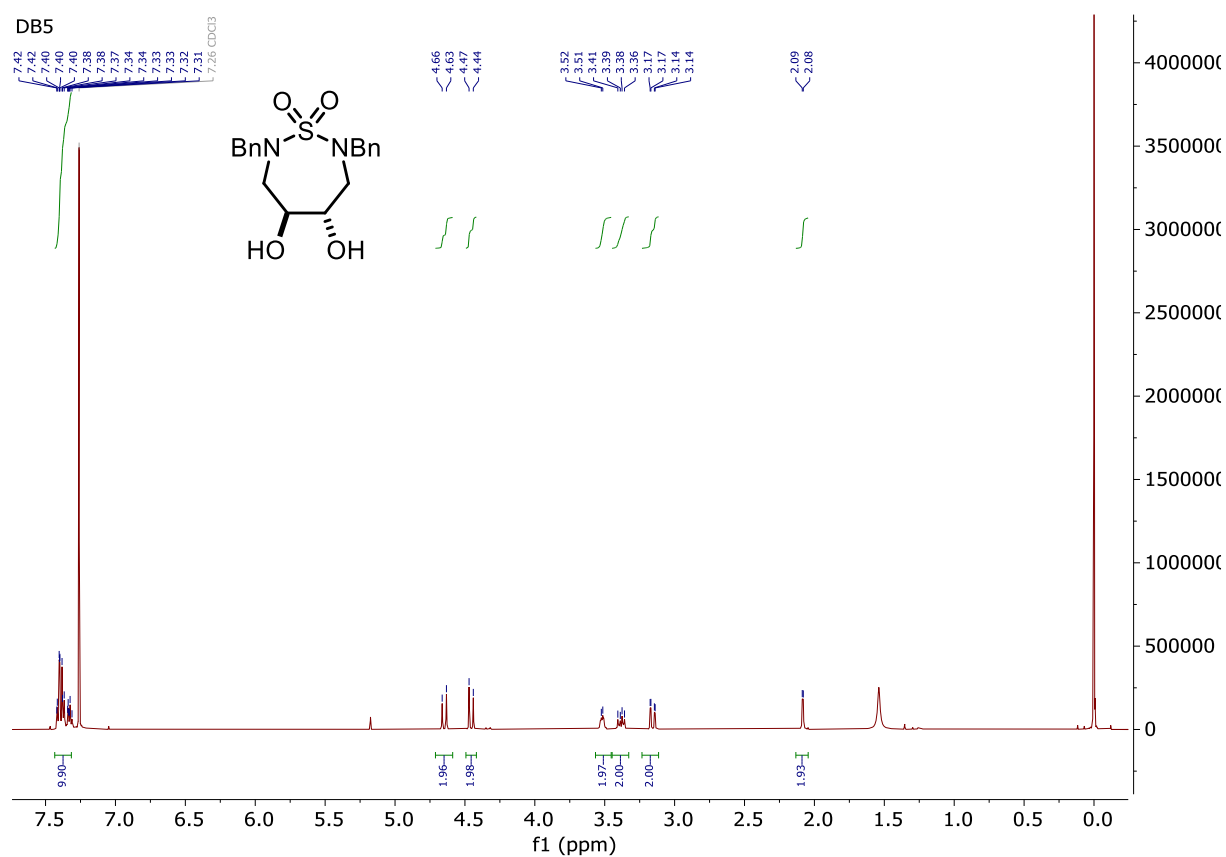
M86



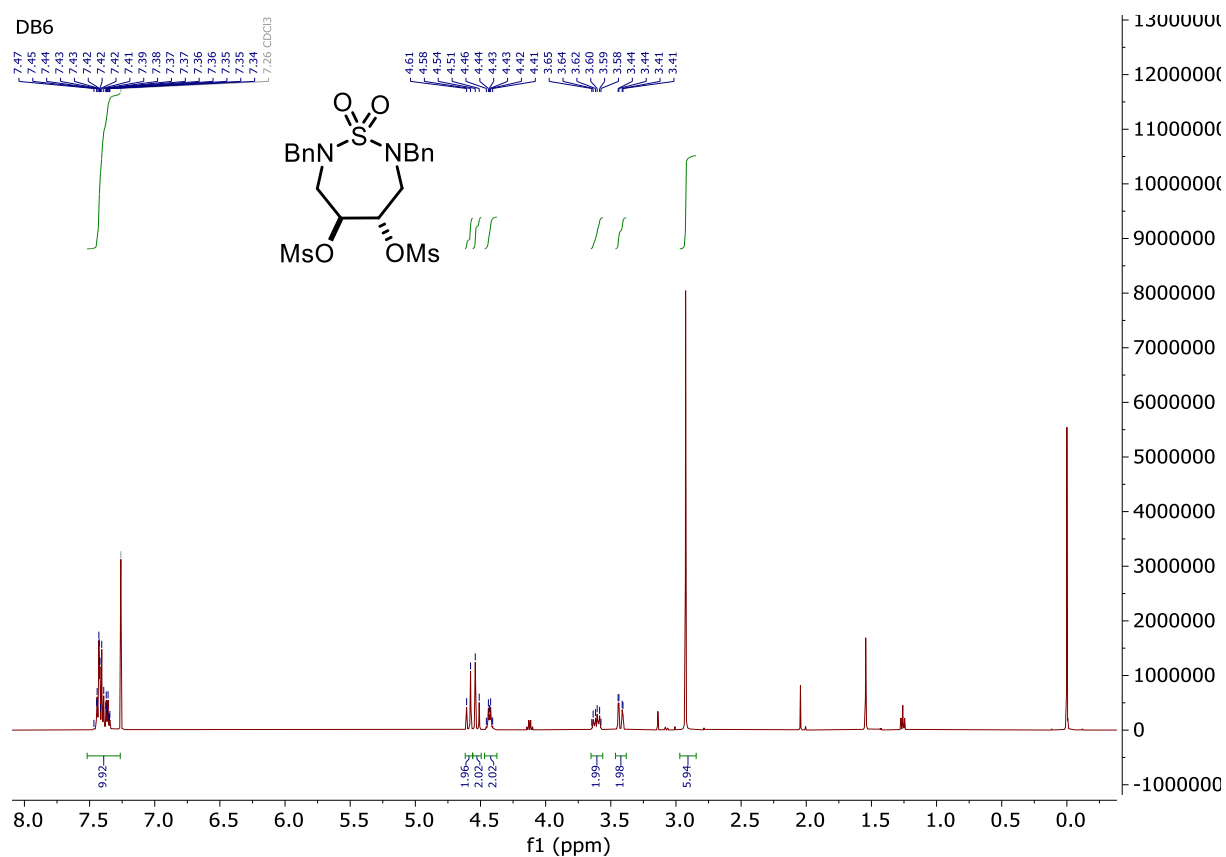
(3*aS*,8*aS*)-5,7-Dibenzyl-2,2-dimethylhexahydro-[1,3]dioxolo[4,5-*d*][1,2,7]thiadiazepine 6,6-dioxide (**DB4**)



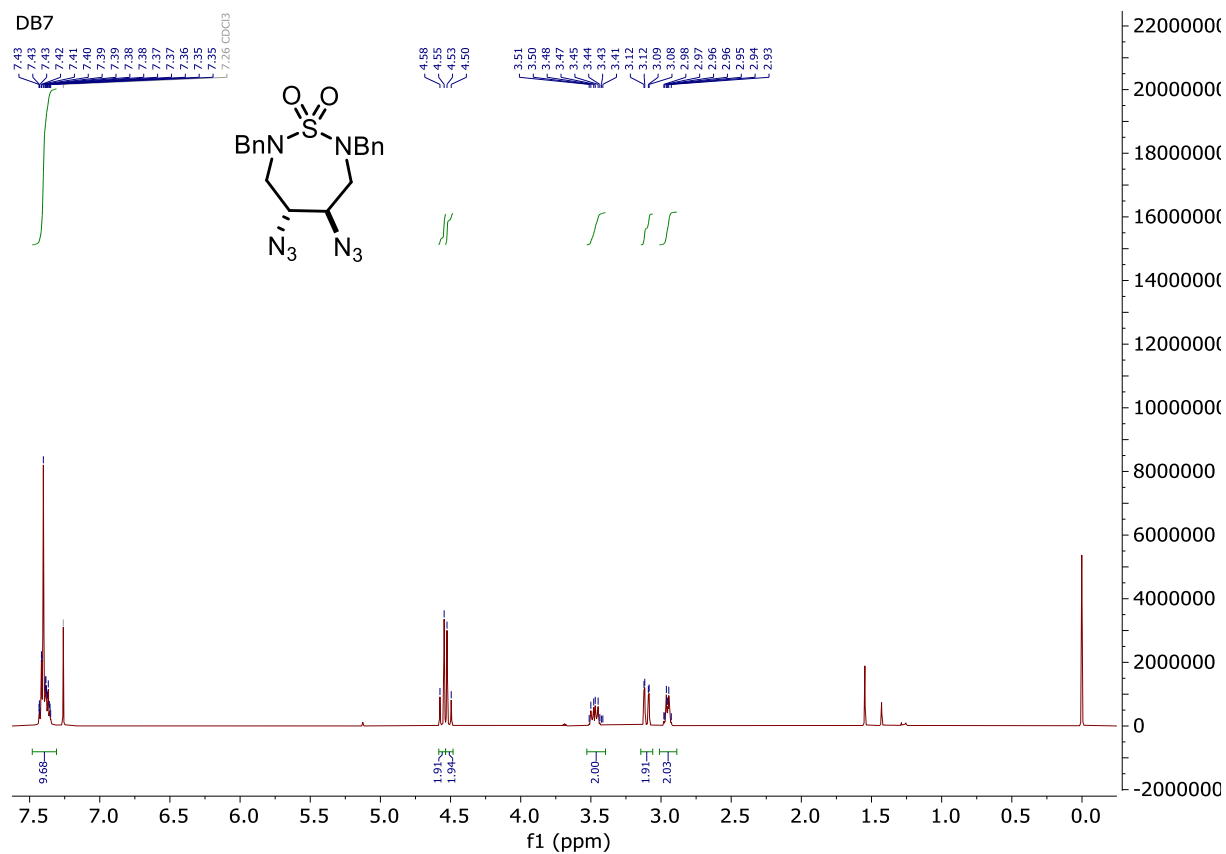
(4*S*,5*S*)-2,7-dibenzyl-4,5-dihydroxy-1,2,7-thiadiazepane 1,1-dioxide (**DB5**)



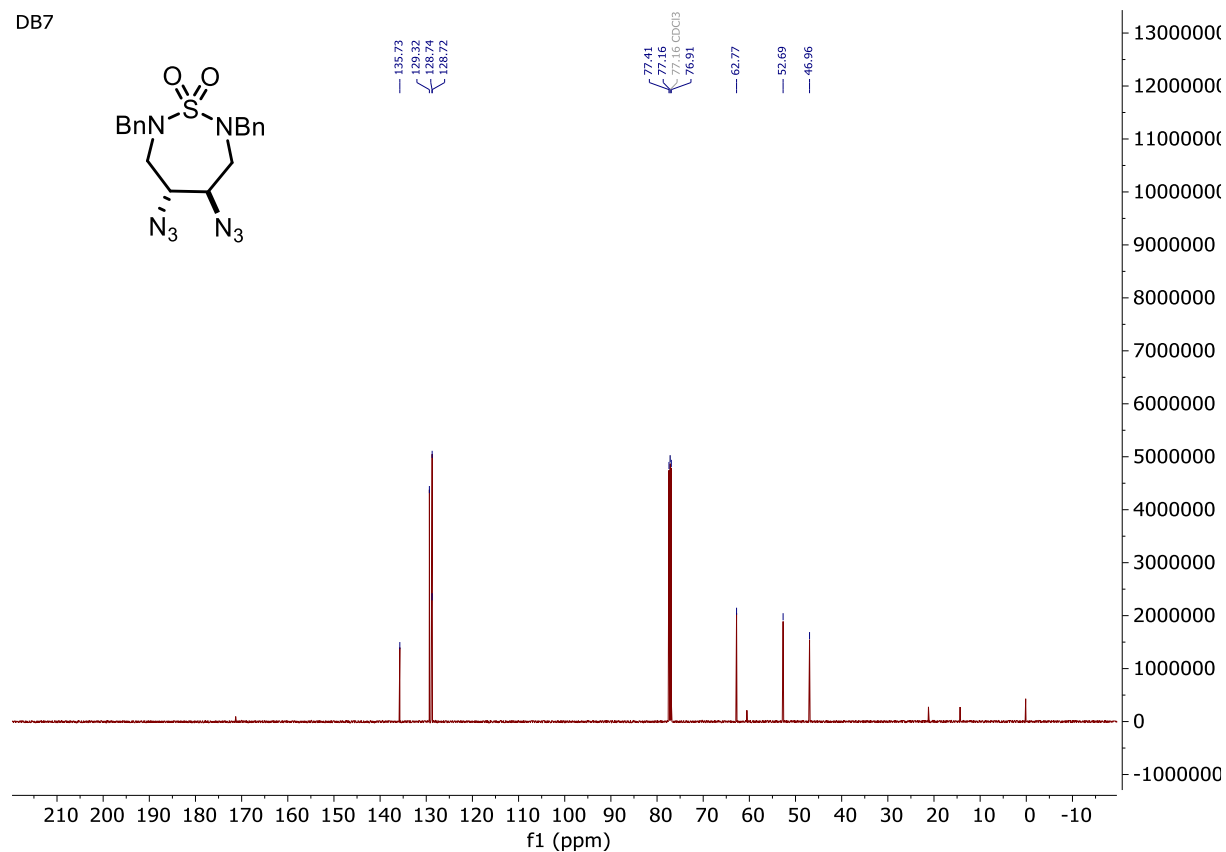
(4*S*,5*S*)-2,7-dibenzyl-1,1-dioxido-1,2,7-thiadiazepane-4,5-diyl dimethanesulfonate (**DB6**)



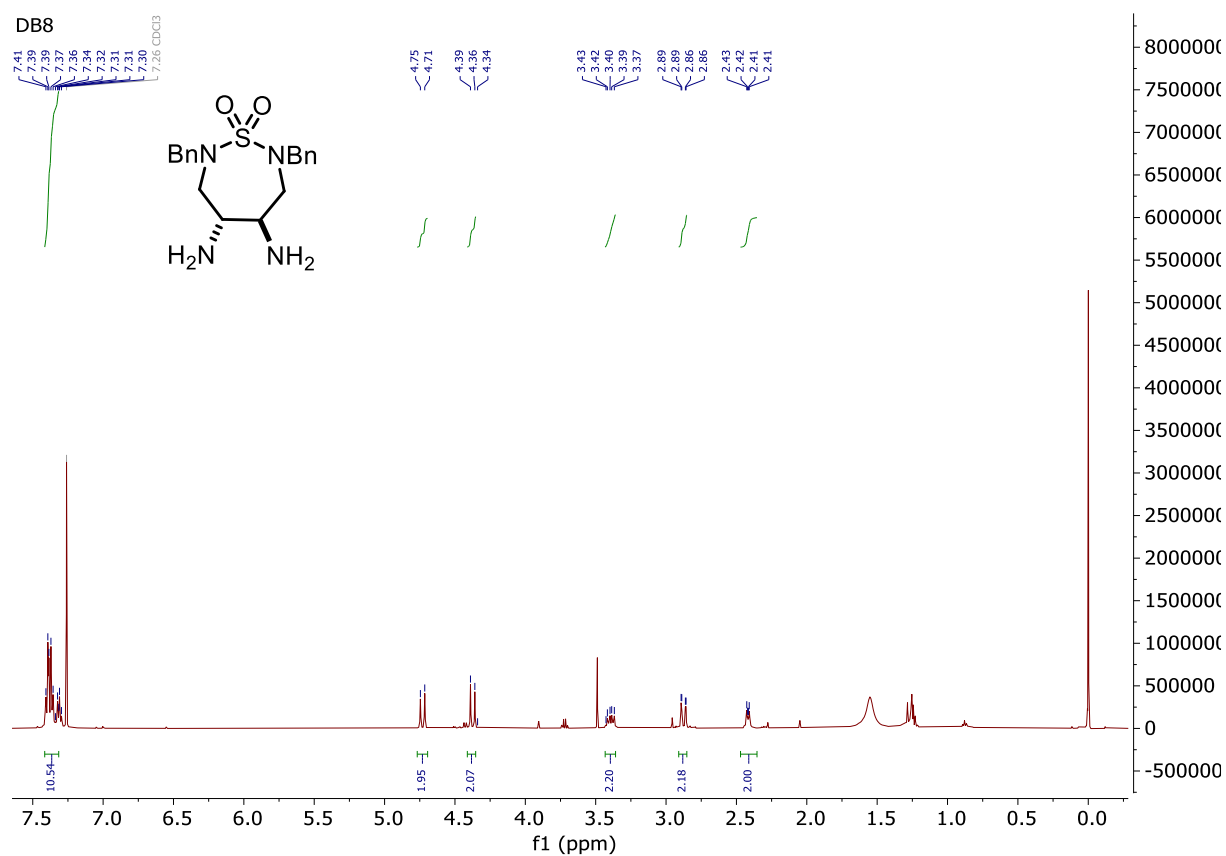
(4*R*,5*R*)-4,5-diazo-2,7-dibenzyl-1,2,7-thiadiazepane 1,1-dioxide (**DB7**)



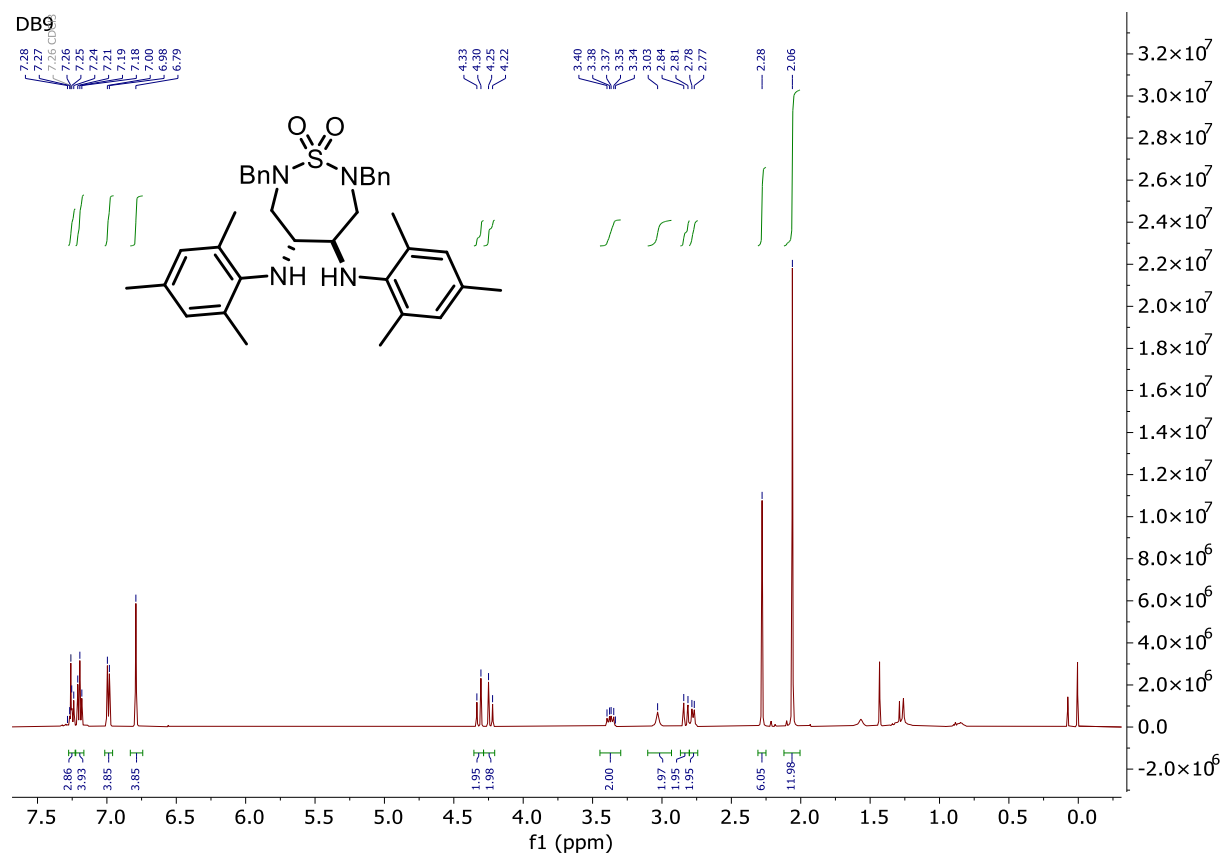
DB7



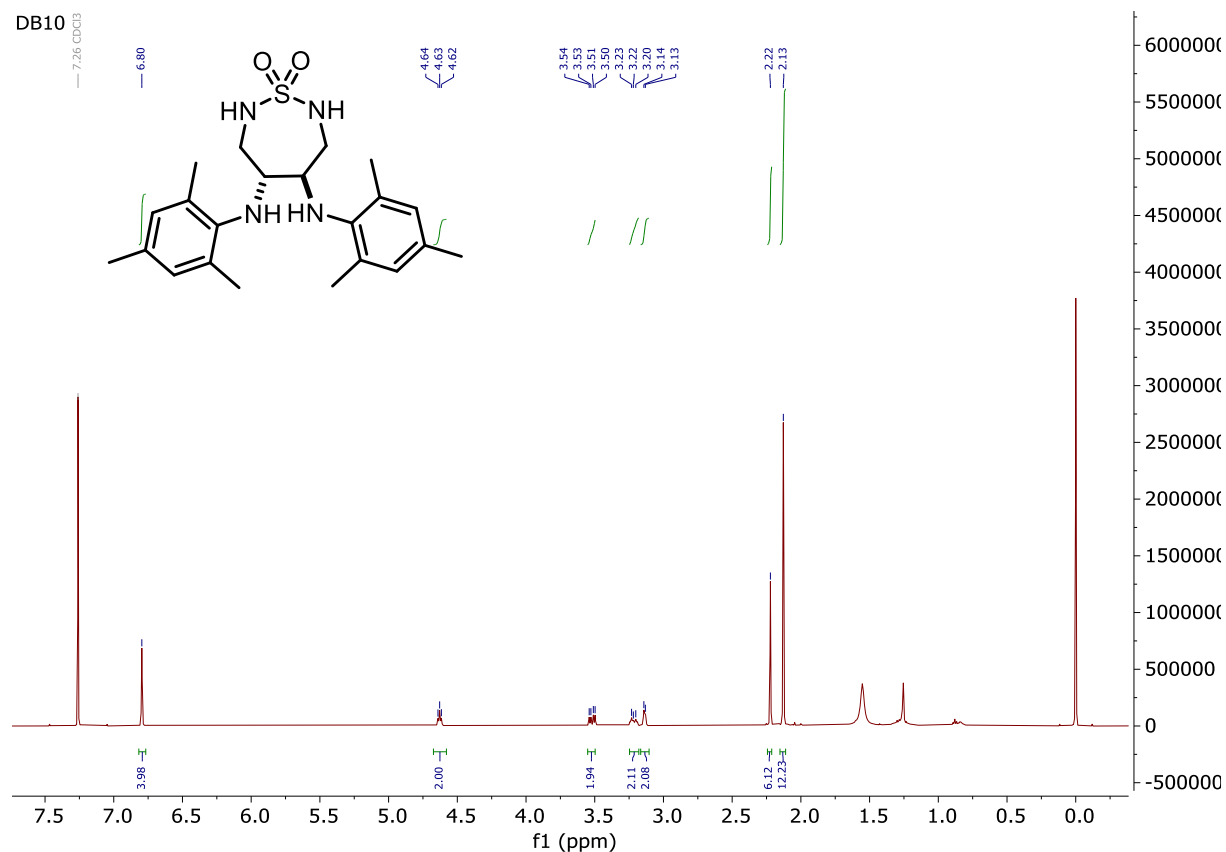
(4*R*,5*R*)-4,5-diamino-2,7-dibenzyl-1,2,7-thiadiazepane 1,1-dioxide (**DB8**)

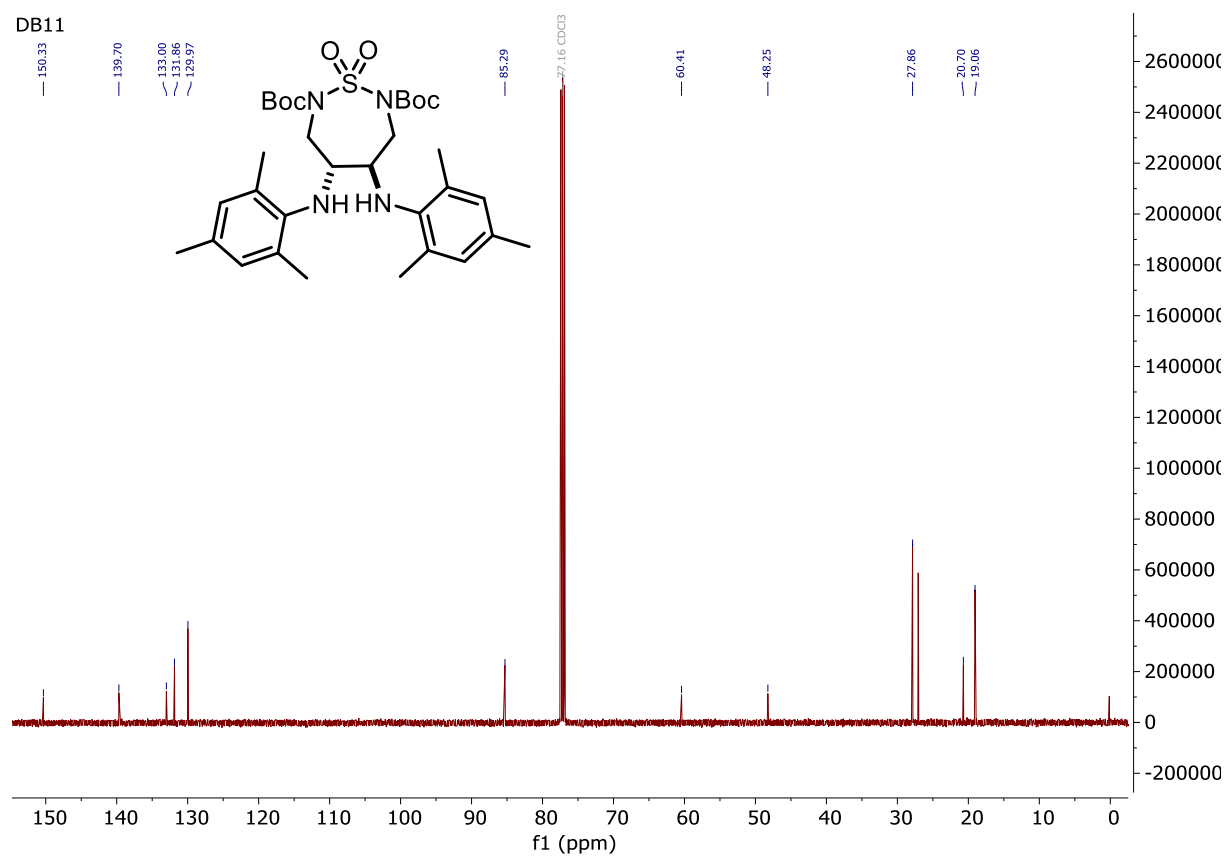
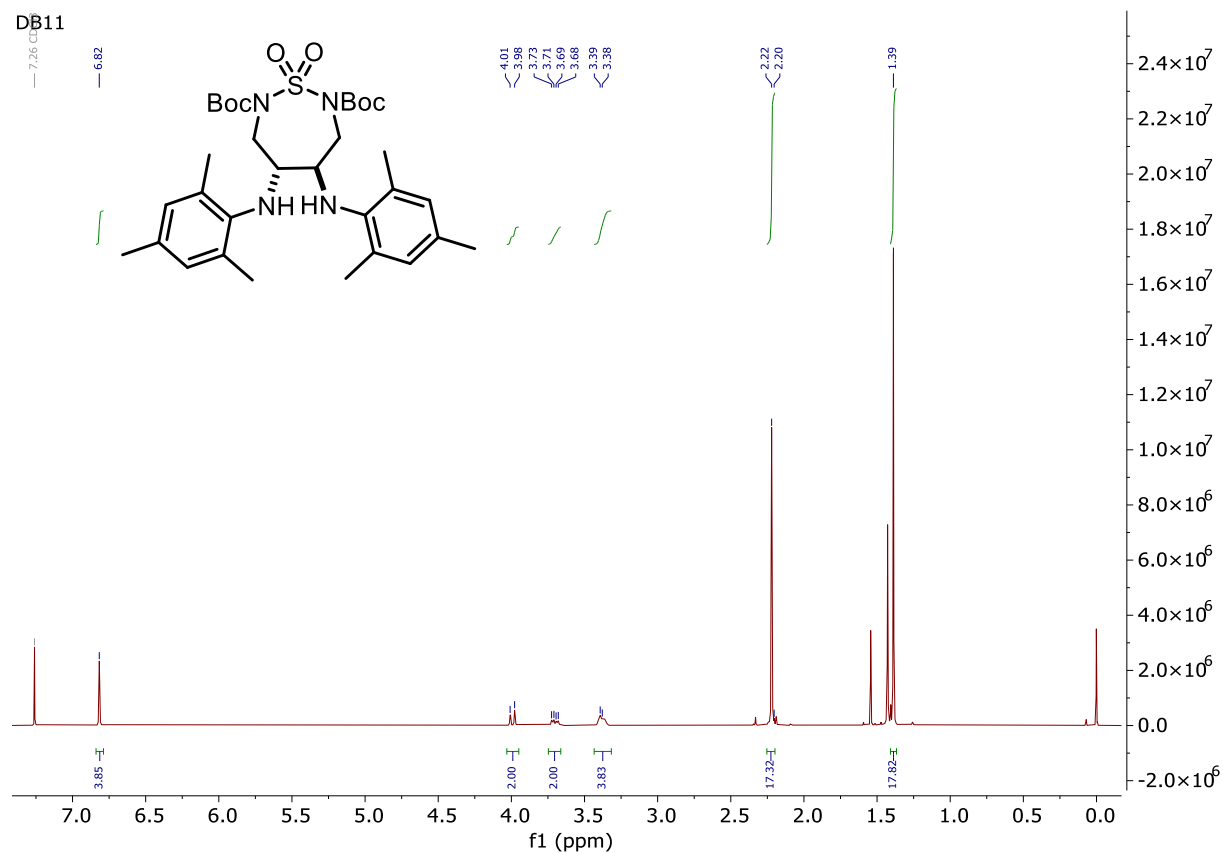


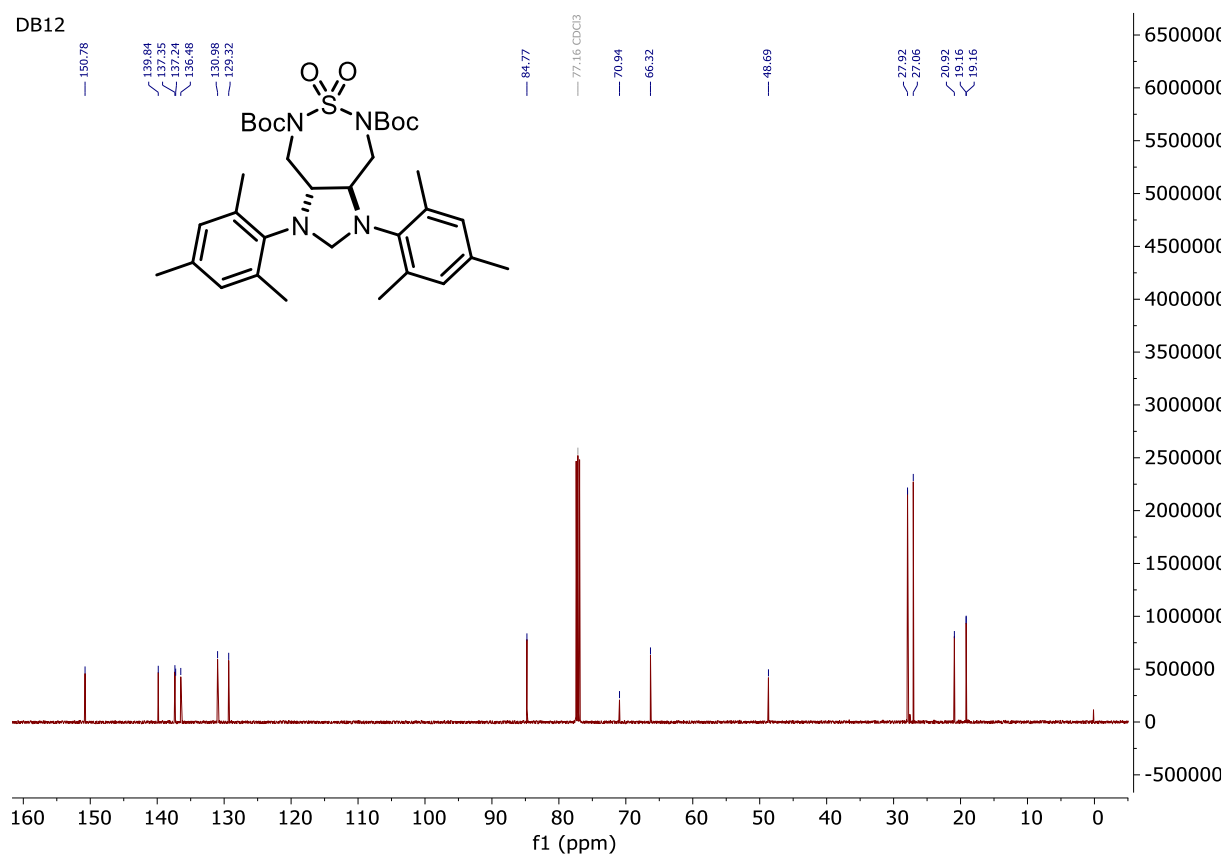
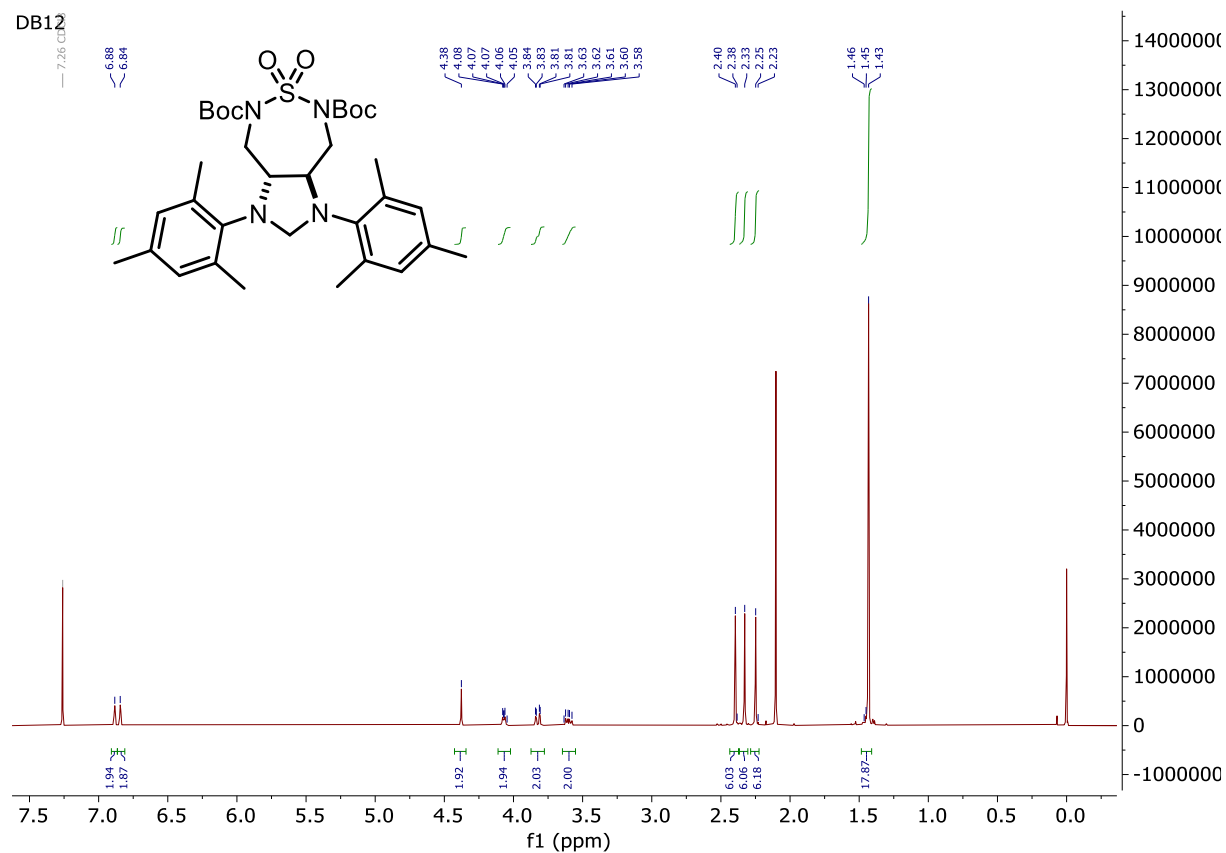
(4*R*,5*R*)-2,7-dibenzyl-4,5-bis(mesitylamino)-1,2,7-thiadiazepane 1,1-dioxide (DB9)



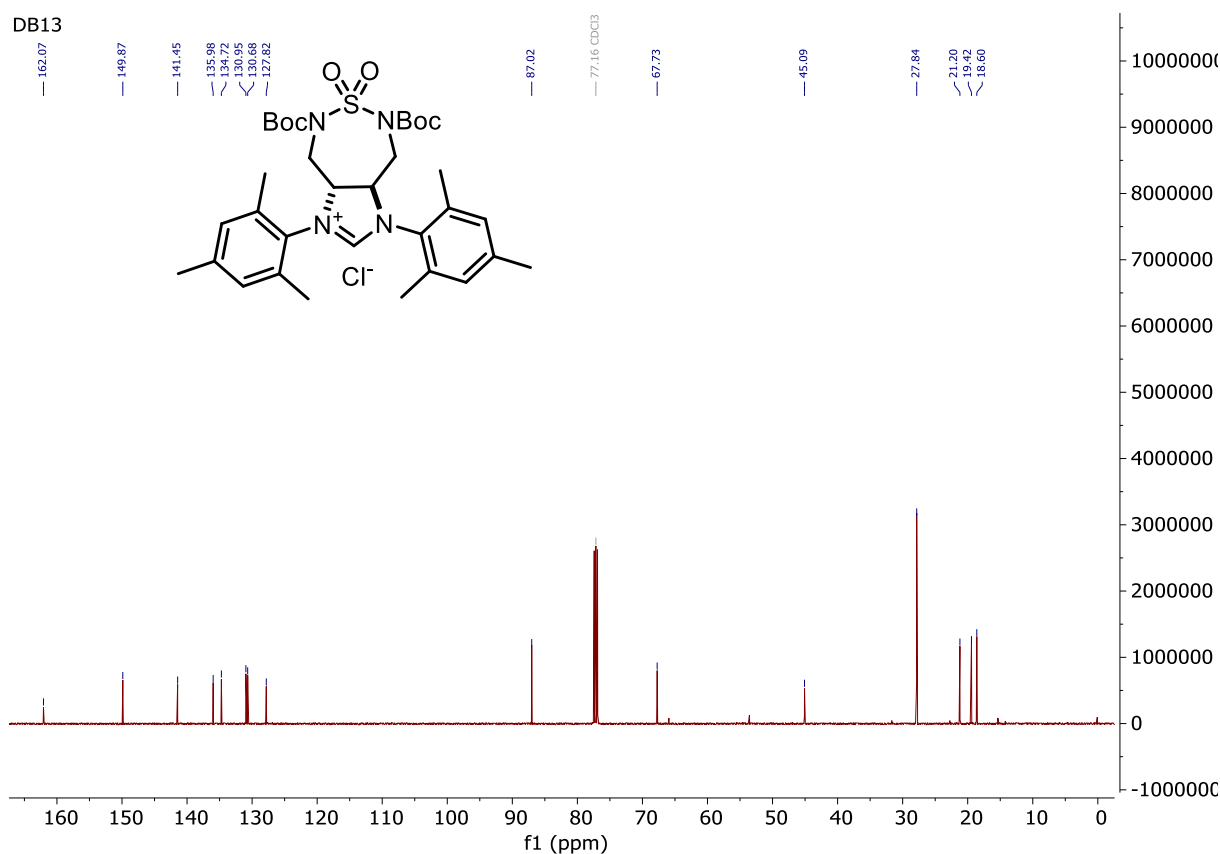
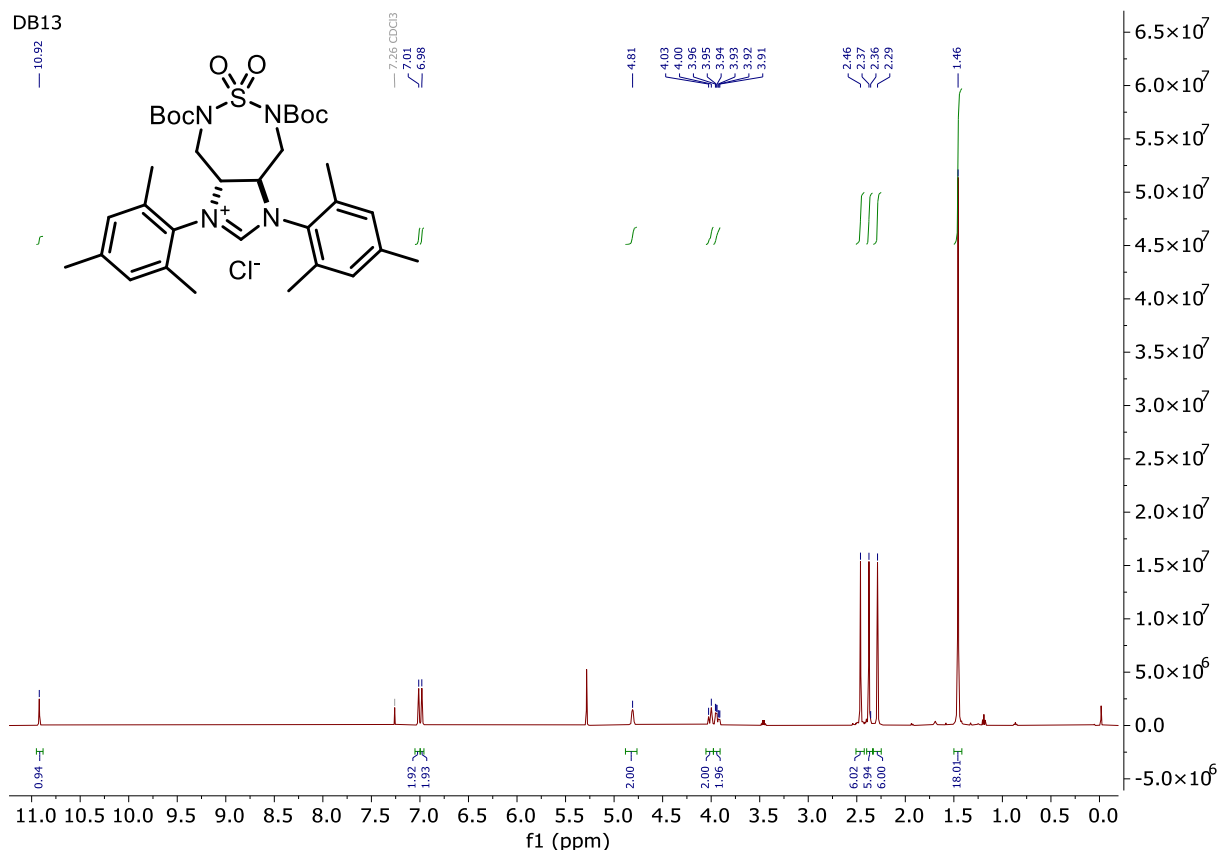
(4*R*,5*R*)-4,5-Bis(mesitylamino)-1,2,7-thiadiazepane 1,1-dioxide (DB10)



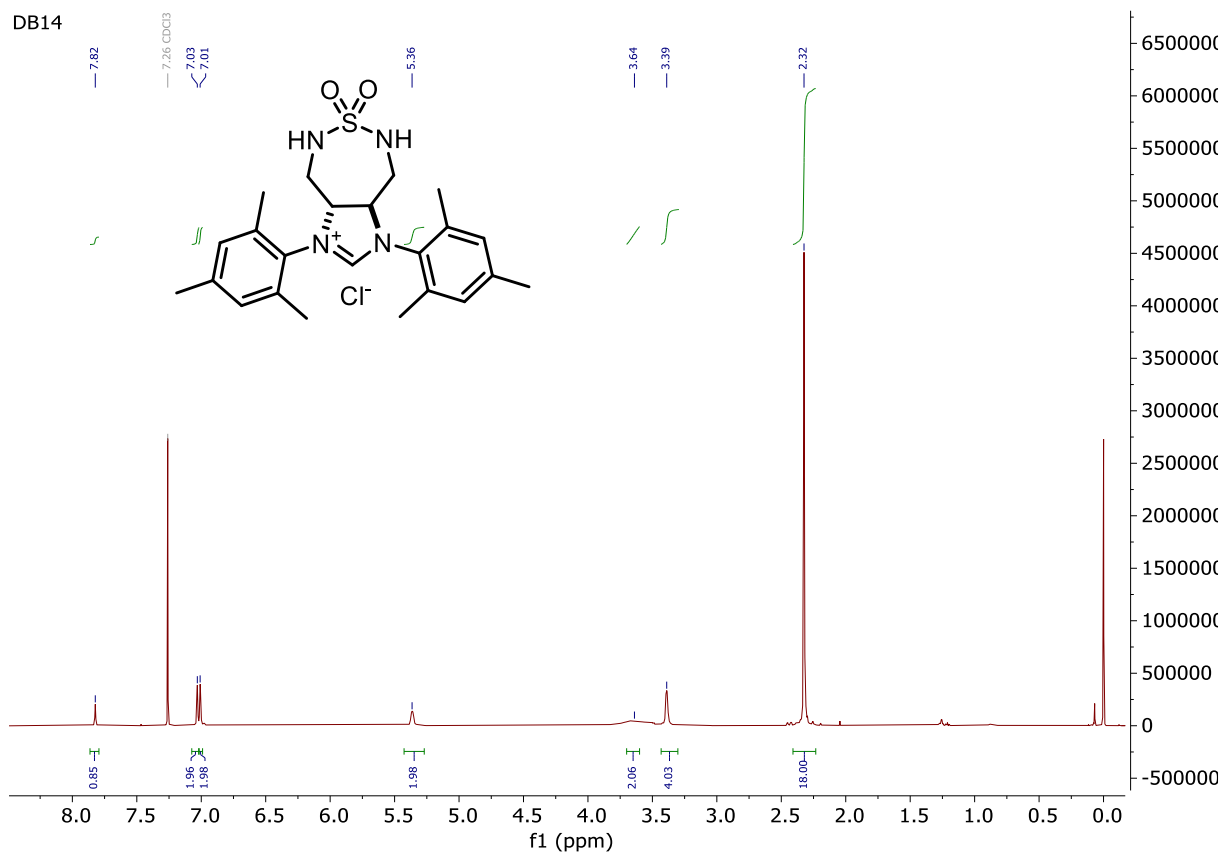
Di-*tert*-butyl (4*R*,5*R*)-4,5-bis(mesitylamino)-1,2,7-thiadiazepane-2,7-dicarboxylate 1,1-dioxide (DB11)

Di-*tert*-butyl (3*aR*,8*aR*)-1,3-dimesitylhexahydro-1*H*-imidazo[4,5-*d*][1,2,7]thiadiazepine-5,7-dicarboxylate 6,6-dioxide (**DB12**)

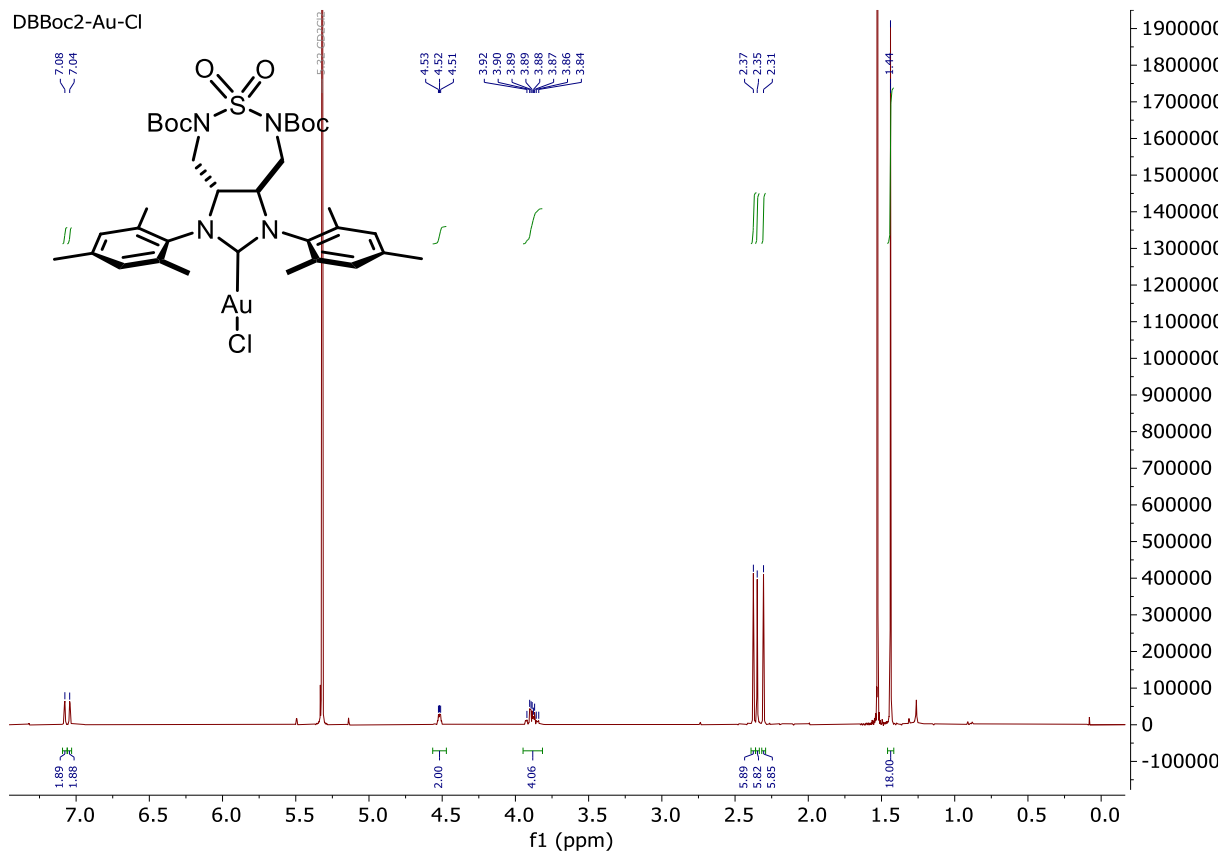
(3a*R*,8a*R*)-5,7-Bis(*tert*-butoxycarbonyl)-1,3-dimesityl-3a,4,5,7,8,8a-hexahydro-1*H*-imidazo[4,5-*d*][1,2,7]thiadiazepin-3-ium 6,6-dioxide chloride (**DB13**)



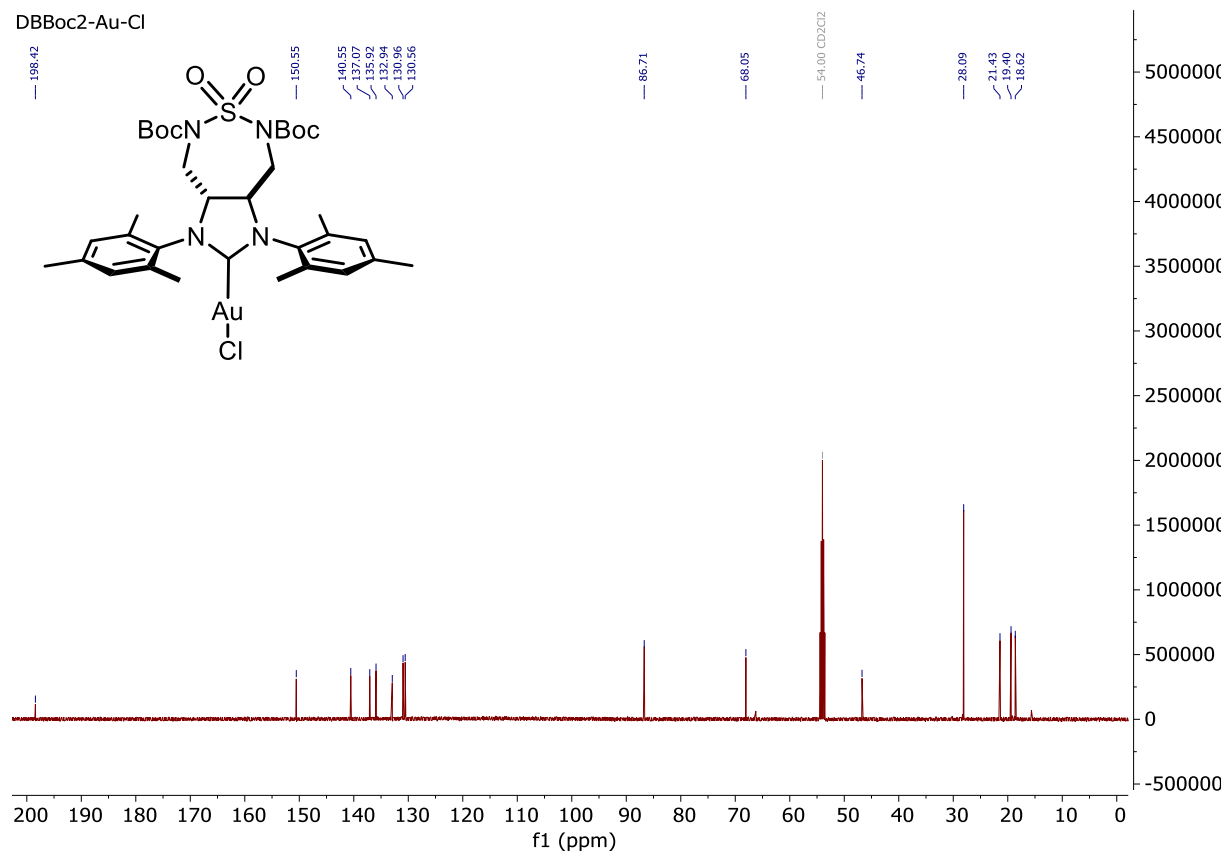
(3*aR*,8*aR*)-1,3-Dimesityl-3*a*,4,5,7,8,8*a*-hexahydro-1*H*-imidazo[4,5-*d*][1,2,7]thiadiazepin-3-ium 6,6-dioxide chloride (**DB14**)



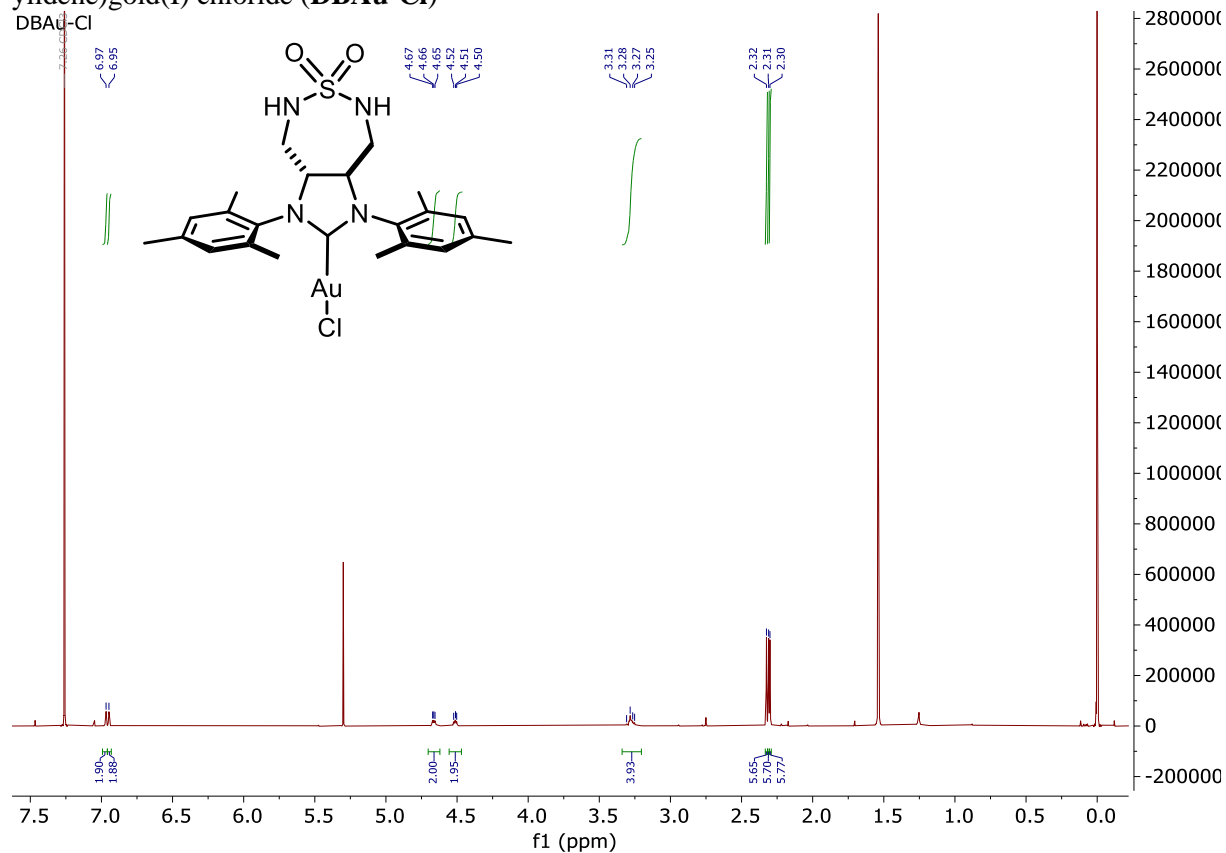
((3*aR*,8*aR*)-5,7-Bis(*tert*-butoxycarbonyl)-1,3-dimesityl-6,6-dioxidoctahydro-2*H*-imidazo[4,5-*d*][1,2,7]thiadiazepin-2-ylidene)gold(I) chloride (**DBBoc2-Au-Cl**)



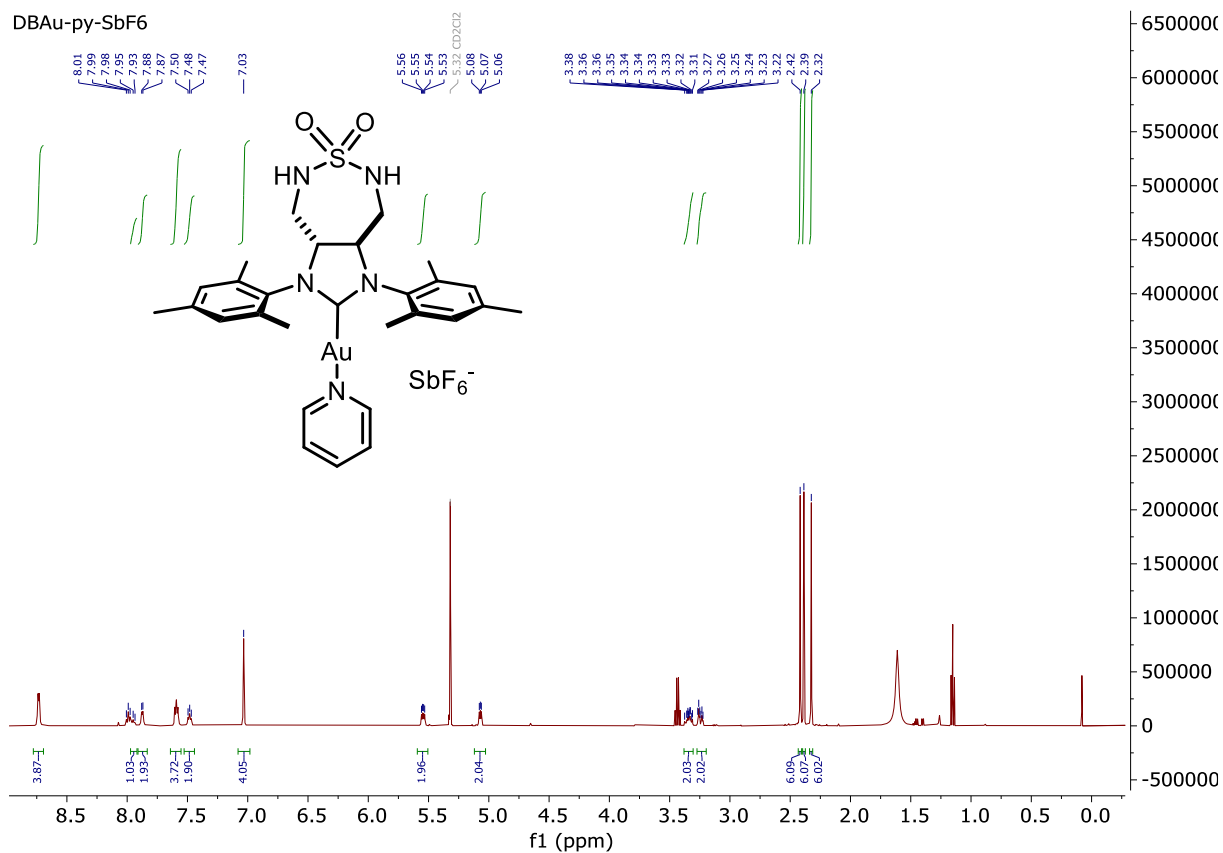
DBBoc2-Au-Cl



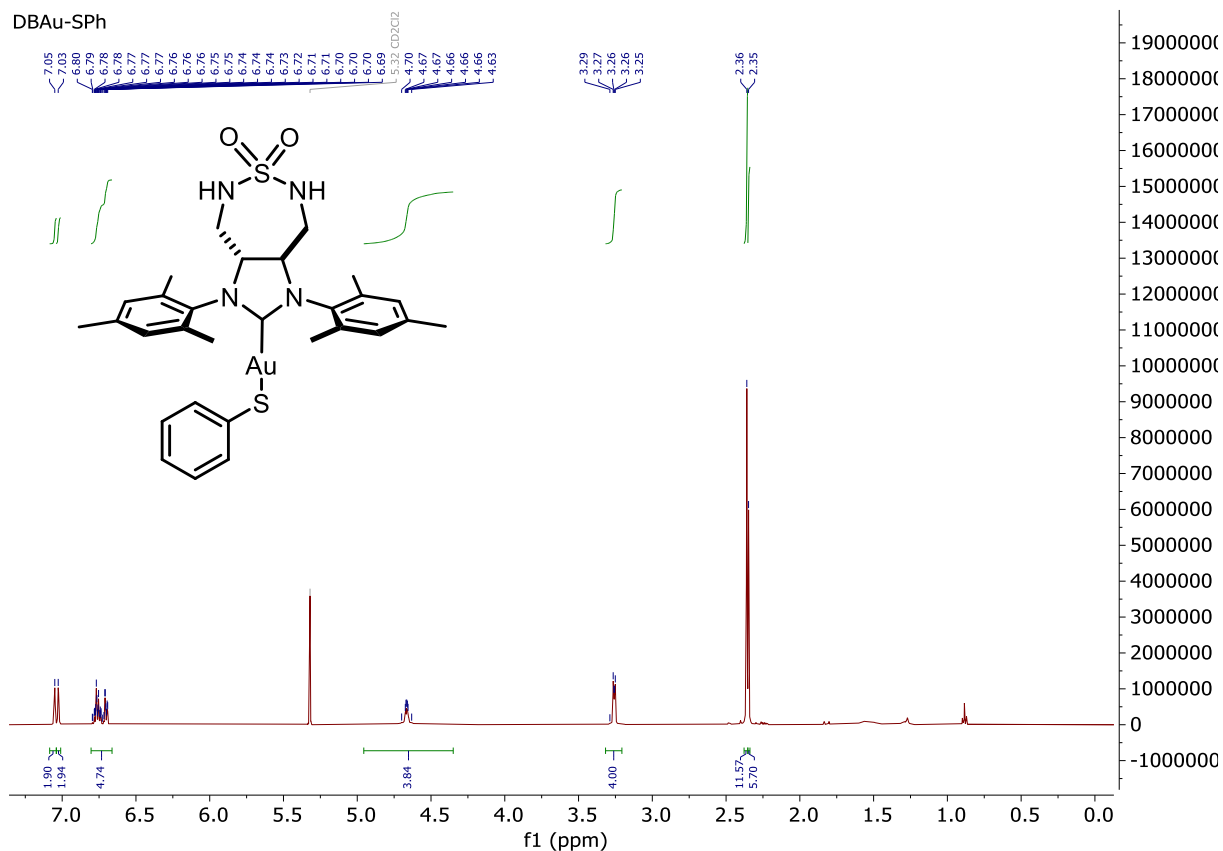
((3a*R*,8a*R*)-1,3-Dimesityl-6,6-dioxidoctahydro-2*H*-imidazo[4,5-*d*][1,2,7]thiadiazepin-2-ylidene)gold(I) chloride (**DBAu-Cl**)

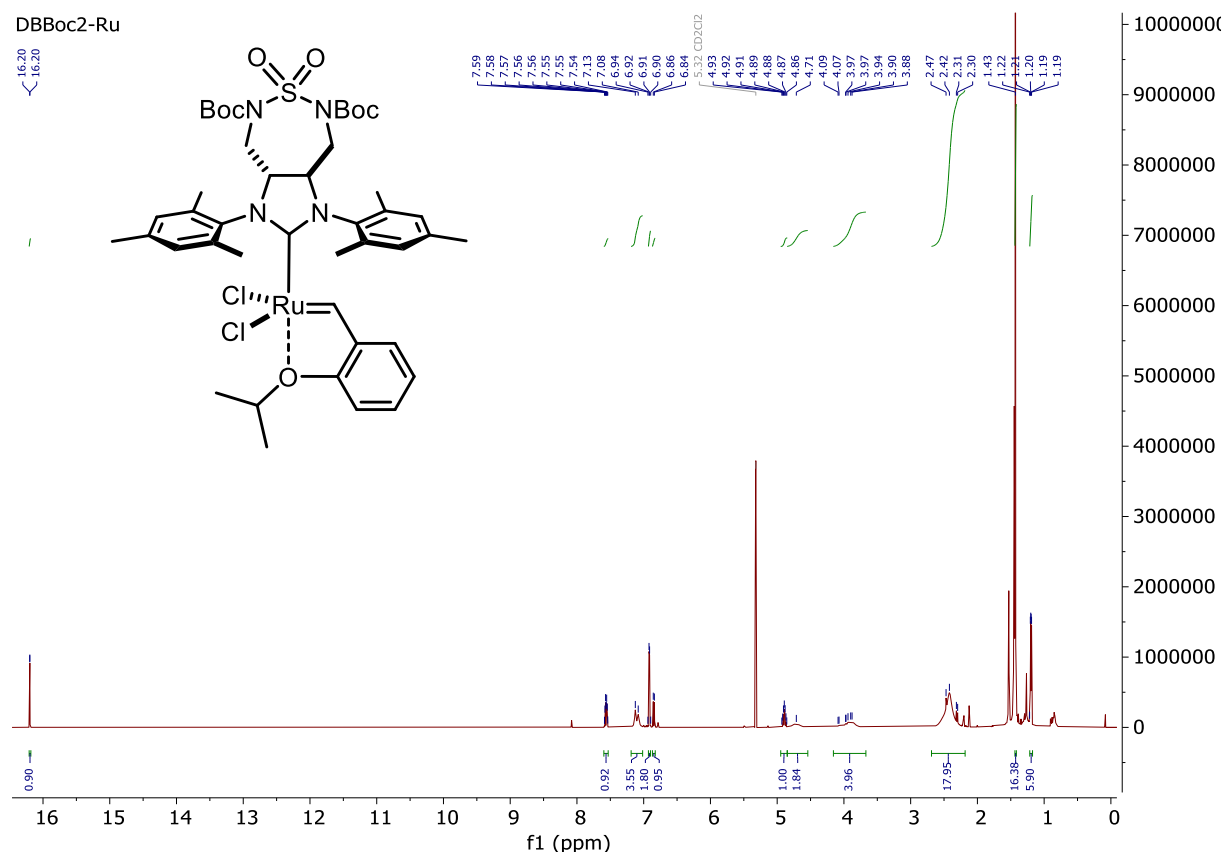
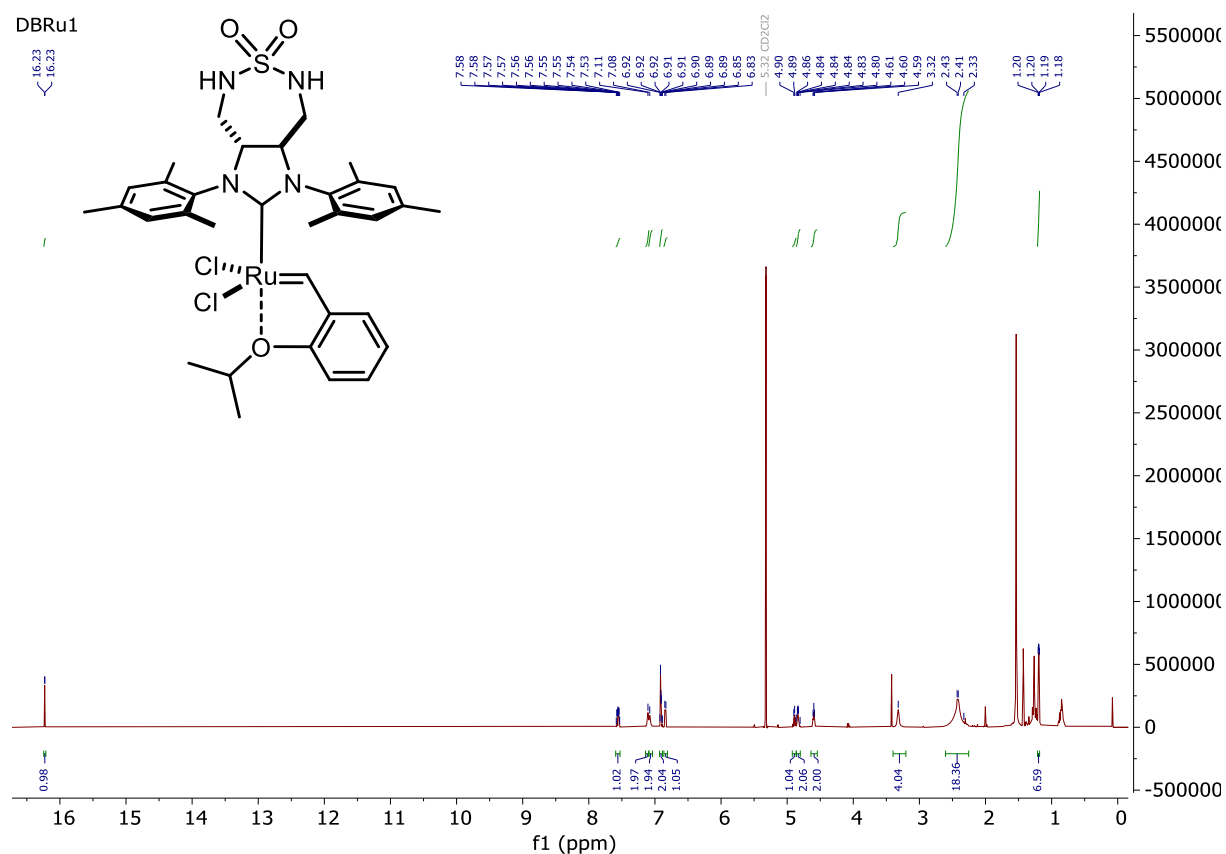


((3*aR*,8*aR*)-1,3-dimesityl-6,6-dioxidoctahydro-2*H*-imidazo[4,5-*d*][1,2,7]thiadiazepin-2-ylidene)(pyridine)gold(I) hexafluoroantimonate (**DBAu-py-SbF₆**)

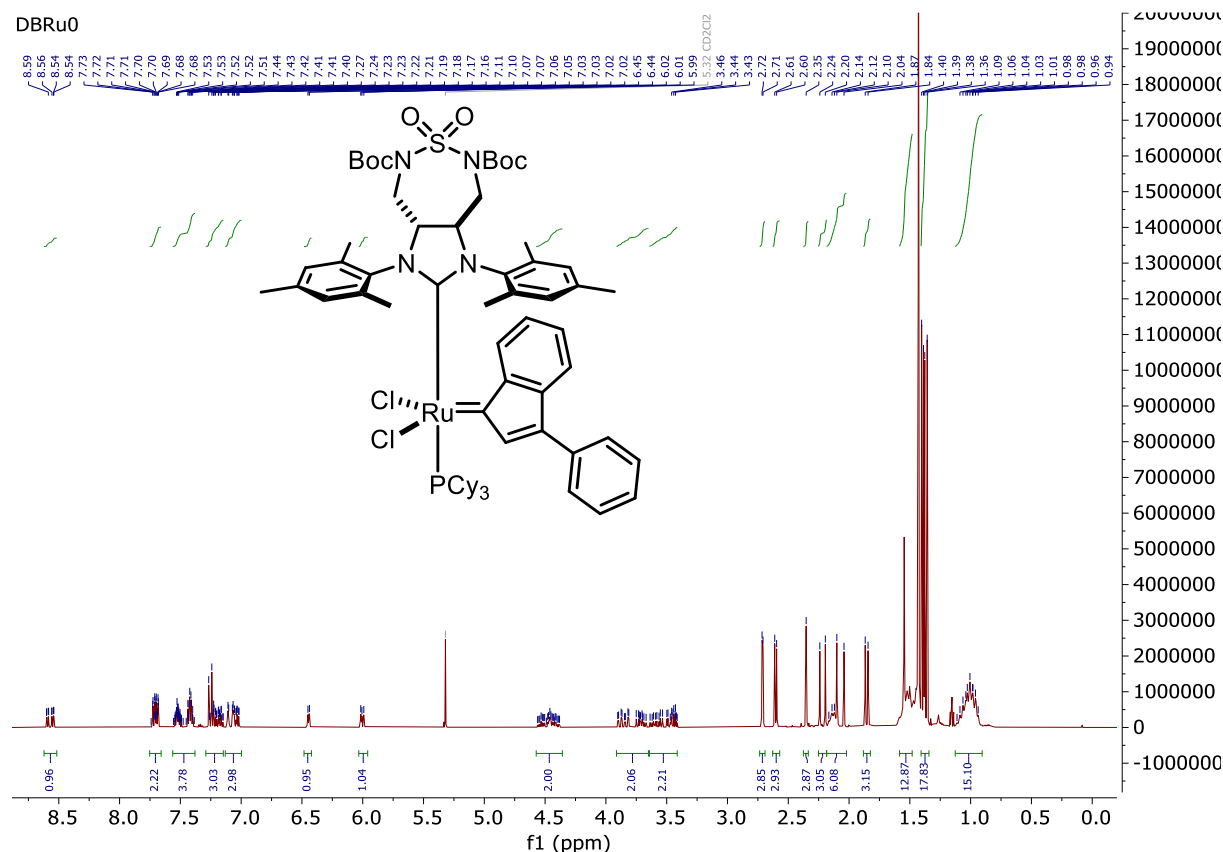


((3*aR*,8*aR*)-1,3-Dimesityl-6,6-dioxidoctahydro-2*H*-imidazo[4,5-*d*][1,2,7]thiadiazepin-2-ylidene)(phenylthio)gold(I) (**DBAu-SPh**)

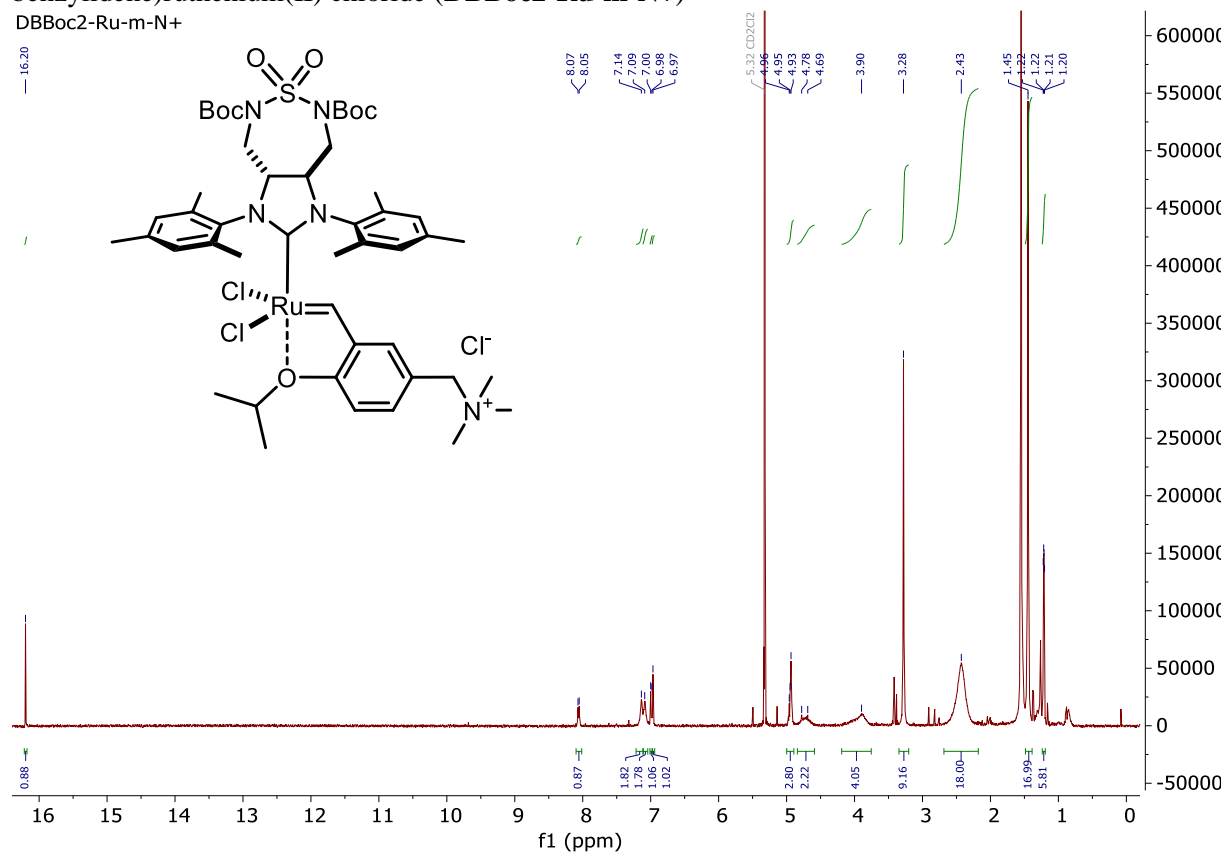


Dichloro((3a*R*,8a*R*)-5,7-bis(*tert*-butoxycarbonyl)-1,3-dimesityl-6,6-dioxidoctahydro-2*H*-imidazo[4,5-*d*][1,2,7]thiadiazepin-2-ylidene)(2-isopropoxybenzylidene)ruthenium(II) (**DBBoc2-Ru**)Dichloro((3a*R*,8a*R*)-1,3-dimesityl-6,6-dioxidoctahydro-2*H*-imidazo[4,5-*d*][1,2,7]thiadiazepin-2-ylidene)(2-isopropoxybenzylidene)ruthenium(II) (**DBRu1**)

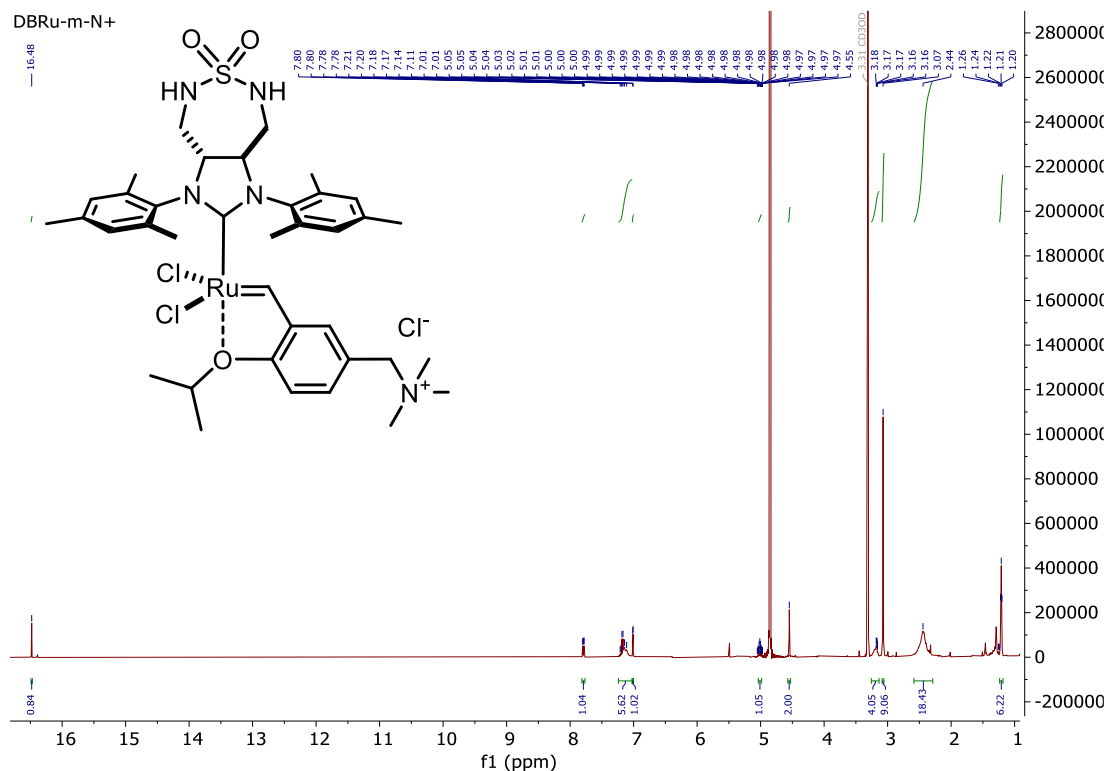
Dichloro((3*aR*,8*aR*)-5,7-bis(*tert*-butoxycarbonyl)-1,3-dimesityl-6,6-dioxidoctahydro-2*H*-imidazo[4,5-*d*][1,2,7]thiadiazepin-2-ylidene)(3-phenyl-1*H*-inden-1-ylidene)ruthenium(II) (**DBRu0**)



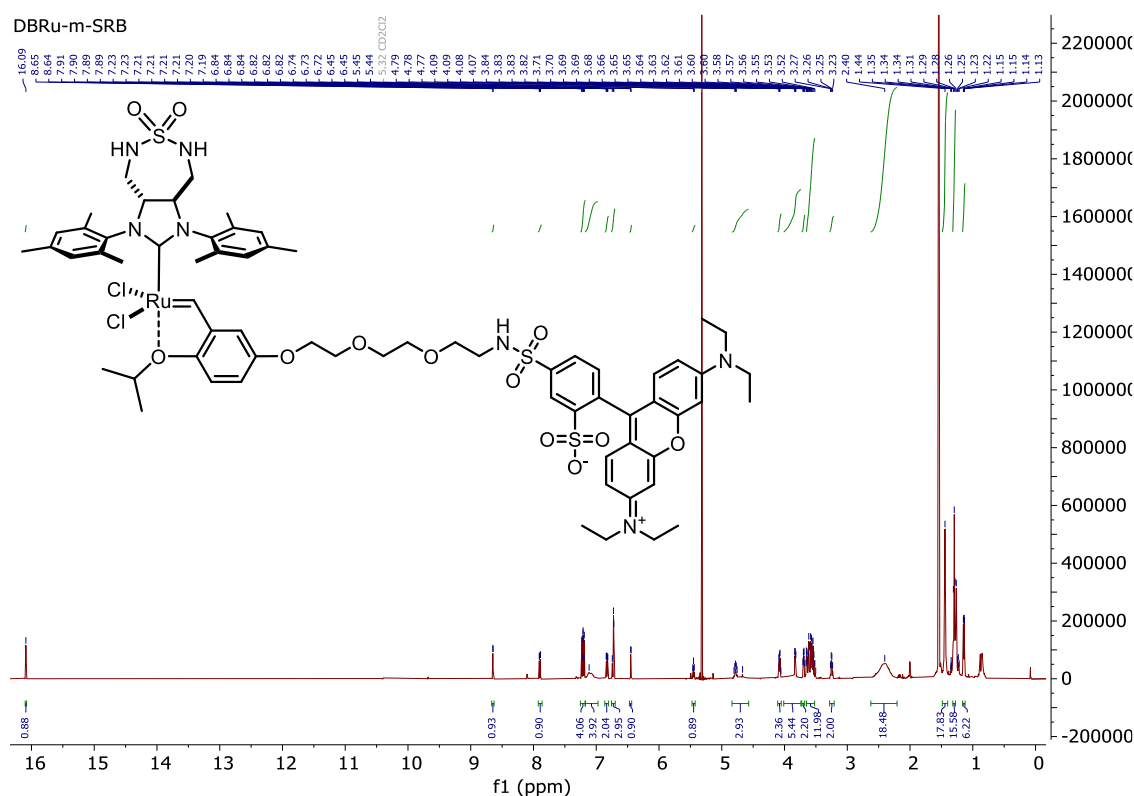
Dichloro((3*aR*,8*aR*)-5,7-bis(*tert*-butoxycarbonyl)-1,3-dimesityl-6,6-dioxidoctahydro-2*H*-imidazo[4,5-*d*][1,2,7]thiadiazepin-2-ylidene)(2-isopropoxy-5-((trimethylammonio)methyl)benzylidene)ruthenium(II) chloride (**DBBoc2-Ru-m-N+**)

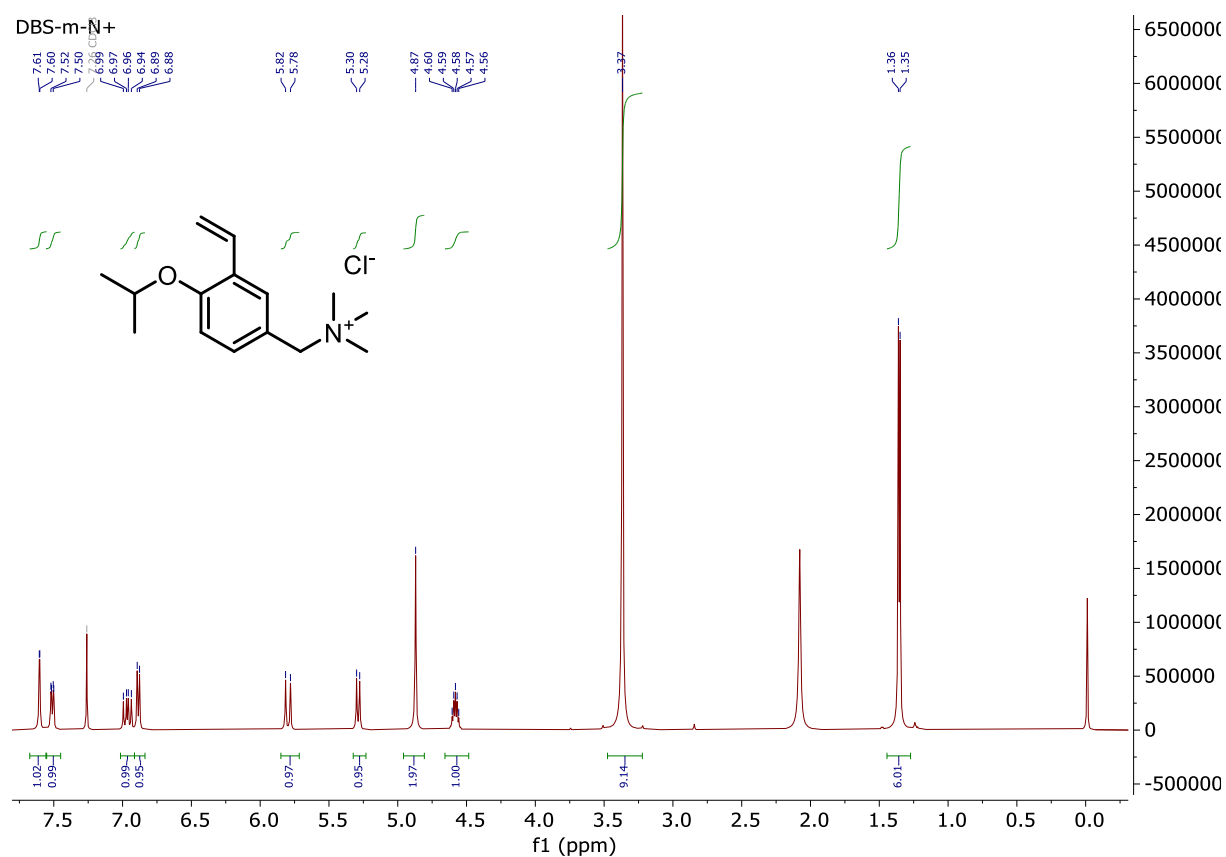
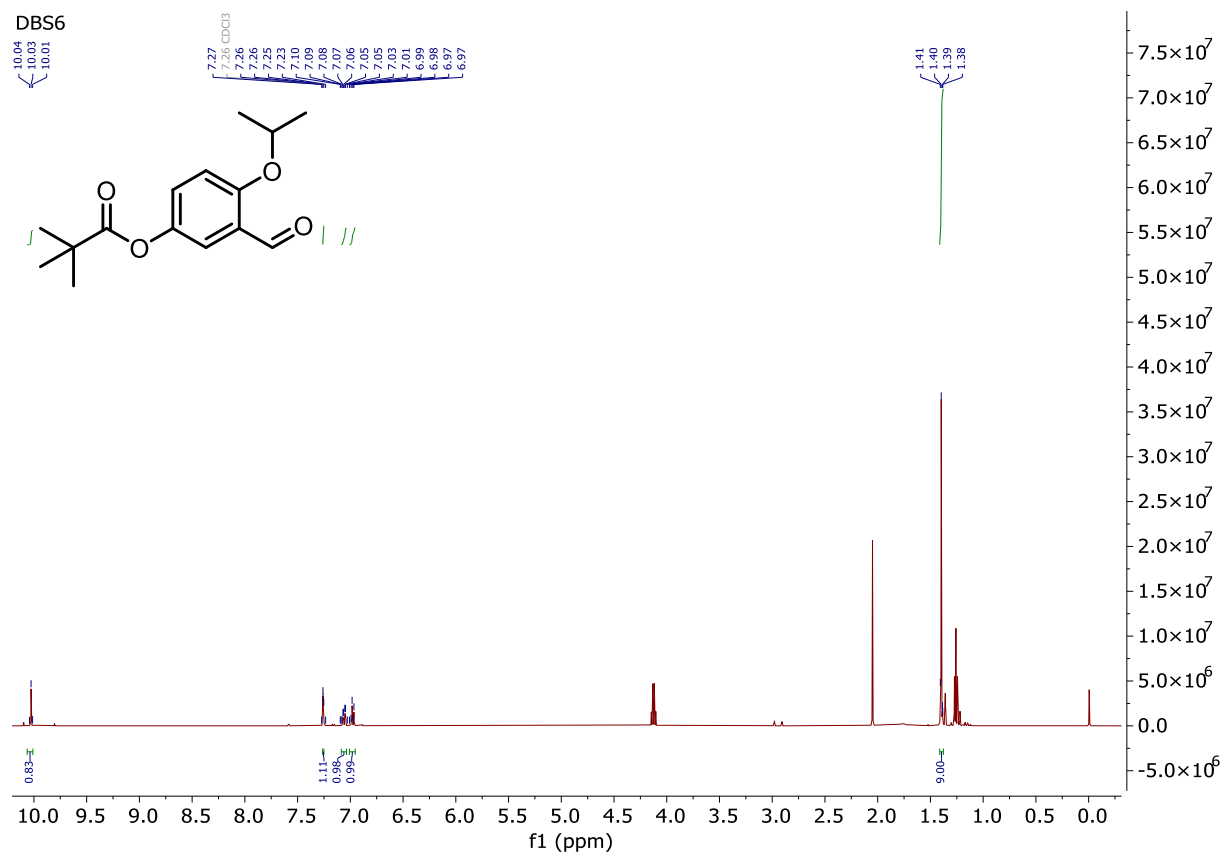


Dichloro((3*aR*,8*aR*)-1,3-dimesityl-6,6-dioxidoctahydro-2*H*-imidazo[4,5-*d*][1,2,7]thiadiazepin-2-ylidene)(2-isopropoxy-5-((trimethylammonio)methyl)benzylidene)ruthenium(II) chloride
(DBRu-m-N+)

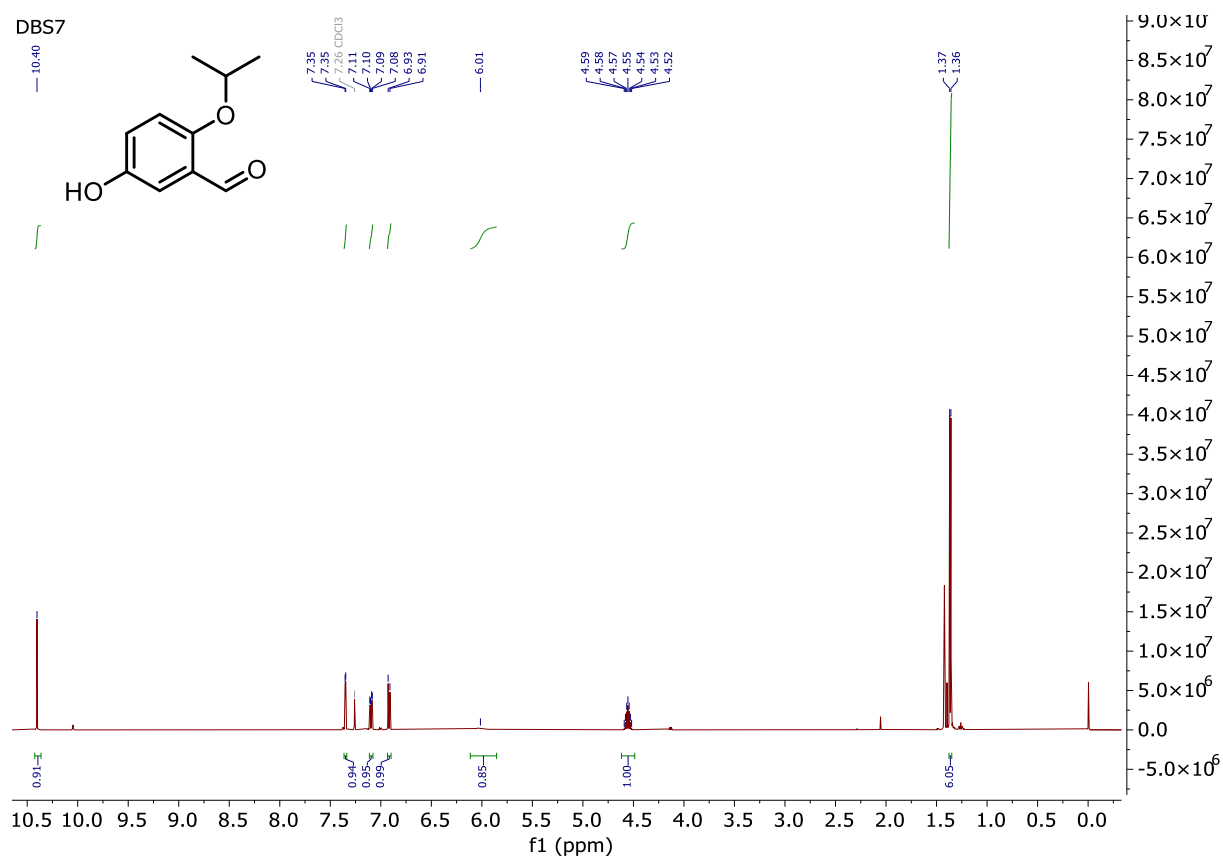


Dichloro(5-(2-(2-((4-(6-(diethylamino)-3-(diethyliminio)-3*H*-xanthen-9-yl)-3-sulfonatophenyl)sulfonamido)ethoxy)ethoxy)ethoxy)-2-isopropoxybenzylidene)((3*aR*,8*aR*)-1,3-dimesityl-6,6-dioxidoctahydro-2*H*-imidazo[4,5-*d*][1,2,7]thiadiazepin-2-ylidene)ruthenium(II) chloride
(DBRu-m-SRB)

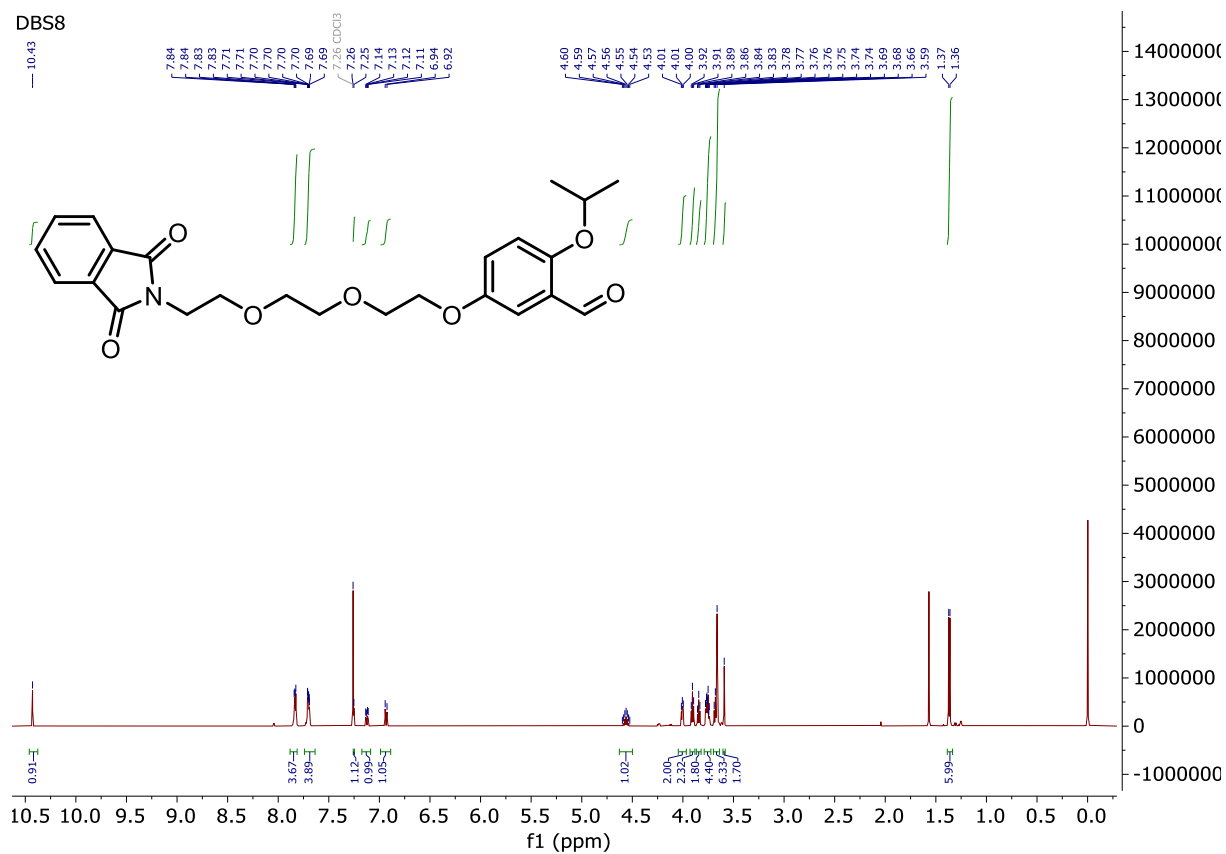


1-(4-Isopropoxy-3-vinylphenyl)-*N,N,N*-trimethylmethanaminium chloride (**DBS-m-N⁺**)3-Formyl-4-isopropoxyphenyl pivalate (**DBS6**)

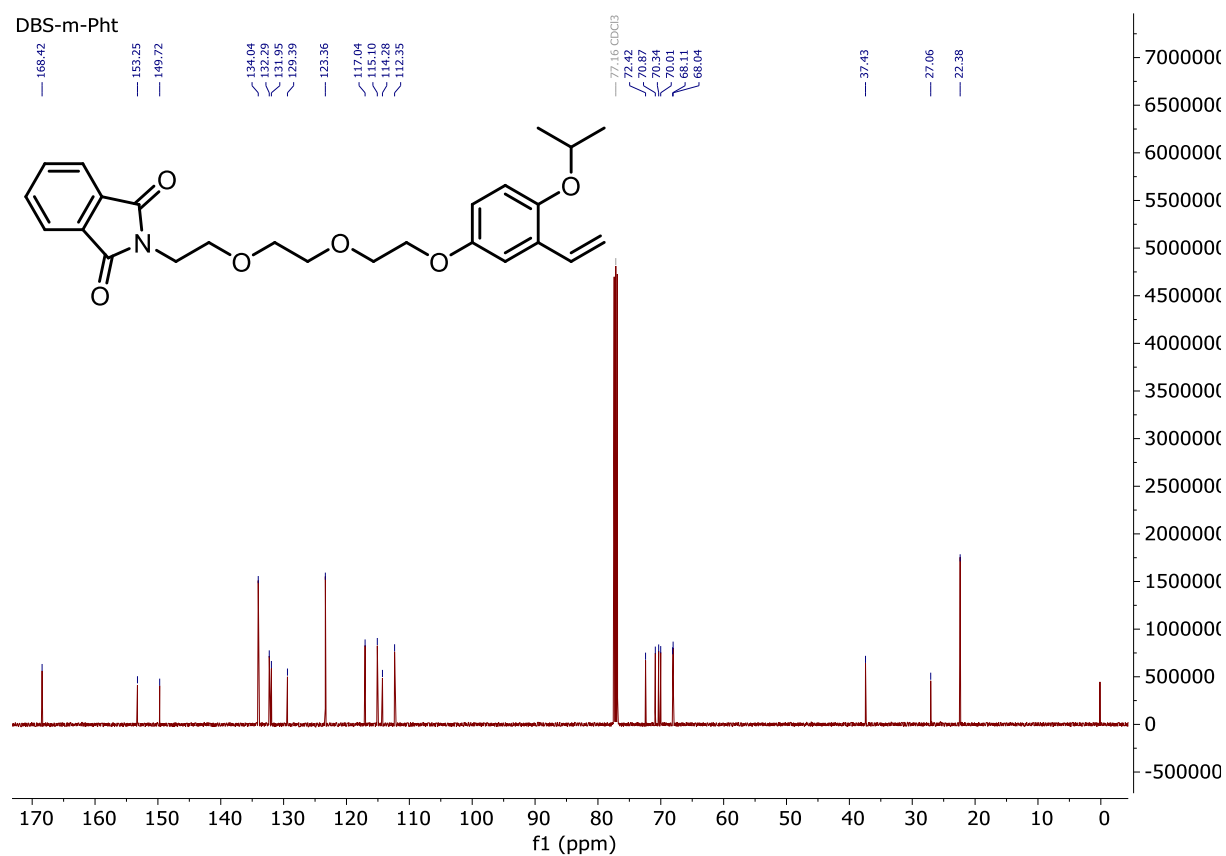
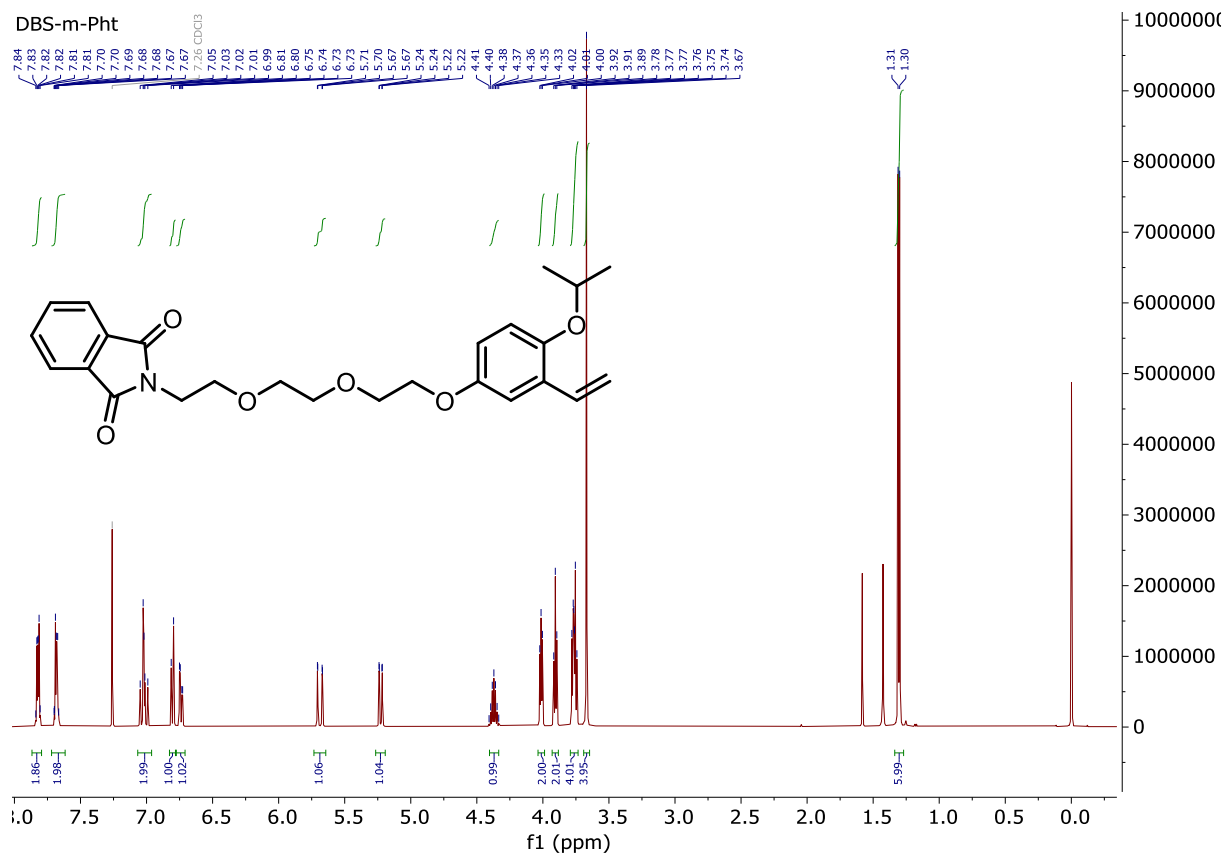
5-Hydroxy-2-isopropoxybenzaldehyde (DBS7)

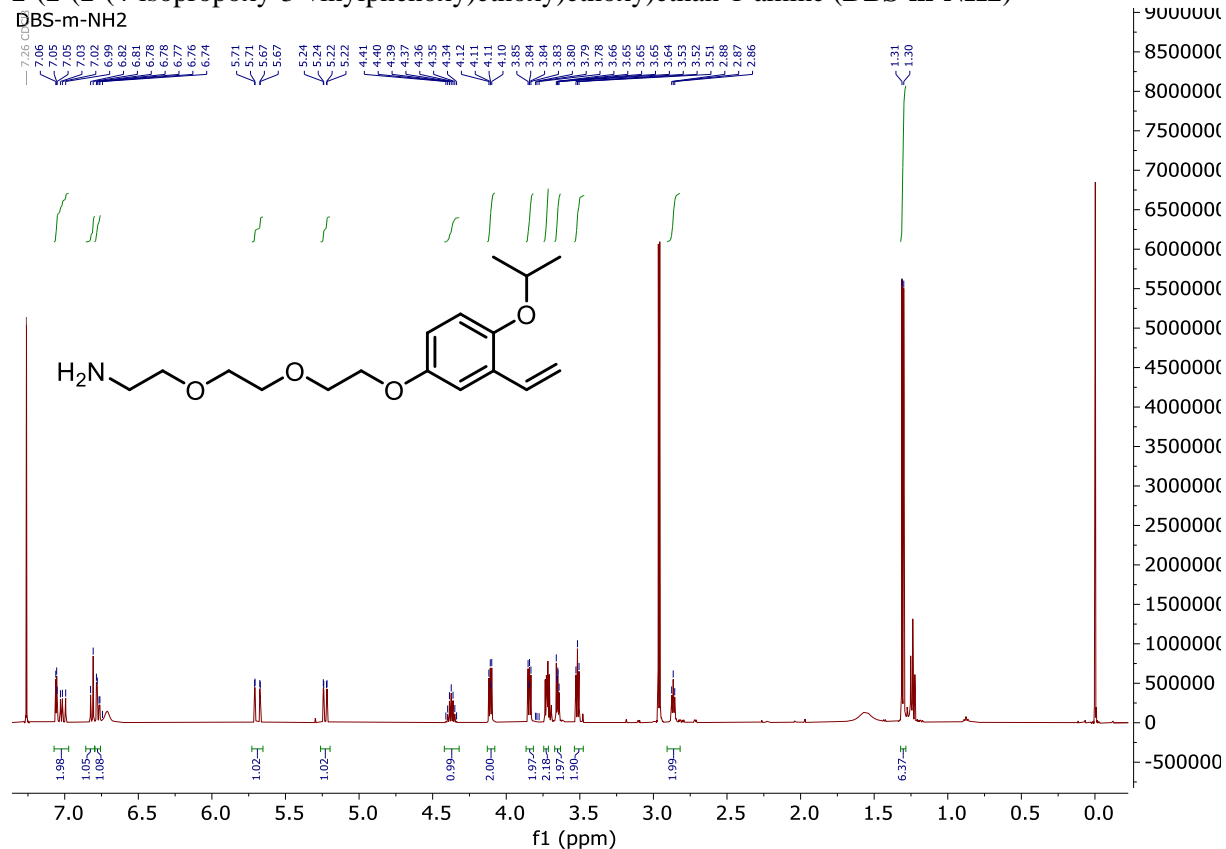
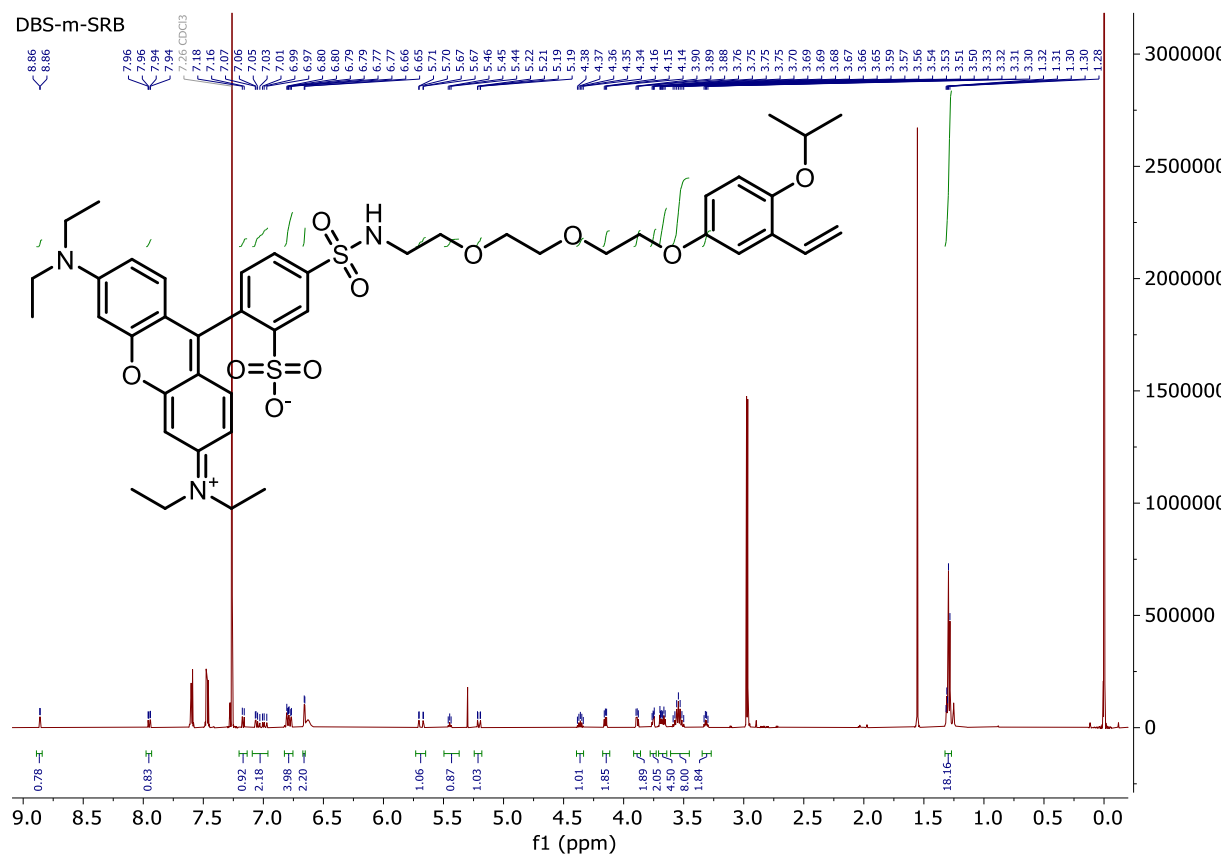


5-(2-(2-(2-(1,3-Dioxoisindolin-2-yl)ethoxy)ethoxy)ethoxy)-2-isopropoxybenzaldehyde (DBS8)

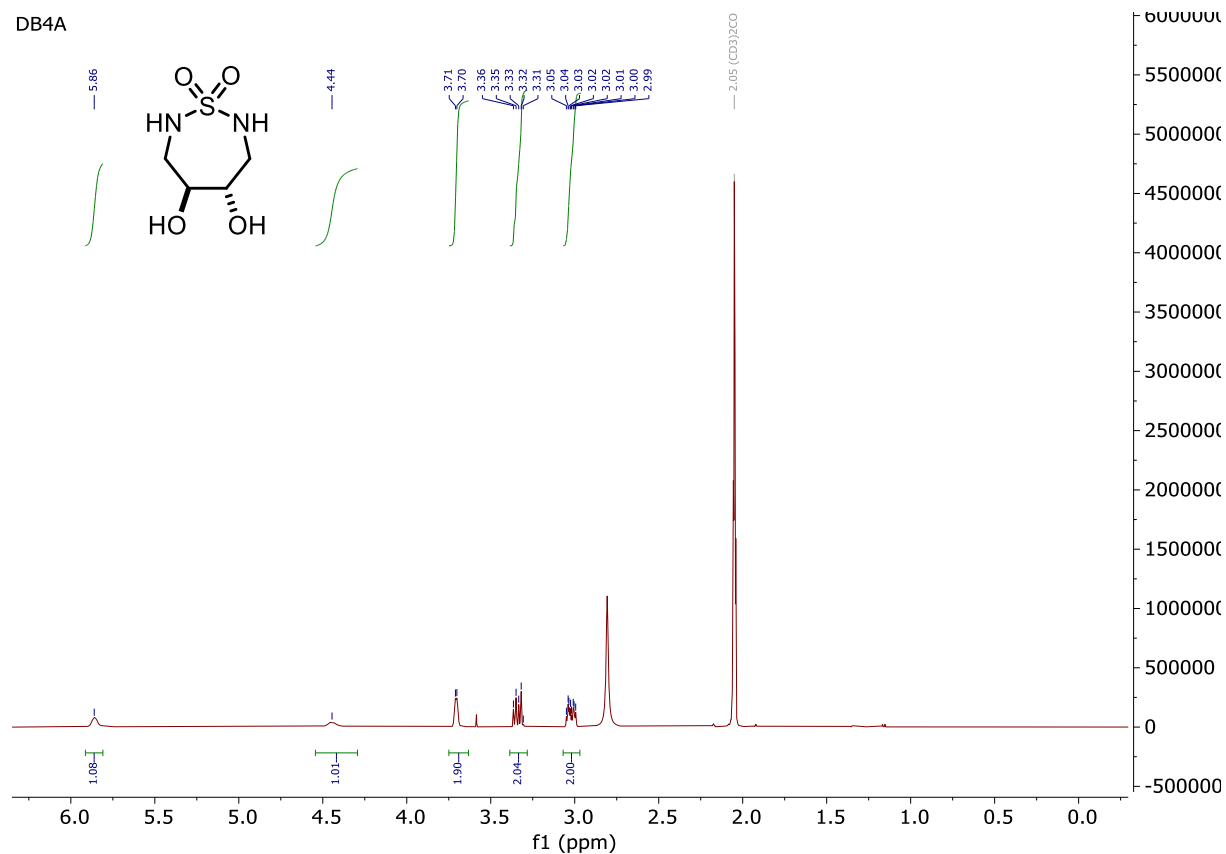


2-(2-(2-(2-(4-Isopropoxy-3-vinylphenoxy)ethoxy)ethoxy)ethyl)isoindoline-1,3-dione (**DBS-m-Pht**)

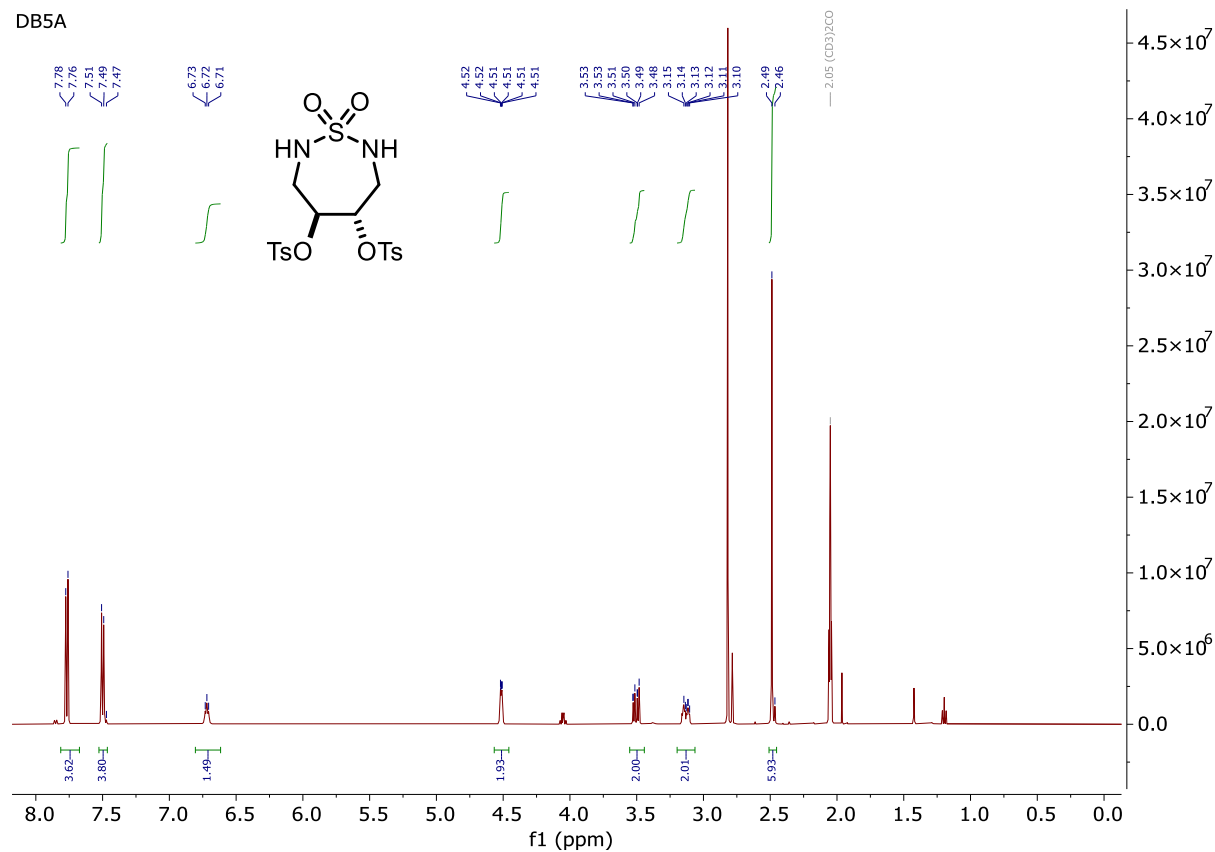


2-(2-(2-(4-isopropoxy-3-vinylphenoxy)ethoxy)ethoxy)ethan-1-amine (**DBS-m-NH2**)2-(6-(Diethylamino)-3-(diethyliminio)-3*H*-xanthen-9-yl)-5-(*N*-(2-(2-(2-(4-isopropoxy-3-vinylphenoxy)ethoxy)ethoxy)ethyl)sulfamoyl)benzenesulfonate (**DBS-m-SRB**)

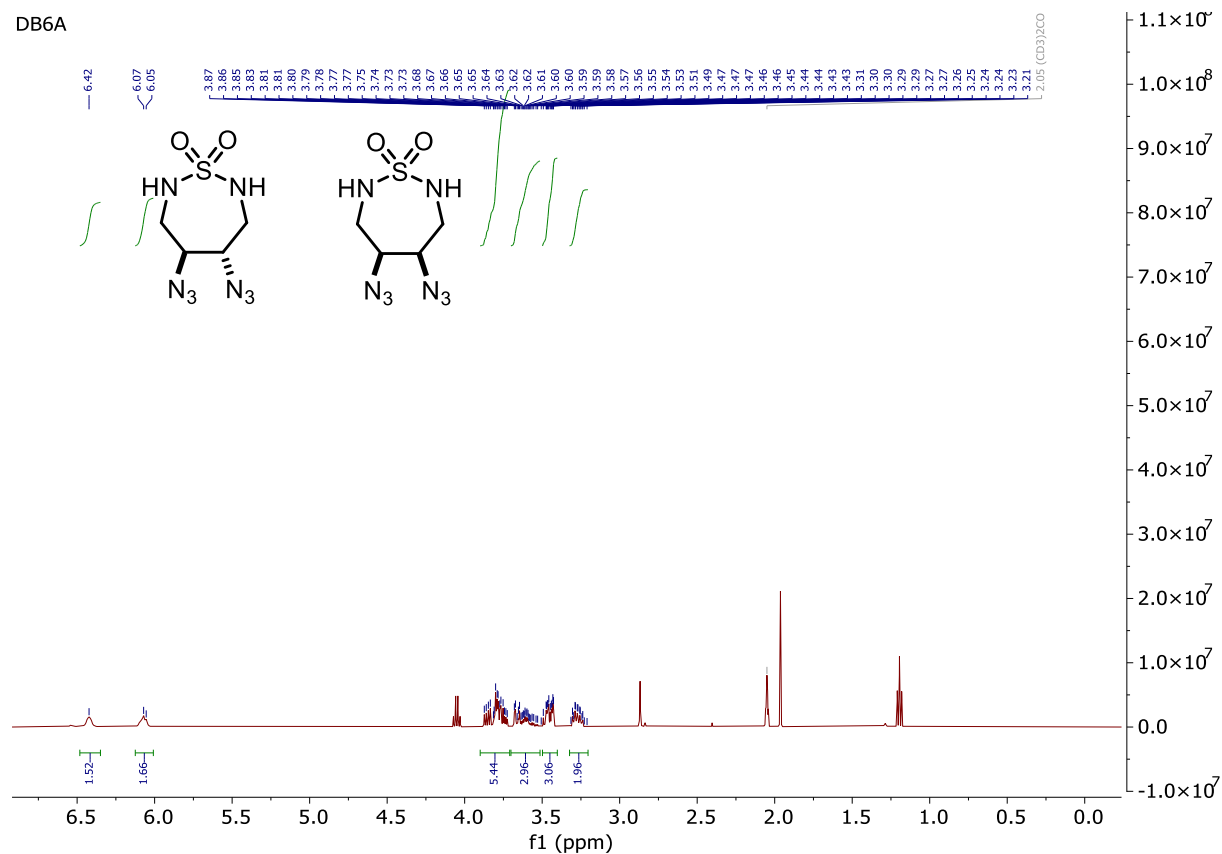
(4*S*,5*S*)-4,5-Dihydroxy-1,2,7-thiadiazepane 1,1-dioxide (DB4A)



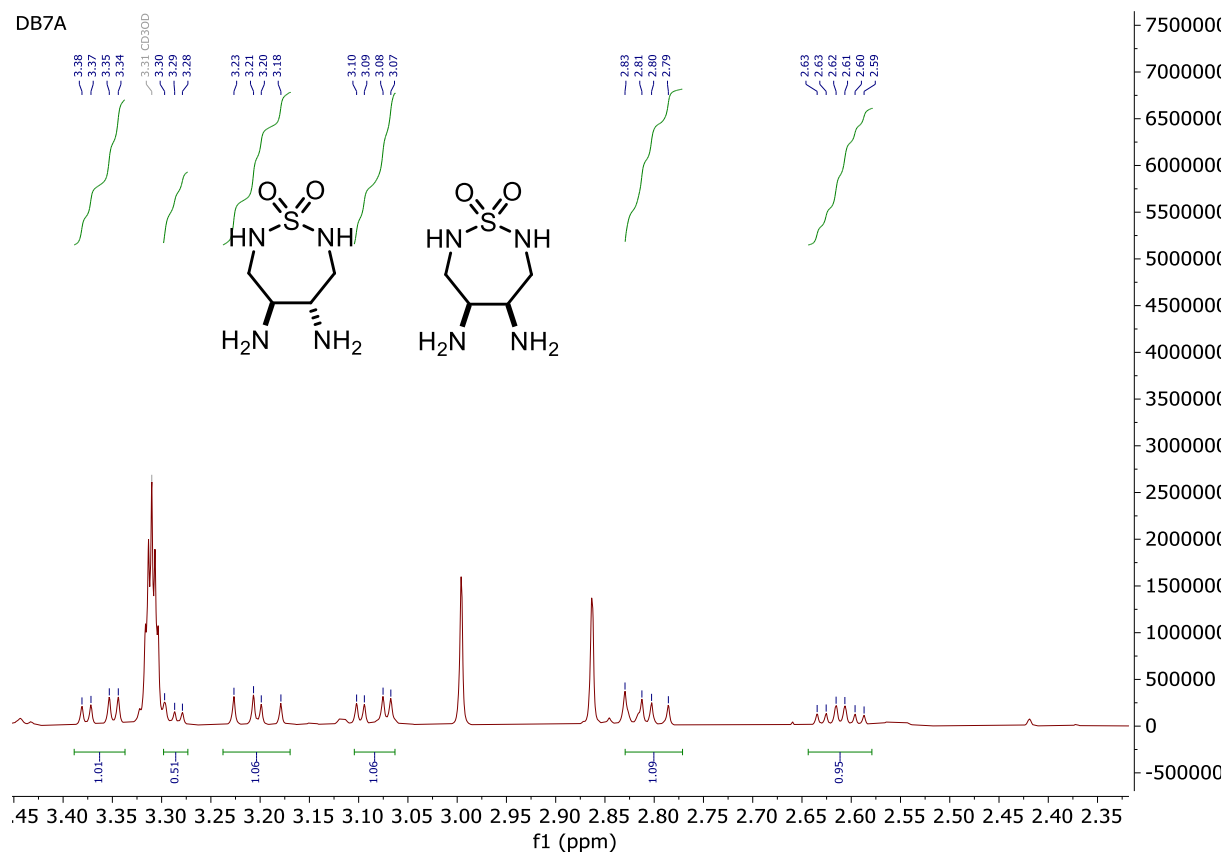
(4*S*,5*S*)-1,1-Dioxido-1,2,7-thiadiazepane-4,5-diyl bis(4-methylbenzenesulfonate) (DB5A)



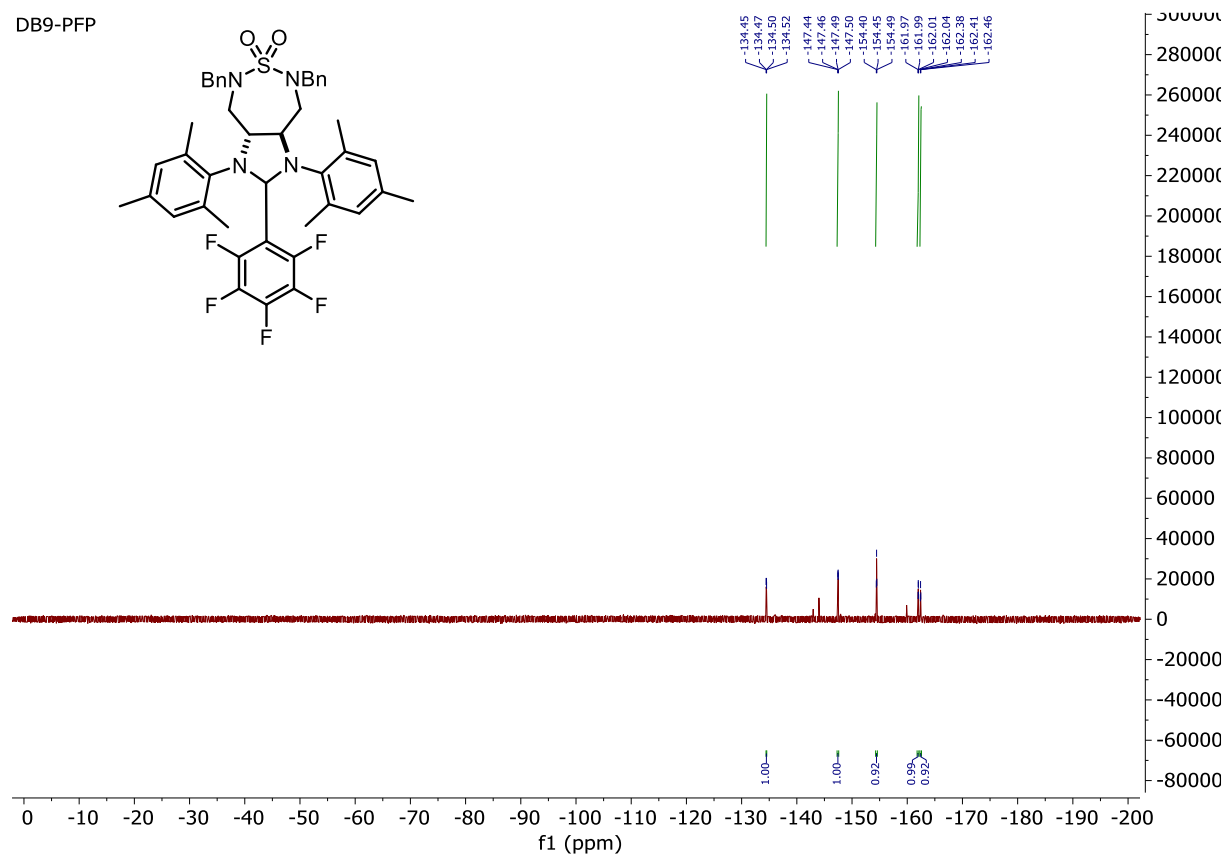
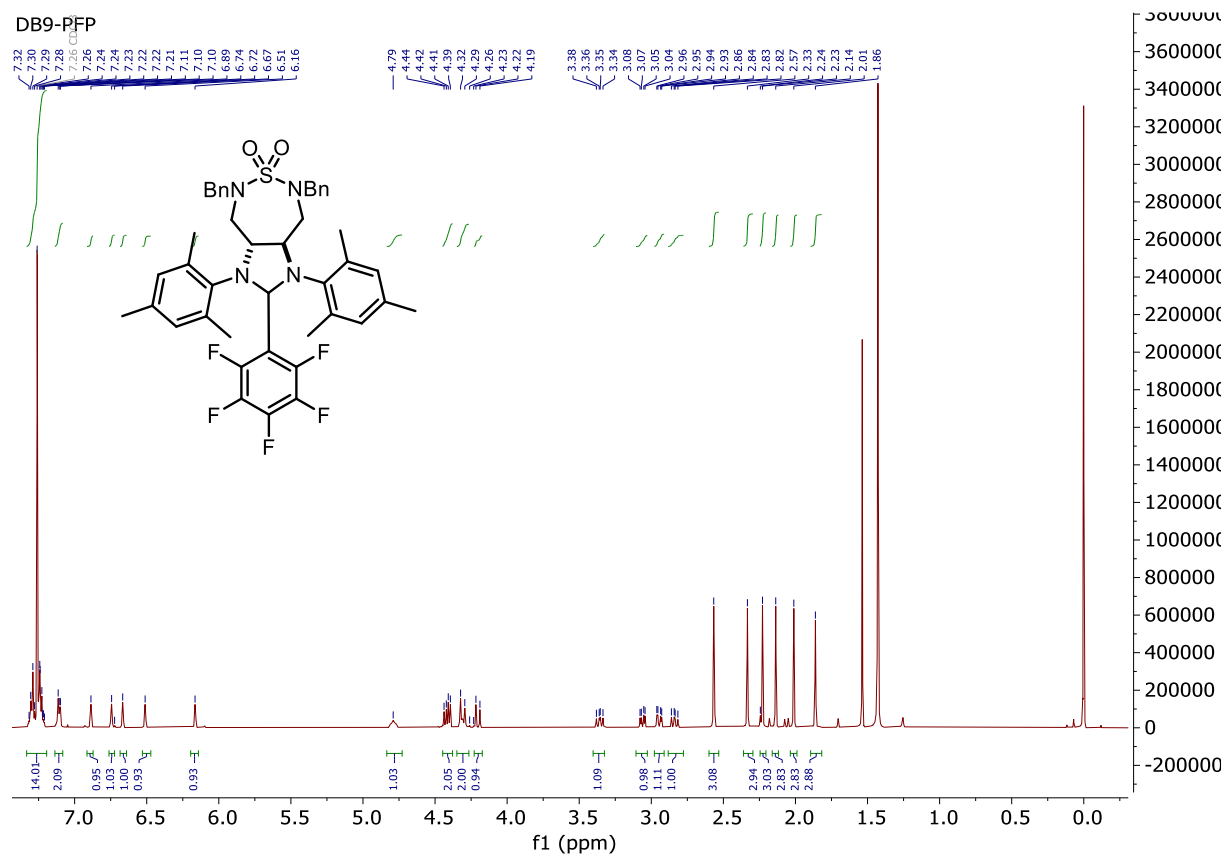
Meso- and rac-4,5-diazo-1,2,7-thiadiazepane 1,1-dioxide (DB6A)

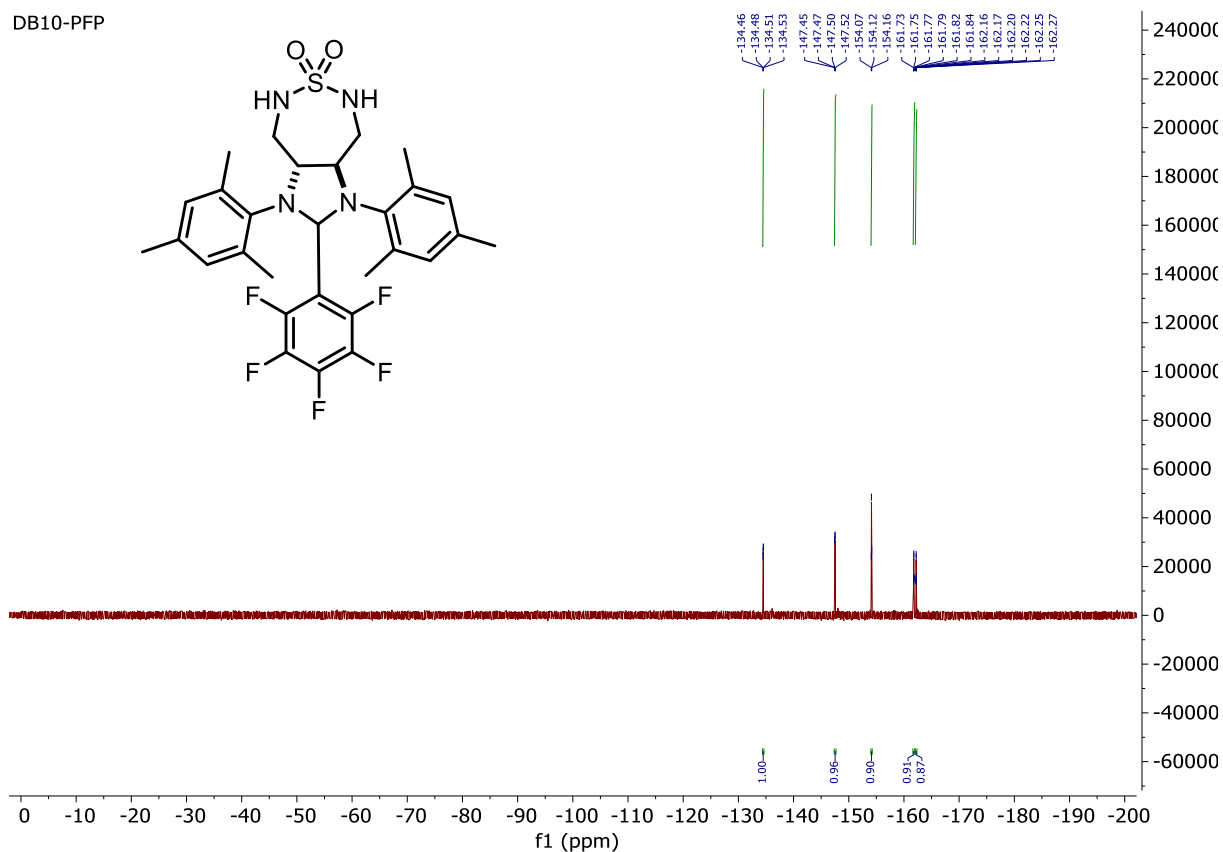
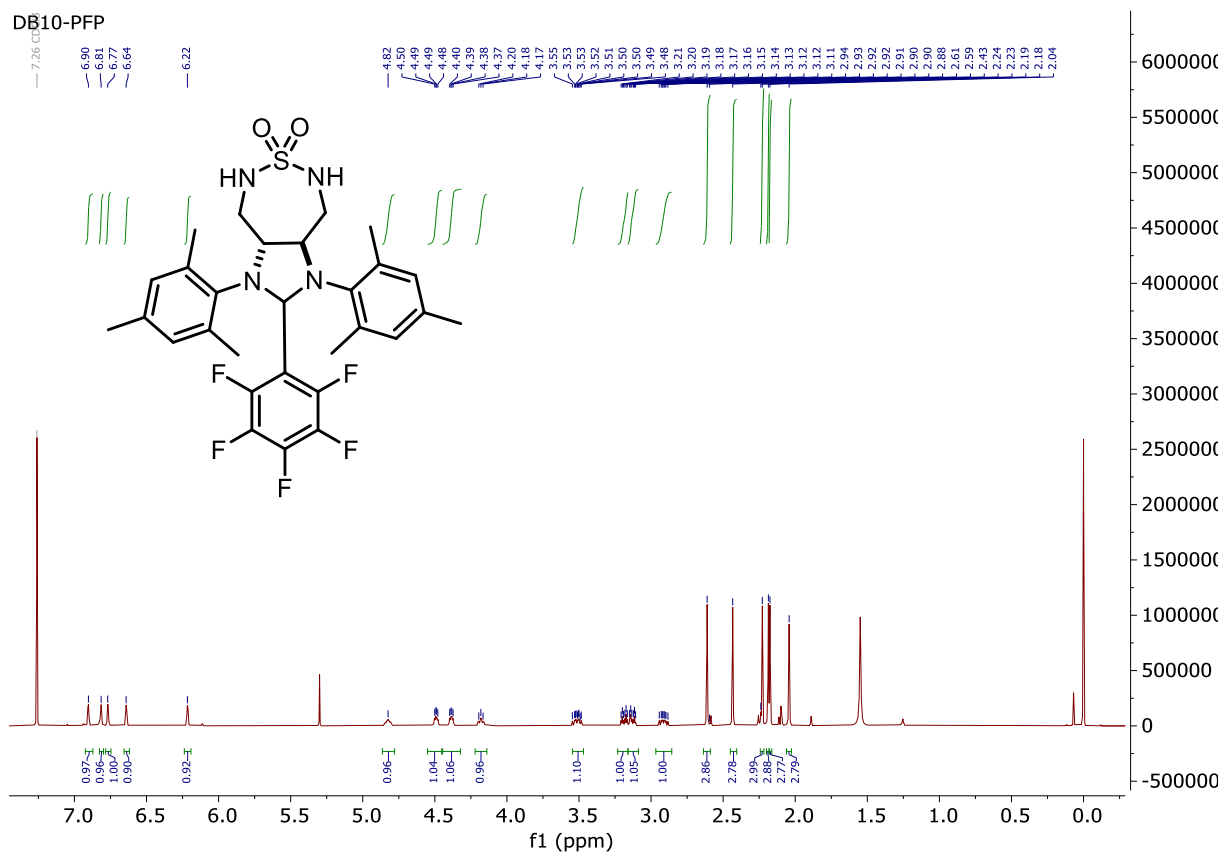


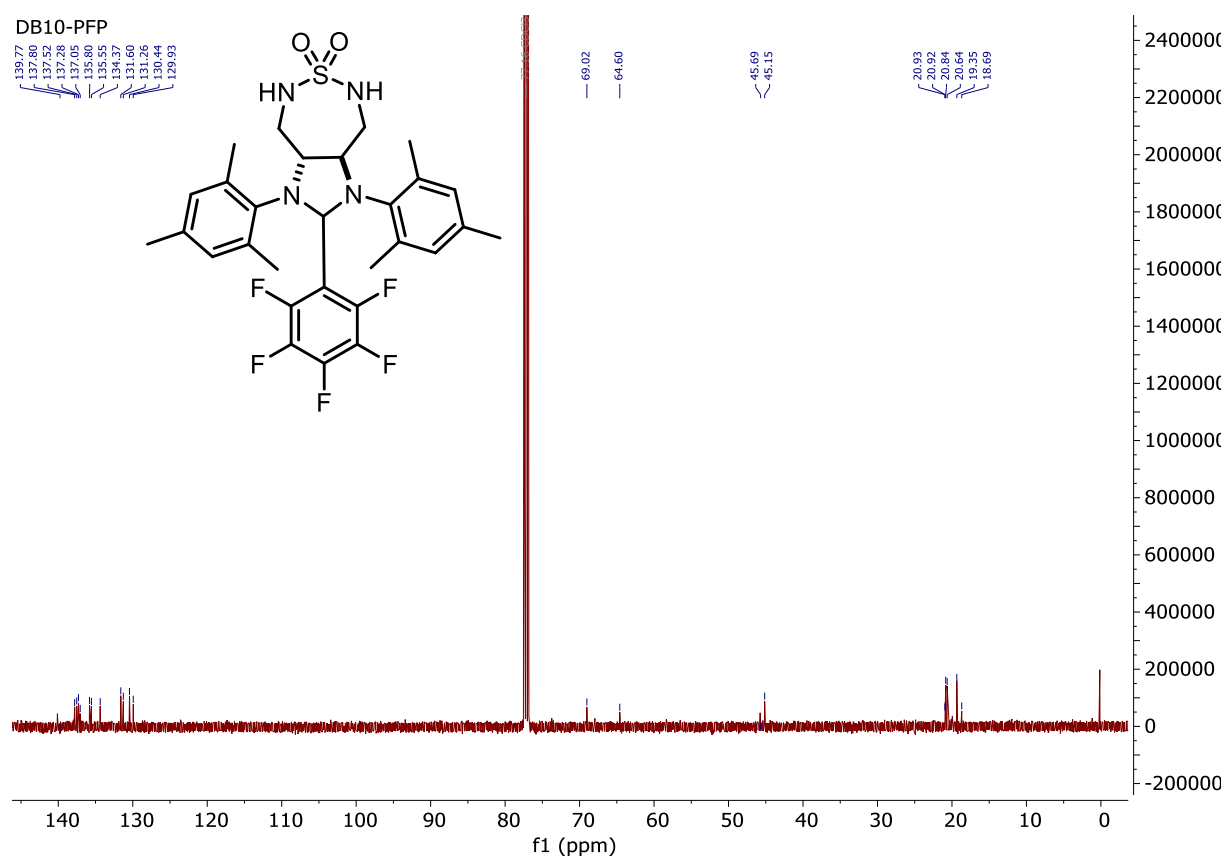
Meso- and rac-4,5-diamino-1,2,7-thiadiazepane 1,1-dioxide (DB7A)



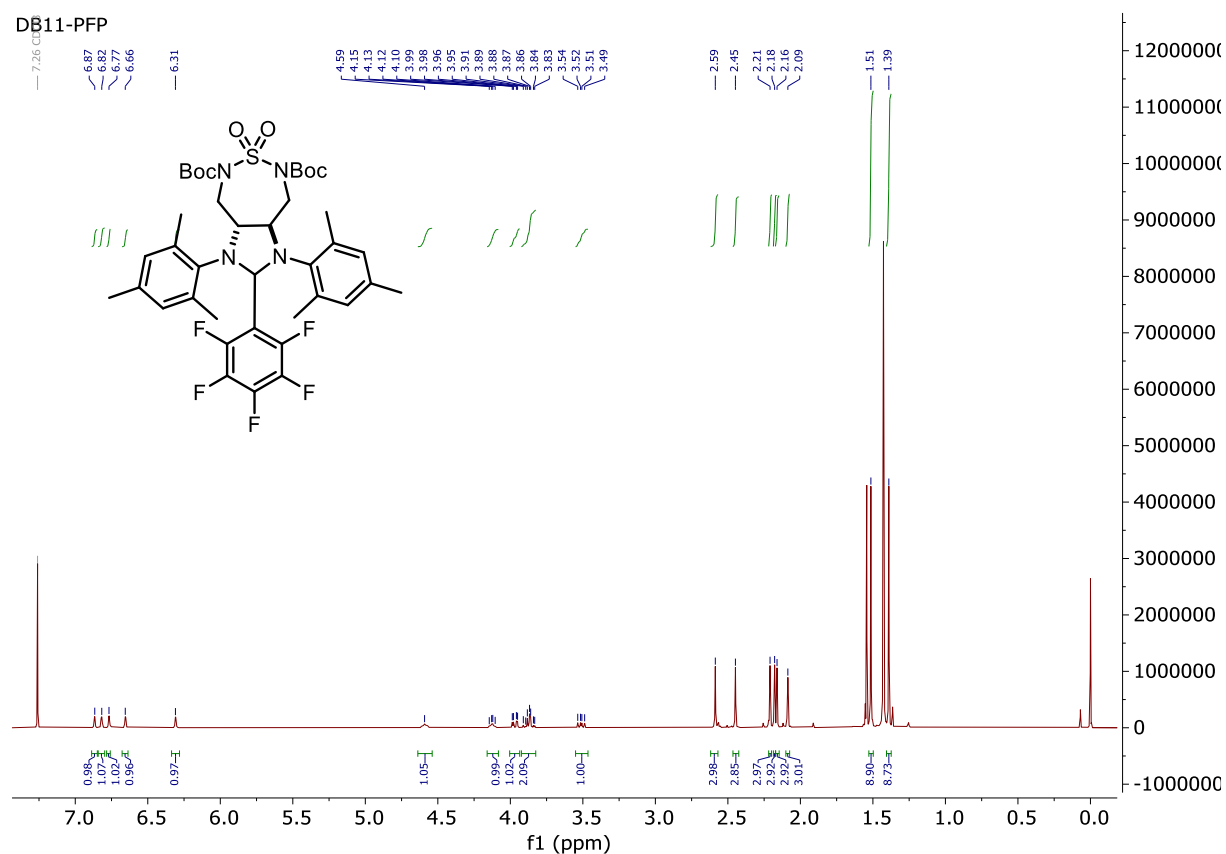
(3*aR*,8*aR*)-5,7-Dibenzyl-1,3-dimesityl-2-(perfluorophenyl)octahydro-1*H*-imidazo[4,5-*d*][1,2,7]thiadiazepine 6,6-dioxide (**DB9-PFP**)



(3*aR*,8*aR*)-1,3-Dimesityl-2-(perfluorophenyl)octahydro-1*H*-imidazo[4,5-*d*][1,2,7]thiadiazepine 6,6-dioxide (**DB10-PFP**)

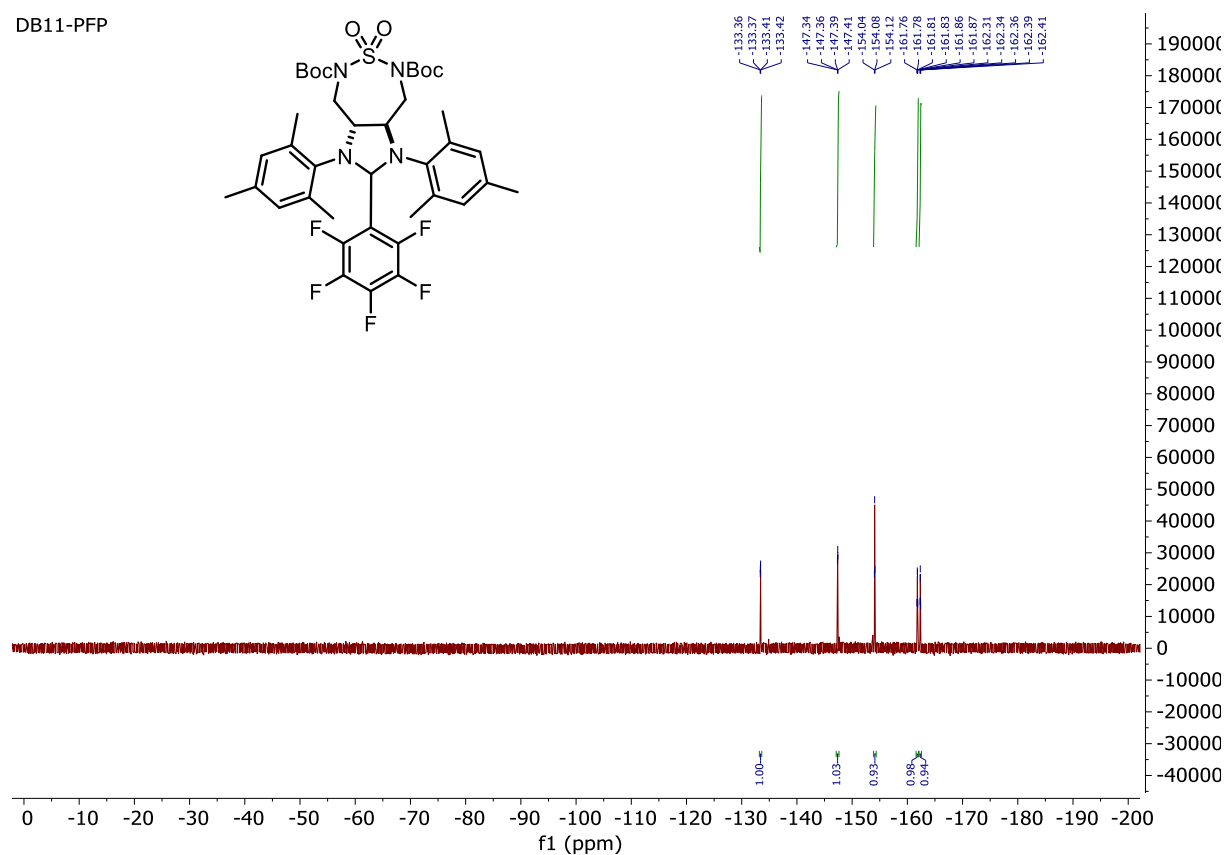


Di-*tert*-butyl (3*aR*,8*aR*)-1,3-dimesityl-2-(perfluorophenyl)hexahydro-1*H*-imidazo[4,5-*d*][1,2,7]thiadiazepine-5,7-dicarboxylate 6,6-dioxide (**DB11-PFP**)

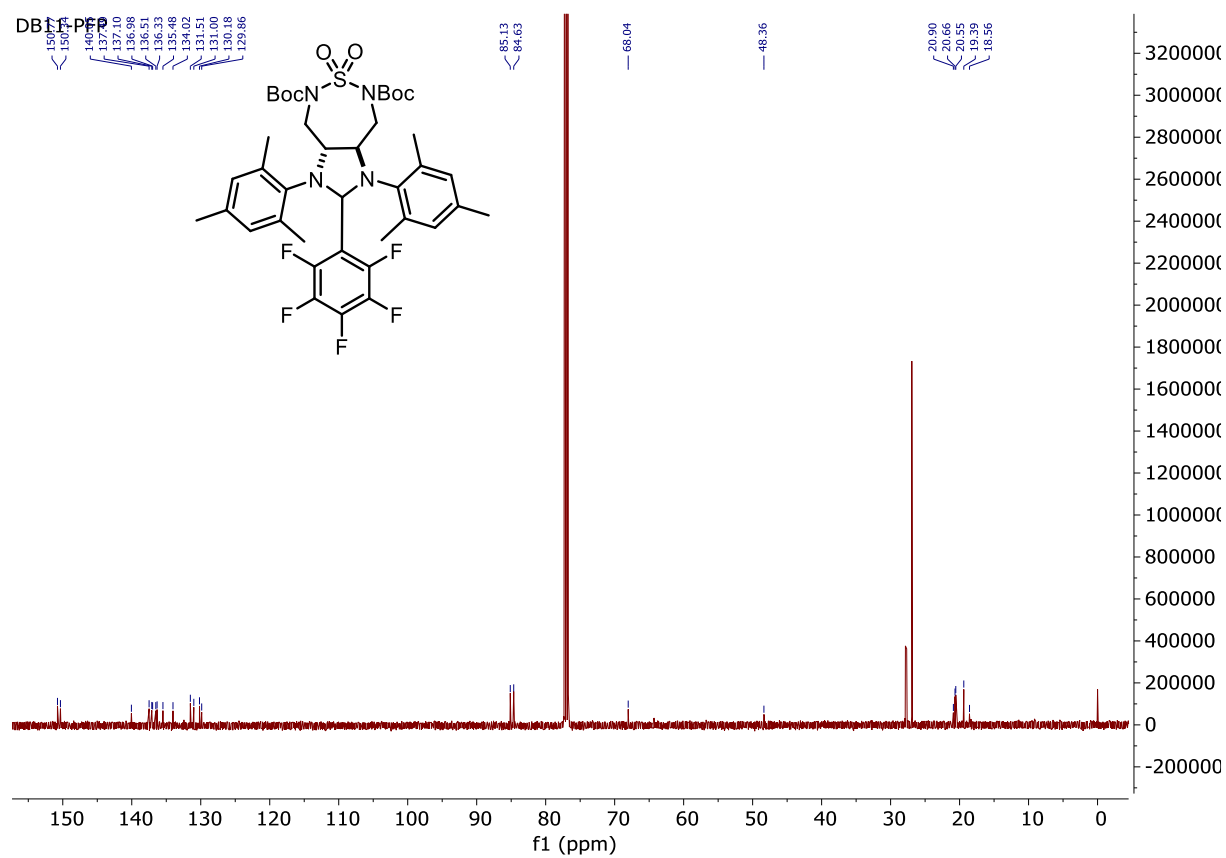


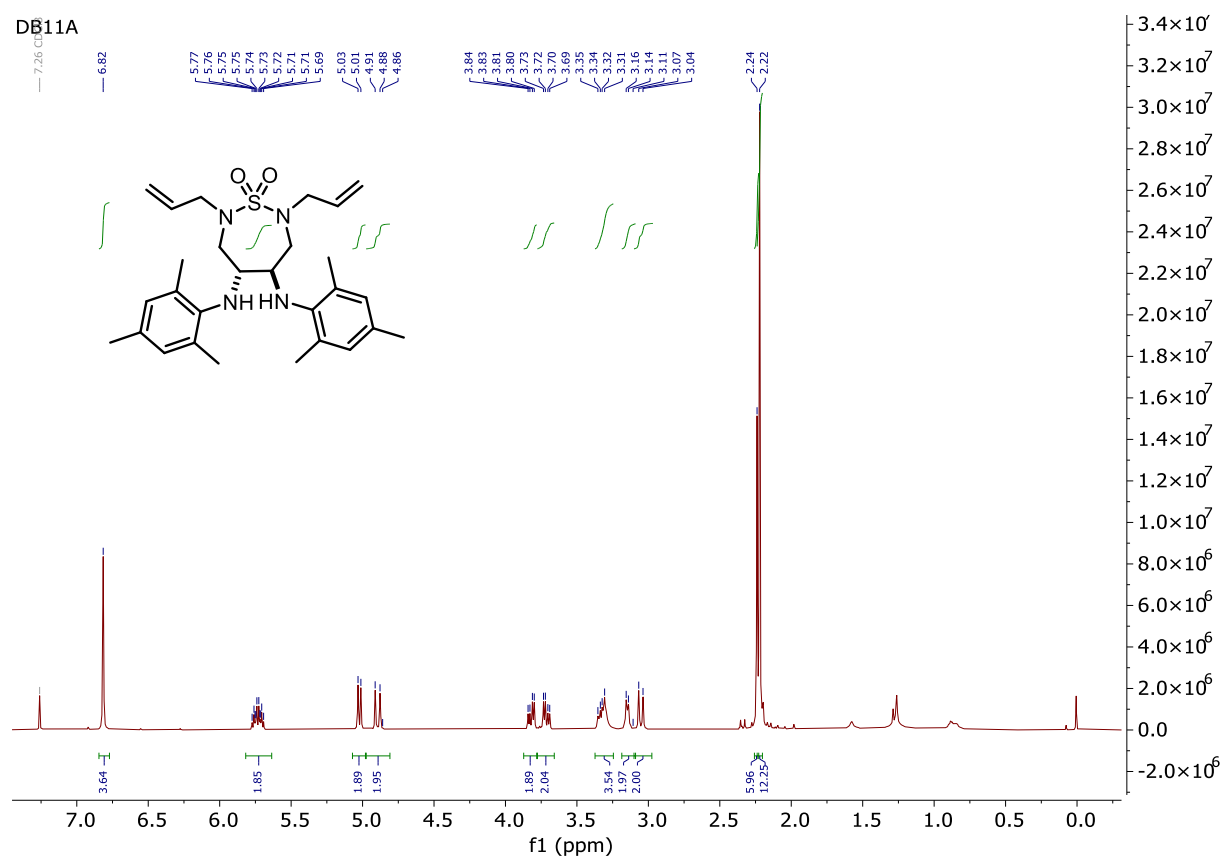
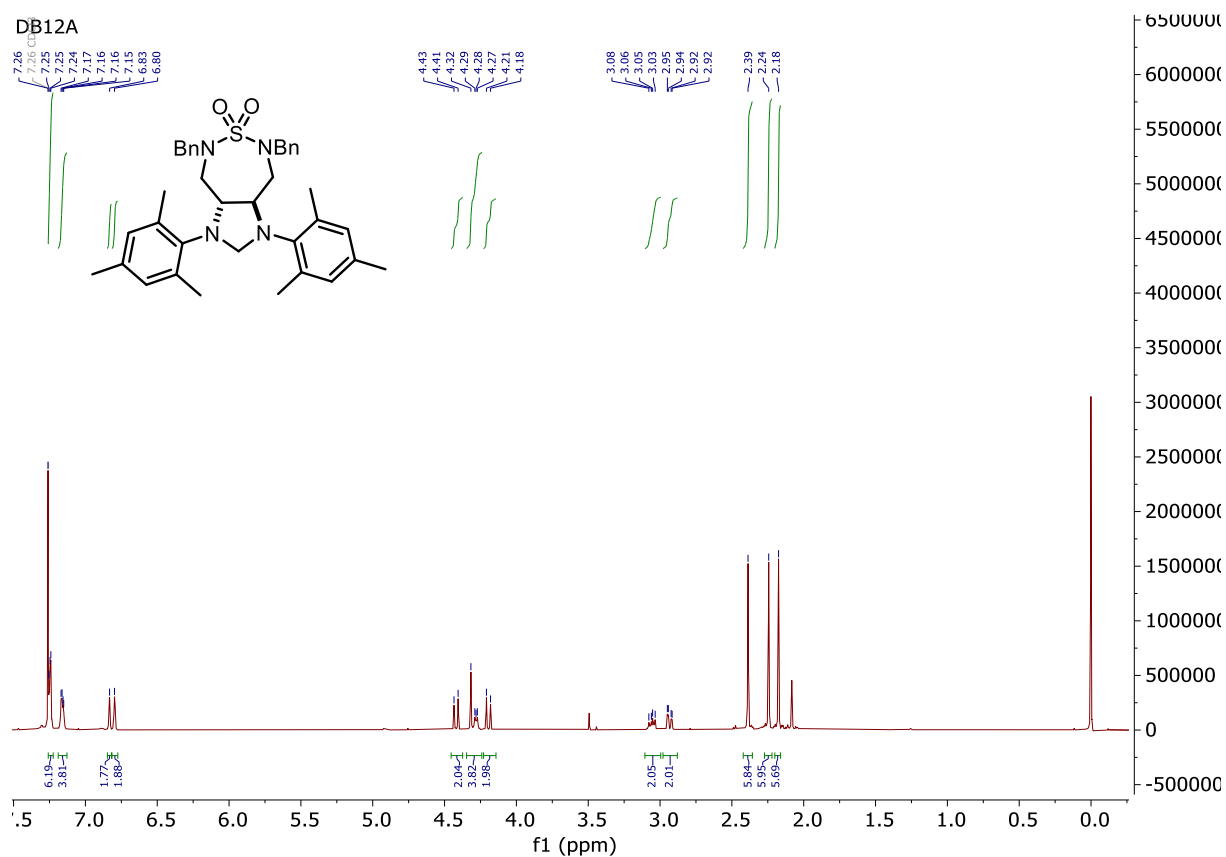
Appendix

DB11-PFP

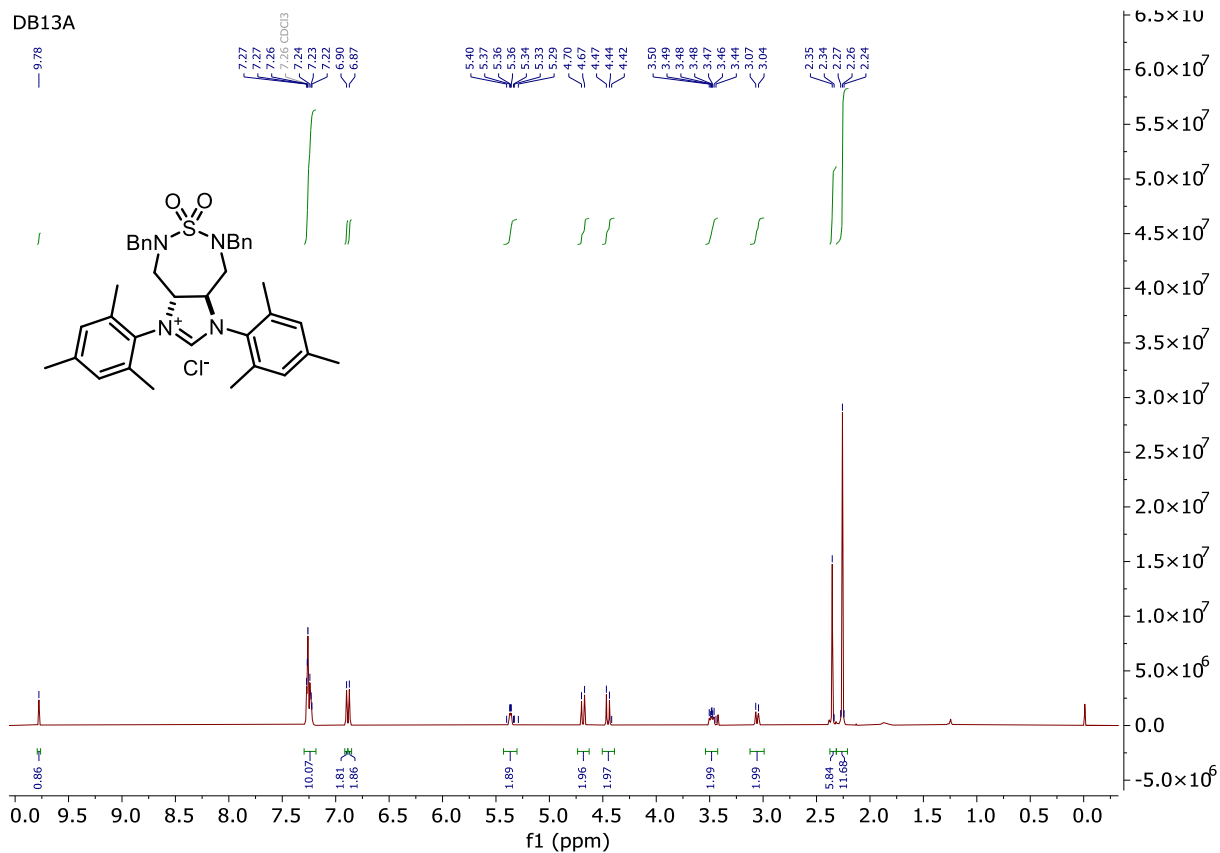


DB11-PFP

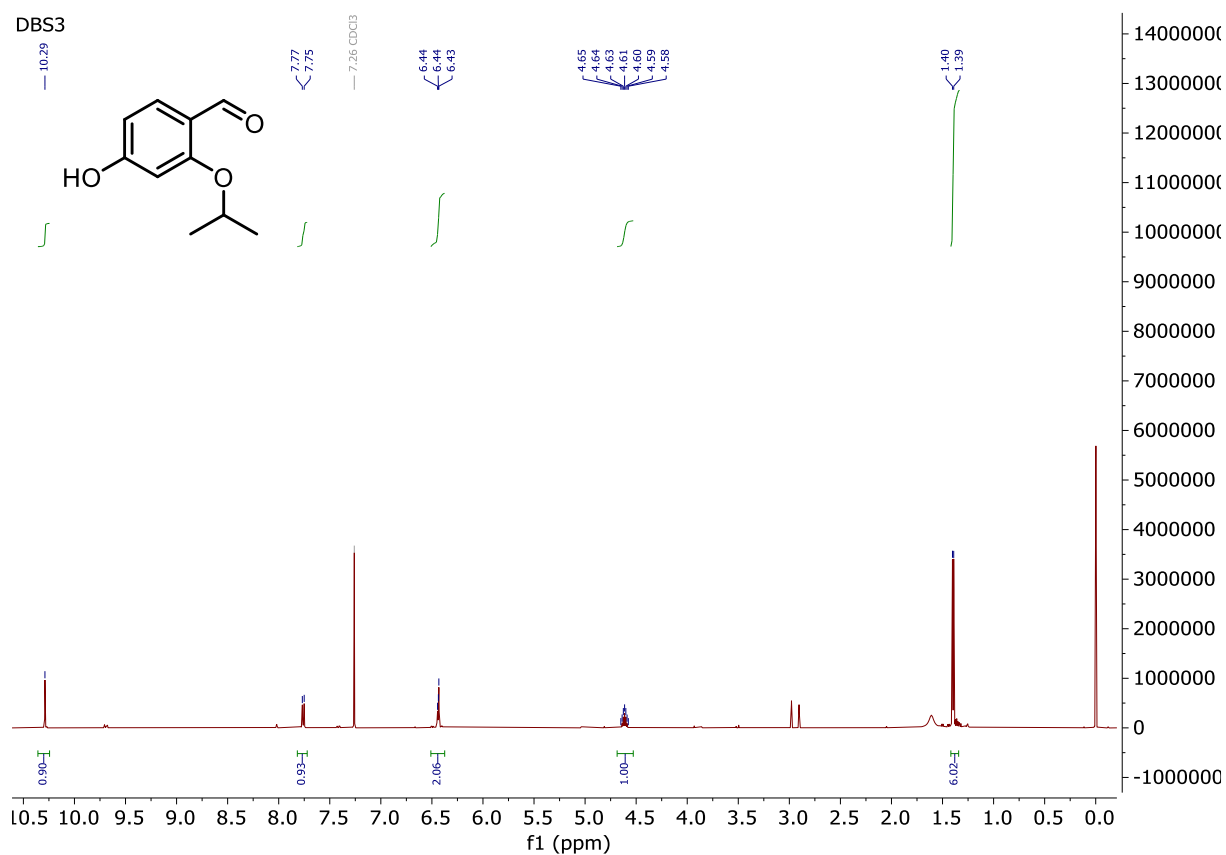


(4*R*,5*R*)-2,7-Diallyl-4,5-bis(mesitylamino)-1,2,7-thiadiazepane 1,1-dioxide (**DB11A**)(3*aR*,8*aR*)-5,7-Dibenzyl-1,3-dimesityloctahydro-1*H*-imidazo[4,5-*d*][1,2,7]thiadiazepine 6,6-dioxide (**DB12A**).

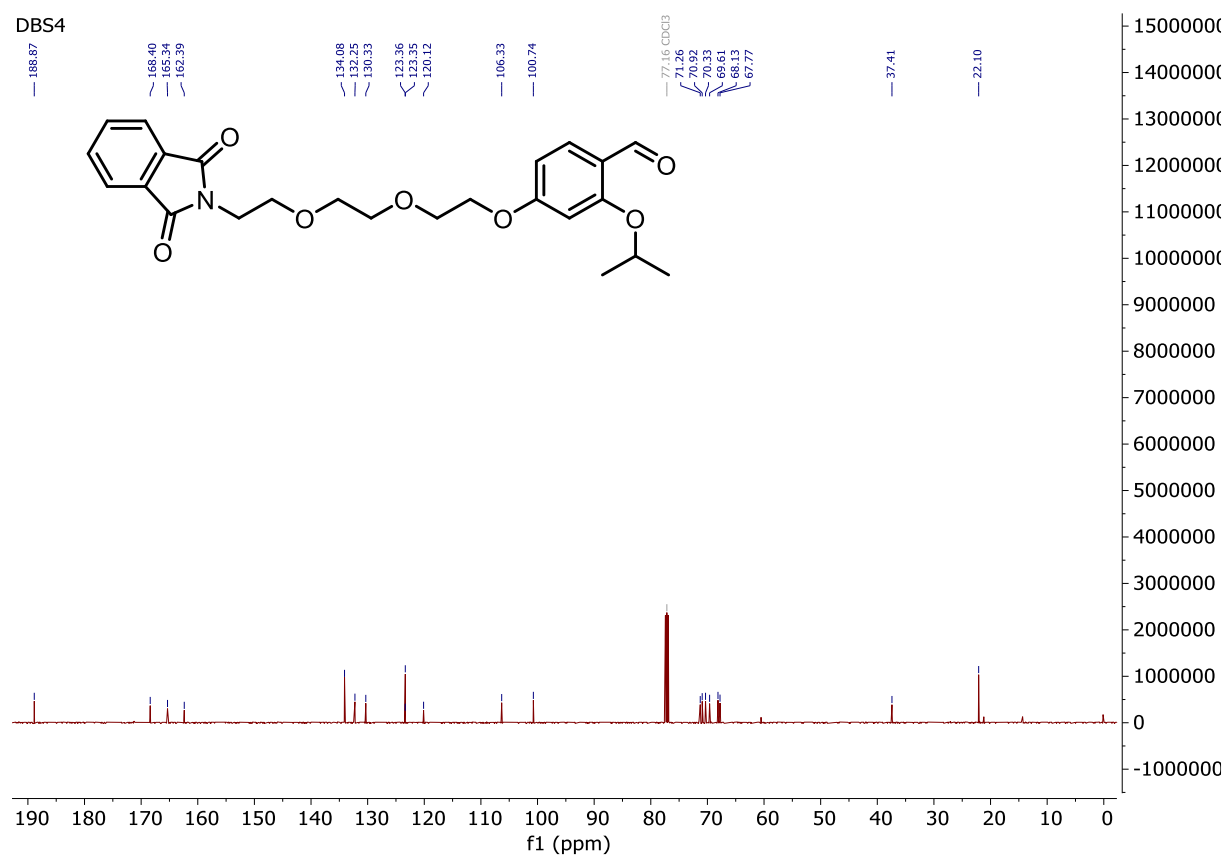
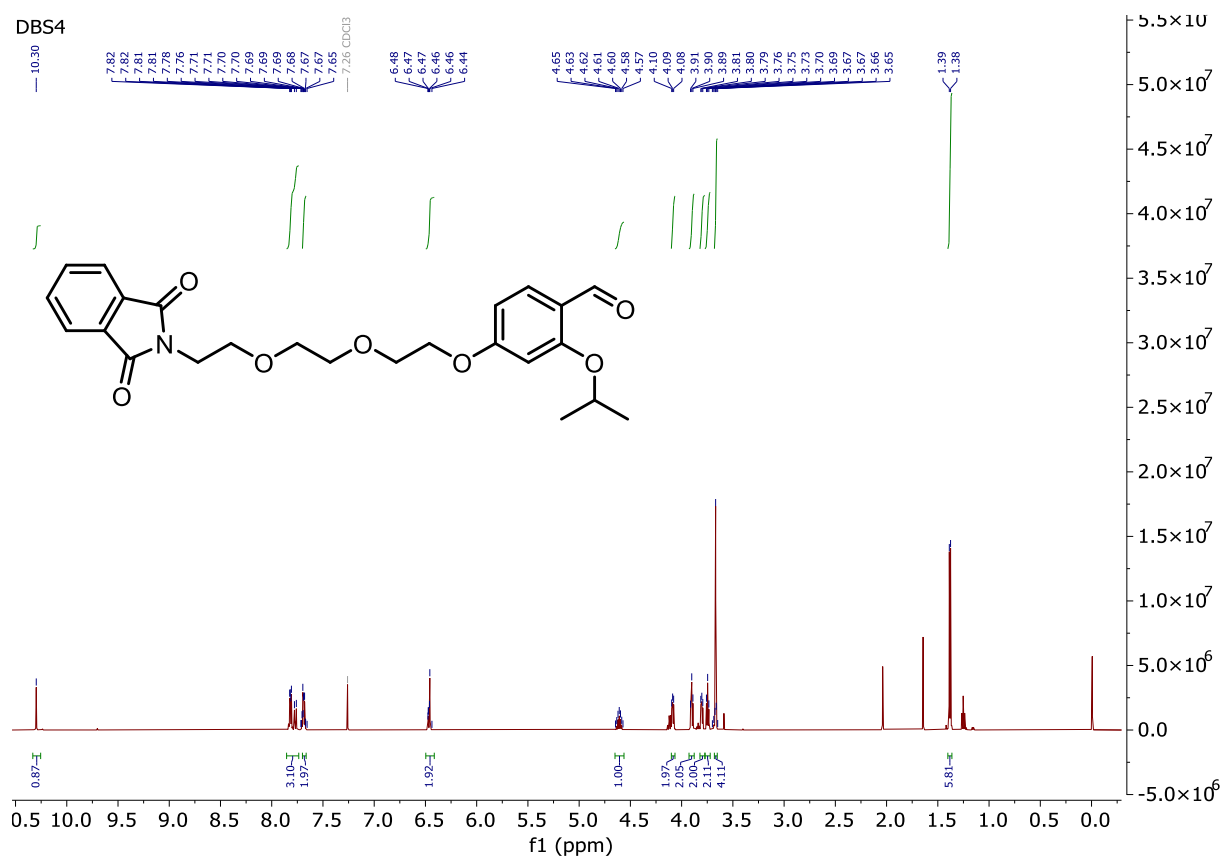
(3a*R*,8a*R*)-5,7-Dibenzyl-1,3-dimesityl-3a,4,5,7,8,8a-hexahydro-1*H*-imidazo[4,5-*d*][1,2,7]thiadiazepin-3-ium 6,6-dioxide (**DB13A**)



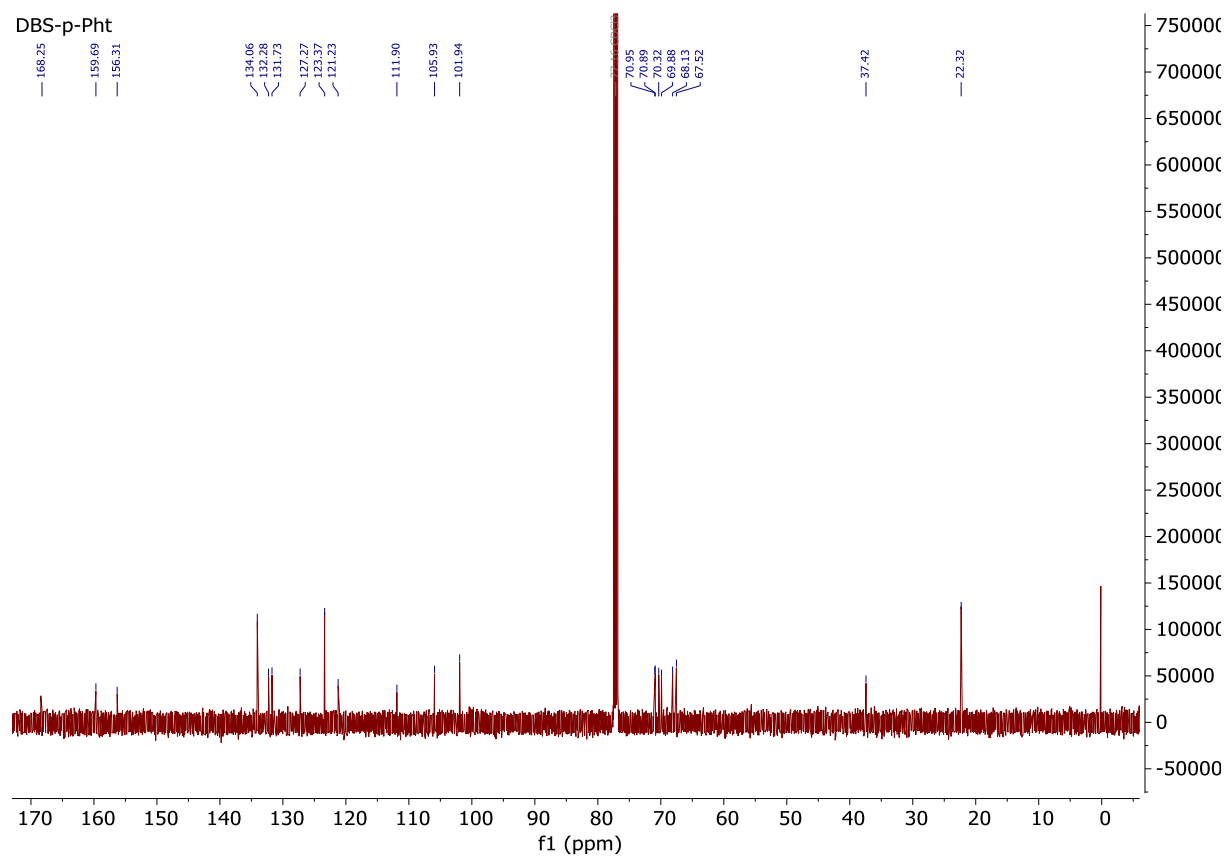
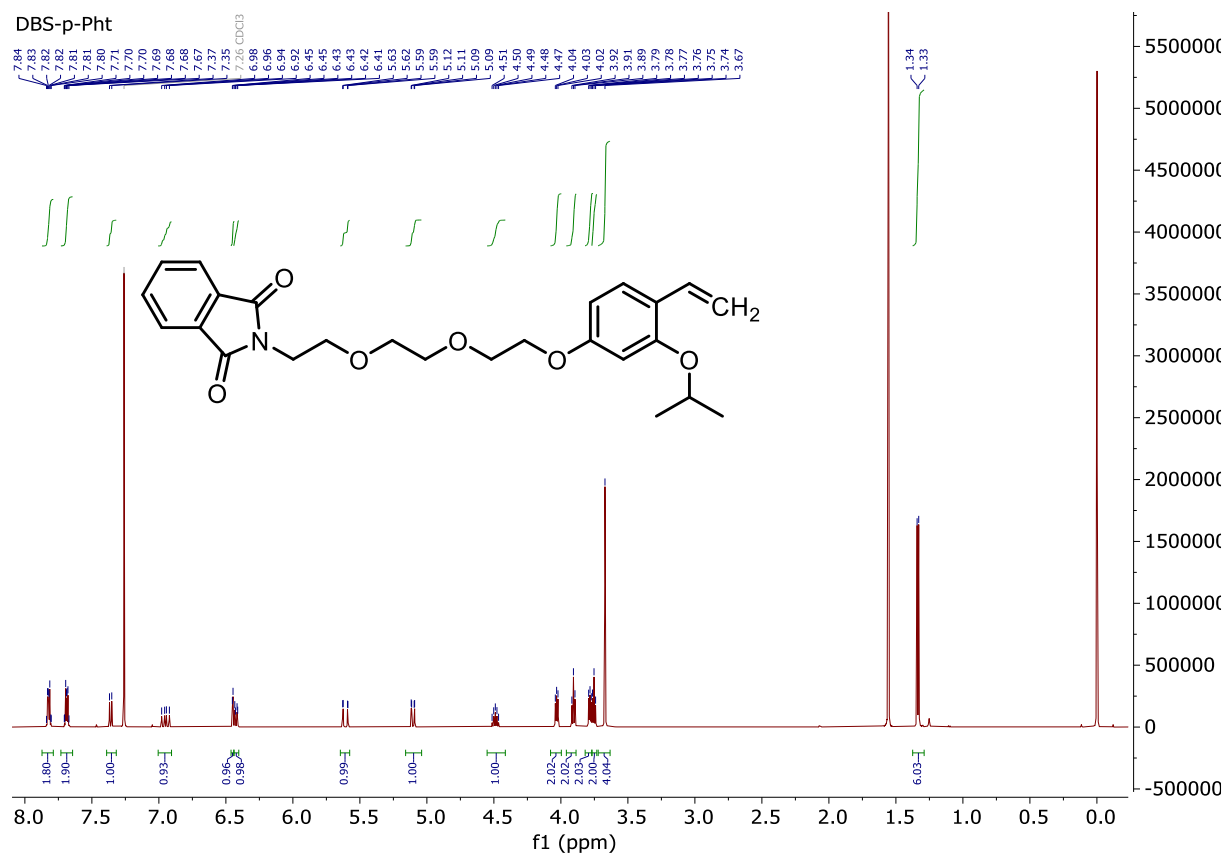
4-Hydroxy-2-isopropoxybenzaldehyde (**DBS3**)

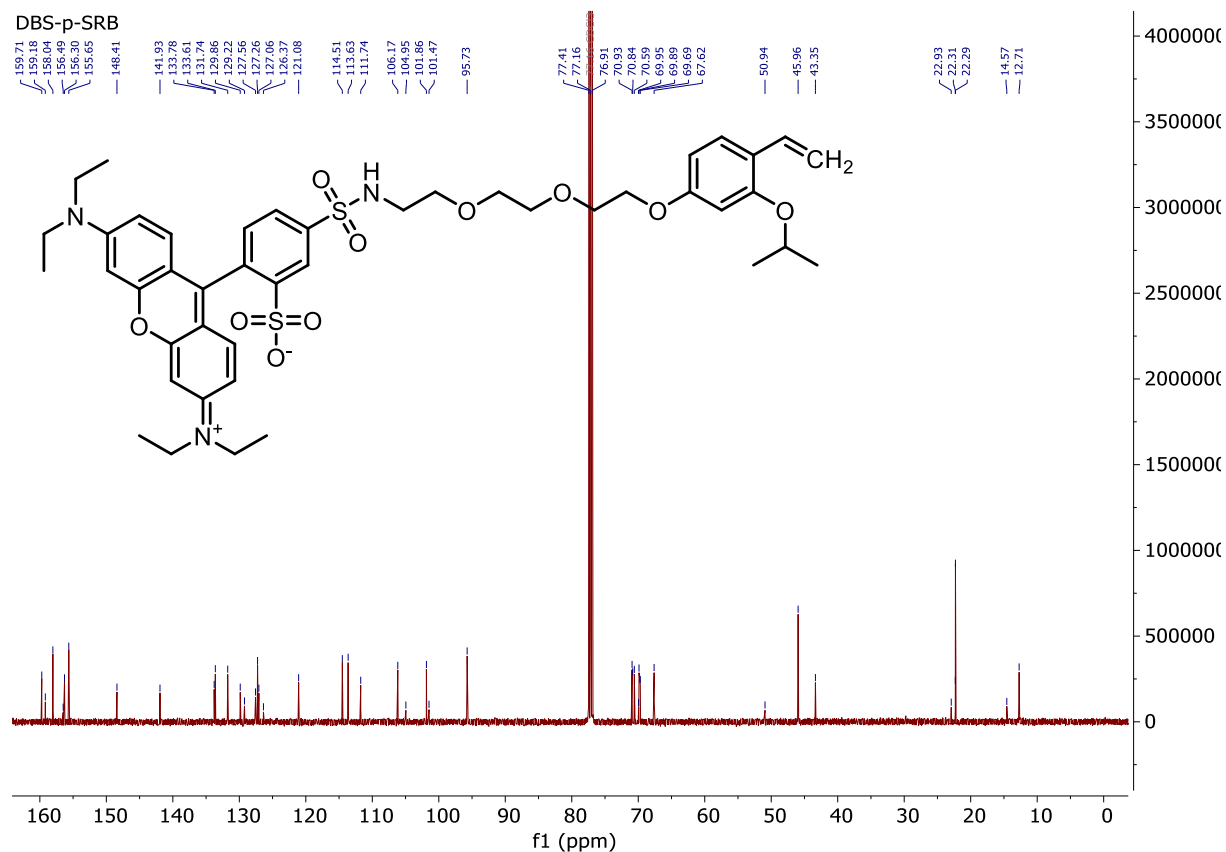


4-(2-(2-(2-(1,3-Dioxoisindolin-2-yl)ethoxy)ethoxy)ethoxy)-2-isopropoxybenzaldehyde (**DBS4**)

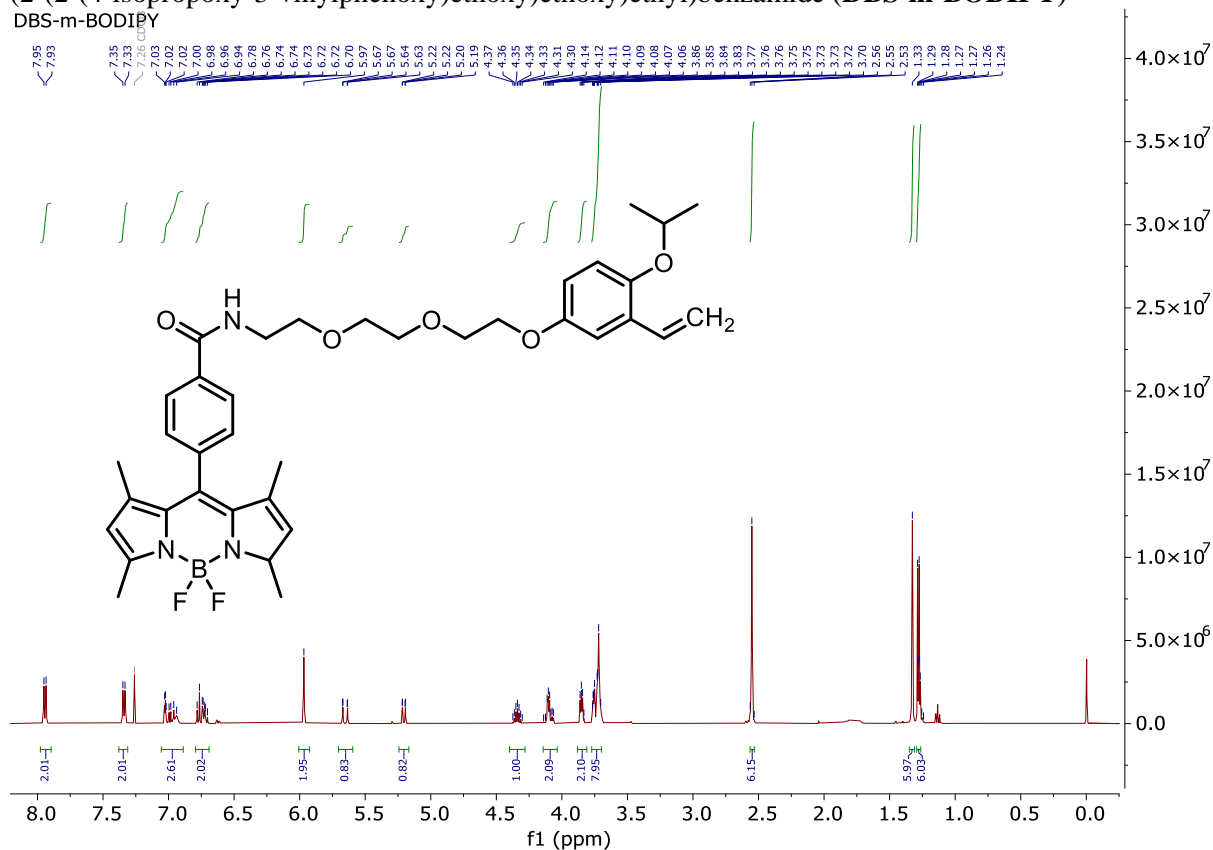


2-(2-(2-(2-(3-Isopropoxy-4-vinylphenoxy)ethoxy)ethoxy)ethyl)isoindoline-1,3-dione (DBS-p-Pht)

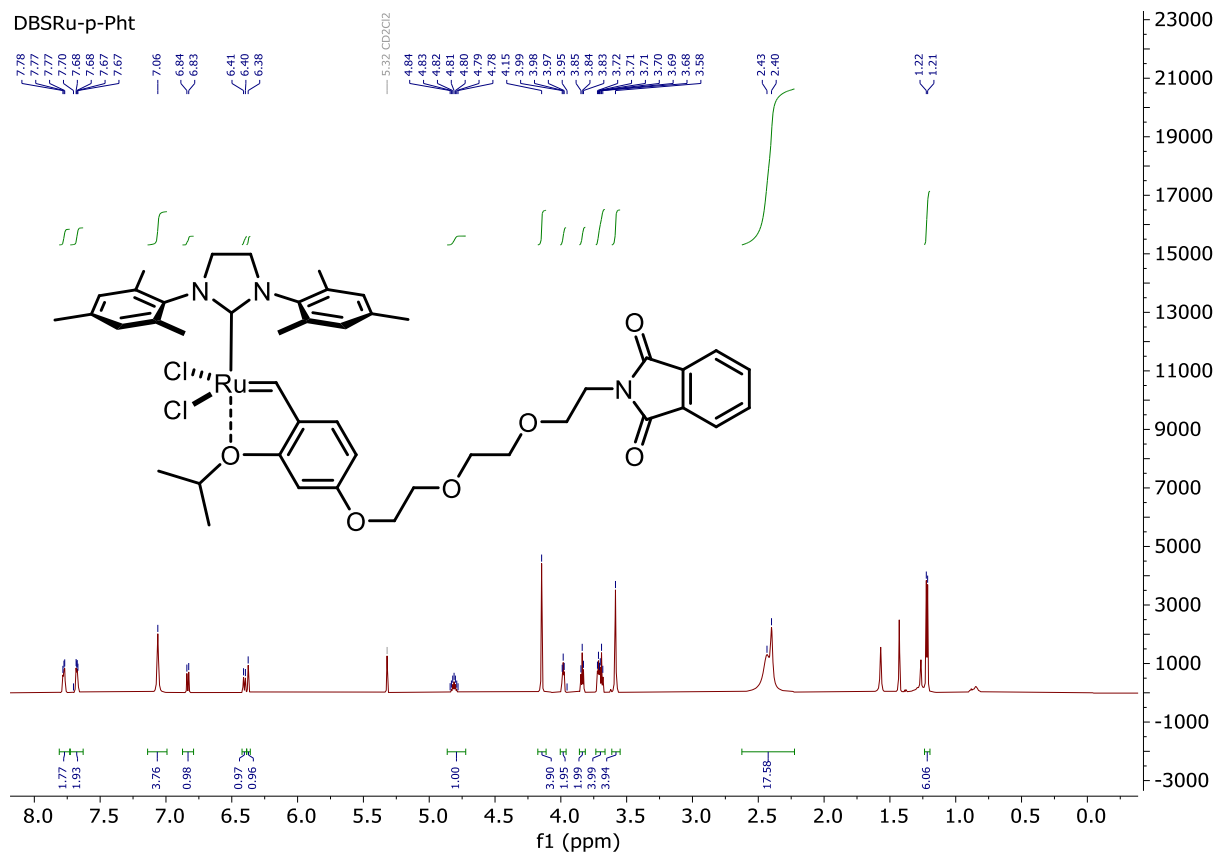




4-(5,5-Difluoro-1,3,7,9-tetramethyl-3*H*,5*H*-5 λ^4 -dipyrrolo[1,2-*c*:2',1'-*f*][1,3,2]diazaborinin-10-yl)-*N*-(2-(2-(2-(4-isopropoxy-3-vinylphenoxy)ethoxy)ethoxy)ethyl)benzamide (**DBS-m-BODIPY**)



Dichloro(1,3-dimesitylimidazolidin-2-ylidene)(4-(2-(2-(2-(1,3-dioxoisindolin-2-yl)ethoxy)ethoxy)ethoxy)-2-isopropoxybenzylidene)ruthenium(II) (**DBRu-p-Pht**)



1H NMR spectrum of compound 10 in CDCl₃.

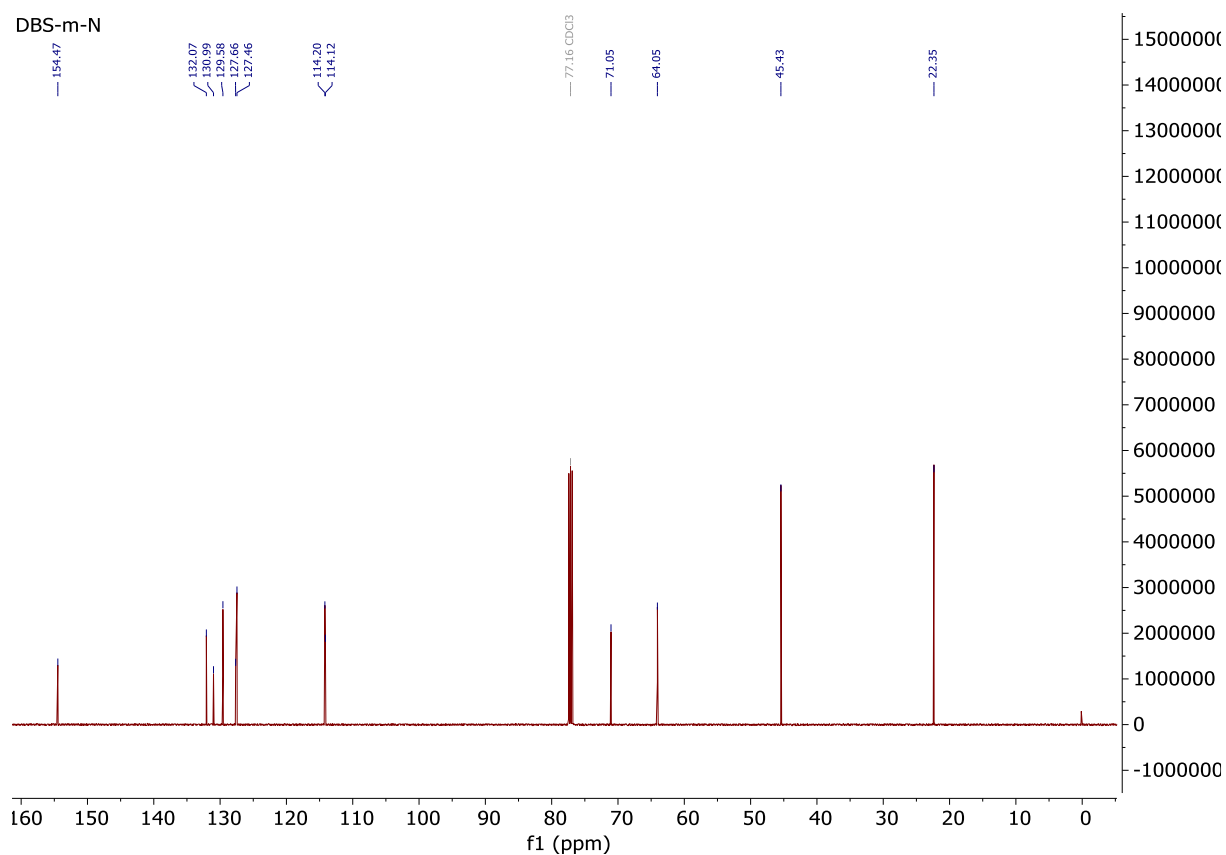
Chemical structure of 10: (dimethylamino)ethyl 2-methyl-4-(prop-1-en-1-yloxy)benzoate

Chemical Shifts (ppm):

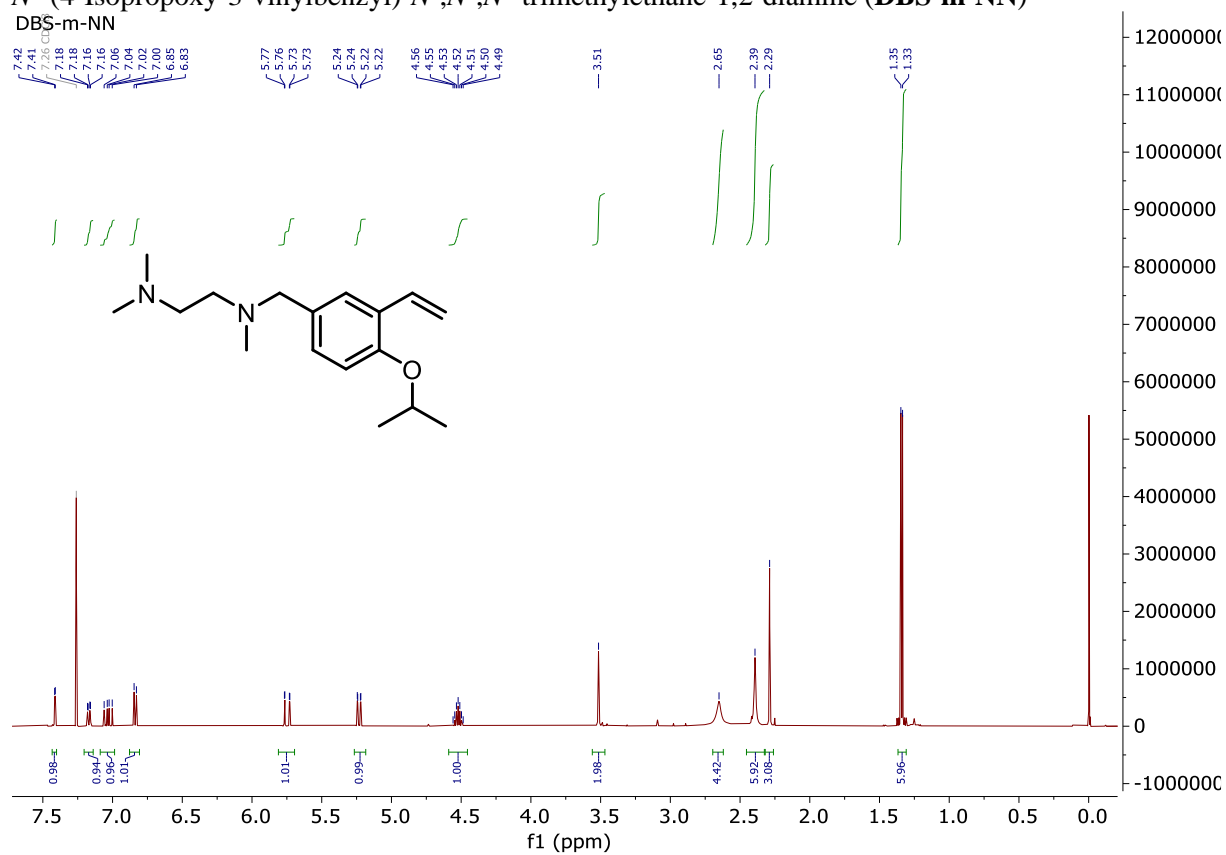
- 7.60, 7.59, 7.59, 7.54, 7.53, 7.53, 7.52 (DBS12)
- 7.26 (CDCl₃)
- 7.00, 6.98, 6.96, 6.94, 6.90, 6.88
- 5.82, 5.82, 5.78, 5.78
- 5.30, 5.29, 5.29, 5.28, 5.28
- 4.62, 4.61, 4.60, 4.58, 4.57, 4.56, 4.55
- 3.82, 3.81, 3.79
- 3.28
- 2.81, 2.80, 2.78
- 2.27, 1.38, 1.38, 1.38, 1.38, 1.38, 1.37, 1.37, 1.37, 1.36, 1.35, 1.34, 1.34, 1.34, 1.34, 1.34, 1.33, 1.33

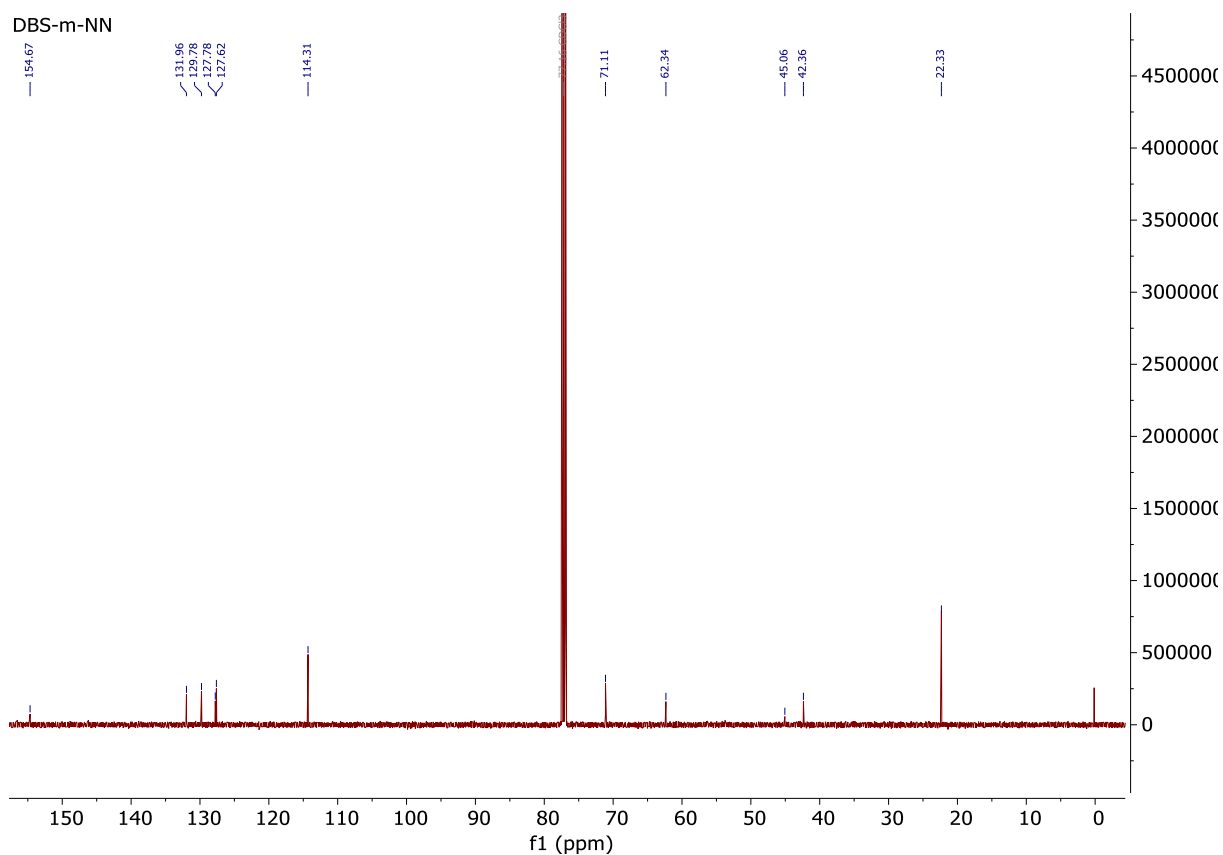
Integration values: 0.99, 0.99, 0.98, 0.98, 0.99, 1.02, 1.94, 1.00, 1.98, 5.80, 2.01, 6.03, 5.84

Appendix

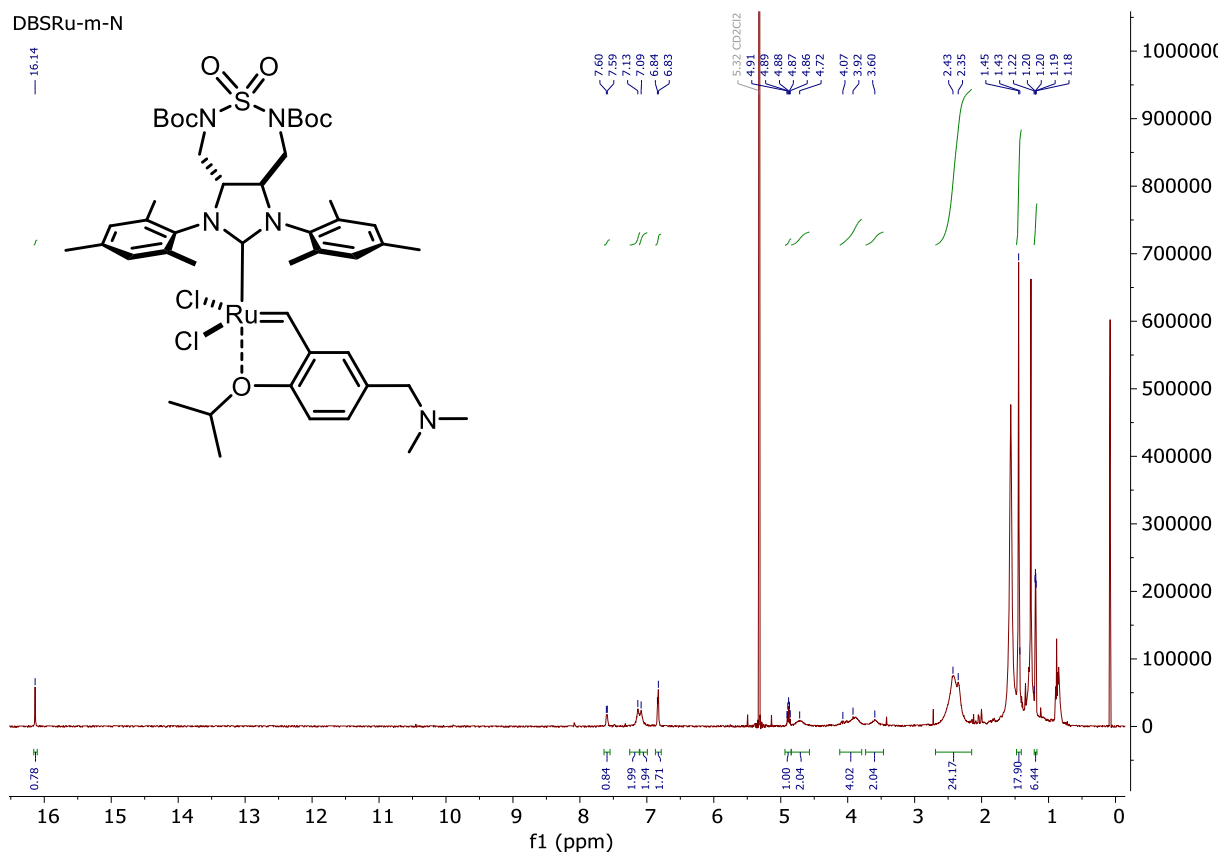


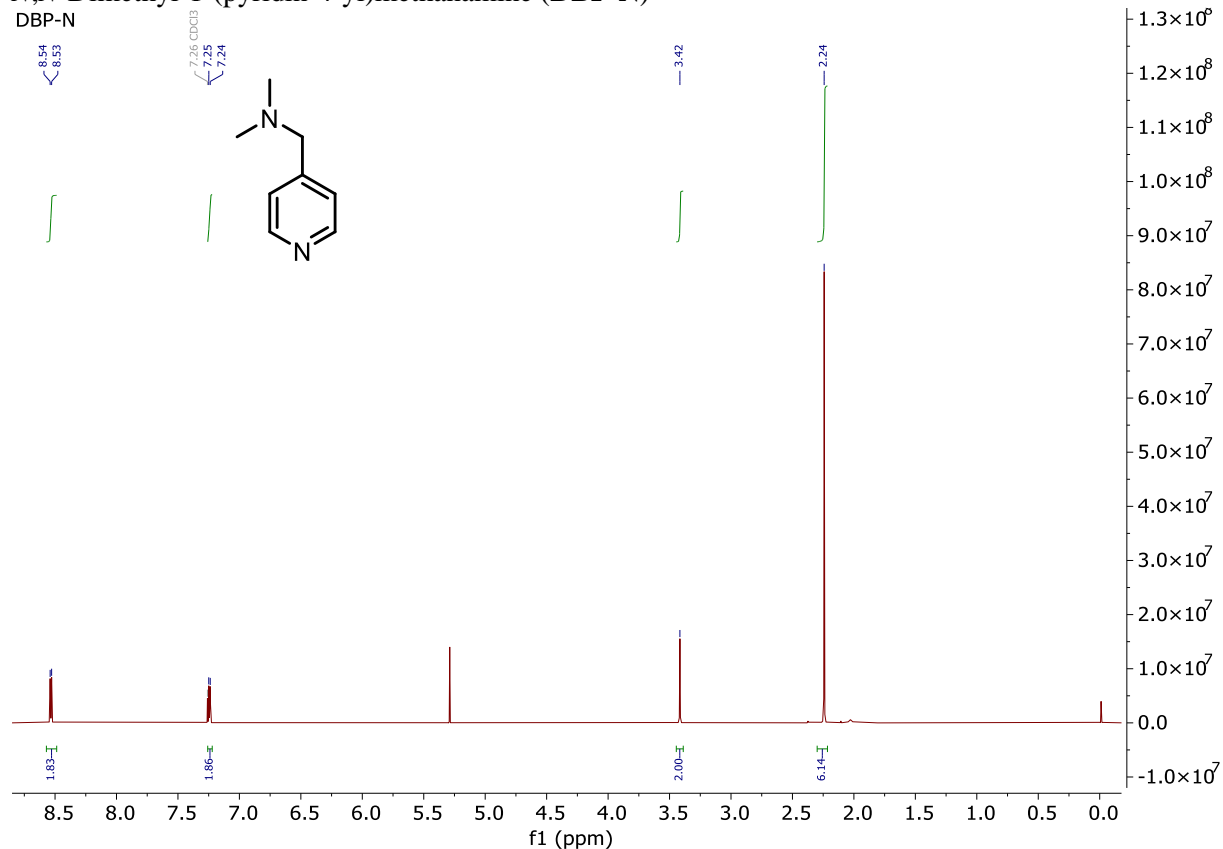
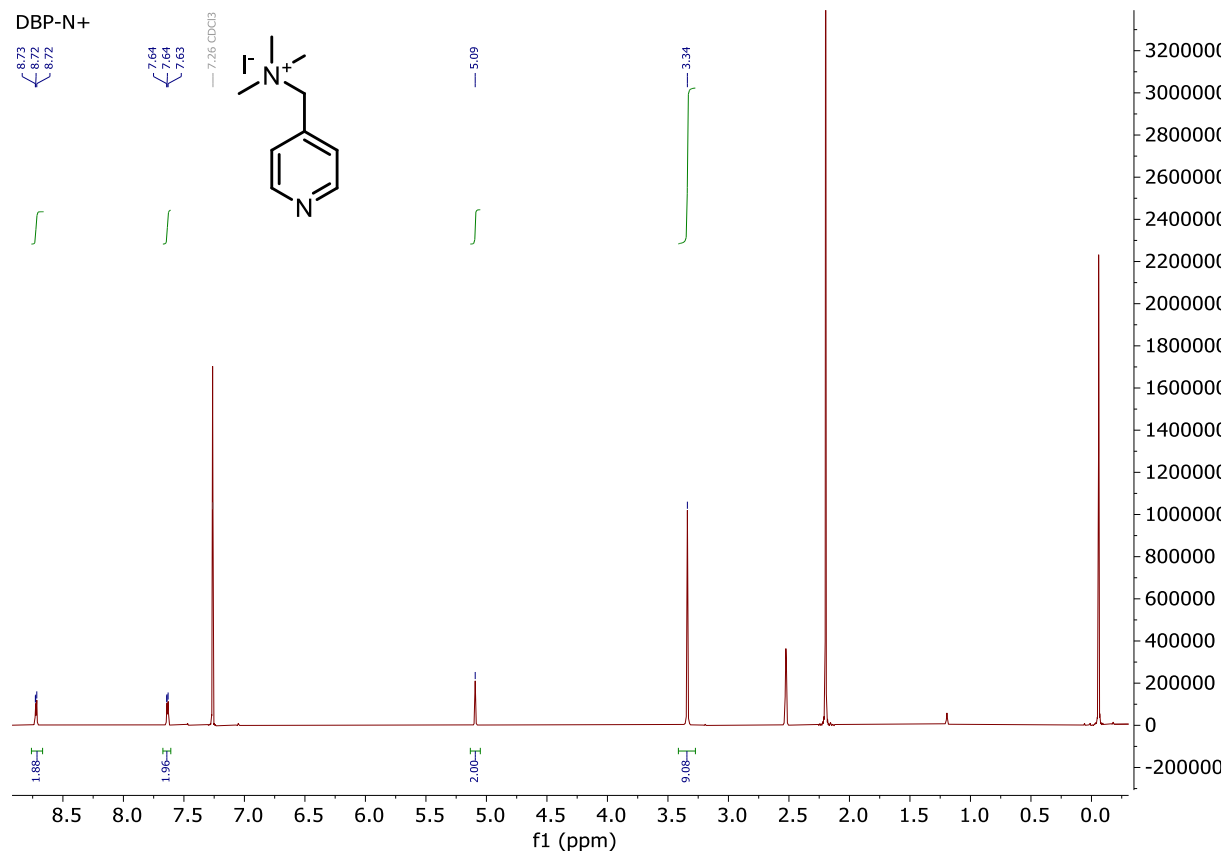
*N*¹-(4-Isopropoxy-3-vinylbenzyl)-*N*¹,*N*²,*N*²-trimethylethane-1,2-diamine (**DBS-m-NN**)

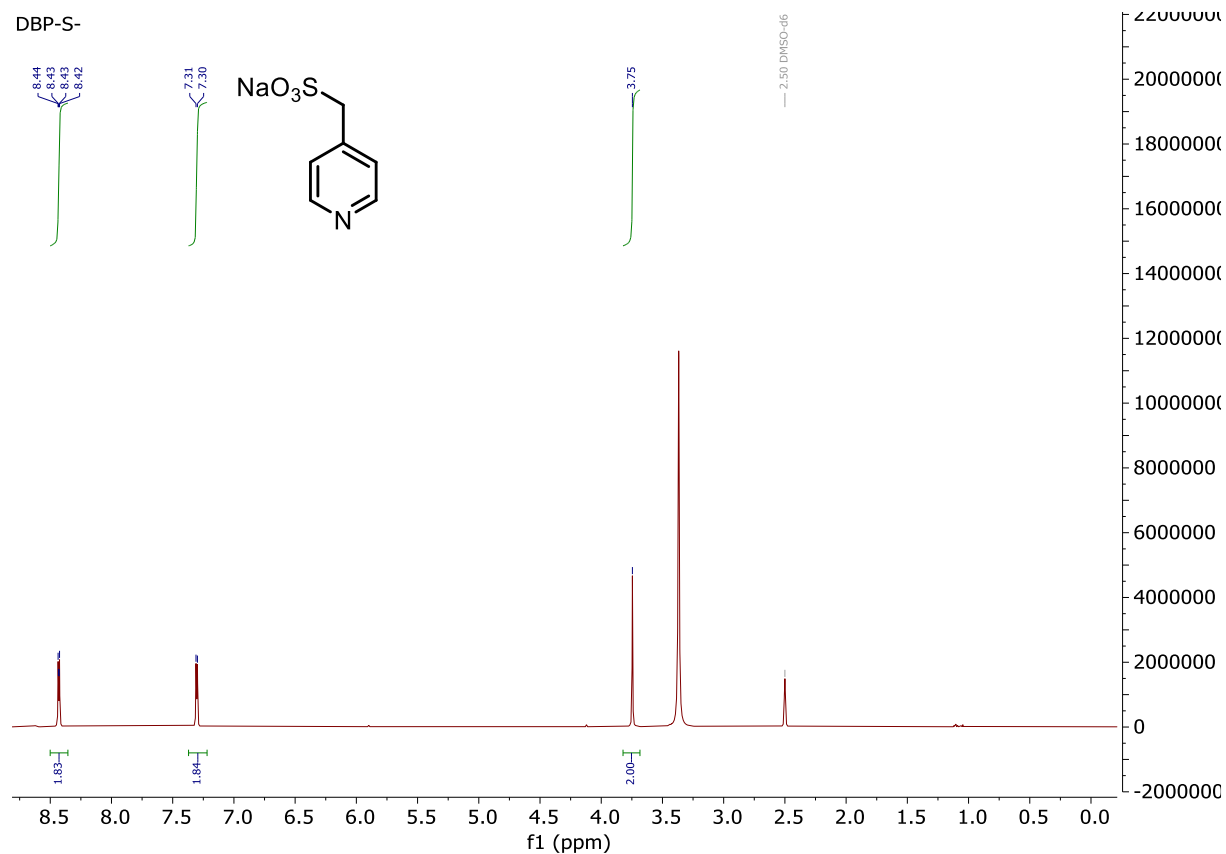
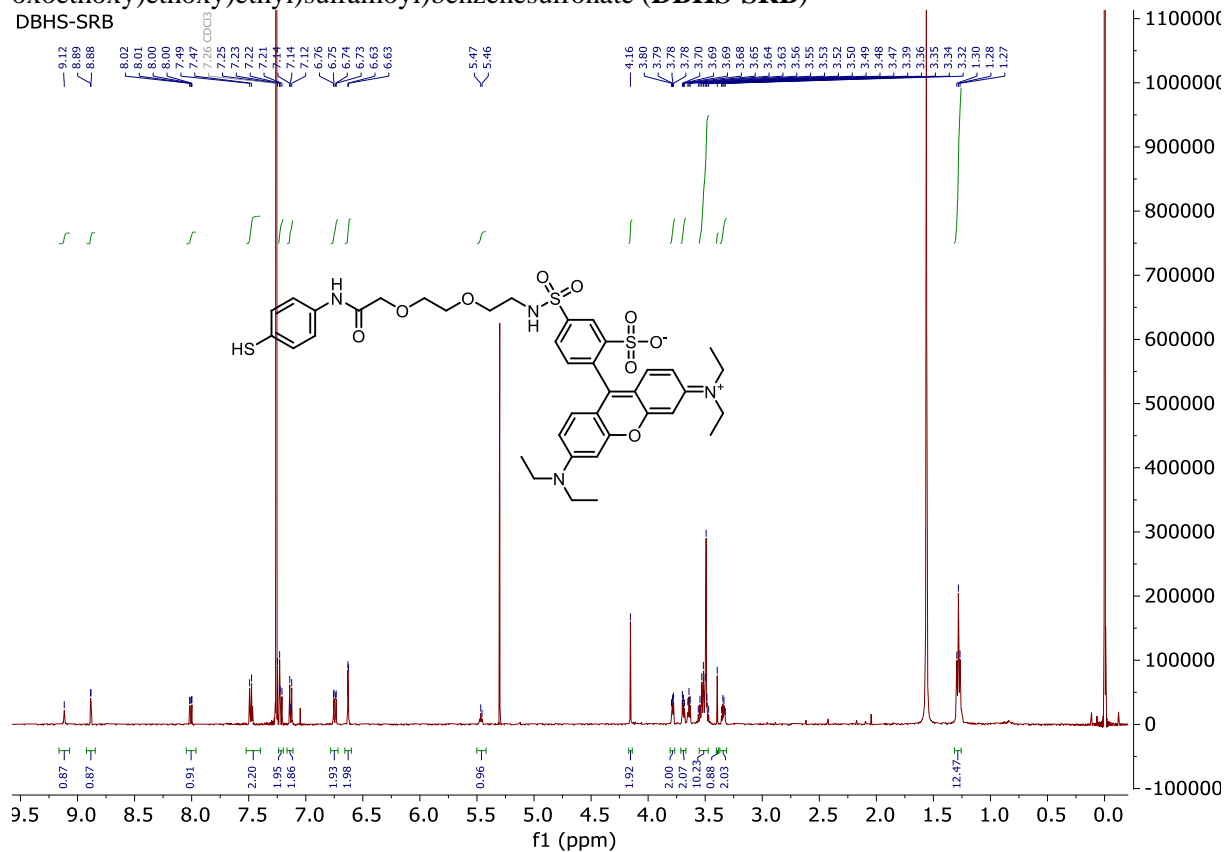


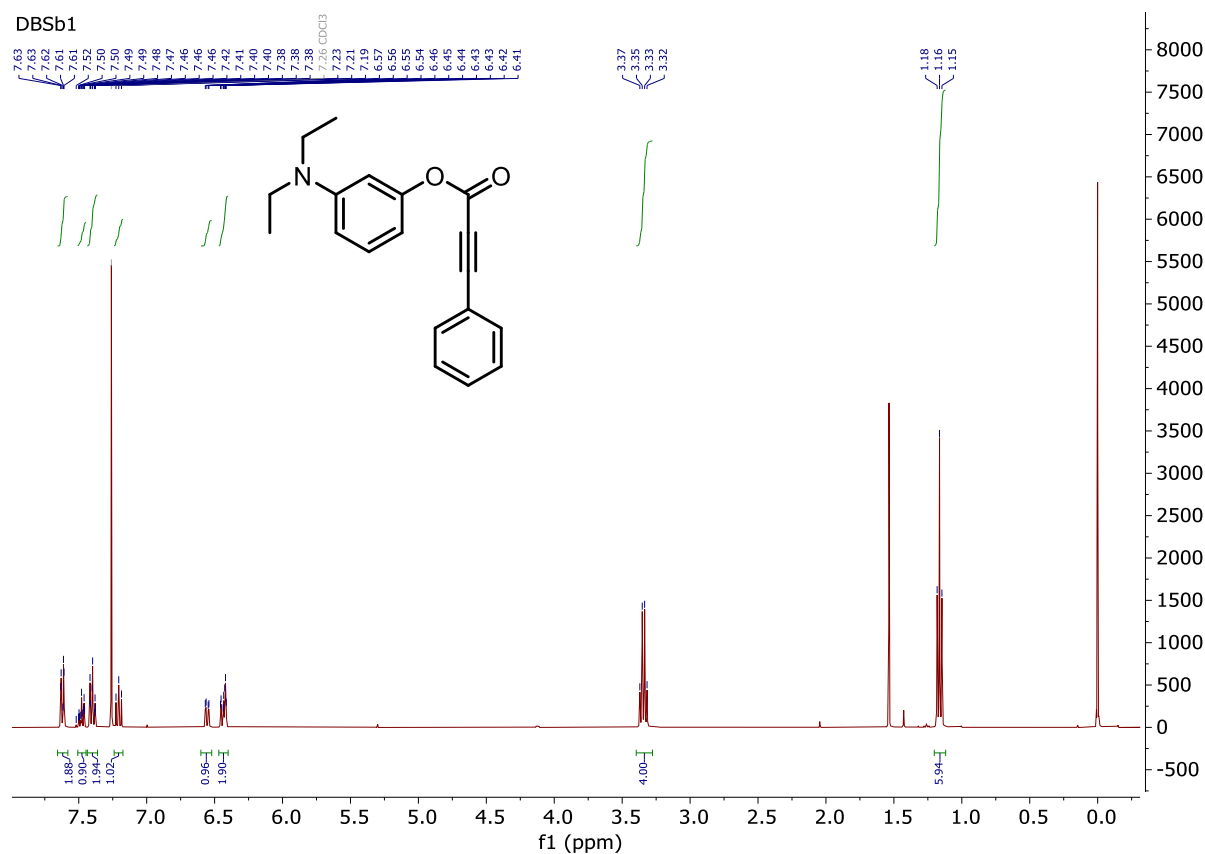
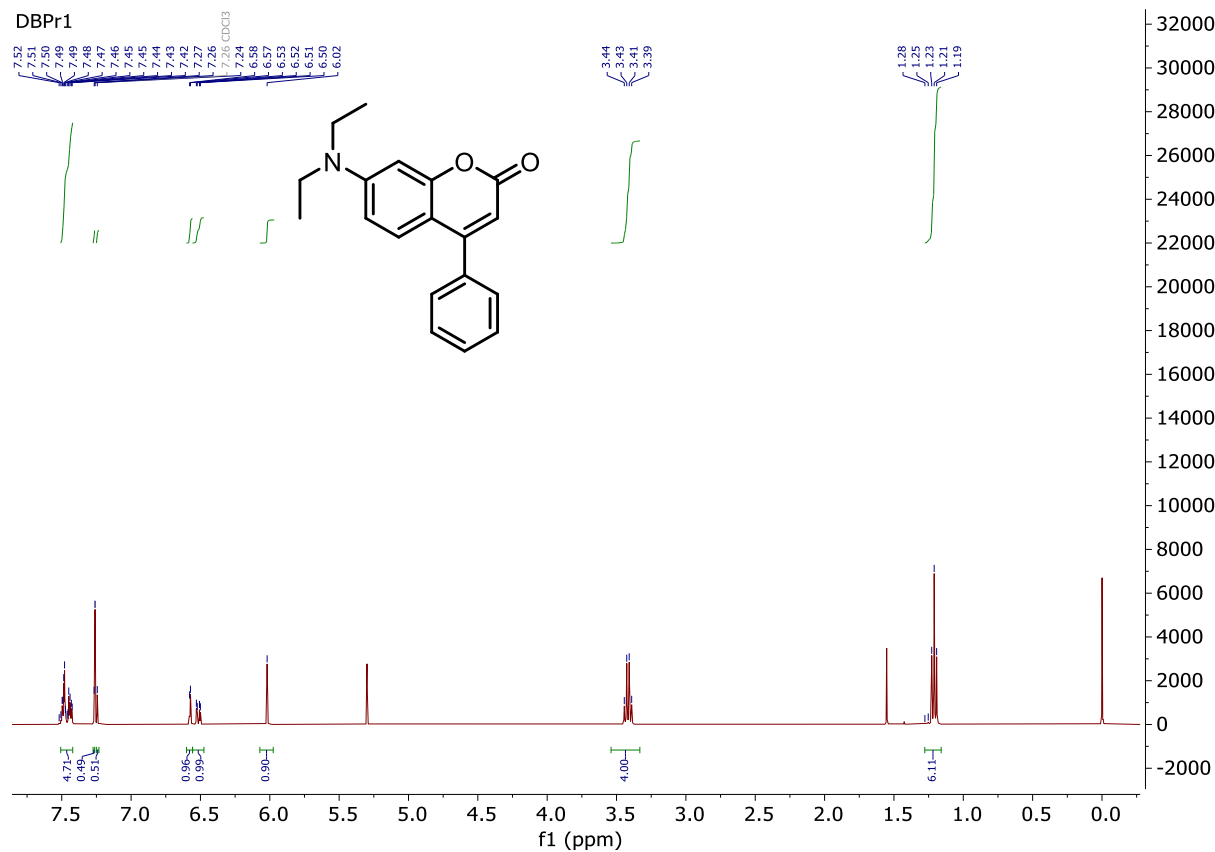


Dichloro((3a*R*,8a*R*)-5,7-bis(*tert*-butoxycarbonyl)-1,3-dimesityl-6,6-dioxidoctahydro-2*H*-imidazo[4,5-*d*][1,2,7]thiadiazepin-2-ylidene)-5-((dimethylamino)methyl)-2-isopropoxybenzylidene)ruthenium(II) (**DBSRu-m-N**)

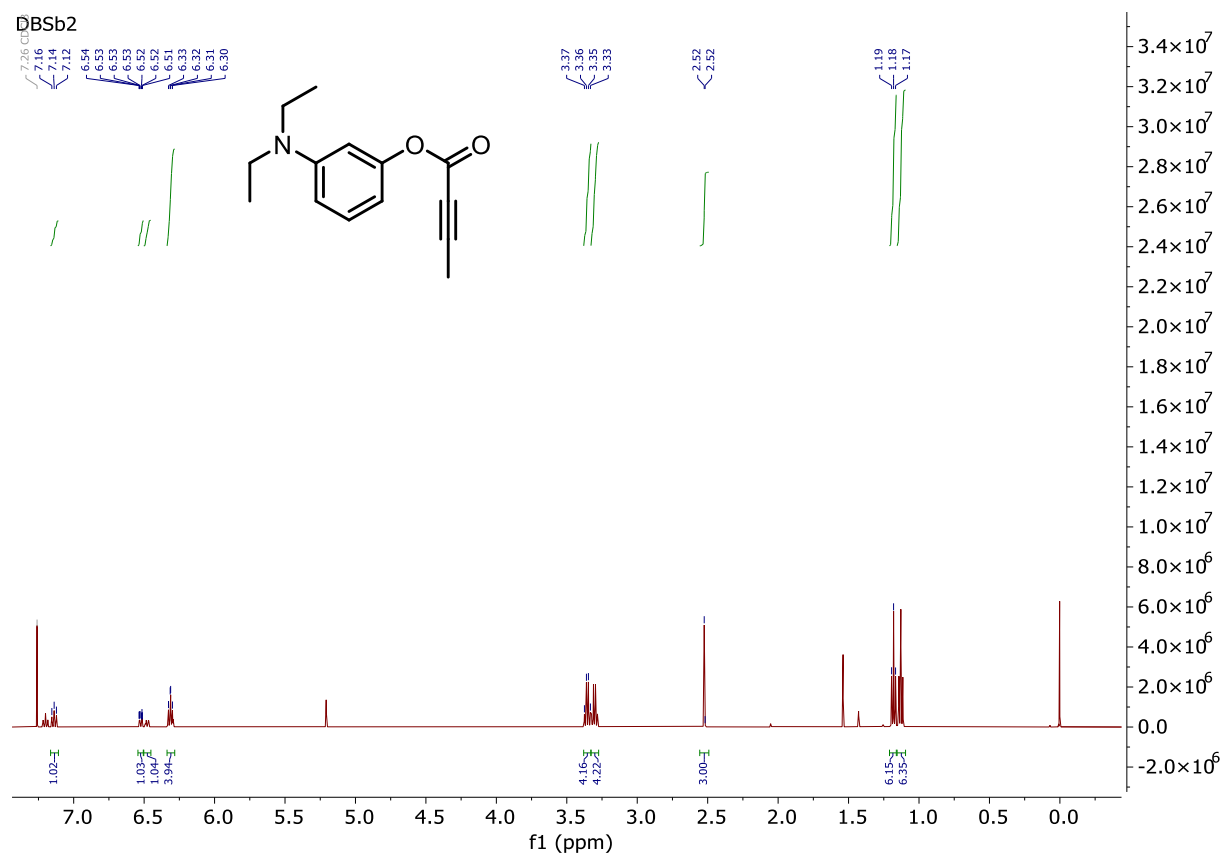


N,N-Dimethyl-1-(pyridin-4-yl)methanamine (**DBP-N**)*N,N,N*-trimethyl-1-(pyridin-4-yl)methanaminium iodide (**DBP-N⁺**)

Sodium pyridin-4-ylmethanesulfonate (**DBP-S-**)2-(6-(diethylamino)-3-(diethyliminio)-3*H*-xanthen-9-yl)-5-(*N*-(2-(2-(2-((4-mercaptophenyl)amino)-2-oxoethoxy)ethoxy)ethyl)sulfamoyl)benzenesulfonate (**DBHS-SRB**)

3-(Diethylamino)phenyl 3-phenylpropiolate (**DBSb1**)7-(Diethylamino)-4-phenyl-2H-chromen-2-one (**DBPr1**)

3-(Diethylamino)phenyl but-2-ynoate (DBSb2)



7-(Diethylamino)-4-methyl-2H-chromen-2-one (DBPr2)

